# Behaviour of displacement piles in overconsolidated clays

by

Andrew John Bond
MA, MSc, DIC, CEng, MICE

12th August 1989

A thesis submitted to the University of London
(Imperial College of Science, Technology, and Medicine)
in partial fulfillment of the requirements for the degree of
Doctor of Philosophy in the Faculty of Engineering

BIBL. LONDIN. UNIV.

# Abstract

## ABSTRACT

The aim of this Thesis is to explain the behaviour of displacement piles in terms of effective stresses.

The Thesis describes a series of field experiments using instrumented piles jacked into London clay. The field work was performed at the test-bed site at Canons Park, north London. A total of five instrumented pile tests were performed, in which earth and pore water pressures were measured along the pile shaft throughout all stages of the pile's lifetime. In addition, the experimental programme involved tests on two (uninstrumented) driven piles, and the excavation of an inspection trench around a driven and a jacked pile.

Volume 1 of the Thesis comprises four parts.

Part I reviews existing methods of pile design; the theoretical behaviour of piles in clays; previous instrumented pile tests; and the ground conditions at Canons Park.

Part II describes the design of the instrumented piles; the strategy behind the programme of field tests; and the experimental procedures that were followed.

Part III presents the results obtained from the instrumented piles during installation, equalization, and load testing. It also includes results from the driven pile tests and the work associated with the inspection trench.

Finally, Part IV compares these results with theoretical predictions of pile behaviour and with the findings of other instrumented pile tests.

Volume 2 contains a series of appendices which provide information in support of the arguments put forward in the main body of the text.

The main conclusions from this research project are that:

i) Piles installed in heavily overconsolidated clays generate *negative* pore pressures along their shafts
ii) The increase in radial stress is heavily dependent on overconsolidation ratio (OCR) and distance behind the pile tip
iii) Residual shearing takes place during pile installation in medium and high plasticity, high OCR clays
iv) Equalization involves both consolidation *and* swelling, and proceeds at a fast pace
v) Load capacity depends on the mode and rate of installation
vi) Shaft capacity is controlled by the *effective* stresses acting at the pile/soil interface
vii) Existing theories of pile behaviour and existing design methods do not reflect these features of soil behaviour

At the end of Chapter 14, a new design method is proposed for displacement piles installed in high OCR clays.

# Acknowledgements

## ACKNOWLEDGEMENTS

The experimental work described in this Thesis was sponsored by the following organizations and companies:

- UK Government's Science and Engineering Research Council (SERC), through the agency of MTD Ltd
- Amoco (UK) Exploration Company
- BP International Ltd
- Conoco (UK) Ltd
- UK Government's Department of Energy
- Exxon Production Research Company
- Mobil Research and Development Corporation
- Saga Petroleum a.s.
- Shell (UK) Ltd

Their support, and that of their representatives, is gratefully acknowledged.

I would like to express my sincere gratitude to Richard Jardine for his encouragement throughout this project, and for his unbounded enthusiasm for the subject of this Thesis. His clear thinking has made a lasting impression on the work described herein, and it has forced me to look beyond the goals I had originally set myself. Richard should also get credit for the many suggestions he has made regarding the contents and presentation of this Thesis. I only hope his eye strain has not been as great as mine.

The success of the field work depended to a great extent on the efforts of my colleagues at Imperial College. Foremost amongst these was Alan Bolsher, whose contribution helped ensure that the Project did not flounder. Other colleagues who assisted in the field work are: Philip Smith; Graham Keefe; Richard Jardine; David French; Paul Bommer; Steve Ackerley; Tim Fitch; Rob Day; George Dounias; Deneys Schreiner; Mahmoud Mahmoud; Luis Bressani; Mike Crilly; Dalmos Nyaoro; Chris Menkiti; Andrew Chipling; Teta Georgiannou; Philippe Caroffe; and Andrew Hernshaw. I would also like to thank Mr Reg Munford of the Building Research

Establishment (BRE) for the many pieces of equipment that he procured, and for his assistance on site. Thanks also go to Messrs Gerwyn Price and John Powell of BRE for sparing so much of their time to this cause.

The surface stress transducers were designed in conjunction with Mr Clive Dalton of Cambridge Insitu, who was always willing to share his considerable experience in this field. I would like to thank Dr Bassett of King's College for his advice on designing the Cambridge load cells. Angus Skinner and Deneys Schreiner also assisted in the design work.

In the laboratory, much of the manufacturing of the equipment was done by Graham Keefe, Alan Bolsher, and Lou Spall. Steve Ackerley and Graham Keefe undertook the strain-gauging and other electrical tasks.

The photographs were produced by Andrew Chipling, whose efforts are greatly appreciated. I thought I knew what I wanted from the photographs, but Andrew inevitably knew better. I commend him on the excellence of his work, and thank him for his friendship. Richard Packer has been very kind throughout this period. Most of the figures herein were produced by Ms Alison Davis - sorry there were so many!

The computing facilities were maintained by David Potts and David Toll; and Mrs Kay Crooks and Miss Jessica Underhill gave unstinting service in the Civil Engineering Library.

I would like to thank Roger Keene for proof-reading the Thesis. Being an intelligent sort of a chap, Roger never let me get away with woolly thinking or muddled arguments. You never know, Rog, you may even have learnt something.

Last but never least, I want to thank Jenny for her patience over the past four years, and especially in recent months (while I have been writing). Her support has kept me going, and her love has kept me sane.

# Volume 1

## Table of Contents

## CHAPTER 1

## Introduction


1.1 THE USE OF DISPLACEMENT PILES IN OVERCONSOLIDATED CLAYS . . . . . 4
1.1.1 The use of displacement piles in civil engineering works 4
1.1.2 Typical ground conditions for displacement piles 5
1.1.3 Assessing the capacity of piles in clays 6
1.2 OVERVIEW OF THE CANONS PARK PROJECT . . . . . 9
1.3 OUTLINE OF THE THESIS . . . . . 10
1.3.1 Aim of the Thesis 10
1.3.2 Volumes 1 and 2 10
1.3.3 Contents of Volume 1: Chapters 1-15 11
1.3.4 Volume 2: Appendices 1-15 13
1.4 NOTES AND REFERENCES . . . . . 15


## CHAPTER 2

## Summary of existing methods of pile design


2.1 INTRODUCTION . . . . . 20
2.1.1 The "Soil Mechanics Triangle" 20
2.1.2 Literature Review (Chapters 2-4) 21
2.1.3 Outline of Chapter 2 21
2.1.4 Poulos's classification of analytical methods 22
2.1.5 Separating shaft capacity from end bearing 23
2.1.6 Co-ordinate system for axi-symmetric problems 24
2.2 "CATEGORY 1" ANALYSES: THE $\alpha$ METHOD . . . . . 26
2.2.1 Basis of the $\alpha$ method 26
2.2.2 Correlations with undrained shear strength 27
2.2.3 Variation of $\alpha$ with the undrained strength ratio 28
2.2.4 Variation of $\alpha$ with pile length 30
2.2.5 Variation of $\alpha$ with set-up time 32
2.3 "CATEGORY 2A" ANALYSES: THE $\beta$ METHOD . . . . . 35
2.3.1 Basis of the $\beta$ method 35
2.3.2 Existing formulae for $\beta$ 36
2.3.3 Discussion of the various formulae for $\beta$ 38
2.3.4 Correlations between $\beta$ and depth 41
2.3.5 General assessment of the $\beta$ method 41
2.3.6 "Local" or "average" values of $\beta$? 43
2.4 "CATEGORY 2B" ANALYSES: EFFECTIVE STRESS METHODS . . . 47
2.4.1 The ESACC programme 47
2.4.2 Philosophy behind the effective stress methods 47
2.4.3 Stress paths followed during a pile's lifetime 48
2.4.4 Differences between the models ESM1-4 49

2.4.5 Assessment of the effective stress methods 50
2.4.6 General comments on the effective stress methods 51
2.5 NOTES AND REFERENCES . . . . . 53


## CHAPTER 3

## Theoretical behaviour of displacement piles in clay


3.1 EXISTING THEORIES OF PILE BEHAVIOUR . . . . . 63
3.2 AN OUTLINE OF THE CAVITY EXPANSION METHOD . . . . . 65
3.2.1 Background to the method 65
3.2.2 Central assumption of all cavity expansion methods 67
3.2.3 Main differences between various cavity expansion methods 67
3.3 AN OUTLINE OF THE STRAIN PATH METHOD . . . . . 69
3.3.1 Background to the method 69
3.3.2 Basic principles of the strain path method 69
3.3.3 Constitutive models 71
3.4 PILE INSTALLATION . . . . . 75
3.4.1 Ground movements induced by pile driving 75
3.4.2 Changes in total stress due to pile installation 79
3.4.3 Pore pressures at the end of pile installation 84
3.4.4 Effective stresses at the end of pile installation 88
3.4.5 Variation of stresses behind the pile tip 92
3.4.6 Discussion 94
3.5 EQUALIZATION STAGE . . . . . 95
3.5.1 Dissipation of excess pore pressures 95
3.5.2 Radial total and effective stresses 103
3.5.3 Orientation of the principal stresses 106
3.5.4 Effective stress paths during equalization 107
3.6 BEHAVIOUR DURING LOADING . . . . . 109
3.6.1 Key assumptions regarding pile loading 109
3.6.2 Drained or undrained loading? 110
3.6.3 Stress changes during drained loading 110
3.6.4 Stress changes during undrained loading 111
3.6.5 Analogy between pile loading and simple shear tests 112
3.6.6 Strain path predictions based on the MIT-E3 model 112
3.6.7 Predictions of the coefficient of friction 113
3.6.8 Orientation of the principal stresses 117
3.6.9 Direction of loading 118
3.6.10 Summary of Section 118
3.7 NOTES AND REFERENCES . . . . . 119

## CHAPTER 4

## Review of instrumented pile tests


4.1 INTRODUCTION . . . . . 128
4.1.1 The purpose of instrumentation 128
4.1.2 Outline of Chapter 4 129
4.2 SURVEY OF PREVIOUS INSTRUMENTED PILE TESTS . . . . . 130
4.2.1 Introduction 130
4.2.2 Categorizing the range of measurements 131
4.2.3 Category A, B, and C tests 132
4.2.4 "Quality" of the test results 134
4.2.5 Main parameters of interest 135
4.2.6 Correlations between the various parameters 138
4.2.7 A note on the meaning of OCR 139
4.3 PILE INSTALLATION . . . . . 141
4.3.1 Pore pressure measurements at the pile shaft 141
4.3.2 Pore pressure measurements in the surrounding soil 146
4.3.3 Radial total stresses 146
4.3.4 Radial effective stresses 151
4.4 EARTH AND PORE PRESSURE EQUALIZATION . . . . . 154
4.4.1 Pore pressure dissipation 154
4.4.2 Changes in total stress 156
4.4.3 Radial effective stresses 158
4.5 PILE LOADING . . . . . 163
4.5.1 Introduction 163
4.5.2 Effective stress data for contractive clays 163
4.5.3 Effective stress data for dilating clays 167
4.5.4 Differences between the behaviour of jacked and driven piles 169
4.5.5 Investigations of particle re-orientation next to piles 170
4.5.6 Other investigations of the clay fabric around piles 174
4.6 NOTES AND REFERENCES . . . . . 177


## CHAPTER 5

## Ground conditions at Canons Park


5.1 INTRODUCTION . . . . . 184
5.1.1 Location and history of the Canons Park site 184
5.1.2 Outline of the Chapter 187
5.2 INVESTIGATIONS OF THE CANONS PARK SITE . . . . . 188
5.2.1 Previous site investigations 188
5.2.2 Boreholes 188
5.2.3 Imperial College laboratory test programme 188
5.2.4 BRE laboratory programme 190
5.2.5 Field tests 191
5.2.6 Previous research into pile behaviour 191
5.3 SOIL PROFILE . . . . . 192
5.3.1 Main strata 192

| | | | |
|---|---|---|---|
| | 5.3.2 | CPT and piezocone profiles | 193 |
| | 5.3.3 | BRE's trial pit through the gravel layer | 195 |
| | 5.3.4 | Piezometer records | 195 |
| 5.4 | SOIL PROPERTIES . . . . . | | 196 |
| | 5.4.1 | Undrained shear strength; water contents; Atterberg limits | 196 |
| | 5.4.2 | In situ horizontal stresses | 198 |
| | 5.4.3 | Overconsolidation ratio | 201 |
| | 5.4.4 | Cavity expansion limit pressure | 205 |
| | 5.4.5 | Soil stiffness | 207 |
| 5.5 | RING SHEAR EXPERIMENTS ON THE LONDON CLAY . . . . . | | 208 |
| | 5.5.1 | Basic shear mechanisms | 208 |
| | 5.5.2 | Sliding shear behaviour | 208 |
| | 5.5.3 | Transitional shear | 209 |
| | 5.5.4 | Special tests to simulate pile installation and loading | 210 |
| | 5.5.5 | Ring-shear data for London clay from Canons Park | 212 |
| 5.6 | NOTES AND REFERENCES . . . . . | | 214 |


## CHAPTER 6

## Design and development of the Imperial College Instrumented Pile


| | | | |
|---|---|---|---|
| 6.1 | INTRODUCTION . . . . . | | 223 |
| 6.2 | INSTRUMENTATION FOR TEST SERIES CP1 . . . . . | | 224 |
| | 6.2.1 | Refurbishment of the Southampton Pile | 224 |
| | 6.2.2 | Main features of Pile CP1 | 224 |
| | 6.2.3 | Saturation of the pore pressure probes | 224 |
| | 6.2.4 | Field performance of the Southampton Pile | 226 |
| 6.3 | MAIN FEATURES OF THE IMPERIAL COLLEGE INSTRUMENTED PILE . . . . . | | 227 |
| | 6.3.1 | General arrangement | 227 |
| | 6.3.2 | Waterproofing the pile | 231 |
| | 6.3.3 | Tests at Canons Park and Labenne | 231 |
| 6.4 | DESIGN OF THE AXIAL LOAD CELLS . . . . . | | 233 |
| | 6.4.1 | General description | 233 |
| | 6.4.2 | Design requirements | 234 |
| | 6.4.3 | Design and manufacture of the Mk III ALCs | 234 |
| | 6.4.4 | Design calculations | 234 |
| | 6.4.5 | Calibration and testing | 235 |
| | 6.4.6 | Field performance | 236 |
| 6.5 | DESIGN OF THE SURFACE STRESS TRANSDUCERS . . . . . | | 237 |
| | 6.5.1 | General description | 237 |
| | 6.5.2 | Design requirements | 241 |
| | 6.5.3 | Design and manufacture of the Mk IV SSTs | 241 |
| | 6.5.4 | Design calculations | 242 |
| | 6.5.5 | Calibration and testing | 243 |
| | 6.5.6 | Cell action effects (under-registration of loads) | 243 |
| | 6.5.7 | Field performance of the surface stress transducers | 245 |
| 6.6 | GENERAL REQUIREMENTS FOR MEASURING PORE PRESSURES . . | | 246 |

6.7 DESIGN OF FAST-ACTING PORE PRESSURE PROBES . . . . . 247
6.7.1 General description 247
6.7.2 Design requirements 247
6.7.3 Design and manufacture of the Mark III PPPs 248
6.7.4 Saturation of the pore pressure probes 251
6.7.5 Calibration and testing 253
6.7.6 Field performance of the fast-acting probes 254
6.8 DESIGN OF THE FLUSHABLE PORE PRESSURE SYSTEM . . . . . 256
6.8.1 General description 256
6.8.2 Design details - pore pressure probes (Mark IV) 256
6.8.3 Design details - half-way housing 258
6.8.4 Calibration and testing 261
6.8.5 Saturation procedure 261
6.8.6 Field performance of the flushable pore pressure system 262
6.9 NOTES AND REFERENCES . . . . . 263


## CHAPTER 7

## Programme of tests at Canons Park


7.1 INTRODUCTION . . . . . 270
7.1.1 The Canons Park Project 270
7.1.2 Outline of Chapters 7 and 8 270
7.2 SCOPE OF THE RESEARCH PROGRAMME . . . . . 272
7.2.1 Programme-of-Works 272
7.2.2 Instrument development 272
7.2.3 Field work at Canons Park 274
7.3 STRATEGY ADOPTED FOR THE PILE TESTS . . . . . 275
7.3.1 Main parameters of interest 275
7.3.2 Pile installation 275
7.3.3 Equalization times 278
7.3.4 Loading direction: first-time loading 278
7.4 NOMENCLATURE . . . . . 279
7.4.1 Main numbering system 279
7.4.2 Individual stages of a Test Series 280
7.4.3 Parameters measured by the Instrumented Pile 280
7.4.4 Leading, following, and trailing instrument positions 281
7.4.5 "Fast" and "slow" jacking rates 281
7.4.6 Short, medium, and long equalization periods 281
7.5 NOTES AND REFERENCES . . . . . 282


## CHAPTER 8

## Instrumented pile tests: test procedures


8.1 GENERAL TEST PROCEDURES . . . . . 286
8.1.1 Introduction 286
8.1.2 Pile preparation 286
8.1.3 Installation of the instrumented piles 286

| | | | |
|---|---|---|---|
| | 8.1.4 | Load testing | 289 |
| | 8.1.5 | Pile extraction | 291 |
| 8.2 | SPECIAL PROCEDURES FOR TEST SERIES CP4 . . . . . | | 293 |
| | 8.2.1 | Introduction | 293 |
| | 8.2.2 | Falling-head permeability test: CP4f/FHK | 293 |
| | 8.2.3 | Hydraulic fracture tests: CP4f/HF | 293 |
| 8.3 | DATA ACQUISITION . . . . . | | 295 |
| | 8.3.1 | Outline of the data acquisition system | 295 |
| | 8.3.2 | Logging intervals | 296 |
| | 8.3.3 | Data reduction | 296 |
| 8.4 | NOTES AND REFERENCES . . . . . | | 298 |


## CHAPTER 9

## Results of instrumented pile tests: pile installation


| | | | |
|---|---|---|---|
| 9.1 | INTRODUCTION . . . . . | | 302 |
| | 9.1.1 | Outline of Chapters 9-14 | 302 |
| | 9.1.2 | Presentation of the data | 302 |
| | 9.1.3 | Coop's test at Canons Park | 303 |
| 9.2 | PORE PRESSURES . . . . . | | 305 |
| | 9.2.1 | Traces from CP5f/IN | 305 |
| | 9.2.2 | Summary diagrams for Test Series CP2-5 | 307 |
| 9.3 | RADIAL TOTAL STRESSES . . . . . | | 309 |
| | 9.3.1 | Traces from experiment CP4f/IN | 309 |
| | 9.3.2 | Summary diagrams for Test Series CP0-5 | 309 |
| | 9.3.3 | The "z/R effect" | 313 |
| | 9.3.4 | Comparison with existing theories | 314 |
| | 9.3.5 | Radial total stresses at the end of installation | 315 |
| 9.4 | RADIAL EFFECTIVE STRESSES . . . . . | | 317 |
| | 9.4.1 | Summary diagrams for Test Series CP2-5 | 317 |
| | 9.4.2 | The z/R effect | 318 |
| | 9.4.3 | Comparison with existing theories | 319 |
| 9.5 | SHEAR STRESSES . . . . . | | 320 |
| | 9.5.1 | Traces from experiment CP4f/IN | 320 |
| | 9.5.2 | Summary diagrams for Test Series CP0-5 | 321 |
| | 9.5.3 | Correlations with the clay's undrained shear strength | 321 |
| | 9.5.4 | The rate effect in terms of average $\alpha$ values | 323 |
| | 9.5.5 | The z/R effect | 325 |
| 9.6 | DISCUSSION . . . . . | | 326 |
| 9.7 | NOTES AND REFERENCES . . . . . | | 328 |

## CHAPTER 10

## Results of instrumented pile tests: equalization period


10.1 INTRODUCTION . . . . . 332
10.2 PORE PRESSURE DISSIPATION . . . . . 333
10.2.1 Typical pore pressure response over the first two days 333
10.2.2 The excess pore pressure ratio, $\Delta u/\sigma'_{vo}$ 334
10.2.3 Values of the coefficient of horizontal consolidation 336
10.3 RELAXATION OF RADIAL TOTAL STRESSES . . . . . 338
10.3.1 Results of long-term experiments CP0 and CP2 338
10.3.2 The normalized horizontal total stress H 338
10.3.3 Radial total stresses after 36h 341
10.4 CHANGES IN RADIAL EFFECTIVE STRESS . . . . . 342
10.4.1 Changes in radial effective stress over the first two days 342
10.4.2 Radial effective stresses after 36h 343
10.4.3 Comparison with existing theories 343
10.5 RESULTS OF SPECIAL TESTS ON PILE CP4f . . . . . 345
10.5.1 Falling-head permeability tests CP4f/FHK 345
10.5.2 Hydraulic fracture tests CP4f/HF 346
10.6 DISCUSSION . . . . . 349
10.7 NOTES AND REFERENCES . . . . . 350


## CHAPTER 11

## Results of the instrumented pile tests: behaviour during load testing


11.1 INTRODUCTION . . . . . 354
11.1.1 Outline of chapter 354
11.1.2 Importance of the rate of installation 354
11.2 LOAD-DISPLACEMENT CHARACTERISTICS . . . . . 356
11.2.1 Fast-jacked pile CP5f 356
11.2.2 Slow-jacked pile CP3fs . 358
11.2.3 Summary of $\alpha$ and $\beta$ values 360
11.3 PORE PRESSURES DURING PILE LOADING . . . . . 363
11.3.1 Load tests on fast-jacked pile CP5f 363
11.3.2 Load tests on slow-jacked pile CP3fs 364
11.3.3 Summary of pore pressure changes 366
11.4 RADIAL TOTAL STRESSES . . . . . 367
11.4.1 Load tests on fast-jacked pile CP5f 367
11.4.2 Load tests on slow-jacked pile CP3fs 368
11.4.3 Summary of radial total stress changes 369
11.5 RADIAL EFFECTIVE STRESSES . . . . . 370
11.6 SHEAR STRESSES . . . . . 372
11.6.1 Shear stresses mobilized by fast-jacked pile CP5f 372
11.6.2 Shear stresses mobilized by slow-jacked pile CP3fs 374

11.7 COEFFICIENTS OF FRICTION . . . . . 376
11.7.1 Introduction 376
11.7.2 Load tests on fast-jacked pile CP5f 376
11.7.3 Load tests on slow-jacked pile CP3fs 378
11.8 EFFECTIVE STRESS PATHS FOLLOWED DURING PILE LOADING . 379
11.8.1 Introduction 379
11.8.2 Load tests on fast-jacked pile CP5f 379
11.8.3 Load tests on slow-jacked pile CP3fs 381
11.9 DISCUSSION . . . . . 383
11.9.1 Key findings from load-displacement data 383
11.9.2 Summary of the behaviour in terms of effective stresses 383
11.10 NOTES AND REFERENCES . . . . . 386


## CHAPTER 12

## Driven pile tests


12.1 INTRODUCTION . . . . . 390
12.2 FABRICATION, INSTALLATION, AND LOAD TESTING . . . . . 391
12.2.1 Fabrication of the driven piles 391
12.2.2 Pile installation 391
12.2.3 Load testing 392
12.2.4 Pile extraction 392
12.3 RESULTS OF TENSION TESTS ON DRIVEN PILES . . . . . 393
12.4 DISCUSSION . . . . . 395
12.5 NOTES AND REFERENCES . . . . . 396


## CHAPTER 13

## Pile inspection trench


13.1 INTRODUCTION . . . . . 400
13.2 GENERAL FEATURES OF THE INSPECTION TRENCH . . . . . 403
13.2.1 Excavation of the inspection trench 403
13.2.2 Sampling/test schedule 405
13.3 SAMPLING AND IN SITU TEST PROCEDURES . . . . . 408
13.3.1 Water content samples (W) 408
13.3.2 Pocket penetrometer tests (PP) 408
13.3.3 Measurements of soil suction 409
13.3.4 Filter-paper samples (FP) 410
13.3.5 Pressure-plate measurements of soil suction 411
13.3.6 Air-dried samples (AD) 412
13.3.7 X-ray specimens (X) 412
13.3.8 Thin-sections (TS) 414
13.4 VARIATIONS IN THE SOIL'S PROPERTIES BETWEEN THE PILES 416
13.4.1 Introduction 416
13.4.2 Water content variation 416
13.4.3 Variations in the soil's consistency 417
13.4.4 Variations in soil suction 418
13.5 EXAMINING THE SOIL FABRIC NEXT TO THE PILES . . . . . 422
13.5.1 Introduction 422

13.5.2 Visual examination 422
13.5.3 X-ray examination 426
13.5.4 Micro-fabric observations 431
13.6 DISCUSSION . . . . . 441
13.7 NOTES AND REFERENCES . . . . . 442

## CHAPTER 14

## Discussion of test results

14.1 INTRODUCTION . . . . . 446
14.1.1 Outline of the chapter 446
14.1.2 Summary of results from Canons Park 446
14.1.3 Comparisons with other high quality field experiments 447
14.1.4 Comparisons with theory 448
14.2 PILE INSTALLATION . . . . . 449
14.2.1 Pore pressure response 449
14.2.2 Radial total stresses 454
14.2.3 Radial effective stresses 458
14.2.4 Coefficients of friction 460
14.3 EARTH AND PORE PRESSURE EQUALIZATION . . . . . 465
14.3.1 Pore pressure dissipation 465
14.3.2 Relaxation of radial total stress 470
14.3.3 Changes in radial effective stress 471
14.4 PILE LOADING . . . . . 473
14.4.1 Introduction 473
14.4.2 Radial effective stress at the end of equalization 474
14.4.3 Changes in radial effective stress during pile loading 478
14.4.4 Coefficients of friction 479
14.5 DESIGN METHOD FOR DISPLACEMENT PILES IN HIGH OCR CLAYS 482
14.5.1 A new design method for high OCR clays 482
14.5.2 Limitations of the new method 483
14.5.3 Determining the parameters needed for the new design method 483
14.5.4 Worked example 485
14.6 NOTES ON THE SELECTED CASE HISTORIES . . . . . 487
14.7 NOTES AND REFERENCES . . . . . 488

## CHAPTER 15

## Conclusions

15.1 INTRODUCTION . . . . . 494
15.2 PRINCIPAL EXPERIMENTAL RESULTS . . . . . 495
15.2.1 Pile installation (495)
15.2.2 Equalization stage (496)
15.2.3 Pile loading (497)
15.3 CONCLUSIONS CONCERNING EXISTING PILE THEORIES . . . . . 499
15.4 SUGGESTIONS FOR FURTHER RESEARCH . . . . . 500

# LIST OF FIGURES: VOLUME 1

## CHAPTER 1


Figure 1.1 Length and diameter of typical tubular steel piles . . . . . 4
Figure 1.2 Typical offshore foundation soil types . . . . 5
Figure 1.3 Distribution of stiff clay deposits in Britain 6
Figure 1.4 Popularity of various methods of assessing pile capacity in clays . . . . . 7
Figure 1.5 The Imperial College Instrumented Pile . . . . 8


## CHAPTER 2


Figure 2.1 Burland's "Soil Mechanics Triangle" . . . . . 20
Figure 2.2 Proportion of load carried by pile shaft (closed-ended piles) . . . . . 24
Figure 2.3 Co-ordinate system for axi-symmetric problems 25
Figure 2.4 Variation of $\alpha$ with $c_{uo}$ . . . . . 27
Figure 2.5 Variation of $\alpha$ with $c_{uo}/\sigma'_{vo}$ . . . . . 29
Figure 2.6 Variation of pile capacity with time . . . . . 33
Figure 2.7 Development of continuous displacement shear next to pile wall . . . . . 38
Figure 2.8 $f_s$ vs $\sigma'_{vo}\sqrt{OCR}$ from timber pile tests . . . . . 39
Figure 2.9 Variation of $\beta$ with $c_{uo}/\sigma'_{vo}$ . . . . . 40
Figure 2.10 Variation of beta with depth of penetration . 41
Figure 2.11 Dependence of $\beta$ on method of calculation: Magnus foundations . . . . . 45
Figure 2.12 Different stages in the life of a pile . . . . 48
Figure 2.13 Stress paths for the ESM models . . . . . 48


## CHAPTER 3


Figure 3.1 Different stages in the life of a pile . . . . 63
Figure 3.2 Predicted de-formations around a "simple pile" 70
Figure 3.3 Ground movements caused by pile driving . . . 76
Figure 3.4 Soil displacements during steady penetration of 60° cone . . . . . 78
Figure 3.5 Changes in total stress caused by cylindrical cavity expansion . . . . . 80
Figure 3.6 Increase in total stress as a function of rigidity index: cavity expansion predictions . 83
Figure 3.7 Vesic's "volume change factor" $\xi_v$ as a function of $I_r$ and $\Delta$ . . . . . 84
Figure 3.8 Excess pore pressures generated during pile installation: SPM and CEM predictions compared 86
Figure 3.9 MIT-E3 predictions for installation pore pressures: strain path method . . . . . 87
Figure 3.10 Effective stresses at the end of pile installation: cavity expansion predictions . . 89
Figure 3.11 Radial effective stresses at the end of pile installation: strain path and cavity expansion predictions compared . . . . . 90
Figure 3.12 MIT-E3 predictions for radial effective stresses following pile installation: strain path method 91

Figure 3.13 Variation in total stresses with distance behind the pile tip during installation: strain path predictions . . . . . 93
Figure 3.14 Pore pressure isochrones during consolidation: CEM initial stresses . . . . . 98
Figure 3.15 Decay of excess pore pressures with time: CEM initial stresses . . . . . 99
Figure 3.16 Pore pressure dissipation at pile wall: SPM initial stresses . . . . . 100
Figure 3.17 Dissipation of pore pressures at various points along a pile shaft . . . . . 101
Figure 3.18 Pore pressure dissipation as a function of Teh's time factor $T^*$ . . . . . 102
Figure 3.19 Changes in radial stress during equalization: initial stresses from SPM . . . . . 104
Figure 3.20 Effective stress paths during equalization: SPM (MIT-E3) predictions . . . . . 107
Figure 3.21 Stress paths followed during pile loading: CEM/MCC predictions . . . . . 111
Figure 3.22 Analogy be-tween un-drained load-ing of a pile and the stress paths in a simple shear test . . 112
Figure 3.23 Stress paths followed during undrained loading: MIT-E3 predictions . . . . . 113
Figure 3.24 Stress states for failure in the soil under two common assumptions . . . . . 115

CHAPTER 4

Figure 4.1 The purpose of instrumentation . . . . . 128
Figure 4.2 PLS cell measurements in Boston blue clay . . . 141
Figure 4.3 Results of Coop's experiment at Canons Park, north London . . . . . 142
Figure 4.4 Excess pore pressure ratio $\Delta u_i/\sigma'_{vo}$ as a function of OCR . . . . . 144
Figure 4.5 Comparison between theoretical and measured values of $\Delta u_i/\sigma'_{vo}$ . . . . . 145
Figure 4.6 Installation excess pore pres-sures versus radial position . . . . . 146
Figure 4.7 Radial total stresses recorded by Johnston in London clay . . . . . 147
Figure 4.8 Normalized horizontal total stress $H_i$ as a function of OCR . . . . . 149
Figure 4.9 Comparison of theoretical and measured values of $H_i$ . . . . . 150
Figure 4.10 Lateral stress coefficient $K_i$ as a function of OCR . . . . . 151
Figure 4.11 Comparison between theoretical and measured values of $K_i$ . . . . . 153
Figure 4.12 Equalization records in lower Boston blue clay 154
Figure 4.13 Equalization records in the Gault clay . . . . 155
Figure 4.14 Increase in $\sigma'_{rr}$ during equalization of Boston blue clay . . . . . 158
Figure 4.15 Lateral stress coefficient $K_o$ as a function of OCR . . . . . 160
Figure 4.16 Comparison of theoretical and measured values of $K_o$ . . . . . 162

Figure 4.17 Piezo-Lateral Stress cell . . . . . 164
Figure 4.18 Effective stress paths followed during load tests in Boston blue clay . . . . . 165
Figure 4.19 Load-displacement curves from Coop's tests in Gault clay . . . . . 168
Figure 4.20 Load-displacement curves from Tomlinson's tests at Stanmore . . . . . 169
Figure 4.21 Fabric disturbance caused by pile driving and jacking, in Martins' laboratory experiments . 172
Figure 4.22 Load-displacement curves for Martins' tests 11, 18, & 191 . . . . . 173

CHAPTER 5

Figure 5.1 Location of the Canons Park site . . . . . 184
Figure 5.2 Plan of the Canons Park site . . . . . 189
Figure 5.3 Soil profile at Canons Park . . . . . 192
Figure 5.4 Results of cone penetration and piezocone tests at Canons Park . . . . . 193
Figure 5.5 Casagrande piezometer readings at Canons Park, 1986-1988 . . . . . 195
Figure 5.6 Summary of soil properties at Canons Park . . 197
Figure 5.7 Self-boring pressuremeter test at Canons Park 198
Figure 5.8 Results of dilatometer tests at Canons Park . 199
Figure 5.9 $K_0$ profile for the Canons Park site . . . . . 200
Figure 5.10 Results of oedometer test on London clay from High Ongar and Canons Park . . . . . 202
Figure 5.11 Limit pressures from self-boring pressuremeter tests at Canons Park . . . . . 206
Figure 5.12 Shear stiffness of the London clay at Canons Park . . . . . 207
Figure 5.13 Special interface ring-shear tests on the London clay from Canons Park . . . . . 211
Figure 5.14 Dependency of stress ratio on rate of displacement in ring shear tests on London clay from Canons Park . . . . . 213

CHAPTER 6

Figure 6.1 Instrumentation for pile CP1 . . . . . 225
Figure 6.2 The Imperial College Instrumented Pile . . . . 227
Figure 6.3 Typical instrument cluster on the Instrumented Pile . . . . . 228
Figure 6.4 Section through an instrument cluster on pile CP2 . . . . . 232
Figure 6.5 Combined axial load cell and pore pressure unit 233
Figure 6.6 The surface stress transducer . . . . . 237
Figure 6.7 The "dogbone" Cambridge earth pressure cell . 238
Figure 6.8 Fast-acting pore pressure probe . . . . . 248
Figure 6.9 Procedure for saturating pore pressure system with silicone fluid . . . . . 252
Figure 6.10 Equipment used to saturate the fast acting pore pressure probes . . . . . 253
Figure 6.11 Typical pore pressures traces during pile installation . . . . . 254
Figure 6.12 Flushable pore pressure probe . . . . . 256

Figure 6.13 General arrangement of flushable pore pressure system . . . . . 257

CHAPTER 7

Figure 7.1 Programme-of-Works for the Canons Park Project 271
Figure 7.2 Piles installed at Canons Park by Imperial College . . . . . 273
Figure 7.3 Programme of pile tests at Canons Park . . . . 276
Figure 7.4 Notation used to describe the pile Test Series 279

CHAPTER 8

Figure 8.1 Loading frame used at Canons Park . . . . . 287
Figure 8.2 Arrangement for installing the instrumented piles . . . . . 288
Figure 8.3 Arrangements for load testing the piles . . . . 290
Figure 8.4 Creep diagram for load test CP5f/L1T . . . . . 292
Figure 8.5 Data acquisition system: from pile to printer . 295
Figure 8.6 Computer programs used for data reduction . . . 297

CHAPTER 9

Figure 9.1 Pore pressures recorded by leading instruments during pile installation, Test CP5f . . . . . 305
Figure 9.2 Pore pressures recorded by following instruments during pile installation, Test CP5f . . . . . 306
Figure 9.3 Summary diagram: pore pressures recorded by leading instruments during installation, Tests CP2-5 . . . . . 307
Figure 9.4 Summary diagram: pore pressures recorded by following instruments, Tests CP2-5 . . . . . 308
Figure 9.5 Radial total stresses recorded during installation of pile CP4f . . . . . 310
Figure 9.6 Summary diagram: radial total stresses recorded by leading instruments during pile installation, Tests CP0-5 . . . . . 311
Figure 9.7 Summary diagram: radial total stresses recorded by following instruments during pile installation, Tests CP0-5 . . . . . 312
Figure 9.8 Variation in radial total stress with distance behind the pile tip, Test CP5f/IN . . . . . 313
Figure 9.9 Variation in radial total stress with distance behind the pile tip, Tests CP2-5 . . . . . 314
Figure 9.10 Radial total stress along the pile at the end of installation, Tests CP0-5 . . . . . 316
Figure 9.11 Summary diagram: radial effective stresses recorded by leading instruments during pile installation, Tests CP2-5 . . . . . 317
Figure 9.12 Summary diagram: radial effective stresses recorded by the following instruments during pile installation, Tests CP2-5 . . . . . 318
Figure 9.13 Variation of radial effective stress with distance behind the pile tip, Test Series CP2-5 319
Figure 9.14 Shear stresses recorded during installation of pile CP4f . . . . . 320

Figure 9.15 Summary diagram: shear stresses recorded by leading instruments during pile installation, Tests CP0-5 . . . . . 322
Figure 9.16 Summary diagram: shear stresses recorded by following instruments during pile installation, Tests CP0-5 . . . . . 323
Figure 9.17 $\alpha$ and $\beta$ values recorded during the final stages of installation, Tests CP0-5 . . . . . 324
Figure 9.18 Variation in shear stress with distance behind the pile tip, Tests CP2-5 . . . . . 325

CHAPTER 10

Figure 10.1 Pore pressure response during first 44h after pile installation, Test CP5f . . . . . 333
Figure 10.2 Excess pore pressure ratio vs log time, Tests CP2-5 . . . . . 335
Figure 10.3 Changes in radial total stress during long-term equalization, Test Series CP0 and CP2 . . . . 339
Figure 10.4 Variation of the normalized horizontal total stress during the equalization period, Tests CP2-5 . . . . . 340
Figure 10.5 Radial total stresses along the pile, 36h after installation, Tests CP2-5 . . . . . 341
Figure 10.6 Changes in radial effective stresses over the first 48h after pile installation, Test CP5f . 342
Figure 10.7 Radial effective stresses acting on the pile, 36h after installation, Tests CP2-5 . . . . . 344
Figure 10.8 Results of falling-head permeability tests CP4f/FHK . . . . . 345
Figure 10.9 Results of hydraulic fracture tests CP4f/HF . 346

CHAPTER 11

Figure 11.1 Complete loading cycle for Pile CP5f . . . . . 357
Figure 11.2 Complete loading cycle for Pile CP3fs . . . . 359
Figure 11.3 Variation in $\alpha$ and $\beta$ values with equalization time . . . . . 361
Figure 11.4 Variations in pore pressure with pile displacement during load test CP5f/L1T . . . . 363
Figure 11.5 Variations in pore pressure with pile displacement during load test CP3fs/L1C . . . 365
Figure 11.6 Radial total stress changes with pile displacement, load test CP5f/L1T . . . . . 367
Figure 11.7 Radial total stress changes, load test CP3fs/L1C . . . . . 368
Figure 11.8 Changes in radial effective stress with pile displacement, load test CP5f/L1T . . . . . 370
Figure 11.9 Variations in shear stresses during load test CP5f/L1T . . . . . 372
Figure 11.10 Shear stresses mobilized during load test CP5f/L1T . . . . . 373
Figure 11.11 Shear stresses mobilized during load test CP5f/L2C . . . . . 374
Figure 11.12 Variations in shear stresses during load test CP3fs/L1C . . . . . 375

Figure 11.13 Coefficients of friction recorded during pile test CP5f/L1T . . . . . 377
Figure 11.14 Coefficients of friction from following and trailing instruments, during load test CP3fs/L1C . . . . . 378
Figure 11.15 Stress paths followed in load tests CP5f/L1T and L2C . . . . . 380
Figure 11.16 Stress paths followed in load tests CP3fs/L1C and L2T . . . . . 382

CHAPTER 12

Figure 12.1 Load-displacement curves for load tests CP6d/L1T and CP7do/L1T . . . . . 394

CHAPTER 13

Figure 13.1 General scheme of the inspection trench . . . . 404
Figure 13.2 Inspection trench: schedule of samples recovered from between the two piles . . . . . 406
Figure 13.3 Filter-paper samples . . . . . 411
Figure 13.4 X-ray and thin-section samples . . . . . 413
Figure 13.5 Variation in water content between driven and jacked piles . . . . . 416
Figure 13.6 Pocket penetrometer readings . . . . . 418
Figure 13.7 Soil suction at 3.86m near to the driven pile . 419
Figure 13.8 Normalized soil suction from filter-paper measurements . . . . . 420

CHAPTER 14

Figure 14.1 Comparison of theoretical and measured values of $\Delta u_i/\sigma'_{vo}$ . . . . . 453
Figure 14.2 Normalized horizontal total stress $H_i$ vs OCR . 454
Figure 14.3 The z/R effect, as measured in Johnston's tests 456
Figure 14.4 Comparison of theoretical and measured values of $H_i$ . . . . . 457
Figure 14.5 Lateral stress coefficient $K_i$ vs OCR . . . . . 459
Figure 14.6 Comparison of measured and theoretical values of $K_i$ . . . . . 460
Figure 14.7 $\alpha$ and $\beta$ values recorded during final stages of pile installation . . . . . 461
Figure 14.8 Profile of $\mu$ during pile installation: leading instruments (CP2f, 4f, & 5f) . . . . . 463
Figure 14.9 Comparison between observed pore pressure decay and simple theoretical decay curves . . . . . 468
Figure 14.10 Changes in $\sigma'_{rr}$ during CP5f/EQ . . . . . 471
Figure 14.11 Lateral stress coefficient $K_c$ vs OCR . . . . . 474
Figure 14.12 Relationship between $K_c$ and z/R for London & Oslo clays . . . . . 476
Figure 14.13 Comparison between measured and theoretical values of $K_c$ . . . . . 477
Figure 14.14 Design chart giving values of $K_c = f(OCR, z/R)$ 485
Figure 14.15 Estimates of skin friction for the Magnus piles 486

# LIST OF TABLES: VOLUME 1

## CHAPTER 2


Table 2.1 Values of $c_h$ (field) for a wide range of clay soils . . . . . 34
Table 2.2 Summary of effective stress models ESM1-ESM4 . 51


## CHAPTER 3


Table 3.1 Summary of cylindrical cavity expansion solutions used for modelling pile installation . . . . . 66
Table 3.2 List of soil models used at MIT with the strain path method . . . . . 72
Table 3.3 Installation pore pressures next to pile wall 88
Table 3.4 Radial effective stresses on pile installation in Boston blue clay (*London clay) . . . . . 92
Table 3.5 Summary of consolidation analyses for piles in clay . . . . . 96
Table 3.6 Time factors at various locations along a 60° cone penetrometer ($T = c_h t/R^2$) . . . . . 102
Table 3.7 Summary of radial total stresses during equalization for Boston blue clay (*for London clay) . . . . . 105
Table 3.8 Summary of radial effective stresses at the end of equalization, for Boston blue clay & *London clay . . . . . 106
Table 3.9 Orientation of principal stresses at the end of equalization . . . . . 107


## CHAPTER 4


Table 4.1 Range of measurements using instrumented piles 131
Table 4.2 Category A, B, and C instrumented pile tests . 132
Table 4.3 Criteria for assessing the quality of instrumented pile test results . . . . . 134
Table 4.4 Results of instrumented pile tests in clay soils . . . . . 136
Table 4.5 Effect of post-depositional processes on geotechnical properties of marine clays . . . 139
Table 4.6 $H_c/H_1$ in contractive clays . . . . . 157
Table 4.7 $K_1/K_c$ for contractive clays . . . . . 159
Table 4.8 Changes in stress during pile loading . . . . 166
Table 4.9 Load tests in the upper and middle layers of Boston blue clay . . . . . 166


## CHAPTER 5


Table 5.1 Results of cone tests at Canons Park . . . . . 194
Table 5.2 Pre-consolidation pressure at Canons Park . . 204
Table 5.3 Variation of OCR with depth . . . . . 205
Table 5.4 Results from interface ring-shear tests on London clay . . . . . 212

CHAPTER 6

Table 6.1 Calibration procedure for surface stress transducer . . . . . 244

CHAPTER 7

Table 7.1 Summary of pile tests at Canons Park . . . . . 275
Table 7.2 Installation details for piles CPO-7 . . . . . 277

CHAPTER 8

Table 8.1 Typical data-logging intervals . . . . . 296

CHAPTER 9

Table 9.1 Summary of alpha values recorded during pile installation . . . . . 327

CHAPTER 10

Table 10.1 Results of hydraulic fracture tests . . . . . 347

CHAPTER 11

Table 11.1 $\alpha$ and $\beta$ values recorded during Test Series CP5f 362
Table 11.2 $\alpha$ and $\beta$ values recorded during Test Series CP3fs . . . . . 362
Table 11.3 Changes in pore pressure during load tests, CP1-5 . . . . . 366
Table 11.4 Changes in radial total stress during load tests, CP1-5 . . . . . 369

CHAPTER 12

Table 12.1 Summary of driven pile tests at Canons Park . . 391
Table 12.2 Results of tension load tests on driven piles . 393

CHAPTER 13

Table 13.1 Orientation of potential shear surfaces on thin-sections . . . . . 432

CHAPTER 14

Table 14.1 Pore pressure response at the leading instrument position during installation of pile CP4f . . . 450
Table 14.2 $H_c/H_i$ and $K_i/K_c$ as recorded in Tests CP2-5 . . . 470
Table 14.3 Statistical analysis of relationship between $K_c$ and OCR . . . . . 484
Table 14.4 Worked example for Magnus foundations . . . . . 485

# LIST OF PLATES: VOLUME 1

## CHAPTER 5


| | | |
|---|---|---|
| Plate 1(a) | General view of the Canons Park site . . . . . | 185 |
| Plate 1(b) | View of the loading frame during pile installation . . . . . | 185 |


## CHAPTER 6


| | | |
|---|---|---|
| Plate 2 | Typical instrument cluster on the Imperial College Instrumented Pile . . . . . | 229 |
| Plate 3(a) | Surface stress transducer showing the "dogbone" load cell . . . . . | 239 |
| Plate 3(b) | Calibration rig for surface stress transducers | 239 |
| Plate 4(a) | Fast-acting pore pressure probe . . . . . | 249 |
| Plate 4(b) | Flushable pore pressure probe . . . . . | 249 |
| Plate 5 | Half-way housing, showing pressure transducers and hydraulic lines . . . . . | 259 |


## CHAPTER 13


| | | |
|---|---|---|
| Plate 6 | Views of the inspection trench: (a) excavation in progress; (b) working platform between the piles . . . . . | 401 |
| Plate 7 | Air-dried samples from (a) driven pile (AD3.10d); (b) jacked pile (AD3.10j) . . . . . | 423 |
| Plate 8 | X-rays of samples adjacent to driven pile: X2.43d; X3.25d . . . . . | 427 |
| Plate 9 | X-rays of samples adjacent to jacked pile: X2.61j; X3.25j . . . . . | 429 |
| Plate 10(a) | Thin-section TSVX2.43d, from adjacent to driven pile . . . . . | 433 |
| Plate 10(b) | Thin-section TSVX3.25d, from adjacent to driven pile . . . . . | 433 |
| Plate 11(a) | Thin-section TSVX2.61j, from adjacent to jacked pile . . . . . | 435 |
| Plate 11(b) | Thin-section TSVX3.25j, from adjacent to jacked pile . . . . . | 435 |
| Plate 12(a) | Thin-section TSV2.43d1, from adjacent to driven pile . . . . . | 437 |
| Plate 12(b) | Thin-section TSV3.25d, from adjacent to driven pile . . . . . | 437 |
| Plate 13(a) | Thin-section TSV2.61j, from adjacent to jacked pile . . . . . | 439 |
| Plate 13(b) | Thin-section TSV3.25j, from adjacent to jacked pile . . . . . | 439 |

# Volume 2

# Table of Contents

## APPENDIX 1

### Cavity expansion solutions


A1.1 FORMULAE FOR INCREASE IN STRESS INSIDE PLASTIC ZONE . . 504
A1.2 NOTES AND REFERENCES . . . . . 507


## APPENDIX 2

### Survey of previous instrumented pile tests


A2.1 INTRODUCTION . . . . . 512
A2.2 SURVEY OF INSTRUMENTED PILE TESTS . . . . . 513
A2.3 NOTES AND REFERENCES . . . . . 518


## APPENDIX 3

### Fundamental properties of London clay


A3.1 INTRODUCTION . . . . . 526
A3.2 COMPOSITION . . . . . 527
A3.3 BEHAVIOUR IN ONE DIMENSIONAL COMPRESSION . . . . . 528
A3.3.1 Introduction 528
A3.3.2 Reconstituted clay 528
A3.3.3 Intact London clay 529
A3.4 BEHAVIOUR IN UNDRAINED SHEAR . . . . . 530
A3.4.1 Reconstituted London clay 530
A3.4.2 Intact Samples 533
A3.5 INTERFACE BEHAVIOUR AT LARGE SHEAR STRAINS . . . . . 534
A3.5.1 The basic shear mechanisms 534
A3.5.2 Sliding shear behaviour 535
A3.5.3 Transitional shear 535
A3.5.4 Special tests to simulate pile installation and testing 536
A3.6 NOTES AND REFERENCES . . . . . 538


## APPENDIX 4

### Geology of the Canons Park area


A4.1 GEOLOGY OF THE STANMORE AREA . . . . . 542
A4.1.1 Six-inch and one-inch geological maps 542
A4.1.2 Well records 542
A4.1.3 Estimating the past overburden 546
A4.2 ESTIMATING THE PRE-CONSOLIDATION PRESSURE OF THE LONDON CLAY . . . . . 547
A4.2.1 From standard oedometer tests 547
A4.2.2 From high pressure oedometer tests 547
A4.3 NOTES AND REFERENCES . . . . . 549

## APPENDIX 5

## Earth and pore pressure cells: a review


A5.1 PILE-MOUNTED EARTH PRESSURES CELLS . . . . . 555
A5.1.1 Introduction 555
A5.1.2 Reese and Seed (1955) 555
A5.1.3 Φien (1962) 556
A5.1.4 Agarwal and Venkatesan (1965) 558
A5.1.5 Koizumi and Ito (1967) 558
A5.1.6 BP/BRE instrumented pile (1976) 558
A5.1.7 Johnston (1979) 559
A5.1.8 Taylor Woodrow's EP cells (1982) 560
A5.1.9 O'Neill et al. (1982) 560
A5.1.10 Maddocks (1983) 561
A5.1.11 Francescon (1983) 562
A5.1.12 The Piezo-Lateral Stress cell 562
A5.1.13 Wersching (1987) 564
A5.1.14 The Oxford University IMP (1987) 565
A5.1.15 NGI's instrumented piles (1989) 566
A5.2 ASSESSMENT OF CELL ACTION EFFECTS . . . . . 569
A5.2.1 Definition of cell action 569
A5.2.2 Factors that affect cell action 570
A5.2.3 Cell action in stiff soils 570
A5.2.4 Comparing designs of earth pressure cell 572
A5.2.5 Cell action effects during pile installation 575
A5.2.6 Laboratory studies of cell action effects 575
A5.3 PILE-MOUNTED PIEZOMETERS . . . . . 578
A5.3.1 Introduction 578
A5.3.2 Reese and Seed (1955) 578
A5.3.3 Hanna (1967) 579
A5.3.4 Kenney (1967) 579
A5.3.5 Laboratory tests at Cambridge University (1981-83) 580
A5.3.6 O'Neill et al. (1982) 580
A5.3.7 The Oxford University IMP (1987) 580
A5.3.8 NGI's instrumented piles (1989) 582
A5.4 RESPONSE TIMES OF PILE-MOUNTED PIEZOMETERS . . . . . 583
A5.4.1 Sources of error in pore pressure measurement 583
A5.4.2 Comparing pile-mounted piezometers 584
A5.5 NOTES AND REFERENCES . . . . . 589


## APPENDIX 6

## Details of instrument design: axial load cells


A6.1 AXIAL LOAD CELLS MKS I-III . . . . . 596
A6.2 TECHNICAL DATA: AXIAL LOAD CELLS . . . . . 597
A6.2.1 General information 597
A6.2.2 Basic properties 597
A6.2.3 Calibration coefficients 598

A6.2.4 Other properties 598
A6.3 DESIGN DRAWING . . . . . 599
A6.4 NOTES AND REFERENCES . . . . . 600

## APPENDIX 7

### Details of instrument design: surface stress transducers

A7.1 SURFACE STRESS TRANSDUCERS MKS I-IV . . . . . 606
A7.1.1 Background 606
A7.1.2 Circuit diagram 607
A7.2 TECHNICAL DATA: SURFACE STRESS TRANSDUCERS . . . . . 608
A7.2.1 General Information 608
A7.2.2 Details of the main housing 608
A7.2.3 Basic features of the load cells 608
A7.2.4 Radial total stress circuits 609
A7.2.5 Shear stress circuits 609
A7.2.6 Calibration coefficients 610
A7.2.7 Load cell compliance 610
A7.3 DESIGN DRAWINGS . . . . . 611
A7.4 NOTES AND REFERENCES . . . . . 617

## APPENDIX 8

### Details of instrument design: pore pressure probes

A8.1 PORE PRESSURE PROBES MKS I-IV . . . . . 624
A8.1.1 Background 624
A8.2 TECHNICAL DATA: PORE PRESSURE PROBES . . . . . 626
A8.2.1 General information 626
A8.2.2 Housing 626
A8.2.3 Pore pressure block 626
A8.2.4 Fluid used in system 626
A8.2.5 Transducer 627
A8.3 DESIGN DRAWINGS . . . . . 628
A8.4 NOTES AND REFERENCES . . . . . 632

## APPENDIX 9

### Notes on instrumented pile tests CP0-5

A9.1 JARDINE'S PILOT TEST (CP0F) . . . . . 638
A9.1.1 Main sequence of events 638
A9.1.2 Instrument performance 639
A9.2 TEST SERIES CP1s - REJUVENATING THE SOUTHAMPTON PILE . . 640
A9.2.1 Aims of the first Test Series 640
A9.2.2 Main sequence of events 640
A9.2.3 Instrument performance 641
A9.3 TEST SERIES CP2f - INAUGURATION OF THE IMPERIAL COLLEGE INSTRUMENTED PILE . . . . . 644

A9.3.1 Aims of the second Test Series 644
A9.3.2 Main sequence of events 645
A9.3.3 Instrument performance 645
A9.4 TEST SERIES CP3fs - PROVING THE SIGNIFICANCE OF JACKING RATE . . . . . 647
A9.4.1 Aims of the third Test Series 647
A9.4.2 Main sequence of events 648
A9.4.3 Instrument performance 648
A9.5 TEST SERIES CP4f - LONG-TERM MEASUREMENTS OF PORE PRESSURE 649
A9.5.1 Aims of the fourth Test Series 649
A9.5.2 Main sequence of events 649
A9.5.3 Special procedure for installing CP4f 650
A9.5.4 Instrument performance 651
A9.6 TEST SERIES CP5f - "CONTROL" EXPERIMENT FOR DRIVEN PILES 652
A9.6.1 Main aims of the fifth Test Series 652
A9.6.2 Main sequence of events 652
A9.6.3 Instrument performance 652
A9.7 ORIENTATION OF INSTRUMENTS . . . . . 653
A9.8 CONFIGURATION OF INSTRUMENTS . . . . . 654
A9.8.1 Test Series CP0-2 654
A9.8.2 Test Series CP3-5 655
A9.9 NOTES AND REFERENCES . . . . . 656

## APPENDIX 10

## Instrument performance (tests CP1-5)

A10.1 INSTRUMENT RELIABILITY: TEST SERIES CP1S . . . . . 660
A10.2 INSTRUMENT RELIABILITY: TEST SERIES CP2F . . . . . 661
A10.3 INSTRUMENT RELIABILITY: TEST SERIES CP3FS . . . . . 662
A10.4 INSTRUMENT RELIABILITY: TEST SERIES CP4F . . . . . 663
A10.5 INSTRUMENT RELIABILITY: TEST SERIES CP5F . . . . . 664

## APPENDIX 11

## Further test results: pile installation

A11.1 PORE PRESSURE RESPONSE DURING PILE INSTALLATION . . . . 668
A11.1.1 Introduction 668
A11.1.2 Test Series CP1s 668
A11.1.3 Test Series CP2f 669
A11.1.4 Test Series CP3fs 670
A11.1.5 Test Series CP4f 671
A11.2 RELIABILITY OF THE PORE PRESSURE READINGS . . . . . 673
A11.3 SUMMARY OF RESULTS FROM CANONS PARK EXPERIMENTS . . . . 675
A11.4 NOTES AND REFERENCES . . . . . 676

APPENDIX 12

Further test results: equalization

A12.1 PORE PRESSURE DISSIPATION CURVES CP1-4 . . . . . 680
A12.2 LONG-TERM MEASUREMENTS WITH FLUSHABLE PROBES . . . . . 684

APPENDIX 13

Further test results: pile loading

A13.1 LOAD-DISPLACEMENT DIAGRAMS . . . . . 688
A13.2 FURTHER INSTRUMENTED PILE DATA: TEST SERIES CP5f . . . . 700
A13.3 FURTHER INSTRUMENTED PILE DATA: TEST SERIES CP3fs . . . 704

APPENDIX 14

Notes on the preparation of thin sections

A14.1 PREPARATION OF THIN SECTIONS . . . . . 710
A14.1.1 Sampling procedure 710
A14.1.2 Sample impregnation 710
A14.2 NOTES AND REFERENCES . . . . . 712

APPENDIX 15

Notes on the measurement of soil suction

A15.1 FILTER PAPER TECHNIQUE . . . . . 716
A15.1.1 Sampling procedure 716
A15.1.2 Testing procedure 716
A15.1.3 Notes on the formulae used to calculate soil suction 717
A15.1.4 Further test results 720
A15.2 PRESSURE-PLATE MEASUREMENTS . . . . . 723
A15.2.1 Testing procedure 723
A15.3 NOTES AND REFERENCES . . . . . 724

# LIST OF FIGURES: VOLUME 2

## APPENDIX 1

Figure A1.1 Relationship between extent of plastic zone and clay's rigidity index . . . . . 506

## APPENDIX 3

Figure A3.1 Schematic map of London clay depositional environment . . . . . 526
Figure A3.2 Grading curve envelope for Canons Park London clay . . . . . 527
Figure A3.3 Mineral suite for typical lower London clay . 527
Figure A3.4 One-dimensional compression and swelling characteristics of London clay . . . . . 528
Figure A3.5 Variation of secant bulk modulus with strain for $K_0$-swelling (reconstituted soil) . . . . . 529
Figure A3.6 Effective stress paths for $K_0$-consolidated reconstituted London clay . . . . . 531
Figure A3.7 Stress-strain curves for $K_0$-consolidated reconstituted London clay: (a) triaxial compression; (b) triaxial extension tests . . 532
Figure A3.8 Normalized undrained stiffness characteristics of reconstituted London clay . . . . . 532
Figure A3.9 Variation of undrained small strain stiffness index with OCR: re-constituted samples . . . . 533
Figure A3.10 Undrained stress paths for intact samples of London clay . . . . . 533
Figure A3.11 Undrained stiffness characteristics of intact samples . . . . . 534
Figure A3.12 Rate effects shown by interface ring shear tests on London clay from Canons Park . . . . . 537

## APPENDIX 4

Figure A4.1 Six-inch geological maps for Canons Park . . . 543
Figure A4.2 Cross-section from Stanmore Common to Hampstead Heath . . . . . 544
Figure A4.3 Construction of the rebound curve for the London clay at Canons Park . . . . . 548

## APPENDIX 5

Figure A5.1 Earth and pore pressure cells employed by Reese and Seed . . . . . 555
Figure A5.2 NGI's earth pressure gauge of the 1960s . . . 556
Figure A5.3 Agarwal and Venkatesan's surface stress transducer . . . . . 557
Figure A5.4 BP's cell for Forties Field . . . . . 558
Figure A5.5 Johnston's Cambridge-type "local load cell" . 559
Figure A5.6 Taylor Woodrow's EP cell . . . . . 560
Figure A5.7 Earth pressure cell designed by Maddocks to measure radial effective stress acting on a pile . . . . . 561

Figure A5.8 The PLS cell . . . . . 563
Figure A5.9 Detail of the Piezo-Lateral Stress cell . . . . 564
Figure A5.10 Wersching's "Boundary Orthogonal Stress Transducer" . . . . . 565
Figure A5.11 Earth pressure cells on the Oxford University model pile . . . . . 565
Figure A5.12 NGI's A-, B-, & C- piles . . . . . 567
Figure A5.13 Instrument units for the NGI's A- & C- piles . 567
Figure A5.14 Cell action effects for rigid piston earth pressure cell . . . . . 569
Figure A5.15 Effect of cell compli-ance, loading platen radius, and soil stiff-ness on cell factor . . 571
Figure A5.16 Cell action effects as determined in laboratory tests at TRRL . . . . . 576
Figure A5.17 Hanna's pile piezometer . . . . . 579
Figure A5.18 Strain-gauged diaphragm pore pressure cell mounted on the Oxford University model pile . . 581
Figure A5.19 Instrument units for the NGI's B- piles . . . . 582
Figure A5.20 Problems associated with measuring pore pressures in soil . . . . . 583

APPENDIX 6

Figure A6.1 Design drawing for Mk III axial load cell . . . 599

APPENDIX 7

Figure A7.1 The "Oval" Cambridge earth pressure cell . . . 606
Figure A7.2 Circuit diagram for surface stress transducers. axial load cells, and pore pressure probes . . 607
Figure A7.3 Surface stress transducer: design drawing AJB/PSST/1 . . . . . 611
Figure A7.4 Surface stress transducer: design drawing AJB/PSST/2 . . . . . 612
Figure A7.5 Surface stress transducer: design drawing AJB/PSST/3 . . . . . 613
Figure A7.6 Surface stress transducer: design drawing AJB/PSST/4 . . . . . 614
Figure A7.7 Surface stress transducer: design drawing AJB/PSST/5 . . . . . 615
Figure A7.8 Surface stress transducer: design drawing AJB/PSST/6 . . . . . 616

APPENDIX 8

Figure A8.1 Pore pressure probes, Mks I and II . . . . . 624
Figure A8.2 Pore pressure probes: design drawing AJB/PPU/1 628
Figure A8.3 Pore pressure probes: design drawing AJB/PPU/2 629
Figure A8.4 Pore pressure probes: design drawing AJB/PPU/3 630
Figure A8.5 Pore pressure probes: design drawing AJB/PPU/4 631

APPENDIX 9


Figure A9.1 Configuration of instruments - Pilot Test . . 638
Figure A9.2 Configuration of instruments - pile CP1 . . . 640
Figure A9.3 Pore pressures recorded during installation, Test CP1 . . . . . 641
Figure A9.4 Erratic pore pressure signals during Test Series CP1s . . . . . 642
Figure A9.5 Erratic pore pressure observations reported by DiBiaggio . . . . . 643
Figure A9.6 Configuration of Pile CP2 . . . . . 644
Figure A9.7 Configuration Pile CP3 . . . . . 647
Figure A9.8 Configuration of Pile CP4 . . . . . 649
Figure A9.9 Orientation of instruments, Test Series CP1-5 653


APPENDIX 11


Figure A11.1 Pore pressures recorded at leading instrument positions during pile installation, Test Series CP1s . . . . . 668
Figure A11.2 Pore pressures recorded at leading instrument positions during pile installation, Test Series CP2f . . . . . 669
Figure A11.3 Pore pressures recorded at leading instrument positions during pile installation, Test Series CP3fs . . . . . 670
Figure A11.4 Pore pressures recorded at leading instrument positions during pile installation, Test Series CP4f . . . . . 672


APPENDIX 12


Figure A12.1 Pore pressure dissipation curves for Test Series CP1s . . . . . 680
Figure A12.2 Pore pressure dissipation curves for Test Series CP2f . . . . . 681
Figure A12.3 Pore pressure dissipation curves for Test Series CP3fs . . . . . 682
Figure A12.4 Pore pressure dissipation curves for Test Series CP4f . . . . . 683
Figure A12.5 Pore pressures recorded by flushable probes in Test Series CP4f . . . . . 684


APPENDIX 13


Figure A13.1 Load-displacement diagram for load test CP1s/L1C . . . . . 688
Figure A13.2 Load-displacement diagram for load test CP2f/L1C . . . . . 689
Figure A13.3 Pattern of loads applied in load test CP2f/L2C 689
Figure A13.4 Load-displacement diagram for load test CP2f/L2C . . . . . 690
Figure A13.5 Load-displacement diagram for load test CP2f/L3T . . . . . 691
Figure A13.6 Load-displacement diagram for load test

CP3fs/L1C . . . . . 692
Figure A13.7 Load-displacement diagram for load test CP3fs/L2T . . . . . 693
Figure A13.8 Load-displacement diagram for load test CP3fs/L3C . . . . . 694
Figure A13.9 Load-displacement diagram for load test CP4f/L1T . . . . . 695
Figure A13.10 Load-displacement diagram for load test CP4f/L2C . . . . . 696
Figure A13.11 Load-displacement diagram for load test CP5f/L1T . . . . . 697
Figure A13.12 Load-displacement diagram for load test CP5f/L2C . . . . . 698
Figure A13.13 Load-displacement diagrams for load tests CP6d/L1T and CP7do/L1T . . . . . 699
Figure A13.14 Variations in pore pressure with pile displacement during load test CP5f/L1T . . . . 700
Figure A13.15 Variations in pore pressure with pile displacement during load test CP5f/L2C . . . . 701
Figure A13.16 Changes in radial total stress, load test CP5f/L2C . . . . . 702
Figure A13.17 Coefficients of friction, load test CP5f/L2C . 703
Figure A13.18 Changes in radial total stress, load test CP3fs/L2T . . . . . 704
Figure A13.19 Coefficients of friction, load test CP3fs/L2T . 705

APPENDIX 15

Figure A15.1 Bench of clay for obtaining filter-paper samples . . . . . 716
Figure A15.2 Filter-paper measurements of soil suction next to the driven pile CP6d . . . . . 721
Figure A15.3 Filter-paper measurements of soil suction next to Kitching's jacked pile . . . . . 722

# LIST OF TABLES: VOLUME 2

## APPENDIX 1

Table A1.1 Formulae for stress changes in plastic zone due to cavity expansion . . . . . 505

## APPENDIX 4

Table A4.1 Well records for Stanmore and surrounding areas 545

## APPENDIX 5

Table A5.1 Properties of various pile-mounted earth pressure cells . . . . . 573
Table A5.2 Response times of various piezometer systems, as used on piles and piezocones . . . . . 586

## APPENDIX 11

Table A11.1 Pore pressure response in CP4f/EQ . . . . . 674
Table A11.2 Summary of results from the Canons Park pile tests . . . . . 675

# List of Symbols

## SYMBOLS AND ABBREVIATIONS

| Symbol | Definition | [SI units] |
|---|---|---|
| A | "compaction factor" (= $K_s/K_0$) (see p37) | [-] |
| AL | axial load (see Table 4.1) | |
| ALC | axial load cell | |
| API | American Petroleum Institute | |
| b | Bishop's parameter (= $[\sigma'_2 - \sigma'_3]/[\sigma'_1 - \sigma'_3]$) | [-] |
| B | Skempton's pore pressure parameter (= $\Delta u/\Delta\sigma$) | [-] |
| $B_q$ | pore pressure parameter for CPTU | [-] |
| BRE | Building Research Establishment | |
| c' | cohesion intercept of Mohr-Coulomb envelope | [kPa] |
| $c_h$ | coefficient of horizontal consolidation (= $k_h/m_v\gamma_w$) | [$mm^2/s$] |
| $c_{uo}$ | undrained shear strength | [kPa] |
| $c_{uo}/\sigma'_{vo}$ | undrained strength ratio | [-] |
| $c_{ups}$ | undrained shear strength in plane strain | [kPa] |
| $c_v$ | coefficient of vertical consolidation (= $k_v/m_v\gamma_w$) | [$mm^2/s$] |
| $C_c$ | compression index (= $\Delta e/\Delta[\log_{10}\sigma'_v]$) | [-] |
| $C_s$ | swelling index (= $\Delta e/\Delta[\log_{10}\sigma'_v]$) | [-] |
| $C_{\alpha e}$ | creep coefficient (= $\Delta e/\Delta[\log_{10}t]$) | [-] |
| CAUTC | anisotropically-consolidated undrained triaxial compression test | |
| CEM | cavity expansion method | |
| $CK_0UDSS$ | $K_0$-consolidated undrained direct simple shear test | |
| $CK_0UTC$ | $K_0$-consolidated undrained triaxial compression test | |
| $CK_0UTE$ | $K_0$-consolidated undrained triaxial extension test | |
| CP1-7 | test numbers | |
| CPT | cone penetration test | |
| CPTU | CPT with measurement of pore pressure (piezocone test) | |
| CSL | critical state line | |
| D | pile diameter | [mm] |
| D/h | diameter/thickness ratio | [-] |
| e | voids ratio | [-] |
| $E_h$ | Young's modulus in horizontal direction | [MPa] |
| $E_v$ | Young's modulus in vertical direction | [MPa] |
| EP | earth pressure (see Table 4.1) | |
| /EQ | equalization stage | |
| ES | effective stress (see Table 4.1) | |
| ESACC | Effective Stress Axial Capacity Co-operative (see p47) | |
| ESM | Effective Stress Model/effective stress method | |
| ESM1-4 | Effective Stress Models 1-4 | |
| f() | function of... | |
| $f()$ | function of... | |
| $f_s$ | shaft friction | [kPa] |
| $100f_s/q_c$ | CPT friction ratio | [-] |
| F | length factor (see p31) | [-] |
| $F_c$ | "correction factor" for alpha method (see p31) | [-] |
| $F_1$ | "correction factor" for alpha method (see p31) | [-] |
| FE | finite element | |
| FSO | full-scale output | |
| G | shear modulus | [MPa] |
| $G_{ur}$ | G from unload-reload curve in SBPM test | [MPa] |
| $G/c_{uo}$ | rigidity index | [-] |
| G/k | rigidity index | [-] |
| GM | ground movements (see Table 4.1) | |

| | | |
|---|---|---|
| h | pile wall thickness | [mm] |
| H | "normalized horizontal total stress" (= $[\sigma_{rr} - u_o]/\sigma'_{vo}$) | [-] |
| $H_c/H_i$ | "relaxation coefficient" | [-] |
| $I_B$ | brittleness index (= 1 - $[\tau_{rz}]_{residual}/[\tau_{rz}]_{peak}$) | [-] |
| $I_L$ | liquidity index (= $[w - w_P]/I_p$) | [%] |
| $I_P$ | plasticity index (= $w_L - w_P$) | [%] |
| $I_r$ | rigidity index (= G/k) | [-] |
| IC | Imperial College | |
| IMP | Oxford University In-situ Model Pile | |
| /IN | pile installation stage | |
| $k_h$ | horizontal permeability | [m/s] |
| $k_v$ | vertical permeability | [m/s] |
| K | "lateral stress coefficient" (= $\sigma'_{rr}/\sigma'_{vo}$) | [-] |
| K | flexibility ratio (see p29) | [-] |
| K' | elastic bulk modulus | [MPa] |
| $K_0$ | coefficient of earth pressure at rest (= $\sigma'_{ho}/\sigma'_{vo}$) | [-] |
| $K_0^{nc}$ | $K_0$ of normally consolidated soil | [-] |
| $K_D$ | horizontal stress index in Marchetti dilatometer test | [-] |
| $K_i/K_c$ | "set-up coefficient" | [-] |
| $K_s$ | earth pressure coefficient (= $\sigma'_{rr}/\sigma'_{vo}$) | [-] |
| kPa | kilopascal (1kPa = $1kN/m^2$) | |
| L | pile length | [m] |
| /LlT | load test | |
| L/D | pile's aspect ratio | [-] |
| LE-PP | linear-elastic/perfectly-plastic | |
| LOC | lightly overconsolidated | |
| $\log_e$ | Naperian (i.e. natural) logarithm | |
| LPC | Laboratoires des Ponts et Chaussées | |
| $m_v$ | volumetric compressibility | [$m^2/kN$] |
| M | critical state parameter (= $6\sin\phi_{tc}/[3 - \sin\phi_{tc}]$) | [-] |
| MCC | Modified Cam Clay constitutive model | |
| MIT | Massachusetts Institute of Technology | |
| MIT-E1 | Effective stress constitutive soil model (out of MIT) | |
| MIT-E2 | Effective stress constitutive soil model (out of MIT) | |
| MIT-E3 | Effective stress constitutive soil model (out of MIT) | |
| MIT-T1 | Total stress constitutive soil model (out of MIT) | |
| MPa | megapascal (1MPa = $1000kN/m^2$) | |
| $N_c$ | bearing capacity factor for pile | [-] |
| $N_k$ | end-bearing coefficient for CPT | [-] |
| NC | normally consolidated | |
| NGI | Norwegian Geotechnical Institute | |
| OC | overconsolidated | |
| OCR | *apparent* overconsolidation ratio (= $\sigma'_{vp}/\sigma'_{vo}$) | [-] |
| $OCR_m$ | *mechanical* overconsolidation ratio (= $\sigma'_{vm}/\sigma'_{vo}$) | [-] |
| p' | mean effective stress | [kPa] |
| $p'_c$ | mean effective stress at end of equalization | [kPa] |
| $p_k$ | soil suction | [kPa] |
| $(p_k)_{ff}$ | soil suction in the far-field | [kPa] |
| $p_{lim}$ | limit pressure from SBPM test | [kPa] |
| $p'_o$ | original mean effective stress | [kPa] |
| $p'_v$ | vertical effective stress (= $\sigma'_{vo}$) (see Figure 2.8) | [kPa] |
| PI | plasticity index (= $I_p$) | [%] |
| PLS | Piezo-Lateral Stress (cell) | |
| PP | pore pressure (see Table 4.1) | |
| $PP^R$ | remote pore pressure (see Table 4.1) | |
| PPI | pocket penetrometer index | |

| | | |
|---|---|---|
| PPP | pore pressure probe | |
| PPU | pore pressure unit | |
| $q_c$ | end-bearing pressure in CPT | [kPa] |
| $q_{toe}$ | end-bearing pressure carried by pile toe | [kPa] |
| $Q_{shaft}$ | axial load carried by pile shaft | [kN] |
| $Q_{toe}$ | axial load carried by pile toe | [kN] |
| $Q_{total}$ | total axial load carried by pile | [kN] |
| r | radial distance from pile centre-line | [m] |
| $r_p$ | radius of plastic zone | [m] |
| R | pile radius (= D/2) | [mm] |
| $R_a$ | centre-line average roughness | [$\mu$m] |
| $R_o$ | overconsolidation ratio (= OCR) (see Figure 2.8) | [-] |
| r/R | normalized radial distance | [-] |
| $r_z/R$ | normalized radius of zone of disturbance (see Table 13.1) | [-] |
| S | undrained strength ratio of normally consolidated clay | [-] |
| S | "sliding" mode of shearing | |
| $S_1$ | "sliding" mode of shearing (against smooth interface) | |
| $S_t$ | sensitivity | [-] |
| SBPM | self-boring pressuremeter | |
| SG | strain gauge (see Table 4.1) | |
| SPM | strain path method | |
| SS | shear stress (see Table 4.1) | |
| SST | surface stress transducer | |
| t | time | [s] |
| $t_{90}$ | time for 90% equalization/response | [s] |
| $t_{95}$ | time for 95% equalization/response | [s] |
| T | time factor (= $c_h t/R^2$) | [-] |
| T | "turbulent" mode of shearing | |
| $T^*$ | Teh's time factor (= $c_h t/R^2\sqrt{(G/k)}$) (see p102) | [-] |
| $T_1$ | time factor T assuming $c_h$ = 1mm$^2$/s | [-] |
| $T^*_{50}$ | $T^*$ after 50% equalization | [-] |
| $T_{95}$ | time factor T for 95% equalization/response | [-] |
| $T_c$ | time factor based on $c_{uo}$ (= $[k_h c_{uo}/\psi_w][t/R^2]$) (see p98) | [-] |
| $T_G$ | time factor based on G (= $[k_h G/\psi_w][t/R^2]$) (see p98) | [-] |
| $T_p$ | time factor based on $p'_o$ (= $[k_h p'_o/\psi_w][t/R^2]$) (see p98) | [-] |
| $T_R$ | "transitional" mode of shearing | |
| TS | temperature sensor | |
| u | pore water pressure | [kPa] |
| $u_o$ | original pore water pressure | [kPa] |
| UC | unconfined compression test | |
| UD | unconsolidated drained | |
| UDTC | unconsolidated drained triaxial compression test | |
| UUTC | unconsolidated undrained triaxial compression test | |
| UUTE | unconsolidated undrained triaxial extension test | |
| v | velocity | [mm/s] |
| $V_i$ | input voltage | [V] |
| $V_o$ | output voltage | [V] |
| VCL | virgin consolidation line | |
| w | water content of soil | [%] |
| $w_{FP}$ | water content of filter paper | [%] |
| $w_L$ | water content at soil's liquid limit | [%] |
| $w_P$ | water content at soil's plastic limit | [%] |
| z | distance behind pile tip | [m] |
| z/R | normalized distance behind pile tip | [-] |

# Chapter 1

# Introduction

# CONTENTS OF CHAPTER 1


1.1 THE USE OF DISPLACEMENT PILES IN OVERCONSOLIDATED CLAYS 4

1.1.1 The use of displacement piles in civil engineering works 4

1.1.2 Typical ground conditions for displacement piles 5

1.1.3 Assessing the capacity of piles in clays 6

1.2 OVERVIEW OF THE CANONS PARK PROJECT . . . . . 9

1.3 OUTLINE OF THE THESIS . . . . . 10

1.3.1 Aim of the Thesis 10

1.3.2 Volumes 1 and 2 10

1.3.3 Contents of Volume 1: Chapters 1-15 11

1.3.4 Volume 2: Appendices 1-15 13

1.4 NOTES AND REFERENCES . . . . . 15

## 1.1 THE USE OF DISPLACEMENT PILES IN OVERCONSOLIDATED CLAYS

### 1.1.1 The use of displacement piles in civil engineering works

Displacement piles are used extensively in the construction of major offshore foundations. The piles are generally very long (typically 30-80m) and have correspondingly large diameters (see Figure 1.1).* The ratio of their length to diameter (the "aspect ratio") is typically between twenty-five and fifty, although in some cases it may exceed one hundred.

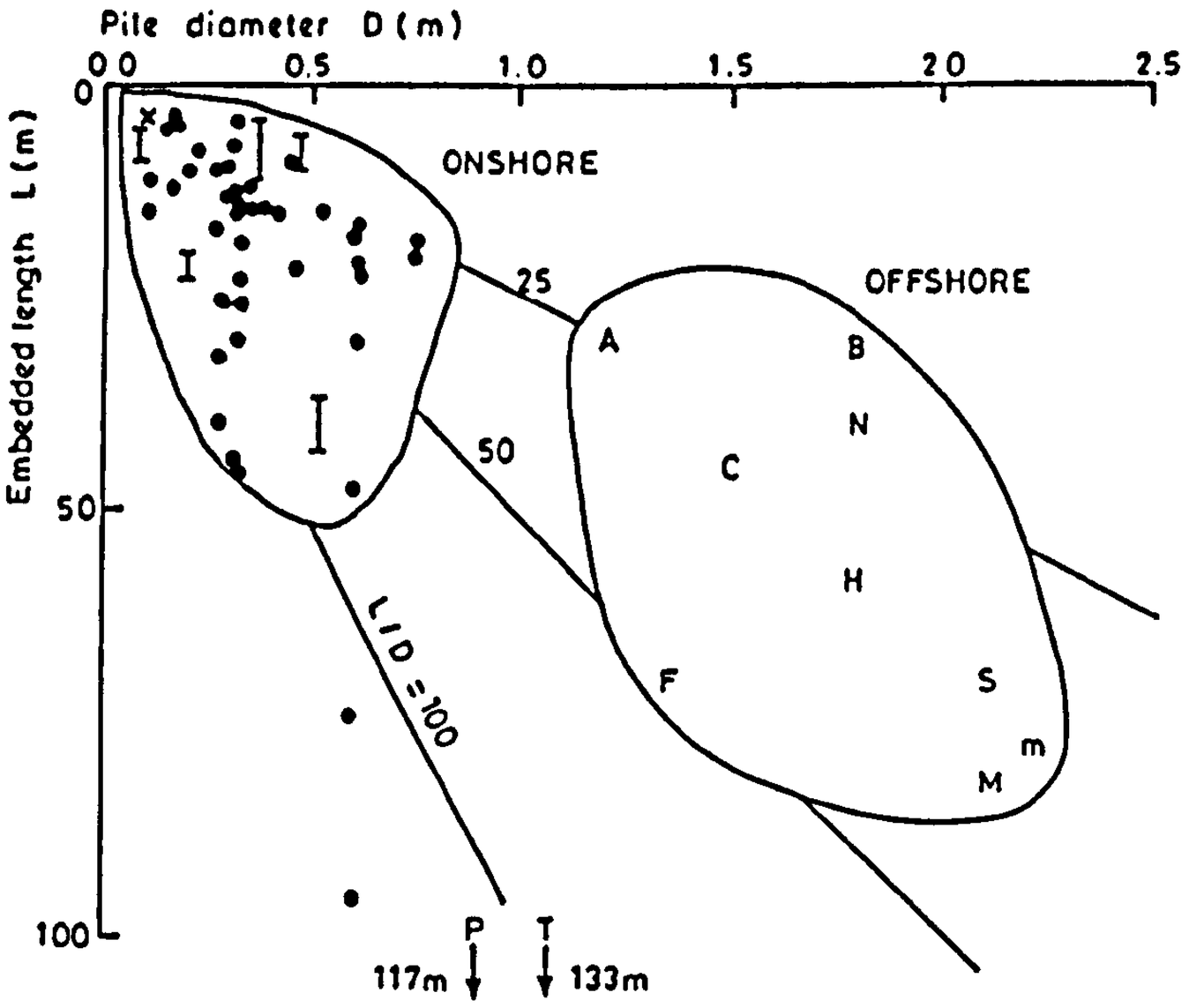



Figure 1.1 Length and diameter of typical tubular steel piles

Invariably the piles are open-ended steel tubes (*pipe* piles), which, because of plugging, are somewhere between *low*-and *full*-displacement piles.

*Onshore* the situation is different. Tubular steel piles find only occasional use, mainly because of the relatively high cost of steel. Instead, the two main forms of displacement pile for land-based work are the pre-cast concrete and the driven cast-in-situ pile (although timber piles were once the most common form of piling). The driven cast-in-situ pile is both cheap and reliable, but it becomes uneconomical once the required penetration exceeds about 18m. Steel H piles and tubular pipes

*The offshore piles included on this diagram are located in the following North Sea oil fields: A - Auk; B - Brent; C - Claymore; F - Forties; H - N.W. Hutton; m - Murchison; M - Magnus; N - Ninian; P - Piper; S - S. Brae; and T - Thistle

can survive fairly heavy driving conditions, and the latter in particular are commonly used for marine structures, such as jetties, piers, and mooring dolphins.[1]

The onshore piles are much shorter than their offshore counterparts, rarely exceeding 50m in length - although their aspect ratios are somewhat higher (typically between twenty-five and one hundred).

### 1.1.2 Typical ground conditions for displacement piles

Typical ground conditions for *offshore* structures are illustrated in Figure 1.2.[2] As the diagram shows, there are many oil and gas platforms in the North Sea that are founded on stiff, to very stiff, over-

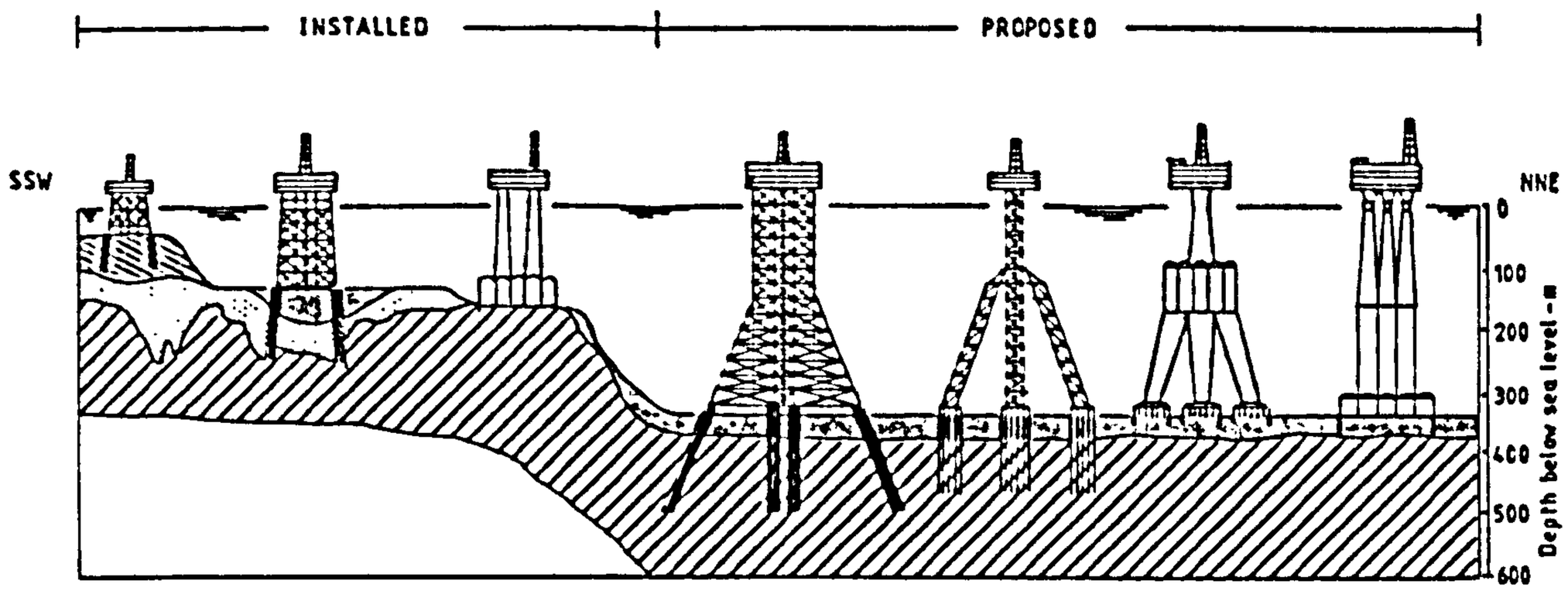



Figure 1.2 Typical offshore foundation soil types

consolidated silty clays (soil type 1); some of them stand on very soft, to soft, normally consolidated clays, overlying stiff clays (soil type 2); and others are supported on fine to course sand (soil type 4).

*Onshore* there are large tracts of land where the superficial deposits are underlain by stiff, overconsolidated clays. Figure 1.3 shows the distribution of these deposits in Great Britain.[3] They include high

plasticity overconsolidated clays, such as the London, Gault, and Oxford clays, as well as many medium to low plasticity glacial tills, e.g. at Garston (in Hertfordshire), Redcar (Yorkshire), and Cowden (North Humberside).

It is obvious from the above that the design of displacement piles in *over-consolidated* clays is highly relevant both to the offshore industry, and also to land-based construction in many parts of the United Kingdom (and elsewhere).

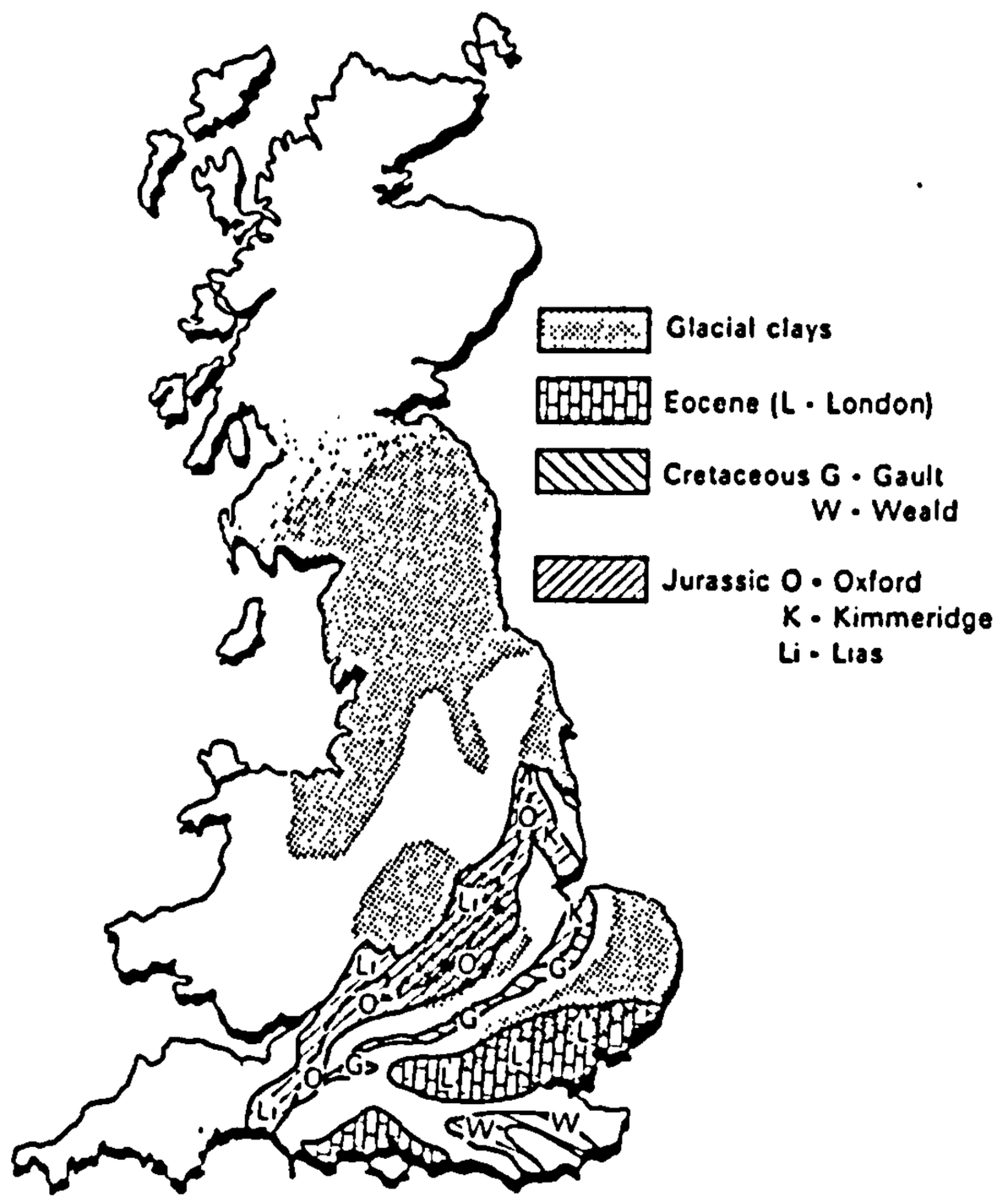



Figure 1.3 Distribution of stiff clay deposits in Britain

The assessment of pile capacity in these soils is not an easy task, and for this reason I have chosen to study the behaviour of displacement piles in *overconsolidated* clays.

### 1.1.3 Assessing the capacity of piles in clays

Methods for assessing the axial capacity of piles driven into cohesive soils vary in their popularity throughout the geotechnical profession, depending on the magnitude and location of the project for which they are needed. The most commonly used procedures fall into the following broad categories:[4]

- Static load tests (†)
- Correlations with $c_{uo}$ or $\sigma'_{vo}$ (†)
- Reliance on local experience (†)
- Prescriptions of the relevant codes-of-practice (†)
- Correlations with in situ tests (†)

- Dynamic measurements/wave equation analysis
- Effective stress methods
- Pile driving formulae (†)

The extent to which these procedures are used is indicated in Figure 1.4, the data coming from a survey[5] of 56 practising engineers across six continents. To predict the capacity of piles, most practitioners rely on empirical methods/"well-winnowed experience" (marked † above); or on experiment/testing (‡). These are two of the key elements in Burland's "Soil Mechanics Triangle",[6] which is described in detail at the beginning of Chapter 2.

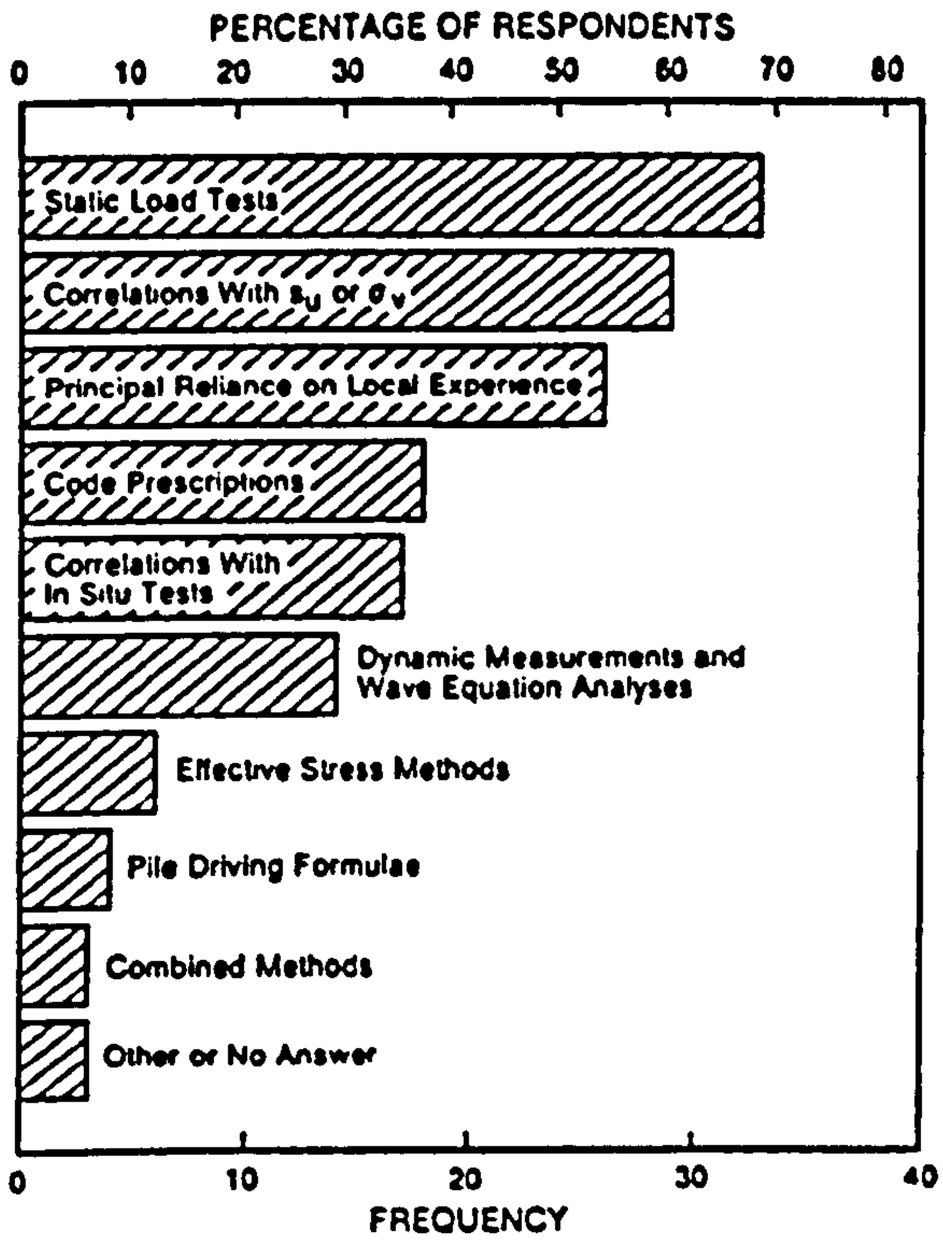



Figure 1.4 Popularity of various methods of assessing pile capacity in clays

The survey also found that confidence in estimating pile capacity is rather low: only 30% of the respondents said that the reliability of their chosen design technique was within ±20%; and as many as 37% thought it was worse than ±30%. Scepticism was highest amongst contractors, of whom 28% perceived an error of more than 50% in estimating pile capacity!

Based on their findings, Focht and O'Neill[7] concluded that:

"The design of piles to carry axial static loads appears to remain essentially an art. ...there is not a universal set of static design rules, based on a fundamental understanding of pile-soil interaction phenomena."

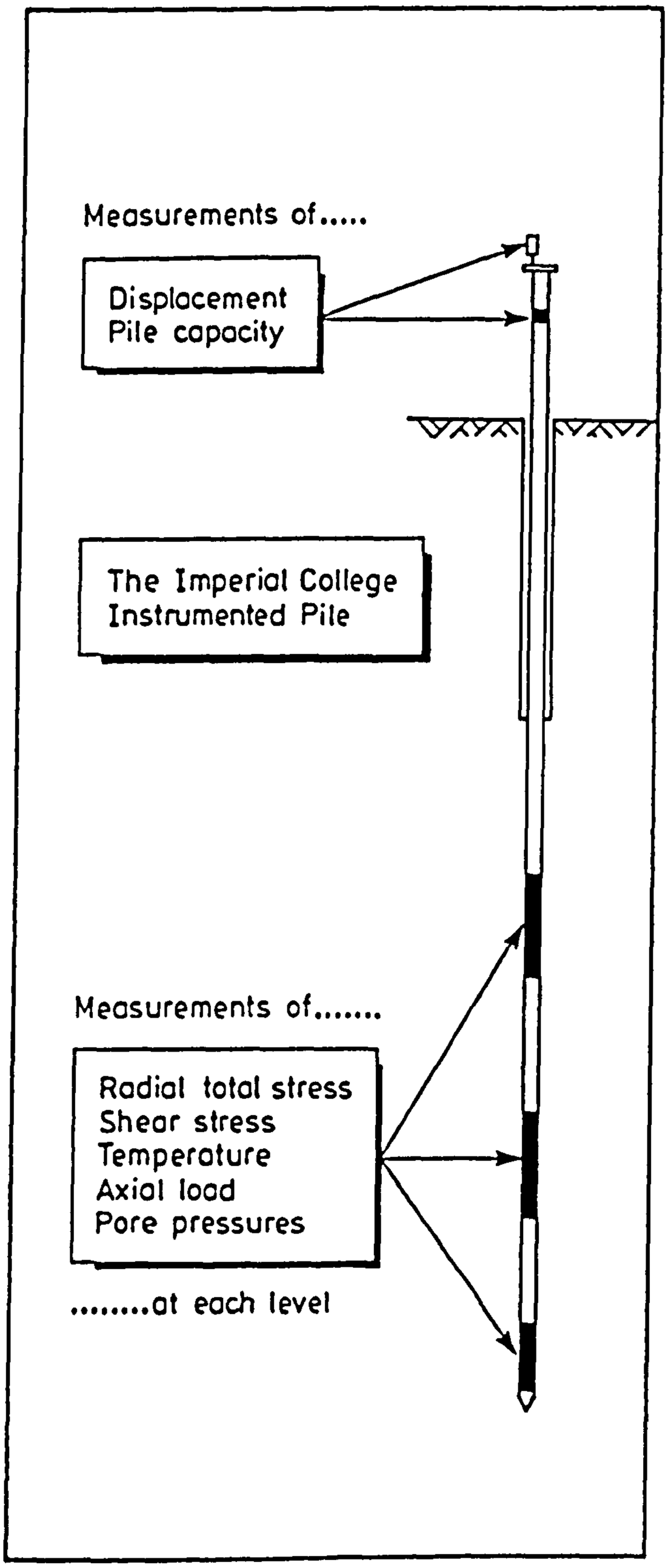



Figure 1.5 The Imperial College Instrumented Pile

## 1.2 OVERVIEW OF THE CANONS PARK PROJECT

The Canons Park Piling Project was set up in 1985 to study the behaviour of large-displacement piles in a heavily overconsolidated clay. Although many pile tests in such clays had previously been reported in the Literature,[8] by 1985 few had encompassed measurements of the effective stresses acting on the surface of a pile. Where this had been attempted[9] great problems had been encountered in obtaining reliable measurements.

The main aim of the Canons Park Project was to obtain high quality data from two specially instrumented model piles (see Figure 1.5) installed at the Building Research Establishment's test-bed site at Canons Park, north London. Each pile was equipped to measure the earth pressures and pore water pressures acting at the boundary between the pile and the surrounding soil. A total of five such experiments were performed between November 1986 and June 1988. In each case the piles were installed by jacking and were load tested within 2½ months of installation.

In addition to the instrumented piles, two uninstrumented driven piles were installed at the site in June 1988, and then load tested in tension. These experiments were designed to assess what effect the method of installation has on the pile's behaviour during load testing.

Finally, an inspection trench was excavated around two of the piles to enable the soil fabric adjacent to them to be examined. The trench also allowed various soil samples to be taken and simple in situ tests to be performed. All of the samples were taken back to the laboratory for testing.

## 1.3 OUTLINE OF THE THESIS

### 1.3.1 Aim of the Thesis

The aim of this Thesis is to provide a clearer understanding of the processes that govern pile behaviour in clay soils, and to contribute towards the establishment of a "universal set of ...design rules",* based on Terzaghi's principle of effective stress.[10]

The principal means of providing this understanding is through instrumented pile tests, in which measurements are made of the effective stresses that act on the pile shaft. A major part of the research described in the Thesis revolves around the design, manufacture, and field testing of an extensively instrumented, closed-ended, steel pile. This equipment, the "Imperial College Instrumented Pile",# was commissioned for a series of experiments in the heavily overconsolidated London clay at Canons Park, north London - a site which has been thoroughly investigated in the past, both by Imperial College and by the Building Research Establishment. Section 1.2 gives a brief overview of the experimental part of the research project.

The manner in which the Thesis has been laid out is described in the following sections.

### 1.3.2 Volumes 1 and 2

The Thesis has been split into two separate volumes, an "engineering" and a "technical" volume. The first describes the essential elements of the programme of research into the behaviour of displacement piles in clay; whereas the second concentrates on more detailed technical aspects of the work (e.g. soil behaviour, theoretical models, instrument design, etc.). The "technical" volume includes data from the experimental programme that would not fit into Volume 1 without interrupting the flow of the Thesis.

---

*See the quotation on page 7

#In fact there are two instrumented piles

Volume 1 comprises fifteen chapters, divided into four main parts; and Volume 2 contains fifteen appendices.

### 1.3.3 Contents of Volume 1: Chapters 1-15

**a) Part I: Review section (Chapters 2-5)**

Part I of the Thesis presents a review of the behaviour of displacement piles in overconsolidated clays (Chapters 2-4), and a summary of the ground conditions at Canons Park (Chapter 5).

Chapter 2 describes two of the most widely-used procedures for estimating the shaft capacity of displacement piles in clays (the alpha and beta methods). The chapter examines the assumptions on which these methods are based, their strengths and weaknesses, and areas in which research is required to improve or extend them (for example, to new field conditions). In addition, the more soundly based (but less popular) "effective stress methods" of pile design are described and discussed in detail.

No attempt is made to review other design procedures. Hence there is no mention of, *inter alia*, pile driving formulae,[11] load transfer methods,[12] or wave equation analyses.[13] The purpose of Chapter 2 is to provide background information which will allow the findings of the current research programme to be judged in the broader context of designing piles in practice.

Chapter 3 concentrates on the *theoretical* behaviour of piles in clay, by reviewing two modern theories (the cavity expansion and strain path methods) that have contributed most to recent debates about pile behaviour. The chapter examines the theories' differences and similarities, and highlights areas where their predictions require verification by independent means (for example, by instrumented pile tests).

To complete the review, Chapter 4 summarizes details of nearly twenty instrumented pile tests in clay soils - tests in which there have been measurements of the *effective* stresses acting on the surface of the pile. The quality of the information has been assessed, and classified on a scale from "poor" to "very good". Results from some of the tests are examined in detail, but the overall synthesis of this body of information is left until Chapter 14, where it is compared with data from the current research programme. One of the purposes of Section 4 is to highlight the difficulties involved in making reliable measurements of effective stresses adjacent to displacement piles.

The general trend of the data is identified and compared with the predictions of the cavity expansion and strain path methods. Suggestions are given for a rational design procedure for piles in clays.

Finally, Chapter 5 reports on the ground conditions at Canons Park, north London (where the current series of instrumented pile tests were performed). The ground conditions were determined in a series of high quality field and laboratory investigations by various organizations, including the Building Research Establishment, Imperial College, and others.

b) Part II: Programme of work (Chapters 6-8)

Part II (Chapters 6 to 8) describes the programme of work that forms the hub of this three-year research project. Chapter 6 recounts the design and development of the Imperial College Instrumented Pile; Chapter 7 the strategy behind the programme of field tests at Canons Park; and Chapter 8 the test procedures that were adopted for the experimental work.

c) Part III: Results of the field experiments (Chapters 9-13)

The results of the experimental work are presented in Part III.

The first three chapters (9-11) cover the instrumented pile tests, deal separately with the three main stages in each experiment, namely: i)

pile installation (Chapter 9); ii) the subsequent equalization period (Chapter 10); and iii) pile loading (Chapter 11).

The testing of two (uninstrumented) driven piles is described in Chapter 12, and the results are discussed with reference to the findings of the instrumented pile tests. The purpose of the driven tests was to assess the influence of the method of installation on the piles' subsequent behaviour during loading.

To conclude Part III, Chapter 13 describes the excavation of an inspection trench around two of the piles, and presents the results of laboratory tests that were performed on samples recovered from the trench. This part of the experimental programme provided an independent check on the findings of the instrumented pile tests, and is regarded as one of the most valuable parts of the experimental programme.

d) Part IV: Discussion (Chapters 14-15)

Chapter 14 compares the results of the research at Canons Park with the findings of previous instrumented pile tests (as reviewed in Chapter 4), and with the predictions of modern theories of pile behaviour (as reviewed in Chapter 3). Finally, Chapter 15 summarizes the main conclusions that arise from this three-year project, and makes suggestions for future research into the behaviour of displacement piles.

### 1.3.4 Volume 2: Appendices 1-15

Volume 2 contains information that could not be fitted into Volume 1 without disrupting the flow of the Thesis. This supplementary material is arranged in a series of appendices, which I have collected together in a separate *reference* volume. The contents of Volume 2 should be clear from the following list of chapter titles:

| | | |
|---|---|---|
| Appendix | 1 | Cavity expansion solutions |
| Appendix | 2 | Survey of previous instrumented pile tests |
| Appendix | 3 | Fundamental properties of London clay |
| Appendix | 4 | Geology of the Canons Park area |

Appendix 5 Earth and pore pressure cells: a review
Appendix 6 Details of instrument design: axial load cells
Appendix 7 Details of instrument design: surface stress transducers
Appendix 8 Details of instrument design: pore pressure probes
Appendix 9 Notes on instrumented pile tests CP0-5
Appendix 10 Instrument performance (tests CP1-5)
Appendix 11 Further test results: pile installation
Appendix 12 Further test results: equalization
Appendix 13 Further test results: pile loading
Appendix 14 Notes on the preparation of thin sections
Appendix 15 Notes on the measurement of soil suction

## 1.4 NOTES AND REFERENCES

[1]Fleming W.G.K., Weltman A.J., Randolph M.F., and Elson W.K. (1985). Piling engineering. Surrey University Press, Glasgow and London/John Wiley and Sons, New York, 380pp.

[2]Figure kindly provided by Fugro-McClelland.

[3]Boden J.B. and Driscoll R.M.C. (1997). House foundations - a review of the effect of clay soil volume change on design and performance. Mun. Engr 4(Aug), pp181-213.

[4]Focht J.A. Jnr and O'Neill M.W. (1985). Piles and other deep foundations. Theme Lecture No 4, Proc. 11th Int. Conf. Soil Mech. & Fdn Engng, San Francisco, 1, pp187-209.

[5]Focht and O'Neill (1985), loc. cit.

[6]See Figure 1 of: Burland J.B. (1987). The Kevin Nash Lecture: The teaching of soil mechanics - a personal view. Proc. 9th Eur. Conf. Soil Mech. & Fdn Engng, Dublin (in press).

[7]Focht and O'Neill (1985), loc. cit., p205.

[8]See, for example, Tomlinson M.J. (1970). Adhesion of piles in stiff clays. CIRIA Report No 26, Construction Industry Research and Information Association, London, 47pp.

[9]See, for example, O'Neill M.W., Hawkins R.A., and Audibert J.M.E. (1982a). Installation of pile group in overconsolidated clay. J. Geotech. Engng Div., Am. Soc. Civ. Engrs, 108(GT11), pp1369-1386.

[10]Terzaghi K. (1936). The shearing resistance of saturated soils and the angle between the planes of shear. Proc. 1st Int. Conf. Soil Mech. & Fdn Engng, Cambridge, 1, pp161-165.

[11]See the useful summary of these formulae in Chapter 1 of: Whitaker T. (1976). The design of piled foundations (2nd edition). Pergamon Press, Oxford, 218pp.

[12]Coyle H.M. and Reese L.C. (1966). Load transfer for axially loaded piles in clay. J. Soil Mech. & Fdns Div., Am. Soc. Civ. Engrs, 92(SM2), pp1-26.

[13]Smith E.A.L. (1960). Pile driving analysis by the wave equation. J. Soil Mech. & Fdns Div., Am. Soc. Civ. Engrs, 86(SM4), pp35-61.

# Chapter 2

# Summary of existing methods of pile design

# CONTENTS OF CHAPTER 2


2.1 INTRODUCTION . . . . . 20
2.1.1 The "Soil Mechanics Triangle" 20
2.1.2 Literature Review (Chapters 2-4) 21
2.1.3 Outline of Chapter 2 21
2.1.4 Poulos's classification of analytical methods 22
2.1.5 Separating shaft capacity from end bearing 23
2.1.6 Co-ordinate system for axi-symmetric problems 24
2.2 "CATEGORY 1" ANALYSES: THE $\alpha$ METHOD . . . . . 26
2.2.1 Basis of the $\alpha$ method 26
2.2.2 Correlations with undrained shear strength 27
2.2.3 Variation of $\alpha$ with the undrained strength ratio 28
2.2.4 Variation of $\alpha$ with pile length 30
2.2.5 Variation of $\alpha$ with set-up time 32
2.3 "CATEGORY 2A" ANALYSES: THE $\beta$ METHOD . . . . . 35
2.3.1 Basis of the $\beta$ method 35
2.3.2 Existing formulae for $\beta$ 36
2.3.3 Discussion of the various formulae for $\beta$ 38
2.3.4 Correlations between $\beta$ and depth 41
2.3.5 General assessment of the $\beta$ method 41
2.3.6 "Local" or "average" values of $\beta$? 43
2.4 "CATEGORY 2B" ANALYSES: EFFECTIVE STRESS METHODS . . . . 47
2.4.1 The ESACC programme 47
2.4.2 Philosophy behind the effective stress methods 47
2.4.3 Stress paths followed during a pile's lifetime 48
2.4.4 Differences between the models ESM1-4 49
2.4.5 Assessment of the effective stress methods 50
2.4.6 General comments on the effective stress methods 51
2.5 NOTES AND REFERENCES . . . . . 53

## 2.1 INTRODUCTION

### 2.1.1 The "Soil Mechanics Triangle"

At the recent European Conference in Dublin, Burland[1] stated that the difficulties encountered by students of soil mechanics could be reduced by emphasizing four separate aspects of the subject:

i) The ground profile
ii) Soil behaviour
iii) Applied mechanics
iv) Empiricism

Burland portrayed the relationship between these topics in the form of a "Soil Mechanics Triangle", as illustrated in Figure 2.1.

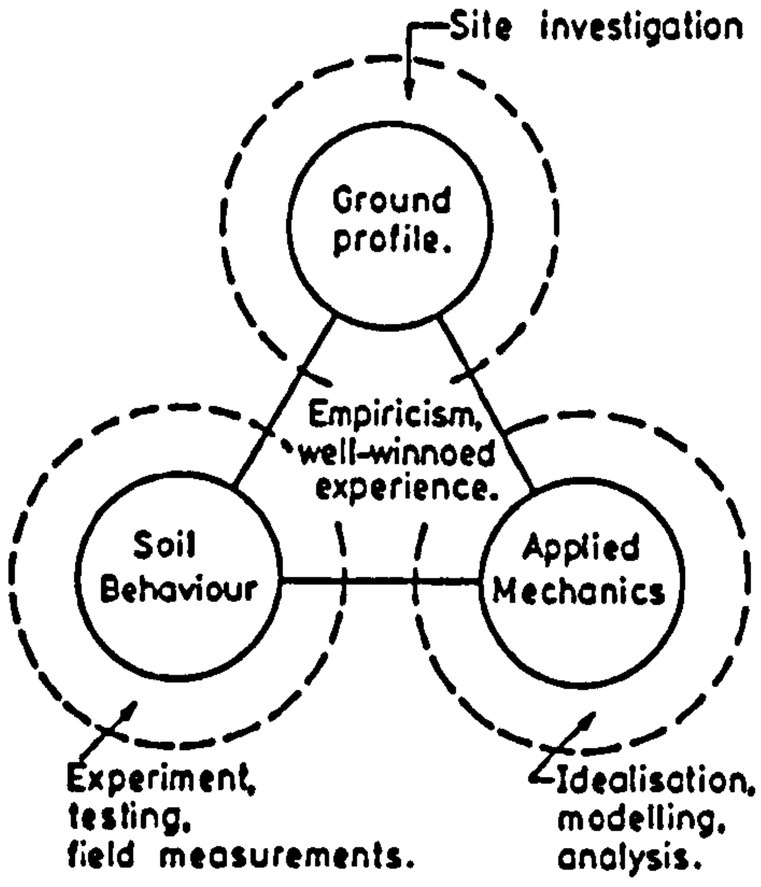



Figure 2.1 Burland's "Soil Mechanics Triangle"

The Soil Mechanics Triangle is an appropriate vehicle for studying the behaviour of piles. Current design methods (as summarized in this chapter) are nearly all based on empiricism and well-winnowed experience (centre). Recent theories of pile behaviour (reviewed in Chapter 3) require idealization, modelling, and quite sophisticated forms of analysis (applied mechanics, bottom right). And much of our knowledge about the way piles perform (see Chapter 4) has been gathered from experiments, testing, and field measurements (soil behaviour, bottom left). Thus, three of the four elements of the Soil Mechanics Triangle provide the information needed for a complete understanding of pile behaviour. (The fourth aspect - information about the ground profile -

is needed in the assessment of all geotechnical phenomena: the investigation of the Canons Park site is described in Chapter 5.)

### 2.1.2 Literature Review (Chapters 2-4)

The next three chapters comprise a Literature Review concerning the behaviour of displacement piles in clay. Each one deals with a particular aspect of the Soil Mechanics Triangle, as described above. In this chapter I summarize some of the most commonly used methods of pile design; in Chapter 3 I discuss the theoretical behaviour of displacement piles in clay; and in Chapter 4 I review the results of various instrumented pile tests.

The aim of the Review is to provide the context in which to judge the findings of the current research project (as described in Chapters 9-13); and to demonstrate the importance of these results in explaining the behaviour of displacement piles in clay.

### 2.1.3 Outline of Chapter 2

I make no attempt herein to discuss every design method that has been proposed for displacement piles in clay. There are many such reviews in the Literature,[2] and to add to these would distract attention from the purpose of the Thesis - which is to explain the physics of pile behaviour in terms of the fundamental properties of clay soils. Nevertheless, it is helpful to examine some of the more common design methods, so that they may be used as "bench-marks" for assessing the results of the pile loading tests that formed part of the field work at Canons Park.

The chapter is split into three main parts. Sections 2.2 and 2.3 describe the essential features of the $\alpha$ and $\beta$ methods; and Section 2.4 summarizes the simple "effective stress methods" of pile design, which have evolved from the development of cavity expansion theory.

## 2.1.4 Poulos's classification of analytical methods

In his recent Rankine Lecture,[3] Poulos introduced a system for classifying analytical and design procedures for piles, according to their level of sophistication and rigour. Three broad categories were proposed, defined as follows:

- Category 1: Empirical procedures
- Category 2: Procedures based on simplified theory or charts
- Category 3: Procedures based on theory

The Category 1 procedures are not based on soil mechanics principles, but depend entirely on correlations with the results of simple in situ or laboratory tests. According to this definition, the alpha method of pile design (described in Section 2.2) is a Category 1 procedure, as are correlations between pile capacity and the results of cone penetration and self-boring pressuremeter tests.

Category 2 methods have a proper theoretical basis, albeit simplified. They involve simple computational methods, but generally do not demand the use of a computer. The required parameters are measured in routine (but relevant) in situ tests. Poulos sub-divided the Category 2 procedures according to the approach adopted for calculating deformations (D) and stability (S):

- 2A: linear-elastic theory (D); rigid-plastic theory (S)
- 2B: non-linear theory (D); elasto-plastic theory (S)

The beta method of pile design (as described in Section 2.3) is a Category 2A procedure; and the "effective stress methods" (described in Section 2.4) are in Category 2B. In all of these procedures the assessment of key parameters relies upon correlations with the results of suitable pile tests - hence these methods are also to some extent empirical in nature.

The main characteristics of the Category 3 methods of analysis are that they are site-specific, based on relatively advanced numerical techniques

(such as the finite element and boundary element methods), and they attempt to build theories from sound soil mechanics principles. In most cases they require the use of a computer. The Category 3 procedures are frequently employed to carry out the parametric studies for developing Category 2 design charts.

Poulos sub-divided the Category 3 procedures as follows:

- 3A: linear-elastic (D) and rigid-plastic (S) models
- 3B: simple non-linear soil models
- 3C: "proper" non-linear constitutive models

The parameters required for the Category 3 procedures are obtained from careful laboratory and/or in situ tests, in which the stress paths followed are designed to match those of the soil next to the pile.

Chapter 3, which reviews the theoretical behaviour of piles, discusses a number of pile theories developed using Category 3C models (such as Modified Cam Clay and those in the MIT-E series).

### 2.1.5 Separating shaft capacity from end bearing

Before proceeding with the Review, I shall define some basic terms and symbols, and attempt to put the calculation of a pile's shaft capacity in context with the problem of estimating its end-bearing.

The pile's overall load capacity, $Q_{total}$, can be split into two separate components, one due to shaft friction ($Q_{shaft}$) and the other due to end-bearing ($Q_{toe}$):

$$Q_{total} = Q_{shaft} + Q_{toe}$$

where $$Q_{shaft} = \pi D L (f_s)_{av}$$

and $$Q_{toe} = q_{toe} \pi D^2/4.$$

In these equations D is the pile's diameter; L its embedded length; $f_s$ is the skin friction on the pile shaft; and $q_{toe}$ the end-bearing pressure.

When loaded in compression, the proportion of load carried by the shaft depends on the pile's "aspect ratio"* (L/D) and also on soil type, but - in clays - is typically greater than 80%, as shown in Figure 2.2.[4]

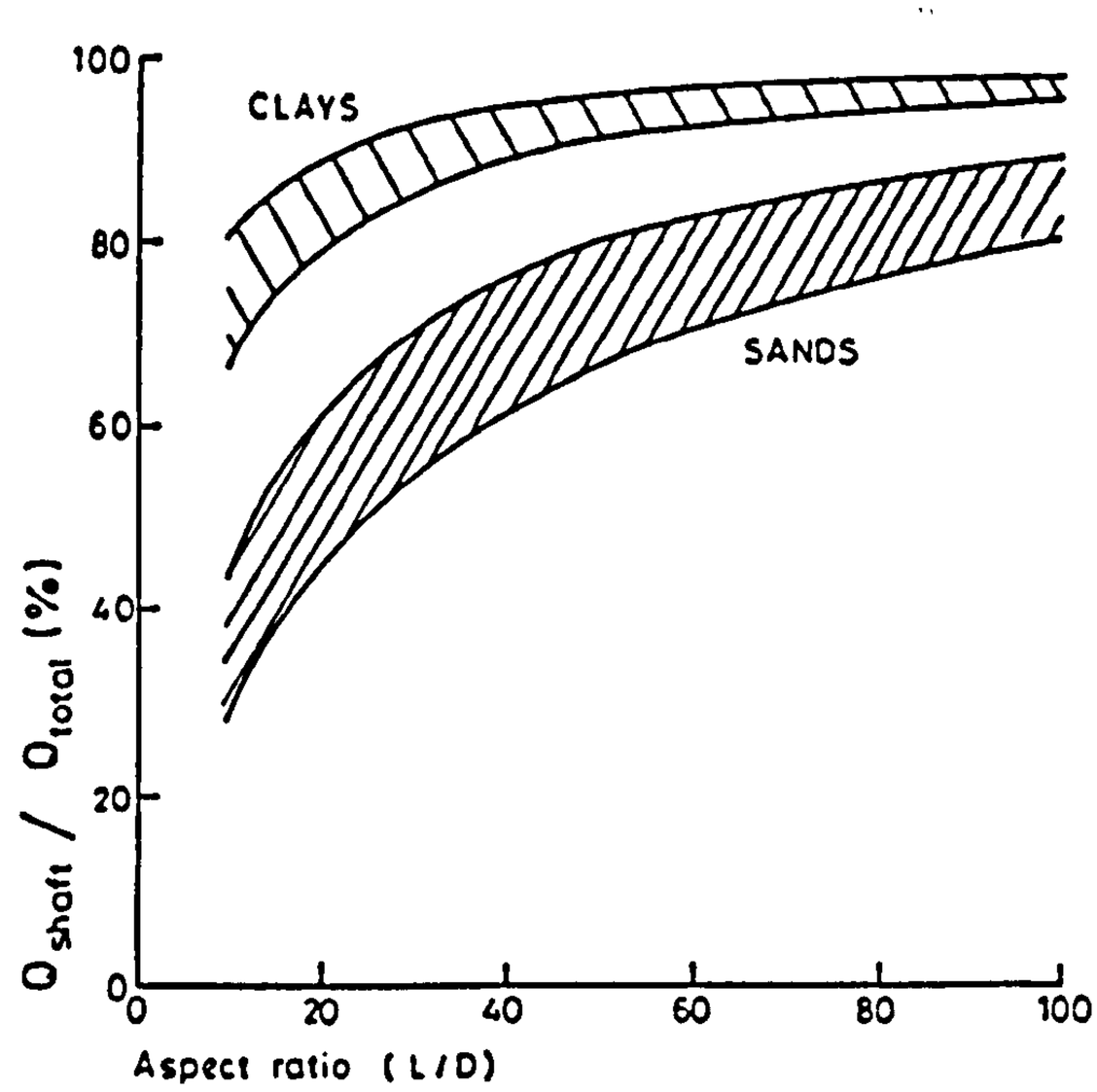



Figure 2.2 Proportion of load carried by pile shaft (closed-ended piles)

This diagram has been drawn for closed-ended piles loaded in compression: open-ended piles carry even less end-bearing, as do tension piles. For these reasons, piles installed in clay soils are commonly referred to as "friction piles".

From the above it is clear that the load capacity of displacement piles in clays is dominated by the mobilization of skin friction along the pile shaft - hence this Thesis concentrates almost exclusively on studying this aspect of pile behaviour.

## 2.1.6 Co-ordinate system for axi-symmetric problems

It is convenient at this point to define the co-ordinate system that will be used throughout the Thesis, and to explain my system of notation for the stresses in the soil around the pile.

Because of axial symmetry there are only four independent stresses to consider (see Figure 2.3): $\sigma_{rr}$, $\sigma_{zz}$, and $\sigma_{\theta\theta}$ are the normal stresses in the radial, vertical, and tangential (hoop) directions. $\tau_{rz}$ is the shear stress acting on vertical and horizontal planes (as shown in the diagram).

---

*Most piles have aspect ratios in the range 25 to 100

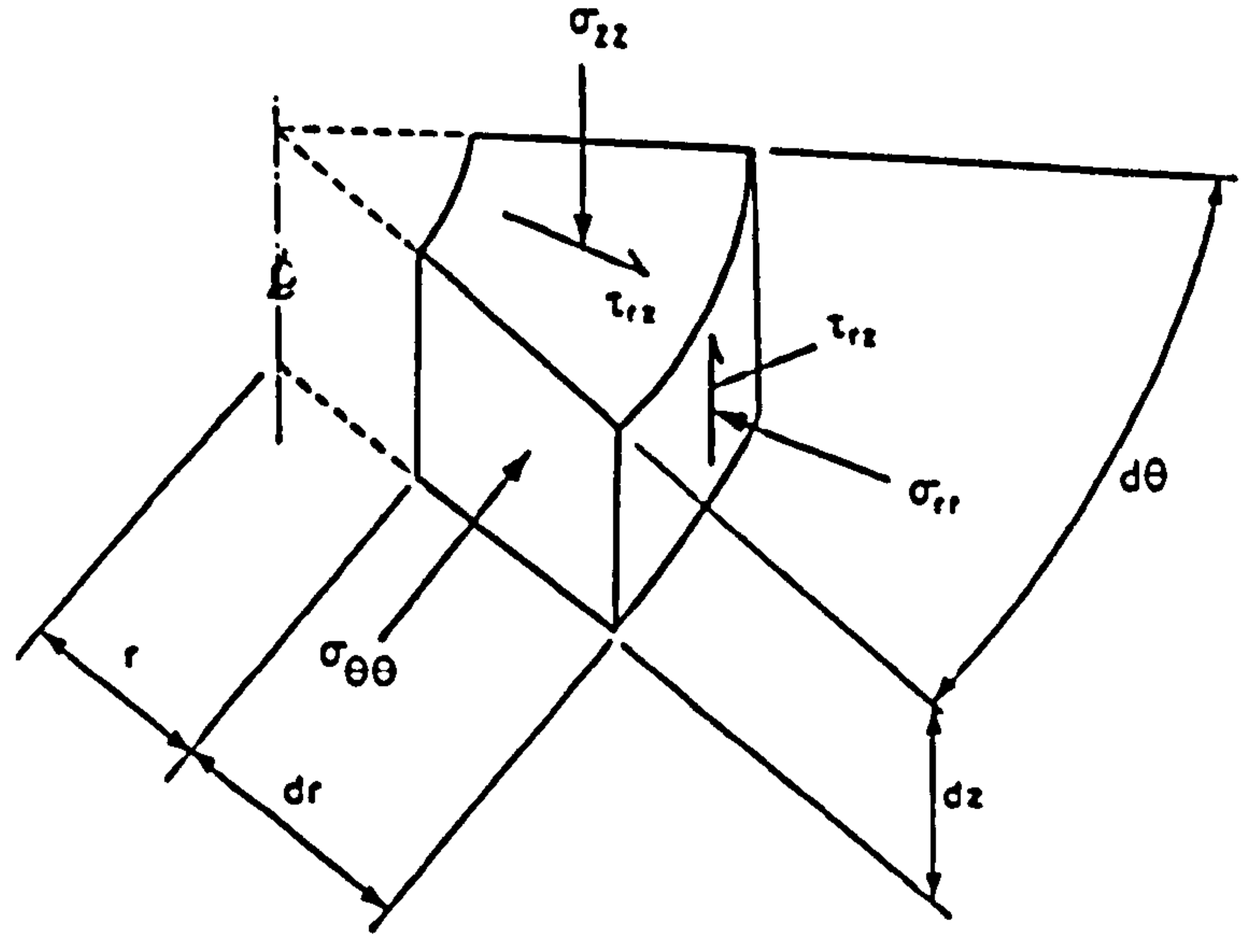



Figure 2.3 Co-ordinate system for axi-symmetric problems

*Effective* stresses are denoted by an apostrophe (e.g. $\sigma'_{zz}$) and *total* stresses by the absence of one (e.g. $\sigma_{rr}$). Pore pressures are represented by the letter u, and hence $\sigma'_{rr} = \sigma_{rr} - u$.

The subscript i denotes conditions at the end of pile installation and c when the subsequent equalization period has been completed. The subscript f denotes conditions at the moment of pile failure in a loading test. Hence the radial effective stresses acting on a pile are, in chronological order: $(\sigma'_{rr})_i = (\sigma_{rr})_i - u_i$; $(\sigma'_{rr})_c = (\sigma_{rr})_c - u_c$; and $(\sigma'_{rr})_f = (\sigma_{rr})_f - u_f$.

## 2.2 "CATEGORY 1" ANALYSES: THE α METHOD

### 2.2.1 Basis of the α method

The most widely used method for estimating the shaft capacity of piles in clay is based on a simple correlation[5,6] between the shaft friction mobilized at failure, $f_s$, and the original (i.e. undisturbed) undrained shear strength of the soil, $c_{uo}$:

$$(f_s)_{av} = \alpha(c_{uo})_{av}.$$

Values of α can be calculated from the results of pile loading tests, provided a suitable assessment of end-bearing is made:

$$\alpha = (Q_{total} - Q_{toe})/\pi DL(c_{uo})_{av}.$$

Since it is uncommon to measure the end-bearing directly (necessitating load cells at the pile's toe), most values of alpha have been calculated assuming that $Q_{toe}$ is given by the equation:[7]

$$Q_{toe} = [N_c(c_{uo})_{toe} + \sigma_{vo}]\pi D^2/4,$$

where $\sigma_{vo}$ is the vertical total stress at the pile toe, and $N_c$ is a bearing capacity factor (usually taken as 9). Values of alpha thus derived lie typically in the range 0.2-1.4, depending on a variety of factors, which include:

- Soil type (normally or over-consolidated)
- Pile type (timber, concrete, steel, etc.)
- Pile geometry (open- or closed-ended tubes; H-section, Franki, tapered piles, etc.)
- Installation method (driven, jacked, bored cast-in-situ)
- Set-up time
- Load test procedures[8] (maintained load, constant rate-of-penetration tests, etc.)

- Method of determining $c_{uo}$ (e.g. field vane, or one of several forms of triaxial test)

Values of alpha have been correlated against a number of soil and pile properties in an attempt to reduce the uncertainty in choosing a value for design. These correlations are reviewed briefly in the following sub-sections.

### 2.2.2 Correlations with undrained shear strength

Many attempts have been made to correlate values of $\alpha$ with the "average" undrained shear strength of the clay soil, with the general conclusion that $\alpha$ reduces significantly as $c_{uo}$ increases (see Figure 2.4). The wide disagreement between the different trend lines demonstrates one of the major difficulties in designing piles by the $\alpha$ method. By way of example, for a pile installed in a stiff clay whose average undrained shear strength equals 100kPa, the curves on Figure 2.4 give $\alpha$ = 0.27 (Flaate[9]), 0.31 (Tomlinson[10]), 0.50 (API[11]), 0.58 (Woodward et al.[12]), and 0.84 (Weltman and Healy[13]).

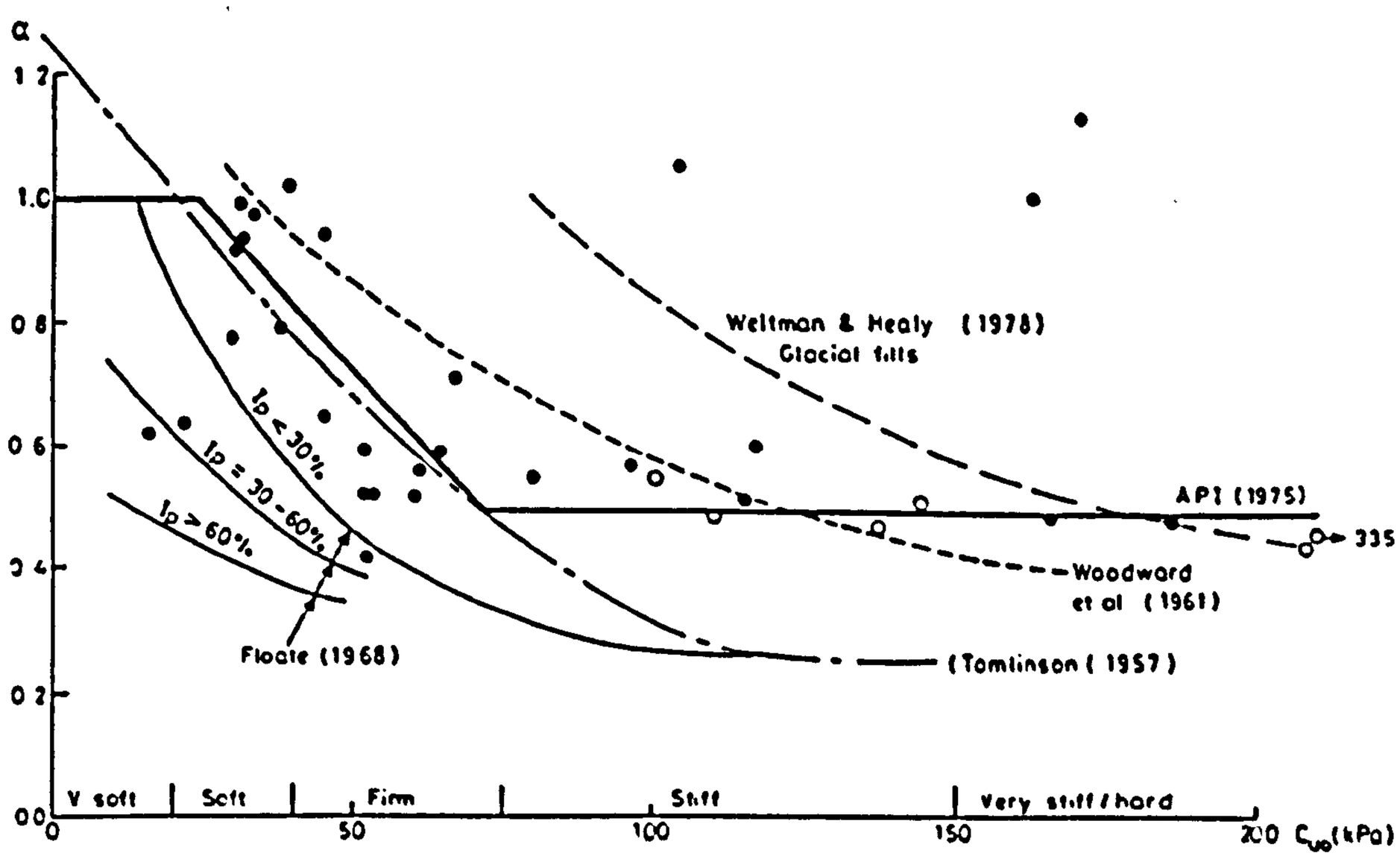



Figure 2.4 Variation of $\alpha$ with $c_{uo}$

Superimposed on Figure 2.4 are the results from load tests on driven steel pipe piles installed in cohesive soils.[14] The large scatter of the data about the design line recommended by the American Petroleum Institute[15] (API) for this type of pile is caused by a number of factors:

- The bearing capacity factor $N_c$ for displacement piles can exceed the value of 9 by as much as 60%,[16,17] resulting in an <u>over</u>-estimate of $\alpha$ of up to 10%
- Back-figured alpha values are sensitive to the estimate of $c_{uo}$, which can vary greatly throughout the deposit
- Values of the clay's undrained shear strength depend on the method of measurement: UK offshore practice is to conduct unconsolidated undrained (UU) triaxial tests,[18] whereas in the United States <u>unconfined</u> compression (UC) tests are more common; the field vane (FV) is often used in sensitive soils because of the problem of recovering "undisturbed" samples; and many research establishments now measure $c_{uo}$ in $K_0$-consolidated undrained triaxial compression ($CK_0UTC$) and direct simple shear ($CK_0UDSS$) tests (e.g. the Norwegian Geotechnical Institute)
- The design rules make no allowance for differences between open- and closed-ended piles; set-up time; or the "direction" of loading (tension or compression)
- Until recently, the alpha method took no account of the over-consolidation ratio (OCR) of the clay or the length of the pile

The undrained shear strength $c_{uo}$ is not a unique soil property, but depends on the method used to measure it. In this Thesis, a distinction is made between the different measurements of $c_{uo}$ by the use of superscripts, for example: $(c_{uo})^{FV}$; $(c_{uo})^{UC}$; $(c_{uo})^{CK_oUTC}$; etc. Whenever the superscript is omitted, either the test method is not relevant to the discussion, or else the strength has been measured in unconsolidated undrained triaxial compression (UUTC).

### 2.2.3 Variation of $\alpha$ with the undrained strength ratio

Recent attempts[19] to rationalize the alpha method have led to a correlation between $\alpha$ and the soil's undrained strength ratio ($c_{uo}/\sigma'_{vo}$),

as shown in Figure 2.5. This relationship can be expressed by two equations:

$$\alpha = S^{0.5}(c_{uo}/\sigma'_{vo})^{-0.5} \quad \text{....for } c_{uo}/\sigma'_{vo} \leq 1.0$$

and $$\alpha = S^{0.5}(c_{uo}/\sigma'_{vo})^{-0.25} \quad \text{....for } c_{uo}/\sigma'_{vo} \geq 1.0$$

where S is the undrained strength ratio for normally consolidated soils - taken as 0.25 for the purposes of this diagram, but generally in the range 0.2-0.45 for anisotropic triaxial compression (CAUTC) tests.[20] Note that the data plotted on Figure 2.5 is based on the results of unconfined compression (UC) tests, i.e. $c_{uo} = (c_{uo})^{UC}$.

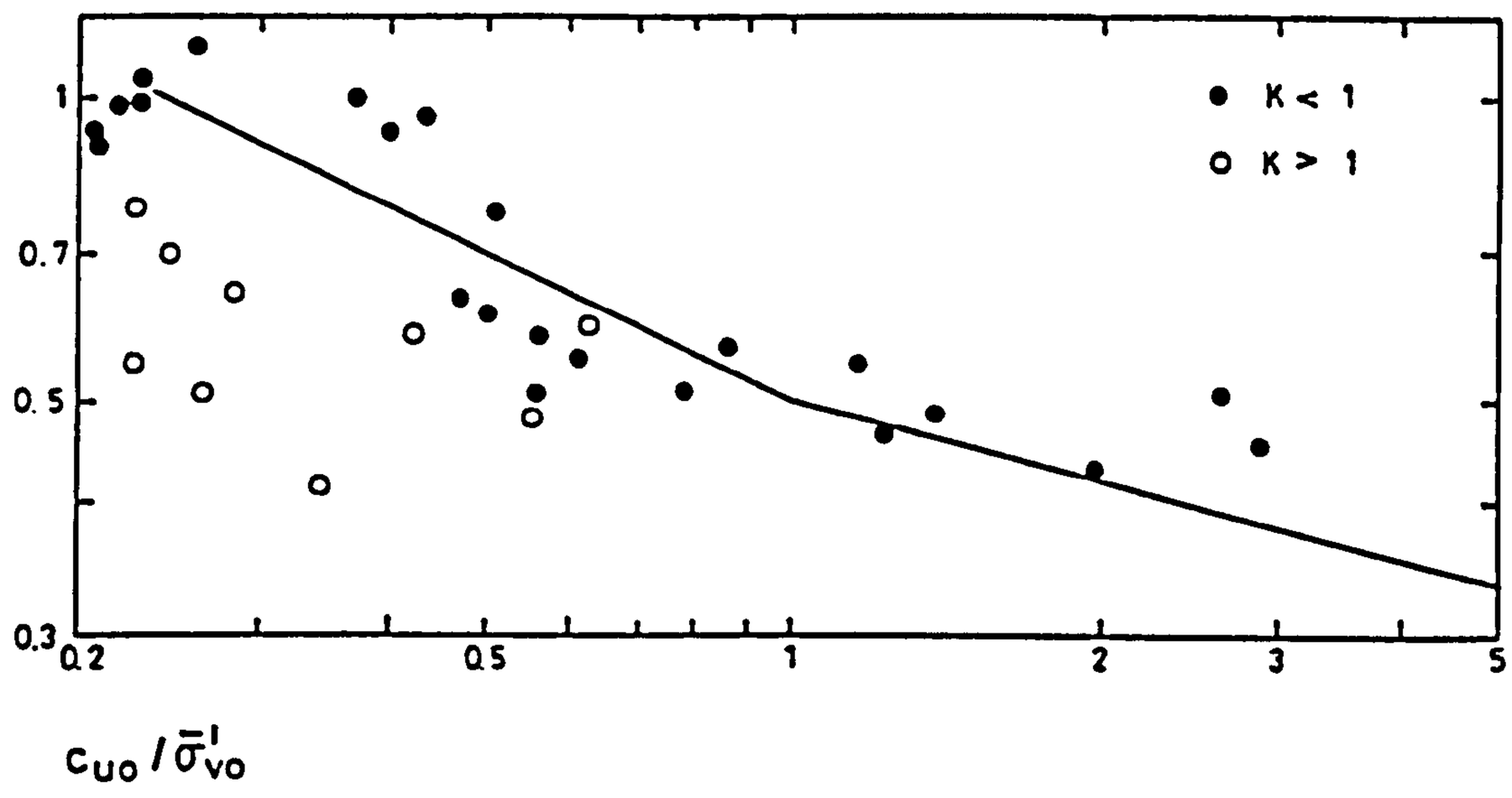



Figure 2.5 Variation of $\alpha$ with $c_{uo}/\sigma'_{vo}$

The various points on this figure have been divided into two groups, according to the value of the "flexibility ratio"[21] K, which reflects the likelihood of progressive failure along the pile (it increases as K increases). For offshore piles K may be as high as five.[22]

The undrained strength ratio $c_{uo}/\sigma'_{vo}$ is known to be a function of the overconsolidation ratio (OCR) of the clay:[23]

$$c_{uo}/\sigma'_{vo} = S(OCR)^A,$$

where $\Lambda$ (= 1 - $\kappa/\lambda$) has been called both the "plastic volumetric strain ratio"[24] and the "strength rebound parameter".[25] $\Lambda$ depends on soil type and the method of measuring $c_{uo}$, but, for anisotropically consolidated natural clays tested in undrained triaxial compression (CAUTC), $\Lambda \approx 0.78$.[26]

From the above, we see that Figure 2.5 takes account of the pre-consolidation of the soil, with normally consolidated clays having $c_{uo}/\sigma'_{vo}$ = 0.2-0.45; lightly overconsolidated clays ($1 < OCR < 4$) $c_{uo}/\sigma'_{vo}$ = 0.35-1.33; and heavily overconsolidated clays ($OCR \geq 8$) $c_{uo}/\sigma'_{vo} > 1.0$. For the London clay at Canons Park, for which $c_{uo}/\sigma'_{vo}$ = 1.94 ±0.42 (see Chapter 5 - $c_{uo}$ from UU tests), the relationship shown in Figure 2.5 predicts that $\alpha$ = 0.42 ±0.03.

### 2.2.4 Variation of $\alpha$ with pile length

A number of studies into the capacity of piles in clays have shown that alpha decreases with increasing pile penetration. Kraft, Focht, and Amerasinghe[27] suggested that the primary causes of this "length effect" are:

- Alterations to the soil fabric as the pile passes a particular soil element
- Strain-softening response of the soil
- Three-dimensional effects (such as the influence of the pile tip and the ground surface)
- Variations in soil properties along the pile's length

Kraft et al. quantified the combined effect of these factors by performing (linear) regression analyses on a data base of 105 pile tests that had previously been reported in the Literature. Their study confirmed that there is a tendency for alpha to reduce as the length of the pile increases:

$$\alpha = 1.336 - 0.126 \log_e(L) \quad \text{...for } c_{uo}/\sigma'_{vo} < 0.4$$

and

$$\alpha = 0.890 - 0.103 \log_e(L) \quad \text{...for } c_{uo}/\sigma'_{vo} > 0.4$$

where the pile's length (L) is in metres, and $c_{uo}$ was measured in unconfined compression (UC) tests. The correlation coefficients* for these equations were rather low (-0.27 and -0.38 respectively), which is a reflection of: i) the small size of the sample (less than 55 data points were selected for this particular analysis); ii) the influence of pile type (concrete, timber, and steel pipe piles were included); and iii) differences in set-up time (28½% less than 25 days; 13½% between 25 and 30 days; and 58% more than 30 days). Accordingly, the scatter of the data about these regression lines is very high, with coefficients of variance (the standard deviation divided by the mean value) of 0.31 and 0.28 respectively. Statistics like these give the pile designer little confidence in using the equations in practice.

The length effect has also been assessed in terms of the pile's aspect ratio (L/D). Semple and Rigden[28] introduced a length factor F into the equation relating $f_s$ to $c_{uo}$:

$$(f_s)_{av} = F\alpha_p(c_{uo})_{av}$$

where $\alpha_p$ is a "peak" value of alpha (which decreases with increasing undrained strength ratio[29]); and F is a function of L/D (F falls as L/D rises[30]). The undrained shear strengths that were used for Semple and Rigden's correlation were mainly values from unconfined compression tests, and they considered driven steel pipe piles only.

Taking this approach one step further, Dennis and Olson[31] introduced *two* "correction factors" into the basic equation relating $f_s$ to $c_{uo}$, as follows:

$$(f_s)_{av} = \alpha F_c F_L (c_{uo})_{av}$$

where $F_c$ "corrects" the measured undrained shear strength to the equivalent unconsolidated undrained (UU) triaxial compression strength

---

*There are at least two definitions of the correlation coefficient, one being the square of the other - Kraft et al. do not say which definition they used

of a high quality sample[32]; and $F_L$ "corrects" for the pile's penetration.[33]

The main problem with all of these studies is that they attempt to determine the effects of a small number of variables (L/D, $c_{uo}$ test method, etc.) when there are several other *independent* variables that may have even greater influence on the pile's capacity (such as set-up time, pile type, etc.). If the number of uncertainties is reduced (by choosing to analyze only those tests on driven pipe piles, say), then the sample size becomes too small for reliable statistical study. This type of approach does not lead to a better understanding of pile behaviour.

## 2.2.5 Variation of $\alpha$ with set-up time

One of the most significant factors that has been neglected in the various studies described above is the influence of set-up time on the derived values of alpha. "Set-up" is the observed increase in total capacity with time, following pile installation.

Figure 2.6 shows the variation of alpha as a function of the time factor $T_1 = c_h t/R^2$, for piles installed in three different *soft* clays.[34] $c_h$ is the coefficient of horizontal consolidation; R the pile's radius; and t the time between installation and loading. The subscript "1" denotes that the time factor has been calculated on the assumption that $c_h = 1mm^2/s$ (field measurements of $c_h$ are not available in all these cases). Each pile was tested in compression on a number of successive occasions, and its capacity was found to increase as shown.

Also plotted on Figure 2.6 is a curve which shows the increase in radial effective stress $\sigma'_{rr}$ on a model pile (the Piezo Lateral Stress cell) installed in the Empire clay.[35] $\sigma'_{rr}$ has been normalized by the radial effective stress at the end of consolidation, $(\sigma'_{rr})_c$. The inference to be drawn from this comparison is that the increase in $\sigma'_{rr}$ is the primary cause of the increase in pile capacity during equalization.

The tendency for the capacity to *increase* is a well-established phenomenon in soft (i.e. normally consolidated) clays. However, in stiff

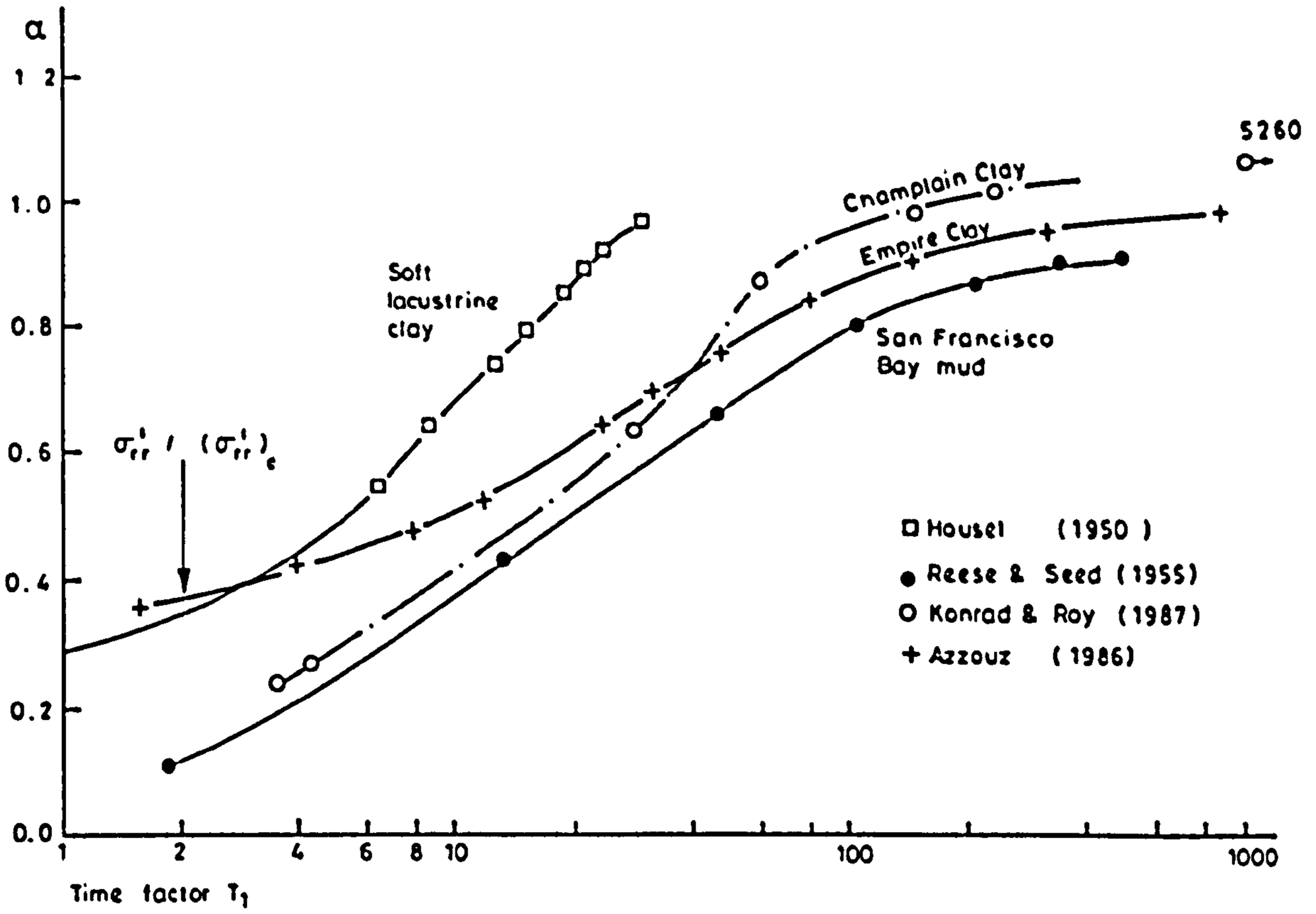



Figure 2.6 Variation of pile capacity with time

(heavily overconsolidated) clays there may be no increase at all and perhaps even a <u>decrease</u> in capacity with time (i.e. negative set-up). See Chapter 4 for further discussion of this point.

It is intriguing to note from Figure 2.6 that the consolidation process proceeds at a very similar rate in the four clays considered. This is because there is very little variation in the value of $c_h$ for a wide range of clay soils. Table 2.1 presents evidence[36] to support this statement, and suggests that $c_h$ falls in the range $0.5 < c_h < 5 mm^2/s$. In the absence of a measured value of $c_h$, there is little error in most cases in assuming $c_h = 1 mm^2/s$ for calculation purposes. To avoid the chance of any misunderstanding, in this Thesis whenever $c_h$ is <u>assumed</u> to be $1 mm^2/s$, the time factor is denoted by the symbol $T_1$.

Table 2.1 Values of $c_h$ (field) for a wide range of clay soils

| Soil | $c_h$ (mm²/s) | Device* | Reference** |
|---|---|---|---|
| Porte Tolle clay | 0.7-1.2 | CPTU | Appendino et al. (1979) |
| | 2.1-3.6 | Pile | |
| Soft org. silty clay | ≈1.9 | SBPM | Clarke et al. (1979) |
| Soft silty clay | 0.44-2.1 | SBPM | |
| Champlain clay | ≈0.5 | Pile | Roy et al. (1981) |
| (Tailings) | 1.6-7.9 | CPTU | Jones and Rust (1982) |
| Cowden glacial till | 0.32 | Pile | Ponniah (1982) |
| Rio de Janeiro soft clay | 0.26-1.02 | CPTU | Rocha Filho & Alencar (1985) |
| Empire clay | 0.45-1.35 | PLS | Azzouz (1986) |
| Soft silty clay | 0.4-3.2 | Probe | Fahey and Foley (1987) |
| Soft lamin. silty clay | 0.74-2.7 | CPTU | Reid and Turnbull (1988) |
| London clay | 0.22-4.4 | CPTU | Long and O'Riordan (1988) |
| London clay | 1.17-2.38 | Pile | This Thesis (see Chapter 10) |

*CPTU - piezocone; SBPM - self-boring pressuremeter; probe - piezo-probe
**See main text for references (note 36)

## 2.3 "CATEGORY 2A" ANALYSES: THE $\beta$ METHOD

### 2.3.1 Basis of the $\beta$ method

The beta method of predicting pile capacity is based on a more "fundamental" approach[37] to the problem than the alpha method, in so much that it relates the skin friction mobilized at failure to the *effective* stresses in the soil (rather than to *total* stresses). The basic equation is:

$$(f_s)_{av} = \beta(\sigma'_{vo})_{av},$$

where $f_s$ is the skin friction; $\sigma'_{vo}$ is the original vertical effective stress in the soil (i.e. prior to pile installation); and $\beta$ is an empirically determined factor, which equals 0.25-0.40 for normally consolidated clays, and up to 2.5 for heavily overconsolidated clays.

Beta has been expressed in terms of various parameters, including the angle of friction at the pile/soil interface ($\delta$); the angle of friction of the soil ($\phi$); an earth pressure coefficient* $K_s$; and the soil's over-consolidation ratio (OCR). The following section summarizes several well-known formulae for $\beta$ in terms of these parameters, and lists the assumptions made in their derivation.

The various formulae are presented in chronological order, and are discussed in more detail in Section 2.3.3.

---

*$K_s$ ($= \sigma'_{rr}/\sigma'_{vo}$) relates the radial effective stress acting on the pile shaft ($\sigma'_{rr}$) to the original vertical effective stress in the soil ($\sigma'_{vo}$); note that the vertical effective stress *at the pile wall* ($\sigma'_{zz}$) is not the same as $\sigma'_{vo}$; $\beta$ is defined in terms of $\sigma'_{vo}$, not $\sigma'_{zz}$

## 2.3.2 Existing formulae for $\beta$

| Author | Assumptions ($c' = 0$ for all) | Formulae ($\beta = \tau_{rz}/\sigma'_{vo}$) |
|---|---|---|
| Burland[38] | Soft clays | |
| | 1) Failure on vertical plane | $\beta = K_s \tan \delta$ |
| | 2) Failure in soil | $\delta = \phi$ |
| | 3) $\sigma'_{rr}$ doesn't change during installation/equalization | $K_s \approx K_0^{nc}$ |
| | 4) Jaky's formula[39] | $K_0^{nc} = (1 - \sin \phi)$ |
| Hence... | | $\beta = (1 - \sin \phi)\tan \phi$ |
| Meyerhof[40] | Stiff clays | |
| | 1) As Burland | $\beta = K_s \tan \delta$ |
| | 2) As Burland | $\delta = \phi$ |
| | 3) Installation increases radial effective stress by up to 100% | $K_s = (1.5 \pm 0.5)K_0$ |
| | 4) Formula for $K_0$ | $K_0 = (1 - \sin \phi)\sqrt{(OCR)}$ |
| Hence... | | $\beta = (1.5 \pm 0.5)(1 - \sin \phi)\tan \phi \sqrt{(OCR)}$ |
| Parry & Swain[41] | Soft clays | |
| | 1) Failure on vertical plane | $(\tau_{rz})_f = (\sigma'_{rr})_f \tan \phi$ |
| | 2) Failure in soil on plane of maximum stress obliquity | $(\sigma'_1 - \sigma'_3)/(\sigma'_1 + \sigma'_3) = \sin \phi$ |
| | 3) At failure $\sigma'_{zz} = \sigma'_{vo}$ | $(\sigma'_{zz})_f = \sigma'_{vo}$; $\sigma'_1 > \sigma'_{zz}$ |
| Hence... | | $\beta = \sin \phi . \cos \phi/(1 + \sin^2 \phi)$ |
| Parry & Swain[42] | Stiff clays | |
| | 1) Radial effective stress at failure is greater than vertical effective stress | $(\sigma'_{rr})_f = n(\sigma'_{zz})_f$, $n > 1$ |
| | 2) As for soft clays | $(\sigma'_1 - \sigma'_3)/(\sigma'_1 + \sigma'_3) = \sin \phi$ |
| | 3) Vertical effective stress at failure is greater than the original vertical effective stress | $(\sigma'_{zz})_f = m\sigma'_{vo}$, $m > 1$ |
| Hence... | | $\beta/m = f(n, \phi)$ |

where $f(n, \phi)$ is a function of n and $\phi$ (see the original paper for details).

## 2.3.2 Existing formulae for $\beta$ (continued)

| Author | Assumptions | Formulae ($\beta = \tau_{rz}/\sigma'_{vo}$) |
|---|---|---|
| Flaate & Selnes[43] | Soft to medium clays | |
| | 1) Failure on vertical plane | $f_s = f(\sigma'_{rr}\tan\delta)$ |
| | 2) Failure in soil | $\delta = \phi$ |
| | 3) Mobilized friction depends on pile length | $f_s \propto \mu_L$ |
| | 4) "Time rate effects" | $f_s \propto \mu_t$ |
| | 5) Original ground stresses in the soil are restored | $\sigma'_{rr} = K_0\sigma'_{vo}$ |
| | 6) Installation pore pressures are $\approx 5\text{-}7c_{uo}$ | $f_s = f(5c_{uo})$ |
| | 7) Formula for $K_0$ | $K_0 = K_0^{nc}/(OCR)$ |
| | 8) Various relationships between main parameters and plasticity index | $K_0^{nc} = f(I_p)$<br>$\tan\phi = f(I_p)$<br>$c_{uo}/\sigma'_{vo} = f(I_p)$ |

Hence... $$\beta = (0.4 \pm 0.1)\mu_L OCR^{0.5},$$

where $\mu_L$ is a function[44] of pile length (and reduces from about 0.75 for a 10m long pile to $\approx$0.5 for much longer piles). Refer to the original paper for further details of this derivation. (Unfortunately, Flaate and Selnes don't give precise details.)

| | | |
|---|---|---|
| Fugro Ltd[45] | All types of clay | |
| | 1) As Burland | $\beta = K_s\tan\delta$ |
| | 2) As Burland | $\delta = \phi$ |
| | 3) Installation increases radial effective stresses | $K_s = AK_0$ |
| | 4) Formula for $K_0$ | $K_0 = (1 - \sin\phi)(OCR)^{0.42}$ |
| | 5) Formula for OCR | $c_{uo}/\sigma'_{vo} = S(OCR)^{0.8}$ |
| | 6) Formula for S | $S = (c_{uo}/\sigma'_{vo})_{nc} = \phi°/100$ |

Hence... $$\beta = A(1 - \sin\phi)\tan\phi(100/\phi°)^{0.525}(c_{uo}/\sigma'_{vo})^{0.525},$$

where $c_{uo}/\sigma'_{vo}$ is the soil's undrained strength ratio; S is the undrained strength ratio for the normally consolidated clay; and A has been termed the "compaction factor". From the results of various pile tests, Fugro obtained the following correlation between A and $c_{uo}/\sigma'_{vo}$:

$$A = 0.75 + 0.2(c_{uo}/\sigma'_{vo})$$

## 2.3.3 Discussion of the various formulae for $\beta$

Most of the formulae for beta assume that failure takes place on a vertical plane in the soil, and not at the pile/soil interface. Parry and Swain's derivation for stiff clays assumes that the peak stress is first reached on failure planes that are *inclined* to the vertical; but, because of the boundary conditions, these planes must re-align themselves parallel to the pile/soil interface for large movements to occur.

The development of a continuous displacement shear next to the pile wall, as envisaged by Parry and Swain, is illustrated in Figure 2.7:

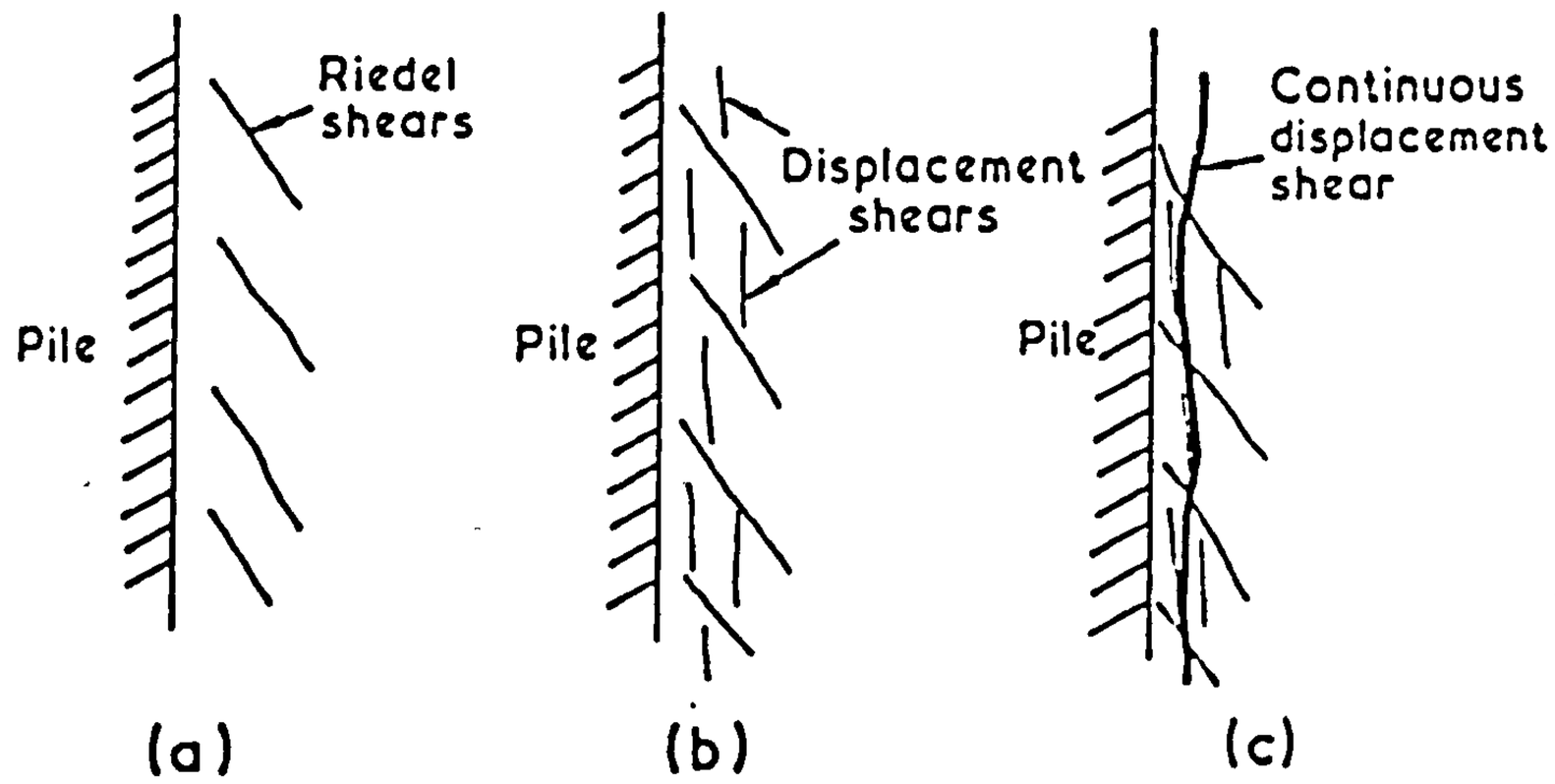



Figure 2.7 Development of continuous displacement shear next to pile wall

> "Adjacent to the soil-pile interface ...surfaces develop which are inclined to the direction of general movement. ...these [Riedel shears] will lie *en echelon* at an angle of some 10° to 30° to the vertical... and have conjugate shears associated with them [Figure 2.7(a)].
>
> "Large slips along the Riedel shears are not possible kinematically and subsequent to initial failure the soil is compelled to develop new slip surfaces parallel or nearly parallel to the soil-pile interface [Figure 2.7(b)]...
>
> "[The displacement shears] will join to form a continuous slip surface [Figure 2.7(c)], or alternatively slip will occur along the soil-pile interface itself."[46]

results of load tests on steel pipe piles (as listed in the API database[49]). Although there is reasonable agreement for all values of $c_{uo}/\sigma'_{vo}$, this is hardly surprising since the "compaction factor" A (= $K_s/K_0$) was back-figured from several of these tests! By comparison, Meyerhof's formula (with a constant value of A = 1.5 ±0.5) shows not only poor agreement with the data for low strength ratios, but also a massive range of possible values for $\beta$. It is clear from Figure 2.9 that the compaction factor has an over-riding influence on beta.

Fugro's equation for $\beta$ as a function of $c_{uo}/\sigma'_{vo}$ results in an almost

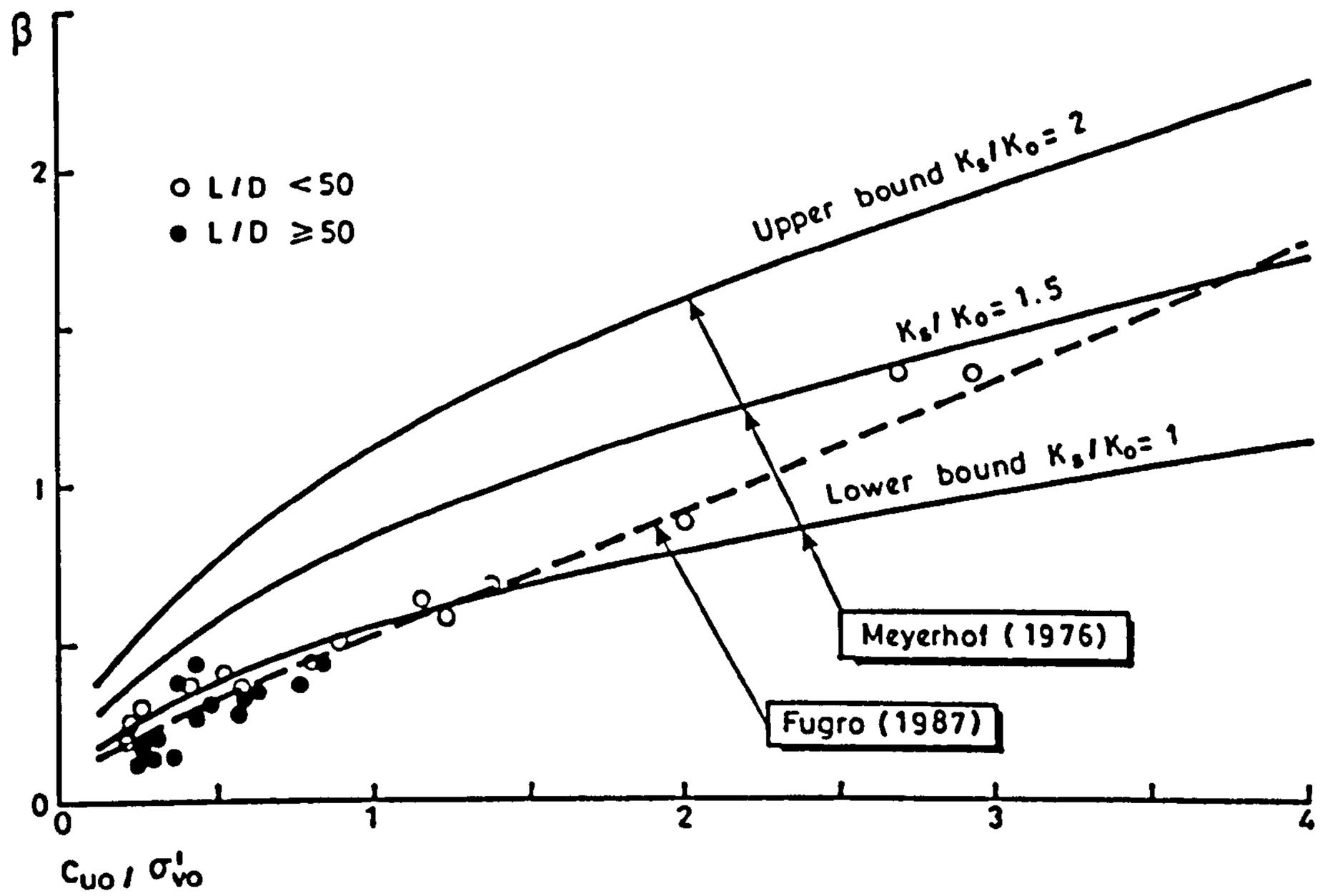



Figure 2.9 Variation of $\beta$ with $c_{uo}/\sigma'_{vo}$

linear relationship between the two parameters:[50]

$$\beta = 0.06 + 0.44(c_{uo}/\sigma'_{vo})$$

Because the data base includes very few pile tests in heavily over-consolidated clays (which have high values of $c_{uo}/\sigma'_{vo}$), this correlation is unduly biased by the results of those tests. If we replace $c_{uo}/\sigma'_{vo}$ with $(c_{uo})_{av}/(\sigma'_{vo})_{av}$ (which is how the strength ratio is normally calculated), and since $\beta = (f_s)_{av}/(\sigma'_{vo})_{av}$, then the equation given above is equivalent to:

This view of the behaviour of displacement piles in clays neglects the potential for a continuous displacement shear to form adjacent to the pile during installation, and for pile loading to re-activate movement along this surface, rather than causing the surrounding soil to fail.

Which angle of friction soil should appear in the equations for $\beta$? The answer depends on the degree of progressive failure that takes place along the pile shaft[47]: if the clay particles are re-aligned in a systematic fashion during pile driving, we should expect friction mobilized on the failure plane to be closer to the residual ($\phi_R$) than to the critical state angle ($\phi_{CS}$). Implicit in all of the equations for $\beta$ is the idea that $\phi = \phi_{CS}$.

For values of $\phi$ between 20° and 30°, the various expressions given in Section 2.3.2 reduce to the following simplified forms ($\beta_{nc}$ is for normally consolidated clays only):

| | |
|---|---|
| Burland | $\beta_{nc} = 0.24\text{-}0.29$ |
| Parry and Swain | $\beta_{nc} = 0.29\text{-}0.35$ |
| Meyerhof | $\beta = (0.40 \pm 0.17)OCR^{0.5}$. |
| Flaate & Selnes | $\beta = (0.4 \pm 0.1)\mu_L OCR^{0.5}$ |
| Fugro Ltd | $\beta = (0.55 \pm 0.01)A(c_{uo}/\sigma'_{vo})^{0.525}$ |

In practice Burland found that $\beta$ varied from 0.25 to 0.40 for piles driven into soft clay. Flaate and Selnes' equation (which is almost identical to Meyerhof's, save for the inclusion of the length factor $\mu_L$) gives a reasonably good fit to the results of over 40 pile tests[48] (mainly on timber piles) in both normally- and over-consolidated clays, as demonstrated in Figure 2.8.

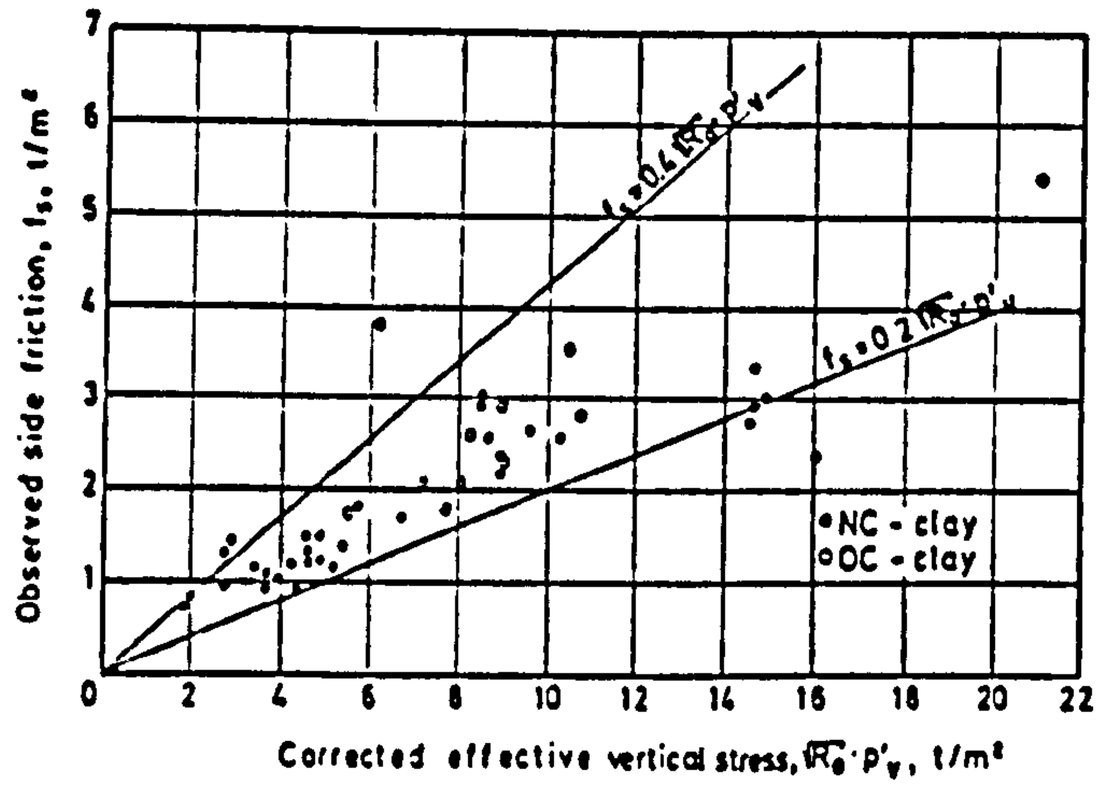



Figure 2.8 $f_s$ vs $\sigma'_{vo}\sqrt{OCR}$ from timber pile tests

Figure 2.9 compares the Fugro relationship for $\beta$ with the

$$(f_s)_{av} = 0.06(\sigma'_{vo})_{av} + 0.44(c_{uo})_{av}$$

i.e. $$\alpha = (f_s)_{av}/(c_{uo})_{av} = 0.06(\sigma'_{vo})_{av}/(c_{uo})_{av} + 0.44$$

In other words, all that this equation really tells us is that $\alpha$ is approximately equal to 0.44 in heavily overconsolidated clays! (For these soils $c_{uo}/\sigma'_{vo} > 1$, and so $0.06(\sigma'_{vo})_{av}/(c_{uo})_{av} << 0.44$.

### 2.3.4 Correlations between $\beta$ and depth

Meyerhof[51] reviewed the data from a wide range of pile tests in soft and medium clays and showed that $\beta$ decreases dramatically once the pile's length exceeds ≈15m (50ft), as shown in Figure 2.10. This diagram clearly demonstrates the enormous scatter in values of $\beta$ for lightly overconsolidated soils ($0.09 \leq \beta \leq 0.5$). As Meyerhof showed in another diagram, the scatter is even greater when stiff clays are considered ($\approx 0.45 \leq \beta \leq 3.1$).

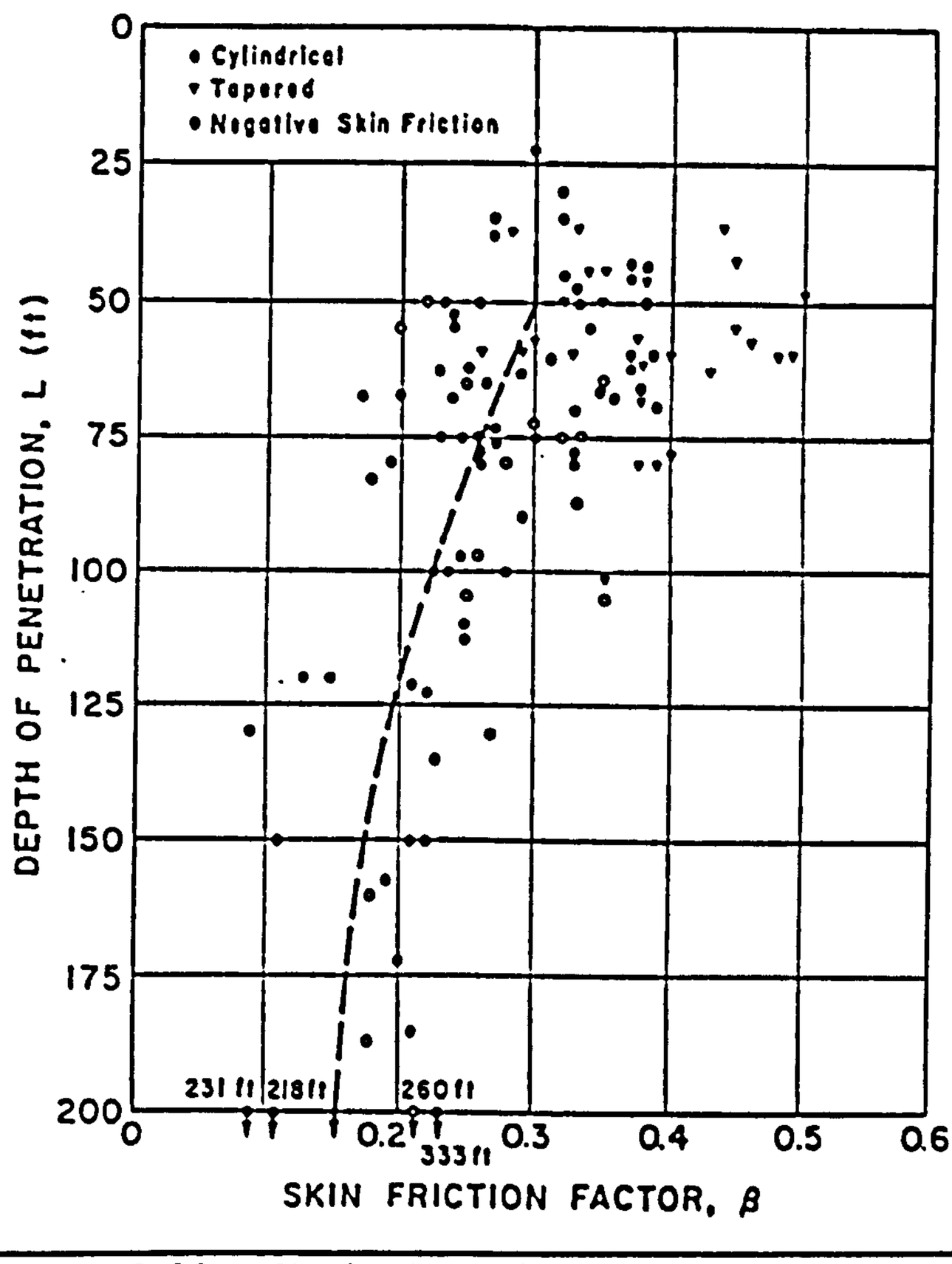



Figure 2.10 Variation of beta with depth of penetration

### 2.3.5 General assessment of the $\beta$ method

Despite its attraction as a "fundamental approach" to estimating shaft friction, the beta method still suffers from many of the handicaps of the

total stress approach (i.e. the alpha method and its derivatives). In particular, it takes no account of the influence on load capacity of, *inter alia*: pile type; pile geometry; installation method*; set-up time; load test procedures; loading history (repeat tests/re-drives); oversized end-plates; and so on.

As an example of the potential importance of just one of these factors, consider the influence of set-up time on the pile capacity of a 2m diameter offshore pile installed in soft clay. As was shown in Section 2.2.5 (see page 32), most piles reach 90% of their ultimate capacity once the time factor $T_1$ equals approximately 100. For a $\phi$2m pile, with $c_h$ = 1mm$^2$/s, this implies that $t_{90} = T_1R^2/c_h \approx 100x1^2/10^{-6}$s = 3.2 years! In other words, the capacity of a large diameter offshore pile, loaded within one year of installation (quite typical), could be much less than its long-term capacity - a fact that is totally ignored in both the alpha and the beta methods.

The large error bands quoted in the equations for $\beta$ warn us that the reliability of this "Category 2A" procedure is not necessarily any greater than that of the $\alpha$ method. The effective stress approach is at least more soundly based, but it is still highly empirical in character (i.e. akin to a Category 1 procedure). Category 2B effective stress methods offer a more rational approach to pile design, and these are discussed at length in Section 2.4.

For the $\beta$ method to offer any real advantage over the $\alpha$ method of pile design, the uncertainty in the value of $K_s/K_0$ must be reduced, and we need to establish whether failure planes are formed in the soil (and at what angle) or at the pile/soil interface. The best - and perhaps the only - way to achieve these aims is to conduct instrumented pile tests, in which there are measurements of the <u>effective</u> stresses acting on the pile; and to examine the soil's fabric around piles, in order to uncover the failure surfaces.

---

*To a certain extent the method does distinguish between bored and displacement piles

Chapter 4 reviews a number of previous instrumented pile tests, and endeavours to establish more appropriate values for $K_s/K_0$ for a wide range of clays. In Chapters 9 to 11, I present the results of instrumented pile tests in the heavily overconsolidated London clay; and in Chapter 13 I describe the investigation of the soil's fabric around two in situ piles.

### 2.3.6 "Local" or "average" values of $\beta$?

Finally, I wish to discuss a subtle point regarding the way in which the undrained strength ratio ($c_{uo}/\sigma'_{vo}$) is used to select appropriate values of beta for design. The discussion has particular relevance to problems involving layered soil profiles.

The theoretical basis of the beta method is that the *local* skin friction on the pile is related to the *local* vertical effective stress, via a parameter $\beta$:

$$(f_s)_{local} = \beta(\sigma'_{vo})_{local},$$

where the subscript "local" is used to denote stresses acting at a specific point below ground level (as opposed to average values of stress).

Now the *average* skin friction acting on the pile is given by the following equation:

$$(f_s)_{av} = (1/L)\int_L (f_s)_{local} dz = (1/L)\int_L \beta(\sigma'_{vo})_{local} dz,$$

where, for typical ground conditions, $(\sigma'_{vo})_{local} \approx \gamma' z$ and $\gamma'$ is the submerged unit weight of the soil (circa 10kN/m$^3$).

According to the correlation shown in Figure 2.9, $\beta$ is related to $c_{uo}/\sigma'_{vo}$ by some constant $\psi$:

$$\beta \approx \psi(c_{uo}/\sigma'_{vo}),$$

where, as discussed in Section 2.3.3, $\psi$ is similar to an alpha value for the pile. Indeed, if we substitute this equation into the previous one for $(f_s)_{av}$, and assume that $\psi$ is constant with depth, we obtain:

$$(f_s)_{av} = (1/L)\int_L \psi (c_{uo}/\sigma'_{vo})_{local} (\sigma'_{vo})_{local} dz$$
$$(f_s)_{av} = (1/L)\psi \int_L (c_{uo})_{local} dz$$

which is the basic equation of the alpha method.

The question now arises: how do we select a value for $\beta$ when we have a layered soil profile? Or when $c_{uo}/\sigma'_{vo}$ varies significantly with depth (as is common in an overconsolidated clay)?

Figure 2.11 illustrates the problem by considering the ground conditions at an offshore site in the North Sea (Magnus). The soil at this site consists primarily of very stiff to hard silty clays, and over the depths of interest comprises eight distinct soil strata (A-H).

The left hand diagram of Figure 2.11 shows the variation of the clay's undrained shear strength ($c_{uo}$) with depth, for the eight layer sequence.[52] This profile represents the "best estimate" of $c_{uo}$ in each horizon. The middle diagram shows the variation of the undrained strength ratio ($c_{uo}/\sigma'_{vo}$) based on this idealized profile. Over the depths 1 to 82m, the average undrained shear strength is 262kPa, and the average vertical effective stress 476kPa, so that $(c_{uo})_{av}/(\sigma'_{vo})_{av} = 0.55$. However, the average value of the undrained strength ratio, $(c_{uo}/\sigma'_{vo})_{av}$, is 1.08! After all, there is no *a priori* reason why the ratio of two averages should equal the average of the corresponding ratio.*

The right hand diagram of Figure 2.11 shows how the value of the skin friction ($f_s$) depends on the method chosen for calculating $\beta$:

---

*The ratio of the two averages is:

$$(c_{uo})_{av}/(\sigma'_{vo})_{av} = (1/L)\int_L c_{uo} dz + (1/L)\int_L \sigma'_{vo} dz$$

and the average of the corresponding ratio:

$$(c_{uo}/\sigma'_{vo})_{av} = (1/L)\int_L (c_{uo}/\sigma'_{vo}) dz$$

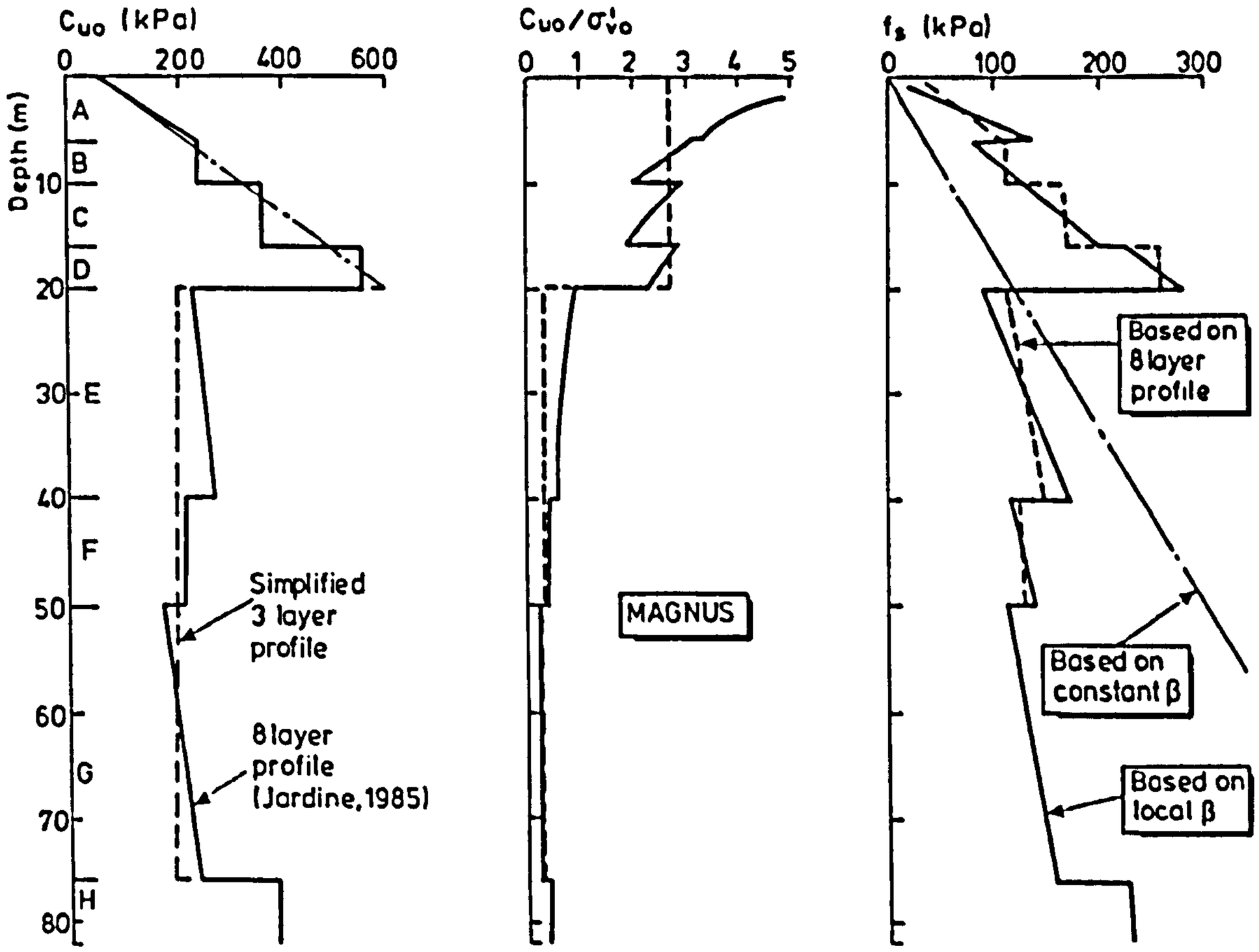



Figure 2.11 Dependence of $\beta$ on method of calculation: Magnus foundations

- Method 1 (full line) is based on "local" values of $\beta$ (i.e. $f_s = \beta_{local}\sigma'_{vo}$, where $\beta_{local}$ depends on the *local* value of $c_{uo}/\sigma'_{vo}$, calculated at 1m intervals)
- Method 2 (broken line) is based on *average* values of $\beta$ for each stratum, i.e. $(c_{uo}/\sigma'_{vo})_{av}$ has been calculated for all eight soil layers, A to H, giving eight different values of $\beta$ (i.e. $\beta_A$, $\beta_B$, ...$\beta_H$)
- Method 3 (chain-dotted) is based on a single value of $\beta$ (= 0.535) for the whole profile, calculated from the average value of $c_{uo}/\sigma'_{vo}$ (= 1.08)

The average skin friction acting on the pile is 144kPa according to the first method; 146kPa according to the second; and 255kPa according to the third (i.e. 77% higher!).

Although few geotechnical engineers would choose to average the undrained strength ratio after the style of Method 3, it is not at all clear how detailed the stratification should be if such horrendous inconsistencies in the calculated skin friction are to be avoided. Would a three-layer profile like the one shown on Figure 2.11 produce reasonable results? Is even an *eight*-layer profile sufficiently detailed?

Clearly great care is needed in using the beta method in practice. This applies to <u>any</u> design method in which the local skin friction is assumed to be proportional to the depth below ground surface (the alpha method does not make this assumption, and hence does not suffer from the problem).

Existing data-bases of pile loading tests invariably contain only *one* entry for each load test - even when the soil is layered, or its over-consolidation ratio (and hence undrained strength ratio) varies with depth. One entry implies one (constant) value of $\beta$ along the pile, and one ("average") value of $c_{uo}/\sigma'_{vo}$ to characterize the soil (i.e. $\beta$ has been determined by Method 3 above). Since most sites possess a layered soil profile, the engineer is more likely to adopt Method 1 in order to design his piles. Hence the data-bases are <u>not</u> consistent with the likely design method.

## 2.4 "CATEGORY 2B" ANALYSES: EFFECTIVE STRESS METHODS

### 2.4.1 The ESACC programme

In 1978, a major programme of research was launched to improve existing methods for predicting the axial capacity of piles in clays.[53] The project, the "Effective Stress Axial Capacity Co-operative" (ESACC), produced three generations of effective stress methods (ESM2, 3, and 4), which were variations on a model (ESM1) that had been developed during an earlier research programme.

The effective stress methods are based on concepts embodied in Critical State Soil Mechanics,[54] and incorporate several features of soil behaviour that are predicted by analytical work into cavity expansion theory (see Chapter 3). They are what Poulos has called "Category 2B" procedures (see Section 2.1.4). Although the models are not described in their entirety herein, the principles behind them are discussed in some detail.

### 2.4.2 Philosophy behind the effective stress methods

The effective stress methods (ESMs) attempt to follow the changes in effective stress in the soil during three distinct stages in the pile's "history" (as illustrated in Figure 2.12):

i) Pile installation
ii) Earth and pore pressure equalization
iii) Pile loading

The philosophy behind the ESMs is founded on the assumptions that:

- The soil next to the pile is failed and remoulded to a critical state during pile installation
- Following installation the soil consolidates
- During loading to failure, the soil is once again sheared to a critical state condition

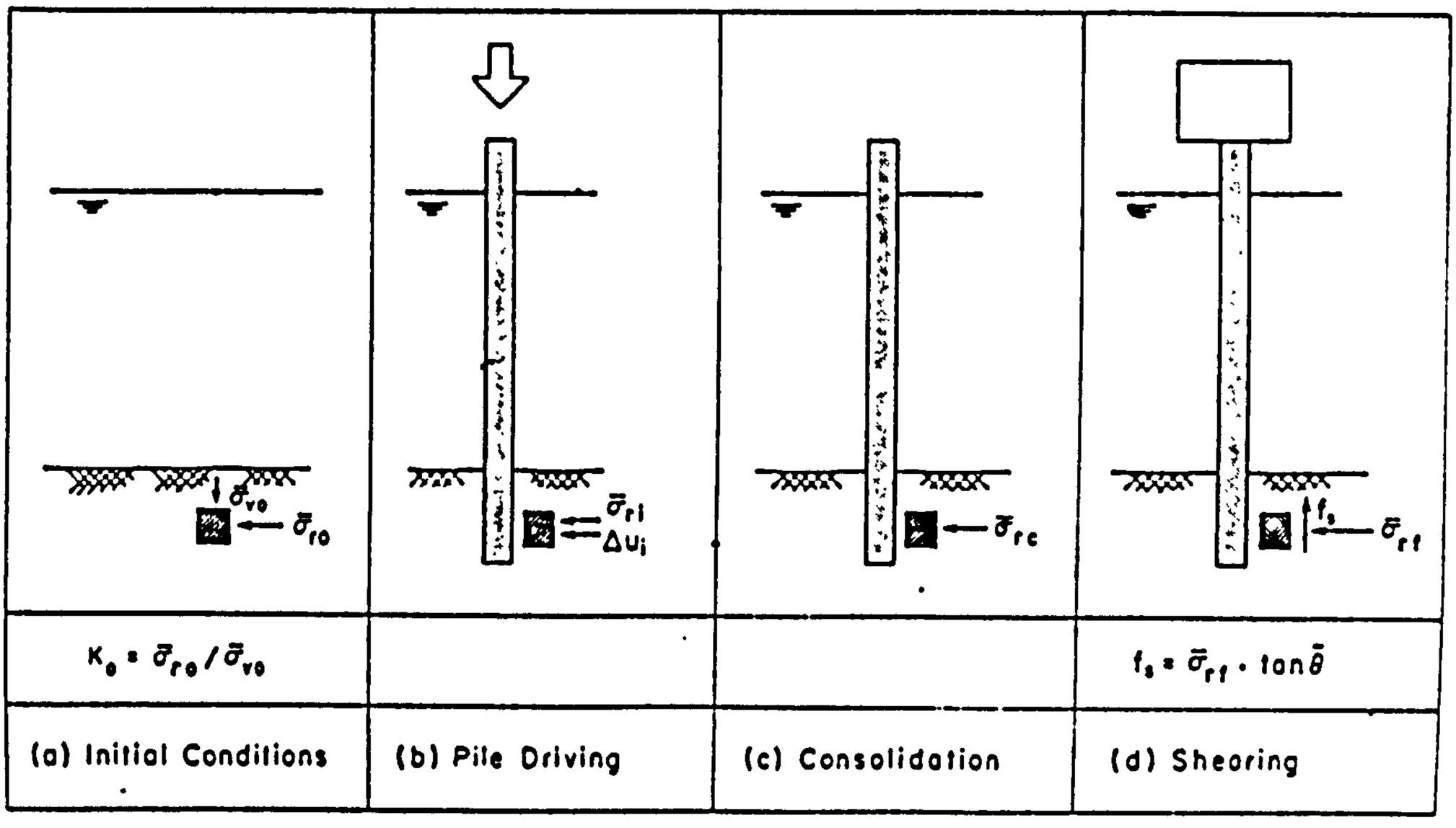



Figure 2.12 Different stages in the life of a pile

## 2.4.3 Stress paths followed during a pile's lifetime

The stress paths followed by the soil during the various stages of a pile's lifetime are shown schematically in Figure 2.13, for a normally- and an over-consolidated clay.

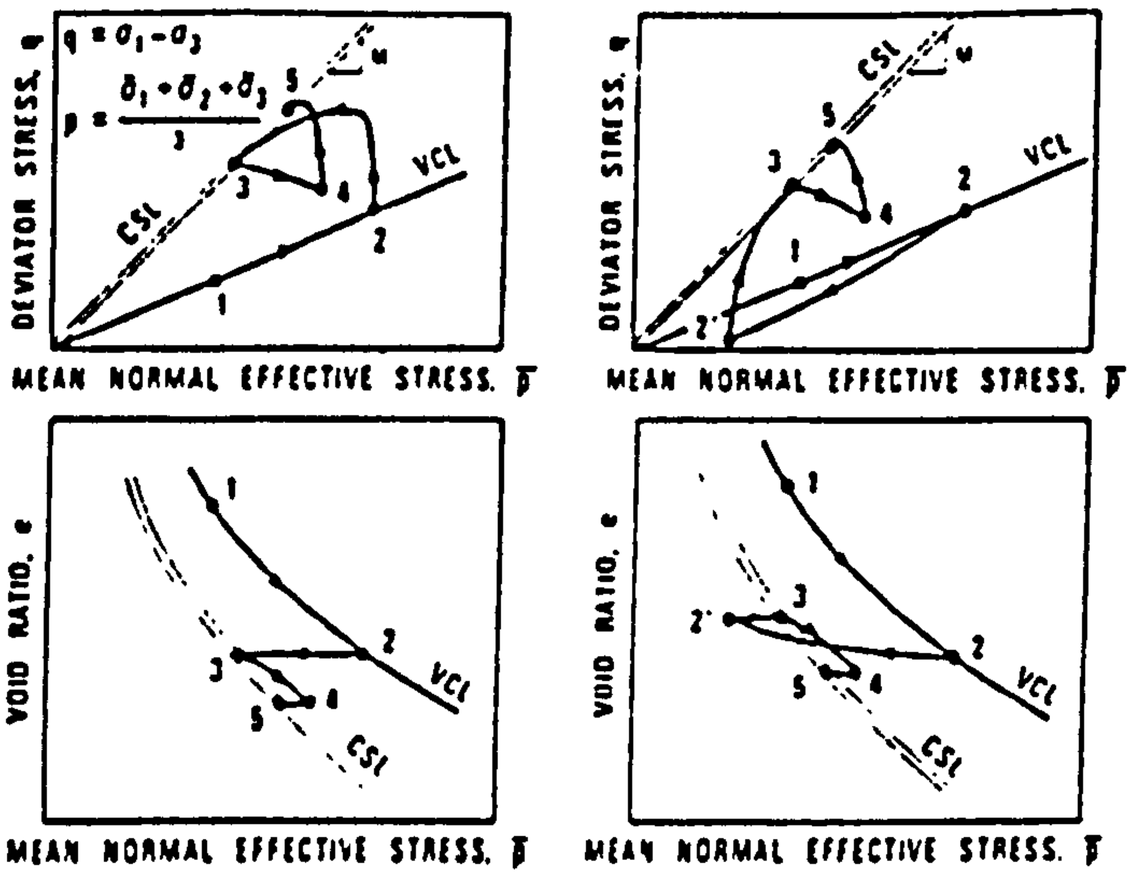



Figure 2.13 Stress paths for the ESM models: (left) normally consolidated; (right) over-consolidated clay

The geological consolidation and swelling of the clays are represented by the paths 1-2 and 1-2-2' (respectively). Pile *installation* causes the stresses to follow paths such as 2-3 (or 2'-3); during *consolidation* 3-4; and during pile *loading* 4-5.

Although these diagrams neglect several important features of soil behaviour (such as the

possible formation of residual shear surfaces next to the pile), they do at least give an idea of the type of behaviour that might be expected from piles installed in clay.

### 2.4.4 Differences between the models ESM1-4

a) Basic form of the equations

The main differences between the models ESM1-4 is the way in which they calculate the stress changes during consolidation and pile loading, and also in their degree of empiricism.

According to these models, the equation for the limiting skin friction along a pile shaft has the following basic form:

$$f_s = [p'_c](p'_f/p'_c)\Psi(\delta \text{ or } \phi),$$

where $p'_c$ is the mean effective stress at the end of consolidation (equalization); $p'_f$ is the mean effective stress at pile failure; and $\Psi(\delta$ or $\phi)$ is a trigonometric function of $\delta$ or $\phi$.

b) Pile installation

In all four cases, pile installation is modelled as the plane strain expansion of a cylindrical cavity. ESM1 utilizes a linear-elastic/perfectly-plastic (LE-PP) soil model; whereas for the remainder a version of Modified Cam Clay[55] (MCC) is employed.

c) Equalization

The mean effective stress after equalization $p'_c$ is written as:[56]

$$p'_c = \eta p'_i + \xi(u_i - u_o)$$

where $p'_i$ and $u_i$ represent the mean effective stress and pore pressure in the soil at the end of pile installation; $u_o$ is the original pore water pressure; and $\eta$ and $\xi$ are empirically determined parameters.

The soil is assumed to be in a critical state condition at the end of installation, so that $p'_i$ equals the mean effective stress at the critical state (for undisturbed soil), i.e. $p'_i = p'_{cs}$. (In ESM4 the soil is considered to be thoroughly remoulded by the action of installing the pile, and $p'_i$ is replaced by $(p'_{cs})_r$, the mean effective stress (at the critical state) for remoulded soil.) For ESM3 and ESM4 an adjustment factor $\eta$ is used to account for the stress state after installation being different to $p'_{cs}$ [or $(p'_{cs})_r$] as determined in triaxial compression tests. Values of $\eta$ are given in Table 2.2. (For ESM1 and 2, $\eta = 1$.)

According to Kraft,[57] pile installation induces enough pore pressure to reconsolidate the soil during the equalization period to the $K_0$-consolidation line of the *remoulded* soil. This idea is incorporated in ESM4 by replacing $(p'_{cs})_r$ with $(p'_k)_r$, where $(p'_k)_r$ is the mean effective stress on the $K_0$-consolidation line (for the remoulded soil).

d) Pile loading

The effective stress models make a number of different assumptions regarding the failure conditions during pile loading. ESM1 and ESM3 assume zero change in mean effective stress (i.e. $p'_f/p'_c = 1$), whereas in ESM2 and ESM4 $p'_f/p'_c$ is given by the relative spacing of the failure and consolidation lines in e vs p' space (i.e. on a plot of voids ratio vs mean effective stress).

The equations for $\Psi$ (see Table 2.2) also differ according to the assumptions made regarding: the magnitude of the intermediate effective stress ($\sigma'_2$); the orientation of the failure surface; and whether failure is governed by the angle of friction of the soil ($\phi$) or that at the pile/soil interface ($\delta$).

## 2.4.5 Assessment of the effective stress methods

The accuracy of these effective stress models was assessed during the ESACC project by comparing their predictions of shaft capacity with the results of tests on:

Table 2.2 Summary of effective stress models ESM1-ESM4 (Kraft, 1982)

| Parameter | Model | | | | | |
|---|---|---|---|---|---|---|
| | ESM1 | ESM2 | ESM3 | | ESM4 | |
| | | | Driven | Jacked | Driven | Jacked |
| $\eta$ | 1.0 | 1.0 | 0.6 | 0.9 | 0.6 | 1.0 |
| $\xi$ | 0.3 | 0.4-0.78 | 0.25 | 0.6 | 0.3 | 0.7 |
| $p'_f/p'_c$ | 1 | $p'_{cs}/p'_c$ | 1 | | $(p'_{cs})_r/(p'_k)_r$ | |
| $\Psi$ | $\frac{1}{2}M_1\cos\delta$ | $\sin\phi\cos\phi$ | $\tan\delta$ | | $\sin\phi$ | |

$M_1 = 6\sin\delta/(3 - \sin\delta)$

i) $\phi$19mm model piles jacked into kaolin[58]

ii) $\phi$114mm piles jacked/driven into San Francisco Bay mud[59]

iii) $\phi$356mm piles driven into the Empire clay[60]

(These tests are reviewed in Chapter 4.)

The performance of ESM1-ESM4 was found to be on a par with conventional approaches (based on the API code[61] and the $\lambda$ method[62]), but was not significantly better.

### 2.4.6 General comments on the effective stress methods

The main problem faced by someone attempting to use these effective stress models is in finding answers to the following questions:

- Does failure occur in the soil or at the pile/soil interface?
- If it occurs in the soil, does it do so on a vertical or an inclined surface?
- Does the mean effective stress change significantly during pile loading?
- What values should be adopted for the empirical parameters $\eta$ and $\xi$?

The fact that ESM1-4 adopt a variety of differing assumptions demonstrates that the answers to these questions are still open to debate (see Chapter 3 for further discussion of these points).

Parry and Swain[63] made these comments about effective stress methods of design:

> "In view of the present lack of experimental data on effective stress conditions around piles in stiff clays it would be inadvisable to rely solely on any effective stress method of calculating skin friction."

Although aimed primarily at the $\beta$ method, this statement is equally true for the more sophisticated effective stress methods described in this section.

The ESMs incorporate a number of rather questionable assumptions regarding the state of stress in the soil, with little or no experimental evidence to support (or deny) the validity of the assumptions. In addition, they ignore several important features of soil behaviour, such as the dependency of strength on the rate of shearing; strain-softening behaviour after the soil's peak strength has been reached; and so on. Although they give an improved understanding of pile behaviour over that provided by purely empirical approaches, the ESMs involve too many simplifications to give a true reflection of the behaviour of piles in clay.

Assessing the overall impact of the ESMs, Kraft concluded that:[64]

> "...the effective stress methods developed during ESACC cannot yet be used alone as design tools because the available pile load test data with well-documented data on the soil properties are inadequate to test fully the validity of the ESM."

This is reflected in the fact that less than 15% of practitioners use effective stress methods for assessing the axial capacity of piles (see Chapter 1).

## 2.5 NOTES AND REFERENCES

[1]Burland J.B. (1987). The Kevin Nash Lecture: The teaching of soil mechanics - a personal view. Proc. 9th Eur. Conf. Soil Mech. & Fdn Engng, Dublin (in press).

[2]For example, see: St John H.D. (1980). A review of current practice in the design and installation of piles for offshore structures. Dept of Energy Offshore Technology Paper, no 5, Construction Industry Research and Information Association, London, 150pp.

[3]Poulos H.G. (1989). Pile behaviour - theory and application. The 29th Rankine Lecture (22nd March 1989). Géotechnique (in press).

[4]Figure 2.2 portrays the function $Q_{shaft}/Q_{total} = 1/(1 + k(q_{toe}/f_s)/(L/D))$, for various values of (L/D). The value of $(q_{toe}/f_s)$ has been taken as 10-20 (for clays) and 50-100 (for sands). See Fleming W.G.K., Weltman A.J., Randolph M.F., and Elson W.K. (1985). Piling engineering. Surrey University Press, Glasgow and London/John Wiley and Sons, New York, 380pp: "Whereas the ratio of end-bearing pressure to skin friction may be typically 50-100 for piles in sand, the corresponding range is 10-20 for piles in clay" (p107).

[5]Tomlinson M.J. (1957). The adhesion of piles driven in clay soils. Proc. 4th Int. Conf. Soil Mech. & Fdn Engng, London, 2, pp66-71.

[6]Skempton A.W. (1959). Cast in-situ bored piles in London Clay. Géotechnique, 9, pp153-173.

[7]Skempton A.W. (1951). The bearing capacity of clays. Building Research Congress, London, 1, pp180-189.

[8]Weltman A.J. (1980). Pile load testing procedures. DOE and CIRIA Piling Development Group, Report PG7, Construction Industry Research and Information Association, London, 52pp.

[9]Flaate K. (1968). Baereevne av Friksjonspeler i Leire. Beregning av Baereevne pa grunnlag av Geotekniske Undersokelser, Oslo Veglaboratoriet, Norway. (Curves and reference as cited by Kavvadas (1982) - see Chapter 3 for reference.) Flaate used values of $c_{uo}$ determined by the field vane.

[10]Tomlinson (1957), loc. cit.

[11]American Petroleum Institute (1975). API RP2A, Recommended practice for planning, designing, and constructing fixed offshore platforms. American Petroleum Institute, Dallas, Texas.

[12]Woodward R.J., Lundgren R., and Boitano J.D. (1961). Pile loading tests in stiff clays. Proc. 5th Int. Conf. Soil Mech. & Fdn Engng, Paris, 2, pp177-184.

[13]Weltman A.J. and Healy P.R. (1978). Piling in boulder clay and other glacial tills. DoE/CIRIA Report PG5, London.

[14]As taken from the 1982 API data base, compiled by: Olson R.E. and Dennis N.D. (1982). Review and compilation of pile test results, axial pile capacity. PRAC Project 81-29, American Petroleum Institute, Dallas, Texas, 297pp.

The results of the load tests are listed in Table 1 of: Semple R.M. and Rigden W.J. (1984). Shaft capacity of driven pipe piles in clay. Proc. Symp. on Codes and Standards, Am. Soc. Civ. Engnrs National Convention, San Francisco. In "Analysis and design of pile foundations" (ed. J.R. Meyer), Am. Soc. Civ. Engnrs, New York, pp59-79. Repeated in Ground Engng, 19(1), Jan, pp11-19.

[15]American Petroleum Institute (1975), loc. cit.

[16]For example, Cooke and Price measured the end-bearing of a pile jacked into London clay, and obtained $N_c$ = 14. Cooke R.W. and Price G. (1973). Strains and displacements around friction piles. Proc. 8th Int. Conf. Soil Mech. & Fdn Engng, Moscow, 2, pp53-60.

[17]Roy et al. measured $N_c$ values of 16.8-18 in the soft sensitive Champlain clay (n.b. $c_{uo}$ was determined by field vane). See: Roy M., Blanchet R., Tavenas F., and La Rochelle P. (1981). Behaviour of a sensitive clay during pile driving. Can. Geotech. J., 18(1), pp67-85.

[18]Clarke J., Rigden W.J., and Senner D.W.F. (1985). Reinterpretation of the West Sole platform 'WC' pile load tests. Géotechnique, 35(4), pp393-412. The tests are usually performed on $\phi$38mm specimens cut from U100 samples.

[19]The following papers take different approaches to the problem, but come to broadly the same conclusion regarding the variation of $\alpha$ with $c_{uo}/\sigma'_{vo}$: Semple and Rigden (1984), loc. cit.; and Randolph M.F. and Murphy B.J. (1985). Shaft capacity of driven piles in clay. Proc. 17th Offshore Technology Conf., Houston, Texas, 1, pp371-378 (Paper OTC 4883).

[20]Mayne P.W. (1988). Determining OCR in clays from laboratory strength. J. Geotech. Engng, Am. Soc. Civ. Engrs, 114(1), pp76-92.

[21]$K = \pi D f_s L^2/(AE)_{pile}\Delta w_R$, where $\Delta w_R$ = displacement required for the skin friction to reduce to a residual value. See: Randolph M.F. (1983). Design considerations for offshore piles. Proc. Conf. on Geotech. Practice in Offshore Engng, Austin, Texas, pp422-439.

[22]Randolph and Murphy (1985), loc. cit.

[23]Ladd C.D., Foott R., Ishihara K., Schlosser F., and Poulos H.G. (1977). Stress-deformation and strength characteristics. State-of-the-Art Report. Proc. 9th Int. Conf. Soil Mech. & Fdn Engng, Tokyo, 2, pp421-494.

[24]Wroth C.P. (1984). The interpretation of in situ soil tests. The 24th Rankine Lecture. Géotechnique, 34(4), pp449-489.

[25]Mayne (1988), loc. cit.

[26]Mayne (1988), loc. cit.

[27]Kraft L.M., Focht J.A., and Amerasinghe S.F. (1981). Friction capacity of piles driven into clay. J. Geotech. Engng Div., Am. Soc. Civ. Engrs, 107(GT11), pp1521-1541.

[28]Semple and Rigden (1984), loc. cit.

[29]$\alpha_p$ = 1.0 for $c_{uo}/\sigma'_{vo} \leq 0.35$; 1.39 - 1.11($c_{uo}/\sigma'_{vo}$) for $0.35 \leq c_{uo}/\sigma'_{vo} \leq 0.8$; and 0.5 for $c_{uo}/\sigma'_{vo} \geq 0.8$.

[30]F = 1.0 for L/D ≤ 50; (1.21 - 0.0043(L/D)) for 50 ≤ L/D ≤ 120; and 0.7 for L/D ≥ 120.

[31]Dennis N.D. and Olson R.E. (1983a). Axial capacity of steel pipe piles in clay. Proc. Conf. on Geotech. Practice on Offshore Engng, Austin, Texas, pp370-388.

[32]$F_c$ = 1.1 for unconfined compression (UC) tests on high quality samples; 1.8 for the same tests on samples taken with typical driven samplers; and 0.7 for in situ vane shear strengths (FV). A "high quality sample" is defined as one that is obtained using a 75mm diameter, pushed, thin-walled sampler.

[33]$F_L$ = 1.0 for L ≤ 30.48m; (0.035L - 0.067) [L in metres] for 30.5 ≤ L ≤ 53.34m; and 1.8 for L ≥ 53.34m.

[34]Data taken from: Housel W.S. (1950). Discussion of paper by Cummings, Kerkoff, and Peck (1948). Trans. Am. Soc. Civ. Engnrs, 115, pp339-346; Reese L.C. and Seed H.B. (1955). Pressure distribution along friction piles. Proc. Am. Soc. for Testing Materials, 55, pp1156-1182; and Konrad J.-M. and Roy M. (1987). Bearing capacity of friction piles in marine clay. Géotechnique, 37(2), pp163-175.

[35]Azzouz A.S. (1986). Role of load tests in friction pile design. J. Geotech. Engng, Am. Soc. Civ. Engrs, 112(4), pp407-423.

[36]The references to accompany Table 2.1 are as follows:
Roy M., Blanchet R., Tavenas F., and La Rochelle P. (1981). Behaviour of a sensitive clay during pile driving. Can. Geotech. J., 18(1), pp67-85.
Rocha Filho P. and Alencar J.A. (1985). Piezocone tests in the Rio de Janeiro soft clay deposit. Proc. 11th Int. Conf. Soil Mech. & Fdn Engng, San Francisco, 2, pp859-862.
Reid J.M. and Turnbull K.W. (1988). An example of the use of cone penetration testing in the design of underground structures and temporary works in cohesive soils. Proc. Instn Civ. Engnrs Geotechnology Conf. on Penetration Testing in the UK, Univ. of Birmingham, Paper 28 (in press), Thomas Telford Ltd.
Long M.M. and O'Riordan N.J. (1988). The use of piezocone in the design of a deep basement in London Clay. Proc. Instn Civ. Engnrs Geotechnology Conf. on Penetration Testing in the UK, Univ. of Birmingham, Paper 19 (in press), Thomas Telford Ltd.
Jones G.A. and Rust E. (1983). Piezocone probe (CUPT) for subsoil identification. Proc. Int. Symp. Soil and Rock Investigations by In-Situ Testing, Paris, 2, pp303-308.
Clarke B.G., Carter J.P., and Wroth C.P. (1979). In situ determination of the consolidation characteristics of saturated clays. Proc. 7th Eur. Conf. Soil Mech. & Fdn Engng, Brighton, 2, pp207-211.

Appendino M., Jamiolkowski M., and Lancellotta R. (1979). Pore pressure of NC soft silty clay around driven displacement piles. Proc. Conf. on Recent Developments in the Design and Construction of Piles, Instn Civ. Engnrs, London, pp169-175.
Azzouz A.S. (1986). Role of load tests in friction pile design. J. Geotech. Engng, Am. Soc. Civ. Engrs, 112(4), pp407-423.
Fahey M. and Foley P.A. (1987). In situ measurement of the coefficient of consolidation. Proc. 9th Eur. Conf. Soil Mech. & Fdn Engng, Dublin, 1, pp29-33.
Ponniah D.A. and McAnoy R. (1982). Pile jacking in glacial tills. Proc. 2nd Int. Conf. Num. Methods in Offshore Piling, Austin, Texas, pp137-146.

[37]Burland J.B. (1973). Shaft friction of piles in clay - a simple fundamental approach. Ground Engng, 6(3), May 1973, pp30-42.

[38]Burland (1973), loc. cit.

[39]Jaky J. (1944). A Nyugalmi Nyomas Tenyezoje (Hungarian). Magyar Mernok-es Epitesz-Egylet Kozlonye, pp355-358.

[40]Meyerhof G.G. (1976). Bearing capacity and settlement of pile foundations. The 11th Terzaghi Lecture. J. Geotech. Engng Div., Am. Soc. Civ. Engrs, 102(GT3), pp197-228.

[41]Parry R.H.G. and Swain C.W. (1977a). Effective stress methods of calculating skin friction on driven piles in soft clay. Ground Engng, 10(3), 1977, pp24-26.

[42]Parry R.H.G. and Swain C.W. (1977b). A study of skin friction on piles in stiff clay. Ground Engng, 10(8), 1977, pp33-37.

[43]Flaate K. and Selnes P. (1977). Side friction of piles in clay. Proc. 9th Int. Conf. Soil Mech. & Fdn Engng, Tokyo, 1, pp517-522.

[44]$\mu_L = (L + 20)/(2L + 20)$, where L is in metres.

[45]Fugro Ltd (1987). Tension piles in clay: state of the art review. Report no 85/3310 for Den Norske Stats Oljeselskap, Norway, 54+pp.

[46]Parry and Swain (1977b), loc. cit.

[47]Meyerhof (1976), loc. cit.

[48]Flaate K. (1972). Effects of pile driving in clays. Can. Geotech. J., 9(1), pp81-88.

[49]Randolph and Murphy (1985), loc. cit.

[50]The linear relationship was first suggested by Burland, in work commissioned by Fugro.

[51]Meyerhof (1976), loc. cit.

[52]Jardine R.J. (1985). Investigations of pile-soil behaviour, with special reference to the foundations of offshore structures. PhD Thesis, Univ.

of London (Imperial College), 2 vol., 789pp. See Chapter 6 and, in particular, Figure 10.4.

[53]Kraft L.M. Jr (1982). Effective stress capacity model for piles in clay. J. Geotech. Engng Div., Am. Soc. Civ. Engrs, 108(GT11), pp1387-1404.

[54]Schofield A.N. and Wroth C.P. (1968). Critical state soil mechanics. McGraw-Hill, London, 310pp.

[55]Roscoe K.M. and Burland J.B. (1968). On the generalized stress-strain behaviour of 'wet' clay. In "Engineering Plasticity", ed. J. Heyman and F.A. Leckie, Cambridge Univ. Press, pp535-610.

[56]Kraft (1982), loc. cit.

[57]Kraft (1982), loc. cit., p1394.

[58]Steenfelt J.S., Randolph M.F., and Wroth C.P. (1981). Instrumented model piles jacked into clay. Proc. 10th Int. Conf. Soil Mech. & Fdn Engng, Stockholm, 2, pp857-864.

[59]Kirby R.C. and Rousel G. (1979). ESACC Project, field model pile load test, Hamilton Air Force Base Test Site, Novato, California. Woodward-Clyde Consultants, Clifton, New Jersey.

[60]Cox W.R., Kraft L.M., and Verner E.A. (1979). Axial load tests on 14-inch pipe piles in clay. Proc. 11th Offshore Technology Conf., Houston, Texas, 2, pp1147-1158 (Paper OTC 3491).

[61]American Petroleum Institute (1980). API RP2A (11th edition), Recommended practice for planning, designing, and constructing fixed offshore platforms. American Petroleum Institute, Dallas, Texas.

[62]Kraft L.M., Focht J.A., and Amerasinghe S.F. (1981). Friction capacity of piles driven into clay. J. Geotech. Engng Div., Am. Soc. Civ. Engrs, 107(GT11), pp1521-1541.

[63]Parry and Swain (1977b), loc. cit., p35.

[64]Kraft (1982), loc. cit., p1401.

# Chapter 3

# Theoretical behaviour of displacement piles in clay

CONTENTS OF CHAPTER 3


3.1 EXISTING THEORIES OF PILE BEHAVIOUR . . . . . 63

3.2 AN OUTLINE OF THE CAVITY EXPANSION METHOD . . . . . 65

3.2.1 Background to the method 65

3.2.2 Central assumption of all cavity expansion methods 67

3.2.3 Main differences between various cavity expansion methods 67

3.3 AN OUTLINE OF THE STRAIN PATH METHOD . . . . . 69

3.3.1 Background to the method 69

3.3.2 Basic principles of the strain path method 69

3.3.3 Constitutive models 71

3.4 PILE INSTALLATION . . . . . 75

3.4.1 Ground movements induced by pile driving 75

3.4.2 Changes in total stress due to pile installation 79

3.4.3 Pore pressures at the end of pile installation 84

3.4.4 Effective stresses at the end of pile installation 88

3.4.5 Variation of stresses behind the pile tip 92

3.4.6 Discussion 94

3.5 EQUALIZATION STAGE . . . . . 95

3.5.1 Dissipation of excess pore pressures 95

3.5.2 Radial total and effective stresses 103

3.5.3 Orientation of the principal stresses 106

3.5.4 Effective stress paths during equalization 107


continued...

3.6 BEHAVIOUR DURING LOADING . . . . . 109

3.6.1 Key assumptions regarding pile loading 109

3.6.2 Drained or undrained loading? 110

3.6.3 Stress changes during drained loading 110

3.6.4 Stress changes during undrained loading 111

3.6.5 Analogy between pile loading and simple shear tests 112

3.6.6 Strain path predictions based on the MIT-E3 model 112

3.6.7 Predictions of the coefficient of friction 113

3.6.8 Orientation of the principal stresses 117

3.6.9 Direction of loading 118

3.6.10 Summary of Section 118

3.7 NOTES AND REFERENCES . . . . . 119

## 3.1 EXISTING THEORIES OF PILE BEHAVIOUR

Modern theories of pile behaviour attempt to follow the changes in earth and pore water pressures during the three main stages in the life of the pile: installation, the subsequent equalization period, and throughout pile loading. This sequence is illustrated in Figure 3.1, for the case of an offshore pile.

A sound theory of pile behaviour, based on Terzaghi's principle of effective stress,[1] must predict the radial effective stresses $\sigma'_{rr}$ during each of the stages illustrated in the diagram: (a) prior to pile

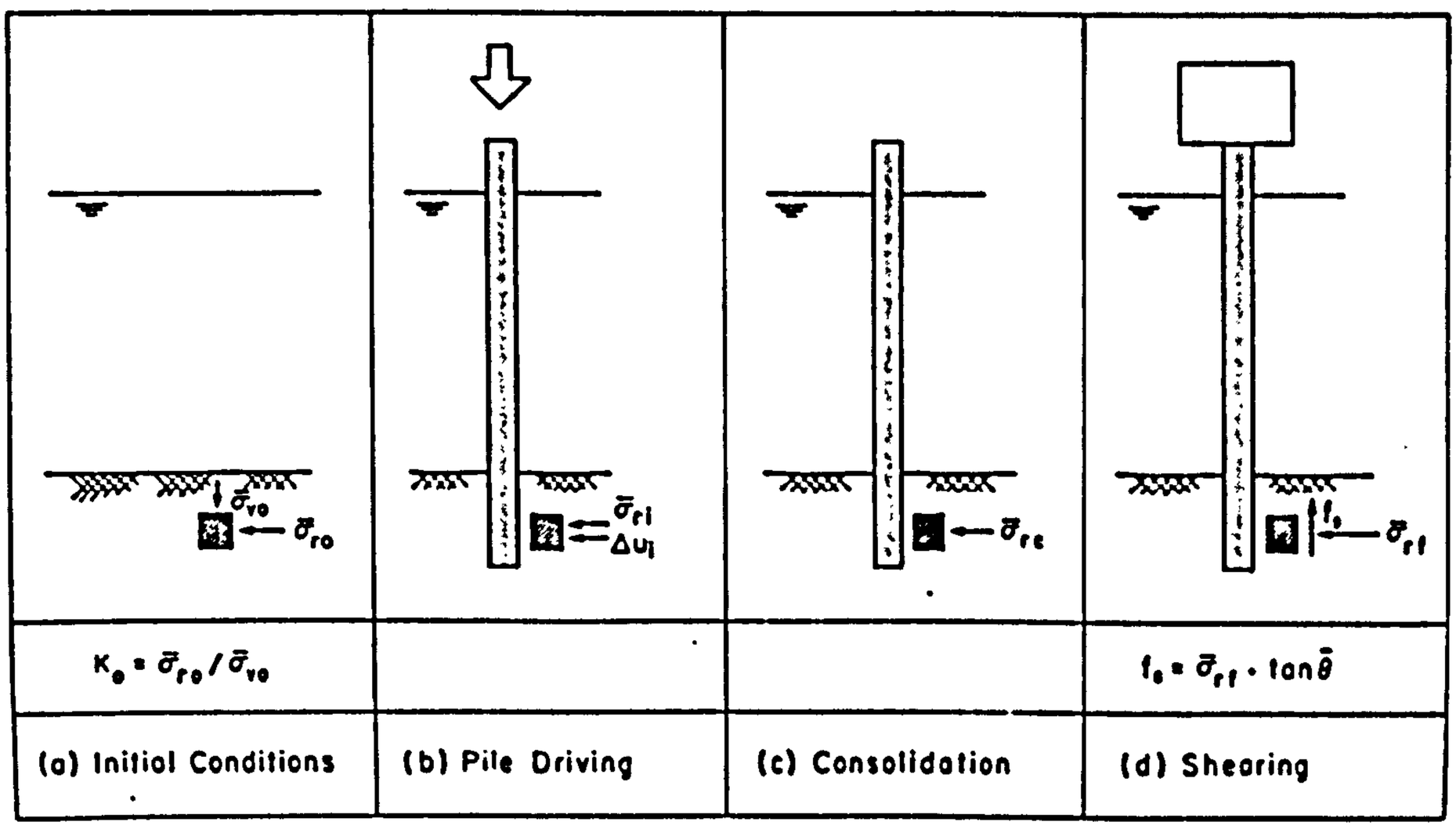



Figure 3.1 Different stages in the life of a pile

installation, when the radial effective stress equals the original horizontal effective stress in the soil, $\sigma'_{ho}$; (b) at the end of driving, when $\sigma'_{rr} = (\sigma'_{rr})_i$; (c) at the end of "consolidation",* when $\sigma'_{rr} = (\sigma'_{rr})_c$; and (d) at the moment of failure during loading, when $\sigma'_{rr} = (\sigma'_{rr})_f$.

This Chapter presents a review of the theoretical behaviour of displacement piles in clay, considering the three main stages in the

*The term "equalization" is preferable to "consolidation", since the soil surrounding the pile inevitably undergoes some degree of swelling as well as consolidation, following pile installation

pile's life in chronological order. Section 3.4 deals with installation; Section 3.5 equalization; and Section 3.6 pile loading.

Before proceeding with this Review, it is helpful to summarize the main features of the two theories of pile behaviour that are considered herein. Section 3.2 gives an outline of the cavity expansion method (CEM) of analysis, and Section 3.3 an outline of the more recent strain path method (SPM). Both theories have evolved sufficiently to furnish predictions for the behaviour of piles in normally- and lightly over-consolidated clays; but at present only the cavity expansion method can be applied to piles in heavily overconsolidated clays.

One of the purposes of this Review is to highlight differences between the predictions of the two theories, and to comment on their suitability for predicting the behaviour of displacement piles in heavily over-consolidated clays. The results of instrumented pile tests (reviewed in the next chapter) enable the validity of the theories to be tested, and help to suggest areas in which they might be further developed and improved.

## 3.2 AN OUTLINE OF THE CAVITY EXPANSION METHOD

### 3.2.1 Background to the method

Cavity expansion methods were first developed in the mid-1940s, in the study of metal indentation,[2] but it was not until Gibson and Anderson[3] published their interpretation of the pressuremeter test, in 1961, that they found widespread popularity in the field of soil mechanics. Since that time several papers have been published (see Table 3.1) in which pile installation is treated as the process of expanding a cylindrical cavity in a semi-infinite soil medium. The pile's shaft capacity can then be obtained from the estimate of the radial effective stress acting on the pile wall after consolidation - provided the angle of shaft friction is known. A similar approach can be used to estimate the pile's end-bearing capacity (from the pressure needed to expand a spherical cavity).

In 1970, Butterfield and Bannerjee[4] published the first[5] complete analysis of pile installation modelled as the expansion of a cylindrical cavity; but the method was given its greatest impetus by Randolph, Carter, and Wroth, working at Cambridge University in the late 1970s. The results of the Cambridge studies form the backbone of the "effective stress methods" of pile behaviour, which are reviewed in Chapter 2. Throughout the 1980s, the theory has been further developed and refined, with much of the recent work taking place at Massachusetts Institute of Technology (MIT).

The use of cavity expansion methods (CEMs) in the analysis of deep foundations has been criticized by Baligh[6] as entering "...a retrogressive stage sometimes generating more distractions and confusion than providing useful answers". However, he also admits that:

> "...the utilization of CEM in pile foundation analyses up to, say 1975,* represented a definite improvement over methods available at the time."

---

*When the first steps were taken towards developing the strain path method (see Section 3.3)

Table 3.1 Summary of cylindrical cavity expansion solutions used for modelling pile installation

| Authors | Initial stresses | Stress-strain model/yield function* | Shear strength (k)# | Notes$ (proposed application) |
|---|---|---|---|---|
| Bishop, Hill, & Mott (1945) | Ignored | LE-PP/pseudo von Mises | $(2/\sqrt{3})c_{utc}$ | Closed-form; 1-phase only (metal indentation) |
| Hill (1950) | Ignored | LE-PP/Tresca | $c_{utc}$ | Closed-form; 1-phase only (metal indentation) |
| Gibson & Anderson (1961) | $\sigma_{rr} = \sigma_{\theta\theta}$ | LE-PP/Tresca | $c_u$ | Closed-form; 1-phase only (PM test) |
| Ladanyi (1963) | Isotropic | Non-linear stress-strain curve from txl tests | $c_{utc}$ | Numerical integration of equilibrium equations (PM test) |
| Nishida (1964) | $K_0$-stresses | LE-PP/Tresca | $c_u$ | Closed-form (driven piles) |
| Butterfield & Bannerjee (1970) | Isotropic | LE-PP/von Mises | $c_u$ | Closed-form; large strain; shaft friction+ (driven piles) |
| Vesic (1972) | Isotropic | LE-PP/Mohr-Coulomb | $c + \sigma'_{ho}\tan\phi$ | Closed-form; large strain; compressible** (PM test; driven piles) |
| Randolph & Wroth (1979) | Ignored | LE-PP/Tresca | $c_{utc}$ | Closed-form (driven piles) |
| Carter, Randolph, & Wroth (1979) | Model (a) Ignored | LE-PP/Tresca | "Strength in pure shear" | FE analysis (driven piles) |
| | Model (b) $K_0$-stresses | MCC/von Mises | $c_{ups} = (2/\sqrt{3})c_{utc}$ | |
| Wroth, Carter, & Randolph (1979); Randolph, Carter, & Wroth (1979) | $K_0$-stresses | MCC/von Mises | $c_{ups} = (2/\sqrt{3})c_{utc}$ | FE analysis (driven piles) |
| Kavvadas (1982) Whittle (1987) | $K_0$-stresses | MIT-E1 MIT-E3 | | FE analysis (driven piles) |

*LE-PP = linear-elastic/perfectly plastic; MCC = Modified Cam-Clay

#$c_u$ = undrained strength of soil (Paper does not say how determined); $c_{ups}$ = undrained strength in plane strain; $c_{utc}$ = in triaxial compression

$All solutions assume the following (unless otherwise stated):

Saturated, incompressible, isotropic, homogeneous, non-viscous, weightless, infinite, two-phase material
Plane strain deformation
Small strain formulation
Shaft friction ignored at cavity wall

"1-phase only" = pore pressures not considered (total stress analysis)

+Solution takes account of shear stresses on surface of pile
N.b. there is an error in Butterfield & Banerjee's calculations: conservation of volume not satisfied; extent of plastic zone over-estimated by factor of $2/\sqrt{w_p}$ (where $w_p = 1 - (\alpha R/r_p)^2$)

**Solution takes account of soil compressibility

### 3.2.2 Central assumption of all cavity expansion methods

The basic premise of all cavity expansion methods is that pile installation displaces the soil primarily in the radial direction* (except near the pile toe and the ground surface). As such, the installation process can be modelled as the monotonic expansion of a (long) cylindrical cavity, which starts from an infinitely small initial radius. The main advantage of this approach is that it simplifies the mathematics involved in formulating the problem. In essence, the cavity expansion method is a one-dimensional simplification of a highly complicated, two-dimensional process.

Other assumptions of existing cavity expansion solutions are summarized in Table 3.1, together with details of the initial stresses and stress-strain relationships that have been used in these studies. Table 3.1 lists only those Papers that are concerned with modelling pile installation.#

### 3.2.3 Main differences between various cavity expansion methods

As Table 3.1 reveals, various techniques have been used to solve the cavity expansion problem:

- Closed-form solutions employing a simple linear-elastic/ perfectly-plastic soil model[7,8,9,10,11,12]
- Numerical integration of the equilibrium equations using laboratory-determined stress-strain curves[13]
- Finite element methods, utilizing sophisticated elasto-plastic, work-hardening soil models[14,15]

---

*The evidence to support this key assumption is examined in detail in Section 3.4.1.a.

#Plus one or two of the early landmark publications - there are several Papers that deal with the interpretation of the pressuremeter test

Some comments are worth making regarding particular features of the solutions listed in Table 3.1:

- In most of the early work the initial stresses in the soil were either ignored or considered isotropic ($\sigma'_{vo} = \sigma'_{ho}$); this greatly simplifies the mathematics of the closed-form solutions
- Few of the early Papers specify how the clay's undrained strength should be determined, i.e. whether in triaxial compression or plane strain (note that the strength in plane strain is about 15% higher than that in triaxial compression)
- Only one Paper (Butterfield and Bannerjee's) accounts for the influence of shaft friction on the total stresses mobilized at the pile wall: this factor alone could affect the results by up to 11%
- Vesic's solution takes account of volume changes in the soil during undrained compression - i.e. it assumes that the soil is compressible rather than incompressible; the net effect is for the soil's stiffness to be reduced by a factor $\xi_v$ that depends on the magnitude of the soil's compressibility (see Section 3.4.2.b for details)
- Although the more recent finite element (FE) studies incorporate more realistic soil models than the earlier solutions, there is little difference between the results obtained using the simple linear-elastic/perfectly-plastic models and using isotropic elasto-plastic models, such as Modified Cam Clay (see Section 3.4.2.a)
- Only when an anisotropic soil model is employed (such as one of the MIT models) is there a significant difference between the results of the simple analyses and the more sophisticated solutions (see Section 3.4 et seq.)

## 3.3 AN OUTLINE OF THE STRAIN PATH METHOD

### 3.3.1 Background to the method

The strain path method[16] (SPM) was developed over the period 1975-1985, by Baligh and his colleagues at the Massachusetts Institute of Technology (MIT). Their aim was to provide an analytical technique that would facilitate the understanding and prediction of the behaviour of "deep" foundations, in the same way that the stress path method[17] assists the analysis of "shallow" foundations. As Baligh points out, these two methods are virtually identical in concept, except for one fundamental aspect: "shallow" foundations are stress-controlled in nature, whilst "deep" foundations are strain-controlled.

### 3.3.2 Basic principles of the strain path method

Due to the severe kinematic constraints that exist during pile installation, soil deformations and strains are, by and large, independent of the shearing resistance of the soil.* In other words, pile installation is essentially a strain-controlled process. The strain path method hinges on the assumption that the soil deformations can be estimated with a reasonable degree of accuracy without the need to consider constitutive relations for the soil.

The principal steps in the strain path method are as follows:[18]

i) Estimate the initial stresses $(\sigma_{ij})_o$ and initial pore pressures $u_o$ in the soil

ii) Estimate the soil velocities $v_i$ from the stream lines formed by an incompressible, inviscid fluid flowing around the pile (see Figure 3.2)

iii) Integrate the velocities to obtain the soil deformations

---

*This is only true over the central portion of long piles - close to the ground surface the problem is more likely to be stress-controlled (akin to a shallow foundation)

iv) Differentiate the velocities to obtain the strain rates $\dot{\epsilon}_{ij}$

v) Determine the strain paths $\epsilon_{ij}$ along the streamlines by integrating the strain rates $\dot{\epsilon}_{ij}$

vi) From an appropriate constitutive model, compute the effective stresses in the soil $\sigma'_{ij}$

vii) From the equilibrium equations, calculate the pore pressures u

viii) Finally, calculate the total stresses from the sum of the pore pressures and effective stresses $\sigma_{ij}$ (= $\sigma'_{ij}$ + $u\delta_{ij}$, where $\delta_{ij}$ is the Kronecker delta [equals 0 for i ≠ j and 1 for i = j])

The key step in this procedure is, of course, Step ii, in which the soil velocities are estimated *without reference to the properties of the soil*. This "decoupling" drastically simplifies the problem of modelling pile installation.

Figure 3.2 illustrates the stream lines obtained around an idealized "simple pile",[19] during steady penetration into saturated clay. Deformation patterns have also been derived for 18 and 60° cones (see Table 3.2), and for the flat-ended wall of a sampling tube.

(The soil *deformations* that are predicted by applying Step iii to the streamlines around the 60° cone are presented later - see Figure 3.4.)

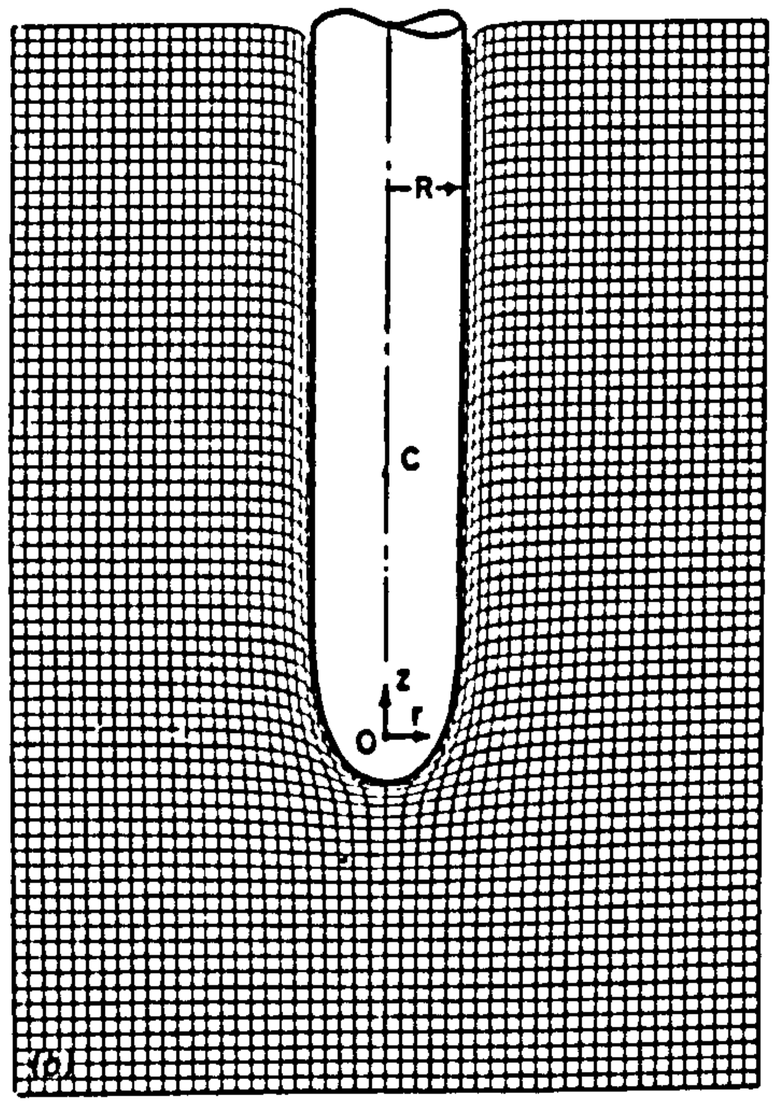



Figure 3.2 Predicted deformations around a "simple pile"

## 3.3.3 Constitutive models

### a) Models used in studies of driven pile behaviour

Another key decision in the strain path method is the choice of constitutive model to describe the soil behaviour (Step vi). There are basically two alternatives. The first is to use a total stress model, describing the soil's (deviatoric stress)-strain behaviour, together with a separate model for predicting the shear-induced pore pressures.[20] The second option is to employ an (effective stress)-strain model.

The various constitutive models that have been used to date are listed in Table 3.2. Although I do not intend to discuss each one in detail, it is worthwhile emphasizing the main differences between the various models, and, in particular, what effect these differences may have on the resultant predictions of pile behaviour.

### b) Limitations of the Modified Cam Clay model

The Modified Cam Clay (MCC) model was developed[21] at Cambridge University in the mid-1960s, since when it has become one of the more popular elasto-plastic models for solving boundary value problems in geomechanics.[22] MCC was designed for isotropically-consolidated clays on the "wet" side of the critical state line (i.e. normally- or lightly over-consolidated clays, which *contract* on yielding in undrained compression). This is the model that was used by Randolph, Carter, and Wroth[23] in their finite element studies of the cavity expansion problem (see Table 3.1).

The principal limitations of MCC are as follows:[24]

- For normally consolidated (NC) and lightly overconsolidated (LOC) clays (i.e. OCR < 2), MCC does not predict strain softening behaviour
- The model over-predicts the value of $K_0$ (one of the key parameters defining the in situ stress state of the soil)

Table 3.2 List of soil models used at MIT with the strain path method

| Model | As employed by... | Pile | Comments |
|---|---|---|---|
| PR | Baligh (1986) | Simple | Prandtl-Ruess model (linear-elastic/perfectly-plastic): 2 parameter (G, k) total stress model; isotropic hardening; associated flow rule |
| MIT-T1 | Levadoux (1980) | 18/60° | Prevost-Levadoux-Baligh model: deviatoric total stress model with multiple nested yield surfaces; used in conjunction with separate model for shear-induced pore pressures; associated flow rule |
| MCC | Kavvadas (1982) | 60° | Modified Cam Clay: 5 parameter ($e_o$, $\lambda$, $\kappa$, 2G/K, M) effective stress model for NC/LOC clays; isotropic hardening; associated flow rule |
| MIT-E1 | Kavvadas (1982) | 60° | 13 parameter effective stress model for NC clays; anisotropic hardening; non-associated flow rule |
| MIT-E2 | Azzouz & Baligh (1984) | 60° | Slightly modified version of MIT-E2, used to describe the behaviour of plastic Empire clay |
| MIT-E3 | Whittle (1987) | Simple | 15 parameter effective stress model for OC clays; anisotropic hardening; bounding surface plasticity; "perfectly hysteretic" model; non-associated flow rule |

- MCC is an <u>isotropic</u> soil model, whereas most soils are highly anisotropic in nature
- Some versions of the model are not properly formulated for plane strain conditions: the magnitude of the intermediate effective stress at failure may be pre-determined by the shape assumed for the plastic potential in the deviatoric plane, in conjunction with the angle of dilation at failure[25]

## c) Development of more realistic soil models: the MIT-E series

Research at MIT during the last decade has led to the development of a series of anisotropic effective stress models, known as MIT-E1, E2, and E3. MIT-E1 was conceived in the early 1980s, primarily to describe the behaviour of normally consolidated and lightly overconsolidated clays.[26] MIT-E2 followed in 1984, but was designed specifically to model the plastic Empire clay, rather than as a general purpose effective stress model.[27] The latest in the series, MIT-E3, characterizes the behaviour of overconsolidated (OC) clays and rectifies some of the deficiencies of its predecessor, MIT-E1.

For example, contrary to observed behaviour (and in common with Modified Cam Clay) MIT-E1 presumes that:[28]

- There are no plastic strains <u>within</u> the yield surface
- There is no coupling between volumetric and shear response until yield occurs - i.e. the model predicts no shear-induced pore pressures during undrained loading of an OC clay (and so there is a linear stress-strain response prior to yield)

MIT-E3 rectifies these shortcomings and incorporates several other important features of soil behaviour (see Appendix 3), including:

- Anisotropic hardening (†)
- Undrained brittleness at low overconsolidation ratios (†)
- Small-strain (i.e. pre-yield) non-linearity in undrained shear
- Irrecoverable straining pre-yield

(The symbol † indicates those features that are included in MIT-E1, release 2.) However, MIT-E3 also neglects certain features of soil behaviour, including:

- Rate effects
- The formation of residual shear surfaces

The findings of the experimental programme that is described in Chapters 9-12 suggest that these last two features have a controlling influence on the behaviour of piles in heavily overconsolidated clays.

MIT-E3 has been validated by the results of laboratory tests on clays with OCRs up to 8. A special feature of the model is that it depicts their behaviour during cyclic loading. However, it has not yet been extended to cater for heavily overconsolidated soils (OCRs > 8), such as the London clay. Details about this latest model have only recently appeared in the Literature (1988).[29]

## 3.4 PILE INSTALLATION

### 3.4.1 Ground movements induced by pile driving

**a) Cavity expansion predictions**

According to the cavity expansion hypothesis, the ground movements induced by pile driving are purely radial in direction and are given by the equation:[30]

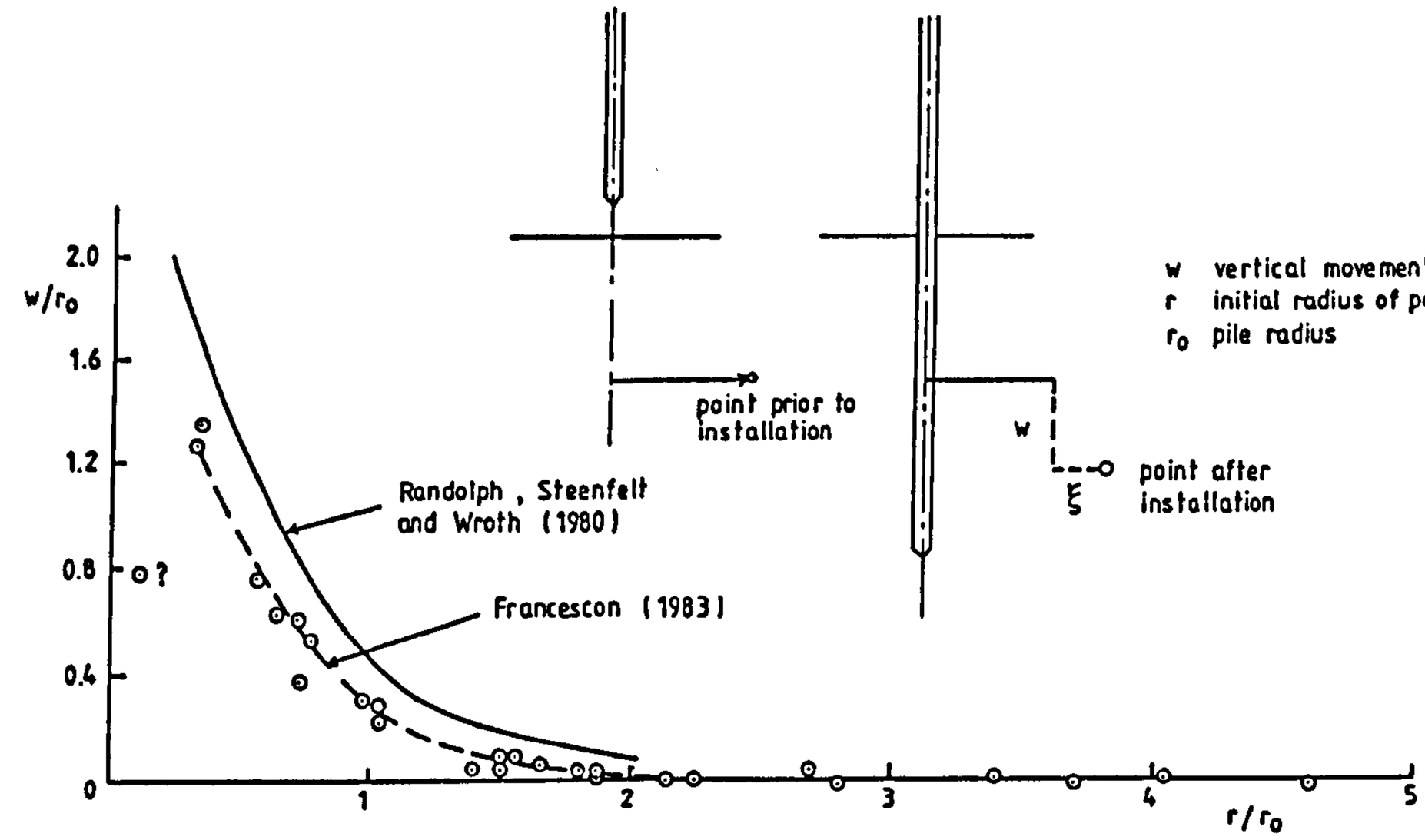
$$\xi/R = [(r/R)^2 + \rho]^{\frac{1}{2}} - r/R,$$

where $\xi$ is the radial movement of a point originally at distance r from the centre-line; R is the pile's outer radius; and $\rho$ is an "area ratio" (for thin-walled piles equals 2h/R, where h is the wall thickness). The ratio $\rho$ equals the pile's enclosed volume ($\propto \pi R^2$) divided by the volume of soil it displaces ($\propto 2\pi Rh$). For closed-ended piles, $\rho = 1$; whereas for open-ended piles with typical values of D/h (25-45), $\rho = 0.09$-$0.16$.

Figure 3.3 compares the cavity expansion prediction for closed-ended piles with the soil movements observed in both laboratory and field experiments.

The laboratory tests[31,32] (points ∘ and •) were conducted at Cambridge University on $\phi$19mm cone-ended model piles, jacked into kaolin; radiographic techniques were used to follow the movement of lead shot and thread which had been placed in the soil prior to consolidation (from slurry). The test chamber was 250mm in diameter, i.e. 13 times larger than the pile itself. (The effect of the chamber walls should be to *reduce* the soil movements caused by installing the model pile.)

The field tests[33] (points Δ) were performed in the heavily over-consolidated London clay at Hendon, on $\phi$168mm cone-ended steel piles; horizontal movements were measured by four $\phi$15mm probes that had been pre-installed in the ground at a depth of 2.1m. Access to the soil was obtained from the corner of a 4m deep trench, located 1.7m away from the



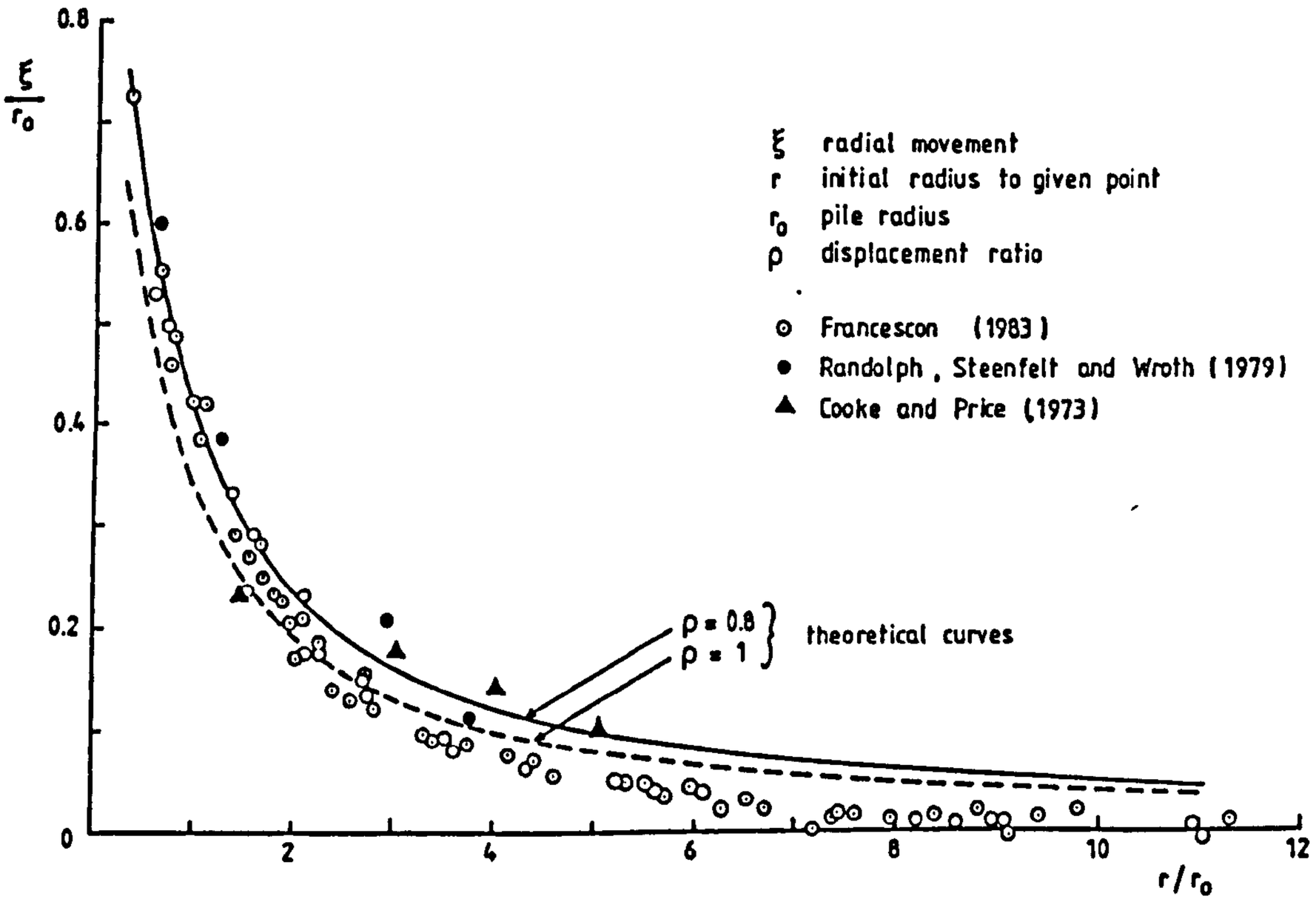




Figure 3.3 Ground movements caused by pile driving:
(Top) Vertical soil movements
(Bottom) Radial soil movements

pile (i.e. at $r/R \approx 20$). The trench was dug some nine months in advance of the field tests - during which time it would have caused stress relief in the surrounding clay (of an unknown amount).

Inspection of Figure 3.3 reveals:

- The observed <u>radial</u> movements ($\xi$) are significantly less than the movements predicted by the theoretical curve for $\rho = 1$ (except, perhaps, for $r/R < 1$, where there is reasonable agreement)
- The effect of the parameter $\rho$ is to reduce the radial movements (compare the theoretical curve for $\rho = 0.8$ with that for $\rho = 1$)
- There are large components of <u>vertical</u> movement (w), ignored in the cavity expansion method, extending to a distance of about twice the radius of the pile

Steenfelt et al.[34] believed that the curve for $\rho = 0.8$ gave a good fit to the horizontal displacements measured in their tests (although the scatter was high); and they suggested that the "missing" 20% of displaced volume must be accommodated by vertical soil movement below the pile tip. Francescon,[35] however, showed that there are significant radial movements *towards the pile* (i.e. negative $\xi$) as the soil consolidates following pile installation. Since they were taken after full equalization, the final set of radiographs record the ground movements due to installation and consolidation *combined*. When the results are adjusted to "correct" for this effect, the curve for $\rho = 1$ provides a good fit to the data.

b) Strain path predictions

As mentioned in Section 3.3, the strain path method takes full account of the two-dimensional nature of pile installation (except near the ground surface). Figure 3.2 (see page 70) presents a picture of the stream lines around an idealized "simple pile",[36] during steady penetration into a saturated clay. Strain path predictions for the *displacements* during steady penetration (of a 60° cone) are shown in Figure 3.4, for five elements of soil (labelled A-E). Initially these points were located at distances of 1, 2, 3, 4, and 5 times the cone

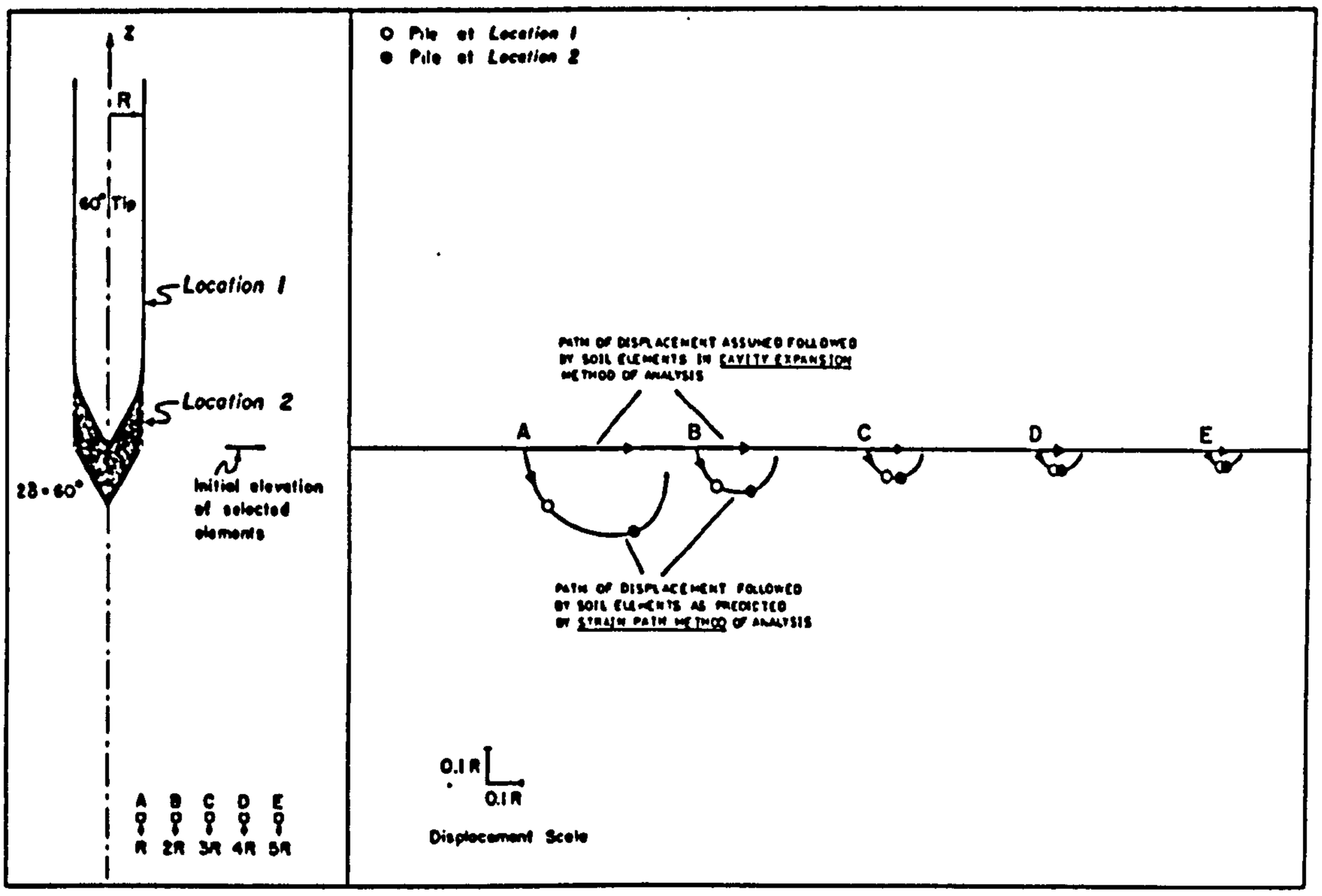



Figure 3.4 Soil displacements during steady penetration of 60° cone

radius from its centre-line. Several features are worth noting:

- There are large radial *and* downward movements of the soil during cone penetration; the radial movements are monotonic
- The downward movement increases dramatically as the cone tip advances towards the soil, attaining a maximum value when its shoulder reaches the same level as the soil elements
- At the same time there are large outward radial movements, most of which occur as the cone face passes the level of the soil particles
- Once the shoulder has passed, the soil <u>rebounds</u> in the vertical direction, but continues to be displaced outwards

Similar "trajectories" to those shown in Figure 3.4 were observed in laboratory tests on $\phi$8mm model piles, jacked into kaolin.[37] The piles were split in half, longitudinally, and installed in a semi-circular prism of clay against a perspex plate. The surface of the clay was marked with grid lines and photographs were taken of these lines before and after pile installation. By carefully measuring the distortion of the grid lines on these photographs, the movement of different soil elements

could be deduced. The accuracy of the experimental technique can be questioned, especially since the effect of the perspex plate is unknown. Nevertheless, the model tests did show significant downward movement of the soil and that the majority of the radial displacement occurs as the pile tip passes the current level of the soil particles. However, there was only a small amount of vertical rebound once the pile tip had passed below the level of interest.

c) Residual shear surfaces next to displacement piles

Both the cavity expansion and strain path methods assume that the soil behaves as a continuum when it is sheared by the pile during installation. Neither theory allows for the possible formation of residual shear surfaces close to the pile, despite evidence from laboratory tests which suggests that a highly polished principal displacement shear does form (see Chapter 4). (See also Appendix 3 for a discussion of the shear behaviour of London clay at large displacements.)

### 3.4.2 Changes in total stress due to pile installation

a) Cavity expansion predictions

Figure 3.5 shows four different predictions for the changes in total stress caused by pile installation, based on the cavity expansion method of analysis. The changes in stress ($\Delta\sigma_{11}$) have been normalized by some measure of the soil's undrained shear strength (herein given the symbol k); and the radial distance (r) by the radius of the pile (R). In some cases k equals the undrained shear strength in triaxial compression, $c_{utc}$, and in others the strength in plane strain, $c_{ups}$ - see Table 3.1 for details.

The four solutions show very similar characteristics, the essential difference between them being the extent ($r_p$) of the plastic zone surrounding the pile ($r_p/R$ = 4, 7, 9, and 14). Most cavity expansion analyses (see Table 3.1) conclude that $r_p/R$ is uniquely defined by the soil's rigidity index $I_r$, as follows:

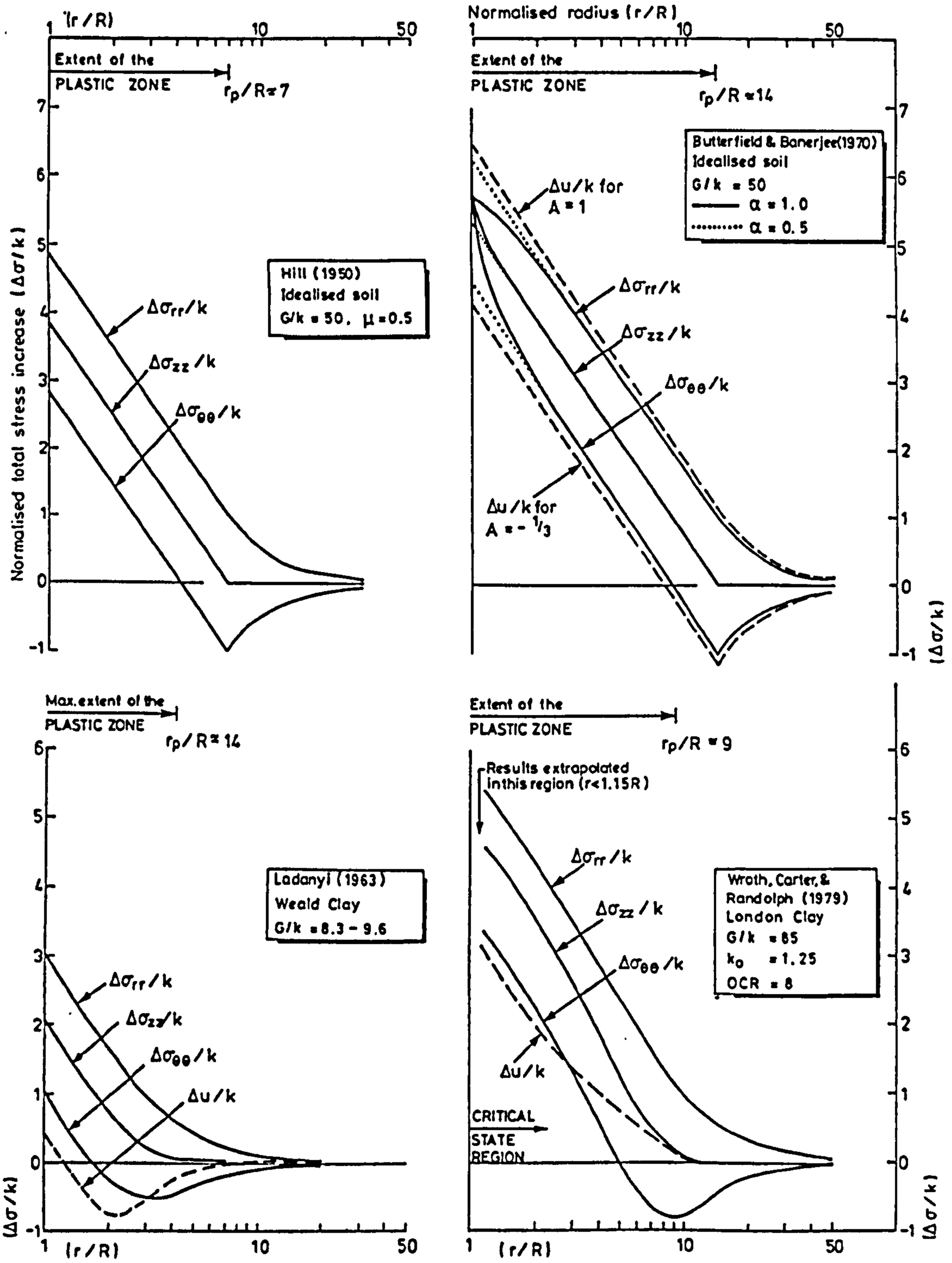



Figure 3.5 Changes in total stress caused by cylindrical cavity expansion

$$r_p/R = \sqrt{I_r} = \sqrt{(G/k)}$$

where G is the elastic shear modulus of the soil and $I_r = G/k$.

As discussed in Chapter 2, a clay's undrained shear strength depends on the method used to measure it and also on sampling procedures. Consequently the uncertainty in the value of $c_{uo}$ can be as high as ±50%.

When we consider the soil's shear modulus, we encounter an even greater problem. Most soils possess highly non-linear stress-strain characteristics prior to yield, with the tangent modulus decreasing by a factor of perhaps a hundred as the strain increases from 0.002% to 4%. Hence choosing a suitable value for the shear modulus G is really rather difficult:

> "...in most soils it would be wrong to associate G with the current in situ stress state since this would result in low, unrealistic values of G, hence low values of the ratio [G/k], at high values of OCR..."[38]

Ladanyi[39] suggests taking a secant modulus $G^{sec}$ (measured over the stress range 0 to ½$c_u$) from laboratory determined stress-strain curves. This would have the greatest bearing on the value of G for normally consolidated clays (which have highly non-linear stress-strain curves). Randolph et al.[40] state that shear stiffnesses are best obtained from in situ tests (plate loading or pressuremeter), "although high quality triaxial tests - particularly with $K_0$ consolidation - may also yield reasonable values for G."

High quality triaxial tests at Imperial College[41] (see also Appendix 3) have shown that many soils display highly non-linear stress-strain characteristics *prior to yield* (i.e. in the elastic range). With moduli that depend on the strain level at which they are measured, it is not at all clear how G should be selected for the cavity expansion methods.

Although the variations of stress with radial position are of great academic interest, from a practical point of view it is the stresses at

the pile wall that are of primary importance. The simple linear-elastic/perfectly-plastic (LE-PP) models generally predict the following relationships between $\Delta\sigma_{ii}/k$ and $r_p/R$ (see Appendix 1 for further details):

$$(\Delta\sigma_{rr}/k)_{wall} = 2Ln(r_p/R) + 1$$
$$(\Delta\sigma_{zz}/k)_{wall} = 2Ln(r_p/R)$$
$$(\Delta\sigma_{\theta\theta}/k)_{wall} = 2Ln(r_p/R) - 1$$

Since $r_p/R$ equals the square root of the rigidity index $I_r$ (= G/k), it follows that:

$$(\Delta\sigma_{rr}/k)_{wall} = Ln(G/k) + 1, \text{ etc.}$$

Despite incorporating a more realistic soil model and $K_0$ initial stresses, the finite element (FE) analyses conducted by Randolph, Carter, and Wroth produce essentially the same results as the simpler closed-form solutions (with a LE-PP model) - provided the same value of G/k is used in both types of analysis.

Figure 3.6 illustrates this point, by comparing Hill's LE-PP solution with the Cambridge predictions for London clay and Boston blue clay (BBC). The normalized total stress changes ($\Delta\sigma_{ii}/k$) from the FE studies agree with Hill's equations to within ±5% for $\Delta\sigma_{rr}/k$ and to within ±8% for $\Delta\sigma_{\theta\theta}/k$. The two methods differ only in their predictions for $\Delta\sigma_{zz}/k$ (and hence $\Delta u/k$). Note that this conclusion holds for a wide range of initial overconsolidation ratios (OCRs from 1 to 32).[42]

Also shown on Figure 3.6 are the results of Ladanyi's analysis for the expansion of a cylindrical cavity in highly overconsolidated Weald clay (OCR = 24), and normally consolidated Drammen clay. Ladanyi's results are in excellent agreement with Hill's relationships for $\Delta\sigma_{rr}/k$.

The key conclusions to be drawn from Figure 3.6 are that:

- There is little difference between the simple closed-form solutions (using a LE-PP model) and the more sophisticated FE

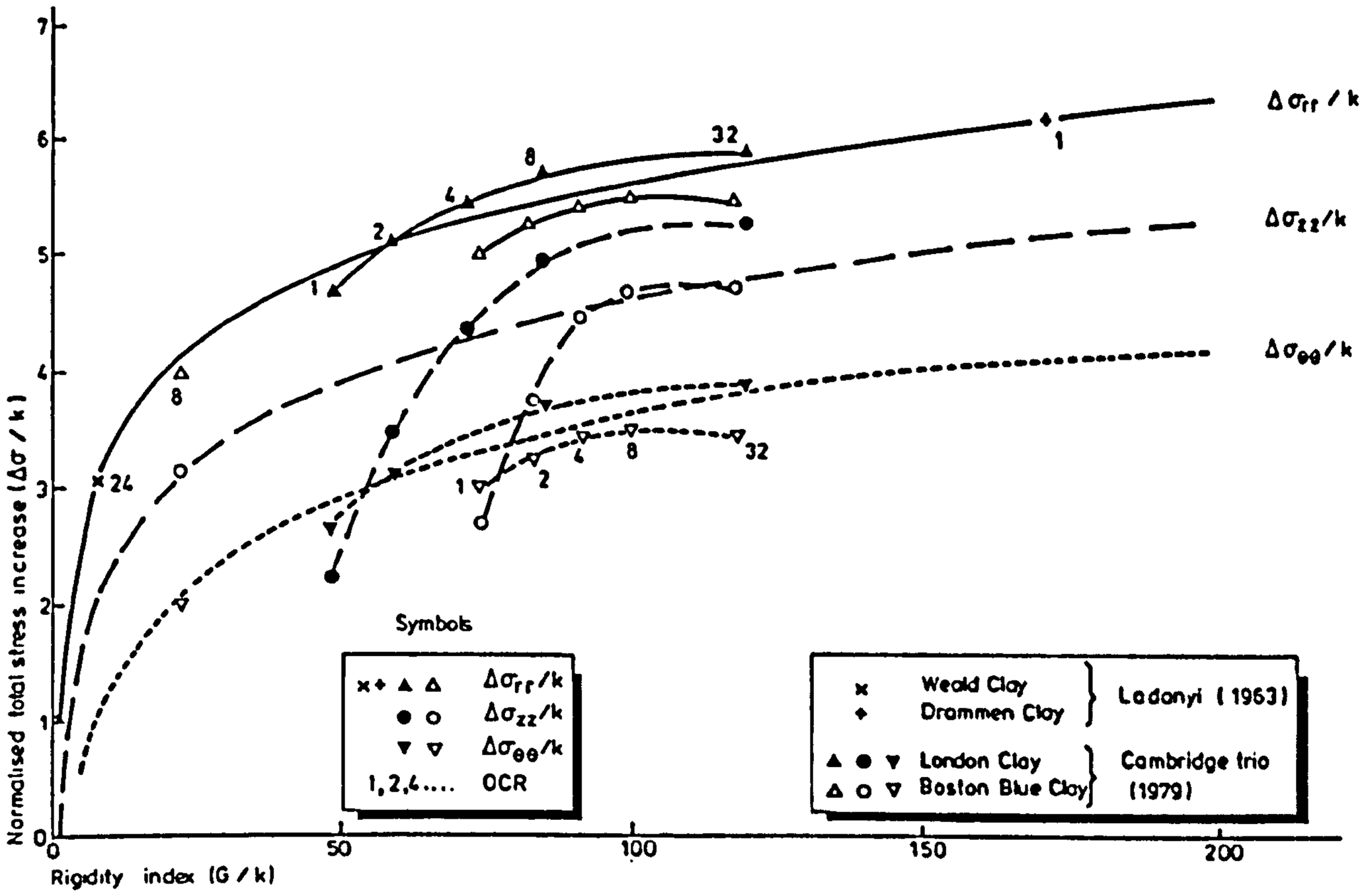



Figure 3.6 Increase in total stress as a function of rigidity index: cavity expansion predictions

analyses (incorporating Modified Cam Clay)

- The rigidity index has over-riding control of the cavity expansion process

Kavvadas[43] has come to broadly the same conclusion:

> "...predictions obtained by the [Modified] Cam-Clay model for the expansion of a cylindrical cavity are practically the same as those predicted with the elastic perfectly-plastic model. This is due to the overriding influence of the relationship between [$(\sigma_{rr} - \sigma_{\theta\theta})/2$, i.e. k] and $\epsilon_r$ [radial strain] on the results... this relationship is virtually the same in the two models."

b) Effect of soil compressibility

Although they are usually considered incompressible (with Poisson's ratio equal to one half), most clay soils are in fact *partially* compressible, owing to sand or silt seams embedded in their fabric or to incomplete saturation (due to gas in the pore fluid, for example).[44] The inherent

compressibility of the soil skeleton and the pore water ensures that real soils are not truly incompressible even when fully saturated.[45]

Vesic[46] took account of soil compressibility in his analysis of the cavity expansion problem, by including a parameter $\Delta$ in the equations, where $\Delta$ is the average volumetric strain in the plastic zone. The nett effect of $\Delta$ was to reduce the soil's "operational" rigidity index by a factor $\xi_v$, to:

$$I_{rr} = \xi_v I_r,$$

where $I_{rr}$ (the "reduced" rigidity index) replaces $I_r$ in the equations for $\Delta\sigma_{11}/k$. Vesic called $\xi_v$ the "volume change factor"; values of $\xi_v$ as a function of $\Delta$ and $I_r$ are given in Figure 3.7, and Appendix 1 includes a diagram which shows the dramatic influence of $\Delta$ on the cavity expansion predictions for $\Delta\sigma_{rr}/k$.

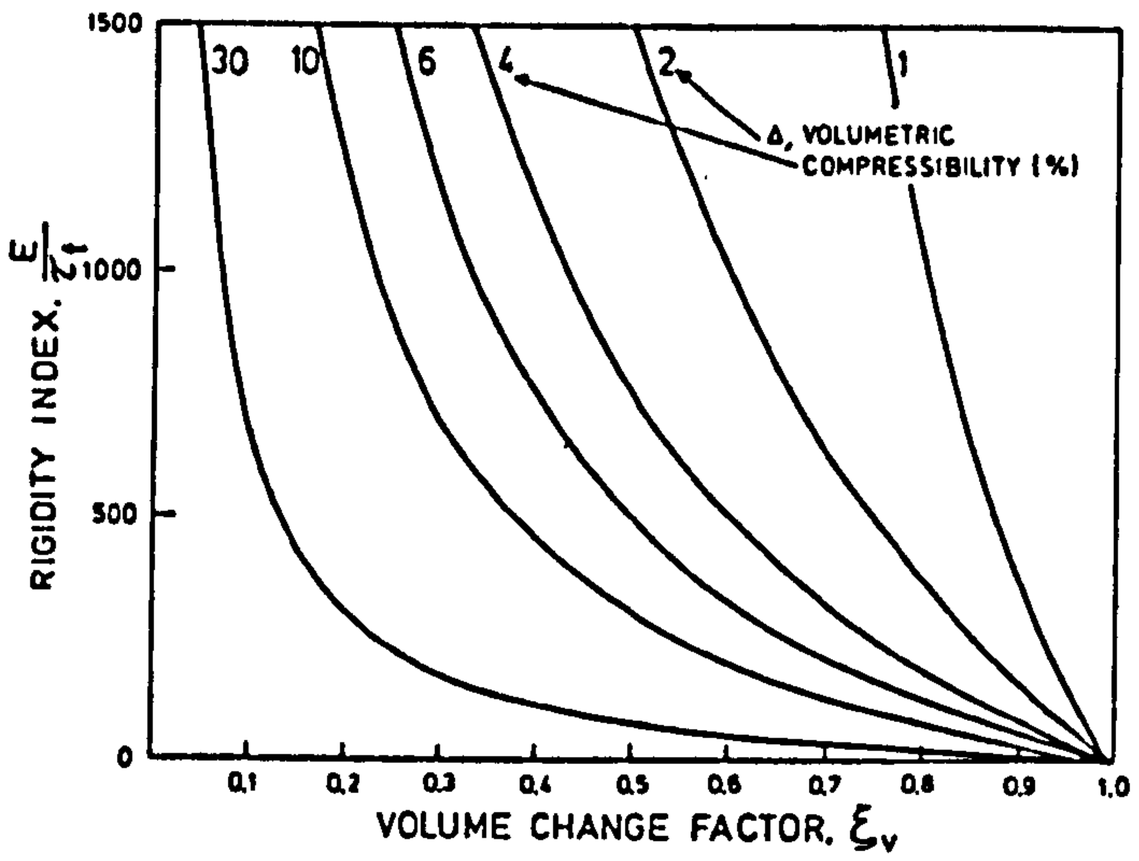



Figure 3.7 Vesic's "volume change factor" $\xi_v$ as a function of $I_r$ and $\Delta$

Unfortunately, Vesic gave no indication of the likely value of $\Delta$ (and hence $\xi_v$) for clay soils, although for medium dense sands he gives examples in which $\Delta = 0.75$ and 1.15%. His analysis does, however, suggest that real soils will mobilize smaller total stresses during pile installation than the cavity expansion methods predict (convention is to assume the soil is incompressible, i.e. $\Delta = 0$).

### 3.4.3 Pore pressures at the end of pile installation

#### a) Cavity expansion predictions

Superimposed on Figure 3.5 (see page 80) are the predictions for the normalized excess pore water pressures at the end of pile installation

$\Delta u_i/k$, as obtained in four separate analyses. The predicted pore pressures are dissimilar in several respects, for the following reasons:*

- Butterfield & Bannerjee's closed-form analysis takes account of shear-induced pore pressures by incorporating Henkel's pore pressure parameter[47] $\alpha_H$ in the equation for $\Delta u_i/k$; hence it predicts pore pressures in the <u>elastic zone</u> as well as in the plastic zone
- Ladanyi's analysis also accounts for shear-induced pore pressures, but on the basis of the soil's behaviour in consolidated undrained triaxial compression tests; note that the Weald clay is heavily overconsolidated (OCR = 24) and, as a consequence, $\Delta u_i$ is <u>negative</u> for $1.2 < r/R < 7$
- Wroth et al.'s analysis suggests that $(\Delta u_i)_{max} = (p'_o - p'_f) + kLn(G/k)$, where $p'_o$ and $p'_f$ are the original and final mean effective stresses in the soil; Wroth et al. assumed that G/k increases with OCR, and, since $(p'_o - p'_f)$ reduces, it turns out that the normalized excess pore pressure $\Delta u_i/k$ is almost unaffected by the soil's past history (laboratory tests at Imperial College[48] indicate that G/k <u>falls</u> with increasing OCR)

It is clear from Figure 3.5 that there are significant differences between the four independent predictions, even though they are all based on the cavity expansion hypothesis. Evidence is needed from instrumented pile tests to determine which (if any) of these predictions is correct.

b) Strain path predictions

Analyses based on the strain path method suggest that the excess pore pressures generated during pile installation are quite unlike those predicted by the cavity expansion method. Figure 3.8 compares the two predictions for a <u>normally consolidated clay</u> according to three different soil models: MIT-E1 (full line); MIT-T1 (broken line); and Modified Cam Clay (chain-dotted). (Note that on this figure $\Delta u_i = (u - u_o)$ has been

---

*N.b. the excess pore pressure comprises two independent components: a total stress component ($\Delta u_{ts} = \Delta p = [\Delta\sigma_{rr} + \Delta\sigma_{zz} + \Delta\sigma_{\theta\theta}]/3$); and a shear-induced component ($\Delta u_s$)

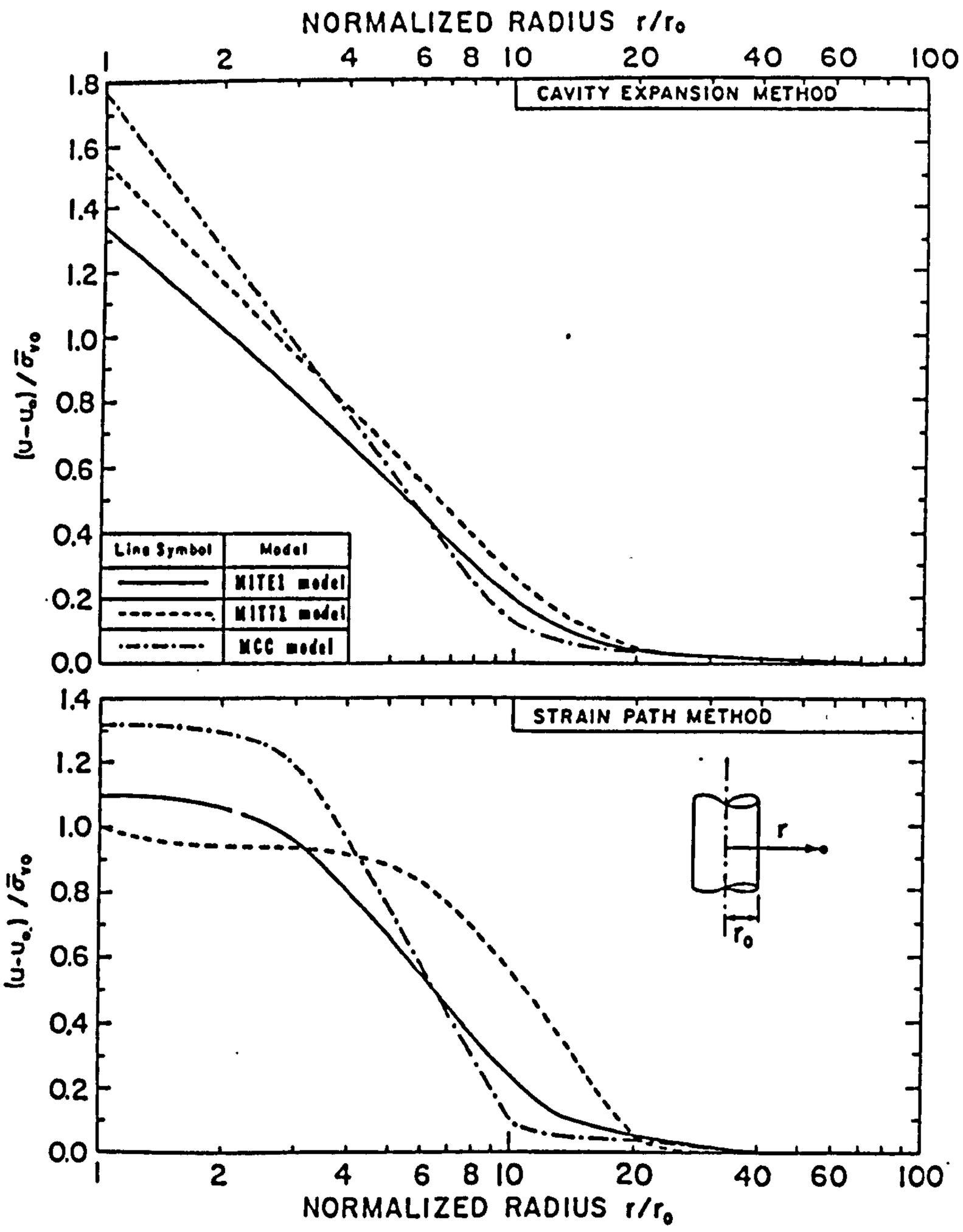



Figure 3.8 Excess pore pressures generated during pile installation: SPM and CEM predictions compared

normalized by $\sigma'_{vo}$ rather than by k.)

Although the choice of soil model affects the results in both cases, there is clearly a significant difference between the SPM and CEM predictions. With the MIT-E1 model, $\Delta u_i/\sigma'_{vo}$ at the pile wall is only 1.1 according to SPM, but is ≈1.34 according to CEM (i.e. a 22% difference). The distributions of excess pore pressure with radial position are also very different: this is important, since the shape of the initial isochrone has a major influence on the dissipation of excess pore pressures following pile installation.

The latest SPM predictions, as obtained with the MIT-E3 model, allow the effect of the overconsolidation ratio (OCR) to be assessed. As Figure 3.9 reveals, the normalized excess pore pressures $\Delta u_i/\sigma'_{vo}$ increase sharply as OCR increases, but only for soil close to the pile ($r/R < 6$). Further away from the pile the OCR has little or no effect on the excess pore pressures. The sharp jump in $\Delta u_i/\sigma'_{vo}$ from OCR = 2 to OCR = 4 warns against extrapolating these results to higher OCRs. Another important difference from the earlier SPM predictions is the distribution of pore pressures with radial position. With the MIT-E1 model (for example) there was a

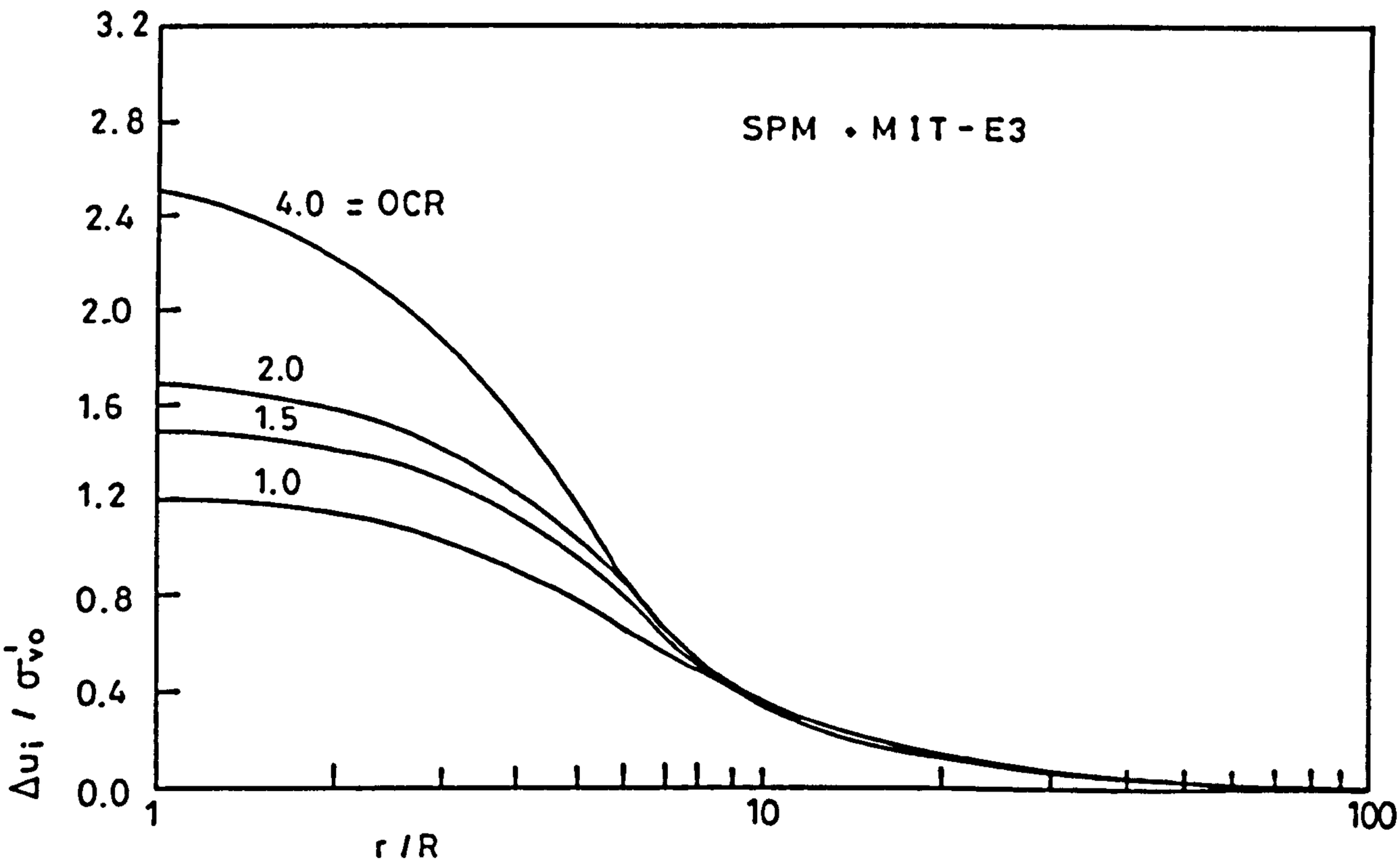



Figure 3.9 MIT-E3 predictions for installation pore pressures: strain path method

distinct "plateau" in $\Delta u_i/\sigma'_{vo}$ for r/R less than about 2-3 (refer to Figure 3.9) - with MIT-E3 the pore pressures show a systematic fall as r/R increases. This will have a significant effect on the rate at which the excess pore pressures dissipate with time (see Section 3.5.1.d).

c) Summary of various predictions

Table 3.3 summarizes various predictions for $\Delta u_i/\sigma'_{vo}$ at the pile wall, obtained using the cavity expansion and strain path methods. The soil

properties assumed were either those of the sensitive Boston blue clay ($S_t \approx 7$) or those of the insensitive London clay. The evidence from instrumented pile tests to support or deny these predictions is examined in Chapter 4.

### 3.4.4 Effective stresses at the end of pile installation

#### a) Cavity expansion predictions

The distribution of effective stresses at the end of cavity expansion are shown in Figure 3.10 for two cases: (left) for a normally consolidated clay (OCR = 1); and (right) for an overconsolidated clay (OCR = 8). The predictions come from the FE analyses performed by Randolph et al.[49] using the Modified Cam Clay model (representing Boston blue clay). The following points should be noted:

- The normalized effective stresses next to the pile are those pertaining to critical state conditions ($\sigma'_{rr}/k = \sqrt{3}/M + 1$; $\sigma'_{zz}/k = \sqrt{3}/M$; and $\sigma'_{\theta\theta}/k = \sqrt{3}/M - 1$, where $M = 6\sin\phi_{tc}/[3 - \sin\phi_{tc}]$)
- Because of this, the normalized effective stresses next to the pile are the same for both the normally consolidated (NC) and the overconsolidated (OC) clay - but only because they have the same initial undrained triaxial compression strength (M is the same for both)
- In both cases the radial effective stress is the major and the hoop stress the minor principal stress (i.e. $\sigma'_{rr} > \sigma'_{zz} > \sigma'_{\theta\theta}$)
- For the OC clay, varying the rigidity index G/k ($G/c_u$ on Figure 3.10) has no effect on the stresses in the critical state region, but <u>does</u> affect the stresses in the elastic zone

Table 3.3 Installation pore pressures next to pile wall

| OCR | Soil model | $\Delta u_i/\sigma'_{vo}$ SPM | $\Delta u_i/\sigma'_{vo}$ CEM |
|---|---|---|---|
| 1.0 | MCC | - | 0.97* |
| | MCC | 1.25 | 1.32 |
| | MIT-E1 | 0.98 | 1.30 |
| | MIT-E3 | 1.20 | 1.49 |
| 1.5 | MIT-E3 | 1.49 | 2.08 |
| 2.0 | MCC | - | 1.48* |
| | MCC | - | 2.39 |
| | MIT-E3 | 1.68 | 2.42 |
| 4.0 | MCC | - | 2.35* |
| | MCC | - | 4.33 |
| | MIT-E3 | 2.50 | 3.65 |
| 8.0 | MCC | - | 3.89* |
| | MCC | - | 7.48 |
| 32.0 | MCC | - | 9.76* |
| | MCC | - | 23.4 |

Predictions for Boston blue clay (*London clay)

Table 3.4 Radial effective stresses on pile installation in Boston blue clay (*London clay)

| OCR | $K_0$ | Soil model | $K_i = (\sigma'_{rr})_i/\sigma'_{vo}$ SPM | CEM |
|---|---|---|---|---|
| 1.0 | 0.62* | MCC | - | 0.91* |
| | 0.53 | MCC | 0.27 | 0.84 |
| | 0.53 | MIT-E1 | 0.06 | 0.49 |
| | 0.48 | MIT-E3 | 0.08 | 0.45 |
| 1.5 | 0.55 | MIT-E3 | 0.17 | 0.70 |
| 2.0 | 0.72* | MCC | - | 1.43* |
| | 0.70 | MCC | - | 1.47 |
| | 0.58 | MIT-E3 | 0.20 | 0.85 |
| 4.0 | 0.94* | MCC | - | 2.29* |
| | 1.00 | MCC | - | 2.71 |
| | 0.75 | MIT-E3 | 0.28 | 1.44 |
| 8.0 | 1.25* | MCC | - | 3.80* |
| | 1.35 | MCC | - | 4.91 |
| 32.0 | 2.15* | MCC | - | 10.4* |
| | 2.75 | MCC | - | 16.7 |

clays ($K_i \approx 0.07$ for the MIT models), and are well below the original horizontal effective stress $\sigma'_{ho}$ in the over-consolidated clays ($K_i < K_0$) - at least for OCRs up to 4. (Strain path predictions have not yet been published for <u>insensitive</u> soils, such as the London clay.) These results are in strong contrast to the cavity expansion predictions, which suggest that $K_i$ is greater than $K_0$ for both the sensitive Boston blue clay and the insensitive London clay. $K_i$ is very much greater than $K_0$ in the heavily overconsolidated soils (OCR $\geq$ 8).

### 3.4.5 Variation of stresses behind the pile tip

So far, I have been comparing predictions of the earth and pore pressures generated by pile installation for positions located far behind the pile tip. For the cavity expansion methods this is the only place where predictions are possible. However, the two-dimensional nature of the strain path solutions allow the variation of stresses to be determined over the full length of the pile.

Figure 3.13 shows how the normalized total stresses at the pile wall, $(\sigma_{ii} - u_o)/\sigma'_{vo}$, vary with (the normalized) distance behind the pile tip, $z/R$, for a <u>normally</u> consolidated clay ($K_0 = 0.537$). As the diagram reveals, all three total stresses fall dramatically with increasing values of $z/R$, particularly so for $0 \leq z/R \leq 5$. For example, $H_i = ([\sigma_{rr}]_i - u_o)/\sigma'_{vo} \approx 3.0$ for $0 \leq z/R \leq 1.5$; whereas $H_i = 1.65$ at $z/R = 5$ and 1.3 at $z/R = 10$.

elsewhere in the plastic zone MCC predicts larger radial stresses ($K_i$ up to 0.3 larger) than the MIT models

- Another important difference between the CEM and SPM predictions is the relative magnitudes of the radial, vertical, and hoop stresses: at the pile wall, $\sigma'_{rr} > \sigma'_{zz} > \sigma'_{\theta\theta}$ according to the cavity expansion method, whereas $\sigma'_{zz} > \sigma'_{\theta\theta} > \sigma'_{rr}$ according to the strain path method

The results obtained with the latest constitutive model, MIT-E3, are shown in Figure 3.12. The soil's OCR clearly has a strong influence on the radial effective stresses in the soil, although the dependency of $K_i$

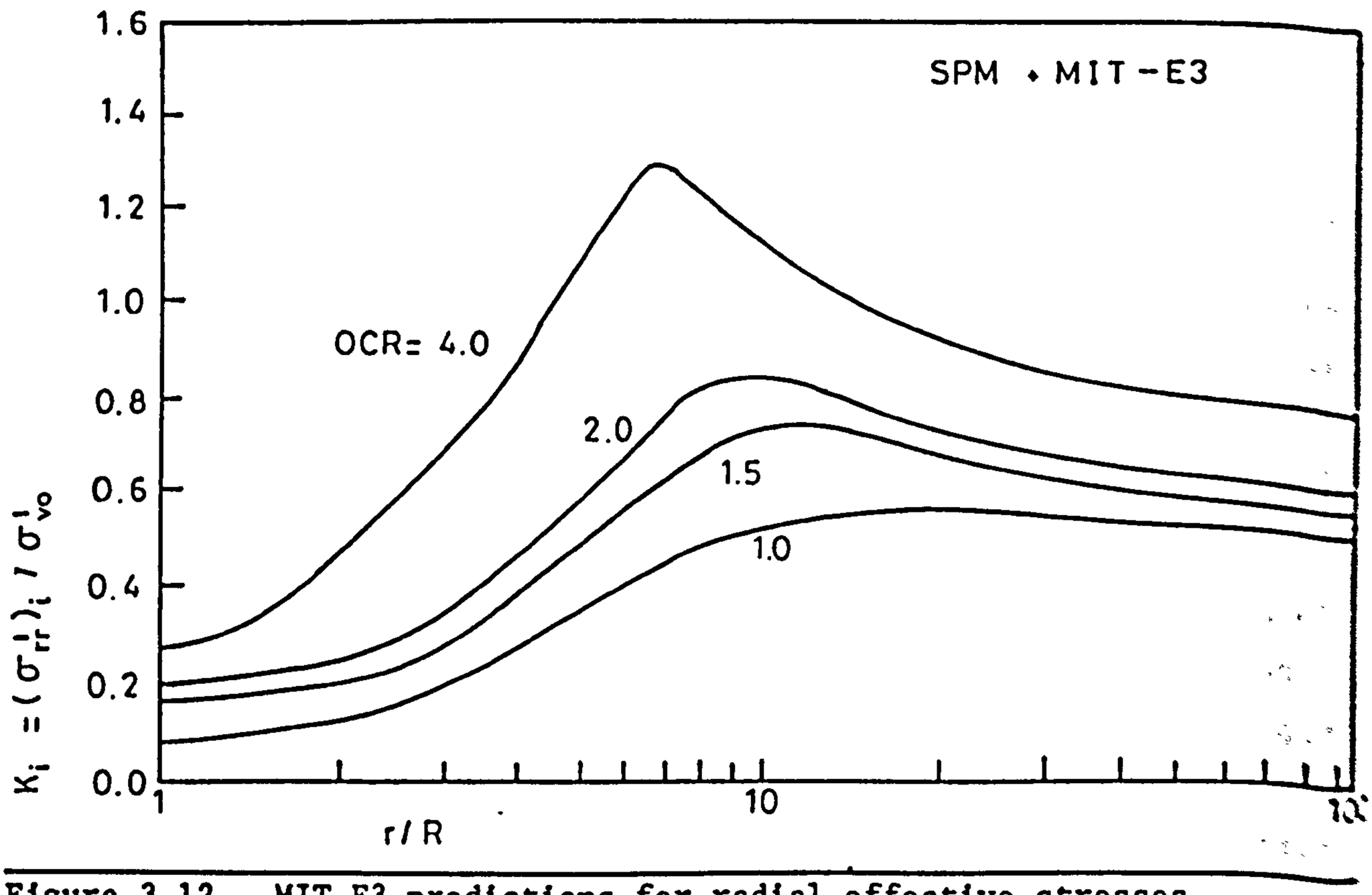



Figure 3.12 MIT-E3 predictions for radial effective stresses following pile installation: strain path method

(= $\sigma'_{rr}/\sigma'_{vo}$) on OCR is <u>least</u> significant at the pile wall (r/R = 1). The results for the normally consolidated clay are fairly close to those obtained with MIT-E1.

Table 3.4 summarizes the values of $K_i$ that have been obtained using the strain path and cavity expansion methods. The inference from the strain path solutions is that the radial effective stresses mobilized during pile installation are close to zero in normally consolidated sensitive

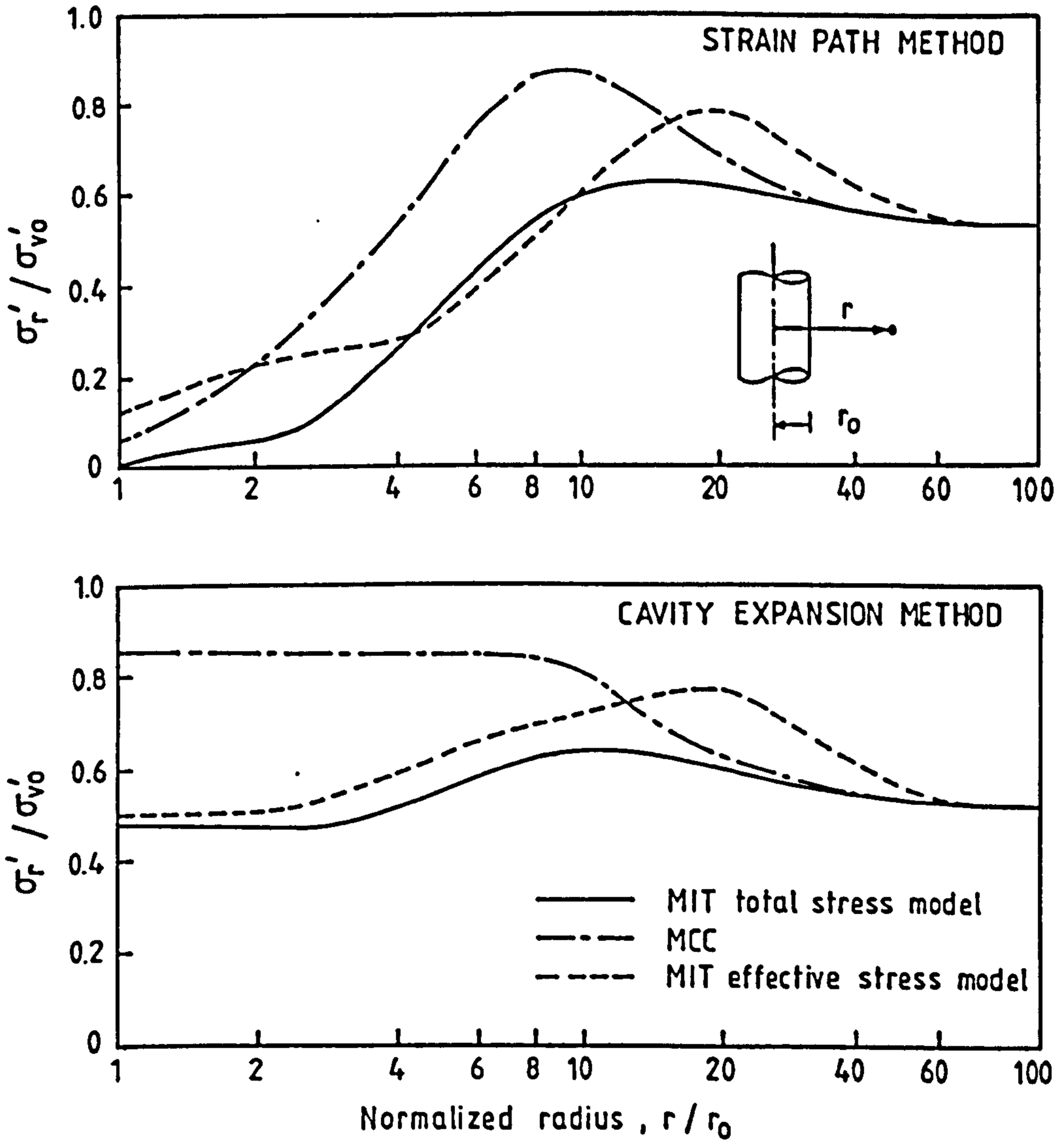



Figure 3.11 Radial effective stresses at the end of pile installation: strain path and cavity expansion predictions compared

for normally consolidated sensitive Boston blue clay. Three predictions are shown for each analytical method: one for the effective stress model MIT-E1; one for Modified Cam Clay (MCC); and one for the total stress model MIT-T1.

Several important points arise from this comparison:

- The strain path method (SPM) predicts far lower radial effective stresses than the cavity expansion method (CEM) throughout the "plastic zone" ($r/R < 10$)
- The SPM predictions with all three soil models are in reasonable agreement with each other next to the pile wall ($r/R = 1$), but

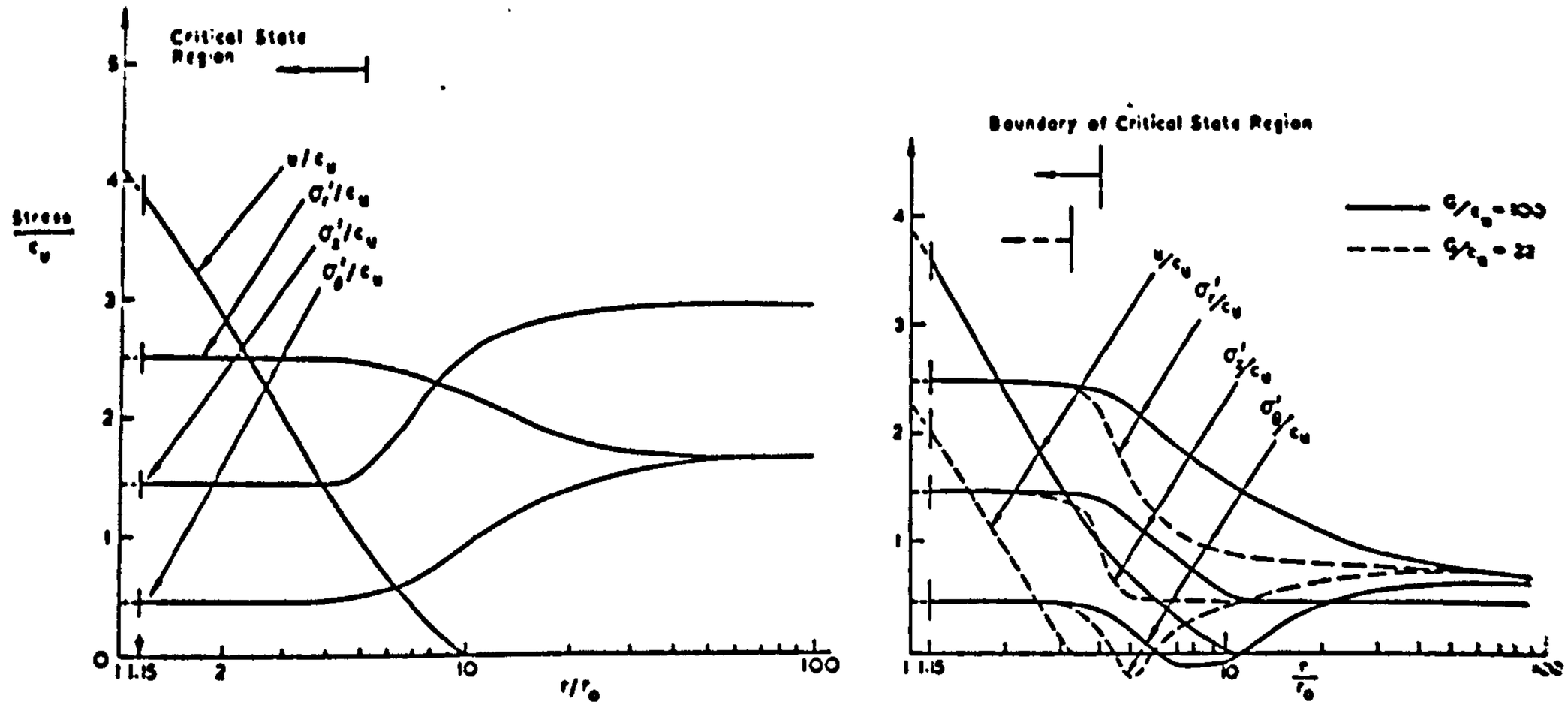



Figure 3.10 Effective stresses at the end of pile installation: cavity expansion predictions for (left) OCR = 1 clay ($K_o$ = 0.55, G/k = 74); and (right) OCR = 8 clay ($K_o$ =1.35, G/k = 22 and 100)

- Tensile hoop stresses ($\sigma_{\theta\theta}'/k < 0$) are predicted for the OC clay for r/R = 6 to r/R ≈ 10-11
- Since soils do not usually sustain tensile stresses, this implies that pile installation might create vertical cracks in OC clays, leading (perhaps) to faster dissipation of excess pore water pressures (Randolph et al. believed that these cracks will be "self-healing", i.e. will close up, during the consolidation phase)

Recent work at MIT suggests that important features of the constitutive model can strongly influence the cavity expansion predictions for the radial effective stress at the end of installation. The value of $K_i$ next to pile wall is significantly higher according to the (isotropic) Modified Cam Clay model than according to the (anisotropic) MIT models: i.e. $K_i \approx 0.86$ as opposed to $\approx 0.5$, for $r/R < 3$ (see Figure 3.11 below).

b) Strain path predictions

Strain path predictions for the radial effective stresses at the end of pile installation are very different to those based on cavity expansion theory, as demonstrated in Figure 3.11. The diagram shows the variation in $K_i = (\sigma_{rr}')_i/\sigma_{vo}'$ with the normalized radius r/R ($r/r_o$ on the diagram)

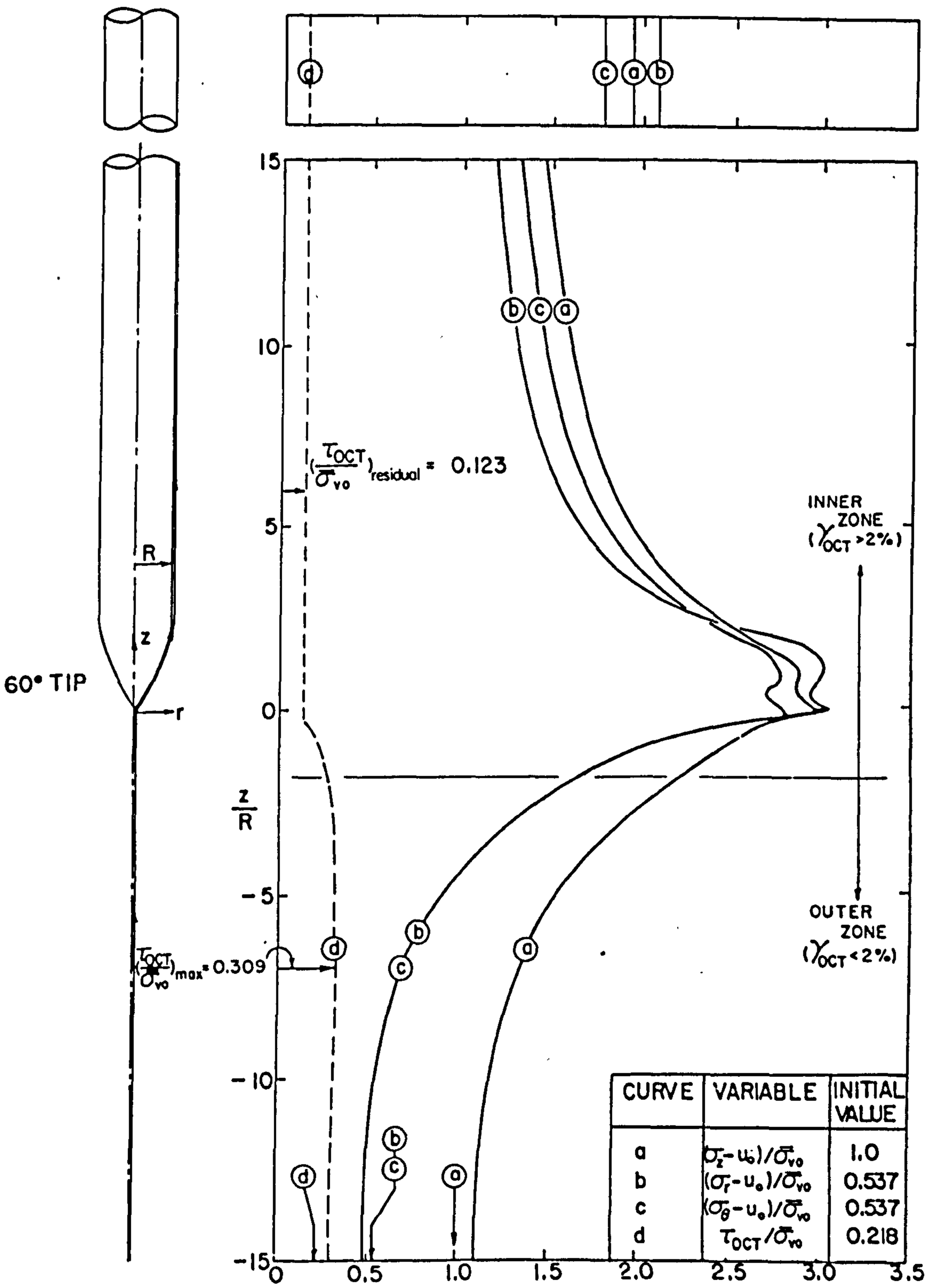



Figure 3.13 Variation in total stresses with distance behind the pile tip during installation: strain path predictions

The tendency for $(\sigma_{11} - u_o)/\sigma'_{vo}$ to fall with distance behind the pile tip* will have a overwhelming effect on the behaviour of short piles (L/D < 10, say), and could have a significant influence on that of long piles. Since the stresses acting on short piles are also greatly affected by the proximity of the ground surface (where $\sigma'_{zz} = 0$), we should expect the strain path predictions for these piles to be in error. There is currently no theory of pile behaviour than can cope adequately with ground surface effects.

### 3.4.6 Discussion

It is clear from the previous sections that the choice of soil model has a significant effect on the predictions of both the cavity expansion and the strain path methods: the key difference between MCC and the two MIT-E models is that the former employs an isotropic hardening rule whereas the latter adopt one that is anisotropic. Since soils are inherently anisotropic (as well as being non-linear and brittle) in their response to loading, the results using the MIT-E models are likely to be far more reliable than those using MCC.

Even more important than the choice of soil model is the choice of the analytical technique with which to study pile installation. As Figure 3.11 demonstrates, there are enormous differences between the strain path and cavity expansion predictions for $K_i$, which is one of the key parameters governing pile behaviour.

Finally, the "z/R effect" is obviously very important when it comes to interpreting the results of instrumented pile tests, even more so when the pile is short. Great care is needed in comparing measurements of stress when the instruments are located close to (within ten pile radii, say) the pile tip.

---

*Termed the "z/R effect" in this Thesis, its magnitude was a key discovery of the instrumented pile tests at Canons Park (see Chapter 9)

## 3.5 EQUALIZATION STAGE

### 3.5.1 Dissipation of excess pore pressures

#### a) Consolidation theory

There are two main theories to describe the consolidation of soils: the Terzaghi/Rendulic "uncoupled" approach, which supposes that the total stress in the soil ($\sigma$) remains everywhere constant, so that strains are caused only by changes in pore pressure (u); and Biot's "coupled" theory, in which the continual interaction between the soil and the pore water pressure is included in the formulation.

There are certain problems in which the total stresses are not constant and yet both approaches lead to the same governing equations.[50] One problem in which this is true is the case of one-dimensional consolidation around a cylindrical pile - but only when the soil is homogeneous, isotropic, and linear-elastic. In these circumstances the consolidation process is practically unaffected by coupling between $\sigma$ and u.[51] Of course, real soils are not isotropic or linear-elastic (let alone homogeneous), and so analyses based on the Terzaghi/Rendulic theory can only be approximations to the behaviour of real soils.

There have been several studies of consolidation around piles, including uncoupled and coupled analyses using linear and non-linear soil models. Table 3.5 summarizes the key features of several of these studies.

#### b) Factors controlling pore pressure dissipation

There are a number of factors that influence the dissipation of excess pore pressures around single piles, the foremost amongst these being:

- The initial distribution of excess pore pressures, $\Delta u_i$, as a function of radial position, i.e. $\Delta u_i = f(r/R)$
- The soil's horizontal permeability, $k_h$
- The soil's compressibility, $m_v$

Table 3.5 Summary of consolidation analyses for piles in clay

| Reference | Type of analysis* | Soil model† | Initial stresses‡ | Assumptions |
|---|---|---|---|---|
| Soderberg (1962) | Uncoupled 1D (FD) | Isotropic linear-elastic | CEM (LE-PP) & "viscous" model | $c_h$ = constant |
| Torstensson (1977) | Uncoupled 1D (FD) | Isotropic linear-elastic | CEM (LE-PP) | Not known |
| Randolph & Wroth (1979) | Uncoupled 1D (CF) | Isotropic linear-elastic | CEM (LE-PP) | $k_h$, G, $\nu$ constants (hence $m_v$ and $c_h$ too) |
| Carter et al. (1979) | Coupled 1D (FE) | Isotropic linear-elastic | CEM (LE-PP) | $k_h$, G, $\nu$ constants (hence $m_v$ and $c_h$ too) |
| | | MCC | CEM (MCC) | $k_h$, G = constants ($m_v$ and $c_h$ vary) |
| Randolph et al. (1979) | Coupled 1D (FE) | MCC | CEM (MCC) | $k_h$, G = constants ($m_v$ and $c_h$ vary) |
| Kavvadas & Baligh (1982) | Coupled 1D (FE) [NON-CAP] | MCC MIT-E1 | SPM & CEM (MIT-E1 & MCC) | $k_h$ = constant ($m_v$ and $c_h$ vary) |
| Levadoux and Baligh (1986) | Uncoupled 2D (FE) [ADINAT] | Isotropic linear-elastic | SPM (MIT-T1) | $c_h$ = constant |
| | Coupled 2D (FE) | Isotropic linear-elastic | SPM (MIT-T1) | $c_h$ = constant |
| Teh (1987) | Uncoupled 2D (FD) | Aniso-tropic linear-elastic | SPM (LE-PP) | $k_h$, G, $\nu$ constants (hence $m_v$ and $c_h$ too) |
| Whittle (1987) | Coupled 1D (FE) [NON-CAP] | MIT-E3 | SPM (MIT-E3) | $k_h$ = constant ($m_v$ and $c_h$ vary) |

*1D = one-dimensional; 2D = two-dimensional axi-symmetric analysis
CF = closed form; FE = finite element; FD = finite difference solution
[name] = name of computer program

†LE-PP = linear-elastic/perfectly-plastic model; MCC = Modified Cam Clay; MIT-T1 = MIT total stress model; MIT-E1 and -E3 = MIT effective stress models

‡CEM = cavity expansion method; SPM = strain path method

- The radius of the pile, R

As Table 3.5 reveals, the soil's permeability is commonly assumed to be a constant. In this case, the combined effect of $k_h$ and $m_v$ on the consolidation process may be represented by one parameter, the coefficient of horizontal consolidation, $c_h$, which is defined as follows:

$$c_h = k_h/m_v\gamma_w$$

where $\gamma_w$ is the unit weight of water.

Linear consolidation analyses assume $c_h$ to be constant, whereas in non-linear studies it is a function of the effective stress in the soil (and hence also a function of time). Because of the disturbance caused by pile installation, $c_h$ also varies with radial position - although this is usually ignored.

For $c_h$ to remain constant during equalization, the ratio of $k_h$ to $m_v$ must remain constant. The compressibility of the clay at any stage is a function of its stress history, stress level, and stress increment; whereas its permeability depends on its current voids ratio.

> "When the clay is in a normally consolidated state, the changes in compressibility and permeability are self compensating such that c remains sensibly constant. On the other hand, if a clay is loaded to effective stress levels exceeding the maximum past pressure, [$\sigma'_{vp}$, the pre-consolidation pressure], or is unloaded near [$\sigma'_{vp}$], severe nonlinearities arise during consolidation. Therefore, linear solutions are reasonably applicable to normally consolidated states or to overconsolidated states involving relatively small stress increments away from [$\sigma'_{vp}$] (i.e. when the OCR is large)."[52]

According to the linear analyses, the combined effect of $c_h$ and pile radius on the rate of consolidation can be represented[53] by a non-dimensional time factor:

$$T = c_h t/R^2 = (k_h/m_v\gamma_w)(t/R^2)$$

where t is the time since the start of consolidation. An alternative definition of T is needed for the non-linear theories, since $c_h$ varies during the equalization period. The options include:

| | |
|---|---|
| Carter et al.'s[54] | $T_G = (k_h G/\gamma_w)(t/R^2)$ |
| Randolph et al's[55] | $T_c = (k_h c_{uo}/\gamma_w)(t/R^2)$ |
| Kavvadas & Baligh's[56] | $T_p = (k_h p'_o/\gamma_w)(t/R^2)$ |

where the subscripts G, c, and p denote whether G, $c_{uo}$, or $p'_o$ appears in the equation, and the other symbols have their usual meanings (see the List of Symbols ~~Glossary~~ for further clarification).

The remainder of this section discusses the effect that the initial pore pressure distribution, $\Delta u_i = f(r/R)$, has on the consolidation process.

c) Initial pressures based on cavity expansion method

Figure 3.14 shows the radial distribution of excess pore pressures in the soil at four different moments during equalization, as given by a linear consolidation analysis[57] in which the initial pore pressures (isochrone 1)

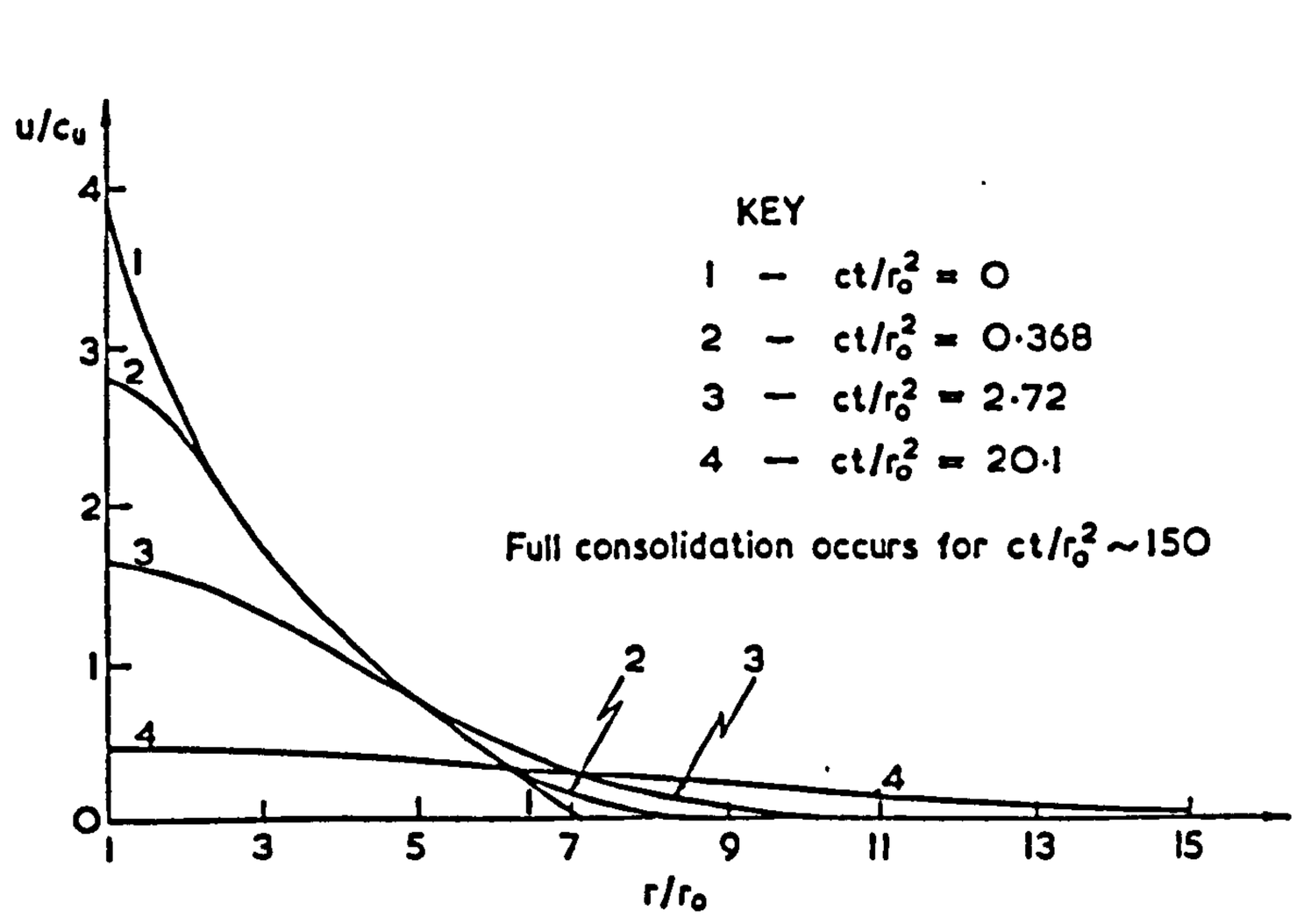



Figure 3.14 Pore pressure isochrones during consolidation: CEM initial stresses

were predicted by the cavity expansion method. There are two main features to note (n.b. the normalized radius r/R is denoted $r/r_o$ on this diagram):

- The pore pressure close to the pile wall (r/R = 0) initially falls very rapidly, but reduces more slowly as time proceeds

- As water flows outwards, so the pore pressures <u>increase</u> in the elastic zone ($r/R > \approx 6$) - i.e. in this region the soil swells rather than consolidates

Figure 3.15 shows the fall in excess pore pressure as a function of the time factor T (= $c_h t/R^2$), for a wide range of values of rigidity index $I_r$ (= $G/c_u$ on this figure).[58] As explained in Section 3.4.3.a, cavity expansion predictions for the pore pressures generated during pile installation are, to all intents and purposes, controlled by the value of the rigidity index. In fact, as Figure 3.15 shows, the influence of $I_r$ on the pore pressures around the pile remains undiminished throughout the equalization period, affecting both the magnitude of $\Delta u/c_{uo}$ and the time taken to reach equilibrium conditions. ($\Delta u/c_{uo}$ is close to zero at T ≈ 55 for $I_r$ = 25, but, for $I_r$ = 400, T ≈ 3000 when $\Delta u/c_{uo} \approx 0$.)

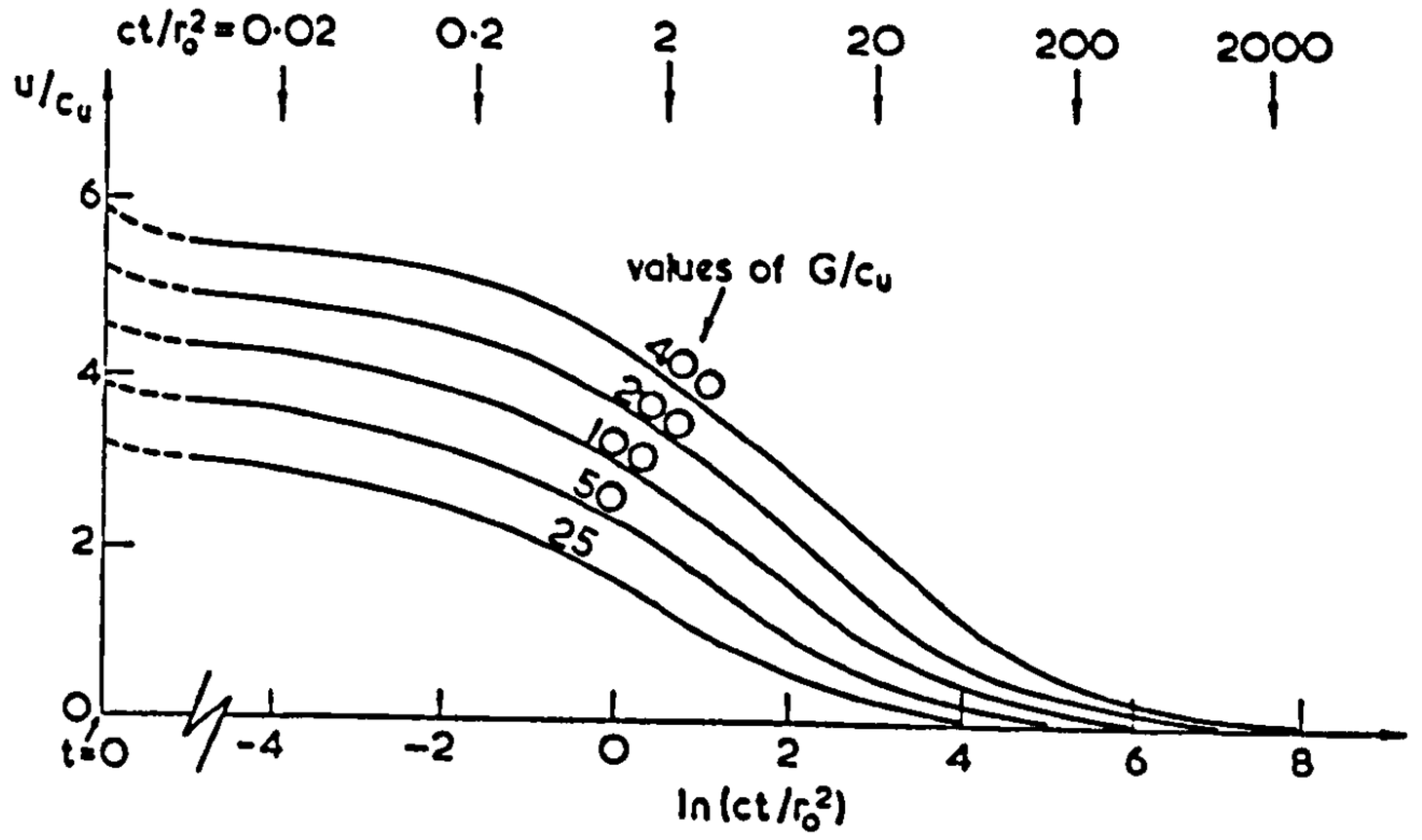



Figure 3.15 Decay of excess pore pressures with time: CEM initial stresses

d) Initial pressures based on strain path method

Figure 3.16 illustrates the effect of overconsolidation ratio (OCR) on the decay of pore pressures next to the pile wall, for OCRs up to 4.0. The initial pore pressures for this analysis[59] were obtained by the strain path method, using the MIT-E3 soil model (with parameters appropriate to Boston blue clay). Also shown are three separate predictions for the pore pressure decay in a normally consolidated clay (OCR = 1), as given by the Modified Cam Clay (MCC), MIT-E1, and MIT-E3 models. For the purposes of this comparison, the excess pore pressures $\Delta u$ have been normalized by the excess pore pressures at the end of pile installation $\Delta u_i$.

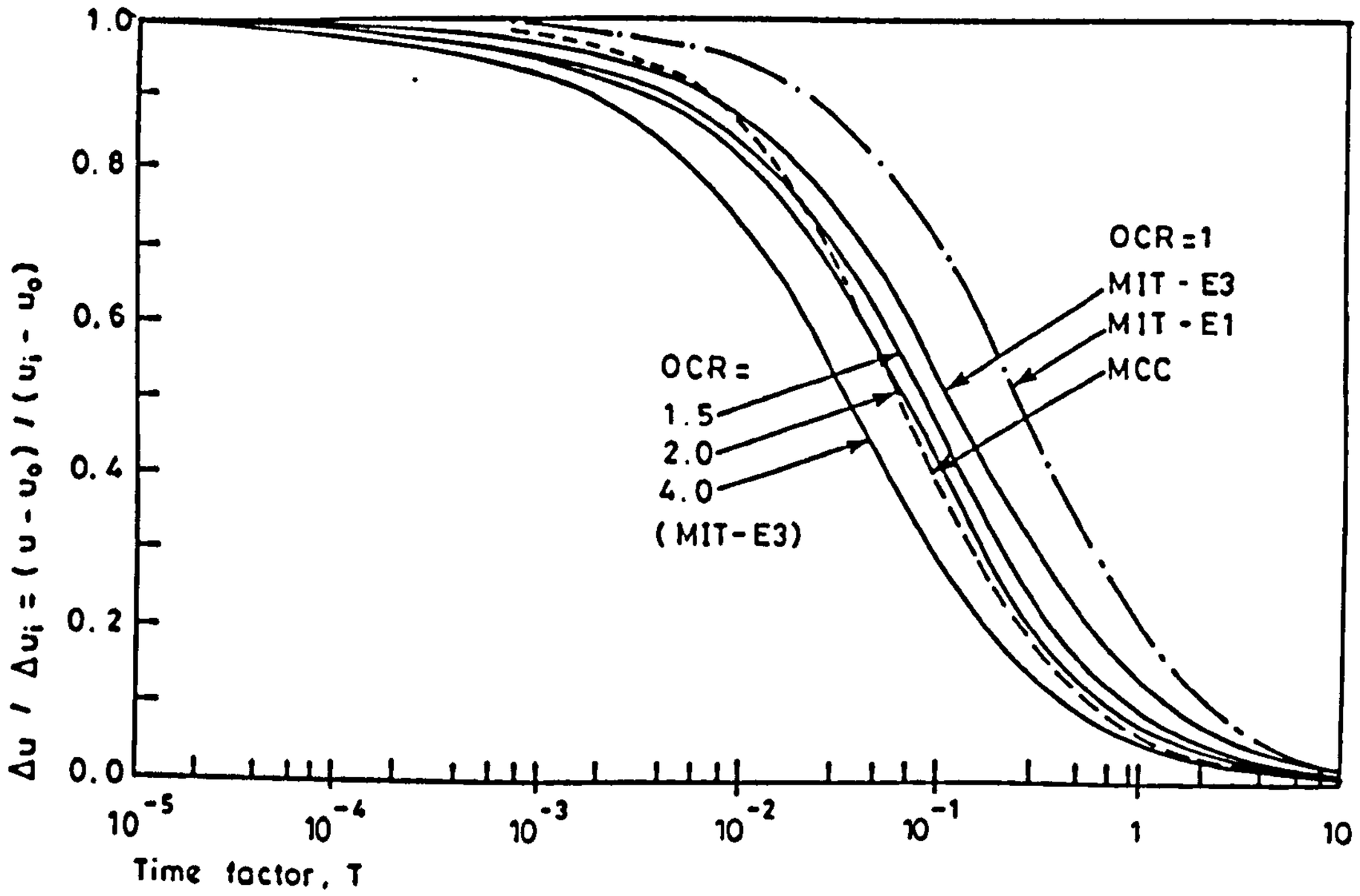



Figure 3.16 Pore pressure dissipation at pile wall: SPM initial stresses (time factor = $T_p$)

Figure 3.16 raises the following points of interest (note that this diagram uses the time factor $T_p$):

- Initially, there is little change in the pore pressures next to the pile ($\Delta u/\Delta u_i > 0.9$ for $T_p < \approx 0.003$)
- Ninety percent of the excess pore pressures have dissipated once the time factor exceeds approximately one ($\Delta u/\Delta u_i < 0.1$ for $T_p > \approx 1$)
- The higher the OCR the <u>faster</u> the pore pressures dissipate
- Fifty percent dissipation occurs at time factors $(T_p)_{50} \approx 0.115$, 0.085, 0.07, and 0.035 (respectively) for OCRs 1, 1.5, 2, and 4 (MIT-E3 predictions): it would be unwise to extrapolate this trend beyond OCR = 4, since it is not obvious if there is an asymptotic value for $(T_p)_{50}$
- The rate of dissipation in the normally consolidated clay is much faster according to MIT-E3 than according to its predecessor, MIT-E1: this is caused by differences between the models' predictions for the shape of the initial pore pressures isochrone ($\Delta u_i = f[r/R]$)

- Modified Cam Clay produces even faster dissipation of pore pressures - mainly because it predicts the steepest gradients for $\Delta u_i$ of all the constitutive models

e) **Dissipation rates at different points along the pile**

Figure 3.17 illustrates the effect of distance behind the pile tip on the rate of dissipation of installation pore pressures. The diagram plots decay curves for six different locations along a cone-ended penetrometer: at the tip (T); on the cone face (F); at the cone's shoulder (S); and at three positions behind the tip (B1-B3). The initial pore pressures were calculated using a linear-elastic/perfectly-plastic soil model in conjunction with the strain path method.[60]

The rate at which the excess pore pressures decay near the bottom of the "pile" is clearly influenced by the position relative to the tip. However, the close agreement of the curves marked B1, B2, and B3 indicates that along the <u>shaft</u> the dissipation process is largely unaffected by z/R (for $z/R \geq 6.7$, and perhaps also for smaller values of z/R).

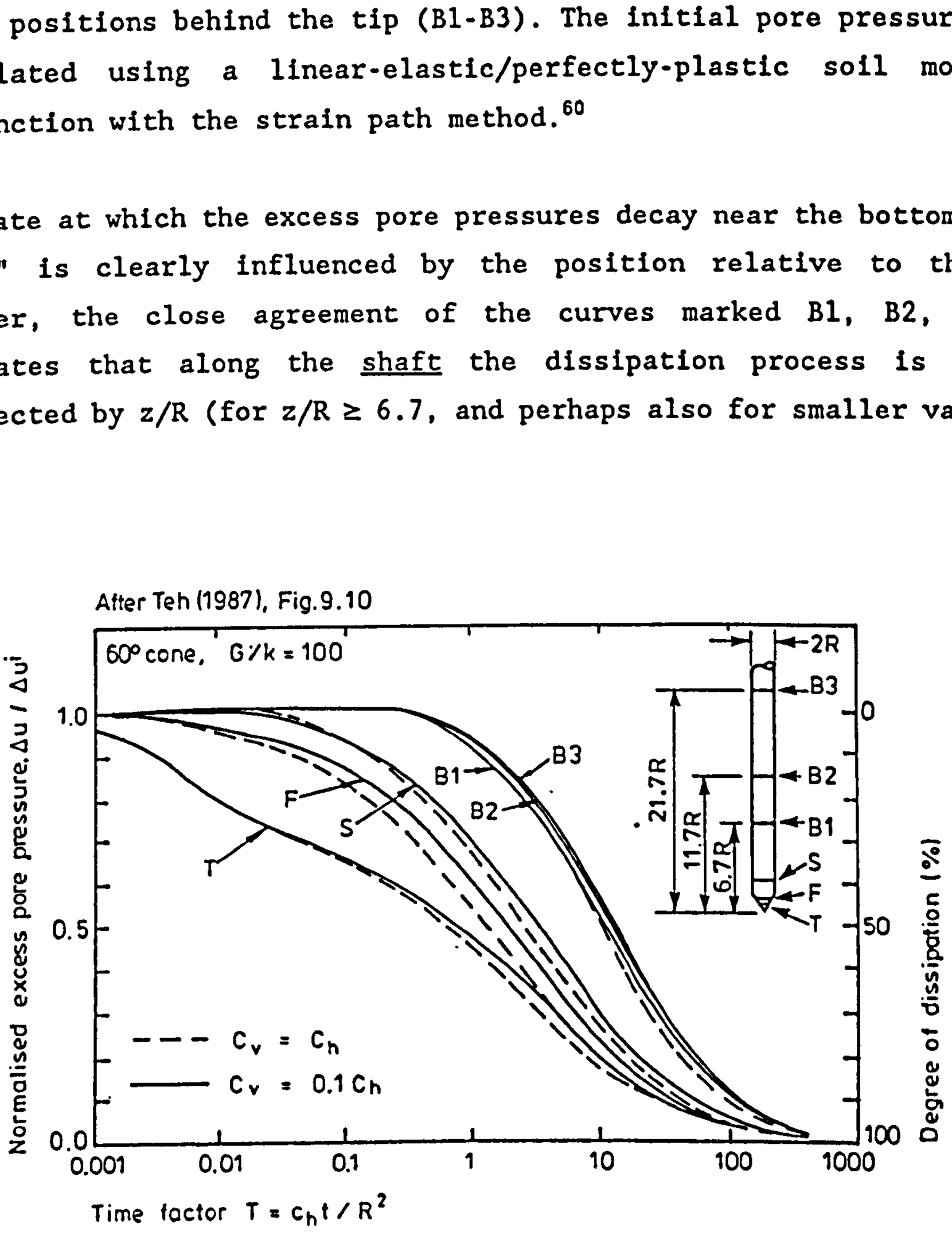



**Figure 3.17** Dissipation of pore pressures at various points along a pile shaft

Figure 3.17 also demonstrates how little the coefficient of vertical consolidation ($c_v$) affects the rate of dissipation, provided the time factor is defined in terms of $c_h$ (the horizontal coefficient). This has also been found by Levadoux and Baligh.[61]

The time factors predicted[62] by MIT-T1 for consolidation around a 60° cone penetrometer (installed in Boston blue clay) are listed in Table 3.6. The initial pore pressures were given by the strain path method.

Table 3.6 Time factors at various locations along a 60° cone penetrometer ($T = c_h t/R^2$)

| Location | z/R | $T_{20}$ | $T_{40}$ | $T_{50}$ | $T_{60}$ | $T_{80}$ |
|---|---|---|---|---|---|---|
| Shaft | 10 | 7.3 | 22 | 33 | 47 | 114 |
| Shoulder | 1.7 | 0.69 | 3.0 | 5.6 | 10 | 39 |
| Cone tip | 0 | 0.44 | 1.9 | 3.7 | 6.5 | 27 |

Figure 3.17 was drawn for a soil whose rigidity index (G/k) equals 100. When the dissipation curves for soils with other values of G/k are compared, there is a significant scattering of the results. Teh[63] attempted to counter this effect by defining a modified time factor $T^*$, as follows:

$$T^* = c_h t/R^2 / (G/k)$$

(N.b. since Teh's was a linear analysis, $c_h$, G, and k are all constants.)

Figure 3.18 demonstrates the relationship between $\Delta u/\Delta u_i$ and $T^*$ for location B1, for a wide range of values of G/k (from 25

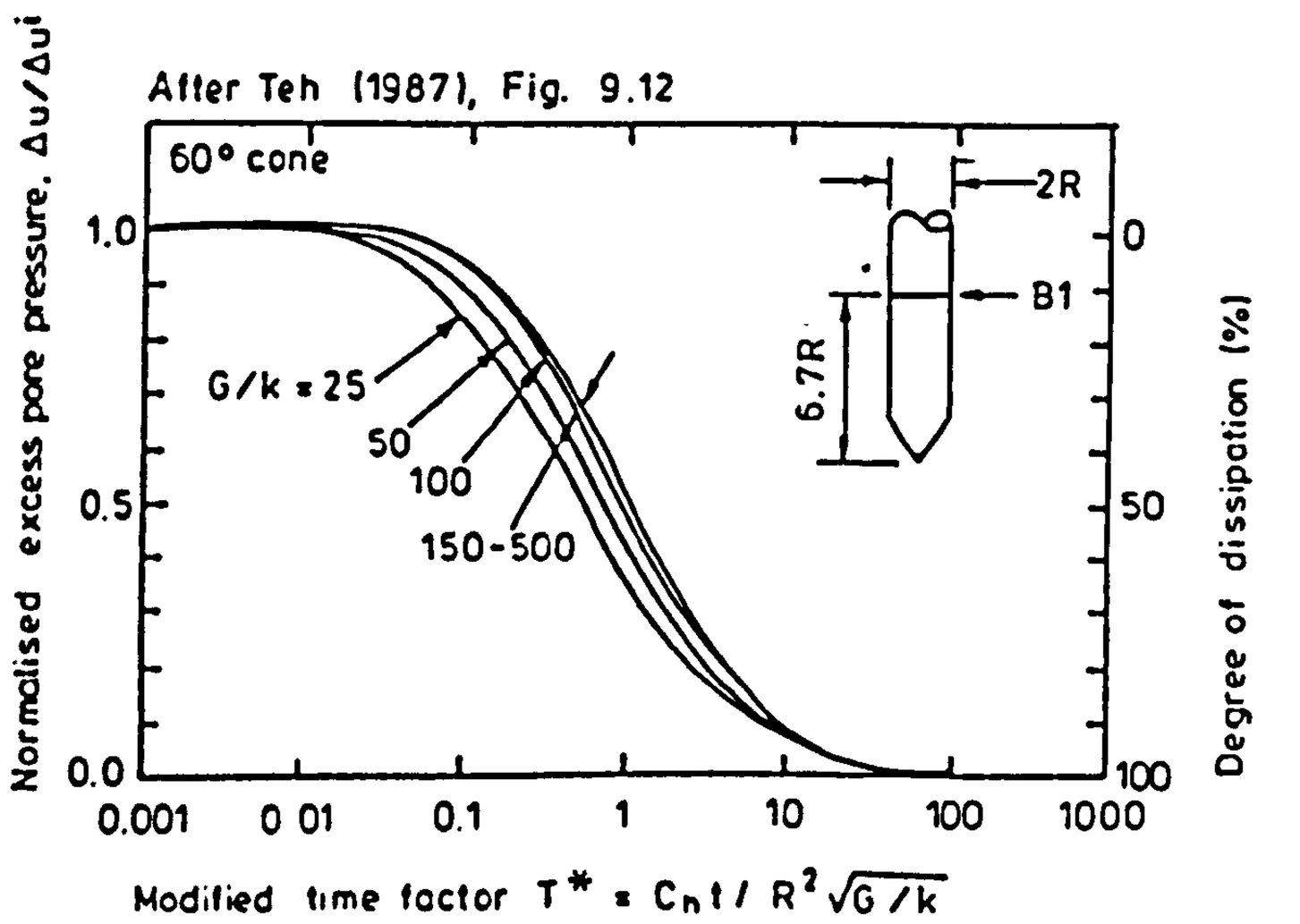



Figure 3.18 Pore pressure dissipation as a function of Teh's time factor $T^*$

to 500). The curves are reasonably close to one another, $T^*_{50}$ varying by a factor of two at most. Unfortunately, when the modified time factor is used the agreement between the dissipation curves for positions B1, B2, and B3 is not as good as that shown on Figure 3.17.

### 3.5.2 Radial total and effective stresses

a) Uncoupled consolidation analyses

The uncoupled consolidation analyses assume that there are no changes in total stress during the equalization period. This is not borne out by the experimental evidence from instrumented pile tests (see Chapters 4 and 10). Hence this section considers the results of the coupled analyses only.

b) Coupled consolidation analyses

Figure 3.19 illustrates how the radial total stress* ($\sigma_{rr}$) falls and the radial effective stress# ($\sigma'_{rr}$) rises during the equalization period for a point far behind the pile tip (z/R = 200). These predictions were obtained using a coupled consolidation analysis with the non-linear MIT-E3 constitutive model (input parameters appropriate for Boston blue clay). The (assumed) initial stresses in the soil were those given by the strain path method for the end of pile installation. The figure shows the results of four separate analyses, with OCRs equal to 1, 1.5, 2, and 4.

---

*$\sigma_{rr}$ (minus the original pore water pressure, $u_o$) has been normalized by its initial value at the start of equalization (also minus $u_o$). This ratio (which Whittle gives the symbol R) may be expressed in terms of the "normalized horizontal total stress" (H), defined here as:

$$H = (\sigma_{rr} - u_o)/\sigma'_{vo},$$

where $\sigma'_{vo}$ is the original vertical effective stress in the soil. It follows that:

$$R = (\sigma_{rr} - u_o)/((\sigma_{rr})_i - u_o) = H/H_i$$

#$\sigma'_{rr}$ has been normalized by the value at the <u>end</u> of equalization $(\sigma'_{rr})_c$; note that $\sigma'_{rr}/(\sigma'_{rr})_c = K/K_c$, where $K$ $(= \sigma'_{rr}/\sigma'_{vo})$

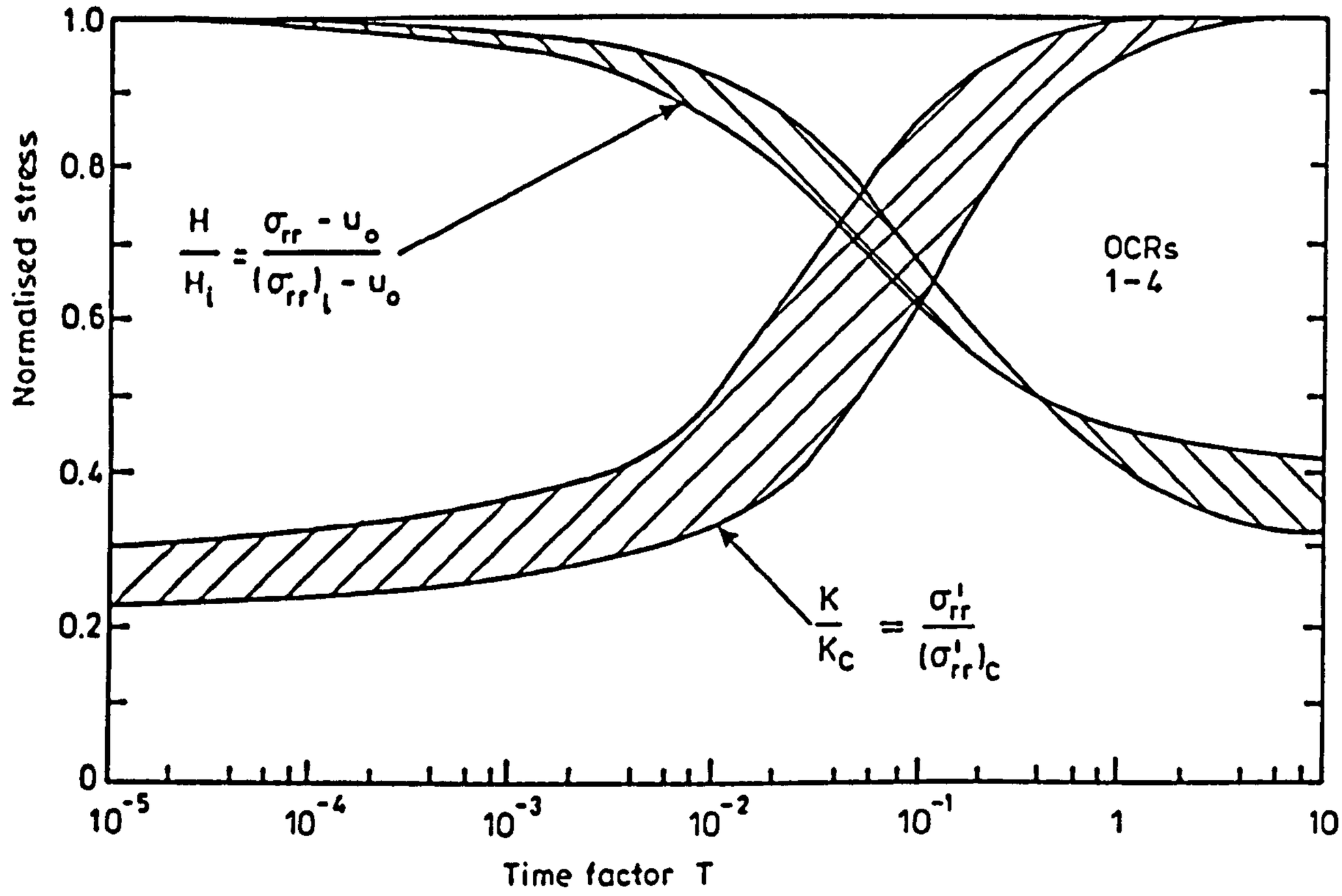



Figure 3.19 Changes in radial stress during equalization: initial stresses from SPM

The most striking conclusion to be drawn from Figure 3.19 is the relative insensitivity of both $H/H_i$ and $K/K_c$ to the value of OCR. This suggests that, provided we have reliable predictions for the <u>installation</u> stresses around a pile, then it is a fairly easy matter to obtain the stress conditions at the end of equalization (for a low OCR clay).

Furthermore, Figure 3.19 suggests that, for a sensitive clay with low OCR (less than 4), the normalized horizontal total stress at the end of equalization is only 35% of its value at the beginning, i.e.:

$$H_c/H_i = 0.35 \pm 0.06$$

(This also implies that the assumption made in linear consolidation analyses - that $\sigma_{rr}$ remains constant - is grossly in error.)

At the same time, the radial effective stress ($\sigma'_{rr}$) increases four fold, i.e.:

$$K_i/K_c = 0.25 \pm 0.04$$

This is the "set-up" effect in normally to lightly over-consolidated clays.

Table 3.7 summarizes various predictions for the "relaxation coefficient" $H_c/H_i$ and the "set-up coefficient" $K_i/K_c$, as obtained in coupled consolidation analyses using the Modified Cam Clay, MIT-E1, and MIT-E3

Table 3.7 Summary of radial total stresses during equalization for Boston blue clay (*for London clay)

| OCR | Soil model | $H_c/H_i$ SPM | $H_c/H_i$ CEM | $K_i/K_c$ SPM | $K_i/K_c$ CEM |
|---|---|---|---|---|---|
| 1-32 | MCC | - | 0.87 ±0.03* | - | 0.57* |
| 1-32 | MCC | 0.83# | 0.82 ±0.04 | 0.21# | 0.49 |
| 1 | MIT-E1 | 0.38 | 0.45 | 0.15 | 0.61 |
| 1-4 | MIT-E3 | 0.35 ±0.06 | 0.37# | 0.25 ±0.04 | 0.63# |

#At OCR = 1 only

models. All of the studies assume implicitly that z/R is large enough for the influence of the pile tip to be negligible. The initial stresses in the soil were obtained by either strain path or cavity expansion methods. There are two main points to note:

- The predictions for $H_c/H_i$ are controlled by features of the <u>soil model</u>, and are not particularly sensitive to the assumed initial stress conditions (i.e. whether obtained by the SPM or CEM)
- The predictions for $K_i/K_c$ are not greatly influenced by the choice of soil model, but they depend strongly on the <u>assumed initial stress conditions</u> (SPM or CEM)

The results of the instrumented pile tests at Canons Park allow $H_c/H_i$ and $K_i/K_c$ to be assessed for a heavily overconsolidated clay (refer to Chapter 14).

Finally, Table 3.8 gives the values of $K_c$ at the end of equalization, according to the various consolidation analyses mentioned above (by definition, $H_c = K_c$). Not only does $K_c$ vary from one soil model to the next, but it also depends to a large extent on the method used to analyze

Table 3.8 Summary of radial effective stresses at the end of equalization, for Boston blue clay & *London clay

| OCR | $K_0$ | Soil model | $K_c = (\sigma'_{rr})_c/\sigma'_{vo}$ SPM | CEM |
|---|---|---|---|---|
| 1.0 | 0.62* | MCC | - | 1.60* |
| | 0.53 | MCC | 1.26 | 1.46 |
| | 0.53 | MIT-E1 | 0.40 | 0.80 |
| | 0.48 | MIT-E3 | 0.37 | 0.72 |
| 1.5 | 0.55 | MIT-E3 | 0.58 | - |
| 2.0 | 0.72* | MCC | - | 2.50* |
| | 0.70 | MCC | - | 3.01 |
| | 0.58 | MIT-E3 | 0.70 | - |
| 4.0 | 0.94* | MCC | - | 4.01* |
| | 1.00 | MCC | - | 5.55 |
| | 0.75 | MIT-E3 | 1.13 | - |
| 8.0 | 1.25* | MCC | - | 6.66* |
| | 1.35 | MCC | - | 10.05 |
| 32.0 | 2.15* | MCC | - | 18.2* |
| | 2.75 | MCC | - | 34.2 |

pile installation. $K_c$ is, in many ways, the single most important parameter that these studies attempt to predict - clearly there is a long way to go before we can have confidence in choosing a suitable value of $K_c$ for design purposes.

### 3.5.3 Orientation of the principal stresses

According to consolidation analyses based on CEM initial stresses, at the end of equalization the soil adjacent to the pile is in a normally consolidated condition, irrespective of its original overconsolidation ratio (i.e. its OCR prior to pile installation). These studies also suggest that the radial stress is the *major* principal stress; and that the vertical and hoop stresses are equal *minor* principal stresses. Furthermore, the ratio of these stresses is close to the value of $K_0$ for the *undisturbed* normally consolidated clay. In other words:

$$(\sigma'_{rr})_c > (\sigma'_{zz})_c = (\sigma'_{\theta\theta})_c \approx K_0^{nc}(\sigma'_{rr})_c \ .$$

According to Whittle's[64] consolidation analyses, based on SPM initial stresses and using the MIT-E3 model, the principal stresses obey the following relationship:

$$(\sigma'_{rr})_c > (\sigma'_{zz})_c > (\sigma'_{\theta\theta})_c \approx K_0^{nc}(\sigma'_{rr})_c$$

The key difference between the cavity expansion and strain path predictions is the value of the vertical effective stress $(\sigma'_{zz})_c$.

Table 3.9 Orientation of principal stresses at the end of equalization

| Prediction/ assumption | $\sigma'_1$ | $\sigma'_3$ | Bishop's* b | $\sigma'_{zz}/\sigma'_{rr}$ | $\sigma'_{\theta\theta}/\sigma'_{rr}$ |
|---|---|---|---|---|---|
| MIT-E3/SPM† | $\sigma'_{rr}$ | $\sigma'_{\theta\theta}$ | 0.84-0.7 | 0.92-0.85 | 0.51 ±0.01 |
| MCC/CEM‡ | $\sigma'_{rr}$ | $\sigma'_{zz} = \sigma'_{\theta\theta}$ | 0 | 0.65 | 0.65 |
| $\beta$ method assumes... | $\sigma'_{zz}$ | $\sigma'_{rr} = \sigma'_{\theta\theta}$ | 0 | $1/K_0^{nc}$ | 1 |

$K_0^{nc}$ = †0.48; ‡0.55 (for Boston blue clay); *b = $(\sigma'_2-\sigma'_3)/(\sigma'_1-\sigma'_3)$

Table 3.9 summarizes these results and compares them with the stress conditions assumed in the beta method of pile design (see Chapter 2). There are clearly major differences between the three cases. However, it is not at all clear what significance these differences may have on pile behaviour during subsequent loading. This is a subject worthy of further research.

### 3.5.4 Effective stress paths during equalization

Figure 3.20 shows the effective stress paths that are followed by soil elements next to the pile wall during the equalization period. The re-compression curves (bottom diagram) of all four clays (OCRs 1-4) are roughly parallel to the virgin $K_0$-consolidation line of the undisturbed clay. However, whereas predictions based on Modified Cam Clay suggest that the re-compression

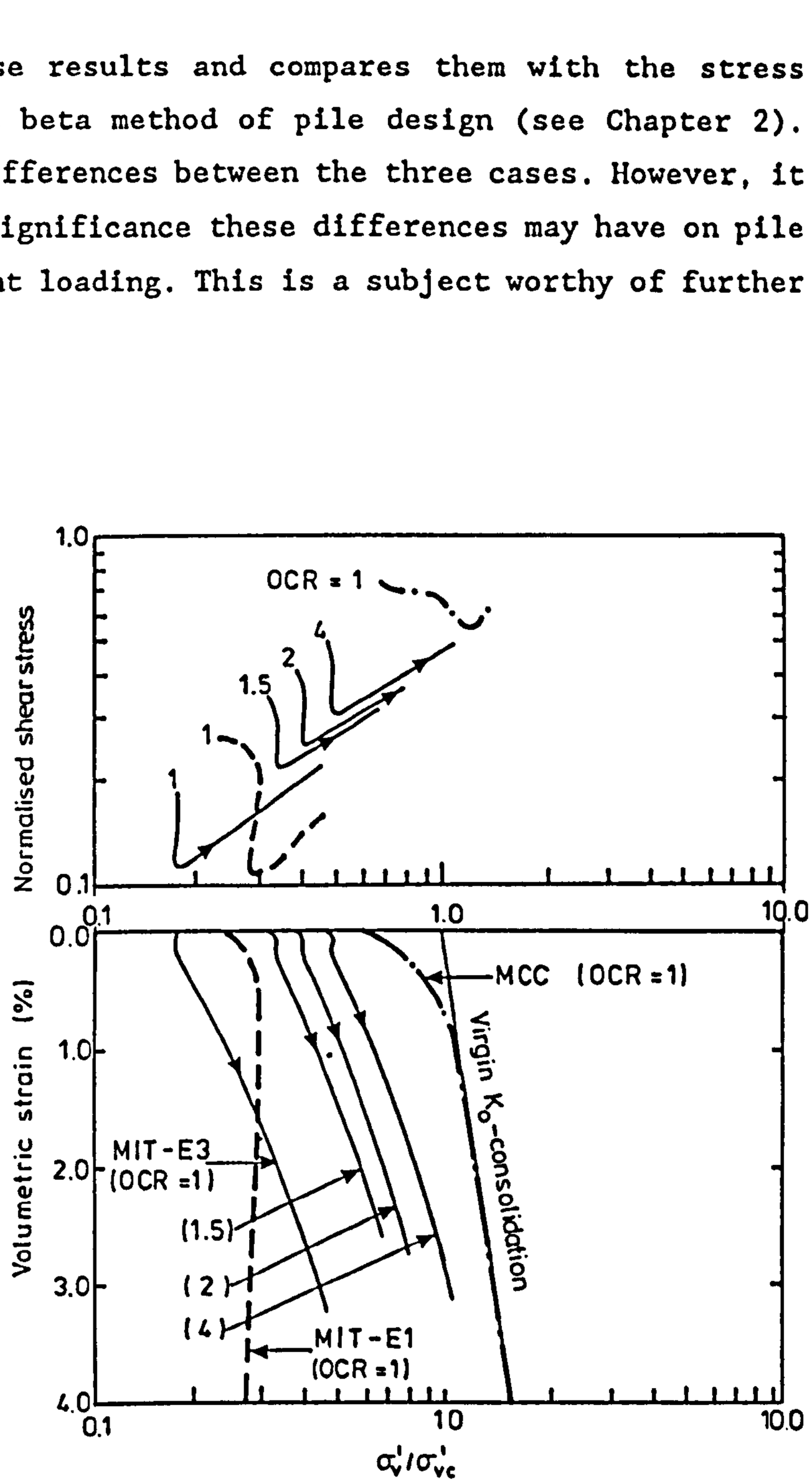



Figure 3.20 Effective stress paths during equalization: SPM (MIT-E3) predictions

curve eventually follows the $K_0$-consolidation line, according to MIT-E3 the re-compression curve runs parallel to the $K_0$-line but with a lower value of mean effective stress at any given voids ratio (see Figure 3.20). This behaviour reflects the intense shearing of the soil during pile installation, which completely alters the anisotropic structure of the clay next to the pile shaft, and thereby erases the soil's "memory" of its previous stress history.

## 3.6 BEHAVIOUR DURING LOADING

### 3.6.1 Key assumptions regarding pile loading

Although great efforts have been made to predict the stresses around driven piles at the end of installation and the subsequent equalization period, the same attention has not been given to predicting the soil's response to pile loading. The few studies that exist shed some light on the factors that govern this response, but there remain several unanswered questions that must be addressed if we are to obtain a clearer understanding of the problem.

The parameter of greatest importance is the average shaft friction mobilized at failure, $(f_s)_{av} = (1/L)\int_L \tau_{rz} dz$. The shear stress $\tau_{rz}$ is related to the radial effective stress ($\sigma'_{rr}$) and the coefficient of friction ($\mu$) *at the pile wall*, as follows:

$$\tau_{rz} = (\sigma'_{rr})_f \mu$$

where the subscript f denotes the stress state at failure.

But how do we determine the value of $\tau_{rz}$ when $(\sigma'_{rr})_f$ and $\mu$ depend on a large number of independent factors whose influence on pile behaviour is only poorly understood? These include:

- The degree of drainage (as governed by the rate of loading)
- The value of the radial effective stress $(\sigma'_{rr})_c$ at the end of equalization (see Section 3.5.2)
- Changes in $\sigma'_{rr}$ during pile loading
- Whether failure occurs in the soil itself or at the pile/soil interface
- Whether a residual shear surface was formed next to pile during installation
- The orientation of the principal stresses ($\sigma'_1$, $\sigma'_2$, and $\sigma'_3$)
- The direction of loading (i.e. tension or compression)

- Whether the soil is normally or over-consolidated state at the end of equalization

The remainder of this chapter comprises a series of essays on several of these topics, the purpose being to identify those aspects of pile behaviour where there is a consensus of opinion, and those which are still open to debate.

### 3.6.2 Drained or undrained loading?

There is little experimental evidence to suggest whether pile loading is an undrained, drained, or partially-drained process. The degree of drainage depends not only on the soil's permeability, but also on the rate at which the loads are applied. For example, it is common to assume that undrained conditions prevail during cyclic storm loading of offshore platforms; but that the foundations are drained when structures are commissioned over long periods of time (i.e. several months). When it comes to pile loading tests in clay soils, it is not at all certain what the degree of drainage is.

### 3.6.3 Stress changes during drained loading

Potts and Martins[65] conducted a parametric study into the behaviour of piles during drained and undrained loading, using the Modified Cam Clay model. They considered the case of i) a bored pile; and ii) a driven pile (for which they adopted cavity expansion initial stresses*). According to the latter analysis, the magnitude of the radial effective stress falls by 30-40% during drained loading, whereas the changes in $\sigma'_{zz}$ and $\sigma'_{\theta\theta}$ are insignificant in comparison (both increase by less than 4%). In other words:

$$(\sigma'_{rr})_f/(\sigma'_{rr})_c = 0.65 \pm 0.05$$

$$(\sigma'_{zz})_f/(\sigma'_{zz})_c \approx 1$$

and

$$(\sigma'_{\theta\theta})_f/(\sigma'_{\theta\theta})_c \approx 1$$

---

*$(\sigma'_{rr})_c = K_0^{nc}(\sigma'_{\theta\theta})_c = K_0^{nc}(\sigma'_{zz})_c$

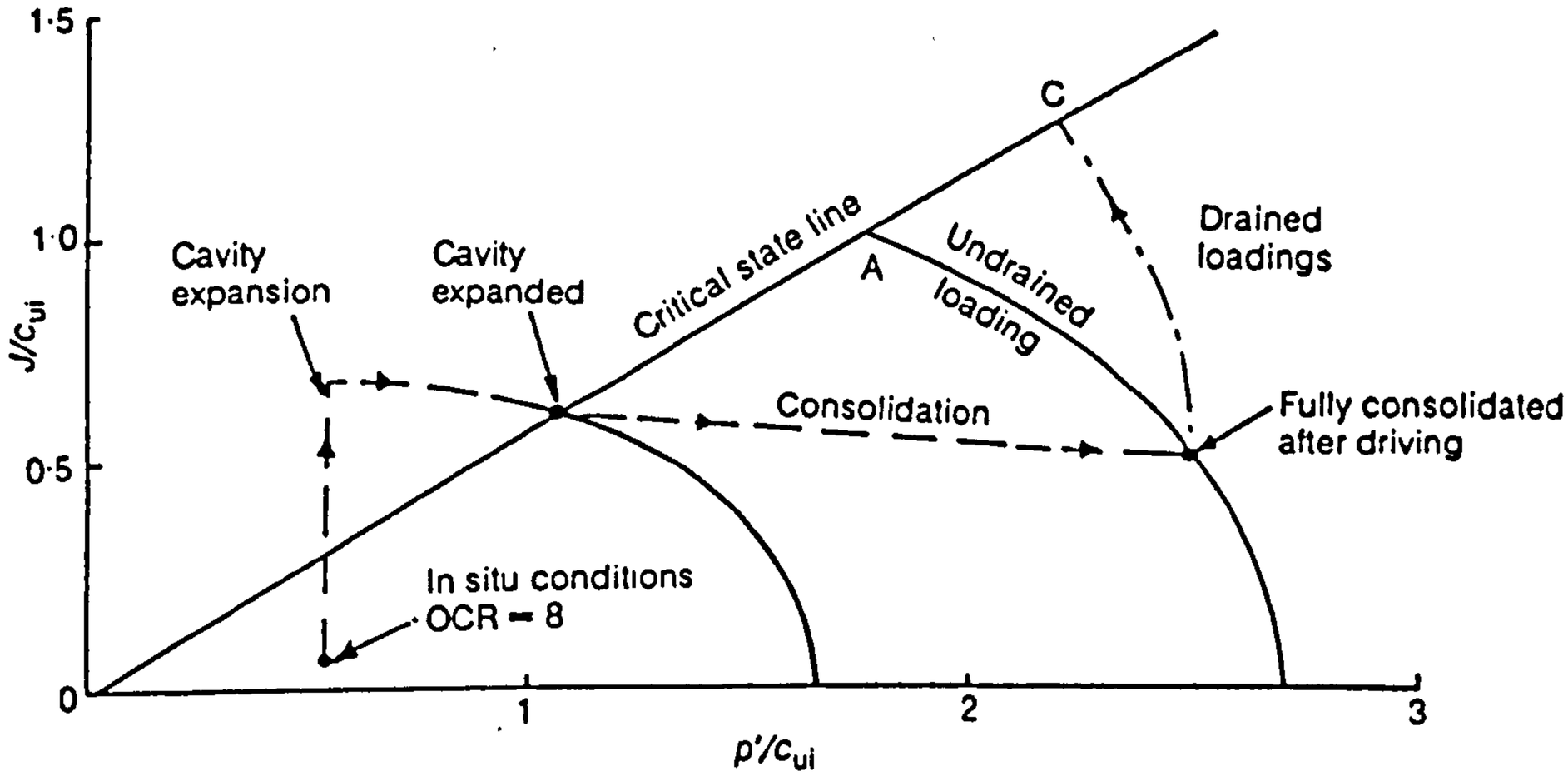



Figure 3.21 Stress paths followed during pile loading: CEM/MCC predictions

The stress paths followed during drained loading are illustrated in Figure 3.21.

### 3.6.4 Stress changes during undrained loading

Figure 3.21 also shows the stress paths followed during *undrained* loading of a driven pile, according to the analysis by Potts and Martins (described in the previous section). The changes in effective stress are much more pronounced than for the drained case: the radial effective stress falls by ≈60%, and the vertical and hoop effective stresses drop by ≈20%. In other words:

$$(\sigma'_{rr})_f/(\sigma'_{rr})_c \approx 0.4$$

$$(\sigma'_{zz})_f/(\sigma'_{zz})_c \approx 0.8,$$

and

$$(\sigma'_{\theta\theta})_f/(\sigma'_{\theta\theta})_c \approx 0.8$$

(Note, however, that these changes would be far less dramatic if the soil were in an overconsolidated state at the end of equalization.)

The pore pressures generated on undrained loading are much smaller and far more localized than those produced on pile driving: hence the time required for the pore pressures to dissipate is short. Thus it is questionable whether pile loading is *entirely* undrained.

### 3.6.5 Analogy between pile loading and simple shear tests

Randolph and Wroth[66] argued that the mode of shearing around a pile is very similar to that in a simple shear test - as illustrated in Figure 3.22. The radial effective stress ($\sigma'_{rr}$) and shear stress ($\tau_{rz}$) acting on the pile are analogous to $\sigma'_y$ and $\tau_{yx}$ in the laboratory situation.

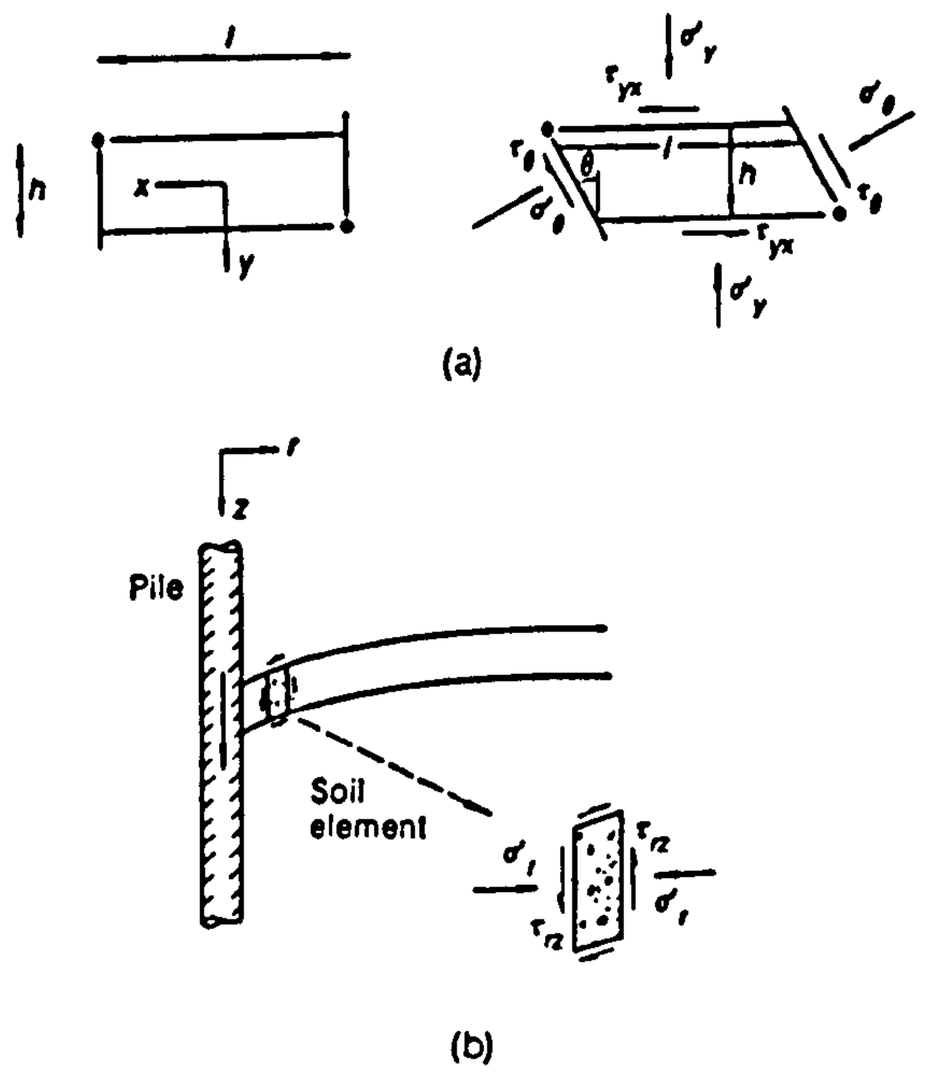



Figure 3.22 Analogy between undrained loading of a pile and the stress paths in a simple shear test

Experimental evidence supports the hypothesis that failure in the simple shear tests is initiated by the formation of rupture planes parallel to the original direction of the major principal stress, $\sigma'_1$ (i.e. $\sigma'_y$). Randolph and Wroth argued that, in the case of a driven pile, $\sigma'_1 = \sigma'_{rr}$, and hence failure in the soil occurs when one of the planes of maximum stress obliquity is *horizontal* - even though during plunging failure the rupture surface must be *vertical* (parallel to the pile wall). For Randolph and Wroth's hypothesis to hold, the principal stresses must rotate following the onset of failure, and $\tau_{rz}$ must fall from a maximum to an "ultimate" value, given by $\tau_{rz}/\sigma'_{rr} = \tan \phi$.

### 3.6.6 Strain path predictions based on the MIT-E3 model

The stress paths followed during undrained loading, according to the MIT-E3 constitutive model, are shown in Figure 3.23 for four different over-consolidation ratios.[67] The initial stresses were those given by the strain path method, allowing for full consolidation after pile installation. On this diagram, the shear stress $\tau_{rz}$ and the radial effective stress $\sigma'_{rr}$ have both been normalized by the original vertical

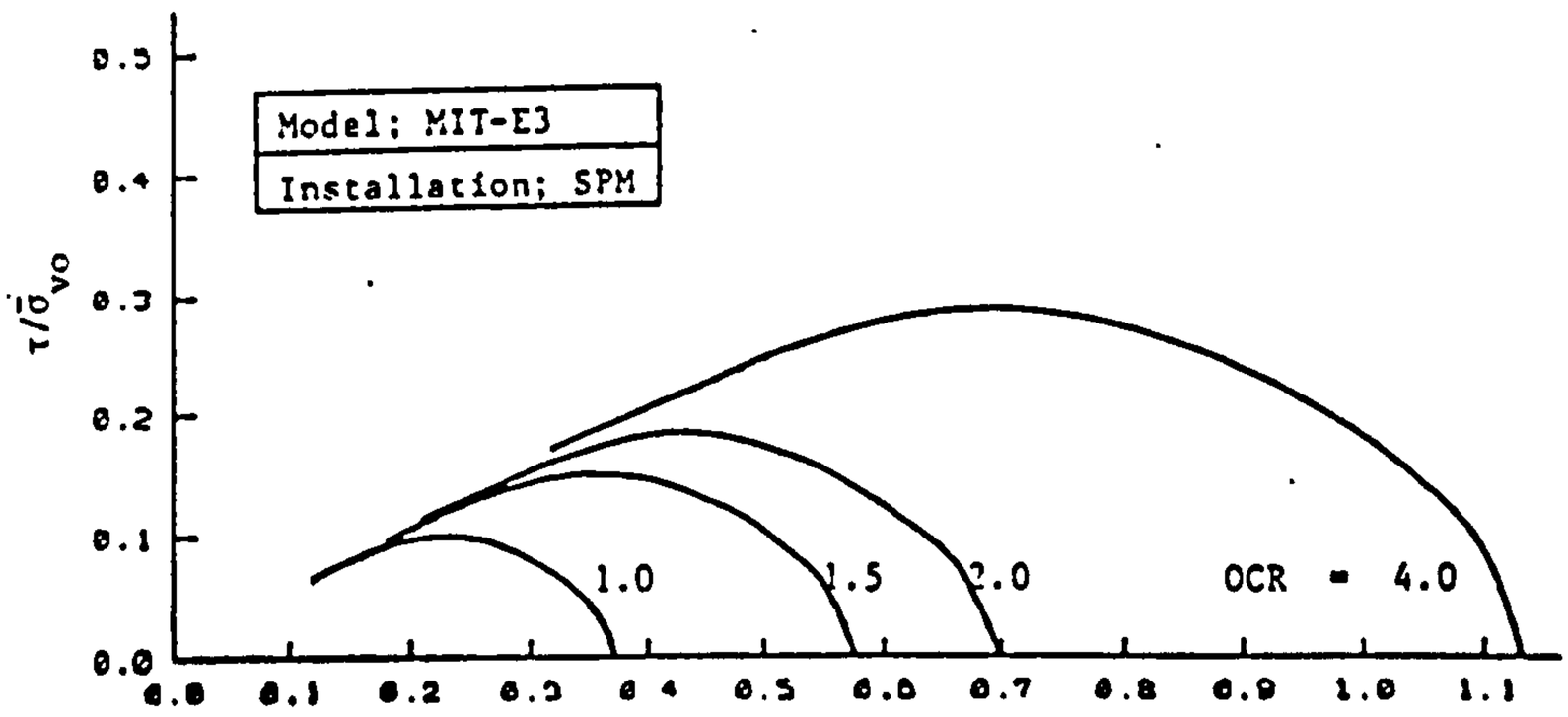



Figure 3.23 Stress paths followed during undrained loading: MIT-E3 predictions

effective stress, $\sigma'_{vo}$. If they had been normalized by $(\sigma'_{rr})_c$ instead, then the four curves would virtually coincide.

If failure occurs when the shear stress $\tau_{rz}$ reaches a maximum, then:

$$(\tau_{rz})_f/(\sigma'_{rr})_c = \rho = 0.26 \pm 0.01$$

and $$(\sigma'_{rr})_f/(\sigma'_{rr})_c \approx 0.6$$

### 3.6.7 Predictions of the coefficient of friction

a) Introduction

Most soils when sheared either dilate or contract, and, in order to satisfy the boundary conditions at the pile/soil interface, complex stress changes may take place next to the pile wall during loading. The results of any analysis of this process are governed by the kinematic aspects of the chosen constitutive law.[68] The following paragraphs summarize predictions of the coefficient of friction ($\mu$), based on a number of different assumptions, and discusses whether there is any experimental evidence to support or deny them.

b) Sliding at the pile/soil interface

If pile failure occurs as a result of slippage between the soil and the pile wall, then the coefficient of friction is given by the equation:

$$\mu = \tan \delta$$

where $\delta$ is the angle of friction at the pile/soil interface. Implicit in this formula is the assumption that the soil surrounding the pile does not reach a limiting stress condition before slippage occurs. Situations in which $\delta$ is very much smaller than the soil's friction angle ($\phi$) could cause the pile's load capacity to be limited by interface sliding. For example, it appears that in the Building Research Establishment's pile tests at Cowden the presence of mill varnish on the piles' outer surface had a significant (and detrimental) effect on their overall load capacity.[69]

In cases where interface sliding occurs it seems likely that the pile's surface roughness will have an important bearing on the angle of friction mobilized at the pile wall (i.e. on the ratio $\delta/\phi$).

c) Failure in the surrounding soil (continuum shearing)

The alternative to sliding at the pile/soil interface is for failure to occur *in the soil itself* (at a short distance from the pile wall). Assuming that the stresses acting on the failure surface are given by the Mohr-Coulomb criterion, $(\tau/\sigma'_n)_f = \tan \phi$, then the stresses at the interface ($\tau_{rz}$, $\sigma'_{rr}$) can be determined <u>provided the orientation of the failure surface is known</u>. Figure 3.24 illustrates two common assumptions regarding the stress states at failure:

- Case (a): failure occurs on a vertical shear surface, when the Mohr's circle first touches the Coulomb envelope (point A); hence $\mu$ ($= \tau_{rz}/\sigma'_{rr}$) $= \tan \phi$
- Case (b): failure occurs on an inclined surface, with the maximum shear stress acting on a vertical plane (point A); hence $\mu = \sin \phi$

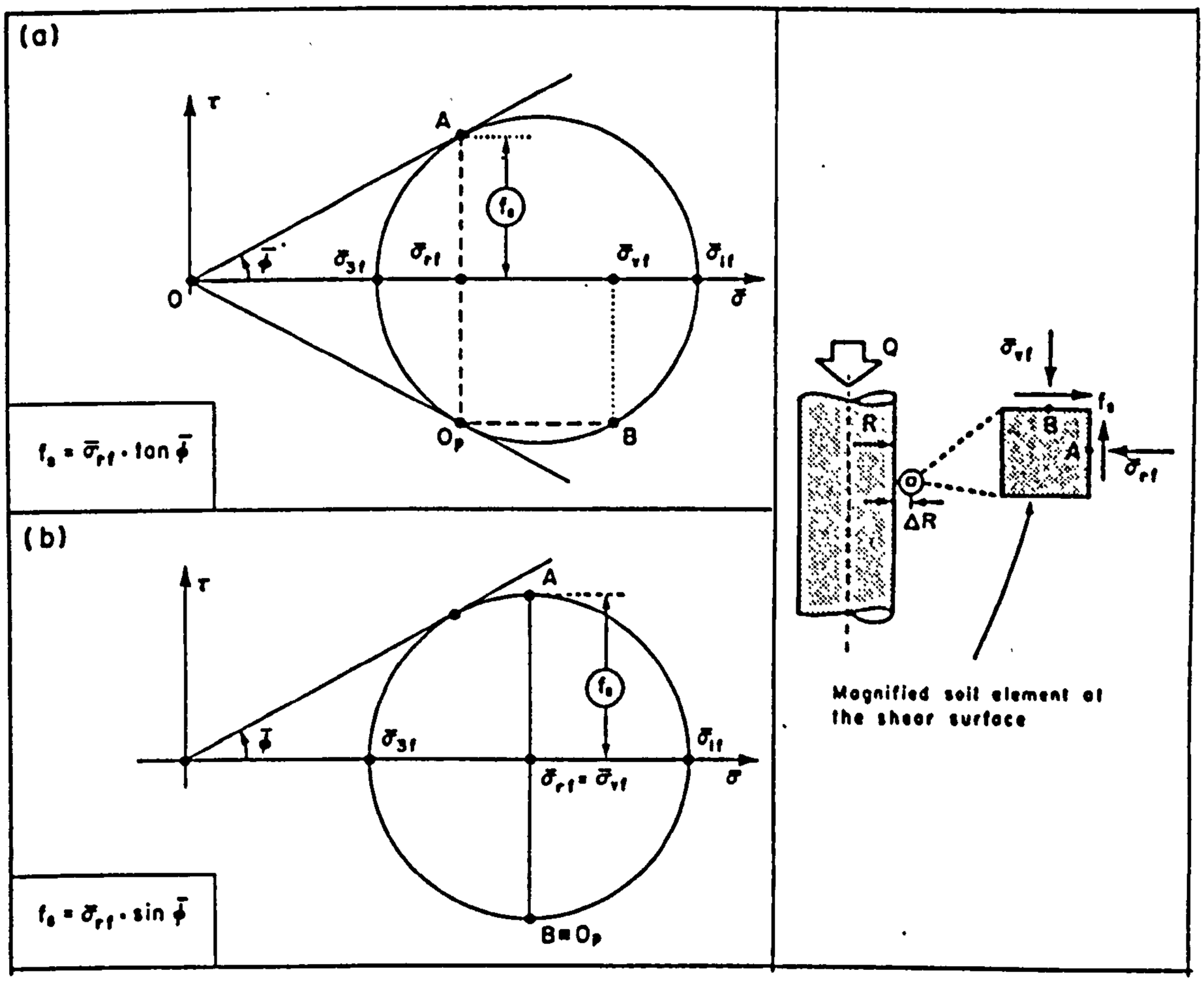



Figure 3.24 Stress states for failure in the soil under two common assumptions

From the results of direct simple shear (DSS) tests on Boston blue clay, Baligh and Kavvadas[70] argued that significant rotation of the principal stresses takes place during pile loading; and that - at failure - the magnitude of $\mu$ is somewhere between the two values given above, i.e. $\sin \phi < \mu < \tan \phi$. (Note that for $\phi$ = 20-30°, $\sin \phi$ is 6-13% smaller than $\tan \phi$.)

As mentioned earlier, the results of any analysis of pile loading will be influenced by details of the constitutive law used to model soil behaviour. If the soil is <u>isotropic elastic</u>, then the radial and vertical effective stresses remain constant[71] during pile loading and hence $(\sigma'_{rr})_f - (\sigma'_{rr})_c$. However, this assumption leads to an equation for $\mu$ which is in strong disagreement with the results of DSS tests and model pile tests, and hence is unacceptable.[72]

If the soil obeys the Mohr-Coulomb criterion, and is elastic up to failure, then the coefficient of friction $\mu$ is strongly dependent on the value of $\sigma'_{rr}/\sigma'_{zz}$ at the beginning of pile loading. This is contrary to the results of Martins' laboratory experiments,[73] on model piles installed in kaolin (see Chapter 4).

Elasto-plastic models (such as Modified Cam Clay) that assume the soil reaches a critical state condition* at failure predict a unique value of $\mu$ at peak load, independent of the initial stress conditions:

$$\mu = \sin \phi$$

This result is a direct consequence of assumptions regarding the directions of the principal stress and strain increments and would hold for *any* elasto-plastic soil model that made the same assumptions. (See the paper by Potts and Gens[74] for further details.) Since clays that dilate on shearing tend to form rupture planes before they reach critical state conditions, it might be argued that this result is not relevant to heavily overconsolidated clays. However, according to the consolidation analyses described in Section 3.5.4, the soil next to the pile wall is in a *normally* consolidated state at the end of equalization, irrespective of its initial overconsolidation ratio. Hence it is possible that this result may hold for a wide range of initial OCRs. Interestingly, the results of Martins' model pile tests are in close agreement with this equation for $\mu$.

d) Failure in the soil on a residual shear surface

Finally, we should consider the possibility of failure occurring along a residual shear surface close to and parallel with (but not at) the pile/soil interface. (The case of sliding at the interface is dealt with in Section 3.6.7.b.) The skin friction mobilized by the pile is controlled by the residual shear strength of the clay, and is given by:

---

*In other words undergoes no change in volume on further shearing; since the vertical ($\epsilon_{zz}$) and hoop ($\epsilon_{\theta\theta}$) strains are zero at the pile wall, so too is the radial strain $\epsilon_{rr}$

$$\mu = \tan \phi_R$$

where $\phi_R$ is the (residual) angle of friction on the shear surface.

Laboratory experiments have shown that - when sheared to large displacements - clay soils can form highly polished failure planes, with residual angles much smaller than the soil's critical state angle ($\phi_{cs}$).

The likelihood of residual shearing occurring depends on the clay's mineralogy and on the proportion of platy particles that it contains. Typically, it affects medium and high plasticity clays ($I_p > 26\%$) subject to large deformations. The *rate* of displacement can have a marked influence on the value of $\phi_R$: at slow rates "sliding" can occur between the particles (with $\phi_R << \phi_{cs}$), whereas at fast rates "turbulent" shearing takes place (with $\phi_R \approx \phi_{cs}$). Between these extremes there is a "transitional" mode, part sliding, part turbulent, in which $\phi_R$ is strongly dependent on the rate of displacement. See Chapter 5 and Appendix 3 for a more detailed explanation of these phenomena.

### 3.6.8 Orientation of the principal stresses

The orientation of the principal stresses at the end of equalization could have a significant effect on a pile's behaviour during loading.

Potts and Martins' study (see Section 3.6.3) considered two of the three cases listed in Table 3.9, i.e.:

$$K(\sigma'_{zz})_c = (\sigma'_{rr})_c = (\sigma'_{\theta\theta})_c$$

and

$$K(\sigma'_{zz})_c = (\sigma'_{rr})_c = K(\sigma'_{\theta\theta})_c$$

where values of K equal to 0.5, 1.0, and 2.0 were considered. However, Whittle's[75] strain path solution based on the MIT-E3 model suggests that the stresses at the end of equalization are given by:

$$K_0^{nc}(\sigma'_{zz})_c = 0.9K_0^{nc}(\sigma'_{rr})_c = (\sigma'_{\theta\theta})_c$$

Further research is needed to assess the significance of this particular combination of stresses on the pile's behaviour during loading.

### 3.6.9 Direction of loading

None of the theories discussed herein makes any distinction between compression and tension loading. In all cases it is assumed that there are no residual shear stresses acting on the pile, and that the soil's angle of friction is the same for both cases. Further research is needed to assess whether these are reasonable assumptions and whether they have any bearing on the predictions of pile capacity.

### 3.6.10 Summary of Section 3.6

A pile's shaft capacity during loading depends on the shear stress mobilized at the pile wall ($\tau_{rz}$). This is related to the radial effective stress at the pile/soil interface ($\sigma'_{rr}$) and the coefficient of friction ($\mu$). At failure:

$$\tau_{rz} = \mu(\sigma'_{rr})_f$$

According to the theories outlined in this section:

$$(\sigma'_{rr})_f/(\sigma'_{rr})_c = 0.4\text{-}0.7$$

depending on the drainage conditions and on how the pile loading process has been modelled. The friction coefficient $\mu$ is governed by how and where failure occurs, and could be given by any one of the following equations. For failure...

At the pile/soil interface: $\mu = \tan \delta$

In the soil: $\sin \phi_{cs} \leq \mu \leq \tan \phi_{cs}$

On a residual surface: $\mu = \tan \phi_R$

The following chapter examines the results of instrumented pile tests in clay soils, to see what evidence there is to support one or other of these predictions of pile behaviour.

## 3.7 NOTES AND REFERENCES

[1]Terzaghi K. (1936). The shearing resistance of saturated soils and the angle between the planes of shear. Proc. 1st Int. Conf. Soil Mech. & Fdn Engng, Cambridge, 1, pp161-165.

[2]Bishop R.F., Hill R., and Mott N.F. (1945). The theory of indentation and hardness tests. Proc. Phys. Soc., 57, Part 3, No 321, pp147-159; Hill R. (1950). The mathematical theory of plasticity. Oxford Univ. Press, London, 356pp.

[3]Gibson R.E. and Anderson W.F. (1961). In-situ measurement of soil properties with the pressuremeter. Civ. Engng & Publ. Works Review, 56(658), May 1961, pp615-618.

[4]Butterfield R. and Bannerjee P.K. (1970). The effect of porewater pressures on the ultimate bearing capacity of driven piles. Proc. 2nd Southeast Asian Conf. Soil Mech. & Fdn Engng, Singapore, pp385-384.

[5]Nishida appears to have worked on the problem a few years earlier than Butterfield and Bannerjee (whose paper was published in 1970). See: Nishida Y. (1962). Correspondence. Géotechnique, 13(1), pp90.

[6]Baligh M.M. (1985). Strain path method. J. Geotech. Engng, Am. Soc. Civ. Engrs, 111(9), pp1108-1136. See p1110.

[7]Bishop, Hill, and Mott (1945), loc. cit.; Hill (1950), loc. cit.

[8]Gibson and Anderson (1961), loc. cit.

[9]Nishida Y. (1964). A basic calculation of the failure zone and the initial pore pressure around a driven pile in clay. Proc. 2nd Asian Regional Conf. Soil Mech. & Fdn Engng, Tokyo, 1, pp217-219.

[10]Butterfield and Bannerjee (1970), loc. cit.

[11]Vesic A.S. (1972). Expansion of cavities in infinite soil mass. J. Soil Mech. & Fdns Div., Am. Soc. Civ. Engrs, 98(SM3), pp265-290.

[12]Randolph M.F and Wroth C.P. (1979). An analytical solution for the consolidation around a driven pile. Int. J. Num. & Anal. Methods in Geomechanics, 3, pp217-229.

[13]Ladanyi B. (1963). Expansion of a cavity in a saturated clay medium. J. Soil Mech. & Fdns Div., Am. Soc. Civ. Engrs, 89(SM4), pp127-161.

[14]Carter J.P., Randolph M.F., and Wroth C.P. (1979). Stress and pore pressure changes in clay during and after the expansion of a cylindrical cavity. Int. J. Numer. Anal. Methods Geomech., 3, pp305-322.
Randolph M.F., Carter J.P., and Wroth C.P. (1979). Driven piles in clay - the effects of installation and subsequent consolidation. Géotechnique, 29(4), pp361-393.

Wroth C.P., Carter J.P., and Randolph M.F. (1979). Stress changes around a pile driven into cohesive soil. In "Recent developments in the design and construction of piles", Instn Civ. Engnrs, London, pp345-354.

[15]Including the MIT-E models reviewed in Section 3.3.

[16]Baligh (1985), loc. cit.

[17]Lambe T.W. (1967). The stress path method. J. Soil Mech. & Fdns Div., Am. Soc. Civ. Engrs, 93(SM6), pp309-331.

[18]This is a simplified version of the presentation given by Baligh (1985), loc. cit., p1113 and Figure 1.

[19]Baligh M.M. (1984). The Simple-Pile Approach to pile installation in clays. In "Analysis and Design of Pile Foundations" (ed. J.R. Meyer). Proc. Symp. on Codes and Standards, ASCE National Conv., San Francisco, 1984, pp310-330.

[20]Levadoux J.-N. (1980). Pore pressures in clays due to cone penetration. PhD Thesis, Massachusetts Institute of Technology, Cambridge, Mass.

[21]Roscoe K.M. and Burland J.B. (1968). On the generalized stress-strain behaviour of 'wet' clay. In "Engineering Plasticity", ed. J. Heyman and F.A. Leckie, Cambridge Univ. Press, pp535-610.

[22]Gens A. and Potts D.M. (1987). The use of critical state models in numerical analysis of geotechnical problems: a review. In "Computational Plasticity", ed. D.R.J. Owen et al., Pineridge Press, pp1491-1525.

[23]Randolph, Carter, and Wroth (1979), loc. cit.

[24]Kavvadas M. (1982). Non-linear consolidation around driven piles in clays. PhD Thesis, Mass. Inst. of Technology, 592pp. See p254.

[25]Potts D.M. and Gens A. (1984). The effect of the plastic potential in boundary value problems involving plane strain deformation. Int. J. Num. & Anal. Methods in Geomechanics, 8, pp259-286.

[26]Kavvadas (1982), loc. cit.

[27]Azzouz A.S. and Baligh M.M. (1984). Behavior of friction piles in plastic Empire clays. Research Report No R84-14, MIT Dept Civ Engng, Cambridge, Mass., 2 vols, 619pp.

[28]Whittle A.J. (1987). A constitutive model for overconsolidated clays with application to the cyclic loading of friction piles. ScD Thesis, Massachusetts Institute of Technology, 641pp. See p149.

[29]Whittle A.J., Baligh M.M., Azzouz A.S., and Malek A.M. (1988). A model for predicting the performance of TLP piles in clays. Proc. 5th Int. Conf. on the Behaviour of Offshore Structures (BOSS '88), Delft, pp97-112. Elsevier, Amsterdam.

[30]Randolph M.F., Steenfelt J.S., and Wroth C.P. (1979). The effect of pile type on design parameters for driven piles. Proc. 7th Eur. Conf. Soil Mech. & Fdn Engng, Brighton, 2, pp107-114.

[31]Steenfelt J.S., Randolph M.F., and Wroth C.P. (1981). Instrumented model piles jacked into clay. Proc. 10th Int. Conf. Soil Mech. & Fdn Engng, Stockholm, 2, pp857-864.

[32]Francescon M. (1983). Model pile tests in clay. Stresses and displacements due to installation and axial loading. PhD Thesis, Univ. of Cambridge, 110pp + figures.

[33]Cooke R.W. and Price G. (1973). Strains and displacements around friction piles. Proc. 8th Int. Conf. Soil Mech. & Fdn Engng, Moscow, 2, pp53-60.

[34]Steenfelt, Randolph, and Wroth (1981), loc. cit.

[35]Francescon (1983), loc. cit., pp52-53.

[36]Baligh (1984), loc. cit.

[37]Randolph, Steenfelt, and Wroth (1979), loc. cit.

[38]Randolph, Carter, and Wroth (1979), loc. cit., p365.

[39]Ladanyi (1963), loc. cit., p157.

[40]Randolph, Carter, and Wroth (1979), loc. cit., p372.

[41]Jardine R.J., Fourie A., Maswoswe J., and Burland J.B. (1985). Field and laboratory measurements of soil stiffness. Proc. 11th Int. Conf. Soil Mech. & Fdn Engng, San Francisco, 2, pp511-514.

[42]Randolph, Carter, and Wroth (1979), loc. cit., investigated the effect of different values of G for overconsolidated Boston Blue Clay (OCR = 8). The first value was based on the relationship $G = 0.5K_{max}$ (where $K_{max}$ = the maximum value of the elastic bulk modulus ever reached during the soil's history), from which G/k = 100 (Case D). The second value of G was based on the current mean effective stress in the soil (see p368), from which G/k = 22 (Case F). As Figure 3.6 shows, the value of G/k governs the changes in total stress acting at the pile wall.

[43]Kavvadas (1982), loc. cit.

[44]Massarsch K.R. (1976). Soil movements caused by pile driving in clay. Report No 6, Dept of Soil and Rock Mechanics, Roy. Inst. of Technology, Sweden, 269pp.

[45]Bishop A.W. and Hight D.W. (1977). The value Of Poisson's ratio in saturated soils and rocks stressed under undrained conditions. Géotechnique, 27(3), pp369-384.

[46]Vesic (1972), loc. cit.

[47]Henkel D.J. (1960). The shear strength of saturated remoulded clays. Proc. Research Conf. Shear Strength of Cohesive Soils, Boulder, Colorado, p551ff.

[48]Jardine R.J. (1985). Investigations of pile-soil behaviour, with special reference to the foundations of offshore structures. PhD Thesis, Univ. of London (Imperial College), 2 vol., 789pp. See Figure 7.36.

[49]Randolph, Carter, and Wroth (1979), loc. cit.

[50]Sills G.C. (1975). Some conditions under which Biot's equations of consolidation reduce to Terzaghi's equation. Géotechnique, 25(1), pp129-132.

[51]Levadoux J.-N. and Baligh M.M. (1986). Consolidation after undrained piezocone penetration. I: Prediction. J. Geotech. Engng, Am. Soc. Civ. Engrs, 112(7), pp707-726.

[52]Levadoux J.-N. and Baligh M.M. (1980). Pore pressures during cone penetration in clays. MIT Research Report No R80-15. Order no 666, 310pp. See p723.

[53]Soderberg L.O. (1962). Consolidation theory applied to foundation pile time effects. Géotechnique, 12(3), pp217-225.

[54]Carter, Randolph, and Wroth (1979), loc. cit.

[55]Randolph, Carter, and Wroth (1979), loc. cit.

[56]Kavvadas M. and Baligh M.M. (1982). Non-linear consolidation analyses around pile shafts. Proc. 3rd Int. Conf. on the Behaviour of Offshore Structures (BOSS '82), Boston, 1, pp325-337. Hemisphere Pub., Washington.

[57]Randolph and Wroth (1979), loc. cit.

[58]Randolph and Wroth (1979), loc. cit.

[59]Whittle (1987), loc. cit.

[60]Teh C.-I. (1987). An analytical study of the cone penetration test. DPhil Thesis, Univ. of Oxford.

[61]Levadoux and Baligh (1986), loc. cit.

[62]Baligh M.M. and Levadoux J.-N. (1986). Consolidation after undrained piezocone penetration. II: Interpretation J. Geotech. Engng, Am. Soc. Civ. Engrs, 112(7), pp727-745.

[63]Teh (1987), loc. cit.

[64]Whittle (1987), loc. cit.

[65]Potts D.M. and Martins J.P. (1982a). The shaft resistance of driven piles in clay. Proc. 2nd Int. Conf. on Num. Methods in Offshore Piling, Austin, Texas, pp215-238.

[66]Randolph M.F. and Wroth C.P. (1981). Application of the failure state in undrained simple shear to the shaft capacity of driven piles. Géotechnique, 31(1), pp143-147.

[67]Whittle (1987), loc. cit.

[68]Potts D.M. and Martins J.P. (1982b). The shaft resistance of axially loaded piles in clay. Géotechnique, 32(4), pp369-386.

[69]Ove Arup and Partners (1986). Research on the behaviour of piles as anchors for buoyant structures. Dept of Energy, Offshore Technology Report, OTH 86 215. HMSO, London, 80pp.

[70]Baligh M.M. and Kavvadas M. (1980). Axial static capacity of offshore friction piles in clays. I. Evaluation of existing methods. Research Report No R80-32, Massachusetts Institute of Technology, Cambridge, Mass., 221pp. See Chapter 6 and especially p143.

[71]Lopez F. de Rezende (1979). The undrained bearing capacity of piles and plates studied by the finite element method. PhD Thesis, Univ. of London (Imperial College).

[72]See Baligh and Kavvadas (1980), loc. cit., pp141-146. The equation is:

$$\mu = \sqrt{[(s'\sin\phi/\sigma'_{rr})^2 + (t/\sigma'_{rr})^2]}$$

where $s' = \frac{1}{2}(\sigma'_{zz} + \sigma'_{rr})$ and $t' = \frac{1}{2}(\sigma'_{zz} - \sigma'_{rr})$. For this equation to match the results of DSS tests would require angles of friction in excess of 45°.

[73]Chandler R.J. and Martins J.P. (1982). An experimental study of skin friction around piles in clay. Géotechnique, 32(2), pp119-132.

[74]Potts and Martins (1982b), loc. cit.

[75]Whittle (1987), loc. cit.

# Chapter 4

# Review of instrumented pile tests

# CONTENTS OF CHAPTER 4


4.1 INTRODUCTION . . . . . 128
4.1.1 The purpose of instrumentation 128
4.1.2 Outline of Chapter 4 129
4.2 SURVEY OF PREVIOUS INSTRUMENTED PILE TESTS . . . . . 130
4.2.1 Introduction 130
4.2.2 Categorizing the range of measurements 131
4.2.3 Category A, B, and C tests 132
4.2.4 "Quality" of the test results 134
4.2.5 Main parameters of interest 135
4.2.6 Correlations between the various parameters 138
4.2.7 A note on the meaning of OCR 139
4.3 PILE INSTALLATION . . . . . 141
4.3.1 Pore pressure measurements at the pile shaft 141
4.3.2 Pore pressure measurements in the surrounding soil 146
4.3.3 Radial total stresses 146
4.3.4 Radial effective stresses 151
4.4 EARTH AND PORE PRESSURE EQUALIZATION . . . . . 154
4.4.1 Pore pressure dissipation 154
4.4.2 Changes in total stress 156
4.4.3 Radial effective stresses 158
4.5 PILE LOADING . . . . . 163
4.5.1 Introduction 163
4.5.2 Effective stress data for contractive clays 163
4.5.3 Effective stress data for dilating clays 167
4.5.4 Differences between the behaviour of jacked and driven piles 169
4.5.5 Investigations of particle re-orientation next to piles 170
4.5.6 Other investigations of the clay fabric around piles 174
4.6 NOTES AND REFERENCES . . . . . 177

# 4.1 INTRODUCTION

## 4.1.1 The purpose of instrumentation

Instrumented pile tests, in which there are measurements of effective stresses in the soil, are the only reliable method of confirming (or denying) the conclusions of theoretical studies into the behaviour of piles. Instrumentation can transform a complex array of physical quantities (see Figure 4.1[1]) into valuable and highly prized technical information, which itself can lead to a clearer perception of the physics of a problem, and hence ultimately to better design procedures. Since the physics of pile behaviour are not well understood, the importance of instrumented pile tests cannot be over-emphasized.

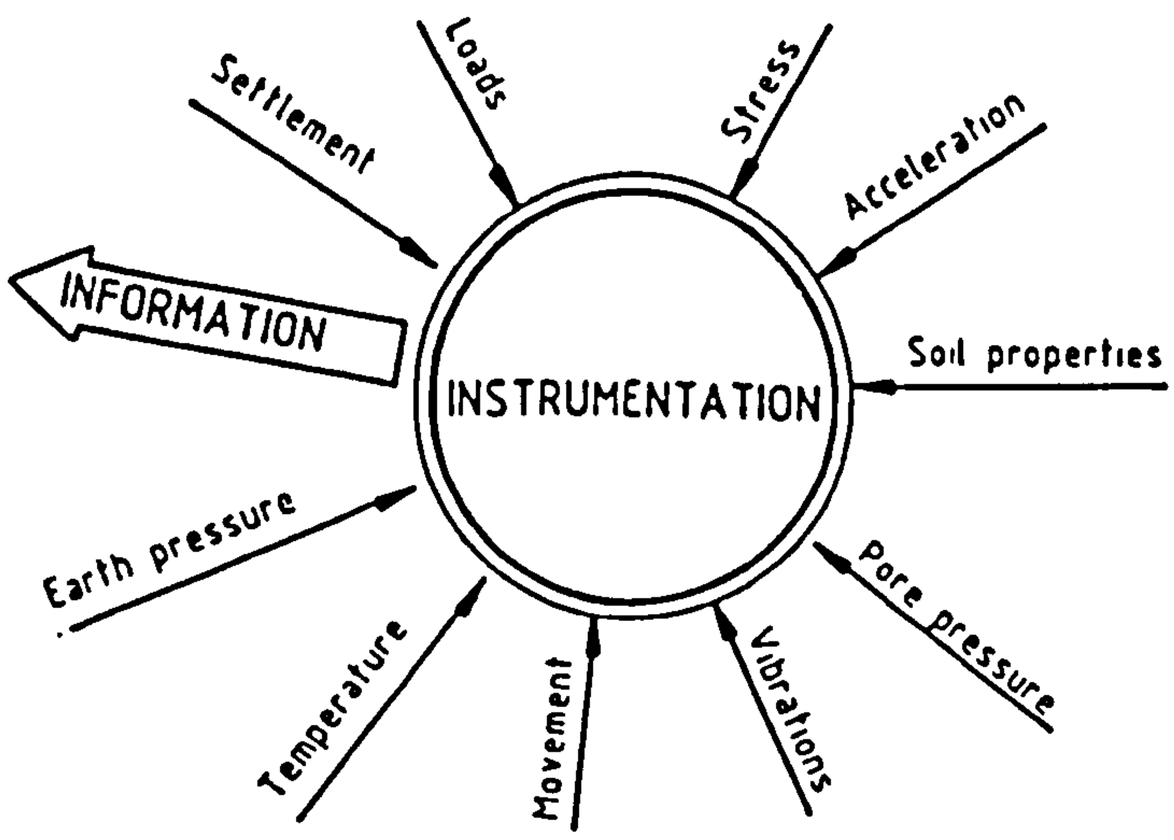



Figure 4.1 The purpose of instrumentation

Successful instrumented pile tests depend on high quality instrumentation being used *in sufficient numbers* for the independent variables that govern pile behaviour to be identified. Ideally, the piles would be installed in representative soil profiles; be as close to full-scale as possible; and be designed to withstand the rigours of potentially arduous field conditions. The readings obtained would be interpreted with a clear understanding of how the instruments interact with - and hence change - the physical quantities they attempt to measure.

### 4.1.2 Outline of Chapter 4

This review of instrumented pile tests is based on a survey of more than fifty such experiments in clay soils. The tests are listed in Appendix 2, together with detailed information about the instrumentation, load tests, soil types, etc., in each case.

The aim of the present chapter is two-fold.

- To identify those experiments that help us to understand pile behaviour in terms of effective stress
- To describe the key features of this behaviour throughout the three main stages in the life of a pile, namely: installation, equalization, and load testing

Chapter 4 is set out as follows.

Section 4.2 identifies those experiments in which measurements have been made of the radial total stresses or pore pressures acting on the pile shaft. The calibre of the data obtained in these experiments is assessed and the results of the better quality tests are summarized in terms of four key parameters that govern pile behaviour.

Sections 4.3 to 4.5 concentrate on the information that can be gleaned from the various instrumented pile tests surveyed in Section 4.2. The variation of the key parameters with the soil's overconsolidation ratio (OCR) is examined in detail. In addition, features of pile behaviour that are relevant to the experiments at Canons Park (see Chapters 9-13) are described and explained in terms of effective stresses.

## 4.2 SURVEY OF PREVIOUS INSTRUMENTED PILE TESTS

### 4.2.1 Introduction

Although literally hundreds of instrumented pile tests in clay soils have been reported in the Literature, there are less than two dozen cases in which earth and pore water pressures have been measured next to the pile shaft. Most of these experiments were performed in soft, normally- or lightly over-consolidated clays, and several of the so-called over-consolidated soils derive their apparent pre-consolidation from chemical processes (such as leaching, cementation, aging, etc.), rather than from the removal of overburden. Consequently there are few (if any) reliable instrumented pile tests in heavily, *mechanically*, overconsolidated clays.

The survey includes more than fifty instrumented pile tests in clay soils (technical details are given in Appendix 2). It includes every test in which measurements were made of the effective stresses acting on the pile shaft*; and most of the tests where measurements were made of the pore pressures acting next to the pile itself or in the surrounding soil. The survey also includes experiments which involved extensive measurements of the variation of axial load along the pile; and of the *deep* ground movements caused by pile installation and load testing (not just surface movements).

Unfortunately, in several cases the quality of the data obtained was not good enough to provide a clear picture of the behaviour of piles in terms of *effective* stresses, and hence some of the conclusions that have been drawn from this data may be misleading.

In assessing the information provided by these experiments, I have found it helpful to categorize the tests according to the overall scope of the measurements. Five categories (A-E) have been used, as explained below (see Section 4.2.2).

---

*Except for a few unpublished case histories

Finally, I have made an attempt to assess the quality of the data, and to rate its reliability on a scale from "very good" to "poor". Section 4.2.4 gives further details of this assessment.

### 4.2.2 Categorizing the range of measurements

The instrumented pile tests listed in Appendix 2 have been divided into five categories, as defined in Table 4.1.

Table 4.1 Range of measurements using instrumented piles

| Category† | Definition‡ |
|---|---|
| A | Measurements of effective stresses next to the pile (EP and PP cells (or ES cells) essential; may carry SS cells) |
| B | Measurements of pore pressures next to the pile (PP cells essential; often includes $PP^R$) |
| C | Measurements of pore pressures in the soil surrounding the pile ($PP^R$, but without any instrumentation on the pile) |
| D | Measurements of axial load distribution along the pile (AL cells or SG essential at several levels, not just at the pile head and toe) |
| E | Measurement of ground movements around the pile (various devices, all designated GM herein) |

†Whenever a test falls into more than one category, the higher category takes precedence

‡Notation: EP = earth pressure; PP = pore pressure; $PP^R$ = "remote" PP instruments (i.e. not at the pile wall, but in the surrounding soil); SS = shear stress; ES = effective stress; AL = axial load; SG = strain gauges; GM = ground movements

This chapter concentrates on the results of the Category A, B, and C tests - and in particular on those in Category A.

### 4.2.3 Category A, B, and C tests

Table 4.2 lists all the Category A, B, and C pile tests that appear in the main survey. Alongside each entry brief details are given about the following:

- The site where the experiments were performed
- The piles' length to diameter ratios (L/D); how they were installed (d - driven; j - jacked; f - free-fall); and whether they were open- (o) or closed- (c) ended, or both types were used (b)
- The instruments employed (see Table 4.1 for an explanation of the abbreviations)
- The quality of the data obtained (see Section 4.2.4)

Table 4.2 Category A-, B, and C instrumented pile tests

| No | Authors (date) | Site [laboratory] | Pile L/D Inst'n End dtls | EP | PP | AL SG | SS | $PP^R$ | Quality of data obtained |
|---|---|---|---|---|---|---|---|---|---|
| **Category A-** | | | | | | | | | |
| 22 | Johnston (1972); Butterfield & Johnston (1973, 1980) | Sports Ground, Southampton University, England | 34½ j c | ✓ | x | ✓ | ✓ | x | Fair |
| **Category B** | | | | | | | | | |
| 23 | Hanna (1967) | Lambton, Ontario, Canada | 13 d o | x | ✓ | x | x | x | Poor |
| 24 | Airhart et al. (1969) | Beaumont, Texas, USA | 37½ d c | x | ✓ | ✓ | x | x | Fair* |
| 25 | Ismael & Klym (1979) | Pickering, Ontario, USA | ? d o | x | ✓ | x | x | ✓ | Fair* |
| 26 | Appendino, Jamiolkowski, & Lancellotta (1979) | Porto Tolle, Italy | 79 d c | x | ✓ | ✓ | x | ✓ | Good |
| 27 | Grosch & Reese (1980) | Sabine, Texas, USA | 31 j c | x | ✓ | ✓ | x | x | Fair |
| 28 | Roy et al. (1981); Konrad & Roy (1987) | St Alban, Quebec, Canada | 30 j c | x | ✓ | x | x | ✓ | V.good* |
| **Category C** | | | | | | | | | |
| 29 | Bjerrum & Johannessen (1960) | Southern Norway | 100-115 d o | x | x | x | x | ✓ | Good* |
| 30 | Milligan, Soderman, & Rutka (1962) | Pic River, Ontario, Canada | ? d H | x | x | x | x | ✓ | Poor |
| 31 | Lo & Stermac (1964) | Toronto, Ontario, Canada | 7-39 d c | x | x | x | x | ✓ | Poor |
| 32 | Orrje & Broms (1967) | Gothenburg, Sweden | ? d c | x | x | x | x | ✓ | Fair |
| 33 | Burghignoli & Caruana (1979) | [Univ. of Rome, Italy] | 6.7 j c | x | x | x | x | ✓ | Good |
| 34 | Blanchet, Tavenas, & Garneau (1980) | Maskinongé, Quebec, Canada | ≈51 d c | x | x | x | x | ✓ | V.good |

Table 4.2 (cont.) Category A instrumented pile tests

| No | Authors (date) | Site [laboratory] | Pile L/D | Inst'n | End dtl | EP | PP | AL | SG | SS | $PP^R$ | Quality of data obtained |
|---|---|---|---|---|---|---|---|---|---|---|---|---|
| 1 | Reese & Seed (1955)<br>Seed and Reese (1955) | San Francisco, California, USA | 30 | d | c | ✓ | ✓ | ✓ | | x | x | Good/fair |
| 2 | Koizumi & Ito (1967) | Otemachi, Tokyo, Japan | 18½ | j | c | ✓ | ✓ | ✓ | | x | ✓ | Good/fair |
| 3a | Kenney (1967) | Kjelsås, Oslo, Norway | 19 | f | o | | | | | | | |
| b | | Manglerud III, Oslo, Norway | 21 | f | o | ✓ | ✓ | x | | x | x | Good |
| c | | Tønsberg, Oslo, Norway | 13 | f | o | | | | | | | |
| 4 | Sutton et al. (1979) | FD Platform, Forties Field, North Sea | 52 | d | o | ✓ | ✓ | ✓ | | x | x | Fair |
| 5 | Rigden et al. (1979)<br>Gallagher & St John (1980) | Cowden, North Humberside, England | 20 | d | b | ✓ | ✓ | ✓ | | x | x | Poor |
| 6 | Steenfelt, Randolph, & Wroth (1981) | [Cambridge Univ., England] | ≈20 | j | c | ✓ | ✓ | ✓ | | x | ✓ | Good (EP failed) |
| 7 | O'Neill et al. (1982a,b) | Beaumont, Texas, USA | 37 | d | c | ✓ | ✓ | ✓ | | x | ✓ | Fair |
| 8 | McAnoy et al. (1982)<br>Ponniah & McAnoy (1985) | Cowden, North Humberside, England | 52 | j | o | ✓ | ✓ | ✓ | | x | ✓ | Good/fair |
| 9 | Francescon (1983) | [Cambridge Univ., England] | <21 | j | c | ✓ | ✓ | ✓ | | ✓ | ✓ | V. good |
| 10 | Azzouz & Morrison (1988) | Saugus, Massachusetts, USA | ≈50 | j | c | ✓ | ✓ | ✓ | | x | x | V. good |
| 11 | Morrison (1984) | MIT Campus, Massachusetts, USA | ≈50 | j | c | ✓ | ✓ | ✓ | | x | x | V. good |
| 12 | Karlsrud & Haugen (1985a,b) | Haga, near Oslo, Norway | 34 | j | c | ✓ | ✓ | ✓ | | x | x | Good |
| 13 | Nauroy, Brucy, & Le Tirant (1985) | Cran, Brittany, France | 62 | d | c | ✓ | ✓ | ✓ | | x | x | Good |
| 14 | Jardine (1985) | Canons Park, London, England | 31 | j | c | ✓ | ✓ | ✓ | | ✓ | x | Fair/poor |
| 15 | Azzouz & Lutz (1986) | Empire, Louisiana, USA | 49 | j | c | ✓ | ✓ | ✓ | | x | x | V. good |
| 16 | BRE (1986) | Cowden, North Humberside, England | 32-48 | d | b | ✓ | ✓ | ✓ | | x | ✓ | EP and PP failed |
| 17a | Coop (1987) | Madingley, Cambridge, England | (13) | j | b | ✓ | ✓ | ✓ | | x | x | V. good |
| b | | Canons Park, London, England | | | | | | | | | | |
| c | | Huntspill, Somerset, England | | | | | | | | | | |
| 18 | This thesis | Canons Park, London, England | 31-40 | j | c | ✓ | ✓ | ✓ | | ✓ | x | V. good |
| 19a | BP (unpublished) | Pentre, Shropshire, England | 52½ | d | o | ✓ | ✓ | ✓ | | x | x | ? |
| b | | Tilbrook Grange, Cambs., England | 39½ | | | | | | | | | |
| 20a | NGI (unpublished) | Onsøy, Norway | 15-148 | d | b | ✓ | ✓ | ✓ | | x | x | ? |
| b | | Lierstranda, Norway | | d | b | | | | | | | |
| c | | Pentre, Shropshire, England | | d | c | | | | | | | |
| 21 | NGI (unpublished) | Tilbrook Grange, Cambridge, England | 43-64 | d | b | ✓ | ✓ | ✓ | | x | x | ? |

## 4.2.4 "Quality" of the test results

Taking measurements of the earth and pore pressures next to displacement piles is not an easy task. Consequently the quality of the results varies greatly from test to test, depending on the design of the instrumentation, and also on the particular soil being investigated.* Many of the early experiments with instrumented piles produced data which is of poor quality, which can confuse our understanding of pile behaviour if it is not recognized as such. Therefore I have made my own assessment of the data quality in the Category A, B, and C tests in an attempt to separate the good from the bad.

Table 4.3 Criteria for assessing the quality of instrumented pile test results

| Quality | Definition |
|---|---|
| Very good | Stable, consistent, repeatable, and frequent readings throughout all stages of the experiment (installation, equalization, and load testing); fast pore pressure response times essential |
| Good | Stable, consistent, and repeatable readings for the end of installation (not during), and throughout equalization and load testing |
| Fair | Data marred by one of the following problems: slow pore pressure response times; instability; large zero shifts; inconsistent results; etc. |
| Poor | A combination of problems rendering the data largely unusable |
| Failed | Tests in which the instrumentation system failed, producing no results at all |

The criteria that I have used to make this assessment are set out in Table 4.3. In some cases (those marked * in Table 4.2) I have been guided by the ratings given, in a similar "quality control" exercise, by Levadoux and Baligh.[2]

---

*For example, an earth pressure cell installed in a soft clays may be far too compliant for accurate measurements in stiff soils; the importance of cell action effects and response times is discussed at length in Appendix 5

### 4.2.5 Main parameters of interest

The Category A pile tests provide vital information about the earth and pore water pressures acting on the pile shaft, throughout all stages of the pile's lifetime. These tests permit the following key parameters to be assessed:[3]

- The normalized horizontal total stress, $H = (\sigma_{rr} - u_o)/\sigma'_{vo}$
- The excess pore pressure ratio, $\Delta u/\sigma'_{vo} = (u - u_o)/\sigma'_{vo}$
- The lateral stress coefficient, $K = \sigma'_{rr}/\sigma'_{vo} = H - \Delta u/\sigma'_{vo}$
- The coefficient of friction, $\mu = (\tau_{rz})_f/(\sigma'_{rr})_f$

Particular attention should be paid to the values of the first three parameters during pile installation (i.e. $H_i$; $\Delta u_i/\sigma'_{vo}$; and $K_i$), and to the lateral stress coefficient at the end of equalization ($K_c$). Finally, and most importantly, we need to know the values of the last two coefficients *at the point of failure* during pile loading (i.e. $K_f$ and $\mu$).

Theoretical predictions for the values of these parameters are given in Chapter 3, where it is shown that the changes in radial stress during the equalization period may be expressed most conveniently by two ratios:

$$H_c/H_i \text{ and } K_i/K_c$$

which I have called the "relaxation" and "set-up" coefficients.

Table 4.4 summarizes the values of four key parameters ($H_i$, $\Delta u_i/\sigma'_{vo}$, $K_i$, and $K_c$), as measured in the Category A experiments; and values of $\Delta u_i/\sigma'_{vo}$ from the Category B experiments. Those tests in which the instruments failed and those in which the data was of poor quality have been excluded (i.e. nos 5-6, 16, and 23). Details about Cases 19-21 have yet to be published, and data from the current research programme (Case 18) is presented separately (in greater detail) in Chapters 9-11. Finally, some of the Category B tests (nos 24, 25, and 27) have been omitted from Table 4.4, since the measurements of $\Delta u_i/\sigma'_{vo}$ in these cases are unreliable (owing to the transducers' slow response times).

Table 4.4 Results of instrumented pile tests in clay soils

| No | SOIL TYPE | Depth(m) | z/R | OCR | $K_0$ | $c_{uo}/\sigma'_{vo}$ | $H_i$ | $\Delta u_i/\sigma'_{vo}$ | $K_i$ | $K_c$ |
|---|---|---|---|---|---|---|---|---|---|---|
| 1 | San Francisco Bay mud | 4.3 | 36 | ≈1 | ? | 0.26 | 0.97 | - | - | 0.24 |
| | $I_p$ = 18% [CL] | 4.9 | 28 | | | 0.23 | 1.52 | - | - | 0.28 |
| | $S_t$ = 2 | 5.5 | 20 | | | 0.21 | - | - | - | ?0.54 |
| | $c_{uo}$ ≈ 11.8kPa [UC] | 6.1 | 12 | | | 0.20 | - | - | - | 0.25 |
| | | 6.7 | 4 | | | 0.18 | 2.43 | 2.00 | 0.43 | ?0.14 |
| 2 | Soft plastic clay from Tokyo | | | | | | | | | |
| | $I_p$ = 40-75% [CH] | 3.1 | 17.4 | ≈2.5 | ? | ≈1.0 | 7.35 | 7.35 | ≈0 | 2.2 |
| | $S_t$ = very high | 5.3 | 2.8 | ≈2.5 | ? | ≈0.8 | 7.34 | 7.34 | ≈0 | 2.0 |
| | $c_{uo}$ = 24.5-39.2kPa [UC] | | | | | | | | | |
| 3a | Quick clay from Kjelsås, Oslo | 4.4 | ≈27 | ≈1 | 0.5- | 0.15# | 0.76 | - | - | 0.35 |
| | $I_p$ = 7% [CL] | 5.4 | ≈22 | " | 0.6‡ | ≈0.1 | 0.83 | 0.21 | 0.62 | 0.44 |
| | $S_t$ > 100 | 7.9 | ≈12 | " | " | " | 1.09 | - | - | 0.55 |
| | $c_{uo}$ ≈ 5kPa [FV] | 8.9 | ≈7.5 | " | " | " | 1.52 | 0.66 | 0.85 | 0.66 |
| 4 | North Sea clays, Forties | | | | | | | | | |
| | $I_p$ = medium [CI] | 39 | 46.7 | nc/ | ? | ≈0.29 | ≈2.5 | ≈2.2 | ≈0.3 | - |
| | $S_t$ = ? | 53 | 26.7 | loc | | ≈0.45? | ≈2.7? | ≈1.7 | ≈1.0 | - |
| | $c_{uo}$ ≈ 90kPa <52m; | 68 | 4.4 | | | ≈0.35 | ≈4.2 | ≈3.5 | ≈0.7 | - |
| | ≈190kPa >52m [UC] | | | | | | | | | |
| 7 | Beaumont clay | | | | | | | | | |
| | $I_p$ = 40-50% [CI] | 5.8 | 53.4 | ≈6 | 2.75 | ≈1.07 | ? | ? | ? | 3.48 |
| | $S_t$ = 0.85+ | | | | | | | | | |
| | $c_{uo}$ = 85kPa [UU] | | | | | | | | | |
| | $I_p$ = 12-30% [CL] | 10.4 | 20.0 | ≈4½ | 1.0 | ≈1.26 | ? | ? | ? | 2.05 |
| | $S_t$ = 1.3 | | | | | | | | | ±0.58 |
| | $c_{uo}$ = 160kPa [UU] | 12.5 | 4.5 | ≈4 | 0.9 | ≈1.08 | ? | ? | ? | 2.21 |
| | | | | | | | | | | ±0.63 |
| 8 | Cowden glacial till | | | | | | | | | |
| | $I_p$ = 12-20% [CL] | 9.5 | 5.2 | ≈2? | ? | 0.77 | 8.58 | 1.81 | 6.01 | - |
| | $S_t$ = ? | | | | | | | | | |
| | $c_{uo}$ = 120-150kPa [UU] | | | | | | | | | |
| 9 | Kaolin (lab. tests) | A | ≈15 | 1 | 0.7 | 0.21 | 1.03 | 0.05 | -0.02 | 0.86 |
| | $I_p$ = 31% [CL] | | | 2 | 0.9 | 0.38 | 1.41 | 1.41 | 0.0 | 1.33 |
| | $S_t$ = ? | | | 4 | 1.2 | 0.62 | 1.91 | 1.79 | 0.12 | 1.85 |
| | $c_{uo}$ = 38-46kPa (A) | | | 8 | 1.6 | 1.03 | 3.29 | 2.36 | 0.92 | 2.92 |
| | = 11-55kPa (B) | | | | | | | | | |
| | | B | ≈15 | 1 | 0.7 | 0.22 | 1.20 | 0.99 | 0.21 | 0.67 |
| | | | | 2 | 0.9 | 0.37 | 2.08 | 1.80 | 0.28 | 1.10 |
| | | | | 4.2 | 1.2 | 0.64 | 2.82 | 2.63 | 0.19 | 1.67 |
| | | | | 8.3 | 1.6 | 1.05 | 3.89 | 3.78 | 0.11 | 2.42 |
| | | | | 17 | 2.1 | 1.67 | 5.33 | 6.00 | -0.66 | 3.33 |
| | | | | 50 | 3.8 | 3.8 | 9.50 | 9.88 | -0.38 | 6.84 |
| 10 | Boston blue clay (Saugus) | | | | | | | | | |
| | $I_p$ = 18-27% [CL] | 12- | 50 | 2- | 0.75- | ≈0.36 | 2.2- | 2.0- | ? | ≈0.90 |
| | $S_t$ = ? | 18 | | 4 | 1.0 | | 3.0 | 2.85 | | |
| | $c_{uo}$ ≈ 38-45kPa [UU]** | | | | | | | | | |
| | $I_p$ = 21 ±3% [CL] | 23+ | 50 | 1.20 | 0.55- | <0.20 | 2.2- | 2.0- | 0.05- | 0.60 |
| | $S_t$ = 7 ±2 | | | ±0.1 | 0.70 | | 2.4 | 2.4 | 0.20 | ±0.03 |
| | $c_{uo}$ = 26-43kPa [UU] | | | | | | | | | |
| 11 | Boston blue clay (MIT) | 19.1 | 50 | 2.2 | ? | 0.39 | 2.64 | 2.54 | 0.10 | 0.65 |
| | $I_p$ = 17-24% [CL] | 22.9 | 50 | 1.5 | ? | 0.33 | 2.37 | 1.99 | 0.39 | 0.77 |
| | $S_t$ = 2-3 | 25.9 | 50 | 1.3 | ? | 0.32 | 2.38 | 1.93 | 0.44 | 0.62 |
| | $c_{uo}$ ≈ 80-100kPa [$CK_0UTC$] | 29.0 | 50 | 1.25 | ? | 0.33 | 2.52 | 2.16 | 0.36 | 0.59 |
| 12 | Haga clay | | | | | | | | | |
| | $I_p$ = 15% [CL] | 0.5 | 60.8 | ≈25 | >1.6 | ? | 3.2## | 3.2 | ≈0 | 0.92 |
| | $S_t$ = 5-6 | 1.9 | 42.5 | ≈9 | 1.24 | 1.77++ | 3.6 | 3.6 | ≈0 | 1.24 |
| | $c_{uo}$ ≈ 43kPa [FV]† | 3.4 | 22.9 | ≈4½ | 0.86 | 1.03 | 3.9 | 3.9 | ≈0 | 1.25 |
| | $I_p$ = 35-40% [CI] | | | | | | | | | |
| | $S_t$ = ? | 4.8 | 4.6 | ≈4 | 0.85 | 0.73 | 3.95 | 4.3 | <0 | 1.10 |
| | $c_{uo}$ = 45-55kPa [FV] | | | | | | | | | |
| 13 | Silty clays from Cran, France | | | | | | | | | |
| | $I_p$ ≥ 50% [CH] | 5.3 | 86 | "nc" | ≈0.56‡ | ≈0.8 | ≈2.1¶ | ≈1.5? | 0.1- | §0.39 |
| | $S_t$ = ? | 8.9 | 59 | " | " | ≈0.7 | ≈1.6 | " | 0.3 | 0.45 |
| | $c_{uo}$ = 20-50kPa (2-8m) | 12.5 | 33 | " | " | ≈0.5 | ≈1.4 | " | " | 0.59 |
| | $c_{uo}$ = 50kPa (>11m) [?] | | | | | | | | | |

Table 4.4 (cont.) Results of instrumented pile tests in clay soils

| No | SOIL TYPE | Depth(m) | z/R | OCR | $K_0$ | $c_{uo}/\sigma'_{vo}$ | $H_i$ | $\Delta u_i/\sigma'_{vo}$ | $K_i$ | $K_c$ |
|---|---|---|---|---|---|---|---|---|---|---|
| 14 | London clay, Canons Park | | | | | | | | | |
| | $I_p$ = 42-58% [CI] | 3.0 | 43 | ††40 ±9 | ≈2.7 | ≈2.0 | 5.7 | $u_i<0$ | ? | ? |
| | $S_t$ = ? | 4.0 | 24 | 33 ±7 | ≈2.5 | ≈1.6 | 4.7 | $u_i<0$ | ? | ? |
| | $c_{uo}$ = 60-130kPa [UU] | 5.0 | 4 | 27 ±6 | ≈2.3 | ≈2.1 | 9.0 | $u_i<0$ | ? | ? |
| 15 | Empire clay | | | | | | | | | |
| | $I_p$ = 59 ±7% [CH] | 35- | 95 | 1.7 | ≈0.75 | 0.32‡‡ | 2.74 | 2.20 | 0.54 | 1.54 |
| | $S_t$ = ? | 50 | | ±0.2 | | ±0.03 | | | ±0.01 | |
| | $c_{uo}$ = 20-90kPa [FV] | | | | | | | | | |
| | $I_p$ = 48 ±13% [CH] | 62- | 95 | ≈1.5 | 0.72 | ≈0.29 | 2.40 | 2.02 | 0.38 | 0.90 |
| | $S_t$ = 2 ±1 | 77 | | | ±0.03 | | | ±0.01 | | |
| | $c_{uo}$ = 40-140kPa [FV] | | | | | | | | | |
| 17a | Gault clay, Madingley | | | | | | | | | |
| | $I_p$ = 45-65% [CH] | 4.85 | 22 | ≈22†† | 2.44 | 2.43 | 8.8 ±0.5 | $u_i<0$ | ≈7.0 | ≈6.7 |
| | $S_t$ = ? | | | | | | | | | |
| | $c_{uo}$ = 105-150kPa [UU] (Borehole G) | 5.57 | 5.5 | ≈27 | 2.33 | 2.35 | 8.9 ±0.6 | $u_i<0$ | ≈8.3 | ≈8.1 |
| 17b | London clay, Canons Park | | | | | | | | | |
| | $I_p$ = 42-58% [CI] | 4.07 | 22 | ††32 ±7 | ≈2.5 | ≈1.6 | 7.0 ±0.4 | $u_i<0$ | ≈7.2 | ? |
| | $S_t$ = ? | | | | | | | | | |
| | $c_{uo}$ = 60-130kPa [UU] | 4.73 | 5.5 | 29 ±7 | ≈2.3 | ≈2.3 | 12.6 ±0.1 | $u_i<0$ | ≈13.5 | ? |
| 17c | Soft silty clay from Huntspill, Somerset | | | | | | | | | |
| | $I_p$ = 30-40% [CL/CI] | 7.41 | 22 | 1.2 | ? | 0.43 | 1.10 ±0.10 | 0.86 ±0.11 | ≈0.22 | ? |
| | $S_t$ = ? | | | | | | | | | |
| | $c_{uo}$ = 20-35kPa [CUTC] | 8.07 | 5.5 | 1.1 | ? | 0.44 | 1.74 ±0.09 | ≈1.04 | ≈0.69 | ? |
| 22 | London clay, Southampton | | | | | | | | | |
| | $I_p$ = 41% [CI] | 3.3 | 39 | ? | ? | ≈0.9 | ≈3.75 | - | - | - |
| | $S_t$ = ? | 4.3 | 21 | ? | ? | ≈0.9 | ≈4.53 | - | - | - |
| | $c_{uo}$ = 68 ±19kPa [UU] | 5.1 | 4.6 | ? | ? | ≈0.65 | ≈4.75 | - | - | - |
| 26 | Porto Tolle clay | | | | | | | | | |
| | $I_p$ = 25-40% [CL/CI] | ≈25 | 5 | ≈1 | 0.51 ±0.03 | 0.30¶¶ | - | 1.21-1.62 | - | - |
| | $S_t$ = ? | | | | | | | | | |
| | $c_{uo}$ = 30-70kPa [FV] | | | | | | | | | |
| 28 | Champlain clay, St Alban | 3.05 | 42.9 | ≈2.3 | ? | 0.74¶¶ | - | 1.81 | - | - |
| | $I_p$ = 10-27% [CL] | 4.60 | 29.2 | " | " | 0.76 | - | 2.09 | - | - |
| | $S_t$ = 12-17 | 6.10 | 15.5 | " | " | 0.82 | - | 2.76 | - | - |
| | $c_{uo}$ = 10-28kPa [FV] | 7.60 | 1.3 | " | " | 0.87 | - | 4.02 | - | - |

Plasticity: CL = low; CI intermediate; CH high
Strengths: FV = field vane; UU = unconsolidated undrained triaxial compression; UC = unconfined compression; $CK_0UTC$ = $K_0$-consolidated undrained triaxial compression

*Remoulded samples failed under their own weight

#Based on field vane strengths

+Undisturbed samples failed on slickensides

**$(c_{uo})^{UU} \approx 0.8(c_{uo})^{FV}$

##Assuming $u_o$ = 0 throughout the deposit

††Based on triaxial compression tests

‡The Haga clay is highly anisotropic: $(c_{uo})^{UU} \approx 1.21\text{-}1.44(c_{uo})^{FV}$

‡‡Assuming $K_0 = 1 - \sin\phi$, with $\phi = 26°$

¶Assuming $\gamma = 18kN/m^3$ & water table at ground level

§Based on estimated value of $K_0$ and measurements of $K_c/K_0$

†††Based on high pressure oedometer tests

‡‡Based on $c_{uo}$ from DSS tests

¶¶Based on UU tests

Table 4.4 also gives information about the soil properties at the sites where these experiments were performed, including the clay's plasticity index ($I_p$), its sensitivity ($S_t$), and its undrained shear strength ($c_{uo}$). In addition, details are given about the ground conditions at depths where instruments were located (i.e. where H, $\Delta u/\sigma'_{vo}$, and K were measured). The ground conditions considered most relevant to the present study are the overconsolidation ratio (OCR), the earth pressure coefficient ($K_0$), and the undrained strength ratio ($c_{uo}/\sigma'_{vo}$). (In many cases this information is not quoted in the original papers. Where this is so, I have made my own assessment of the likely values of the missing parameters; this particularly applies to the figures given for the undrained strength ratio, $c_{uo}/\sigma'_{vo}$.)

Finally, the column headed "z/R" records the distance from each instrument to the pile tip (z), normalized by the pile's radius (R).

### 4.2.6 Correlations between the various parameters

As shown later, correlations between the various parameters listed in Table 4.4 reveal a consistent pattern of behaviour, in which the values of $H_i$, $\Delta u_i/\sigma'_{vo}$, $K_i$, and $K_c$ depend principally on three main factors:

- The magnitude of the soil's overconsolidation ratio (OCR)
- The distance between the pile tip and the position where the measurements were made (z/R)
- The soil's sensitivity ($S_t$)

Sections 4.3.1.c, 4.3.3.b, 4.3.4.a, and 4.4.3.e present and discuss the correlations that have been derived using these parameters. Because of the scarcity of data for heavily overconsolidated clays I have chosen to include the results of my own experiments on the diagrams presented in this chapter. Full details about these experiments may be found in Chapters 9-11, and a summary of the results is given in Chapter 14.

## 4.2.7 A note on the meaning of OCR

Although the overconsolidation ratio is commonly used to characterize the mechanical behaviour of soils, the precise meaning of OCR is rather ambiguous. In this thesis, it is defined as the pre-consolidation pressure measured in an oedometer test ($\sigma'_{vp}$), divided by the vertical effective stress that acted on the oedometer sample when it was in the ground ($\sigma'_{vo}$), i.e. OCR = $\sigma'_{vp}/\sigma'_{vo}$.

The commonest form of pre-consolidation is that caused by the erosion of sediment. If no other mechanism is involved, then the pre-consolidation pressure (for a young sediment) is equal to the maximum vertical effective stress that the soil has previously experienced ($\sigma'_{vm}$). However, the true nature of soils is not as simple as this, and various other physical and chemical processes can lead to what is termed "apparent overconsolidation", whereby $\sigma'_{vp} \neq \sigma'_{vm}$. In this context, it is useful to distinguish between the soil's *mechanical* overconsolidation ratio ($OCR_m = \sigma'_{vm}/\sigma'_{vo}$) and its *apparent* OCR ($= \sigma'_{vp}/\sigma'_{vo}$). For most soils, $OCR_m$ can only be determined from a knowledge of the geological history of the deposit.

The processes that lead to an apparent OCR different to $OCR_m$ include *physical* events such as aging, desiccation, freeze-thaw cycles, etc.; and *chemical* processes such as leaching, cementation, and weathering (oxidation, decomposition of minerals, etc.). The effects of these processes on the geotechnical properties of marine clays are summarized

Table 4.5 Effect of post-depositional processes on geotechnical properties of marine clays

| Process | $I_p$ | $I_L$ | $\sigma'_{vp}$ | Compress-ibility | Strength* U | Strength* R | $S_t$ |
|---|---|---|---|---|---|---|---|
| Aging | ~ | ⇓ | ⇑ | ⇓ | ⇑ | ⇑ | ⇑ |
| Desiccation | ~ | ⇓ | ⇑ | ⇓ | ⇑ | ? | ? |
| Leaching | ⇓ | ⇑ | ⇓ | ⇑ | ⇓ | ⇓ | ⇑ |
| Cementation | ⇑ | ? | ⇑ | ⇓ | ⇑ | ⇑† | ⇑ |
| Weathering | ⇑ | ⇓ | ⇑ | ⇓ | ⇑ | ⇕‡ | ⇕‡ |

⇑ Increases; ⇓ decreases; ~ little or no change; ⇕ either ⇑ or ⇓
* Undrained strength: U = undisturbed; R = remoulded
† Depends on amorphous content; ‡ Depends on clay mineral

in Table 4.5, part of which is taken from the excellent review of the engineering geology of (soft) clays by Brenner et al.[4].

Soils with *apparent* OCRs as high as 10-16 can possess many of the characteristics of low OCR clays. For example, the Haga clay (Case 13) is described as "overconsolidated"[5] even though it displays many of the characteristics of a normally consolidated soil. Its apparent over-consolidation (OCR = 4-25 below 1m, depending on depth), has been caused by the removal of salt from its pore water, as well as the erosion of sediment. Consequently the Haga clay is a sensitive material, which laboratory tests show will tend to *contract* on shearing, whereas *mechanically* overconsolidated clays with $OCR_m$ between 4 and 25 tend to *dilate*.

Throughout the remainder of this chapter (and elsewhere in the Thesis), I have chosen to distinguish between *contractive* and *dilating* soils, on the basis of their behaviour during undrained shear. Although in many cases these terms describe clays with low and high OCRs (respectively), we should remember that this is not always the case, especially when the material has high sensitivity.

Finally, I should comment on the values of OCR that I have quoted in Table 4.4 for the London and Gault clays (Cases 14, 17a, and 17b). As discussed in Appendix 4, the standard oedometer test is not a reliable method for measuring the pre-consolidation pressure of high OCR clays, and often leads to OCR being grossly under-estimated. The geological evidence for Canons Park (Cases 14 and 17b) suggests that up to 121m of sediment has been eroded from the site (see Appendix 4). This implies that $OCR_m$ is of order of 20 at 5m depth. Since the London clay has had chance to age (over 30 million years or so), we would expect $\sigma'_{vp}$ to be greater than $\sigma'_{vm}$ (and hence OCR to be > $OCR_m$). *High pressure* oedometer tests[6] confirm this conclusion, implying for Canons Park that OCR = 27-33 at 5m depth. The figures quoted in Table 4.4 for this material (and the Gault clay at Madingley) are therefore based on the results of high pressure oedometer tests.

## 4.3 PILE INSTALLATION

### 4.3.1 Pore pressure measurements at the pile shaft

a) Typical measurements in contractive clays

Reliable measurements of the excess pore pressures generated along the pile shaft *during* installation have been obtained in only a handful of cases, and the vast majority of these tests were performed in soft, normally- or lightly over-consolidated clays (e.g. Cases 10-11, 15, 17c, and 28).

Figure 4.2 shows a typical set of measurements in a soft clay[7] (as recorded at a point fifty radii behind the pile tip). Large, positive excess pore pressures ($\Delta u_i$) were generated throughout the soil profile, these being about 2-2½ times the original vertical effective stress ($\sigma'_{vo}$) at any particular depth. Similar profiles have been recorded in other soft clays.

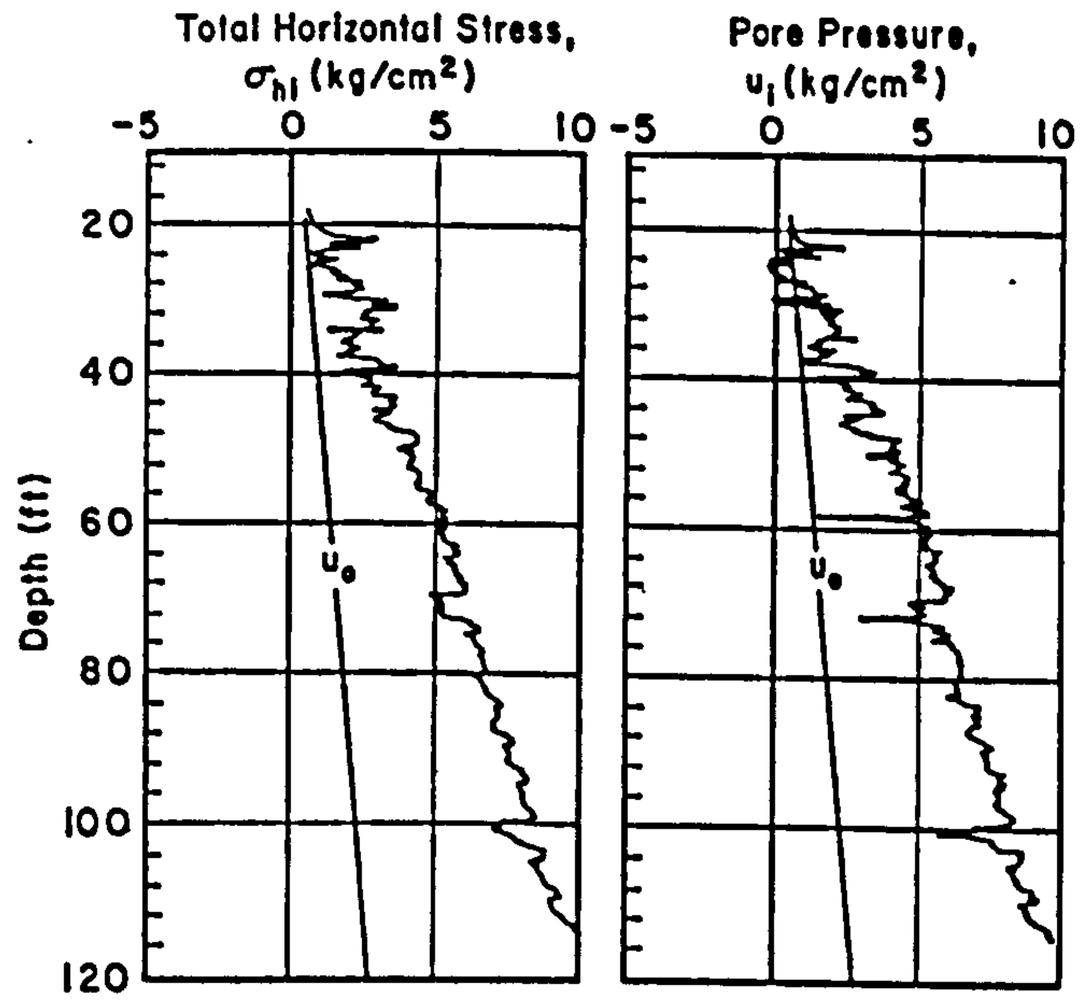



Figure 4.2 PLS cell measurements in Boston blue clay (Case 10)

b) Typical measurements in dilating clays

There are few (if any) pore pressure measurements of comparable quality in stiff, heavily overconsolidated clays. Reliable readings are very difficult to obtain, owing to cavitation of the piezometer fluid during pile installation. For example, consider O'Neill et al.'s experience in the stiff Beaumont clay:

> "During driving, saturation was lost on the piezometers at the surface of the piles. Re-saturation ... was not reached until one to four days after installation so that pore pressures that

> existed immediately after driving at the pile-soil interfaces were not known."[8]

In most of the experiments in high OCR clays, the quality of the data is generally poor to fair (e.g. Cases 4-5, 7-8, 14, and 24-25). Even where the overall quality is very good (e.g. Cases 17a and b), the pore pressure readings are often suspect.

Coop's experiment[9] in the London clay at Canons Park (Case 17b) demonstrates the problems involved. His results are reproduced here as Figure 4.3: the pore pressure readings are shown on the top left-hand diagram, next to the label "PP1".

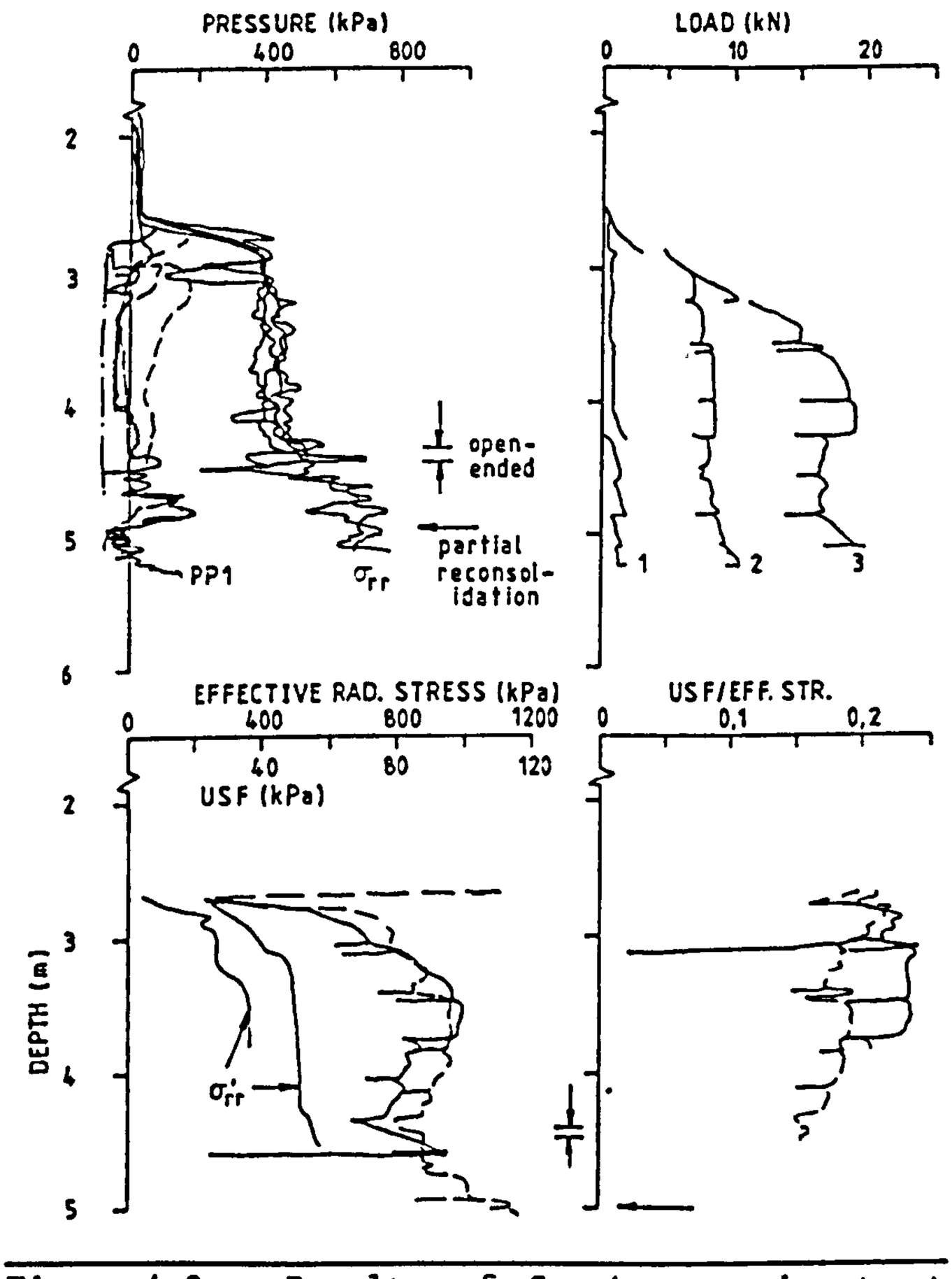



Figure 4.3 Results of Coop's experiment at Canons Park, north London

There are five traces in total,* four of which appear as smooth curves and only one as an irregular profile. Because the London clay at Canons Park contains numerous seams of sand and silt (see Chapter 5), the pore pressure transducers should have recorded highly variable traces, similar to those in Figure 4.2. The smoothness of Coop's traces suggests that the fluid used to saturate his probes cavitated at an early stage

*One at z/R = 0, two at 5.5, and two at 22

during pile installation and did not recover quickly enough to register small fluctuations in pore pressure. The readings are consequently unreliable below a depth of about 3m. The one trace (PP1) that remained "alive" throughout penetration - i.e. responded to the sand and silt seams, and pauses in jacking - was recorded by the transducer located at the pile tip. All the other transducers were located along the pile shaft.

c) Relationship between $\Delta u_i/\sigma'_{vo}$ and OCR

Values of $\Delta u_i/\sigma'_{vo}$ from all the Category A/B pile tests (as listed in Table 4.4) are plotted against OCR on Figure 4.4. Despite the scatter of the data, several important conclusions can be drawn from this diagram:

- Results for the majority of normally-/lightly over-consolidated clays (OCR < 4) fall in the range $1 \leq \Delta u_i/\sigma'_{vo} \leq 3$
- The highest values of $\Delta u_i/\sigma'_{vo}$ (greater than three) were recorded in sensitive clays (the Tokyo [T], Haga [H], and Champlain [Ch] clays, Cases 2, 12, and 28); or in laboratory tests on re-constituted kaolin (Case 9, points x)
- The results for the heavily overconsolidated Gault and London clays (Cases 14, 17a, and 17b) form a group completely separate from the other data; in these high OCR clays, measurements of $\Delta u_i$ are generally <u>negative</u> *while the pile is moving* (they quickly rise to large positive values once penetration ceases)
- There is a tendency for the pore pressures recorded at leading instrument positions ($z/R \leq 10$, points •) to be larger than those measured at other positions along the pile shaft (this cannot be confirmed for the London and Gault clays)

d) Comparisons with theory

The theoretical predictions for $\Delta u_i/\sigma'_{vo}$ are compared with the overall trend of the data in Figure 4.5. They were obtained by the cavity expansion (CEM) and strain path (SPM) methods, using either Modified Cam Clay (MCC) or MIT-E3, and are based on input parameters for Boston blue clay (BBC) or London clay (see Chapter 3 for further details). Neither

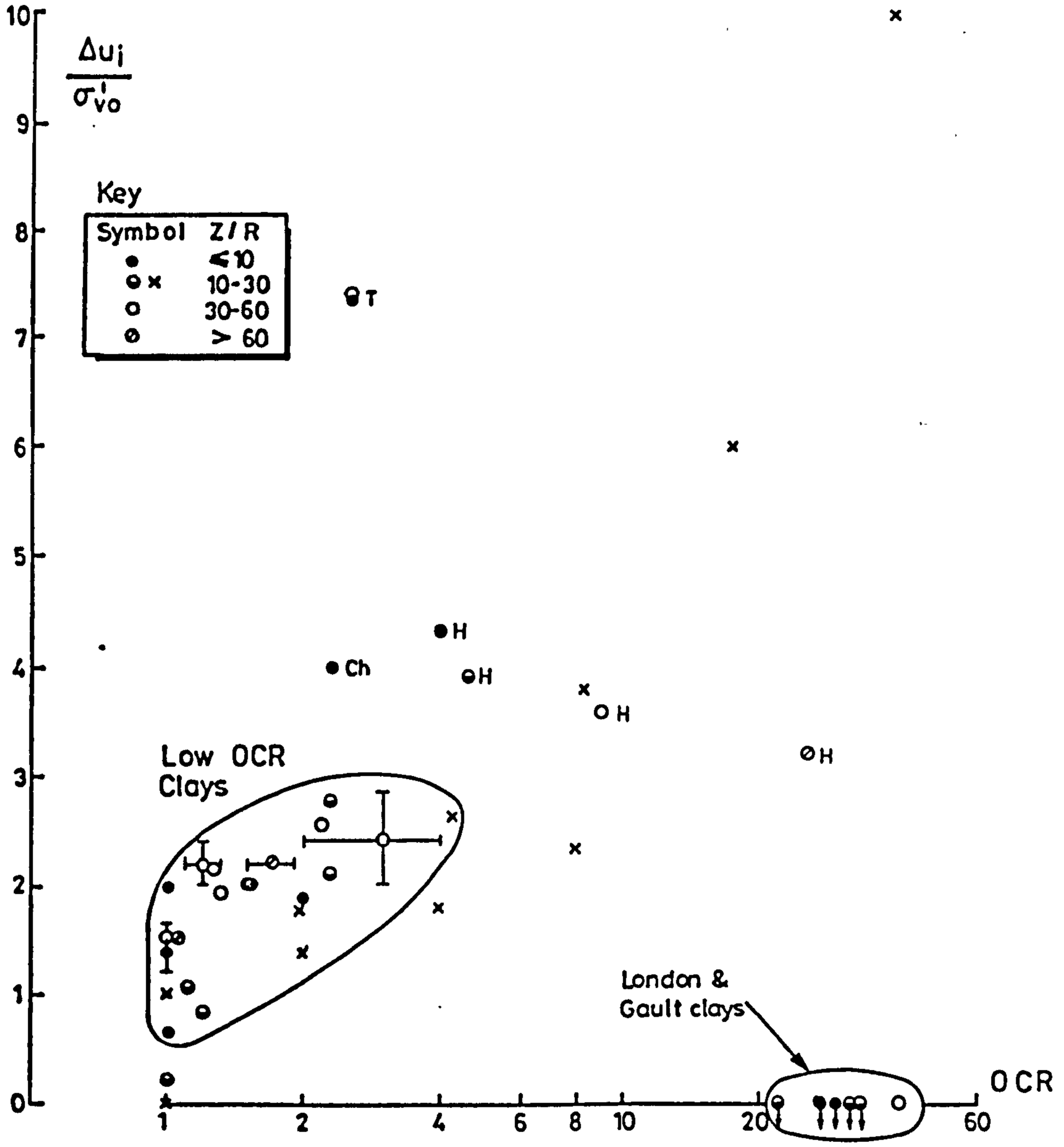



Figure 4.4 Excess pore pressure ratio $\Delta u_i/\sigma'_{vo}$ as a function of OCR

set of predictions allows for possible variations in $\Delta u_i/\sigma'_{vo}$ along the pile shaft: the pressures given are those acting at a point <u>far behind</u> the pile tip (for the SPM, at z/R = 200).

The following points are worth noting:

- The SPM/MIT-E3 curve falls within the spread of the data for OCR ≤ 4, but on average tends to underestimate $\Delta u_i/\sigma'_{vo}$ (strain path predictions have not yet been published for higher OCRs*)

*Professor Whittle and I have recently produced a series of predictions for the London clay, which we hope to publish at a later date

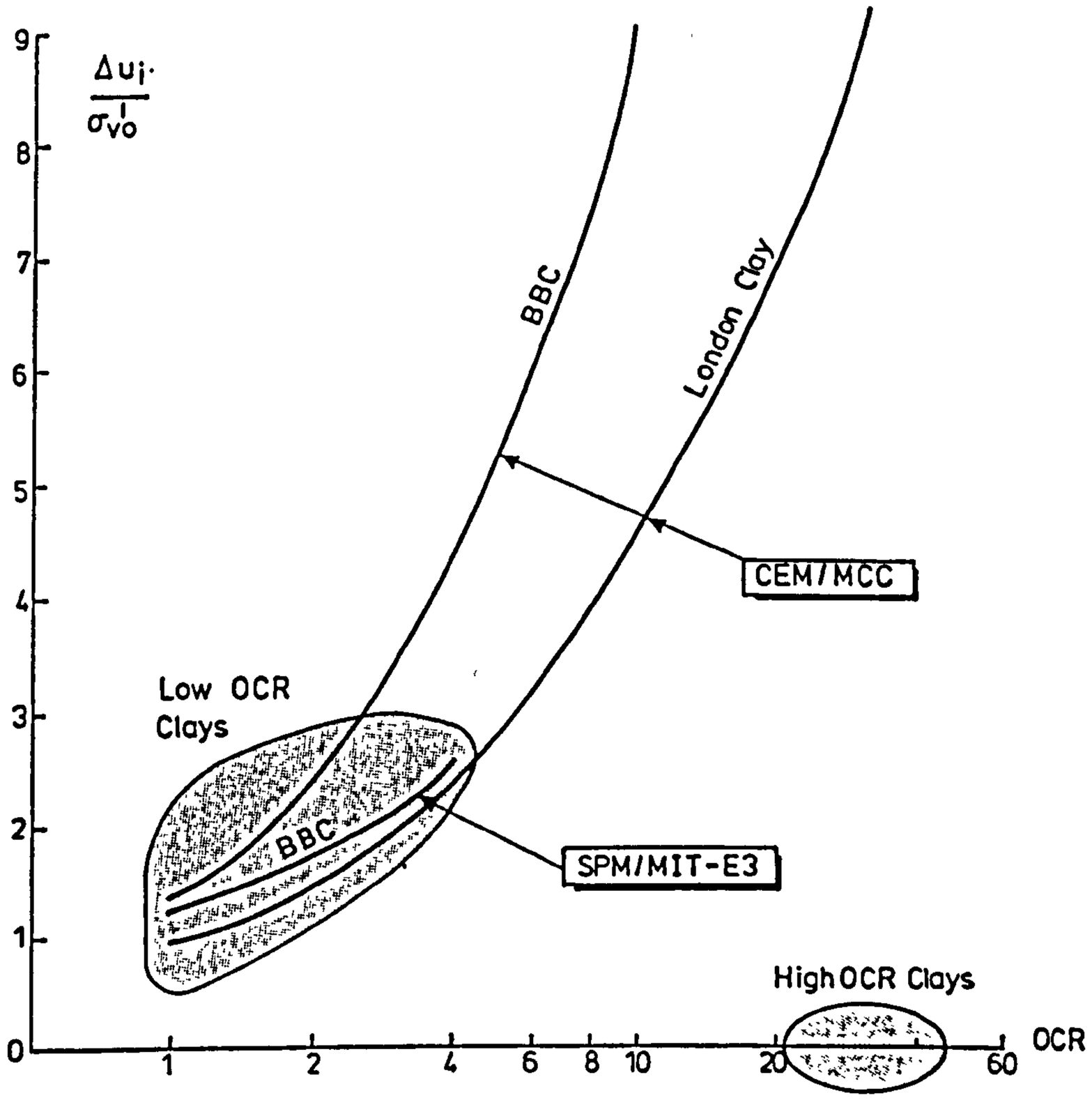



Figure 4.5 Comparison between theoretical and measured values of $\Delta u_i/\sigma'_{vo}$

- The CEM/MCC curves bracket some of the data points at low OCRs (less than 4), but very few points at high OCRs
- The CEM/MCC curves appear to follow the trend of the laboratory results in <u>reconstituted</u> kaolin (points x) over the entire range of OCRs
- The CEM/MCC curve for London clay fails to predict the <u>negative</u> pore pressures measured in the London and Gault clays (i.e. in the *natural*, high OCR materials)
- The experiments in the soft Tokyo clay [T] (which are often cited in support of the cavity expansion predictions) are clearly not representative of the overall trend of the data; the high values of $\Delta u_i/\sigma'_{vo}$ in this case are probably caused by the very high sensitivity of the Tokyo clay

The significance of these results is discussed further in Chapter 14.

### 4.3.2 Pore pressure measurements in the surrounding soil

The variation of $\Delta u_i/\sigma'_{vo}$ with radial distance from the pile wall has a controlling influence on the rate at which the soil surrounding the pile consolidates. This variation can be determined from pore pressure measurements in the surrounding soil (i.e. from Category C experiments).

Figure 4.6[10] illustrates the relationship between $\Delta u_i/\sigma'_{vo}$ and radial position (r/R), as determined in Cases 2, 24-25 and 28-31. Most of the soils tested were soft, normally- or lightly over-consolidated clays. The results show a reasonably consistent pattern, with the largest excess pore pressure occurring at the pile wall and $\Delta u_i/\sigma'_{vo}$ reducing only slightly as r/R increases from 1 to 5. This "plateau" in the pore pressure profile matches the strain path predictions for $\Delta u_i/\sigma'_{vo}$, but not those obtained with the cavity expansion method (see Chapter 3).

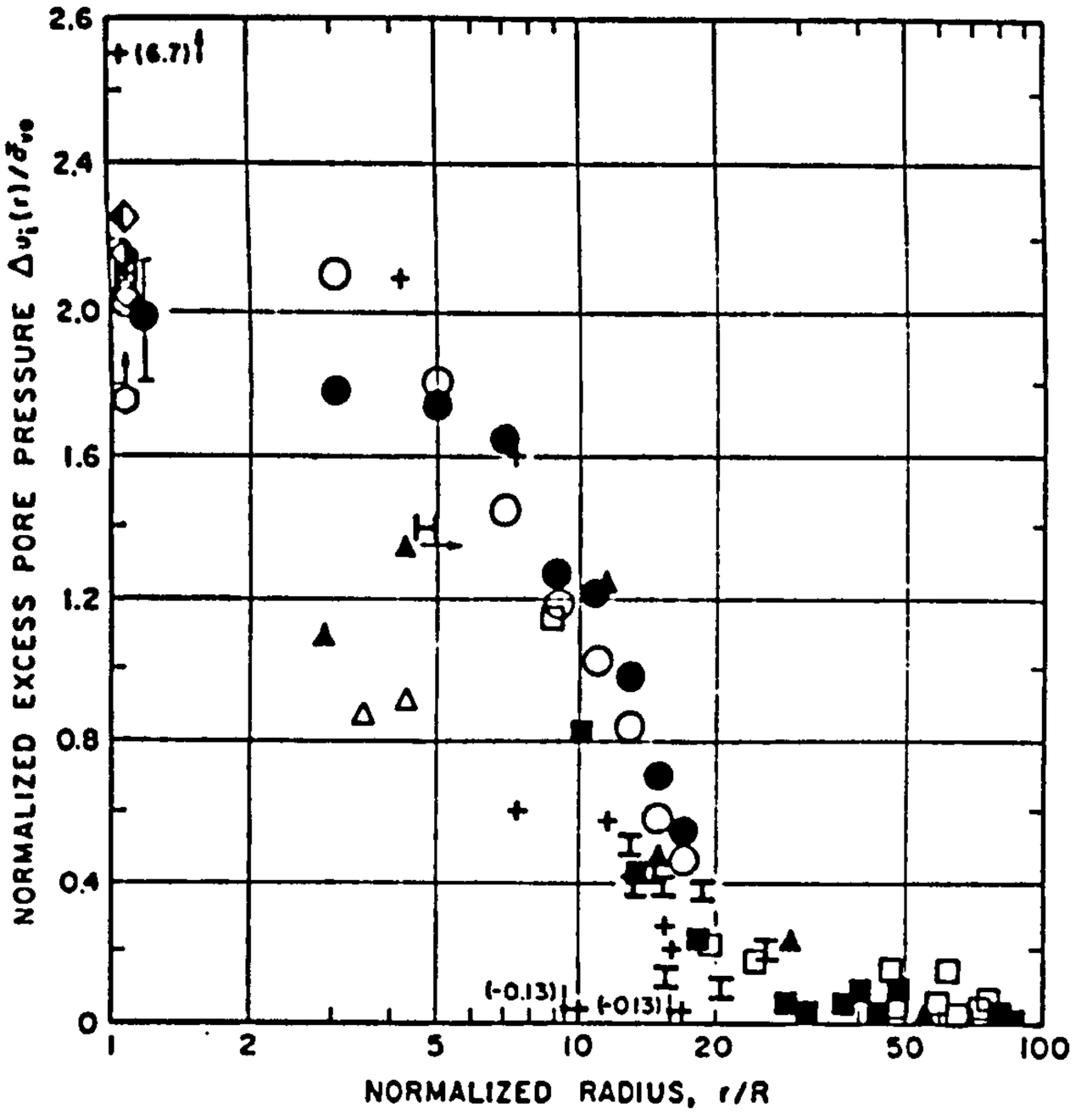



Figure 4.6 Installation excess pore pressures versus radial position

### 4.3.3 Radial total stresses

a) The "z/R effect"

One of the key findings of the experiments at Canons Park (see Chapters 7-13) was the magnitude of the "z/R effect". This is the phenomenon whereby the radial total stress ($\sigma_{rr}$) decreases with increasing distance

(z) behind the pile tip. Other evidence to support the generality of this finding comes from tests in which $\sigma_{rr}$ was measured at several points along the pile shaft.

Reese and Seed made the following comments about the stresses that they recorded in the San Francisco Bay mud (Case 1):

> "...different pressures were measured at the same depth, depending on the distance of the measuring gage [sic] from the pile point... [the] pressures, created at a particular depth by the pile point, [were] partially decayed before the next pressure gage reached that depth."[11]

Reese and Seed believed that the reduced values of $\sigma_{rr}$ were a consequence of the time taken to drive their pile (3 to 4 hours in total, allowing for delays while the instruments were being read). However, the same effect has been recorded in experiments where the pile was installed much faster than this.

Figure 4.7 summarizes the measurements of $\sigma_{rr}$ that were obtained by Johnston[12] in the stiff London clay of the Hampshire Basin. Radial stress cells were located at three separate positions along the pile shaft. The diagram shows results from three tests: the magnitude of $\sigma_{rr}$ at any particular depth clearly reduces as z/R increases. The highest value of radial total stress was recorded by the "leading" instruments, located at z/R = 4.6; and the lowest at the "trailing" position (z/R = 38.8).

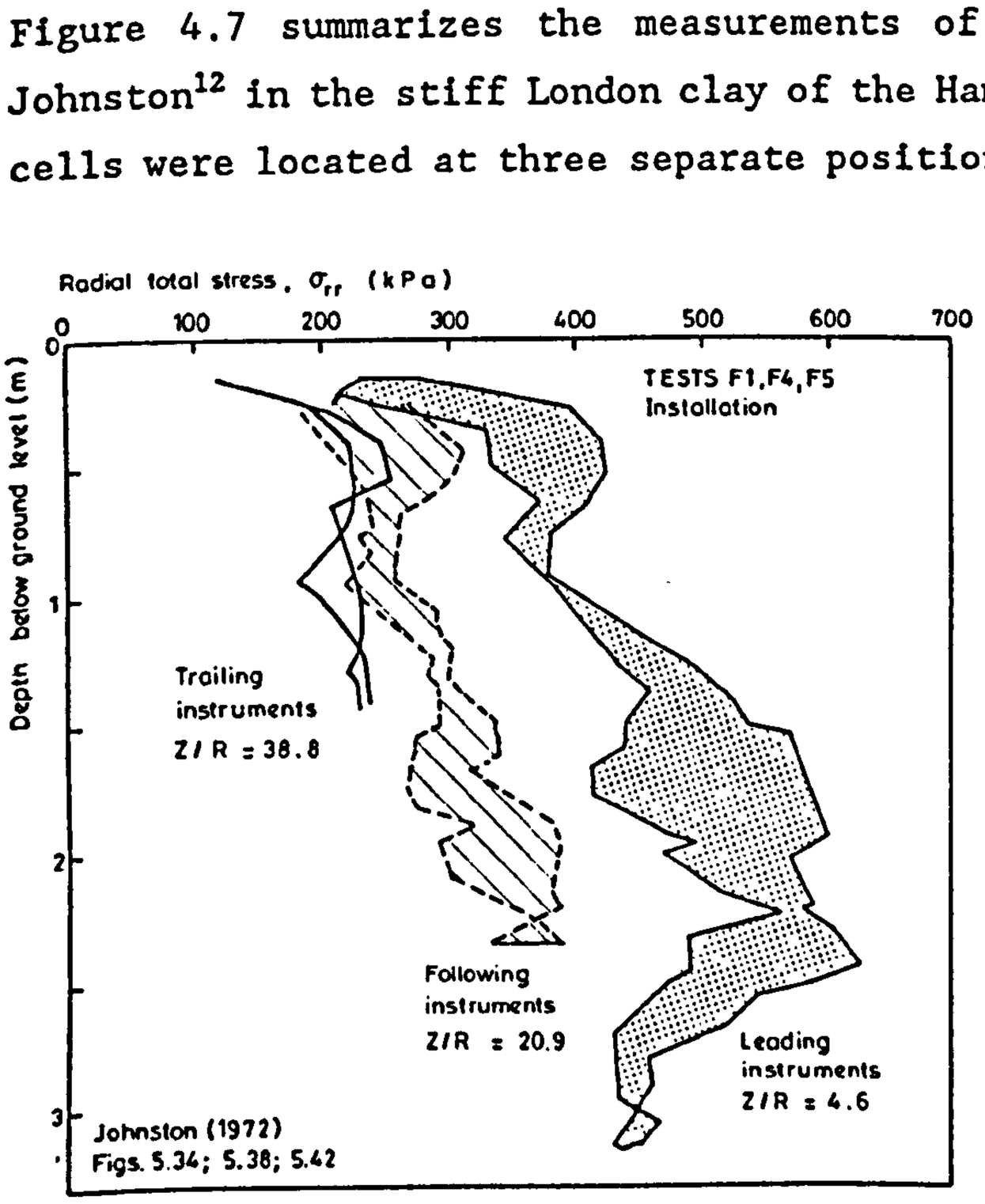



Figure 4.7 Radial total stresses recorded by Johnston in London clay

Similarly, Coop's results[13] in the Gault clay

(Case 17a) reveal a 30% reduction in radial total stress from the leading instrument position (at z/R = 5.5) to the following position (at z/R = 22). By comparison, his results in the London clay (Case 17b, see Figure 4.3) show a very weak z/R effect.

Finally, indirect evidence supporting the z/R hypothesis comes from the series of laboratory experiments conducted at Cambridge University by Steenfelt et al.:

> "One of the striking findings during the tests was that the pore pressures measured along the pile shaft continued to increase after pile installation... A rational explanation would seem to be a tendency for the mean total stress in the clay to decrease as the pile tip continues past that particular location. The effect appears to be confined to a narrow zone around the pile, since even transducers at ½ a pile radius from the shaft... show no corresponding effect."[14]

b) Relationship between $H_i$ and OCR

Unfortunately, the z/R effect makes it particularly difficult to compare values of the normalized horizontal total stress ($H_i$) from different tests, since very few measurements have been made at the same normalized distance behind the pile tip. Nevertheless, it is still possible to uncover certain trends in the data, despite the confusing influence of z/R.

Figure 4.8 shows values of $H_i$, plotted against the soil's over-consolidation ratio, for each of the cases listed in Table 4.4 (circular symbols). Also included on the diagram are the results of my own experiments at Canons Park, which are described in detail in Chapters 9-11 (square symbols). The following points are worth noting from an inspection of Figure 4.8:

- In the normally- and lightly over-consolidated clays (OCRs < 4), the value of $H_i$ is typically in the range $1 \leq H_i < 3$
- In the heavily overconsolidated clays (OCRs > 20), $H_i$ exceeds 2½ and can be as high as 17½; however, the spread of the data is very wide in these soils (partly owing to the large z/R effect)

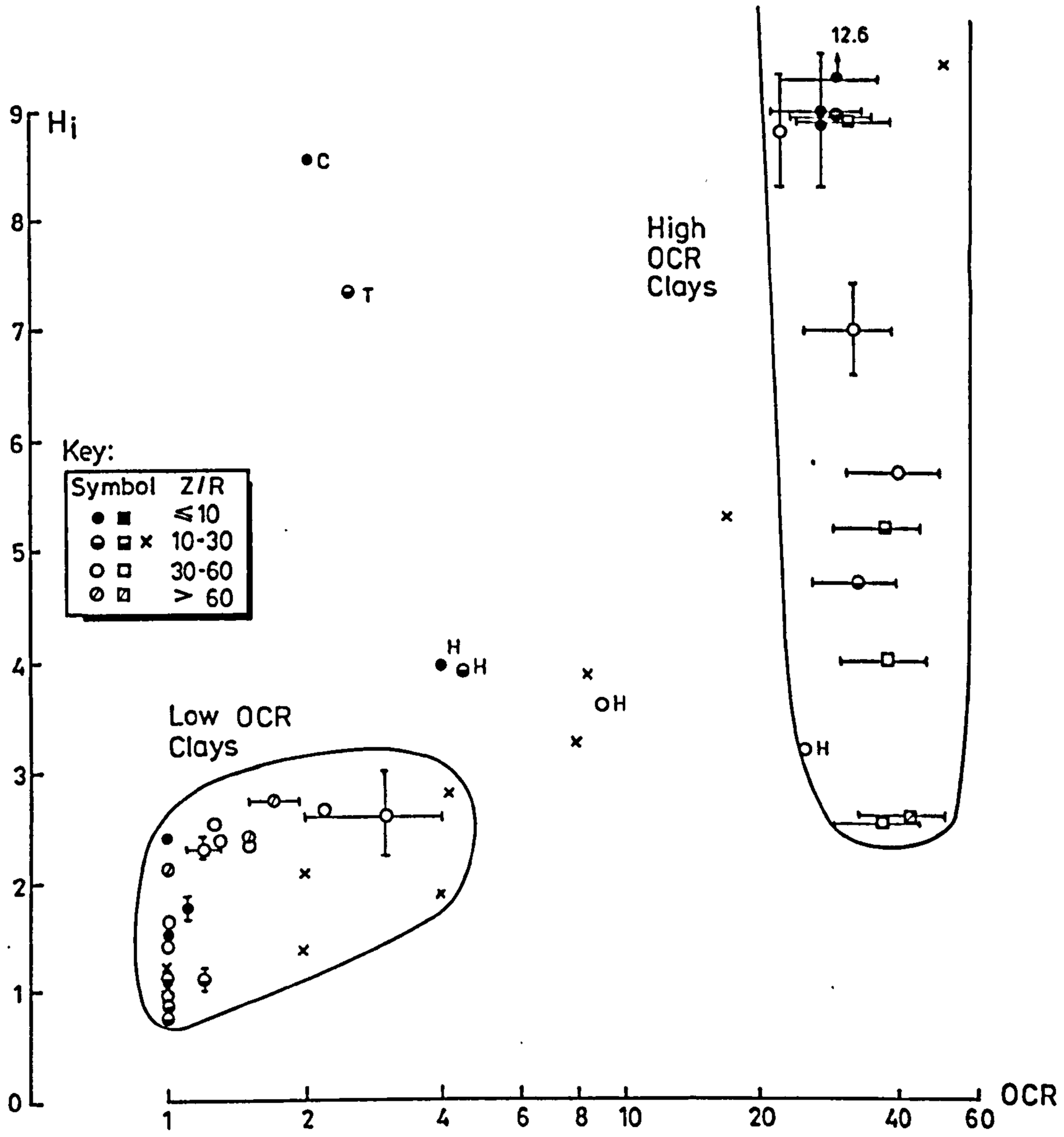



Figure 4.8 Normalized horizontal total stress $H_i$ as a function of OCR

- The data points for the sensitive Tokyo clay [T] and Cowden glacial till [C] do not conform to the trends followed by the other data
- The results for the Haga clay [H] reveal a strong z/R effect (whereby $H_i$ decreases as z/R increases), which almost entirely offsets the tendency for $H_i$ to increase with OCR (at this site OCR varies greatly with depth, and hence also with z/R)
- In general, the radial total stresses measured at leading instrument positions ($z/R \leq 10$, points •) are higher than those recorded at other positions

c) Comparisons with theory

The theoretical predictions for $H_1$ (see Chapter 3) are compared with the overall trend of the data in Figure 4.9:

- The predictions based on the strain path method (curve SPM/MIT-E3) fall within the spread of the data for the low OCR clays, and appear to follow the general trend of the data, which is for $H_1$ to increase with increasing values of OCR
- The cavity expansion method, however, clearly over-estimates the value of $H_1$ once the OCR exceeds 2; the difference between theory and data becomes progressively wider as OCR increases (note that the data *for points far behind the tip* falls near the bottom of the "balloon" for the high OCR clays)

The significance of these results is discussed further in Chapter 14.

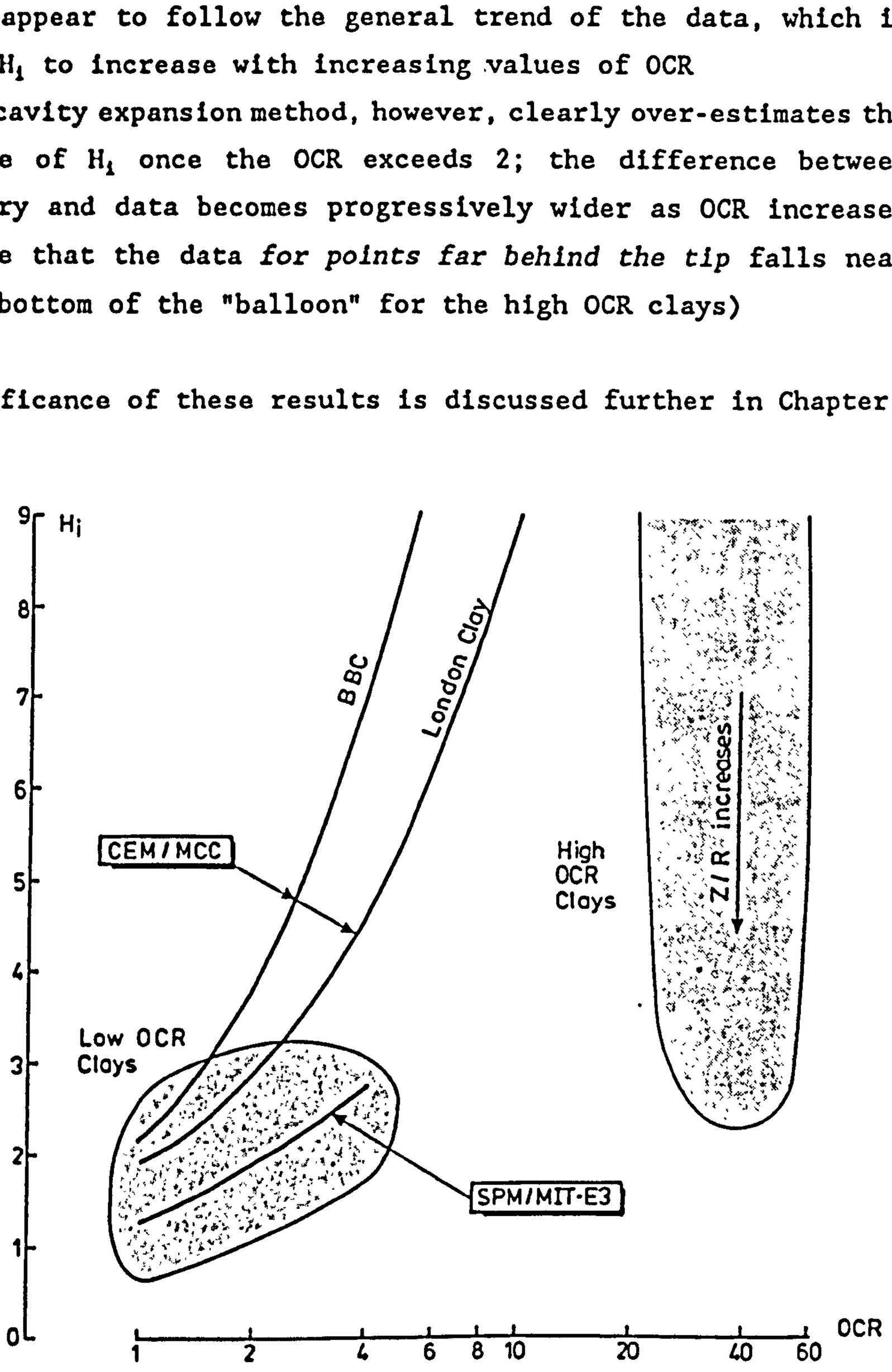



Figure 4.9 Comparison of theoretical and measured values of $H_1$

## 4.3.4 Radial effective stresses

### a) Relationship between $K_i$ and OCR

Figure 4.10 shows values of the lateral stress coefficient $K_i$, plotted against overconsolidation ratio (OCR), for the cases listed in Table 4.4. The results of the experiments at Canons Park (see Chapters 9-11) are also shown on this diagram, and are distinguished by the use of square symbols as opposed to circles.

An inspection of Figure 4.10 reveals the following points of interest:

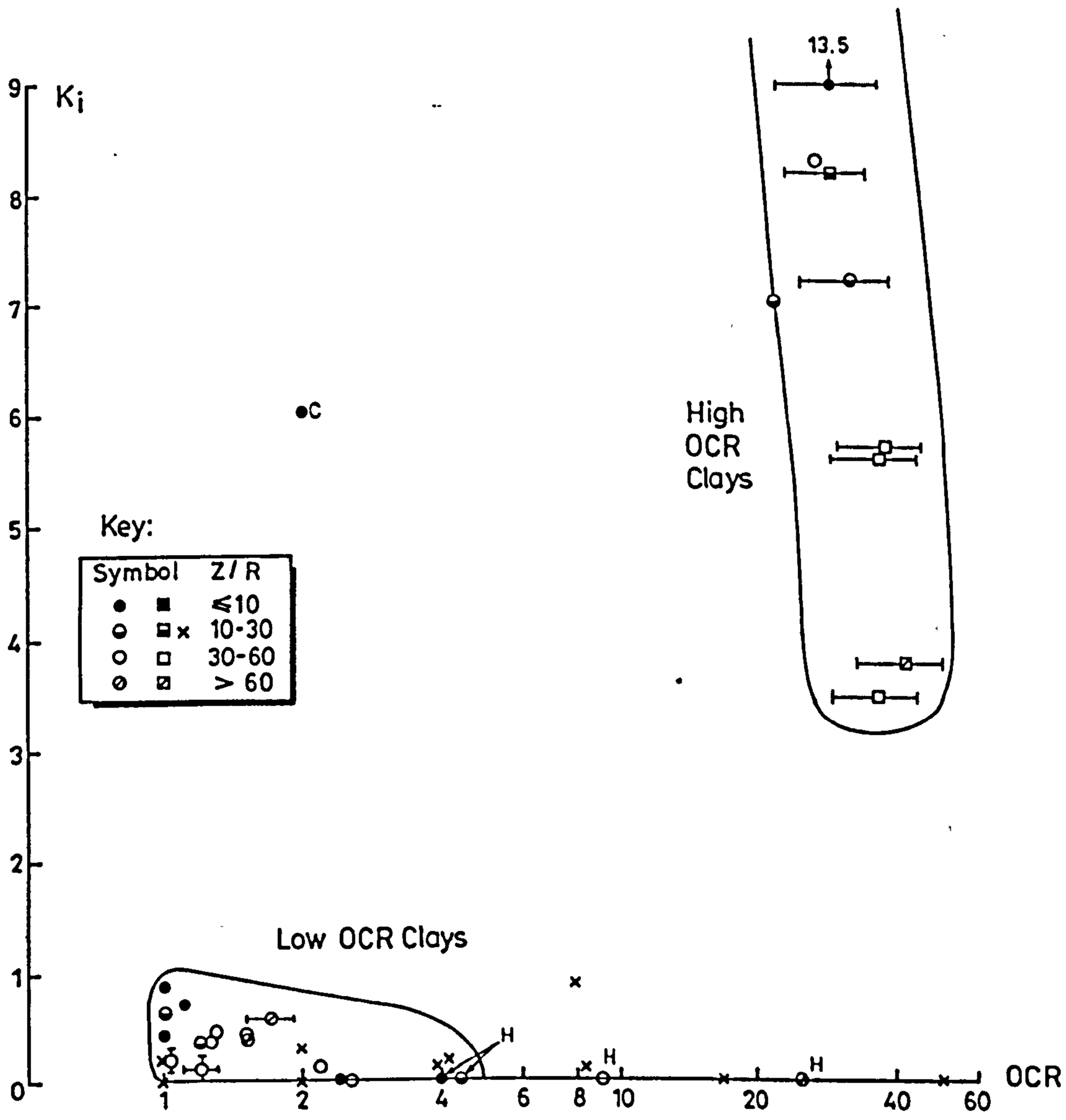



Figure 4.10 Lateral stress coefficient $K_i$ as a function of OCR

- All but one of the data points for the low OCR clays (OCRs < 4) fall within a narrow band, with $K_i$ between 0 and 1; the exception is for a test in the Cowden glacial till [point C, Case 8], a soil which tends to *dilate* when sheared
- The high OCR clays have extremely high values of $K_i$, between 3½ and almost 18), and display a very strong "z/R effect" (whereby $K_i$ reduces with increasing distance behind the pile tip)
- The z/R effect is not so pronounced in the low OCR clays, but the little data that exists (basically Case 3a) <u>does</u> confirm that $K_i$ reduces with increasing z/R
- The few data points with OCR ≥ 4 and $K_i$ < 1 are from field tests in the sensitive Haga clay (points H, Case 13) or from laboratory tests in reconstituted kaolin (points x, Case 9)
- The value of $K_i$ appears to depend on whether the clay *dilates* or *contracts* when sheared: the contractive clays (i.e. the low OCR group plus the Haga clay) have very low values of $K_i$; whereas the dilating clays (the high OCR group plus the Cowden till [Case 8, point C] have high values of $K_i$
- The massive jump in $K_i$ from one group to the other leads to speculation that the behaviour of a pile installed in a dilating soil is fundamentally different from that of one installed in a contractive clay; there may be further discrepancies between their behaviour as a result of the widely different effective stress regimes that exist in the soil that surrounds them

b) Comparisons with theory

The measured values of $K_i$ are compared, in Figure 4.11, with the theoretical predictions based on the cavity expansion and strain path methods (see p143 and Chapter 3).

- The strain path predictions (SPM/MIT-E3) fall within the spread of the experimental data for the low OCR clays, but on average tend to under-estimate $K_i$; predictions are not available for the high OCR materials

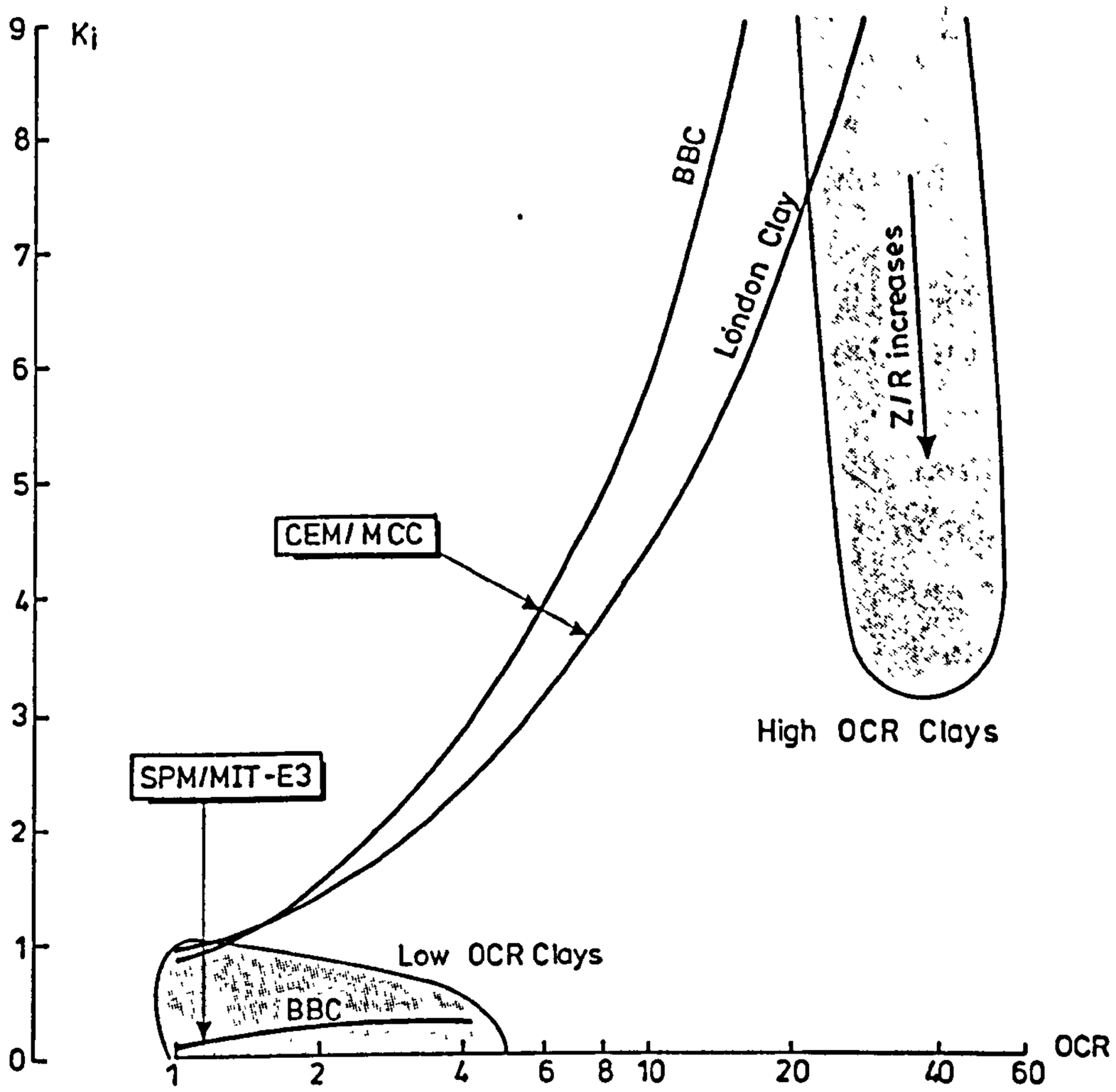



Figure 4.11 Comparison between theoretical and measured values of $K_i$

- The cavity expansion predictions (CEM/MCC) show no agreement with the experimental data, and clearly over-estimate $K_i$ by a large margin over the entire range of OCRs (remember that the data for high z/Rs falls near the bottom of the "balloon" for the high OCR clays)

These results are discussed at greater length in Chapter 14.

## 4.4 EARTH AND PORE PRESSURE EQUALIZATION

### 4.4.1 Pore pressure dissipation

**a) Measurements in contractive clays**

The dissipation of excess pore pressures in the Boston blue clay at Saugus, Massachusetts (Case 10), is illustrated in Figure 4.12 (lower diagram).[15] These results are typical of dissipation records from tests in a wide range of normally- and lightly over-consolidated clays.

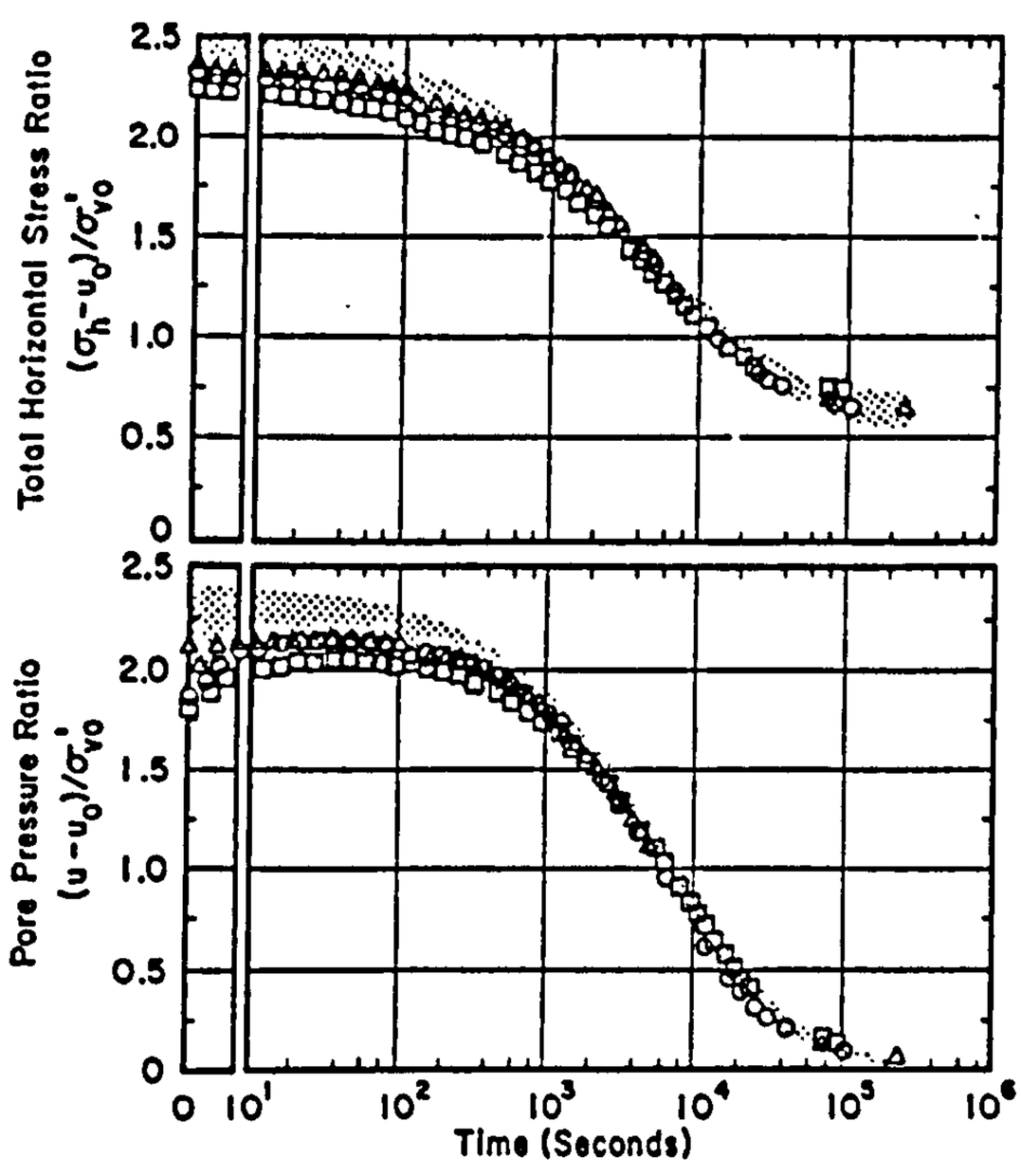



Figure 4.12 Equalization records in lower Boston blue clay

**b) Measurements in dilating clays**

Coop's experiments[16] in the heavily overconsolidated Gault clay show a pattern of behaviour very different from that in the Boston blue clay (see Figure 4.13). The excess pore pressures <u>rise</u> initially and do not reach their maximum values until 1½ to 83 minutes into the equalization period. After 2½h (≈$10^4$s) have elapsed the pore pressures are all falling steadily with time, in a manner similar to that for the Boston blue clay.

The apparent rise in pore pressures during the early stages of equalization may reflect problems of the piezometer system, rather than the true response of the soil. During pile installation, Coop's pore pressure probes suffered from slow response times owing to cavitation of the piezometer fluid (see p142) - therefore we must have reservations about the ability of these probes to register the true response of the soil. Unfortunately, the other Category A/B tests in heavily over-

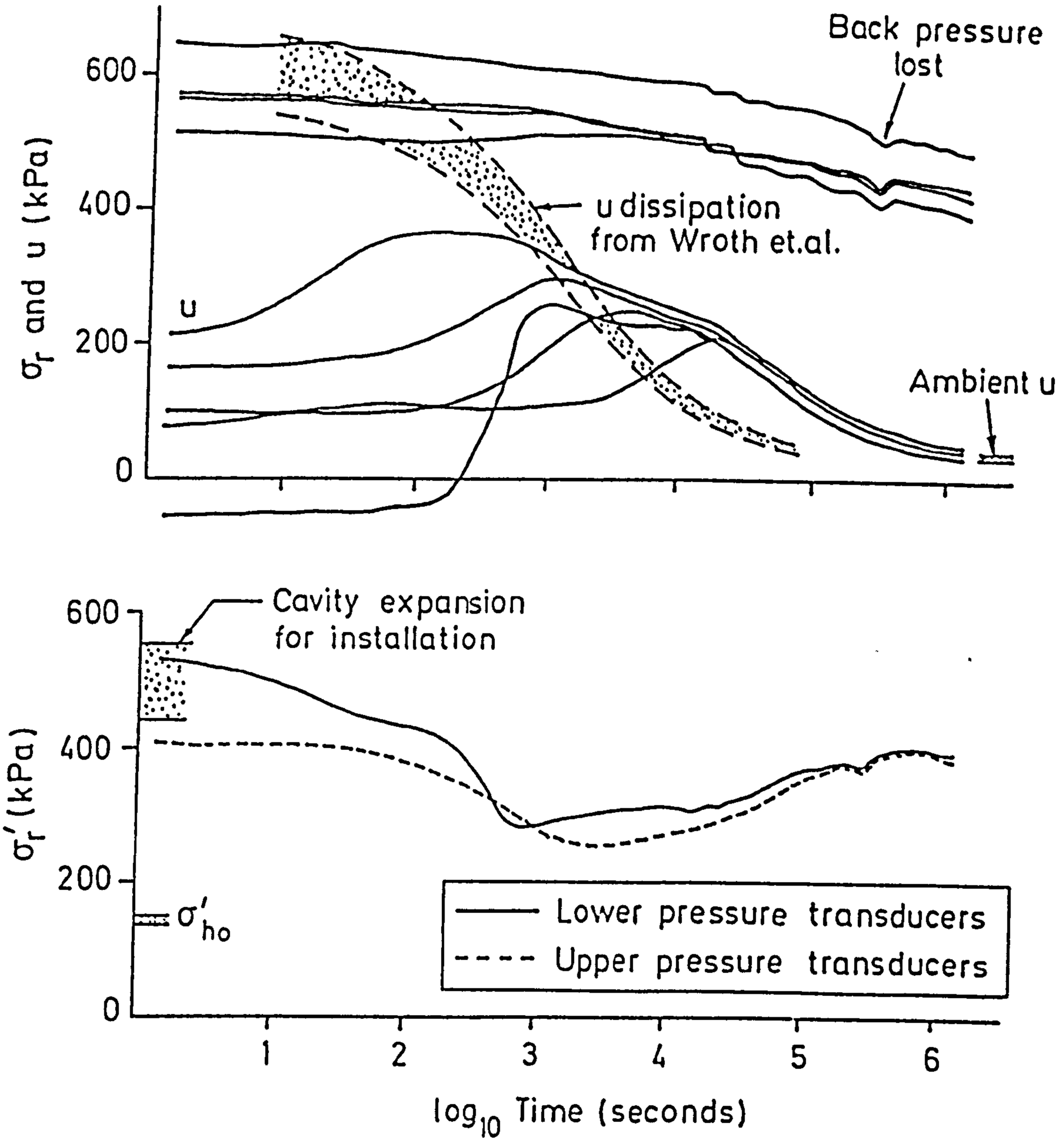



**Figure 4.13** Equalization records in the Gault clay

consolidated clays (Cases 5, 7, 8, 14, and 16) provide only poor quality data and cannot be relied upon to confirm this behaviour.

The results of my experiments in the London clay (see Chapter 10) help to corroborate the trends of Coop's data. Unlike his devices, my pore pressure probes remained "alive" during pile installation, and are therefore considered more reliable. They too gave rise times during equalization of between 3 and 45 minutes at <u>leading</u> instrument positions ($z/R \leq 10$), although the behaviour at the following and trailing positions ($z/R$ = 10-30) was very different (see Chapter 14 for further

discussion of this point). Two of Coop's probes were located at leading positions, and two at following positions. Similar characteristics to these have also been observed in piezocone tests in high OCR clays (where the filter was located behind the cone tip, at z/R = 2.2).[17]

### 4.4.2 Changes in total stress

a) Measurements in contractive clays

Figure 4.12 (upper diagram) shows how the normalized horizontal total stress (H) decreased during equalization in the lightly overconsolidated Boston blue clay. The value of H fell from 2.38 ±0.12 at the start of consolidation to 0.60 ±0.03 at the end.

According to Azzouz and Morrison, these measurements provide "...clear evidence of the importance of soil nonlinearities during consolidation".[18] They certainly invalidate any analysis of pile behaviour that is based on uncoupled (i.e. *linear*) consolidation theory (linear theory predicts no change in H during equalization - see Chapter 3).

b) Measurements in dilating clays

Although the radial total stress has been found to decrease in high OCR clays - witness the data for the Gault clay on p155 (Figure 4.13) - the drop in H is generally more gradual and a smaller proportion of $H_i$ than in low OCR clays. My experiments in the London clay have shown that $\sigma_{rr}$ can also <u>increase</u> during equalization, depending on the position relative to the pile tip (see Chapter 10).

c) Magnitude of the relaxation coefficient $H_c/H_i$

The degree to which the normalized horizontal total stress (H) falls during consolidation can be assessed in terms of the "relaxation coefficient", $H_c/H_i$. Table 4.6 summarizes the values of $H_c/H_i$ <u>for contractive clays</u>, as recorded in the Category A experiments where the full dissipation of excess pore pressures was allowed. The numbers are in

reasonable agreement with each other, with the relaxation coefficient taking the average* value $H_c/H_i$ = 0.32 ±0.21.

Table 4.6 $H_c/H_i$ in contractive clays

| Case | $H_c/H_i$ | Scatter |
|---|---|---|
| 1 | 0.22 | ±0.04 |
| 2 | 0.28 | ±0.02 |
| 3a | 0.48 | ±0.05 |
| 9(A)† | 0.91 | ±0.08 |
| 9(B)† | 0.56 | ±0.03 |
| 10 | 0.30 | ±0.05 |
| 11 | 0.27 | ±0.05 |
| 12 | 0.31 | ±0.04 |
| 13 | 0.30 | ±0.12 |
| 15 | 0.47 | ±0.09 |
| Mean | 0.33 | ±0.23 |

† not included in mean

Data for <u>dilating</u> clays is rather sparse, but where it does exist it indicates that $H_c/H_i$ is much higher than for contractive clays. In the Gault clay (Case 17a), the relaxation coefficient was 0.73 ±0.09. In my experiments at Canons Park, in the London clay, $H_c/H_i$ varied from 0.77 ±0.06 (at $z/R \approx 8$) to 1.35 ±0.31 (at $z/R \approx 50$). The last figure indicates that the radial total stress acting on the pile may in fact <u>increase</u> rather than decrease during equalization (the term "relaxation" is a misnomer in this case). The Canons Park results are discussed at greater length in Chapters 10 and 14.

d) Comparisons with theoretical predictions for $H_c/H_i$

Recalling one of the findings from Chapter 3 (see p105ff): theoretical predictions for $H_c/H_i$ are controlled by features of the constitutive model employed, and not by the method of analysis. Thus both the cavity expansion and strain path methods' prophesy that $H_c/H_i \approx 0.83$ according to Modified Cam Clay (for a wide range of OCRs, from 1 to 32); whereas with MIT-E1 and -E3 they suggest that $H_c/H_i$ = 0.29-0.45 (for OCRs = 1-4).

The test data for the low OCR (i.e. contractive) clays lends little credence to the use of the Modified Cam Clay model, but is in reasonable agreement with those produced with MIT-E1 and -E3. (There are several versions of Modified Cam Clay - these comments pertain solely to the formulation used by the research workers at MIT.)

---

*Values of $H_c/H_i$ from Case 9 (Francescon's laboratory tests) have been ignored, since the radial total stress in this case may be governed by features of the laboratory apparatus

## 4.4.3 Radial effective stresses

### a) Measurements in contractive clays

The way in which the radial effective stress ($\sigma'_{rr}$) varies during equalization depends on the relative magnitude of the changes in radial total stress ($\sigma_{rr}$) and pore pressure (u).

In the Boston blue clay at Saugus (see Figure 4.14), the lateral stress coefficient at the start of equalization ($K_i$) was between 0.05 and 0.2; it decreased slightly during the first ½h ($10^3$s), and then increased monotonically over the next 11½ days ($10^6$ seconds), reaching a final value ($K_c$) of 0.6 ±0.3.

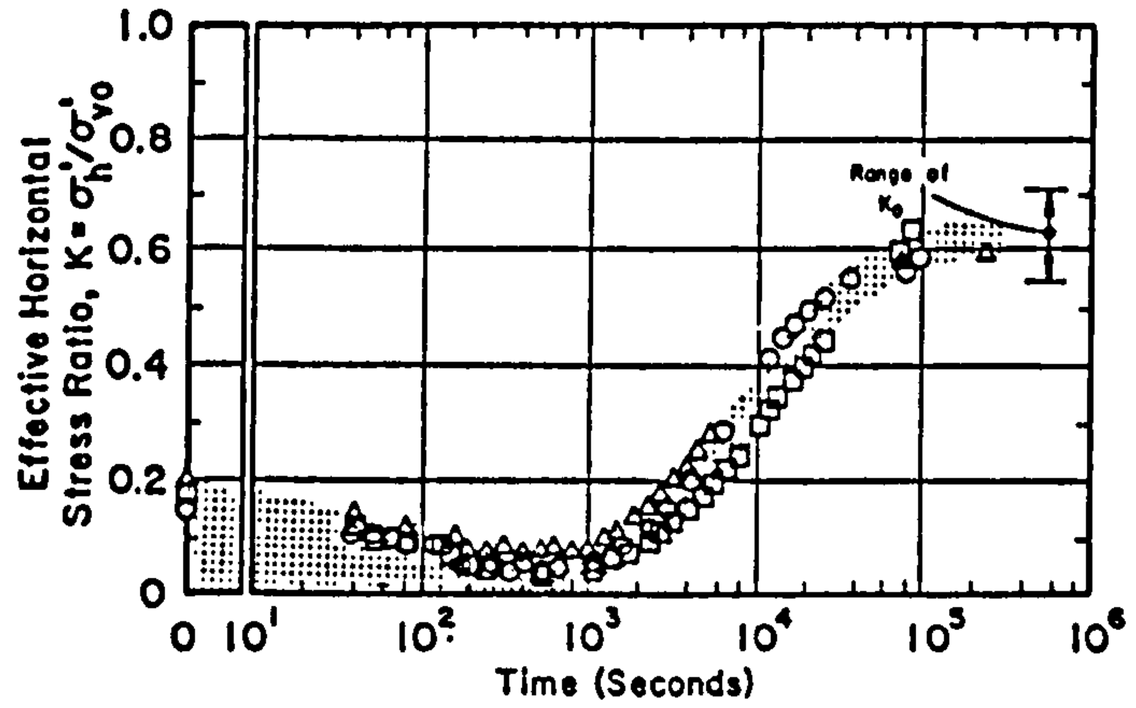



Figure 4.14 Increase in $\sigma'_{rr}$ during equalization of Boston blue clay (for z/R = 50)

### b) Measurements in dilating clays

As Figure 4.13 shows (see p155), the variation of the radial effective stresses during equalization of the Gault clay is rather different from that of the Boston blue clay (BBC).

In the high OCR clay, $K_i$ = 7.0-8.3. During the first ½h ($10^3$s) of equalization, the lateral stress coefficient decreased by between 38 and 47% of $K_i$ (the decrease in the BBC was negligible by comparison). Although, over the next 11½ days ($10^6$ seconds), the radial effective stresses regained between 60 and 90% of the amount that they had fallen, the recovery was not enough for the lateral stress coefficient at the end of equalization ($K_c$) to exceed that at the start ($K_i$). The value of $K_c$ was 4-27% <u>smaller</u> than $K_i$ (i.e. $K_i/K_c$ = 1.05-1.46), whereas in the Boston blue clay it was over three times <u>larger</u> ($K_i/K_c$ = 0.08-0.35).

c) Magnitude of the set-up coefficient $K_i/K_c$

Values of the "set-up coefficient"* ($K_i/K_c$) recorded in contractive clays are summarized in Table 4.7. The scatter of the results is too high to draw any firm conclusions about the magnitude of $K_i/K_c$, although it would appear that the ratio is generally less than about 0.4. The notable exception in Table 4.7 is the value of 1.35 recorded in the Oslo quick clay (Case 3a).

Table 4.7 $K_i/K_c$ for contractive clays

| Case | $K_i/K_c$ | Scatter |
|---|---|---|
| 2 | ≈0.0 | ? |
| 3a | 1.35 | ±0.06 |
| 9(A) | 0.1 | ±0.2 |
| 9(B) | 0.18 | ±0.13 |
| 10 | 0.21 | ? |
| 11 | 0.50 | ±0.35 |
| 12 | ≈0.0 | ? |
| 13 | ≈0.43 | ±0.09 |
| 15 | 0.39 | ±0.04 |

In dilating clays the set-up coefficient generally exceeds one, since the radial effective stress at the end of equalization is less than that at the start. In the Gault clay (Case 17a), $K_i/K_c$ = 1.36 at z/R = 5½, reducing to 1.04 at z/R = 22; and in the London clay (see Chapters 10 and 14), $K_i/K_c$ = 1.25 ±0.22 at z/R ≈ 8, reducing to 0.96 ±0.09 at z/R ≈ 50. In both of these clays the set-up coefficient clearly depends on the value of z/R.

d) Theoretical predictions for $K_i/K_c$

Theoretical predictions for $K_i/K_c$ are given in Chapter 3 (p105ff).

According to the cavity expansion method, for OCRs in the range 1-32 the set-up coefficient equals 0.49-0.63 (depending on which constitutive model is used). These results are generally too high at low OCRs and too low at high ones. (Note, however, that the predictions at high OCRs are for the Modified Cam Clay model only.)

According to the strain path method, at low OCRs (less than four) the set-up coefficient is between 0.15 and 0.29 (depending on soil model) - a result which is in broad agreement with the data given in Table 4.7.

---

*Note that $K_i$ is divided by $K_c$, and not vice versa; a more logical definition of the set-up coefficient would be $K_c/K_i$ - this, however, would create a highly unstable parameter, since $K_i$ is close to zero in contractive clays

Strain path predictions for high OCR clays have not yet been published (see the footnote on page 144).

e) Relationship between $K_c$ and OCR

Figure 4.15 shows the relationship between the lateral stress coefficient at the end of equalization ($K_c$) and the clay's undrained strength ratio ($c_{uo}/\sigma'_{vo}$), as determined in the Category A experiments listed in Table 4.2.

The following points arise from an inspection of Figure 4.15:

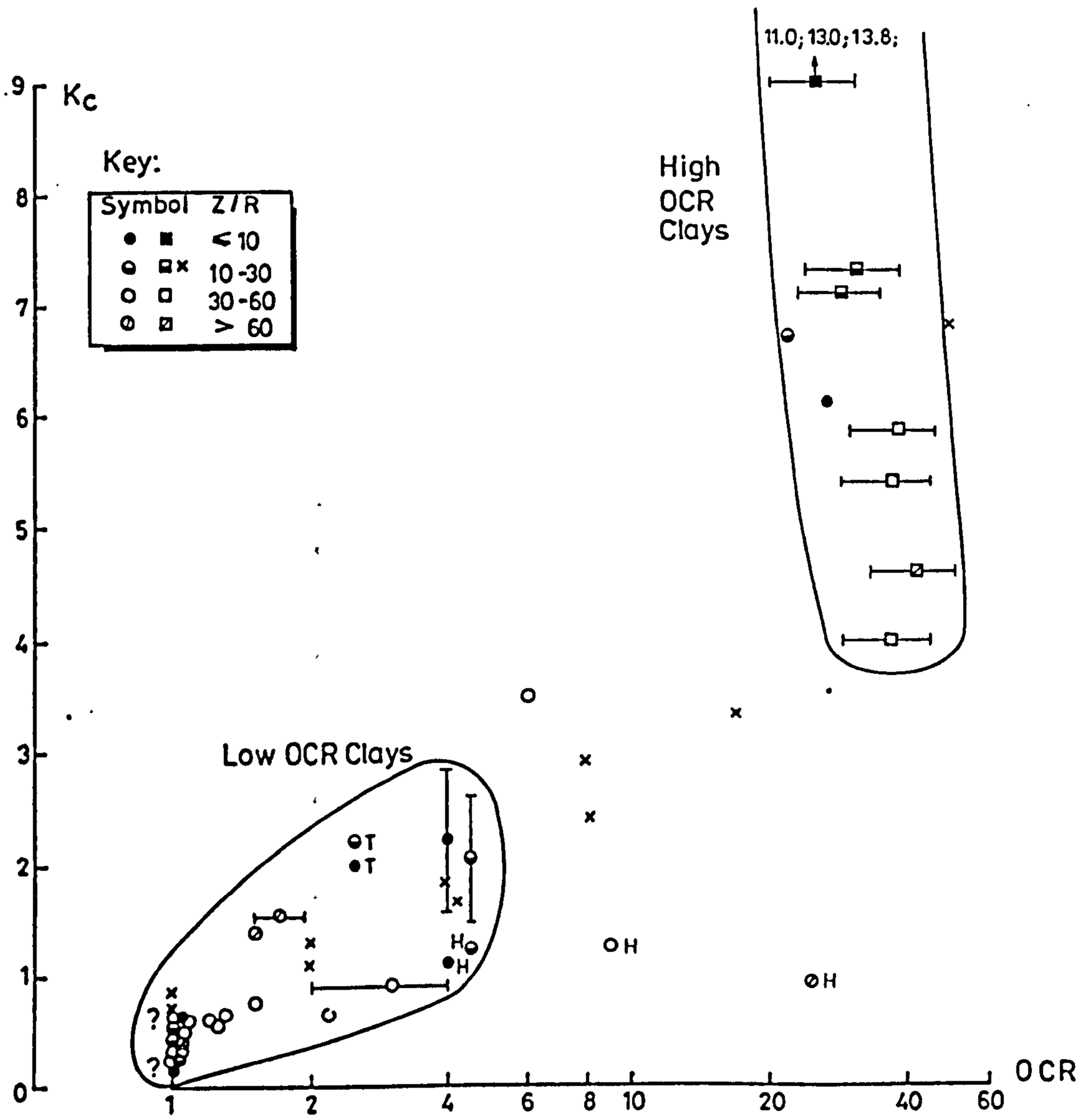



Figure 4.15 Lateral stress coefficient $K_c$ as a function of OCR

- The general trend of the data is for $K_c$ to
  the spread of the data also tends to inc
  once OCR exceeds 10
- The spread of the data at low OCRs (less t
  ≤ 2.25; at high OCRs (greater than 20) it i
- The data points for the sensitive Haga clay
  do not conform to the pattern of the othe
  clay's apparent OCR has been caused by leacl
  the erosion of sediment - consequently the
  on shearing, and behaves more like a low O
  one
- There is a very clear "z/R effect" for the h
  is a vestige of the stress conditions s
  installation; the z/R effect is less pronour
  clays, although the indications are that it

f) Comparison with theory

The theoretical predictions for $K_c$, according to strain path methods (see Chapter 3 and p143), experimental data in Figure 4.16.

- The cavity expansion method (CEM/MCC) clear
  by a large factor, over the entire range
  irrefutable proof that the cavity expansio
  inappropriate for predicting the behaviour
- The curve (SPM/MIT-E3) representing the stra
  (note: for z/R = 200) falls within the spre
  the low OCR clays, tending (on average) to
  predictions are not yet available for highe
- The curve labelled "$K_0$" indicates the likel
  horizontal stresses that existed in the gr
  installation: the line shown represents a c
  angle ($\phi$) of 25°, and assumes that $K_0$ is giv
  Kulhawy[19] equation: $K_0 = (1 - \sin \phi)OCR^{\sin \phi}$
- At low OCRs, $K_c$ generally exceeds $K_0$, althou
  can be significantly lower; at high OCRs

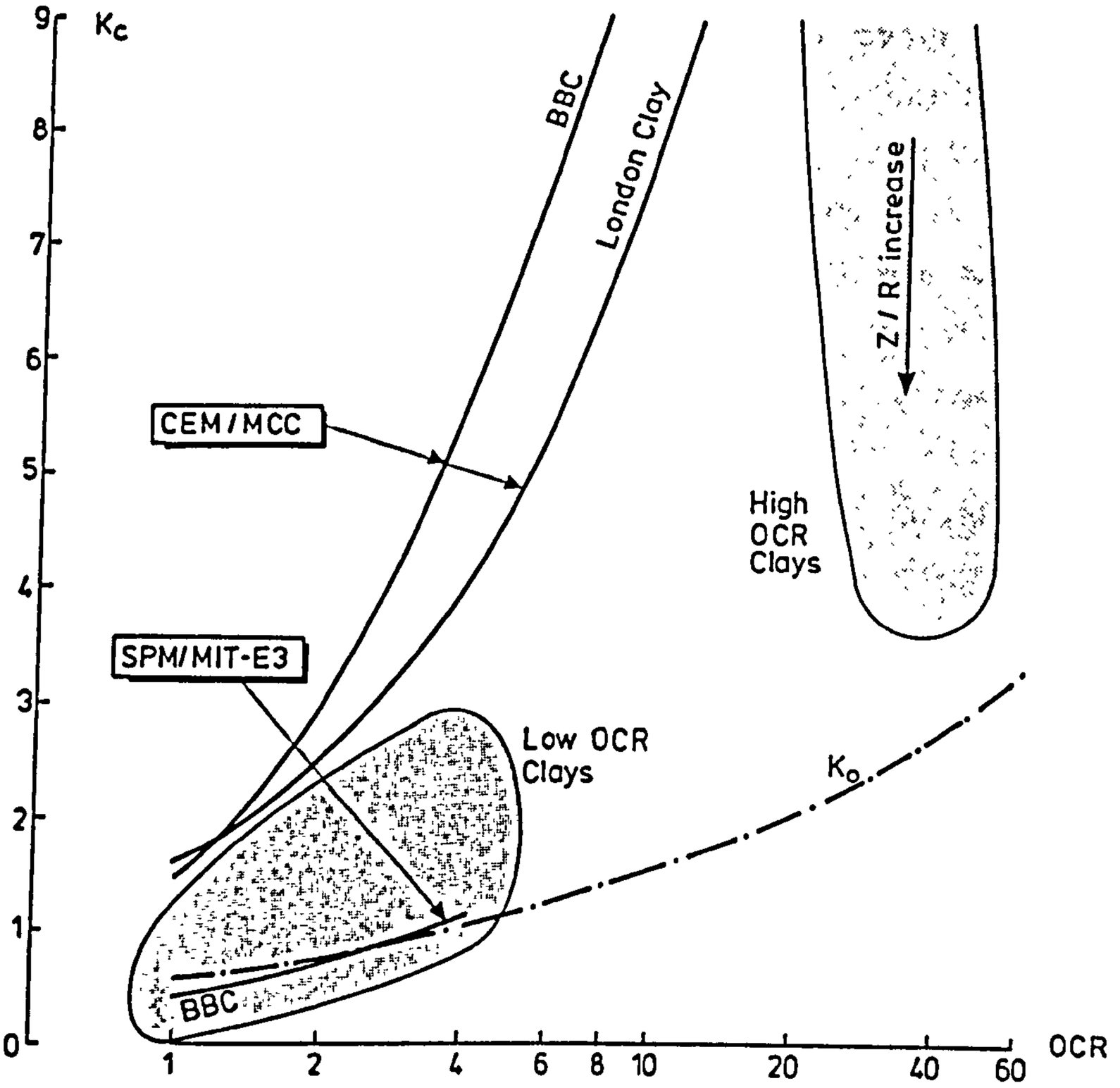



**Figure 4.16** Comparison of theoretical and measured values of $K_c$

greater than $K_0$

- As z/R increases (i.e. we move away from the pile tip), $K_c$ reduces to a value close to - but always above - the value of $K_0$ for the undisturbed ground

These results are discussed at much greater length in Chapter 14.

## 4.5 PILE LOADING

### 4.5.1 Introduction

The parameters that govern the shaft capacity of a pile during loading are the radial effective stress ($\sigma'_{rr}$) and the coefficient of friction ($\mu$) acting at the pile/soil interface:

$$Q_{shaft} = \pi D \int_L \tau_{rz} dz = \pi D \int_L \mu (\sigma'_{rr})_f dz$$

Direct measurements of these parameters *during* pile loading have been reported in only two previous case histories (nos 10 and 17). Neither of these experiments followed standard load test procedures[20]; instead, the piles were loaded very rapidly, effectively under *undrained* conditions. Hence the results of these experiments may not represent the behaviour of most working piles, which are often loaded at much slower rates, under drained or partially drained conditions.

Because there are so few direct measurements of effective stresses during pile loading, we must examine "indirect" evidence regarding the values of $\sigma'_{rr}$ and $\mu$, if we are to understand the fundamentals of pile behaviour. The "indirect" evidence includes comparisons between the load-displacement curves of jacked and driven piles (see Section 4.5.4); and investigations into the disturbance caused to the soil during pile installation (Section 4.5.5). However, we should examine the direct measurements first, before moving on to the "indirect".

### 4.5.2 Effective stress data for contractive clays

a) PLS cell measurements in the Boston blue clay

Morrison[21] conducted a series of experiments in the Boston blue clay, using the Piezo-Lateral Stress (PLS) cell which is illustrated in Figure 4.17. Certain features of this instrument are worth mentioning, since they have a direct bearing on the accuracy of the measurements obtained during pile loading.

The first thing to note is that the porous stone (see detail A of Figure 4.17) has a rough surface finish, whereas the remainder of the PLS cell is very smooth. Therefore the pore pressure measured through the porous stone may be much higher than that acting on the membrane of the radial stress cell (owing to shear-induced pore pressures).

Secondly, the smooth surface finish of the PLS cell is not realistic of working piles, and may lead to artificially low angles of friction ($\mu$) being measured, if sliding takes place at the pile/soil interface.

Thirdly, there are potentially large errors in the values quoted for the coefficient of friction, $\mu$ (= $\tau_{rz}/\sigma'_{rr}$), arising from the variation of shear stress ($\tau_{rz}$) with distance behind the pile tip (i.e. the "z/R effect"). The shear stress is calculated from the difference between the axial stress ($\sigma_a$) acting at the end of the AW drill rod (see Figure 4.17) and the end bearing at the pile tip. $\tau_{rz}$ is therefore an "average" and not a "local" measurement. Since $\sigma'_{rr}$ is a "local" measurement, the value of $\mu$ is probably over-estimated.

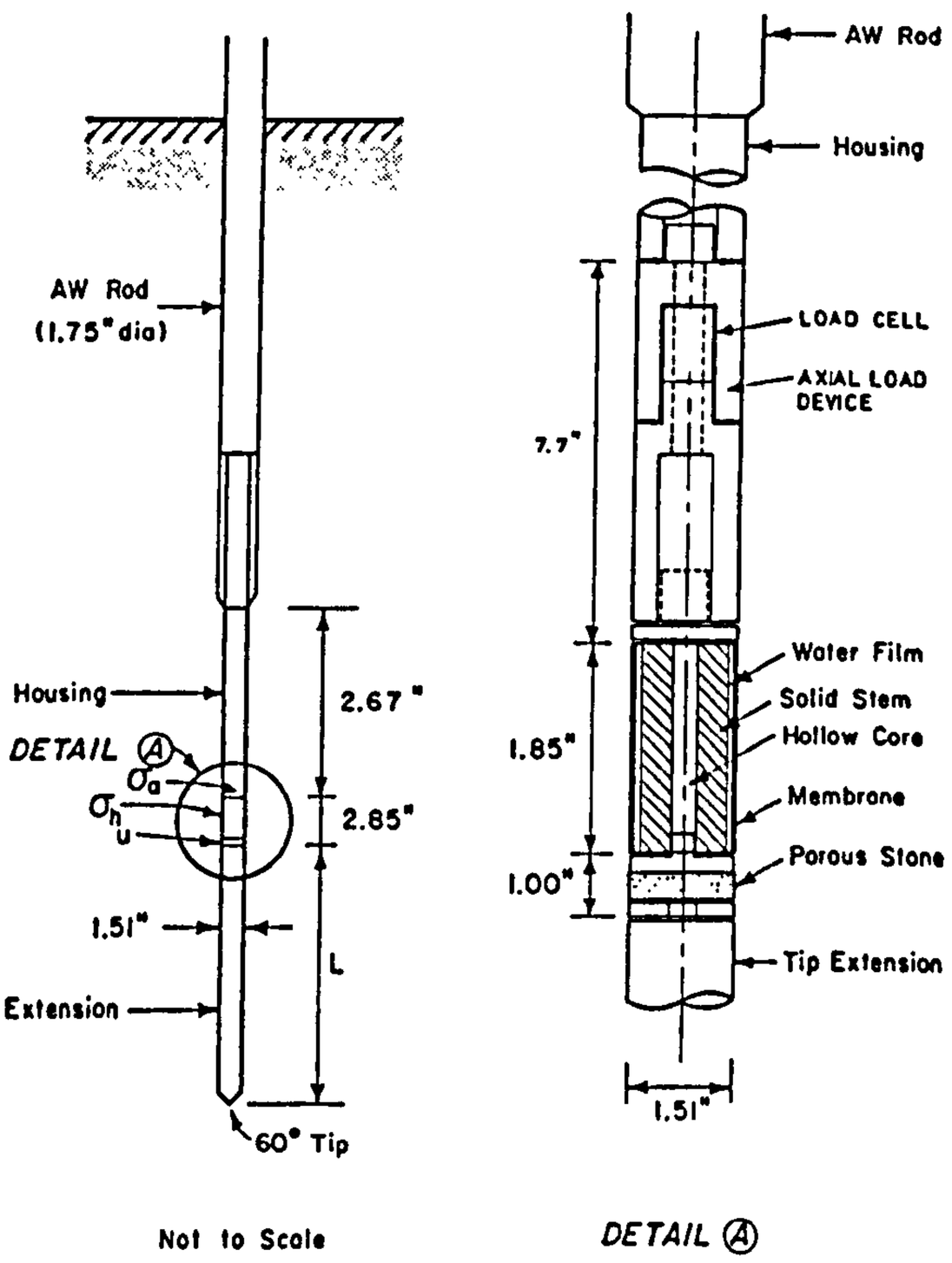



Figure 4.17 Piezo-Lateral Stress cell

(In addition, there are errors in the calculated values of $\tau_{rz}$ owing to differences between the actual and the <u>assumed</u> end bearing ($q_c$) acting at the tip.)

Finally, the arrangements for loading the PLS cell are somewhat primitive, as Morrison himself admits:

> "The process of pile loading was simulated... by applying a compressive or tensile force of sufficient magnitude to induce failure, this being signified by movement [of 13-25mm] of the drill rods at the ground surface... In view of the relatively crude system of loading used in the field, accurate control of deformation is lacking."[22]

As a consequence, accurate measurements of the radial effective stress at failure, $(\sigma'_{rr})_f$, are also lacking.

b) Stress paths from PLS experiments in Boston blue clay

Figure 4.18 shows the effective stress paths that were followed by the Boston blue clay during a typical *compression* load test, as recorded in PLS cell experiments at Saugus, Massachusetts (Case 10). Three curves have been drawn, showing i) the pore pressure (u); ii) the radial total stress ($\sigma_{rr}$); and iii) the radial effective stress ($\sigma'_{rr}$), as functions of the applied shear stress ($\tau_{rz}$). Each parameter has been normalized by the vertical effective stress in the undisturbed ground ($\sigma'_{vo}$).

Initially there is little or no change in any of the parameters (points A to B). However, as the applied shear stress increases beyond point B, the clay starts to contract (B to C), with little change in radial total

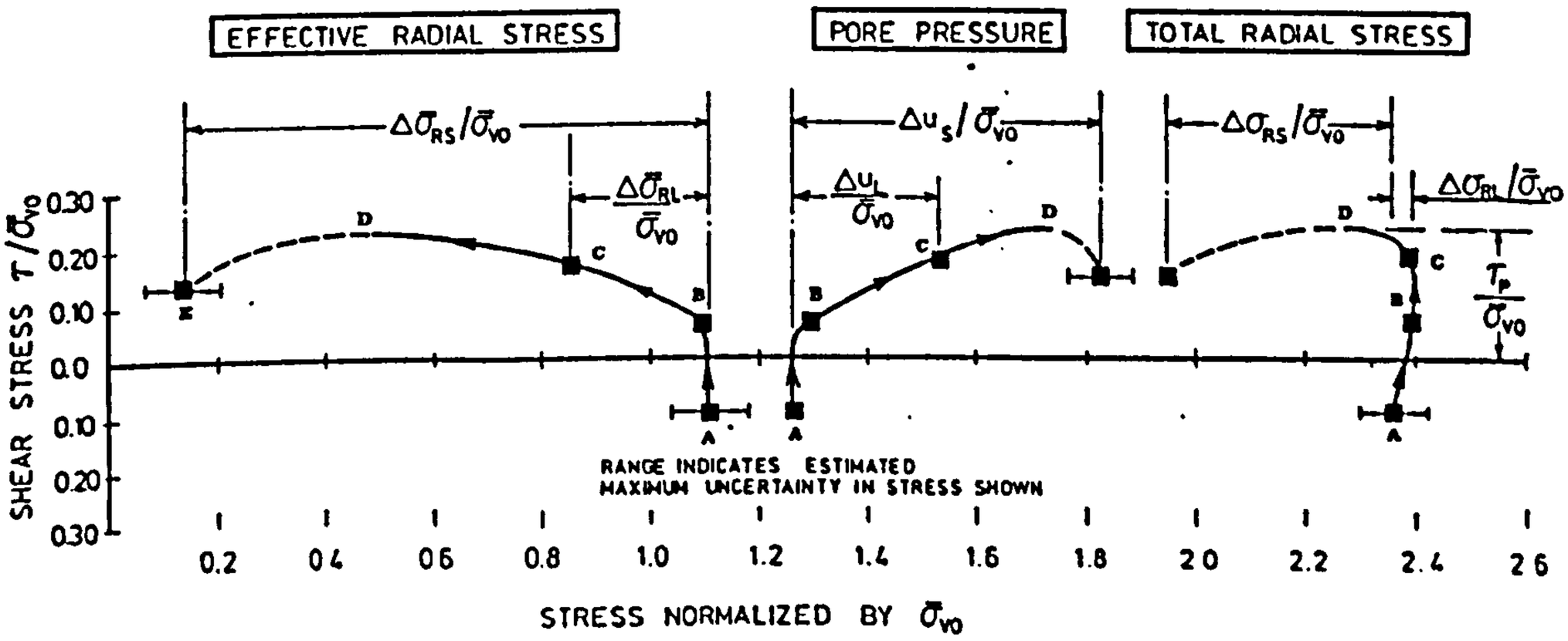



Figure 4.18 Effective stress paths followed during load tests in Boston blue clay

stress; the pore pressure rises as the radial effective stress falls. Failure occurs somewhere around point D. (The reduction in pore pressure after point D is due to the axial load dropping during plunging failure.)

The shape of the effective stress path ($\tau_{rz}/\sigma'_{vo}$ vs $\sigma'_{rr}/\sigma'_{vo}$) is similar to those obtained in direct simple shear tests on normally consolidated Boston blue clay (see Chapter 3).

The magnitude of these changes are summarized[23] in Table 4.8 for first-time loading in compression and tension. In both cases the change in radial total stress is small, and of the same sign, i.e. $\Delta\sigma_{rr}/\sigma'_{vo} \approx -0.1$. The changes in radial effective stress are smaller in tension than in compression, and the changes in pore pressure are consequently bigger. These differences are the result of the clay re-consolidating (during the equalization period) under the influence of a tensile (i.e. downward) shear stress, of magnitude $\tau_{rz}/\sigma'_{vo} = 0.05$-$0.06$.

Table 4.8 Changes in stress during pile loading (Boston blue clay)

| Parameter | Compression test | Tension test |
|---|---|---|
| $\Delta\sigma_{rr}/\sigma'_{vo}$ | -0.13 | -0.05 |
| $\Delta u/\sigma'_{vo}$ | +0.50† | +0.38‡ |
| $\sigma'_{rr}/\sigma'_{vo}$ | -0.65† | -0.43‡ |

Figures ±0.03 except: † ±0.05; ‡ ±0.08

c) Coefficient of friction

Unfortunately, owing to the limitations of the equipment, measurements of the coefficient of friction at the *onset* of failure are not very reliable. For example, Table 4.9 summarizes the values of $(\sigma'_{rr})_f$ and $\mu$ that were recorded in the upper deposits of Boston blue clay. The scatter in the values is too great for firm conclusions to be drawn from this data regarding the magnitude of the coefficient of friction.

Table 4.9 Load tests in the upper and middle layers of Boston blue clay

| Depth (m) | $\beta$ | $\rho$ | † | $\mu$ |
|---|---|---|---|---|
| 10.5 | 0.21 | 0.38 | 0.70 | 0.55 |
| 12.0 | 0.26 | 0.24 | 0.78 | 0.30 |
| 13.6 | 0.22 | 0.28 | 0.45 | 0.62 |
| 19.1 | 0.25 | 0.52 | 0.83 | 0.28 |

$\beta = (\tau_{rz})_f/\sigma'_{vo}$; $\rho = (\tau_{rz})_f/(\sigma'_{rr})_c$
† $= (\sigma'_{rr})_f/(\sigma'_{rr})_c$; $\mu = (\tau_{rz})_f/(\sigma'_{rr})_f$

### 4.5.3 Effective stress data for dilating clays

Coop[24] presents effective stress data from a series of load tests in the heavily overconsolidated Gault clay (Case 17a). A notable feature of these experiments was that the pile's overall load capacity reduced slightly during the equalization period (i.e. there was a *negative* set-up effect).

As discussed in Section 4.5.1, the load tests were performed according to a non-standard procedure: the head of the pile was pushed a distance of 30mm in just over 90 seconds. Hence, the load tests were performed under nominally undrained conditions. Failure of the pile was accompanied by a sudden drop in pore pressure, while the radial total stress transducers* registered little or no change in $\sigma_{rr}$. The coefficient of friction mobilized at failure ($\mu$ = tan 8.4°) was similar in value to that measured during pile installation (tan 5.7° $\leq \mu \leq$ tan 9.6°).

Unfortunately, the way that Coop presents his data does not allow the effective stress paths to be plotted with sufficient accuracy to warrant including them herein. In their stead I have drawn the load-displacement diagram for one of the tests (Test G), since this reveals some interesting features of pile behaviour in dilating clays.

The model pile was installed by jacking at a relatively slow# rate of displacement (nominally 200mm/min); it was load tested after 16 days, twice in compression (L1C and L2C) and then once in tension (L3T). The load-displacement curve for test L1C is shown in Figure 4.19. Note the close agreement between the independent measurements provided by the upper and lower friction sleeves. The following points are also worth mentioning:

---

*These operate as null devices, the radial total stress reacting against a back-pressure inside the pile (see Appendix 5); it is not clear if the measurements of $\sigma_{rr}$ during pile loading were affected by the inevitable lack of control of the back-pressure system

#Relative to the rates for driven piles, and the fast jacking achieved in the tests at Canons Park (see Chapters 7 and 8)

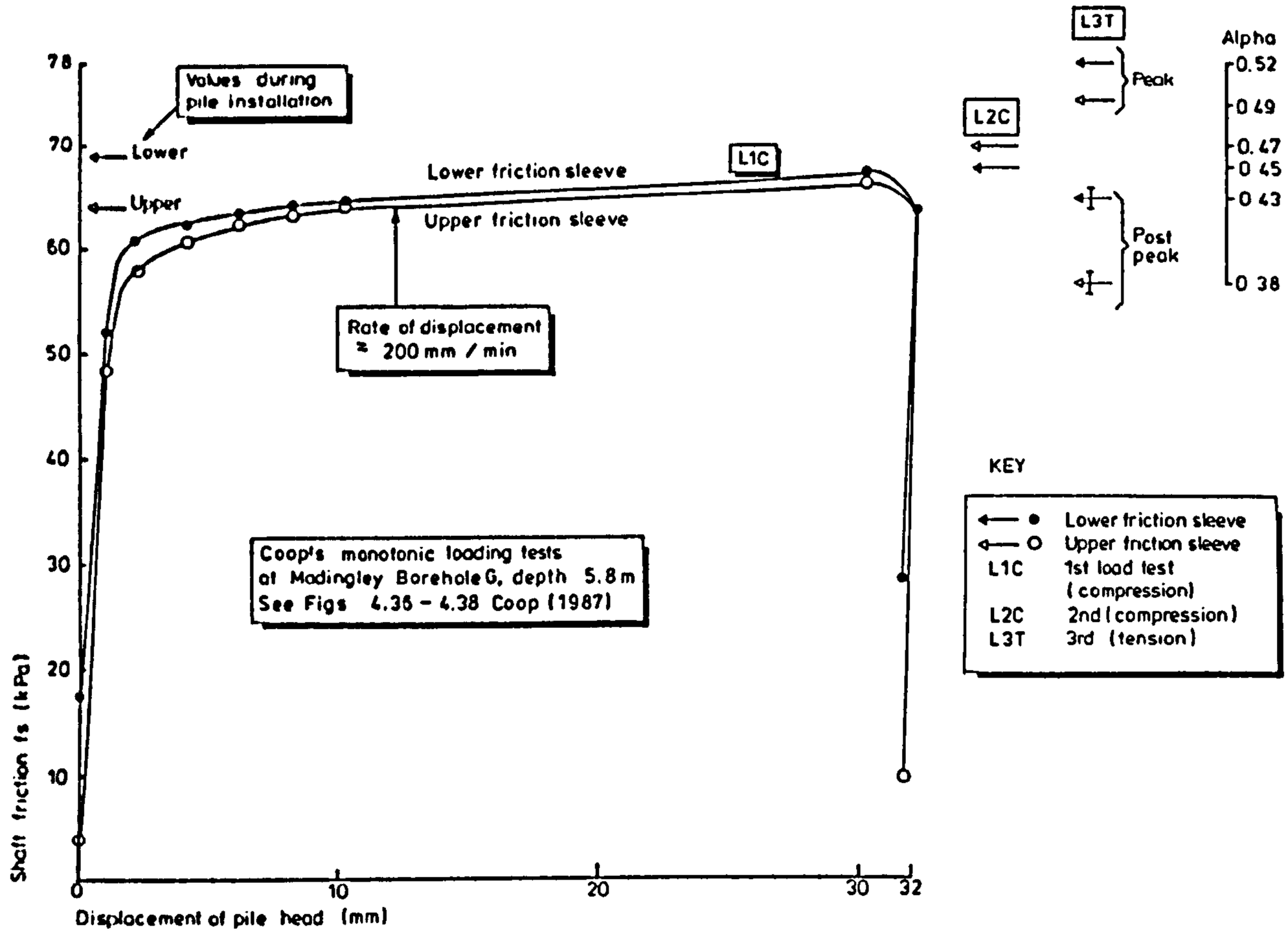



Figure 4.19 Load-displacement curves from Coop's tests in Gault clay

- When loaded in compression the pile's response is ductile (tests L1C and L2C)
- When the loading direction is changed (in L3T), the pile's response becomes brittle
- (Not shown by the diagram.) The radial effective stress acting on the pile at the onset of plunging failure, $(\sigma'_{rr})_f$, is similar to that at the end of equalization, i.e. $(\sigma'_{rr})_f \approx (\sigma'_{rr})_c$

Based on these results Coop concluded that failure of the model pile occurred along a residual shear surface "established during installation".[25] The results of the experiments described in Chapters 9-13 (in the London clay) support this conclusion for heavily over-consolidated clays, but indicate that the *rate* of displacement may have a major influence on the value of $\mu$.

## 4.5.4 Differences between the behaviour of jacked and driven piles

The extensive series of (uninstrumented) pile tests performed by Tomlinson,[26] in the London clay at Stanmore, north London, reveal important differences between the behaviour of jacked and driven piles in stiff clays. Tomlinson tested six driven (DP1-6) and six jacked (JP1-6) piles,* on three separate occasions: 28 days, 3 months, and 1 year after installation. Figure 4.20 shows the load-displacement curves for all thirty-six load tests.

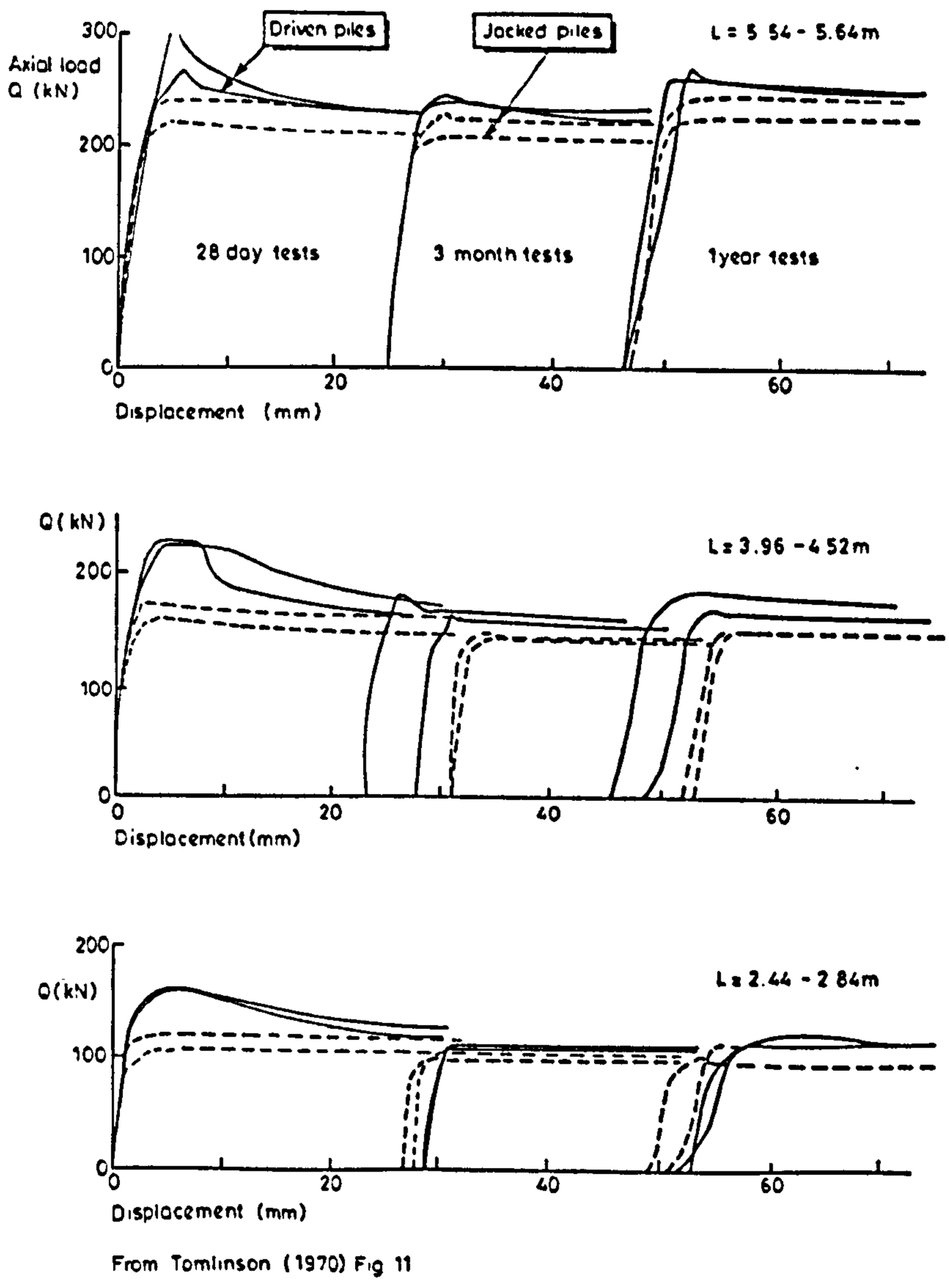



Figure 4.20 Load-displacement curves from Tomlinson's tests at Stanmore

The size and shape of these curves is highly significant:

- The driven piles are very brittle on first loading (the 28 day tests), but become considerably less so on subsequent re-loading
- Conversely, the response of the jacked piles is ductile throughout

*Tomlinson did not record the rate of jacking for these piles; however, it seems likely to have been in the range 50-200mm/min

- The ultimate (i.e. post-peak) capacity of the driven piles is only slightly (≈10%) higher than that of the jacked piles; this is accounted for by slight differences in the piles' lengths
- There is little or no "set-up" in the piles' overall load capacity from one test to another (except for the shortest piles); in general, there is a slight reduction in capacity with repeated loading

The method of pile installation clearly has a profound effect on the 28 day test results. According to Martins,[27] the differences between the response of the driven and jacked piles may be explained by particle re-orientation next to the pile shaft (see Section 4.5.5 below).

### 4.5.5 Investigations of particle re-orientation next to piles

#### a) Experimental programme

Martins[28] conducted a series of laboratory experiments on $\phi$15mm piles installed in normally consolidated kaolin. One of the purposes of the experiments was to investigate the nature of fabric disturbance caused by the installation of full displacement piles. Three methods of installation were examined:

i) Very careful drilling and grouting (Tests 1-15, and 17)
ii) Driving (Tests 16 and 18)
iii) Jacking (Test 19)

The first installation method was designed to cause minimal disturbance to the clay fabric, and is sometimes referred to as the "wished-in-place" method. The average rate of displacement during pile driving was ≈1000mm/min, whereas during jacking it was 4mm/min. Following installation the piles were left overnight to permit excess pore pressures to dissipate, and then loaded under displacement control (at ≈0.25mm/h). The sample was kept fully drained during pile loading.

b) Radial stress measurements

Martins measured the radial total stress acting on two of the drilled-and-grouted piles (7* and 15) by using a specially designed radial stress cell. In these experiments, $\sigma'_{rr}$ fell by 15% as the piles were loaded to their peak capacity (i.e. $(\sigma'_{rr})_f/(\sigma'_{rr})_c = 0.85$), and then fluctuated between $(\sigma'_{rr})_f$ and $(\sigma'_{rr})_c$ during plunging. (Since the experiments were fully drained, the radial effective stress and radial total stress are equal.)

c) Fabric studies

Martins' micro-fabric studies are of great relevance to the experiments at Canons Park (see Chapter 13 in particular). Figure 4.21 shows line drawings of the disturbance caused by pile installation and subsequent load testing, in experiments 18 and 19. This information was determined by examining thin-sections cut from material taken from next to the pile wall. In Test 18 (left) the pile had been driven, and in Test 19 (right) it had been jacked. In both cases the pile had been displaced by more than 10mm during the subsequent load test.

Consider first the fabric of the clay from next to the jacked pile (Figure 4.21 right):

- The single most important feature to note is the "principal displacement shear" that runs parallel to the pile shaft and 0.1-0.5mm away from it; significantly, there is only <u>one</u> such structure, and it is continuous over the full length of the thin-section
- There are a series of Riedel shears, inclined at 20-35° to the vertical, which Martins suggests are relics of the disturbance caused by the pile toe
- The zone of disturbance around the pile extends to just beyond 8mm (i.e. to $r/R \approx 2$): in "Zone C" the clay is undisturbed

*OCR = 5 in this test (only)

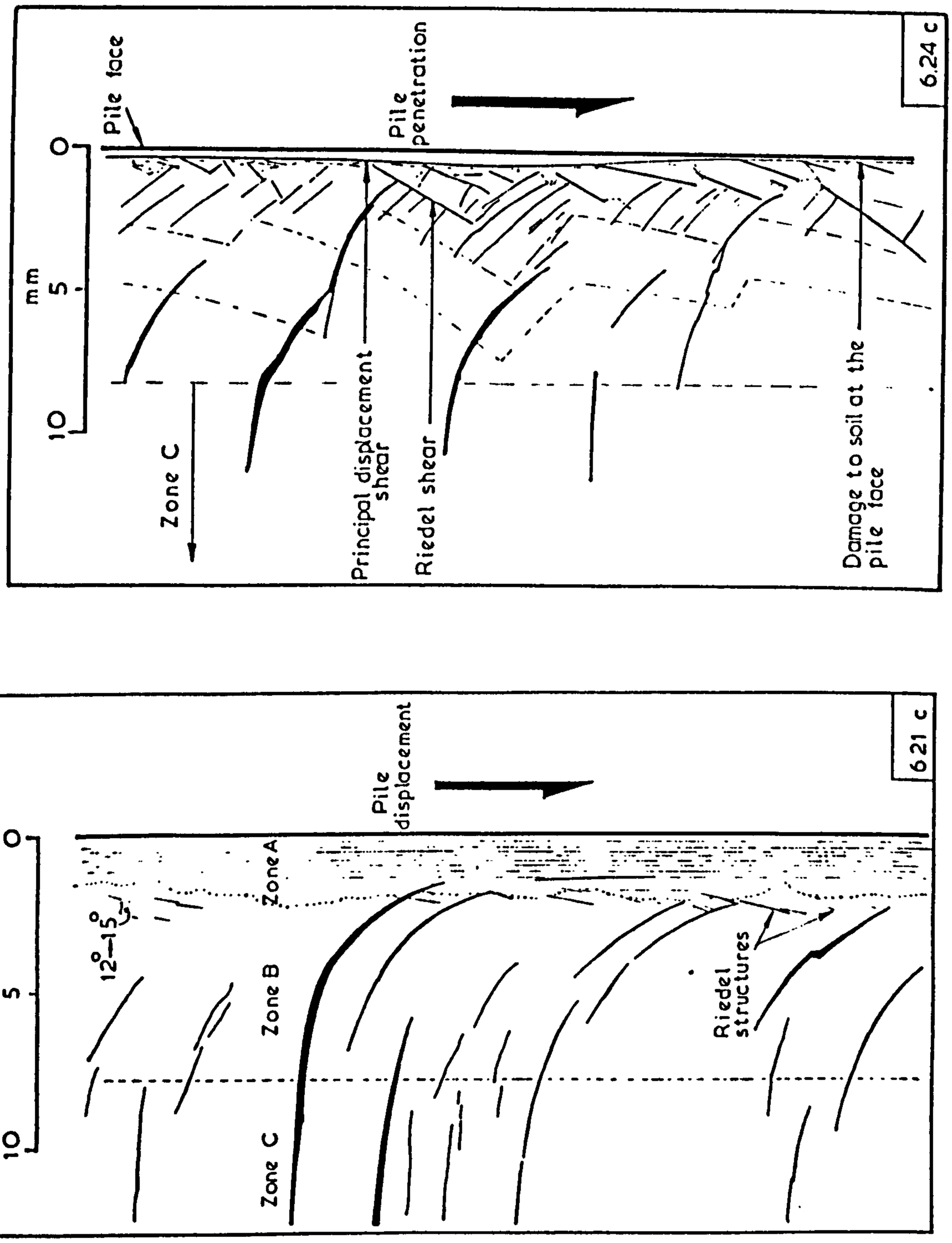



Figure 4.21 Fabric disturbance caused by (left) pile driving and (right) jacking, in Martins' laboratory experiments

The pattern is significantly different when we look at the micro-fabric next to the driven pile (Figure 4.21 ~~right~~ left). As Martins himself notes:

> "...there is no obvious, single, principal displacement shear. Rather, it would seem that the pile displacements were accommodated by slip on combinations of the many shear surfaces present [i.e. in Zone A]"[29]

In Zone A the soil is severely distorted, with almost all the relic Riedel shears being destroyed. This Zone extends to ≈1½mm from the pile wall (i.e. to r/R ≈ 1.2), whereas the overall zone of disturbance (Zones A and B combined) extends to r/R ≈ 2, as for the jacked pile.

d) Load-displacement curves

The load-displacement curves for the two piles are very similar, as can be seen from Figure 4.22. Also shown on this diagram is the curve for one of the drilled-and-grouted piles (Test 11), which was installed with a minimum of disturbance.

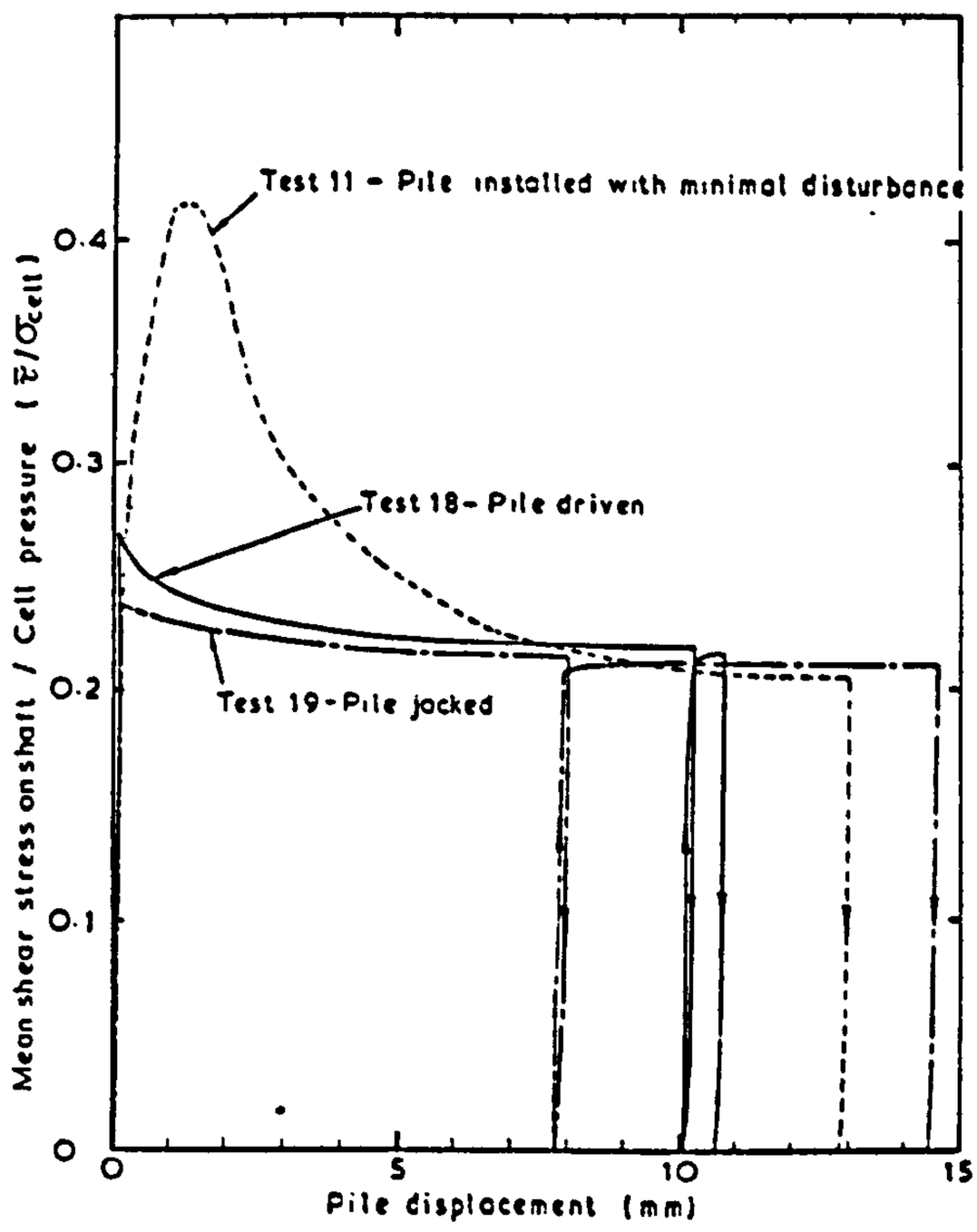



Figure 4.22 Load-displacement curves for Martins' tests 11, 18, & 19

The initial stiffness of the load-displacement curves is similar in all three drained tests (the equivalent rigidity index, $G/c_{uo}$, equals 187-203). The *residual* load capacity (at displacements > 10mm) is likewise very similar: $(\tau_{rz})/\sigma'_{cell}$ = 0.20-0.22. The main difference between the results is in the peak load (and consequently the degree of post-peak brittleness).

Martins explains the differences between the behaviour of the three piles as follows:

"...the installation of a displacement pile into a plastic clay may cause severe disturbance to the micro-fabric of the clay adjacent to the pile. The large relative displacements between the pile and the clay are accommodated by slip within a narrow shear zone, and locally the clay particles are re-oriented to lie sub-parallel to the direction of pile penetration. When the pile is loaded, its shaft capacity is limited by the presence of this shear zone.

> "...the greater peak strengths of driven piles result from rate effects experienced during installation by the clay in the shear zones beside the piles..., and possibly also from the reverse shear that may occur on pile rebound following each blow during driving."[30]

## 4.5.6 Other investigations of the clay fabric around piles

Tomlinson excavated trial pits around several driven and jacked piles that he had installed in the London clay at Stanmore (see Section 4.5.4 above). All of these piles had undergone an additional 70mm displacement during load testing.

Over the lower portions of each pile, Tomlinson discovered a skin of clay between 1 and 6mm thick, which adhered strongly to the pile's surface:

> "In the upper and middle zones [extending to half or two-thirds of the pile depth]... the surface of the clay in contact with the pile was smooth, polished and black in colour. In the lower zone the clay skin, after it had been peeled off the pile, had a matt appearance and carried the pattern of the steel. The outer surface of the skin was smooth and striated with close-spaced vertical lines."[31]

Based on the appearance of the clay fabric in electron micrographs, Tomlinson comments that the "inner surface of the skin of the driven pile [DP6] has a rougher and more ridged appearance than that of the jacked pile [JP5]."[32] Next to JP5, the particles were aligned parallel to the pile surface, whereas next to DP6 they were aligned at 45°.

Kitching[33] attempted to study the soil fabric next to <u>jacked</u> piles, by examining thin-sections of clay under a polarizing microscope. The

samples from which the thin-sections were made were taken using a novel hole cutting device that could be lowered down the inside of the pile. Unfortunately, sampling disturbance makes Kitching's results rather unreliable, although the evidence from his London clay* samples suggests that the clay fabric was aligned parallel to the pile wall within 5-15mm (r/R = 1.05-1.15) of it. Possible "principal displacement shears"[34] could be identified within a few millimetres of the pile wall.

The Building Research Establishment (BRE) excavated an inspection trench around a driven pile that they had installed in the glacial till at Cowden. The pile had been subjected to both tension and compression load tests prior to excavation. The only evidence of any remoulding of the clay was a thin discoloured layer, about 0.1mm thick, immediately adjacent to the pile. The presence of a thin layer of mill varnish (which had not been removed prior to driving) had caused sliding at the pile/soil interface. Further away, there were a number of discrete shear discontinuities, which extended to a radius of about 200mm (r/R ≈ 1.3).[35]

In a similar exercise to that of the BRE, the Norwegian Geotechnical Institute excavated an inspection trench around a jacked pile that had been installed in the sensitive Haga clay (Case 12). This pile was also covered with mill varnish, and when block samples of soil were taken the clay did not stick to the pile surface, but slipped off easily.[36]

The original horizontal layering of the Haga clay was strongly distorted close to the pile wall, and on the basis of shear strength and water content measurements three distinct zones were identified:[37]

- In Zone A (from r/R = 1.0 to 1.2), the clay was extensively remoulded and reconsolidated to a much lower water content than it had originally

*The pile that Kitching used for these experiments was installed in the London clay at Canons Park, close to where my own experiments were performed; at the end of the test programme I excavated an inspection trench around two piles, one of which was Kitching's

- In Zone B (from r/R = 1.2 to ≈3), the clay had been subjected to shear distortion which decreased rapidly with distance from the pile
- In Zone C (r/R > ≈3), the clay was undisturbed by pile installation

The work at Haga is examined in more detail in Chapter 14, where it is compared with my investigations into the fabric around piles installed in the London clay at Canons Park (as described in Chapter 13).

## 4.6 NOTES AND REFERENCES

[1]DiBiaggio E. (1987). More information, reduced costs, better designs and improved safety through instrumentation. Proc. 2nd Int. Symp. on Field Measurements in Geomechanics, Kobe, pp369-384. A.A. Balkema, Netherlands. Also in NGI Publ. No 175, Oslo, 1988.

[2]Levadoux J.-N. and Baligh M.M. (1980). Pore pressures during cone penetration in clays. MIT Research Report No R80-15. Order no 666, 310pp.

[3]Many of these parameters were defined by: Azzouz A.S. and Lutz D.G. (1986). Shaft behavior of a model pile in plastic Empire clays. J. Geotech. Engng, Am. Soc. Civ. Engrs, 112(4), pp389-406.

[4]Brenner R.P., Nutalaya, P., Chilingarian, G.V., and Robertson, J.O. Jr (1981). Engineering geology of soft clay. In "Soft clay engineering", ed. E.W. Brand and R.P. Brenner, Elsevier Scientific Publishing Company, Amsterdam, pp157-238.

[5]See, for example, Karlsrud K. and Haugen T. (1985a). Axial static capacity of steel model piles in overconsolidated clay. Proc. 11th Int. Conf. Soil Mech. & Fdn Engng, San Francisco, 3, pp1401-1406.

[6]The data for the Gault clay was kindly provided by Mr John Powell of the Building Research Establishment. The OCRs for the London clay are based on tests at Imperial College by Som, on samples from High Ongar. See Appendix 4 for a full discussion.

[7]Azzouz A.S. and Morrison M.J. (1988). Field measurements on model pile in two clay deposits. J. Geotech. Engng, Am. Soc. Civ. Engrs, 114(1), pp104-121.

[8]O'Neill M.W., Hawkins R.A., and Audibert J.M.E. (1982a). Installation of pile group in overconsolidated clay. J. Geotech. Engng Div., Am. Soc. Civ. Engrs, 108(GT11), pp1369-1386. Quotation from pp1376-1377.

[9]Coop M.R. (1987). The axial capacity of driven piles in clay. DPhil Thesis, Univ. of Oxford.

[10]Levadoux and Baligh (1980), loc. cit. See Figure 6.29.

[11]Reese L.C. and Seed H.B. (1955). Pressure distribution along friction piles. Proc. Am. Soc. for Testing Materials, 55, pp1156-1182. Quotation taken from p1175.

[12]Johnston I.W. (1972). Electro-osmosis and porewater pressures; their effect on the stresses acting on driven piles. PhD Thesis, Southampton Univ.

[13]Coop (1987), loc. cit.

[14]Steenfelt J.S., Randolph M.F., and Wroth C.P. (1981). Instrumented model piles jacked into clay. Proc. 10th Int. Conf. Soil Mech. & Fdn Engng, Stockholm, 2, pp857-864. See Section 4.2, pp860-861.

[15]Azzouz and Morrison (1988), loc. cit.

[16]Coop (1987), loc. cit.

[17]Lunne T., Powell J.J.M., Quarterman R.S.T., and Eidsmoen T.E. (1986). Piezocone testing in overconsolidated clays. Proc. 39th Can. Geotech. Conf. on 'Insitu Testing and Field Behaviour', Carlton Univ., Ottawa, Canada, pp209-218.

[18]Azzouz and Morrison (1988), loc. cit. See p113.

[19]Mayne P.W. and Kulhawy F.H. (1982). Ko - OCR relationships in soils. J. Geotech. Engng, Am. Soc. Civ. Engrs, 108(GT6), pp851-872.

[20]Such as one of the test procedures described by: Weltman A.J. (1980). Pile load testing procedures. DoE/CIRIA Piling Development Group, Report PG7, Construction Industry Research and Information Association, London, 52pp.

[21]Morrison M.J. (1984). In-situ measurements on a model pile in clay. PhD Thesis, Massachusetts Institute of Technology, c687pp.

[22]Morrison (1984), loc. cit., pp424 and 426.

[23]Morrison (1984), loc. cit. Values quoted on p476.

[24]Coop (1987), loc. cit.

[25]Coop (1987), loc. cit., p434.

[26]Tomlinson M.J. (1970a). Adhesion of piles in stiff clays. CIRIA Report 26, Construction Industry Research and Information Association, London, 47pp.

[27]Martins J.P. (1983). Shaft resistance of axially loaded piles in clay. PhD Thesis, Univ. of London (Imperial College), 435pp.

[28]Martins (1983), loc. cit.

[29]Martins (1983), loc. cit., p187.

[30]Martins (1983), loc. cit., p194.

[31]Tomlinson (1970a), loc. cit., p33.

[32]Tomlinson (1970a), loc. cit., p37.

[33]Kitching D.N. (1983). A study into the microfabric of clays adjacent to jacked piles. MSc Dissertation, Univ. of London (Imperial College), 31pp+.

[34]As described by Skempton, in: Skempton A.W. (1961). Horizontal stresses in an overconsolidated Eocene clay. Proc. 5th Int. Conf. Soil Mech. & Fdn Engng, Paris, 1, pp351-357.

[35]Ove Arup and Partners (1987). Comparison of British and Norwegian research on the behaviour of piles as anchors for buoyant structures. Dept of Energy, Offshore Technology Report, OTH 86 218. HMSO, London, 43pp. See pp19-22.

[36]Ove Arup and Partners (1987), loc. cit. See pp19-22.

[37]Karlsrud and Haugen (1985a), loc. cit.

# Chapter 5

# Ground conditions at Canons Park

# CONTENTS OF CHAPTER 5


5.1 INTRODUCTION . . . . . 184
5.1.1 Location and history of the Canons Park site 184
5.1.2 Outline of the Chapter 187
5.2 INVESTIGATIONS OF THE CANONS PARK SITE . . . . . 188
5.2.1 Previous site investigations 188
5.2.2 Boreholes 188
5.2.3 Imperial College laboratory test programme 188
5.2.4 BRE laboratory programme 190
5.2.5 Field tests 191
5.2.6 Previous research into pile behaviour 191
5.3 SOIL PROFILE . . . . . 192
5.3.1 Main strata 192
5.3.2 CPT and piezocone profiles 193
5.3.3 BRE's trial pit through the gravel layer 195
5.3.4 Piezometer records 195
5.4 SOIL PROPERTIES . . . . . 196
5.4.1 Undrained shear strength; water contents; Atterberg limits 196
5.4.2 In situ horizontal stresses 198
5.4.3 Overconsolidation ratio 201
5.4.4 Cavity expansion limit pressure 205
5.4.5 Soil stiffness 207
5.5 RING SHEAR EXPERIMENTS ON THE LONDON CLAY . . . . . 208
5.5.1 Basic shear mechanisms 208
5.5.2 Sliding shear behaviour 208
5.5.3 Transitional shear 209
5.5.4 Special tests to simulate pile installation and loading 210
5.5.5 Ring-shear data for London clay from Canons Park 212
5.6 NOTES AND REFERENCES . . . . . 214

# 5.1 INTRODUCTION

## 5.1.1 Location and history of the Canons Park site

The Building Research Establishment's test-bed site at Canons Park, north London, is located approximately one mile south-south-east of Stanmore, near the junction of Whitchurch Lane and Honeypot Lane (see Figure 5.1

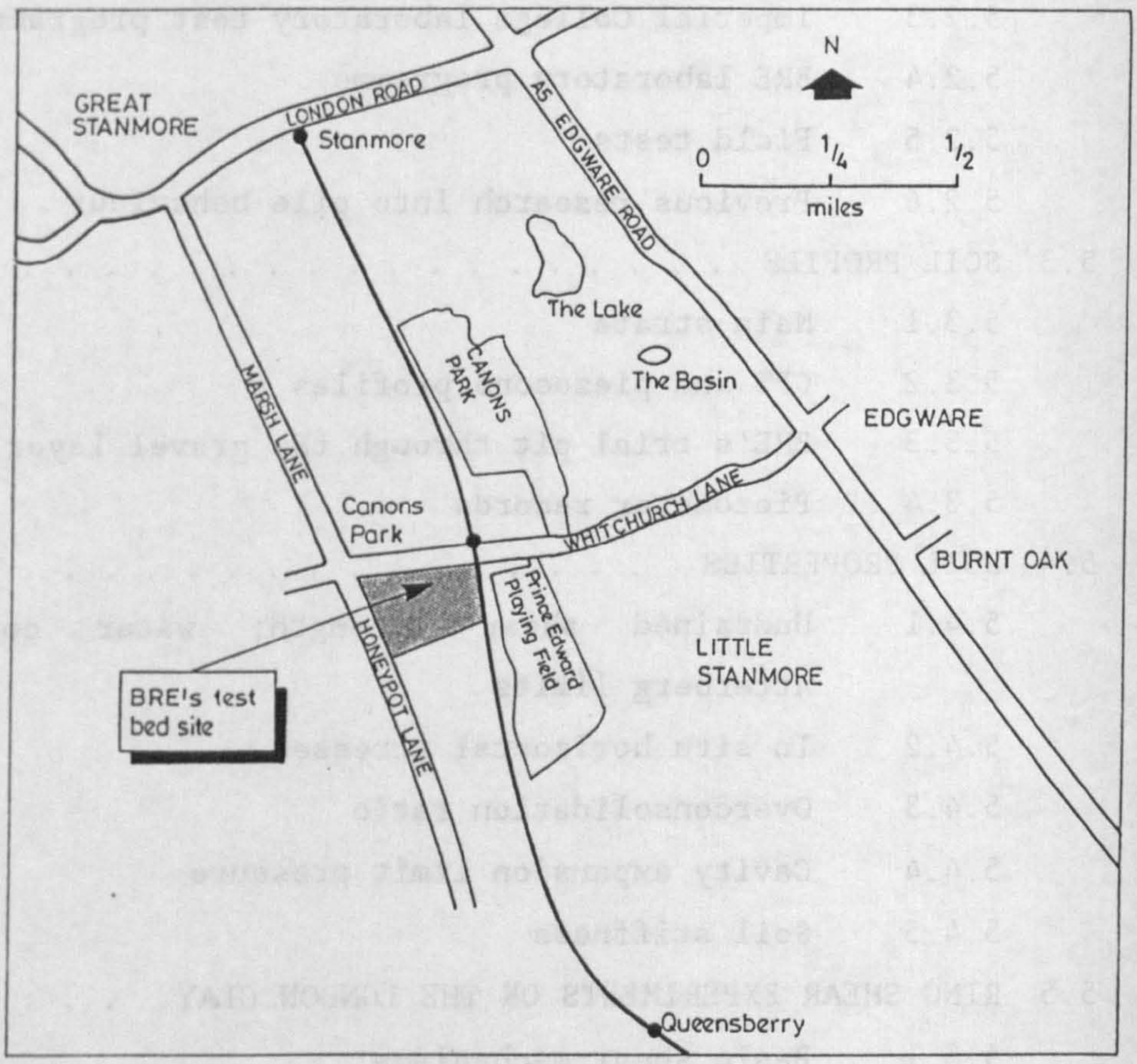



Figure 5.1 Location of the Canons Park site

and Plate 1). The site is situated within the grounds of the Government Depot along Honeypot Lane, at grid reference TQ 181 911. The Depot was built in the early 1940s on one half of Prince Edward's Playing Fields, and is currently used by various Government departments for offices, laboratories, and storage.



Plate 1(a) General view of the Canons Park site [photo: A. Bond]



Plate 1(b) View of the loading frame during pile installation

[photo: A. Bond]

The Canons Park area takes its name from the park which now exists in reduced form north of Whitchurch Lane. Originally, it was an extensive area of some 1590 acres whose boundaries were Whitchurch Lane, the Edgware Road, Marsh Lane, and the London Road. Today most of the area is built-up, with the Underground railway line (overground at this point) running parallel to Marsh Lane and terminating at Stanmore station. This railway passes alongside the site's eastern boundary and a tube station is situated nearby (on Whitchurch Lane). The easy access from Imperial College was one of the reasons for choosing to do field research at Canons Park.

### 5.1.2 Outline of the Chapter

This Chapter is divided into four main parts. Section 5.2 describes the previous investigations of the Canons Park site; Section 5.3 summarizes the ground conditions; Section 5.4 discusses the soil properties, as determined from the site investigations; and Section 5.5 gives details about some special ring shear experiments on London clay which have particular relevance to the instrumented pile tests.

## 5.2 INVESTIGATIONS OF THE CANONS PARK SITE

### 5.2.1 Previous site investigations

The ground conditions at Canons Park have been assessed in two site investigations, one by the Building Research Establishment[1] (BRE) and the other by Imperial College[2] (IC). In addition, various of field tests have been performed, including research into pile behaviour. Figure 5.2 shows a plan of the Canons Park site, with the various boreholes and field tests marked. The following paragraphs summarize the scope of the ground investigations, and Sections 5.3-5.4 present a summary of the results.

### 5.2.2 Boreholes

In 1983 a team from the BRE drilled two boreholes (nos 5-6 on Figure 5.2) under Imperial College supervision. Thin-walled jacked samples were taken throughout both these boreholes, to their full depth of 10m.

The BRE carried out a second survey in 1984 that included four 6.2m deep holes (nos 1-4), and took a total of 28 thick-walled tube samples for subsequent laboratory testing.

### 5.2.3 Imperial College laboratory test programme

A comprehensive testing programme was conducted at Imperial College on the thin-walled samples, including oedometer and triaxial tests on intact samples and triaxial stress-path tests on reconstituted samples (see the box below). The tests were state-of-the-art, employing electro-level gauges[3] (for "local" measurements of the soil's small-strain stiffness) and mid-height pore pressure probes.[4] Full details of this work are given in Jardine's PhD Thesis[5] (and elsewhere[6]).

A wide range of ring shear tests[7,8] have been performed on samples from Canons Park, including recent experiments devised to complement the current programme of pile tests. These experiments will be discussed in detail in Section 5.5.

Key

- • Boreholes
- o Imperial College pile tests
- ■ Other pile tests
- ∇ Cone tests (black = with friction sleeve)
- ⊗ Piezocone test
- Δ Marchetti dilatometer profile (black = offshore DMT)
- x BREcone rate tests
- * Self-boring pressuremeter tests

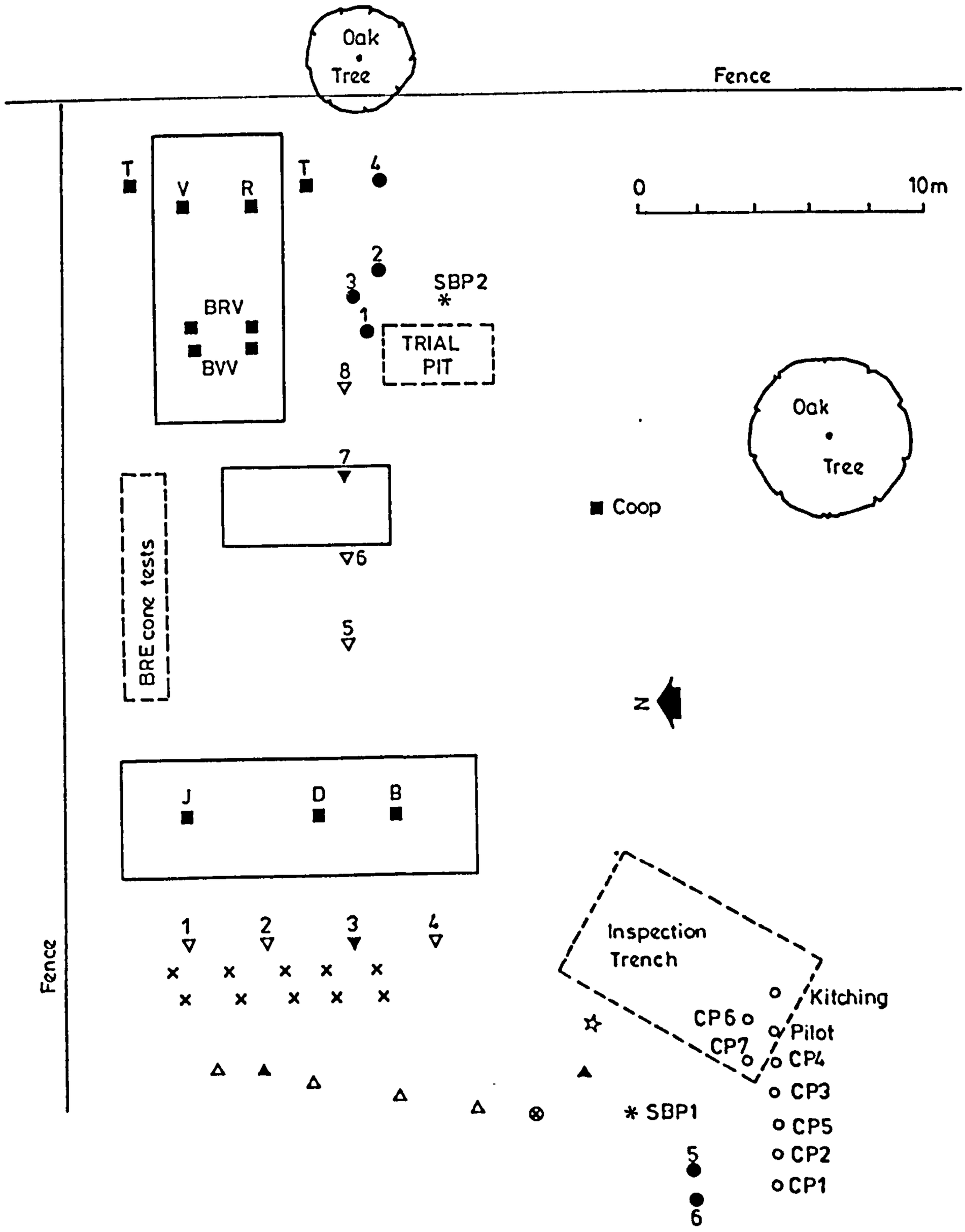



Figure 5.2 Plan of the Canons Park site

## 5.3 SOIL PROFILE

### 5.3.1 Main strata

The test facility at Canons Park is situated on a 22m thick deposit of heavily overconsolidated London clay. At the surface of the London clay are some thin layers of geologically recent deposits, namely: topsoil, gravel, and a silty clay head. Beneath the London clay are the Reading Beds of sand, loam, and pebbles. The London clay itself forms three distinct strata: an upper layer of disturbed material; an intact middle layer which is weathered brown; and the lowest layer, the (intact) blue London clay.

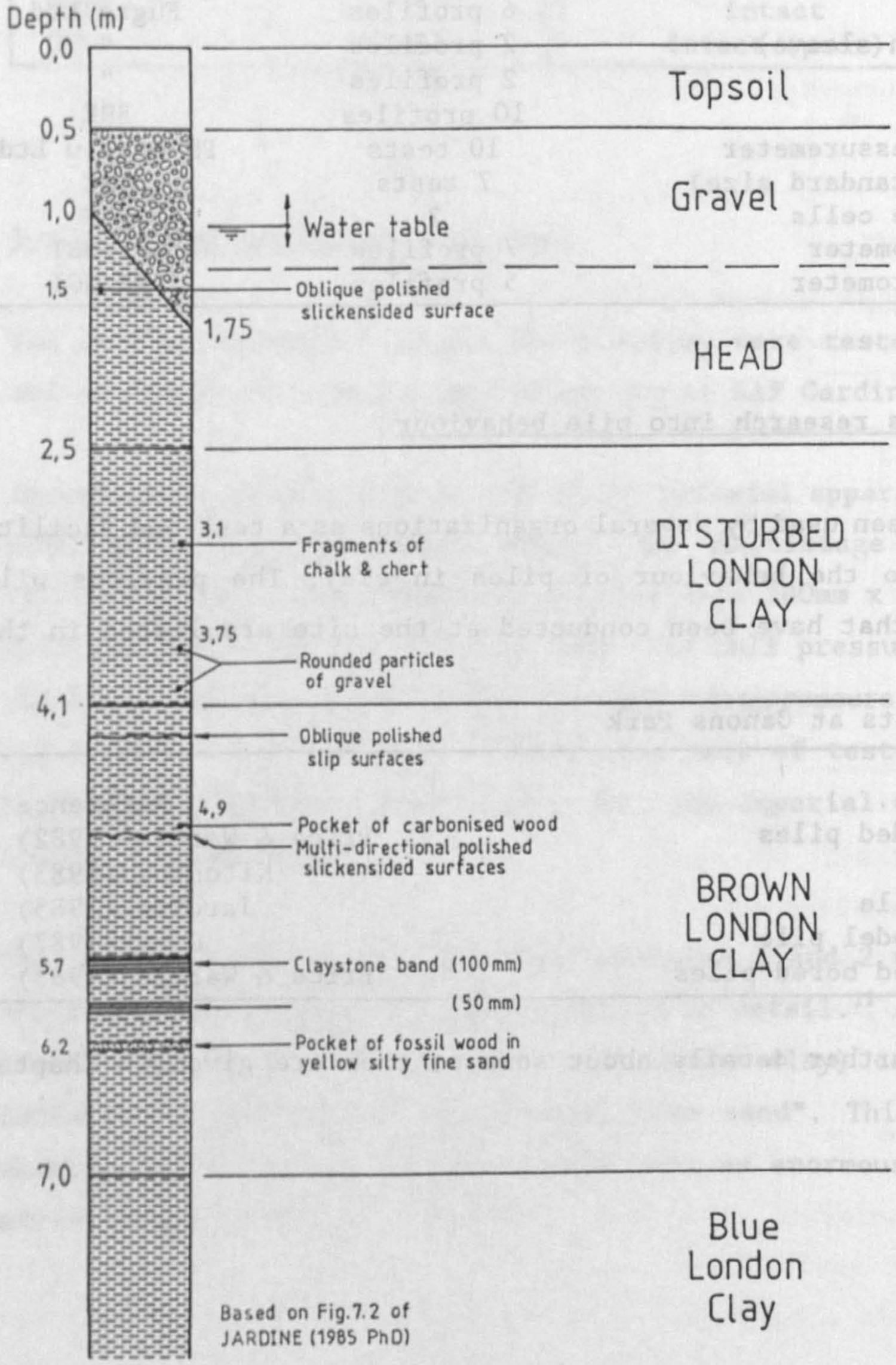



Figure 5.3 Soil profile at Canons Park

Figure 5.3 shows a profile of the ground at Canons Park, to a depth of 8m - this being the depth of interest in the field work. The topsoil and gravel together extend to a depth of 1.0-1.75m.[17]

According to the Geological Memoirs for this area:

> "The main part of the London clay is a stiff clay of dark grey or bluish-grey colour; when exposed at the surface, however, it is brown owing to the conversion of ferrous oxide to ferric oxide by weathering; a few feet down, where the process is not complete, the clay is silty in appearance and is then difficult to distinguish from the alluvial clay that has no doubt been derived from it."[18]

A clay-stone band has been found 5.7m below ground level (see Figure 5.3):

> "...septaria or cement-stones, which are a characteristic feature of the London clay, occur in nodular layers at irregular intervals... They are concretions of argillaceous limestone..."[19]

The water table is around one metre below ground level; and the site is under-drained by the chalk at a depth of ≈45m.

## 5.3.2 CPT and piezocone profiles

Eight cone penetration tests (CPTs) were performed by Fugro Ltd[20] on 4th December 1980, in the positions indicated on Figure 5.2. Sleeve friction was measured to depths of more than 14m in two of the tests (nos 3 and 7), whereas in the others only the end bearing was recorded (to 10m).

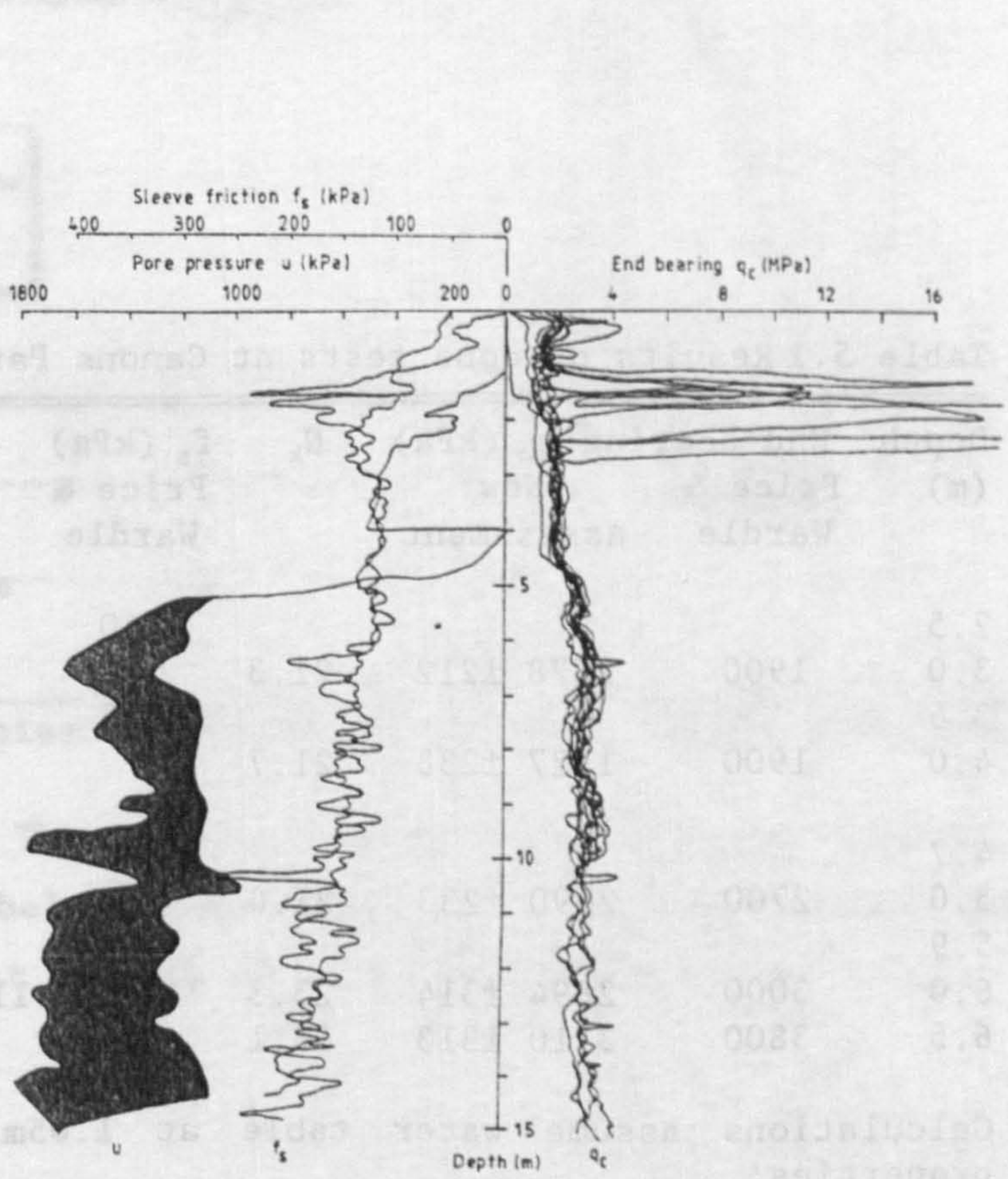



Figure 5.4 Results of cone penetration and piezocone tests at Canons Park

The results of the CPTs are shown in Figure 5.4 together with the traces from two piezocone tests that were commissioned by the BRE in 1987.[21] The boundaries between the head material, the disturbed London clay, and the brown London clay (see Figure 5.3) can be identified from the variation in end bearing ($q_c$); they are 0.5m deeper than indicated by the Imperial College boreholes owing to differences in ground level across the site.

Table 5.1 summarizes the values of end bearing $q_c$, shaft friction $f_s$, and pore pressure u obtained in the cone tests, together with values of the cone factor[22] $N_k$, the pore pressure parameter[23] $B_q$, and the friction ratio $100f_s/q_c$.

Typically these parameters have the following values at Canons Park:

$$N_k = 22 \pm 3$$
$$B_q = 0.31 \pm 0.13$$
$$100f_s/q_c = 5\text{-}8$$

Table 5.1 Results of cone tests at Canons Park

| Depth (m) | End bearing $q_c$ (kPa) Price & Wardle | New assessment | $N_k$ | $f_s$ (kPa) Price & Wardle | u (kPa) | $B_q$ | Friction ratio $100f_s/q_c$ |
|---|---|---|---|---|---|---|---|
| 2.5 | | | | 140 | 420 | 0.27 | 7-9 |
| 3.0 | 1900 | 1678 ±212 | 21.3 | | 470 | 0.31 | 6½-8 |
| 3.5 | | | | 125 | 480 | 0.31 | 6½-8 |
| 4.0 | 1900 | 1727 ±233 | 21.7 | | 520 | 0.34 | 7-7½ |
| 4.7 | | | | 120 | | | 5½-6 |
| 5.0 | 2700 | 2590 ±233 | 21.0 | | 600 | 0.20 | 5½ |
| 5.9 | | | | 125 | | | 4½-5 |
| 6.0 | 3000 | 2894 ±314 | 23.3 | | 1180-1500 | 0.35-0.44 | 5 |
| 6.5 | 3800 | 3110 ±313 | 15.1 | | | | 5-6 |

Calculations assume water table at 1.05m, and the following soil properties:

$c_{uo}$ = 76kPa and $\gamma$ = 19.2kN/m$^3$ for $z \leq 4.5$m
$c_{uo}$ = 119kPa and $\gamma$ = 19.7kN/m$^3$ for $z > 4.5$m

### 5.3.3 BRE's trial pit through the gravel layer

The BRE excavated a 1.5m x 2.5m x 3m deep trial pit at the position indicated on Figure 5.2, with the purpose of examining the layers of gravel and head that overlie the London clay.[24] Unfortunately, the pit was not taken deep enough to provide information about the soil of interest in the pile tests.

### 5.3.4 Piezometer records

Four Casagrande type piezometers were installed at Canons Park prior to 1984, a few metres away from the Imperial College test area (see Figure 5.2). Readings from these piezometers over the period 1986-1988

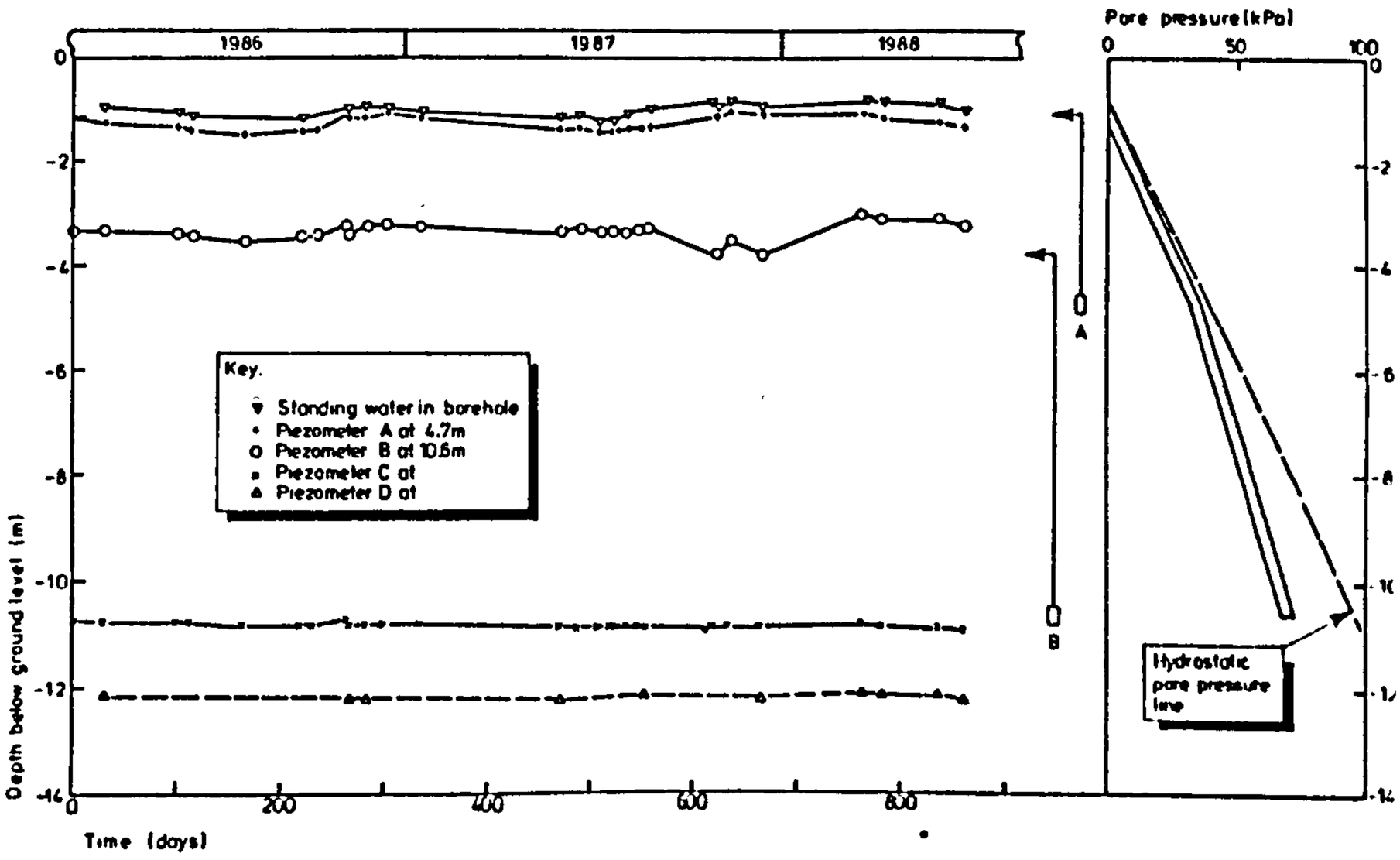



Figure 5.5 Casagrande piezometer readings at Canons Park, 1986-1988

are shown in Figure 5.5. The site is clearly under-drained, with the water table at 1.05 ±0.2m below ground level. The pore pressures are ≈8% below hydrostatic values at a depth of 4.7m; and ≈25% below at 10.6m.

## 5.4 SOIL PROPERTIES

### 5.4.1 Undrained shear strength; water contents; Atterberg limits

Figure 5.6 summarizes the laboratory determinations of undrained shear strength ($c_{uo}$); water content (w); Atterberg limits ($w_P$ and $w_L$); and bulk density ($\gamma$), for the Canons Park site.* The peak strengths in Jardine's triaxial tests give values for the undrained strength ratio ($c_{uo}/\sigma'_{vo}$) of 1.94 ±0.42, for the depths of interest in the pile tests.

In choosing a simplified strength profile through the data, greatest weight has been placed on the results of Jardine's tests on the thin-walled samples. The undrained shear strengths and bulk densities determined on five poor quality samples (points x on Figure 5.6) have been ignored, since they appear unreliable when compared with the higher quality data. The simplified profile of undrained shear strength drawn on Figure 5.6 has been used throughout this Thesis for interpreting the pile tests at Canons Park.

Values of $c_{uo}$ from the pressuremeter tests[25] are also plotted on Figure 5.6, and they exhibit broad agreement with the line through the peak strengths from Jardine's triaxial compression tests.# This is true despite the theoretical objection to using conventional pressuremeter theories for estimating the strength parameters of high $K_0$ materials (such as the London clay).[26]

---

*The values plotted for boreholes 1-4 have been re-interpreted from the data reported by RAF Cardington

#The value for $c_{uo}$ at 4.2m (305kPa) is obviously in error

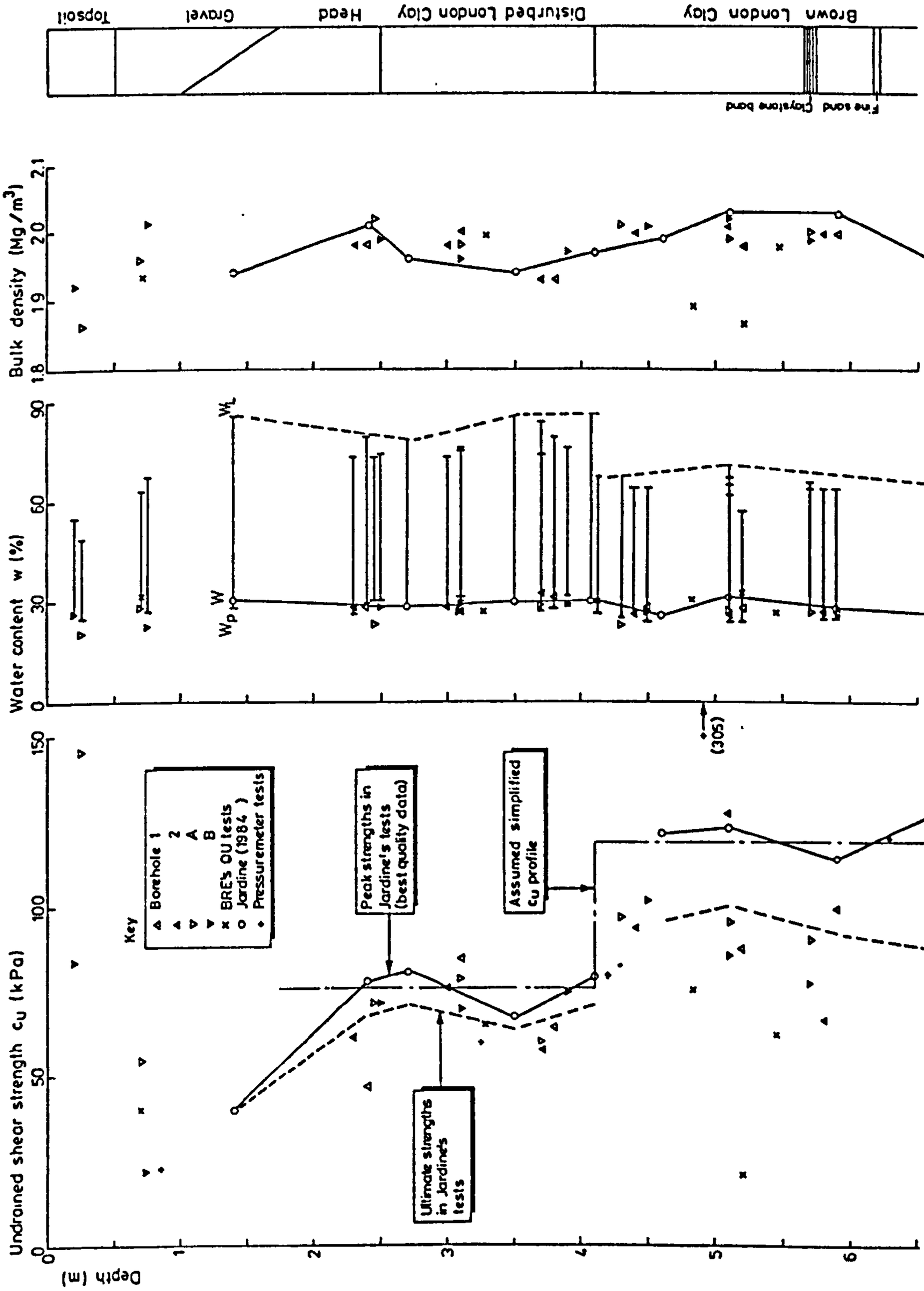



Figure 5.6 Summary of soil properties at Canons Park

## 5.4.2 In situ horizontal stresses

### a) From self-boring pressuremeter tests

Ten self-boring pressuremeter tests were performed by PM Insitu Ltd[27] in June 1984, to a maximum depth of 10.3m. One test was in borehole SBP2 and all the others in SBP1 (see Figure 5.2). A typical stress-strain curve is shown in Figure 5.7: the complete set of curves is included in Jardine's PhD Thesis.[28] Values of $K_0$ were deduced from the lift-off points of individual membrane expansion curves.

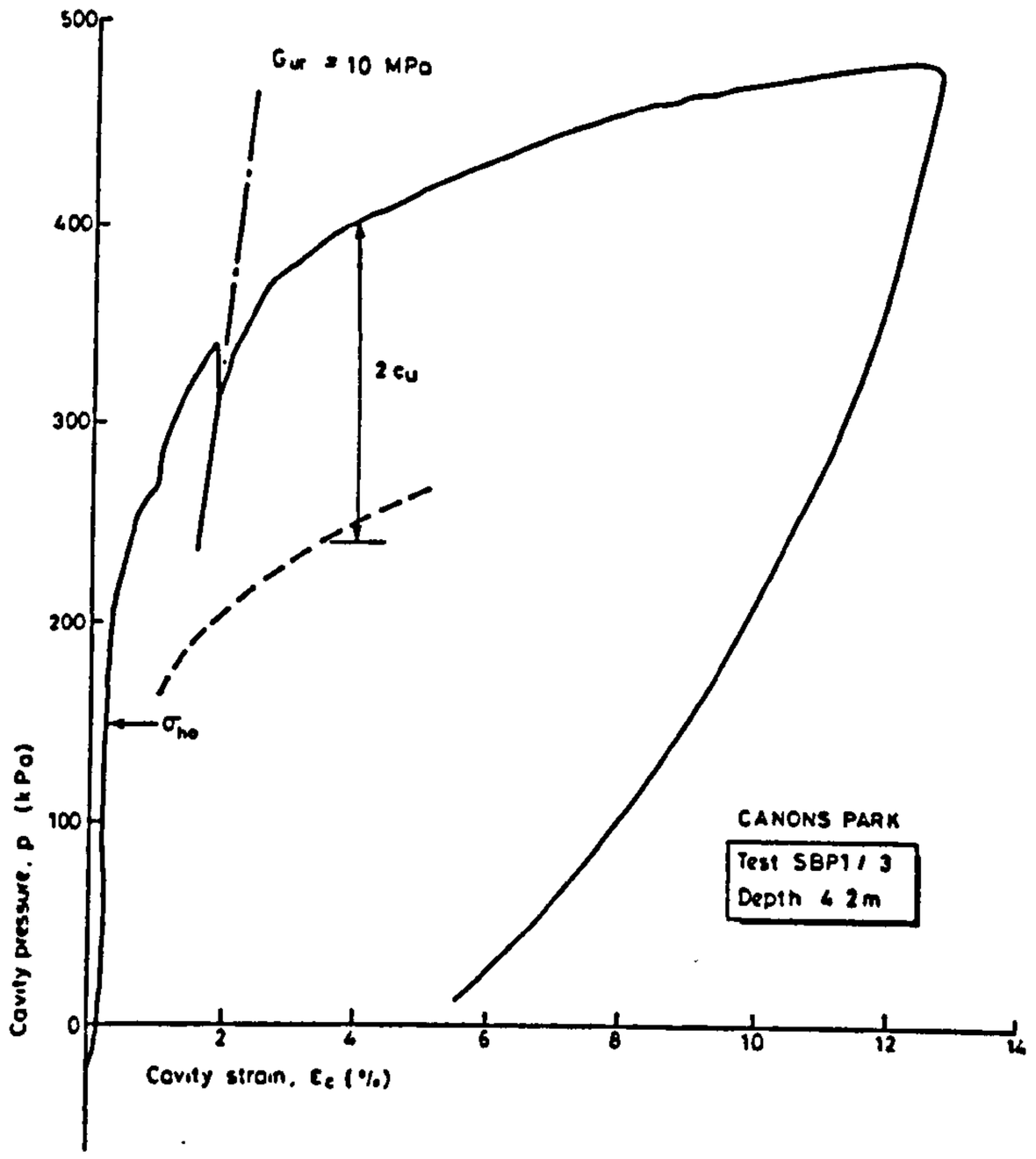



Figure 5.7 Self-boring pressuremeter test at Canons Park

### b) From spade cell experiments

Tedd and Charles[29] report the results of three spade cell experiments at Canons Park, two at 3m and the other at 9m depth; the cells' dimensions were 100mm x 200mm x 5mm thick. These experiments were performed ≈50m west of the Imperial College pile test area (see Figure 5.2). The BRE has recently installed more spade cells at Canons Park and the provisional results from these instruments are included herein.[30]

Spade cells generally overestimate the in situ horizontal stress in stiff clays. Tedd and Charles[31] recommend that estimates of $\sigma_{ho}$ from spade cells should be "corrected" by deducting half the undrained shear strength of the clay (this has the effect of reducing $K_0$ by $\frac{1}{2}c_{uo}/\sigma'_{vo}$). At Canons Park

$c_{uo}/\sigma'_{vo}$ = 1.94 ±0.42, so the correction that has been made to $K_0$ is between -0.8 and -1.2.

c) From Marchetti dilatometer tests

Powell and Uglow[32,33] have performed an extensive series of experiments with the Marchetti dilatometer, at a number of UK sites including Brent Cross and Madingley. Their results for Canons Park are reproduced here

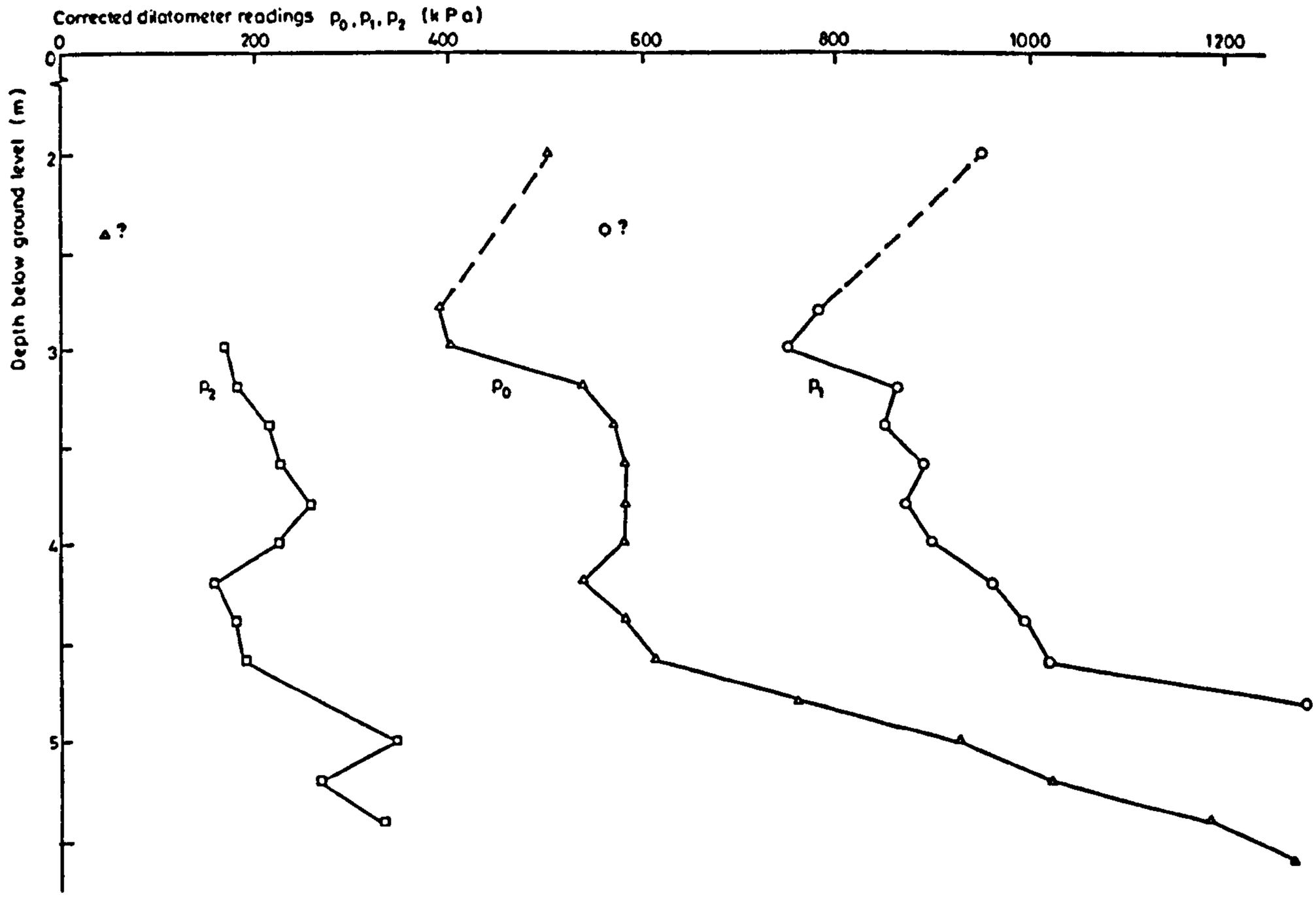



Figure 5.8 Results of dilatometer tests at Canons Park

in Figure 5.8.

Interpretation of the dilatometer test relies on empirical correlations developed by Marchetti for Italian soils. One of the main conclusions from Powell and Uglow's work is that Marchetti's original correlations do not hold for UK soils. They proposed alternative correlations to replace Marchetti's for young clays; but, due to a lack of data, they were unable to do likewise for aged clays (such as the London clay).[34]

Therefore, the values of $K_0$ that are quoted in this Thesis have been calculated from Marchetti's original formula, which is:[35]

$$K_0 = (K_D/1.5)^{0.47} - 0.6$$

where the "horizontal stress index" $K_D$ equals $(p_0 - u_0)/\sigma'_{vo}$ and $p_0$ is the pressure at which the dilatometer membrane lifts off.

### d) Summary of $K_0$ values for the Canons Park site

Figure 5.9 summarizes the values of $K_0$ determined from the experiments described above, and compares them with values calculated from Mayne and Kulhawy's[36] equation relating $K_0$ to OCR:

$$K_0 = (1 - \sin \phi)OCR^{\sin \phi}$$

The OCRs used in this formula were calculated from the preconsolidation pressures deduced from high pressure oedometer tests (see Section 5.4.3 below). Note that Mayne and Kulhawy's equation is strictly only applicable to monotonically unloaded soils, although it has been

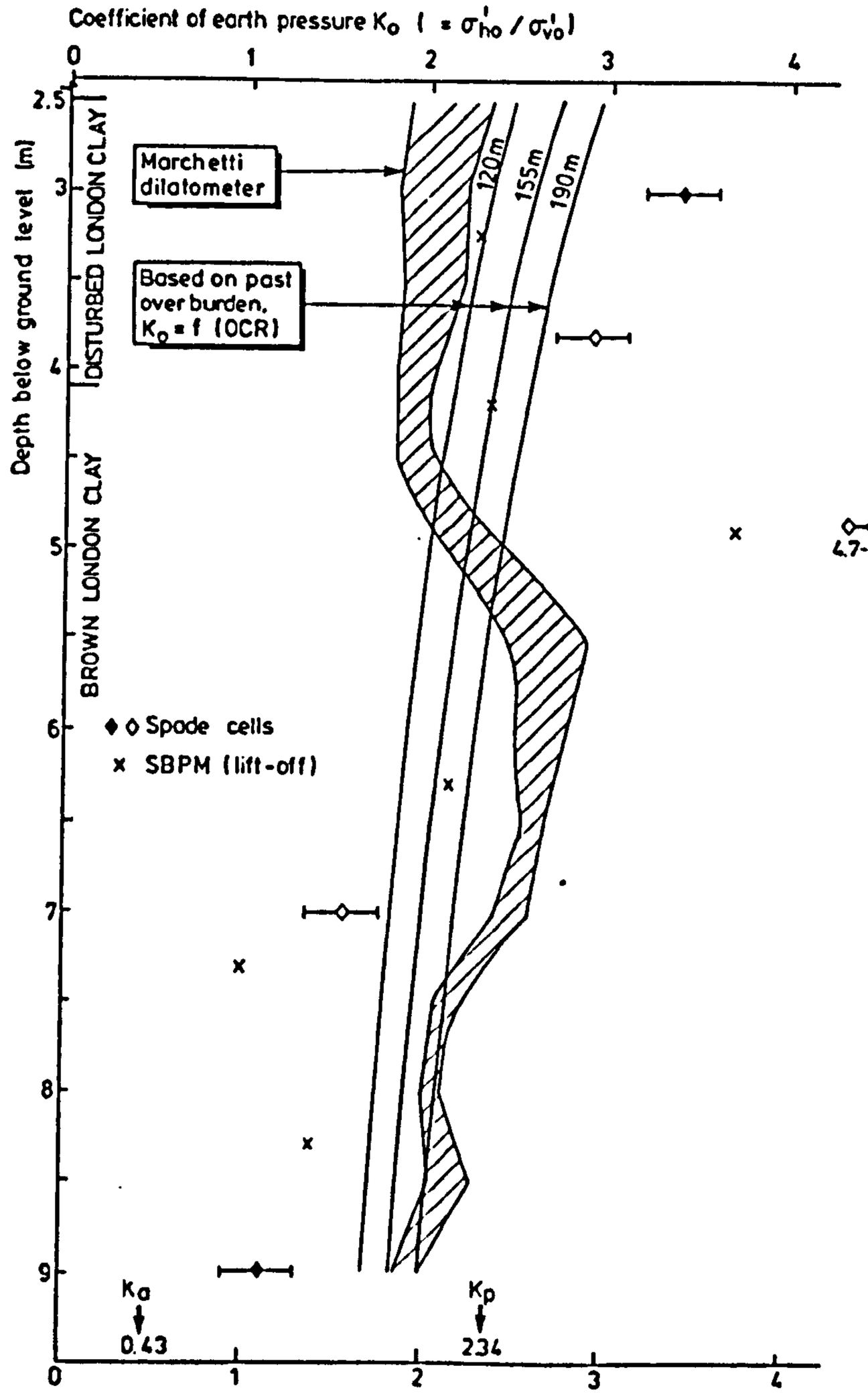



Figure 5.9 $K_0$ profile for the Canons Park site

found to give reasonable estimates for $K_0$ in a variety of other cases.

As Figure 5.9 reveals, there is reasonable agreement between the different estimates of $K_0$. Interestingly, the Marchetti dilatometer profile indicates a sharp rise in $K_0$ from 4.5 to 5.5m depth - this sudden increase in horizontal stress mirrors the jump in radial total stress observed during installation of the instrumented piles at canons Park (see Chapter 9).

### 5.4.3 Overconsolidation ratio

a) From oedometer tests

The overconsolidation ratio (OCR) of the London clay at Canons Park can be estimated[37] from the results of standard oedometer tests, using Casagrande's construction[38] to determine the pre-consolidation pressure ($\sigma'_{vp}$). This approach gives $\sigma'_{vp} \approx 0.6$MPa, and hence an overconsolidation ratio of about 6, for soil at a depth of ≈9m below ground level. However, as Som point out, this method of estimating OCR suffers from one serious drawback:

> "...the Casagrande method of determining the pre-consolidation pressure is not satisfactory. ...for heavily overconsolidated clays the laboratory [voids ratio] vs log [$\sigma'_v$] diagrams show continuous changes of curvature... and often no distinct change of slope can be discerned"[39]

This problem is illustrated in Figure 5.10, which shows the results of i) Jardine's standard oedometer tests; and ii) Som's high-pressure tests on London clay (from High Ongar). The virgin $K_0$-consolidation lines (points O and x) are for tests on re-constituted samples. Both authors did tests on intact samples as well (Jardine's are given by the points • and +; Som's are labelled CRS-HO-1 & 2). The main things to note from Figure 5.10 are as follows:

- The virgin $K_o$-consolidation lines for both the High Ongar and the Canons Park clays are very similar
- So too are the initial loading curves for the intact specimens

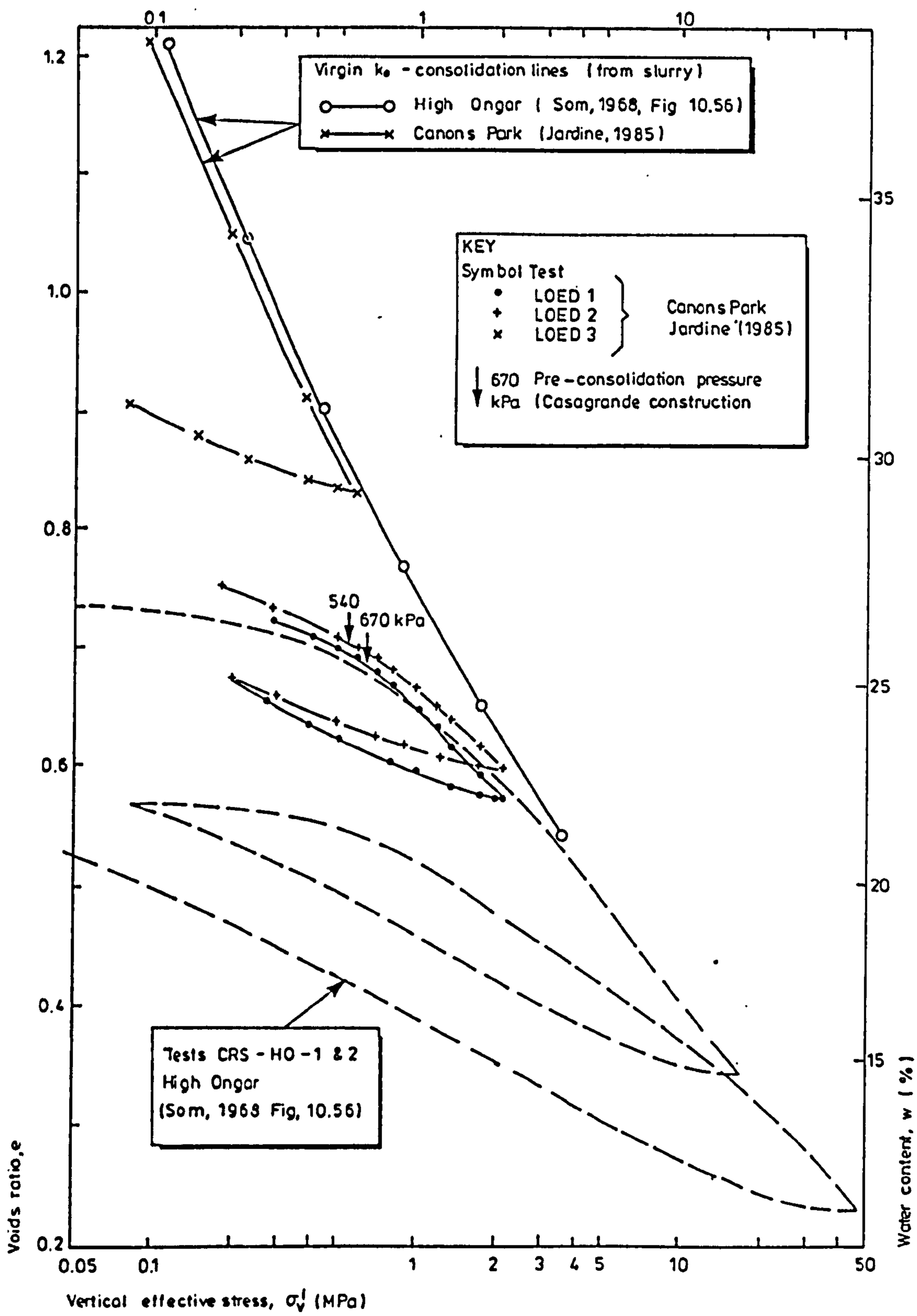



Figure 5.10 Results of oedometer test on London clay from High Ongar and Canons Park

(cf. CRS-HO-1 & 2 with LOED1 and 2)

- The pre-consolidation pressure of the intact clay from High Ongar can be found by extrapolating the virgin consolidation line to the point of intersection with the intact curve (CRS-HO): this gives $\sigma'_{vp} \approx 5MPa$
- The standard oedometer tests clearly under-estimate the true value of $\sigma'_{vp}$ for the Canons Park clay

In his Thesis, Som suggests a method for determining the pre-consolidation pressures of heavily overconsolidated clays by re-constructing the rebound curve for the intact, in situ, material. Based on this construction, $\sigma'_{vp}$ at Canons Park is estimated to be between 1530 and 1870kPa for soil at 9m depth (equivalent to 155-190m of past overburden and an OCR of 16 to 21). See Appendix 4 for details about Som's construction.

b) From the geological evidence

A study of the geological history of the Stanmore area (see Appendix 4) suggests that the Canons Park site was once buried beneath 73-121m of sediment, which implies that the *mechanical* overconsolidation ratio ($OCR_m$) - at a depth of 9m - is somewhere between 8 and 14. Since the London clay is a very old deposit, we would expect the true OCR (i.e. $\sigma'_{vp}/\sigma'_{vo}$) to be greater than $OCR_m$, owing to various aging processes (see Chapter 4).

c) From Marchetti dilatometer tests

Values of OCR have been calculated for Canons Park from the results of Marchetti dilatometer tests, using the following formula:[40]

$$OCR = (0.5K_D)^{1.56}$$

where $K_D$ is the horizontal stress index. Note that this correlation was established with the results of *standard* oedometer tests, and should tend to *under*-estimate the OCR of a heavily consolidated clay (for the reasons given in Section 5.4.3.a above). The reader should also refer to the

discussion on p199 about the validity of Marchetti's correlations in UK soils.

d) Summary of OCR values for the Canons Park site

Table 5.2 summarizes the values of $\sigma'_{vp}$ and OCR determined above. As the table reveals, there is very little agreement between the various estimates of OCR (which illustrates the difficulty in evaluating the

Table 5.2 Pre-consolidation pressure at Canons Park (at 9m depth)

| Method | Overburden (m) | $\sigma'_{vp}$ (MPa) | OCR |
|---|---|---|---|
| Geological records | 73-121 | 0.8-1.3 | 8-14 |
| Standard oedometer | 55-64 | ≈0.6 | ≈6 |
| Rebound reconstruction* | 155-190 | 1.53-1.87 | 16-21 |
| Dilatometer | - | - | 13-16 |

*based on high pressure oedometer tests on reconstituted clay

overconsolidation ratio for heavily overconsolidated clays). A few comments are worth making about these estimates:

- As discussed earlier, standard oedometer tests do <u>not</u> give reliable OCR values for heavily overconsolidated clays
- Preferably, the OCR of a heavily overconsolidated clay would be determined from the results of *high pressure* oedometer tests on intact samples (such tests have not been performed for the Canons Park London clay)
- Som's rebound reconstruction allows a realistic value of OCR to be determined in cases where the results of high pressure oedometer tests are not available; however, the method relies on data for *reconstituted* material, and it is not clear whether it over- or under-estimates $\sigma'_{vp}$ (and therefore OCR) for <u>aged</u> clays
- The geological estimate is subject to great uncertainties, but appears to give a reasonable <u>lower bound</u> figure for OCR (due to aging, the true OCR exceeds the mechanical, i.e. $OCR_m$); note that Skempton reckoned that "erosion has accounted for the removal of about [152m] of sediments"[41] at Bradwell (50 miles

NE of London)

- It is impossible to assess whether the dilatometer's estimate is an upper or lower bound to the true OCR; further research is needed before the dilatometer can be used - with confidence - to determine the OCRs of heavily overconsolidated clays

Based on the arguments set out above, I believe the best estimate of OCR for Canons Park is that given by Som's rebound construction. Since all estimates of OCR are much lower than Som's, and allowing for the uncertainties involved in his method of construction, I have assumed in this Thesis that the total depth of sediment that has been removed from the site is 155 ±35m. Accordingly, the OCR varies with depth as noted in Table 5.3.

Table 5.3 Variation of OCR with depth

| Depth (m) | OCR based on overburden of... 120m | 155m | 190m |
|---|---|---|---|
| 2.5 | 35.7 | 45.9 | 56.1 |
| 3.0 | 31.5 | 40.5 | 49.4 |
| 3.5 | 28.2 | 36.2 | 44.2 |
| 4.0 | 25.5 | 32.7 | 39.9 |
| 4.5 | 23.3 | 29.8 | 36.3 |
| 5.0 | 21.4 | 27.3 | 33.3 |
| 5.5 | 19.8 | 25.3 | 30.8 |
| 6.0 | 18.4 | 23.5 | 28.6 |
| 7.0 | 16.2 | 20.6 | 25.1 |
| 8.0 | 14.5 | 18.4 | 22.4 |
| 9.0 | 13.1 | 16.6 | 20.2 |

### 5.4.4 Cavity expansion limit pressure

The limit pressure ($p_{lim}$), determined from self-boring pressuremeter tests, forms the (putative) upper bound to the radial total stress mobilized against the surface of a displacement pile during installation. I have analyzed the self-boring pressuremeter tests at Canons Park (see Section 5.4.2.a above) in order to obtain $p_{lim}$, by extrapolating the pressure-strain curves (such as the one shown in Figure 5.7) to a cavity strain ($\epsilon_c$) of infinity.[42] Figure 5.11 presents the values of $p_{lim}$ determined in this way, together with contours of cell pressure at various strain levels below $\epsilon_c = \infty$.

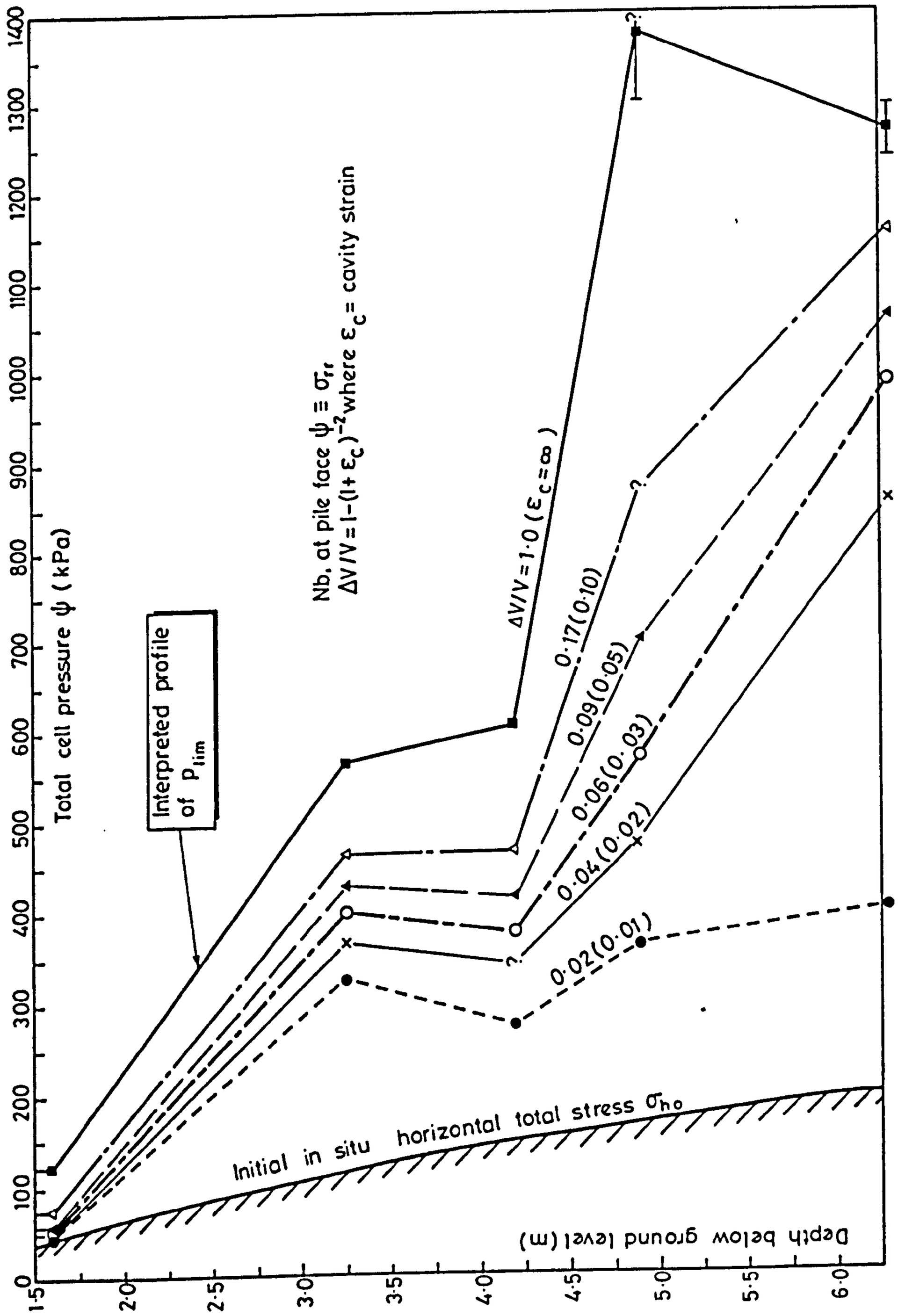



Figure 5.11 Limit pressures from self-boring pressuremeter tests at Canons Park

## 5.4.5 Soil stiffness

Values of the shear modulus from the unload-reload portion of the pressuremeter curves, $G_{ur}$, are compared with laboratory-determined stiffnesses in Figure 5.12. The precise value of $G_{ur}$ obtained from the pressuremeter curve is strongly dependent on the size of the unload-reload loop over which it is measured. Laboratory measurements of small strain stiffnesses[43] have shown that soils do not behave as ideal linear-elastic materials prior to yield (as is commonly assumed). Instead, they exhibit marked non-linearity in the elastic range, their stiffnesses reducing dramatically as the strain level increases. For example, the (intact) brown London clay from Canons Park has a shear stiffness G in undrained triaxial compression of 40-50MPa ($G/c_{uo}$ = 335-445) at 0.01% axial strain; but a stiffness G equal to only 15-20MPa ($G/c_{uo}$ = 125-160) at 0.1% strain.[44] Typically the soil yields at an axial strain of about 1%.

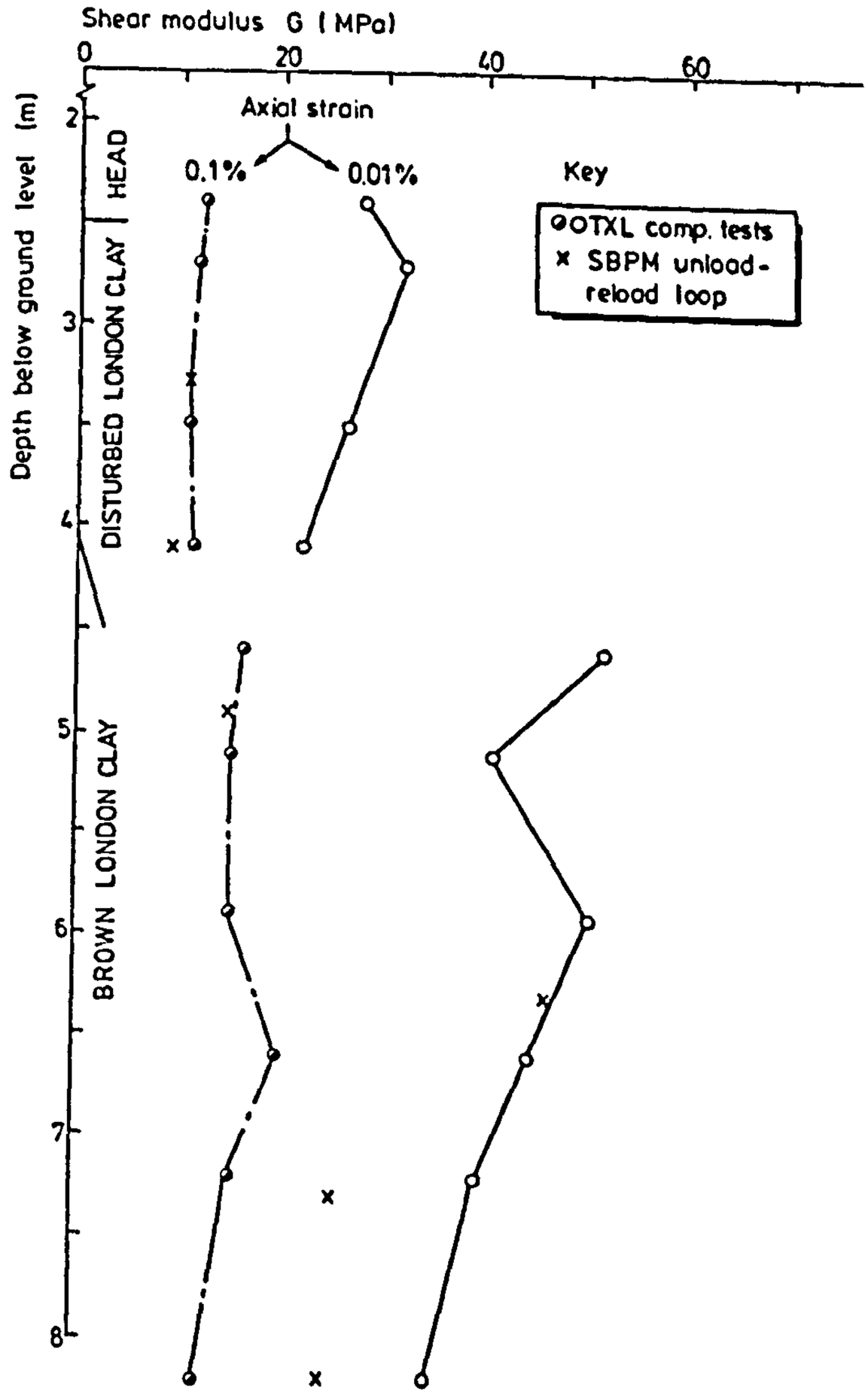



Figure 5.12 Shear stiffness of the London clay at Canons Park

## 5.5 RING SHEAR EXPERIMENTS ON THE LONDON CLAY

### 5.5.1 Basic shear mechanisms

Experiments in the ring shear apparatus at Imperial College have demonstrated how a clay's frictional resistance depends on, amongst other things, the rate of shearing. To understand why certain factors govern the soil's behaviour it is necessary to distinguish between the different shearing mechanisms that are involved.

Lupini[45] described two basic shear mechanisms that govern the behaviour of soils in the ring shear apparatus. "Turbulent" shearing (mode T) occurs typically in soils with a low clay content and hence low plasticity index $I_p$; whereas "sliding" shear (mode S) occurs in soils with a high plasticity index. A "transitional" mode ($T_R$) of shearing exists, part turbulent and part sliding, for soils with intermediate plasticity. Soils which would normally fail in a turbulent manner may also undergo sliding shear when failed against a smooth surface - this mode of behaviour has been designated $S_1$. And when sheared very quickly, soils that normally slide may fail in the transitional - or even turbulent - mode.[46]

The London clay usually fails by shearing in the sliding mode, but may also fail in modes $T_R$ and $S_1$, particularly when loaded at a fast rate. Real piles are not smooth, and so, to prevent the soil from failing prematurely (and artificially) in mode $S_1$, the surfaces of piles CP1-CP7 were deliberately roughened prior to the field experiments, to simulate the roughness of a typical rusty pile.

### 5.5.2 Sliding shear behaviour

Sliding shear involves the formation of a polished surface of strongly oriented clay particles:

> "...an oriented shear surface, once formed, is a permanent feature of the soil and is substantially unaffected by subsequent stress history... When sliding occurs the residual

> friction angle is quite strongly dependent on the normal effective stress."[47]

Typical residual angles of friction for the London clay are between 7 and 11° (for mode S).

> "[A] plastic clay, which suffers preferred particle orientation when sheared to large strains, will be brittle even when sheared after normal consolidation... Once a shear surface has formed, the clay will fail without brittleness on this surface even after overconsolidation [provided that displacement on the surface is monotonic and without reversal]."[48]

Hence, if we suppose that a continuous shear surface forms adjacent to a pile <u>during installation</u>, then in a subsequent first-time load test <u>in compression</u> we would expect the load-displacement curve to display no signs of strain-softening (i.e. we would expect to see a ductile, not a brittle, response to loading). If a shear surface does <u>not</u> form during pile installation then the subsequent load-displacement curve will be brittle. As is shown in Chapter 11, the response of a slow-jacked pile is ductile when tested in first-time compression, whereas the response of a fast-jacked pile is brittle.

### 5.5.3 Transitional shear

Soils undergoing transitional shear exhibit the behaviour observed for both the turbulent* and sliding modes, although in muted form.

> ...transitional behaviour involves discontinuous sliding shear surfaces and pockets of soil behaving in the turbulent mode, both contained within a thick shear zone. ...the effects of increasing normal stress will be to reduce the residual angle in sliding and at the same time to cause a denser packing of the rotund particles and more interference between them. The total effect... may thus be a product of two opposing mechanisms."[49]

The turbulent component may be suppressed when shearing takes place against an interface:

---

*Soils exhibiting turbulent shear show a high residual strength, typically with $\phi_R \approx \phi_{cs}$ (for London clay $\approx 23°$)

"If a soil ... of the turbulent type is sheared against a smooth interface which locally reduces interlocking and interference, then... partial sliding on the boundary might occur, with local orientation of the platy particles and a low residual strength."[50]

### 5.5.4 Special tests to simulate pile installation and loading

A special series of ring-shear tests on the London clay from Canons Park have been performed[51] at Imperial College, in order to complement the field experiments with the instrumented piles. Remoulded samples of the un-weathered London clay were sheared against a stainless-steel interface that had previously been grit-blasted to give the same surface roughness (≈8$\mu$m centre-line average) as the instrumented piles.

Figure 5.13 presents the results of two of these special tests: the broken lines represent the "slow" test (no 40) and the full lines the "fast" test (no 41). The experimental procedure was as follows.

After initial consolidation to a normal stress ($\sigma_n$) of 484kPa, the samples were sheared at a constant velocity in a series of five or six identical stages, each stage involving ≈1m of relative displacement between the soil and the interface (corresponding to the pile/soil interface). The velocity for Test 40 was 110mm/min, whilst that for Test 41 was ten times higher. Between each stage (e.g. for Test 40, numbers 1-6 on the figure) the samples were allowed to consolidate for 10 minutes before being re-sheared. This procedure was designed to simulate the installation of an instrumented pile.

At the end of "pile installation" (in our example at the end of stage 6) the sample was left to consolidate for 16-18h, and was then sheared <u>at a slow rate</u> (≈0.005mm/min) - thereby simulating a subsequent compression load test on the pile. (This stage is not shown on the figure.)

It is clear from Figure 5.13 that the stress ratio ($\tau/\sigma_n$) mobilized at a displacement rate of 1100mm/min (Test 41) is much higher than the value mobilized at 110mm/min (Test 40). This is true both for the "fast peak"

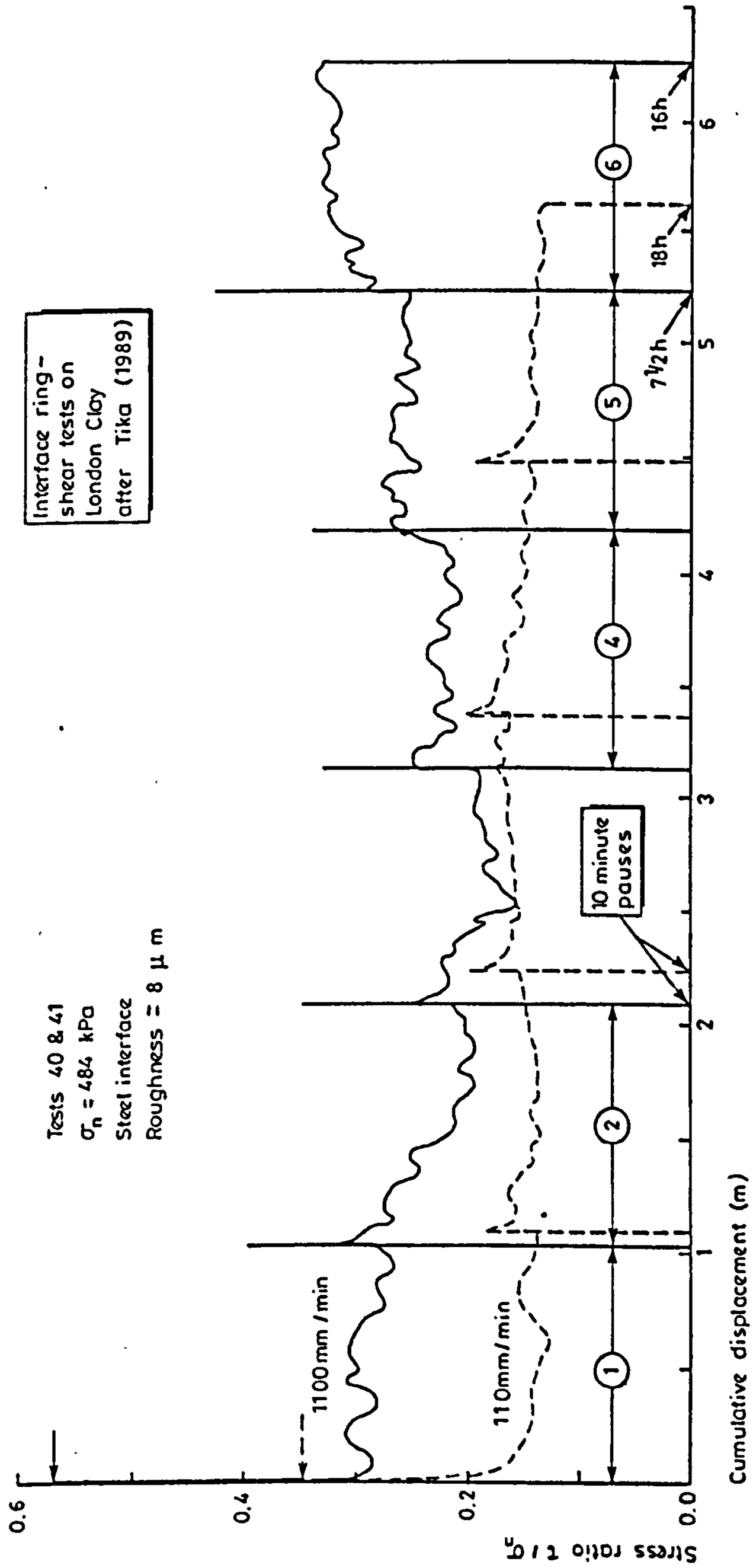



Figure 5.13 Special interface ring-shear tests on the London clay from Canons Park

values, $(\tau/\sigma_n)_{fp}$, at the start of each stage (i.e. the spikes on Figure 5.13) and the "fast minimum" values, $(\tau/\sigma_n)_{fm}$, at the end.

Table 5.4 summarizes the values of the stress ratio measured in these special ring-shear tests on London clay from Canons Park. The "slow peak" and "slow minimum" values, $(\tau/\sigma_n)_{sp}$ and $(\tau/\sigma_n)_{sm}$, were recorded during

Table 5.4 Results from interface ring-shear tests on London clay

| Test no | Rate of displacement (mm/min) | Stress ratio $\tau/\sigma_n$ Fast peak | Fast minimum | Slow peak | Slow minimum |
|---|---|---|---|---|---|
| 40 | 110 | 0.18-0.21 | 0.12-0.14 | 0.195 | 0.158 |
| 41 | 1100 | 0.33-0.43 | 0.15-0.28 | 0.262 | 0.195 |
| 42 | 2600 | 0.36-0.56 | 0.26-0.33 | 0.251 | 0.154 |

"load tests" on each sample (e.g. Stage 7 in Test 41). Assuming the soil is fully drained during the "load tests" allows the angle of friction to be calculated from $\delta = \tan^{-1}(\tau/\sigma_n)$; values of $\delta$ thus calculated are 11.0-14.7° for the slow peak and 8.75-11.0° for the slow minimum.

### 5.5.5 Ring-shear data for London clay from Canons Park

Figure 5.14 compiles data from all the ring shear tests that have been performed on samples of London clay from Canons Park. This includes some earlier tests by Lemos[52] in addition to soil-on-soil tests by Tika.[53]

The white symbols indicate the peak stress ratios recorded during fast shearing stages, $(\tau/\sigma_n)_{fp}$, plotted against the rate of displacement. The black symbols give values of peak stress ratio recorded during slow shear, $(\tau/\sigma_n)_{sp}$, plotted against the rate of displacement in the immediately preceding fast shearing stage. A slow rate is defined as 0.001-0.00625mm/min for this purpose; and a fast rate as > 1mm/min.

Not all of the data is strictly comparable: some of the points shown on the figure are from multiple tests on the same sample, others from single tests; some samples were allowed to consolidate for > 4h before shearing, others were not; some samples were tested against a smooth glass interface, some against roughened steel, and the others against soil; and, finally, the normal stress $\sigma_n$ varies from test to test. These

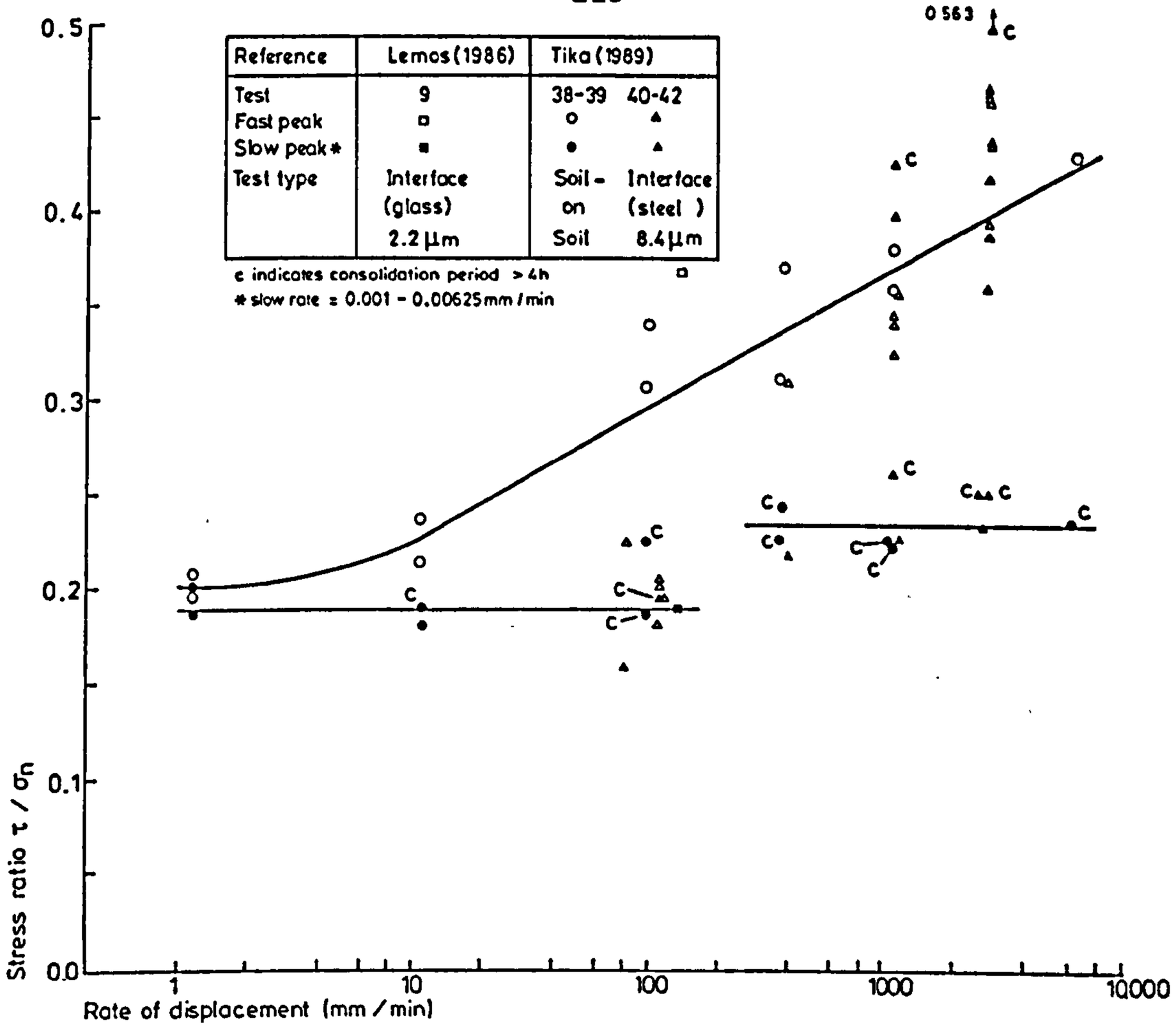



Figure 5.14 Dependency of stress ratio on rate of displacement in ring shear tests on London clay from Canons Park

factors contribute to the scatter that is evident on the diagram. Nevertheless, certain trends are immediately apparent.

There is a strong and consistent tendency for the fast peak values $(\tau/\sigma_n)_{fp}$ to increase with velocity (e.g. $(\tau/\sigma_n)_{fp} = 0.2$ at 1mm/min, rising to 0.4 at 4000mm/min). This rate dependency combines two separate components: a rate effect due to the soil's viscosity and a rate effect due to fabric re-orientation.

The slow peak values $(\tau/\sigma_n)_{sp}$ are considerably smaller than the equivalent fast peak values, as was noted earlier. Since all the slow shearing stages were conducted at (approximately) the same rate, $(\tau/\sigma_n)_{sp}$ should not be affected by the soil's viscosity. Therefore the jump in the value of $(\tau/\sigma_n)_{sp}$ from 0.19 to 0.235 between 110 and 370mm/min is caused by features of the soil's fabric. This jump represents an increase in the angle of friction $\delta$ from $\approx 11°$ to $\approx 13°$.

## 5.6 NOTES AND REFERENCES

[1]Personal communication with Mr Gerwyn Price of BRE. See also: Price G. and Wardle I.F. (1988). Comparison of vertical and shallow angled raked piles under lateral load. TRRL Contractor Report 45, Dept of Transport, Transport and Road Research Laboratory, Crowthorne, Berkshire, 43pp + figures.

[2]Jardine R.J. (1985). Investigations of pile-soil behaviour, with special reference to the foundations of offshore structures. PhD Thesis, Univ. of London (Imperial College), 2 vol., 789pp. See Chapter 7.

[3]Jardine R.J., Symes M.J., and Burland J.B. (1984). The measurement of soil stiffness in the triaxial apparatus. Géotechnique, 34(3), pp323-340.

[4]Hight D.W. (1982). A simple piezometer probe for the routine measurement of pore pressures in triaxial tests on saturated soils. Géotechnique, 32(4), pp396-401.

[5]Jardine (1985), loc. cit. Chapter 7.

[6]Jardine R.J., Fourie A., Maswoswe J., and Burland J.B. (1985). Field and laboratory measurements of soil stiffness. Proc. 11th Int. Conf. Soil Mech. & Fdn Engng, San Francisco, 2, pp511-514.

[7]Lemos L.J.L. (1986). The effect of rate on residual strength of soil. PhD Thesis, Univ. of London (Imperial College), 540+pp.

[8]Tika T. (1989). The effect of fast shearing on the residual strength of soils. PhD Thesis, Univ. of London (Imperial College).

[9]BRE project no GG202. All information (and copies of the test results) kindly provided by Mr Gerwyn Price (personal communication).

[10]As described in the book by Head K.H. (1982). Manual of soil laboratory testing. Volume 2: Permeability, shear strength and compressibility tests. Pentech Press, London. See Section 13.6.5, pp633-636.

[11]A typical description for soil below 4.1m was:

> "CLAY, firm to stiff, fissured, brown, with numerous pockets and partings of yellow silt/fine sand, numerous selenite crystals, and some pieces of mudstone".

[12]Price G. and Wardle I.F. (1982). A comparison between cone penetration test results and the performance of small diameter instrumented piles in stiff clay. Proc. 2nd Eur. Symp. on Penetration Testing (ESOPT II), Amsterdam, 2, pp775-780. A.A. Balkema, Rotterdam, 1982.

[13]Kitching D.N. (1983). A study into the microfabric of clays adjacent to jacked piles. MSc Dissertation, Univ. of London (Imperial College), 31pp+.

[14]Jardine (1985), loc. cit. See Chapter 9.

[15]Coop M.R. (1987). The axial capacity of driven piles in clay. DPhil Thesis, Univ. of Oxford. See Chapter 5.

[16]Price and Wardle (1988), loc. cit.

[17]After the pile test by Kitching (in 1983), seven 2.0m deep cased boreholes were sunk through the topsoil and gravel layers at the site. Throughout the Canons Park Project all of the piles were installed through these boreholes (i.e. directly into the head material).

[18]See pp19-20 of Bromehead C.E.N. (1925). The geology of North London. Memoirs Geol. Survey, England & Wales (explanation of Sheet 256). HMSO, London, 63pp.

[19]Bromehead (1925), loc. cit.

[20]Fugro Limited (1980). Static cone penetration tests at Canons Park, London. Project no U0662. Soils investigation report, 2pp + figures.

[21]Piezocone traces kindly supplied by Mr John Powell of the BRE (personal communication, 1988).

[22]The "cone factor" is defined as $N_k = (q_c - \sigma_{vo})/c_{uo}$ (where the symbols have their usual meanings). The values of $c_{uo}$ that have been used in this formula come from 100mm diameter UU triaxial compression tests.

[23]The pore pressure parameter is defined as: $B_q = (u - u_o)/(q_T - \sigma_{vo})$.

[24]Photographs of the pit are presented by: Price and Wardle (1988), loc. cit.

[25]Calculated by the Gibson/Anderson method. See Gibson R.E. and Anderson W.F. (1961). In-situ measurement of soil properties with the pressuremeter. Civ. Engng & Publ. Works Review, 56(658), May 1961, pp615-618.

[26]Mair R.J. and Wood D.M. (1987). Pressuremeter testing: methods and interpretation. CIRIA Ground Engineering Report: In-situ Testing. CIRIA/Butterworths, London, 160pp. See Appendix A8, pp150-153.

[27]PM Insitu Techniques Ltd (1984). Canons Park - London. Results of self-boring pressuremeter tests. Report no T76-R1, 6pp+.

[28]Jardine (1985), loc. cit., vol. 2, pp769-773.

[29]Tedd P. and Charles J.A. (1981). In situ measurement of horizontal stress in overconsolidated clay using push-in spade-shaped pressure cells. Géotechnique, 31(4), pp554-558.

[30]Results kindly supplied by Mr John Powell of the BRE (personal communication, 1988).

[31]Tedd P. and Charles J.A. (1983). Evaluation of push-in pressure cell results in stiff clay. Proc. Int. Symp. on In Situ Testing, Paris, 2, pp579-584.

[32]Powell J.J.M. and Uglow I.M. (1988a). Marchetti dilatometer testing in UK soils. Proc. 1st Int. Symp. on Penetration Testing, Florida, in press.

[33]Powell J.J.M. and Uglow I.M. (1988b). The interpretation of the Marchetti dilatometer in UK clays. Proc. Instn of Civ. Engnrs' Geotechnology conf. on Penetration testing in the UK, Univ. of Birmingham, July 1988, in press.

[34]Powell and Uglow (1988b), loc. cit. One criticism of Powell and Uglow's approach is that they have correlated the dilatometer parameters (such as the horizontal stress index $K_D$) against (corrected) $K_0$ values determined from spade cell experiments. Spade cells are still widely regarded as giving an overestimate of the true value of $K_0$. Also, the overconsolidation ratios they quote for Canons Park are well in excess of the values deduced from high pressure oedometer tests, and are most probably in error.

[35]Marchetti S. (1980). Insitu tests by flat dilatometer. J. Geotech. Engng Div., Am. Soc. Civ. Engrs, 106(GT3), pp299-322.

[36]Mayne P.W. and Kulhawy F.H. (1982). Ko - OCR relationships in soils. J. Geotech. Engng, Am. Soc. Civ. Engrs, 108(GT6), pp851-872.

[37]Jardine (1985), loc. cit., vol. 1, Section 7.3 (pp159-161); and vol. 2, Figures 7.10, 7.11, and 7.13. Test LOED1 (on soil from 9.4m depth) gave $\sigma'_{vp}$ = 630kPa; test LOED2 (4.7m depth) gave 540kPa. See also Table 9 of: Fourie A.B. (1984). The behaviour of retaining walls in stiff clay. PhD Thesis, Univ. of London (Imperial College), 437pp.

[38]See any standard text book on soil mechanics, for example: Terzaghi K. and Peck R.B. (1967). Soil mechanics in engineering practice (2nd edition). John Wiley and Sons Inc., New York, 729pp.

[39]Som N.N. (1968). The effect of stress path on the deformation and consolidation of London Clay. PhD Thesis, Univ. of London (Imperial College), 2 vols, 409pp + figures. See p224ff.

[40]Marchetti (1980), loc. cit.

[41]Skempton A.W. (1961). Horizontal stresses in an overconsolidated Eocene clay. Proc. 5th Int. Conf. Soil Mech. & Fdn Engng, Paris, 1, pp351-357. Quoted from p352.

[42]For example, see pp51-55 of Mair and Wood (1987), loc. cit.

[43]Jardine et al. (1985), loc. cit.

[44]Jardine (1985), loc. cit., Table 7.4.

[45]Lupini J.F. (1981). The residual strength of soils. PhD Thesis, Univ. of London (Imperial College), 462pp.

[46]Lupini (1981), loc. cit., presents the basic shear mechanisms in terms of the "granular voids ratio" of the soil ($e_g$). This is defined as the volume of platy particles (typically < 2$\mu$m in size) and water, divided by the volume of rotund particles (≥ 2$\mu$m). Turbulent shearing (mode T) typically occurs in soils with $e_g$ < 1¼; whereas "sliding" (mode S) occurs in soils with $e_g$ > 3. The London clay has a granular voids ratio between 2 and 3.

[47]Lupini J.F., Skinner A.E., and Vaughan P.R. (1981). The drained residual strength of cohesive soils. Géotechnique, 31(2), pp181-213. See p206.

[48]Lupini, Skinner, and Vaughan (1981), loc. cit., p185.

[49]Lupini, Skinner, and Vaughan (1981), loc. cit., pp206-207.

[50]Lupini, Skinner, and Vaughan (1981), loc. cit., p205.

[51]Tika (1989), loc. cit.

[52]Lemos (1986), loc. cit.

[53]Tika (1989), loc. cit.

# Chapter 6

# Design and development of the Imperial College Instrumented Pile

CONTENTS OF CHAPTER 6


6.1 INTRODUCTION . . . . . 223
6.2 INSTRUMENTATION FOR TEST SERIES CP1 . . . . . 224
6.2.1 Refurbishment of the Southampton Pile 224
6.2.2 Main features of Pile CP1 224
6.2.3 Saturation of the pore pressure probes 224
6.2.4 Field performance of the Southampton Pile 226
6.3 MAIN FEATURES OF THE IMPERIAL COLLEGE INSTRUMENTED PILE 227
6.3.1 General arrangement 227
6.3.2 Waterproofing the pile 231
6.3.3 Tests at Canons Park and Labenne 231
6.4 DESIGN OF THE AXIAL LOAD CELLS . . . . . 233
6.4.1 General description 233
6.4.2 Design requirements 234
6.4.3 Design and manufacture of the Mk III ALCs 234
6.4.4 Design calculations 234
6.4.5 Calibration and testing 235
6.4.6 Field performance 236
6.5 DESIGN OF THE SURFACE STRESS TRANSDUCERS . . . . . 237
6.5.1 General description 237
6.5.2 Design requirements 241
6.5.3 Design and manufacture of the Mk IV SSTs 241
6.5.4 Design calculations 242
6.5.5 Calibration and testing 243
6.5.6 Cell action effects (under-registration of loads) 243
6.5.7 Field performance of the surface stress transducers 245
6.6 GENERAL REQUIREMENTS FOR MEASURING PORE PRESSURES . . . 246


continued...

6.7 DESIGN OF FAST-ACTING PORE PRESSURE PROBES . . . . . 247
6.7.1 General description 247
6.7.2 Design requirements 247
6.7.3 Design and manufacture of the Mark III PPPs 248
6.7.4 Saturation of the pore pressure probes 251
6.7.5 Calibration and testing 253
6.7.6 Field performance of the fast-acting probes 254
6.8 DESIGN OF THE FLUSHABLE PORE PRESSURE SYSTEM . . . . . 256
6.8.1 General description 256
6.8.2 Design details - pore pressure probes (Mark IV) 256
6.8.3 Design details - half-way housing 258
6.8.4 Calibration and testing 261
6.8.5 Saturation procedure 261
6.8.6 Field performance of the flushable pore pressure system 262
6.9 NOTES AND REFERENCES . . . . . 263

## 6.1 INTRODUCTION

The Pilot Test in the series of experiments at Canons Park was conducted by Jardine[1] in 1984, using an instrumented pile that had originally been designed and manufactured at Southampton University (for research into the effects of electro-osmosis on the load capacity of piles).[2] The Southampton Pile carried a total of five axial load cells and eight "local" load cells.* On its arrival at Imperial College, Jardine decided to refurbish the instrumentation, replace several of the load cells, and to augment the equipment with four pore pressure transducers, so that effective stresses could be calculated.

The results of the Pilot Test (CP0) were sufficiently encouraging for the Canons Park Project to get under way, but further improvements to the equipment were needed: the long-term readings in the Pilot Test had proved unreliable and several instruments had been damaged. Further development of the original equipment was attempted prior to the next experiment (CP1), whilst at the same time work was started on designing a completely new suite of instruments (the "Imperial College Instrumented Pile"). The Southampton Pile was employed in only two tests at Canons Park, CP0 and CP1; its use was discontinued for the remainder in favour of the Imperial College Instrumented Pile.

This Chapter describes the design, development, and field performance of the Imperial College Instrumented Pile. Section 6.2 describes briefly the original (Southampton) pile, concentrating on the instrumentation that was employed during Test Series CP1; and Section 6.3 gives details about the design of the new equipment. The data acquisition system for the Canons Park project is described at the end of Chapter 8.

---

*The "local" load cells measured simultaneously the radial total stresses and the shear stresses acting on the pile; herein these devices are called "surface stress transducers"

## 6.2 INSTRUMENTATION FOR TEST SERIES CP1

### 6.2.1 Refurbishment of the Southampton Pile

The Southampton Pile required extensive refurbishment following completion of the Pilot Test. Two new axial load cells were manufactured; the surface stress transducers were re-designed; and extra pore pressure probes were fitted to the pile. Further details are given in Appendices 6-8.

### 6.2.2 Main features of Pile CP1

For experiment CP1, the Southampton Pile carried instruments at three separate levels, spaced at approximately 1m intervals along the pile's length. Figure 6.1 shows a cut-away section through these instrument "clusters". The middle and top clusters (nos 2 and 3) contained one axial load cell (ALC), two surface stress transducers (SSTs), two pore pressure probes (PPPs), and one temperature sensor (TS). The bottom cluster (no 4) contained an ALC and two PPPs only. In addition, an ALC was mounted at the head of the pile.

### 6.2.3 Saturation of the pore pressure probes

As explained in more detail in Section 6.7.4, the performance of any piezometer system in a strongly dilating material (such as the London clay at Canons Park) is critically dependent on good saturation of the piezometer system and also on the choice of a suitable saturating fluid.

For Test Series CP1 the pore pressure probes were saturated with de-aerated water and typically had 99% response times (in the laboratory) of less than one second. However, during pile installation the fluid in the probes cavitated and their response became extremely sluggish. The probes recovered from these adverse effects when penetration ceased (at the end of installation) but not until several minutes had passed. It was decided, on the basis of this experience, to use a saturating fluid other than water in the remaining tests (CP2-CP5).

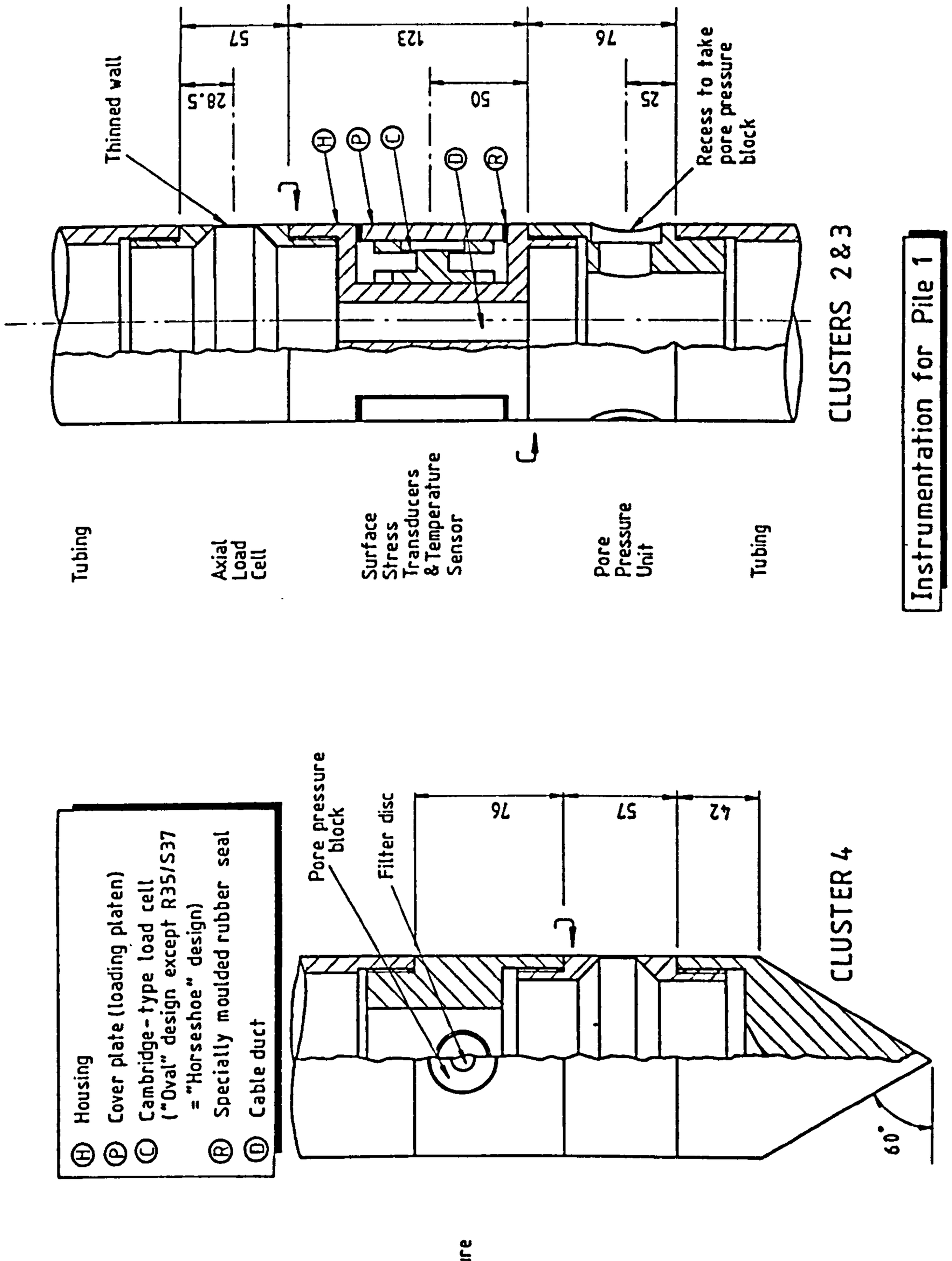



Figure 6.1 Instrumentation for pile CP1

Further details about the pore pressure response during Test Series CP1 are given in Appendix 9.

### 6.2.4 Field performance of the Southampton Pile

Despite considerable efforts to make the Southampton Pile completely waterproof, it proved impossible to seal the pile well enough to prevent the instruments' signals from drifting in the long term (over a period of 80 days). The main culprits were the joints between the various sections of the pile and the housings of the surface stress transducers. As the design of the original equipment was such that no further improvements could be made to it, the only viable option was to design a completely new instrumented pile (as described in Section 6.3).

## 6.3 MAIN FEATURES OF THE IMPERIAL COLLEGE INSTRUMENTED PILE[3]

### 6.3.1 General arrangement

The Imperial College Instrumented Pile is a 7m long, 101.6mm diameter, closed-ended steel pile. There are three instrumented sections (or "clusters") spaced approximately one metre apart along its length, and each one contains:

- A high capacity axial load cell (ALC)
- A surface stress transducer (SST) and temperature sensor (TS)
- A pore pressure unit (PPU) containing two pore pressure probes (PPPs)

Figure 6.2 shows the general arrangement of the instrument clusters along the pile's shaft. In addition to instruments at the top, middle, and bottom of the pile's embedded portion, there is also an axial load cell at the pile head. During loading tests, three displacement transducers are used to measure the vertical movements.

Plate 2 and Figure 6.3 show a typical instrument cluster in exploded view. On the left is an axial load cell (ALC); in the

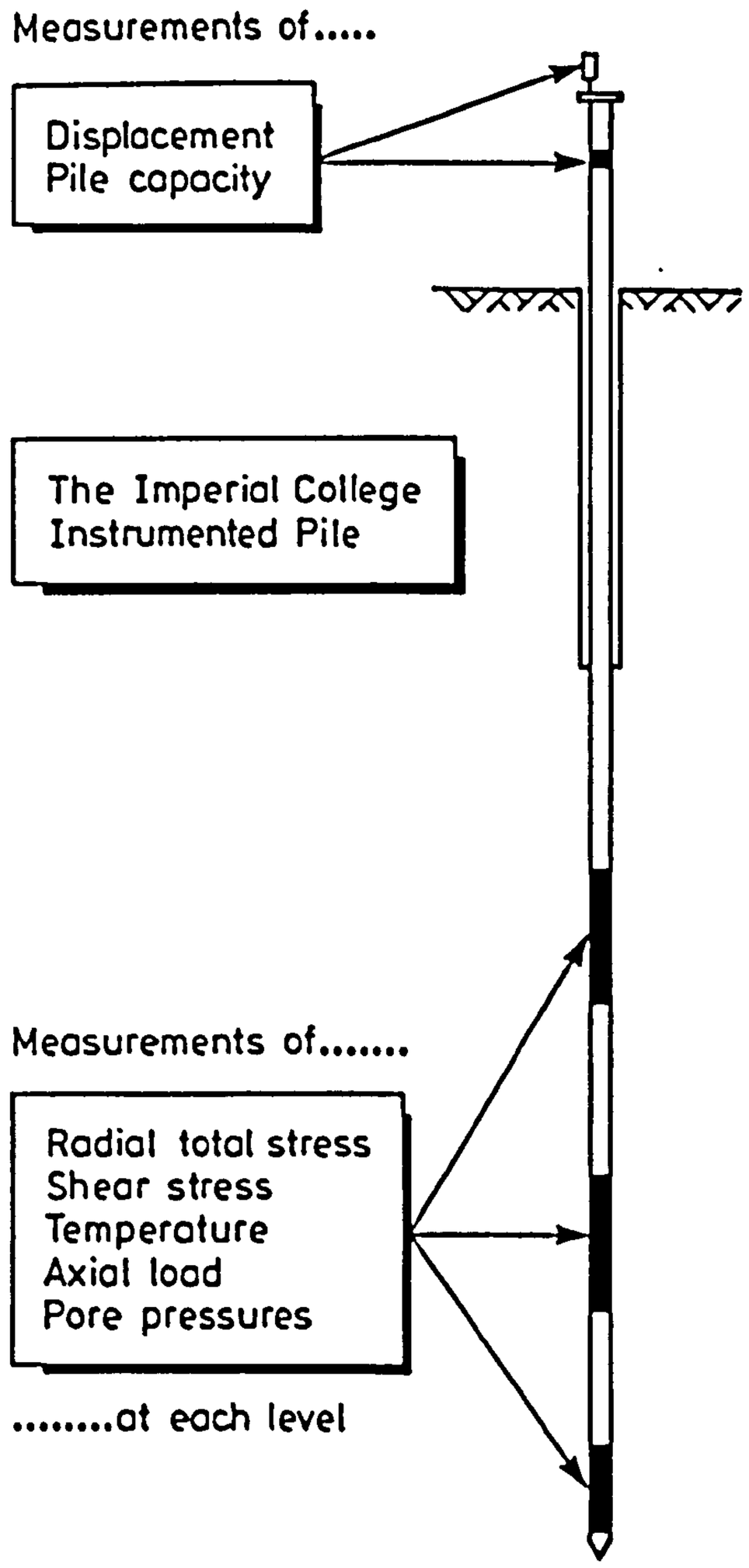



Figure 6.2 The Imperial College Instrumented Pile

centre a pore pressure unit (PPU) with a pore pressure probe hanging from one of its two portholes; and on the right a surface stress transducer (SST) with its cover plate lying to one side. Each surface stress transducer incorporates a temperature sensor (TS) within it.

The instrumented sections of the pile are separated by steel tubing of wall thickness 9.525mm. The ratio of the pile's diameter to its wall thickness is, therefore, D/h = 10.7. Similar tubing is used to connect the top instrument cluster to the axial load cell at the pile head. Each tube is between 660 and 1102mm long, and the various sections of the pile

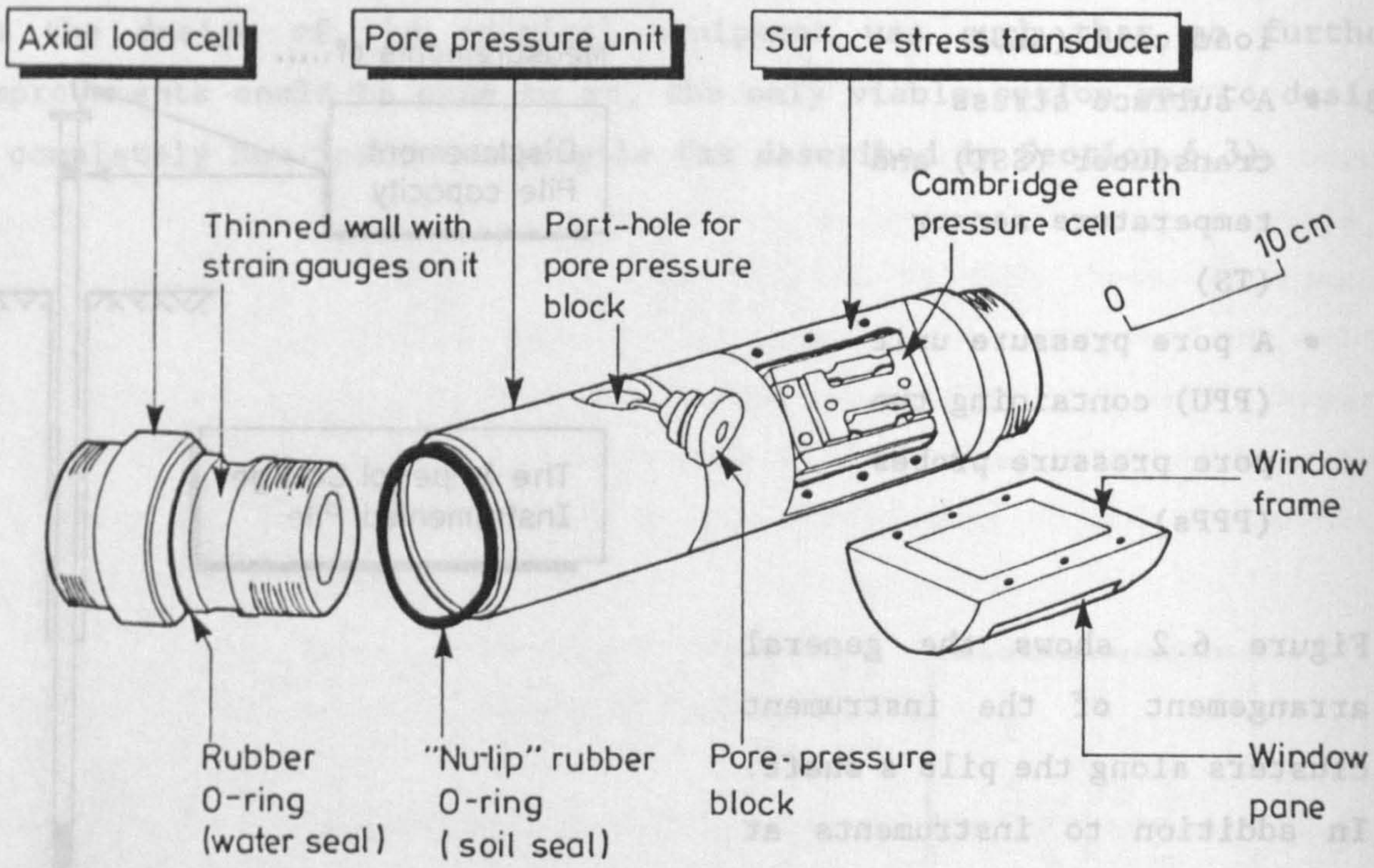



Figure 6.3 Typical instrument cluster on the Instrumented Pile

are connected together by screw threads. The tubes between the instrument clusters have at one end a right-handed thread and at the other a left-handed thread, so that they can be used as turnbuckles. This arrangement helps to prevent the instruments' cables from twisting during pile assembly.

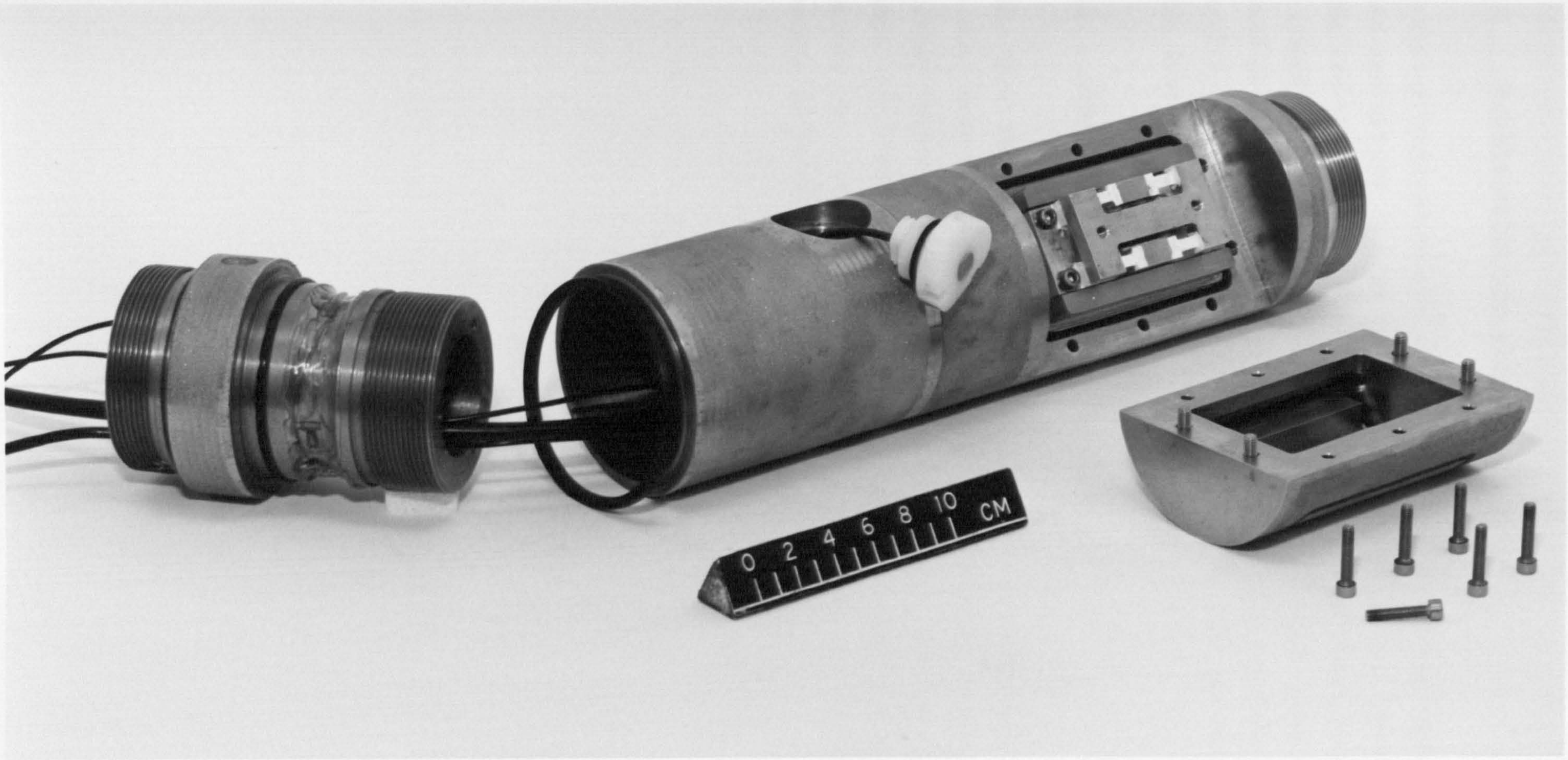



Plate 2 Typical instrument cluster on the Imperial College Instrumented Pile [photo: A. Chipling]

### 6.3.2 Waterproofing the pile

The various instruments are connected together by screw threads which are sealed against the ingress of water in two ways. First, there is a rubber O-ring located at the root of the male thread, as shown in Figure 6.4 by the symbol "O"; second, the threads themselves were coated with either Hylomar gasket sealant or with Bostik 1753 sealing compound.[4] This method of sealing has proved completely sound, with no leakage occurring in any of the Test Series to date.

### 6.3.3 Tests at Canons Park and Labenne

At the time of writing (July 1989), the Imperial College Instrumented Pile has been used in a total of four experiments at Canons Park (as described in the following chapters) and in a further two at a site near Labenne, in France. The results of these latest pile tests (in medium dense and loose sand) will be reported at a later date (the results are currently confidential).

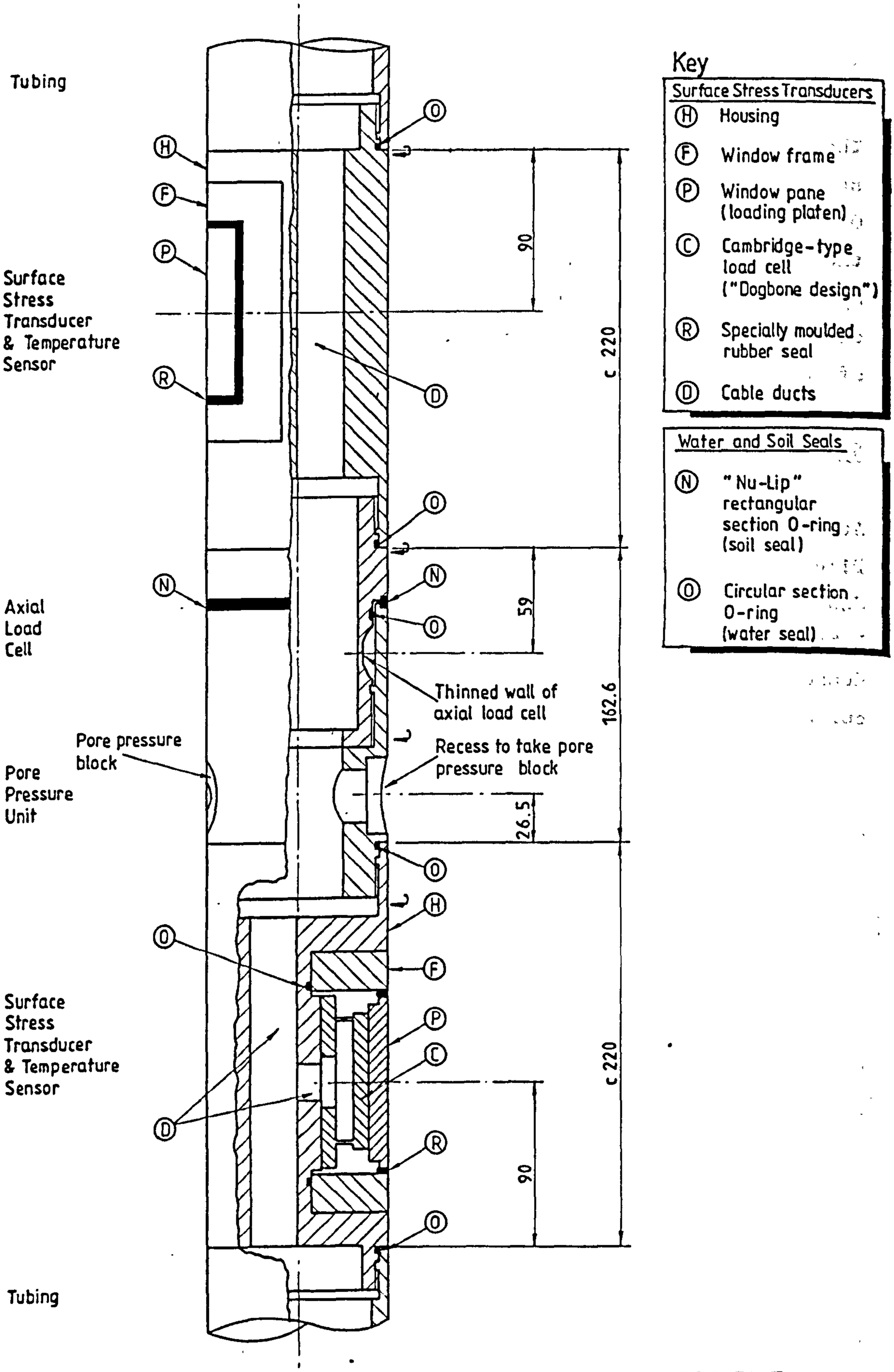



Figure 6.4 Section through an instrument cluster on pile CP2

## 6.4 DESIGN OF THE AXIAL LOAD CELLS

### 6.4.1 General description

The Instrumented Pile carries a total of three axial load cells along its length, in addition to the load cell at the pile's head. Figure 6.5 shows a cut-away view of an axial load cell and the pore pressure unit which is an integral part of it: the bottom part of the load cell (ALC) screws into the top part of the pore pressure unit (PPU). The axial force that bears on the ALC passes through the thinned-wall section and strain gauges arranged in a Poisson bridge[5] convert this force into an electrical signal.

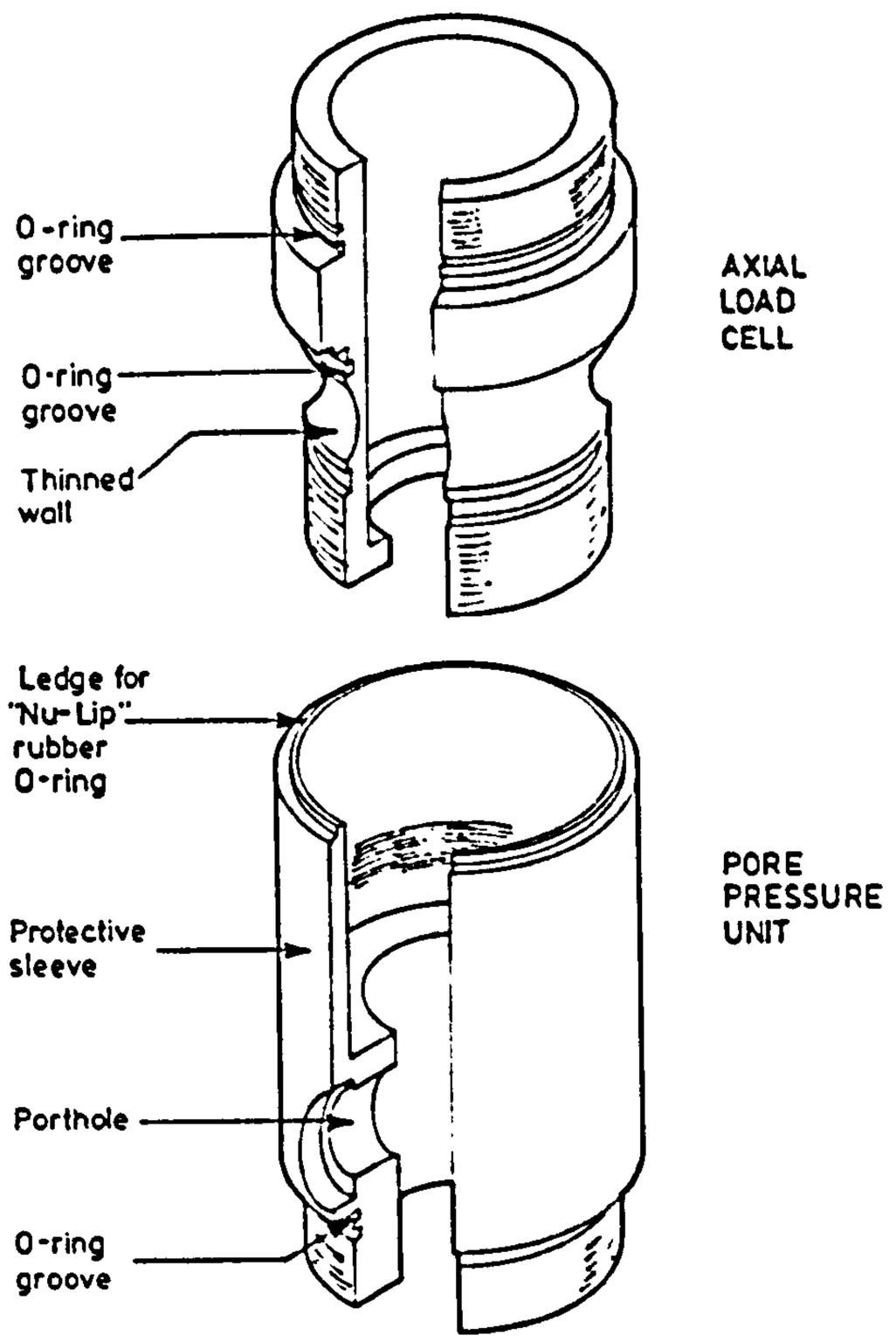



Figure 6.5 Combined axial load cell and pore pressure unit

The thinned-wall itself is prevented from touching the soil outside the pile by the protective sleeve at the top of the pore pressure unit. Neither soil nor water can reach the space directly in front of the strain gauges because of two rubber O-rings. A "Nu-Lip"[6] rectangular section O-ring prevents soil from getting behind the protective sleeve, and a circular section O-ring holds back the water.

A 25m long, four-core, underwater quality cable connects to the Wheatstone bridge and carries the electrical signal from it out of the pile. The cable passes through a small hole in the thinned-wall, and it is firmly clamped at the top of the cell to prevent pulling on the gauges.

### 6.4.2 Design requirements

The axial load cells were designed to meet the following main requirements.

- Load capacity ≥ 200kN
- Linear relationship between signal and load
- Adequate capacity against buckling within the cell's working range
- Zero cross-sensitivity to radial total stresses acting on the pile
- Fast response to changes in load
- Completely reliable waterproofing
- Ease of repair/refurbishment in case of accidents
- Ease of manufacture

### 6.4.3 Design and manufacture of the Mk III ALCs

The axial load cells were designed and manufactured at Imperial College during 1986-7. Detailed design drawings are presented in Appendix 6, which also includes a summary of the cells' technical specifications.

The axial load cells were manufactured from a manganese molybdenum steel, 605M36S, which is known for its good machining properties. Care was taken in the design to ensure that the length of the thinned wall was short, to avoid the cells buckling under working loads.[7] The cell was designed to give a full-scale output of 2mV/V under a load of 200kN.

### 6.4.4 Design calculations

The formula that relates the signal produced by the Poisson bridge to the load applied to the cell is:

$$Q = a_0 + a_1(V_o/V_i)$$

where $a_0$ and $a_1$ are calibration constants; and $V_o$ and $V_i$ are the output and input voltages, respectively.

The coefficient $a_1$ may be estimated from:

$$a_1 = 4\pi RhE/(1+\mu)k,$$

where R is the radius and h the thickness of the thinned wall; E and $\mu$ are the Young's modulus and Poisson's ratio of the steel; and k is the strain gauge factor ($\approx$ 2.1 for metal foil gauges).

This formula (appropriate for thin-walled load cells only) gives[8] $a_1 \approx$ 79MN, whereas in calibration tests $a_1$ has been found to be in the range 93-109MN for the six cells made to date. The difference between the figures is believed to be caused by bending moments acting at the top and bottom edges of the thin-walled section.

### 6.4.5 Calibration and testing

Each axial load cell was calibrated against a 35tonf Amsler loading machine. Separate calibrations were obtained in compression and in tension, there being slight differences (of no more than 3.7%) in the calibration coefficients $a_0$ and $a_1$ for the two cases. The load cells all showed the required sensitivity and gave a linear response to loading. Precise details of each cell's performance are given in Appendix 10. The errors obtained due to non-linearity and hysteresis combined were less than 0.56% of the full-scale output. These values are perfectly acceptable for the purposes of the field experiments.

One of the axial load cells (ALC2) was also tested to determine the following:

- Cross-sensitivity to pressures acting on the protective sleeve
- The proportion of the load carried by the Nu-Lip O-ring

The load cell's cross-sensitivity to pressure on the protective sleeve needs to be small, since large radial total stresses (of up to $\approx$1MPa) may

bear on the pile whilst it is in the ground. The cross-sensitivity was determined by applying a water pressure of 1.1MPa to the combined ALC/PPU. No discernible change in signal from the cell could be measured.

The cell was also calibrated with and without the Nu-Lip O-ring in position. With it present, the output signal was 0.6% lower than that obtained with the O-ring absent. In normal use, therefore, 99.4% of the axial load can be expected to pass through the thinned-wall section.

### 6.4.6 Field performance

The axial load cells have performed extremely well in all the tests series to date (July 1989). They have given very stable signals during both the short- and long-term experiments, and have required little or no attention to keep them functioning properly.

## 6.5 DESIGN OF THE SURFACE STRESS TRANSDUCERS

### 6.5.1 General description

The surface stress transducers (SSTs) are the most complicated of all the instruments that make up the Instrumented Pile. They measure both the radial total stress, $\sigma_{rr}$, and the shear stress, $\tau_{rz}$, acting at specific locations along the pile's surface. Plate 3(a) and Figure 6.6 show two exploded views of the transducer, which consists of four main elements:

- Main housing
- Cambridge-type boundary earth pressure cell
- Window pane (the loading platen)
- Window frame

These four parts fit together as follows. The Cambridge earth pressure cell sits on top of a raised platform in the centre of the SST, and is covered by a two-part "window" that protects it from direct contact with the soil. The window pane and window frame, although manufactured as separate pieces, are joined together by a hot-bonded rubber seal that runs along the edges of the window pane. When the transducer is fully assembled the window frame is bolted down

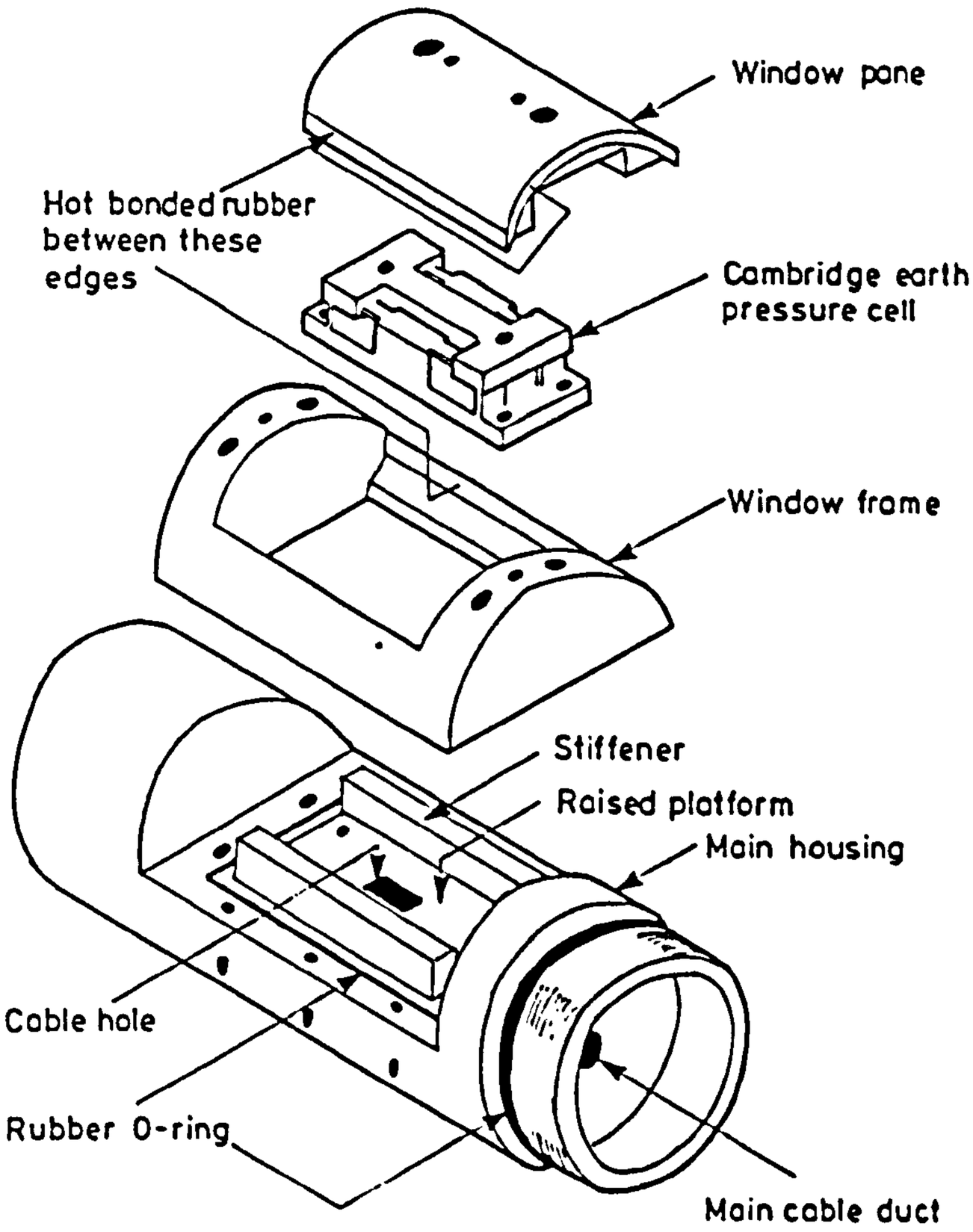



Figure 6.6 The surface stress transducer

onto the main housing, and the window pane onto the top surface of the Cambridge pressure cell. The cell, therefore, is sandwiched between the window pane and the main housing.

Any load that bears on the window pane is transferred to the main housing via the earth pressure cell, save for a small proportion of the load that is lost through the hot-bonded rubber. The earth pressure cell is an intricate device, as revealed in Plate 3(a) and Figure 6.7. Because of the orientation of its strain-gauged webs, the cell can resolve both the normal and the shear stresses acting on it. This type of device was first used in soil mechanics research by Arthur and Roscoe, at Cambridge University.[9] (The particular cell shown in Figure 6.7 is similar to one designed by Stroud.[10])

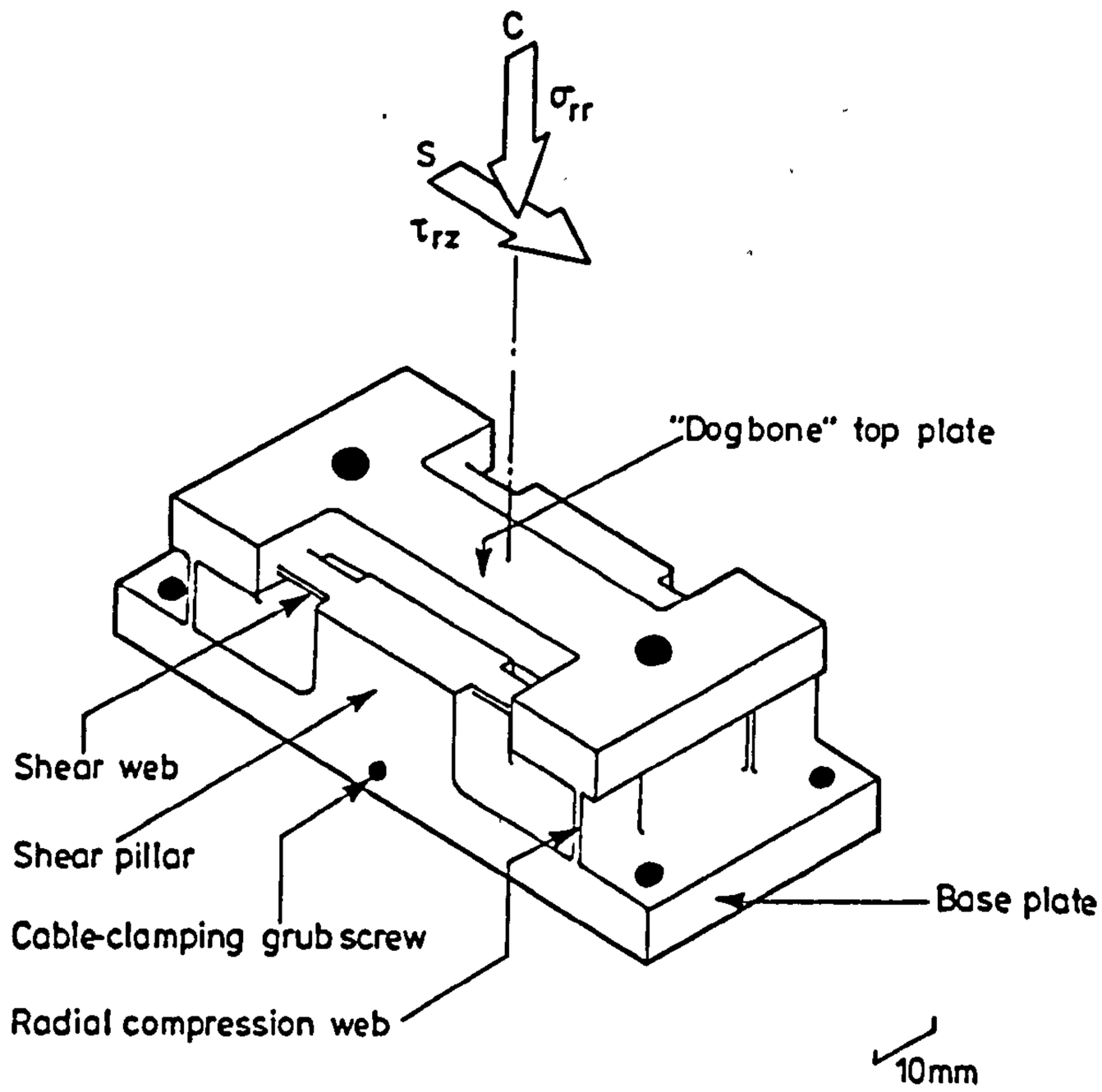



Figure 6.7 The "dogbone" Cambridge earth pressure cell

Water is kept from entering the surface stress transducer by three main seals. The window frame is sealed against the main housing by a large rubber O-ring which fits into the groove surrounding the raised platform. The gap between the window pane and frame is sealed by hot-bonded rubber, as mentioned above. Finally, the bolts which connect the window pane to the Cambridge pressure cell are sealed by Dowty washers and Hylomar gasket sealant.

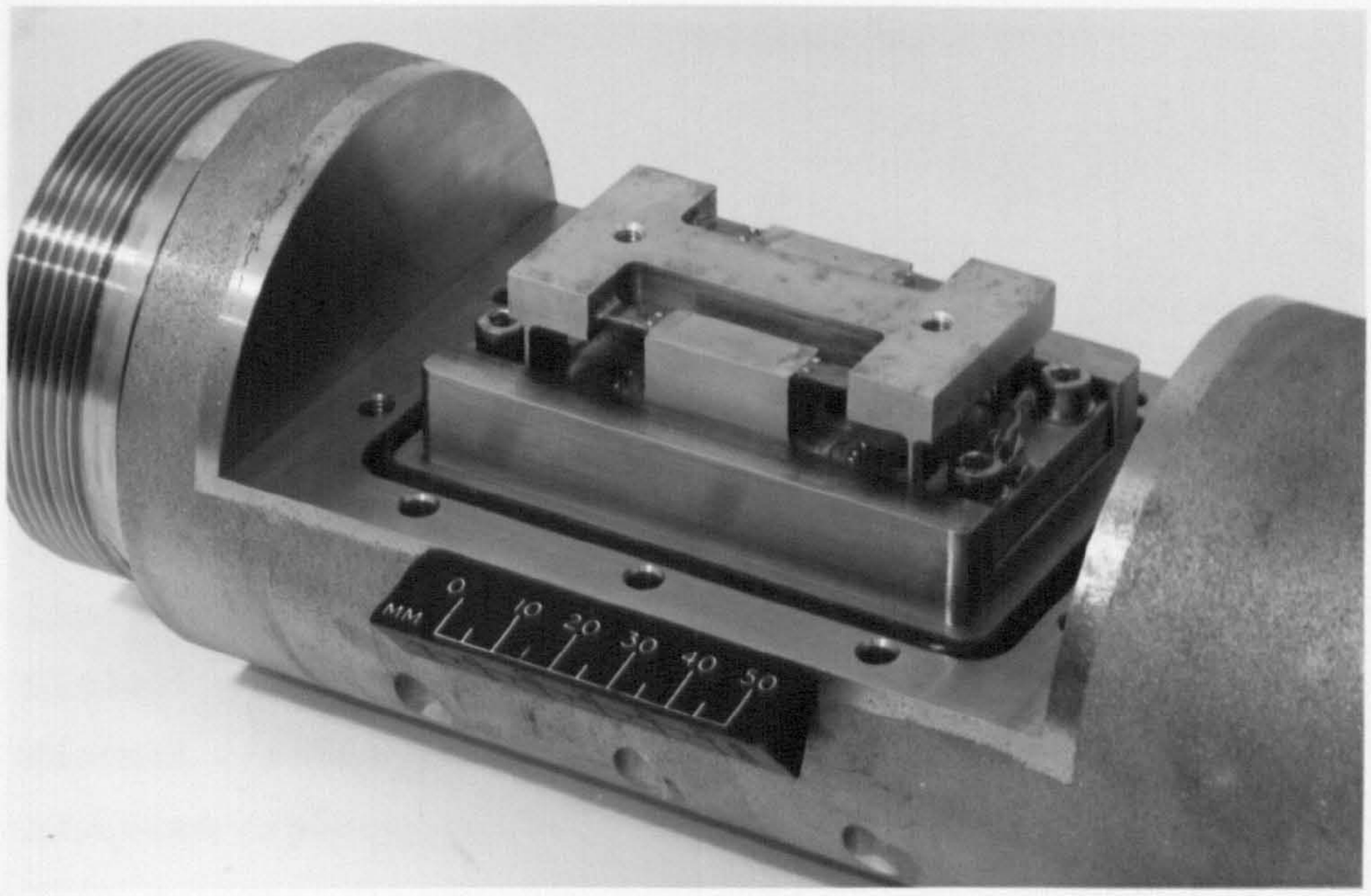



Plate 3(a) Surface stress transducer showing the "dogbone" load cell

[photo: A. Chipling]




Plate 3(b) Calibration rig for surface stress transducers

[photo: A. Chipling]

### 6.5.2 Design requirements

The main requirements for the design of the surface stress transducers were as follows.

- Load capacities: $\sigma_{rr} \geq 870$kPa; $\tau_{rz} \geq 200$kPa
- Linear relationship between signal and load
- Minimal cross-sensitivity between $\sigma_{rr}$ and $\tau_{rz}$
- Minimal compliance, especially to $\sigma_{rr}$
- Adequate capacity against buckling of the cell's webs
- Fast response to changes in load
- Completely reliable waterproofing system
- Ease of assembly and calibration
- Ease of repair/refurbishment in case of accidents
- Robust design, suitable for the demanding conditions likely to be met on site

### 6.5.3 Design and manufacture of the Mk IV SSTs

The surface stress transducers were designed in conjunction with Mr Clive Dalton of Cambridge Insitu Ltd.[11] The design drawings are included in Appendix 7 for reference. Certain features of the design are worth noting here:

- All of the main components were made from stainless steel, save for the earth pressure cells (made from aluminium alloy 2014A)
- The raised platform and the stiffeners on either side of it were designed to increase the housing's resistance to bending, which is a potential problem during the early stages of pile installation (until the SST enters the ground)
- The axis of the cable hole running through the main housing is not concentric with the axis of the pile - consequently, during pile assembly there is the danger that cables running through the hole will become twisted as each section of the pile is screwed into the next; this undesirable (but unavoidable)

feature of the design is mitigated by the use of turnbuckles between each instrumented section

- The surface of the raised platform is a "good quality surface free of machining marks"[12]; the absence of machining marks is important if the pressure cell is to bed down properly onto the platform

The window pane and the window frame were joined together in a hot-bonding process that injects pressurized rubber between their adjoining edges. The two components were held in the correct position relative to one another by an aluminium moulding jig.[13] The Cambridge earth pressure cells - given the name "Dogbone" after the shape of their top plate - were made on a CNC milling machine.

Each cell was wired-up with three independent strain-gauge circuits, two to sense the radial stress and the other to sense the shear stress.[14] A major advantage of the chosen wiring arrangement is that, should one of the compression circuits be lost, the value of $\sigma_{rr}$ can still be estimated from the readings of the other circuit.

### 6.5.4 Design calculations

The relationship between the applied stresses $\sigma_{rr}$ and $\tau_{rz}$ and the signals produced by the Wheatstone bridges is as follows:

$$\sigma_{rr} = c_{11}[\tfrac{1}{2}(V_o/V_i)_{c1} + \tfrac{1}{2}(V_o/V_i)_{c2}] + c_{12}(V_o/V_i)_s$$
$$\tau_{rz} = c_{21}[\tfrac{1}{2}(V_o/V_i)_{c1} + \tfrac{1}{2}(V_o/V_i)_{c2}] + c_{22}(V_o/V_i)_s$$

where $c_{ij}$ are calibration coefficients; $V_o$ and $V_i$ are the output and input voltages, respectively; and the subscripts c1, c2, and s denote the two radial compression circuits and one shear circuit, respectively.

The direct sensitivities $c_{11}$ and $c_{22}$ are typically 2.4$\mu$V/V per kPa radial stress and 15.5$\mu$V/V per kPa shear stress respectively. The cross-sensitivity of $\sigma_{rr}$ to $\tau_{rz}$ (i.e. $c_{12}/c_{22}$) is less than 0.04kPa/kPa; and of $\tau_{rz}$ to $\sigma_{rr}$ (i.e. $c_{21}/c_{11}$) less than 0.005kPa/kPa.

The coefficients $c_{12}$ and $c_{21}$ (representing the cross-sensitivity of one circuit to the other) are not amenable to calculation. However, $c_{11}$ and $c_{22}$ (the direct sensitivities of the circuits) may be estimated from the following formulae:

$$c_{11} = 2n_c w_c t_c E/kA_c$$

and

$$c_{22} = 2n_s w_s t_s E/kA_s$$

where n = the number of webs in the circuit; w = the width of the webs; t = their thickness; E = Young's modulus of the material; k = the strain gauge factor (≈2.1); and A = the "area factor". The area factor equals the plan area of the loading platen in the case of the radial stress webs ($A_c$ = WL) and the curved area in the case of the shear stress cells ($A_s$ = $2RL\sin^{-1}[W/2R]$). (W is the width of the window pane, L its length, and R the radius of the pile.)

The values of $c_{11}$ and $c_{22}$ given by these formulae are: $c_{11}$ = 2.43 ±0.13μV/V per kPa (cf. 2.41 ±0.15μV/V per kPa, as measured during the calibration of the surface stress transducers); and $c_{22}$ = 16.0 ±0.8μV/V per kPa (cf. 15.7 ±2.4μV/V per kPa).

### 6.5.5 Calibration and testing

The transducers were calibrated according to the procedure summarized in Table 6.1. A special calibration rig - as shown on Plate 3(b) - was required to apply shearing and compression forces simultaneously to the transducer's window pane.

### 6.5.6 Cell action effects (under-registration of loads)

An important aspect in the design of earth pressure cells is the assessment of cell action. In order to register a load, the cell's loading platen must deflect by a finite amount under the pressure exerted by the soil. This deflection in turn reduces the earth pressure, leading to an error in the measurement of the true load. In stiff soils the under-registration of pressure is potentially a serious problem: to overcome it the transducer itself must be made as stiff as possible

Table 6.1 Calibration procedure for surface stress transducers

| Step | Stage | Calibration | $\sigma_{rr}$ kPa | $\tau_{rz}$ kPa |
|---|---|---|---|---|
| 1 | Exercise | Sustained loads | 600 | +155 |
| 2 | | Sustained loads | 600 | -155 |
| 3-4 | | Rapid cycling | 600 | ±155 |
| 5 | | Rapid cycling | 0-600 | 0 |
| 6 | Shear calibration | Vary shear stress | 600 | ±155 |
| 7 | | whilst keeping | 480 | ±155 |
| 8 | | radial stress | 360 | ±155 |
| 9 | | constant | 240 | ±155 |
| 10 | Radial stress | Vary $\sigma_{rr}$ whilst | 0-600 | +60 |
| 11 | calibration | keeping $\tau_{rz}$ const | 0-600 | 0 |
| 12 | Eccentric loading | Apply $\sigma_{rr}$ at -e* | 0-600 | 0 |
| 13 | | Apply $\sigma_{rr}$ at +e | 0-600 | 0 |
| 14 | Creep testing | Sustained loads | 600 | -155 |
| 15 | Calibration under water pressure | Re-calibrate & check watertight | 0-700 | 0 |

*Eccentricity e = 16mm

(thereby reducing its sensitivity), and the loading platen as large as possible (in order to avoid arching).

Simple calculations can be used to assess the scale of such under-registration.

The cell's compliance, f, can be defined as the ratio of its deflection, $\delta$, to an applied constant stress, $\sigma$ (i.e. $f = \delta/\sigma$). Provided that a reasonable assessment of the soil's shear stiffness G can be made, the error $\epsilon$ in the reading can be estimated using the theory of elasticity.[15] Unfortunately, the soil's elastic behaviour is highly non-linear and values of G depend on the level of straining involved and the direction of the stress increment (i.e. loading or unloading).[16] A reasonable upper estimate of G for these calculations might be the value equivalent to 0.01% axial strain in a triaxial test. For the London clay at Canons Park this is ≈33MPa, a value not too dissimilar from that used by Maddocks[17] for the Gault clay.

The under-registration of loads has been assessed for these transducers,[18] and is less than -3.8% for $\sigma_{rr}$ and -8.3% for $\tau_{rz}$. There are strong grounds for believing that these figures are gross over-estimates of the under-registration whilst the pile is moving (i.e. during installation).[19]

### 6.5.7 Field performance of the surface stress transducers

The surface stress transducers (SSTs) have performed extremely well in all the Test Series to date. The readings obtained have shown excellent repeatability, with close agreement being found between the data from the two $\sigma_{rr}$ circuits in each cell, and between the measurements of $\tau_{rz}$ and values of skin friction deduced from the axial loads along the pile.

A potential design weakness of the SST is that, owing to its asymmetrical shape, the instrument's main housing tends to bend under axial load. The result is an error in the measured value of $\sigma_{rr}$. Fortunately, the lateral support given to the pile by the ground helps to reduce bending, and as the instrument penetrates further and further into the ground, the error in $\sigma_{rr}$ would be expected to reduce. At Canons Park the error in $\sigma_{rr}$ was negligible (because the London clay is so stiff). However, this was not the case in the loose/medium-dense sand at Labenne (see Section 6.3.3 above), and hence in general the readings of $\sigma_{rr}$ should be corrected for this effect (by running laboratory calibrations to determine the cross-sensitivity to axial load).

## 6.6 GENERAL REQUIREMENTS FOR MEASURING PORE PRESSURES

The requirements of a 'perfect' pore pressure measuring system - one that is both fast-acting and stable over long periods - are in many ways contradictory. For the experiments at Canons Park the system needed to provide:

- Instantaneous response to pore pressure changes during pile penetration
- Immediate recovery from cavitation should negative pore pressures occur in the strongly dilating London clay
- Minimal system compliance, to prevent interference with the pressure being measured
- Accurate and stable long-term performance

The first three requirements demand an extremely stiff pore pressure measuring system, i.e. one with a very small internal volume and low transducer compliance. Unfortunately, such a system is highly susceptible to over-reading in the long-term, once gases diffuse (or otherwise enter) into the cavity.[20] On the other hand, a large volume system - although unable to satisfy the first three requirements in the list above - is less susceptible to the effects of gassing-up and can also be designed to allow for periodic de-airing.

The contradictory requirements of a perfect pore pressure system proved impossible to meet using a single design of probe. The fast-acting instruments described in Section 6.7 were used in all the instrumented pile tests at Canons Park, but they gave unreliable readings in the long-term. To determine the trend of the long-term values of pore pressure, a system that could be flushed with de-aerated water was designed for use <u>in parallel</u> with the fast-acting probes. Further details of this alternative design are given in Section 6.8.

## 6.7 DESIGN OF FAST-ACTING PORE PRESSURE PROBES

### 6.7.1 General description

The Instrumented Pile carries a total of three pore pressure units (PPUs), one per instrument cluster. Each PPU has two portholes oriented at 180° to each other, into which the probes are inserted. Two types of probe exist: a fast-acting probe (as described in this section) and a flushable probe (as described in Section 6.8).

Figure 6.8 and Plate 4(a) show one of the fast-acting probes in exploded view. There are three main components:

- The mounting block (made from acetal copolymer), which carries a sintered stainless steel porous filter in its front face
- A Druck PDCR 81, sub-miniature, semi-conductor pressure transducer, which is glued into a titanium holder
- A thrust ring (acetal copolymer), which clamps the titanium holder into the back of the mounting block

The mounting block and the thrust ring are made from acetal copolymer in order to avoid two-metal corrosion between the various dissimilar metals in the pile.[21] For the same reason, the holder for the transducer is made from titanium to match the casing of the Druck PDCR 81.

### 6.7.2 Design requirements

The general requirements of an ideal pore pressure measuring system have been discussed already (in Section 6.6). The specific demands made on the design of the fast-acting probes were as follows:

- Response time $t_{95} \leq 1s$ (in the laboratory)
- Smallest possible compliance/volume factor
- Immediate recovery from cavitation
- Ease of assembly and saturation in the laboratory
- Ease of insertion into the Pile

- No loss of saturation during transfer from the laboratory to the ground
- Robust design, suitable for use on site
- Ease of repair/refurbishment in case of accidental damage to any of the components
- Porous filter to be changeable

### 6.7.3 Design and manufacture of the Mark III PPPs

The following paragraphs highlight important or unusual features of the fast-acting pore pressure probes: further technical details are given in Appendix 8.

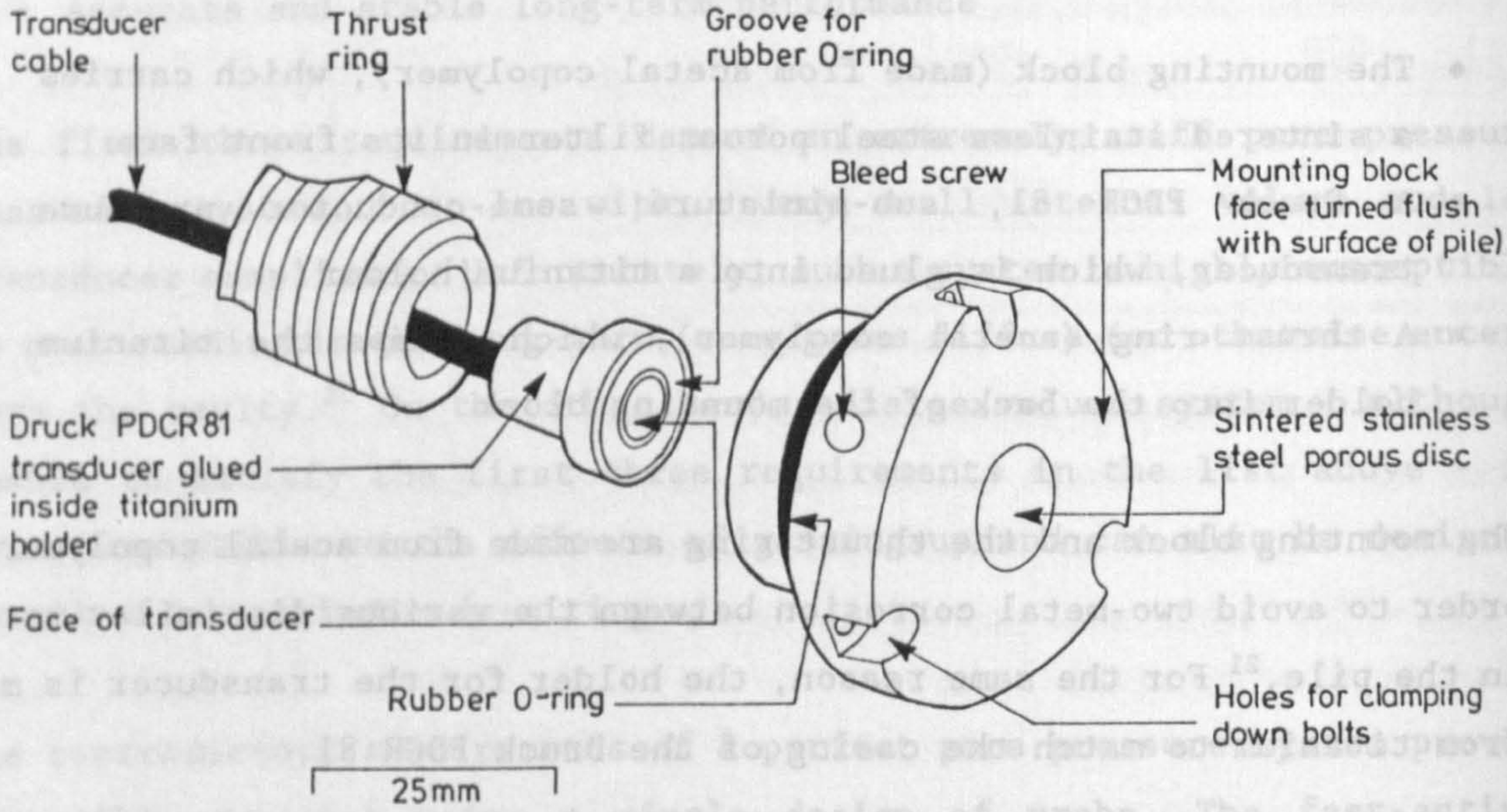



Figure 6.8 Fast-acting pore pressure probe

At the heart of the pore pressure probe is a Druck PDCR 81 pressure transducer, a device that has found wide application in soil mechanics research.[22] It is a very sensitive instrument, giving a full-scale output of ≈15mV/V. However, the feature that makes it particularly suitable for the Instrumented Pile is its small size.

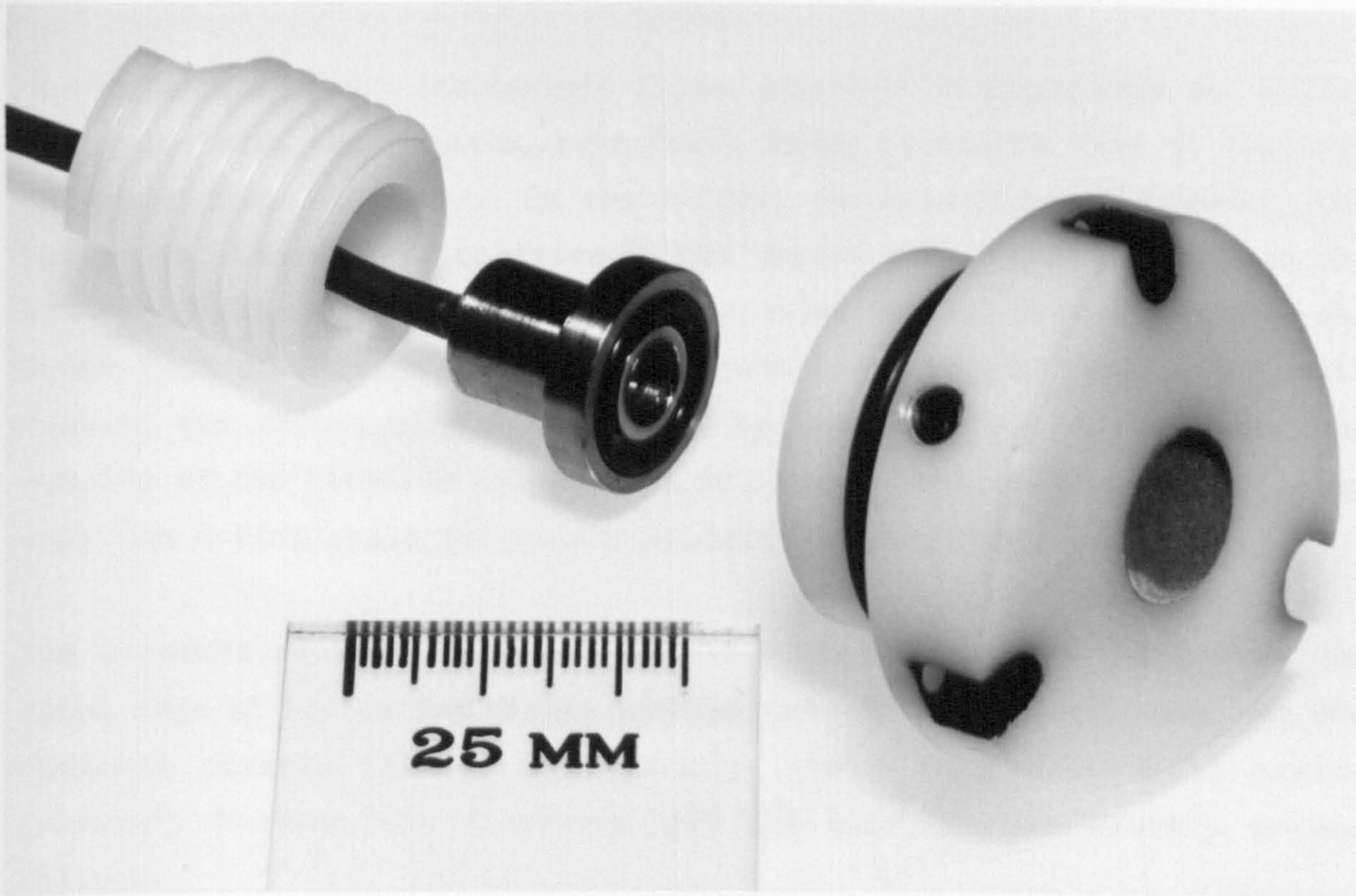



Plate 4(a) Fast-acting pore pressure probe [photo: A. Chipling]

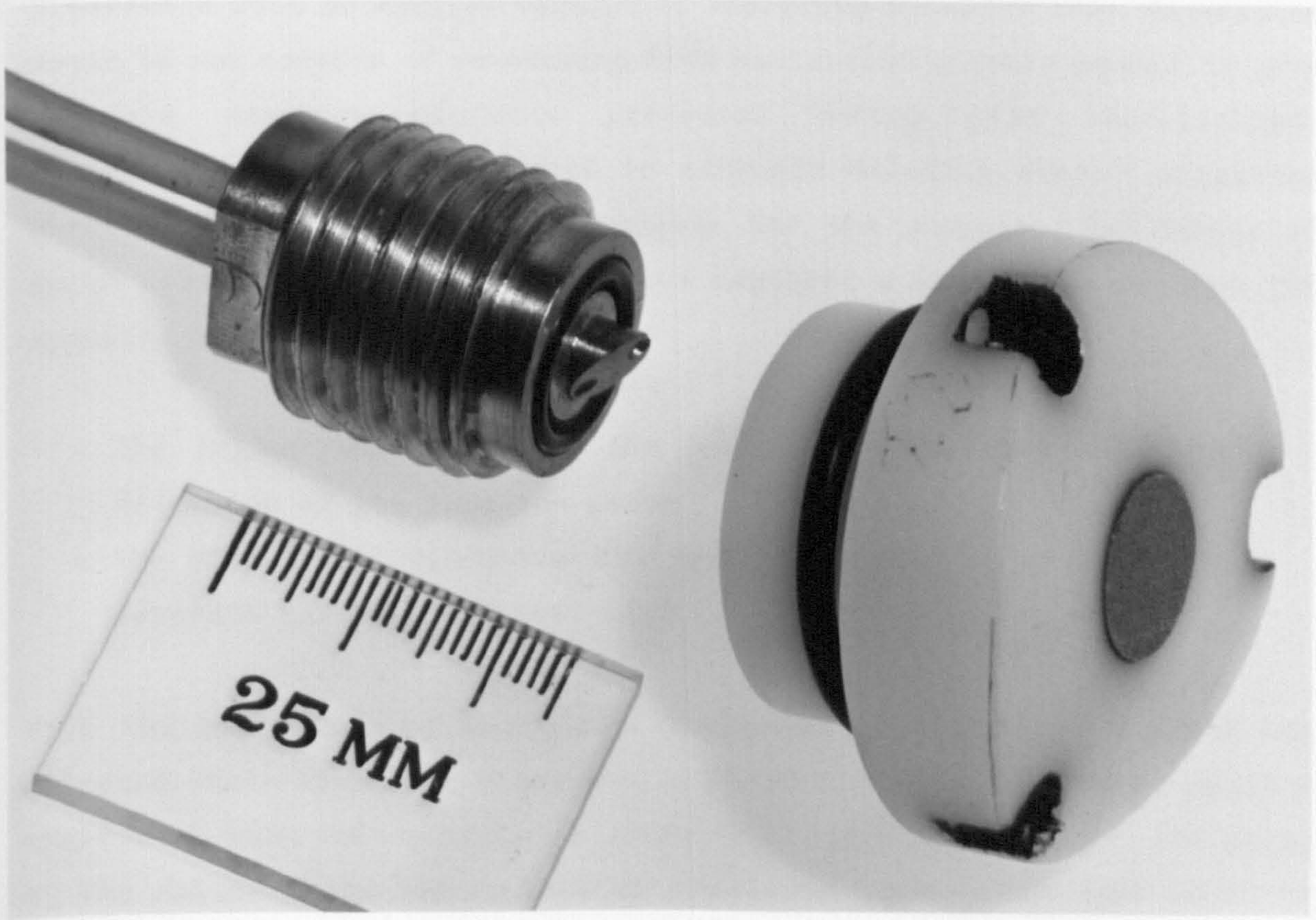



Plate 4(b) Flushable pore pressure probe [photo: A. Chipling]

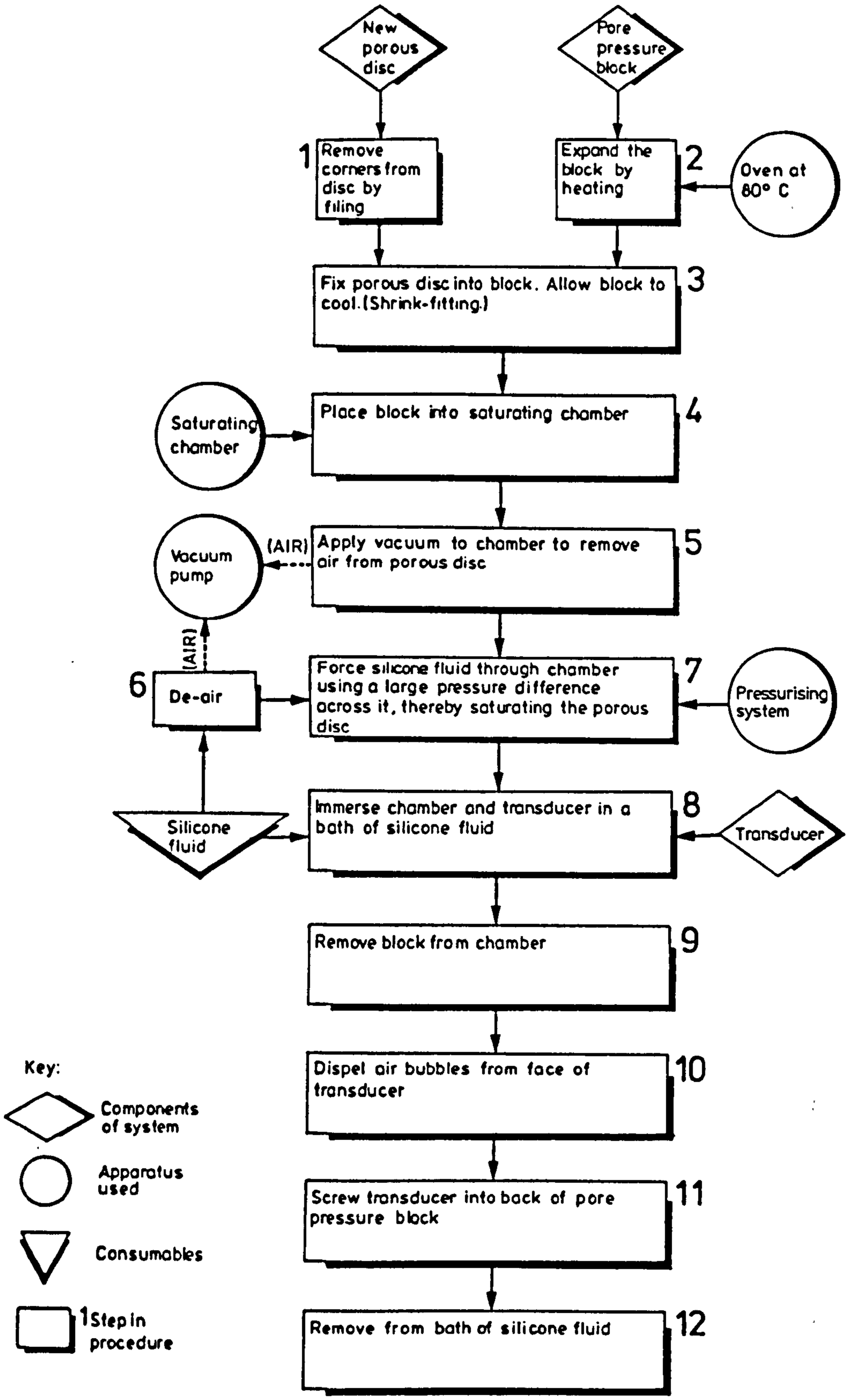



Figure 6.9 Procedure for saturating pore pressure system with silicone fluid

highly effective. Each pore pressure probe is assembled and saturated following the sequence of activities shown in the flow-chart of Figure 6.9, using the equipment illustrated in Figure 6.10.[25]

### 6.7.5 Calibration and testing

All of the pore pressure probes were calibrated in the laboratory, prior to the start of each experiment. They were tested to a gauge pressure of ≈1000kPa using a Budenberg dead-weight tester. The probes give a highly linear response to loading: the combined non-linearity and hysteresis is typically 0.2% of the full-scale output.

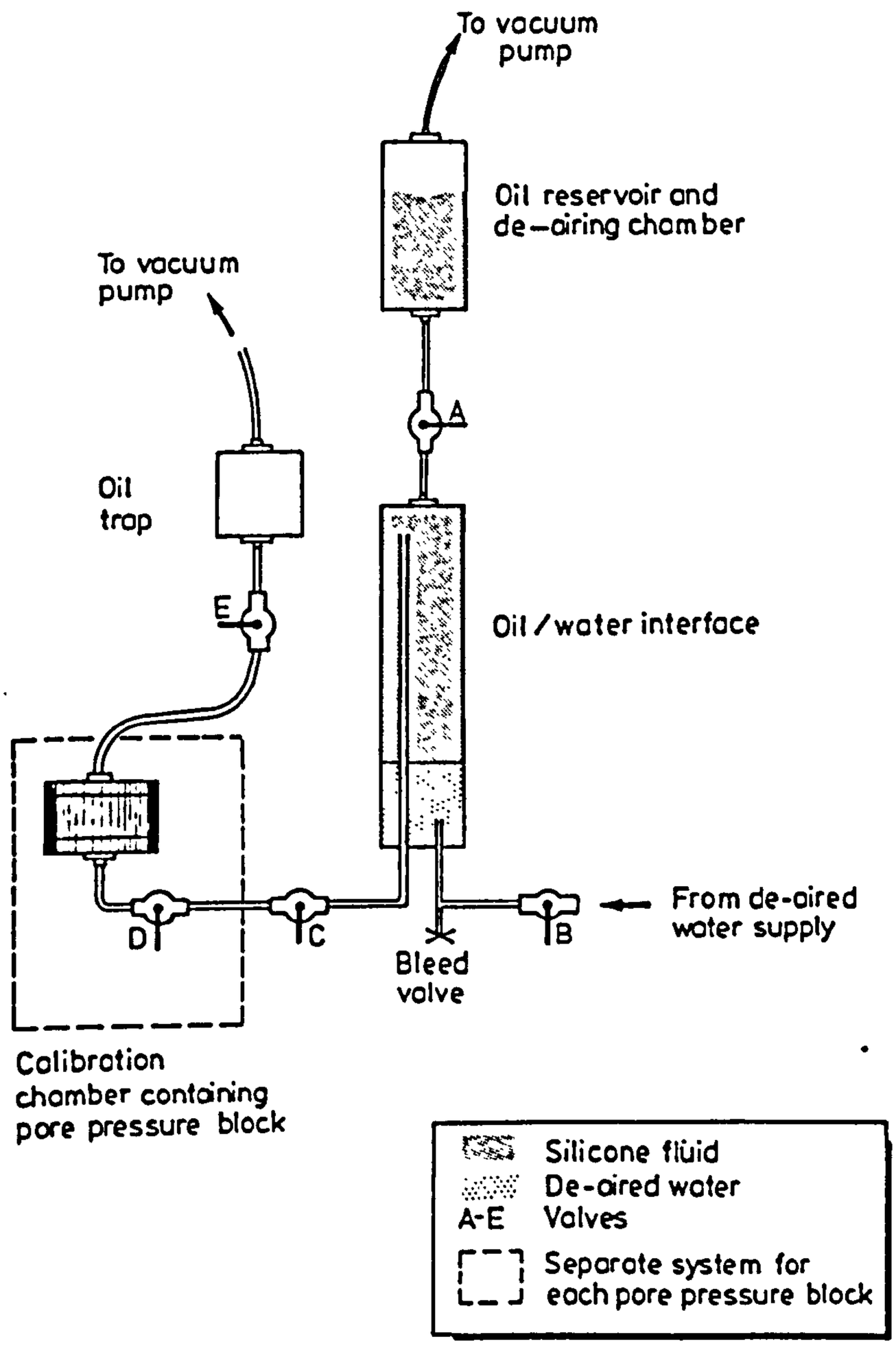



Figure 6.10 Equipment used to saturate the fast acting pore pressure probes

The probes used for Test Series CP2 were also calibrated at pressures below atmospheric, using a mercury manometer. The coefficients obtained agreed to within 0.5% with those obtained at pressures above atmospheric, and I considered it unnecessary to perform any other low pressure calibrations prior to the other experiments.

The probes' response times (in water) were measured in the laboratory prior to Test Series CP2, using an oscilloscope set to resolve to 10ms. Ninety-nine per cent response to a sudden step loading of ±800kPa was obtained within 10-400ms depending on the quality of the saturation procedure - such times are well within the design requirement.

### 6.7.6 Field performance of the fast-acting probes

The probes' field performance during pile installation is best discussed by examining certain aspects of the recorded test data: Figure 6.11 shows a typical pair of traces, as recorded in Test Series CP2f. Note the excellent agreement between the readings from the two probes, which are

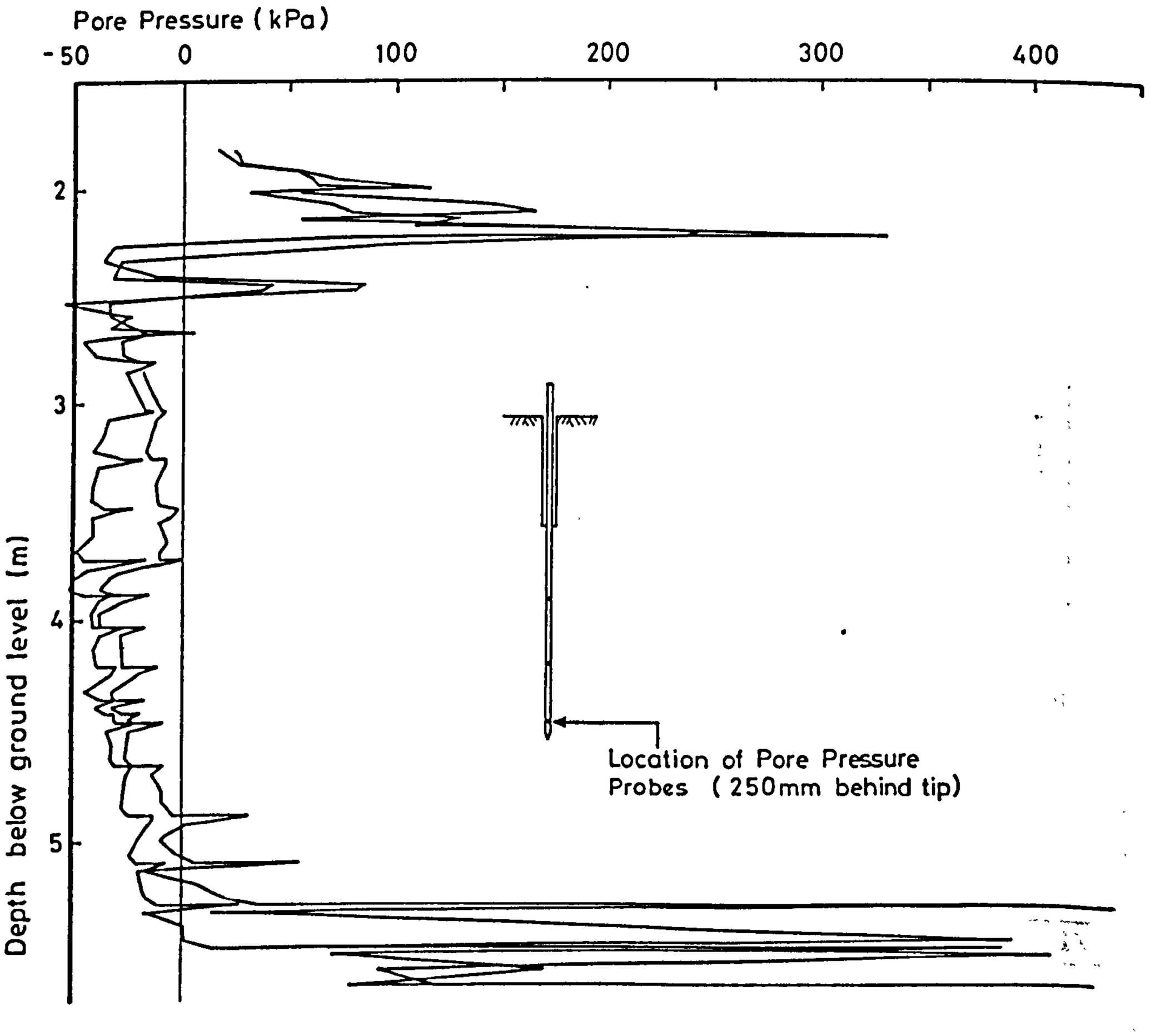



Figure 6.11 Typical pore pressures traces during pile installation (CP2)

from the same level on the pile, but from diametrically opposite locations. The pile enters the ground in a number of discrete pushes, and the signals drop sharply towards -100kPa (gauge) at the start of each push, but move towards (higher) equilibrium values as soon as penetration ceases. The signals from the probes have clearly remained "alive", despite cavitation of the silicone fluid in the probe (or perhaps of the pore water in the soil). The probes used in Test Series CP1 (which were saturated with water) did not give these spiky signals, and failed to respond for some time (typically 10 minutes) after penetration had ceased. The fast-acting probes have been used during installation in Test Series CP2-CP5, and the data has shown excellent repeatability.

Unfortunately, a problem has been encountered with this system during the medium- and long-term experiments (CP2 and CP4). After five days have elapsed, the probes start to be affected by the accumulation of gas within their (extremely small) internal volume. The readings are no longer reliable in absolute terms, although some useful information can still be deduced from changes in signal during pile loading. Other researchers[26] have encountered similar problems, caused by the generation of gases through galvanic action between dissimilar metals. The fast-acting probes were designed specifically to avoid galvanic reaction within the piezo system (hence the use of acetal copolymer), although gases may still build up on other parts of the pile's surface and then diffuse into the piezometer. Further details about this problem are given in Appendix 9.

## 6.8 DESIGN OF THE FLUSHABLE PORE PRESSURE SYSTEM

### 6.8.1 General description

The Instrumented Pile that was used in Test Series CP4 was fitted with three fast-acting and three flushable pore pressure probes (one at each instrument level). The general arrangement of the flushable systems is shown in Figure 6.13.

Each of the flushable probes was linked hydraulically, via two small-bore plastic tubes, to a special housing located half-way along the pile. Three semi-conductor pressure transducers were mounted inside this "half-way housing", where they registered the pressure in one of small-bore tubes (the "down" line). The other tube (the "return" line) passed straight through the housing (see Figure 6.13). Both lines extended up to ground level, where they were sealed by two high quality valves.

### 6.8.2 Design details - pore pressure probes (Mark IV)

Figure 6.12 and Plate 4(b) (on page 249) show one of the flushable pore pressure probes in exploded view. Each probe comprises two main components:

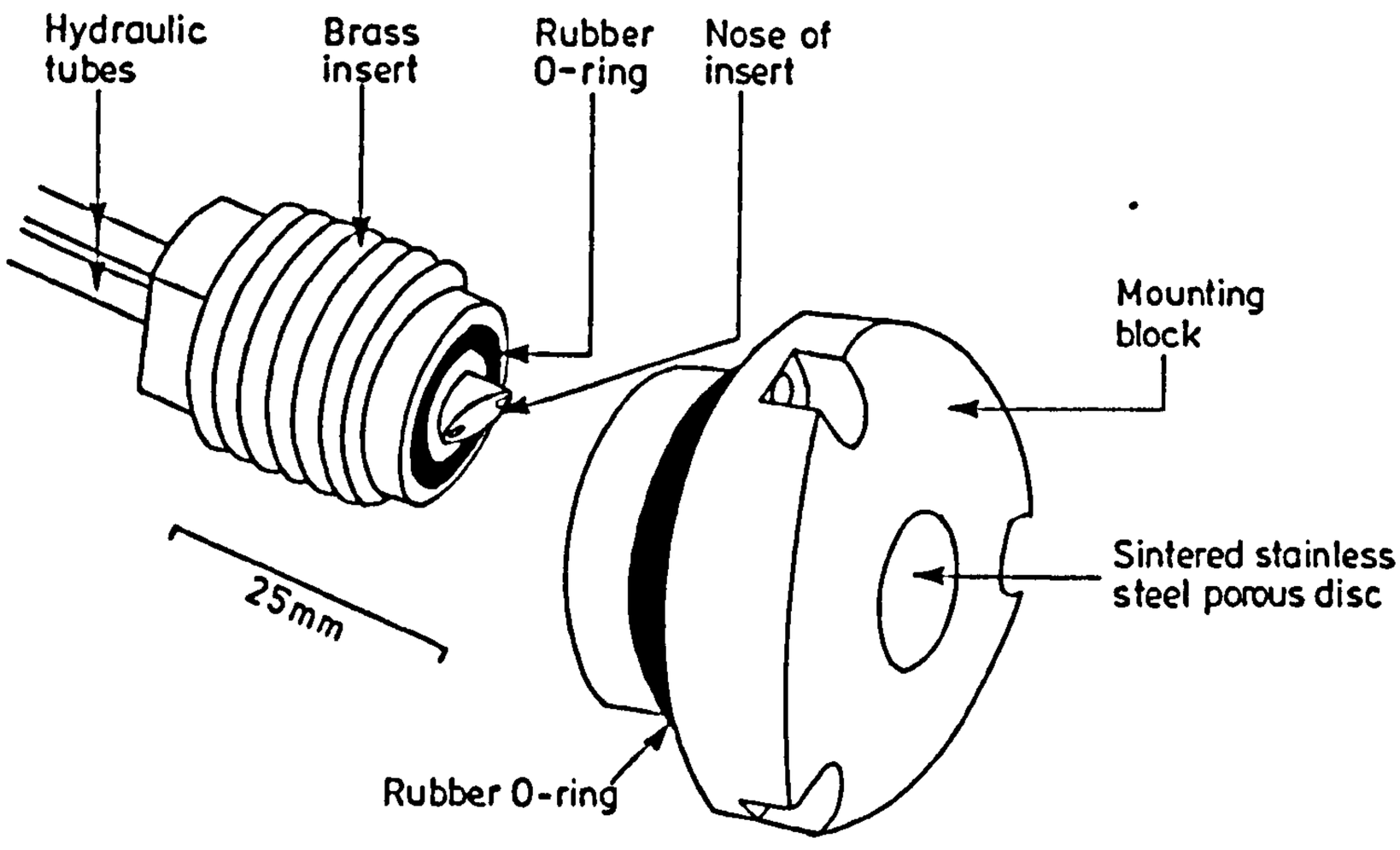



**Figure 6.12 Flushable pore pressure probe**

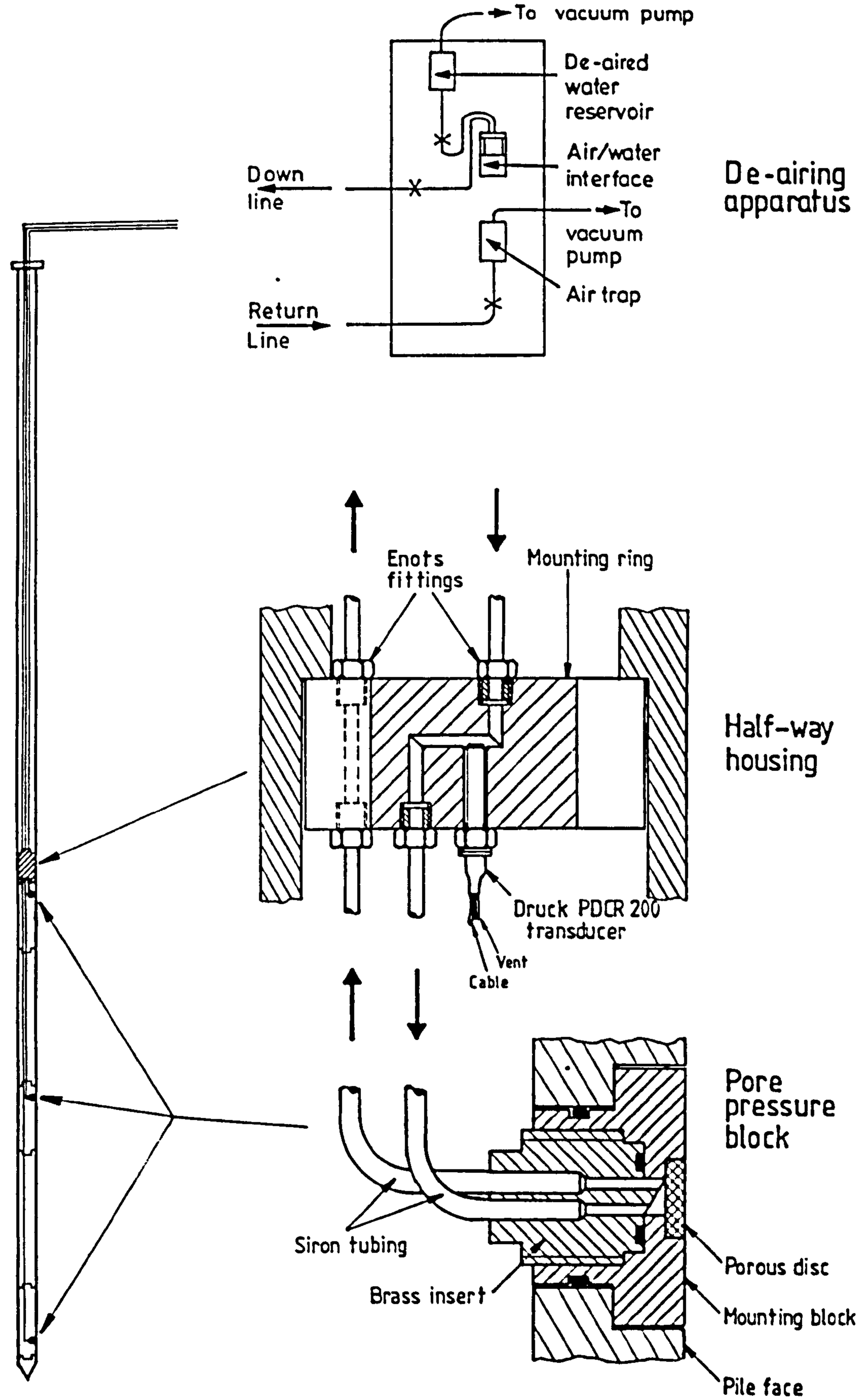



Figure 6.13 General arrangement of flushable pore pressure system

- A mounting block (made from acetal copolymer), with a sintered stainless steel porous filter in its front face (identical to the block used in the fast-acting probe)
- A brass insert, in which are glued the two small-bore tubes

(To distinguish them from the fast-acting versions, the flushable probes have had the letter "F" appended to their channel numbers - e.g. P52F, P54F, and P56F as opposed to P51, P53, and P55.)

### 6.8.3 Design details - half-way housing

The half-way housing is shown on Plate 5 and consists of two brass rings (the lower one is used as a stand). The hydraulic lines connect into the upper ring, which in turn holds three Druck PDCR 200 pressure transducers (identifiable by their white cables). Each transducer is aligned with its pressure-sensing diaphragm pointing upwards (see Figure 6.13), so that if any gas bubbles enter the hydraulic lines they will not collect in the space in front of the diaphragm.

The Druck PDCR 200 pressure transducers are very similar to the PDCR 81s employed in the fast-acting probes: they are extremely small ($\phi$5mm x 19mm long) semi-conductor devices, with a full-scale output of $\approx$15$\mu$V/V.

The hydraulic lines are made from Saren tubing (a form of nylon), with an internal diameter of approximately 1.6mm and a wall thickness of $\approx$0.8mm. In Test CP4 each hydraulic line was closed at ground level by a Hoke valve.

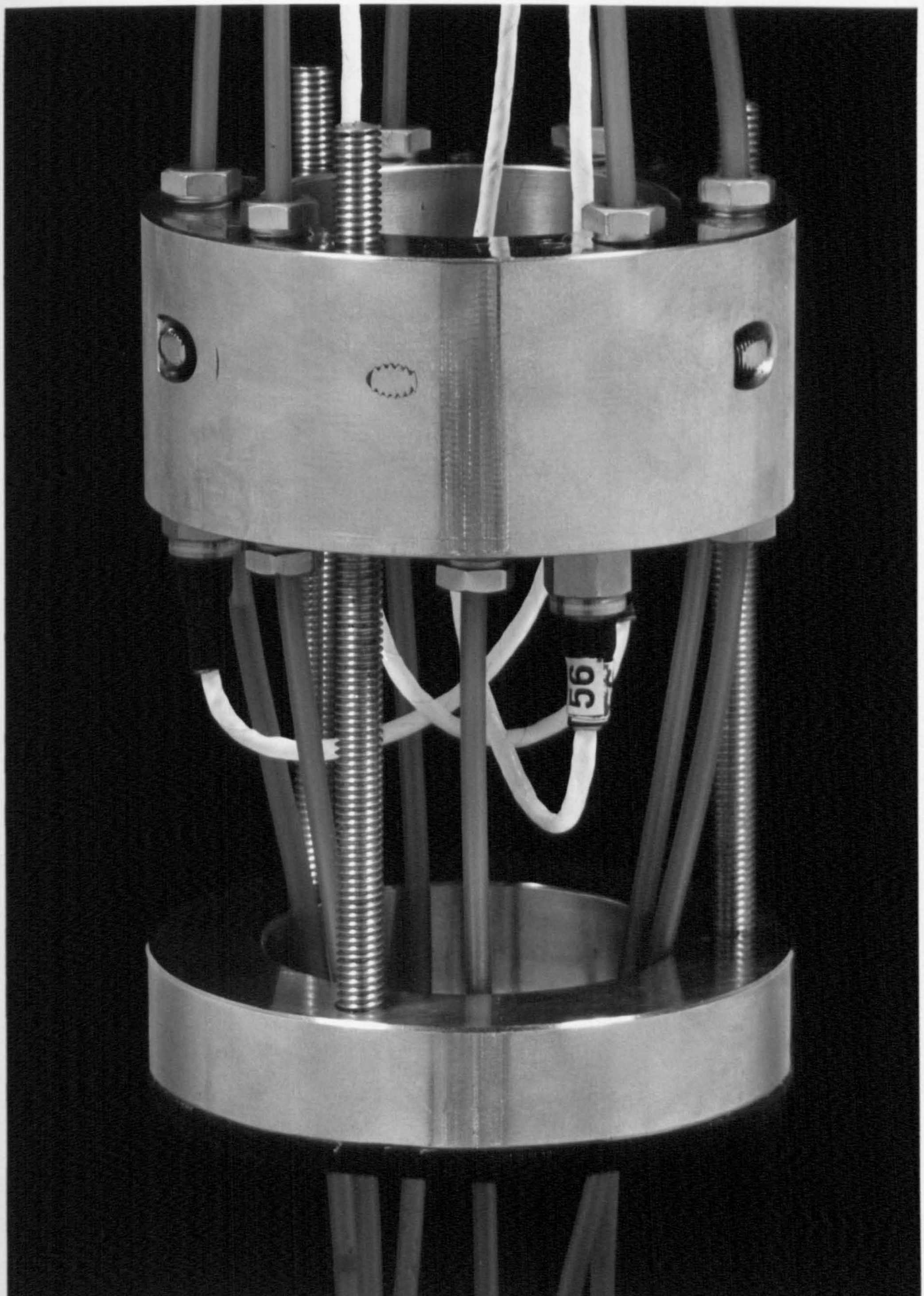


Plate 5 Half-way housing, showing pressure transducers and hydraulic lines [photo: A. Chipling]

### 6.8.4 Calibration and testing

The flushable probes were calibrated in the laboratory up to a gauge pressure of ≈700kPa, using a Budenberg dead-weight tester (as for the fast-acting probes). The internal volume of the hydraulic circuits ranged from 18.5cm$^3$ for the shortest to 28.8cm$^3$ for the longest (98% of which was contributed by the two small-bore tubes in each circuit). The compressibility of the flushable systems was also measured, and was typically of the order of 1mm$^3$/kPa - i.e. many times greater than that of the fast-acting pore pressure probes (for which the compressibility has been estimated[27] as 0.000 29mm$^3$/kPa).

### 6.8.5 Saturation procedure

The pore pressure probes were flushed with de-aerated water (using the de-airing apparatus shown in Figure 6.13) at periodic intervals during Test Series CP4. A special procedure was adopted for de-airing the probes, as described below.

The down line was attached to a "re-charge" cylinder (the air/water interface shown on Figure 6.13) which contained de-aerated water. The return line was connected to a vacuum pump, via a measuring cylinder (which also served as an air trap) containing water. Care was taken to expel all traces of air from the adjoining tubes and valves. The re-charge cylinder was vented to atmospheric pressure.

The vacuum pump was turned on and the valve at the top of the return line was opened, thereby imposing a gauge pressure of about -100kPa to the water inside the piezometer system. Bubbles would start to appear in the water inside the measuring cylinder at this stage. After 30s the valve connected to the down line was opened, and de-aerated water was driven around the hydraulic lines (by the pressure difference between the down line valve and the return line valve) - causing numerous bubbles to appear in the measuring cylinder.

Once ≈120cm$^3$ of de-aerated water had been pumped around the system (typically after < 4 minutes), the return line valve was closed. At this point the head of water in the hydraulic lines would equal the head of water in the re-charge cylinder. Thirty seconds later the down line valve was closed, thereby sealing the hydraulic circuit.

Since the water in the re-charge cylinder was higher than that in the soil adjacent to the pile, on closing the down line valve the pressure recorded by the transducer started to fall towards a value in equilibrium with the pressure in the soil.

### 6.8.6 Field performance of the flushable pore pressure system

No attempt was made to measure pore pressures during pile installation using the flushable systems, since their response times in the London clay were estimated to be of the order of 2½ hours.

During the equalization period, the signals from the pressure transducers fluctuated daily by up to ±30kPa, with the minimum pressure occurring at midday. The period of oscillation was 24h exactly, suggesting that the hydraulic lines were reacting to diurnal changes in the ambient air temperature. Most plastics expand and contract more than water, hence a rise in temperature would reduce the pressure in the hydraulic lines. A simple calculation[28] shows that the magnitude of the fluctuations should be of the order of -3kPa/°C: hence the observed variations in signal are easily explained by assuming changes in ambient temperature of ±10°C. (Pile CP4 was in the ground from the end of March to the beginning of May 1988 - hence such temperature changes are highly plausible.)

Despite such high temperature sensitivity, the flushable pore pressure systems did allow a reasonably good estimate to be made of the pore pressure trends in the medium and long terms, and hence they more than served their purpose. In addition, the flushable probes provided the opportunity to conduct falling-head permeability tests and hydraulic fracture tests on the clay surrounding the pile. In this way, valuable information was obtained to supplement the data gathered with the fast-acting probes.

## 6.9 NOTES AND REFERENCES

[1]Jardine R.J. (1985). Investigations of pile-soil behaviour, with special reference to the foundations of offshore structures. PhD Thesis, Univ. of London (Imperial College), 2 vol., 789pp.

[2]Johnston I.W. (1972). Electro-osmosis and porewater pressures; their effect on the stresses acting on driven piles. PhD Thesis, Southampton Univ.

[3]A shortened version of this section appears in Bond A.J. and Jardine R.J. (1989). Instruments for measuring the effective stresses acting on a pile jacked into overconsolidated clay. Proc. Conf. on Geotech. Instrumentation in Civ. Engng Projects, Nottingham, April 1989 (in press).

[4]Bostik 1753 sealing compound is a solvent-borne nitrile rubber, designed specifically for the sealing of pressurized aircraft cabins.

[5]Four 120Ω gauges oriented in the longitudinal direction to sense the axial strain; and four in the circumferential direction to sense the hoop strain.

[6]Pioneer Western Nu-Lip rectangular section O-ring, no 4-045

[7]See Chajes A. (1985). Stability and collapse analysis of axially compressed cylindrical shells. Chapter 1 (pp1-17) of "Shell Structures. Stability and Strength", ed. R. Narayanan. Elsevier Applied Science Publishers, London, 345pp. Design against buckling of cylindrical shells is not as simple as might first be expected, and a number of semi-empirical rules have been developed to try to quantify the process. The essential point to note is that 'short' shells yield before they buckle, whereas moderately long shells (such as the Mk I and Mk II load cells on the original pile) might buckle before they yield.

[8]For these axial load cells, R = 34mm; h =2.25mm; E = 210GPa; $\mu$ = 0.29; and k = 2.1.

[9]Arthur and Roscoe (1961), loc. cit., reported the development of the first Cambridge-type earth pressure cell.

[10]Stroud M.A. (1971). The behaviour of sand at low stress levels in the simple shear apparatus. PhD Thesis, Univ. of Cambridge.

[11]The surface stress transducers were made by L & C Precision Engineering Ltd, of Baldock, Cambridgeshire, under sub-contract to Cambridge Insitu Ltd.

[12]See design drawing AJB/PSST/1, in Appendix 7.

[13]See drawings AJB/PSST/5 and 6, in Appendix 7.

[14]An alternative wiring arrangement exists that gives only one independent measure of $\sigma_{rr}$, but provides a direct reading of e, the eccentricity of load. Further information on this point, and some helpful advice on the design of Cambridge earth pressure cells, is given by: Bransby P.L. (1972). Cambridge contact stress transducers. Lecture notes for the course "Research techniques and equipment in soil mechanics", Cambridge, March 1972. Cambridge Univ. Engng Dept Report CUED/C-SOILS/LN2.

[15]Poulos H.G. and Davis E.H. (1974). Elastic solutions for soil and rock mechanics. John Wiley & Sons Inc., New York, 411pp.

[16]Jardine R.J., Fourie A., Maswoswe J., and Burland J.B. (1985). Field and laboratory measurements of soil stiffness. Proc. 11th Int. Conf. Soil Mech. & Fdn Engng, San Francisco, 2, pp511-514.

[17]Maddocks D.V. (1983a). A transducer to measure the radial effective soil stress and the pore water pressure acting on the surface of a driven, steel pile. Cambridge Univ. Engng Dept Report CUED/D-SOILS/TR131, 18pp+. Maddocks used G = 30MPa for the Gault clay.

[18]See Appendix 5 and Bond and Jardine (1989), loc. cit., Table 2.

[19]During installation the soil next to the pile is subject to enormous radial and shear strains, and hence its equivalent elastic "stiffness" is almost certainly extremely small. The calculations for the under-registration of stress assume very high stiffnesses (at 0.01% strain), and hence these calculations over-estimate the value of $\epsilon$ during installation by a large amount. Of course, this argument does <u>not</u> hold during equalization or load testing, when the strains imposed on the soil are very much smaller than during installation.

[20]See Hight D.W. (1983). Laboratory investigations of sea bed clays. PhD Thesis, Univ. of London (Imperial College).

[21]DiBiaggio E. (1977). Field instrumentation - a geotechnical tool. Proc. 1st Baltic Conf. on Soil Mech. & Found. Engng, Gdansk, 1, pp29-40.

[22]The Druck PDCR 81 was developed for use in centrifuge tests (see Hird C.C., Marsland A., and Schofield A.N. (1978). The development of centrifugal models to study the influence of uplift pressures on the stability of a flood bank. Géotechnique, 28(1), pp85-106), but it has also been employed in triaxial tests, particularly at Imperial College (see Hight D.W. (1982). A simple piezometer probe for the routine measurement of pore pressures in triaxial tests on saturated soils. Géotechnique, 32(4), pp396-401).

[23]See Lunne T., Powell J.J.M., Quarterman R.S.T., and Eidsmoen T.E. (1986). Piezocone testing in overconsolidated clays. Proc. 39th Can. Geotech. Conf. on 'Insitu Testing and Field Behaviour', Carlton Univ., Ottawa, Canada, pp209-218.

[24]Personal communication with Mr Roy Wakeling of Delft Geotechnics.

[25]This apparatus works as follows:

i) With valves E and D open, but C closed, a vacuum is applied to the calibration/saturation chamber for a minimum period of 2h.
ii) With valve A closed and B open, the silicone oil in the oil/water interface is pressurised to ≈200kPa by the de-aerated water supply.
iii) Valve C is then opened, allowing the silicone oil to enter the saturation chamber.
iv) Valve E is closed once silicone fluid is visible in the oil trap. Valves B, C, and D are then closed.
v) The oil in the oil/water interface is replenished by opening valve A and the bleed valve at the same time. The oil in the top reservoir has previously been de-aerated under a vacuum.

[26]DiBiaggio (1977), loc. cit.

[27]See Appendix 5 and Table 3 of Bond and Jardine (1989), loc. cit.

[28]The change in pressure $\Delta p$ caused by a change in temperature $\Delta T$ is given by the equation $\Delta p/\Delta T = K_w(\Gamma_w - 3\alpha_p)$, where $K_w$ is the bulk modulus of the water (with 0.33% air in it, $K_w \approx 0.03$GPa, ignoring the solubility of air), $\Gamma_w$ is the coefficient of volume expansivity for water ($\approx 2.1 \times 10^{-4}$ per °C), and $\alpha_p$ is the coefficient of linear expansivity for the plastic tubing ($\approx 10^{-4}$ per °C for nylon). The value of $K_w$ comes from: Fredlund D.G. (1976). Density and compressibility characteristics of air-water mixtures. Can. Geotech. J., 13(4), pp386-396. The values of $\Gamma_w$ and $\alpha_p$ come from: Tennent R.M. (1971). (Editor.) Science data book. Oliver & Boyd, Edinburgh, 104pp.

# Chapter 7

## Programme of tests at Canons Park

# CONTENTS OF CHAPTER 7


7.1 INTRODUCTION . . . . . 270
7.1.1 The Canons Park Project 270
7.1.2 Outline of Chapters 7 and 8 270
7.2 SCOPE OF THE RESEARCH PROGRAMME . . . . . 272
7.2.1 Programme-of-Works 272
7.2.2 Instrument development 272
7.2.3 Field work at Canons Park 274
7.3 STRATEGY ADOPTED FOR THE PILE TESTS . . . . . 275
7.3.1 Main parameters of interest 275
7.3.2 Pile installation 275
7.3.3 Equalization times 278
7.3.4 Loading direction: first-time loading 278
7.4 NOMENCLATURE . . . . . 279
7.4.1 Main numbering system 279
7.4.2 Individual stages of a Test Series 280
7.4.3 Parameters measured by the Instrumented Pile 280
7.4.4 Leading, following, and trailing instrument positions 281
7.4.5 "Fast" and "slow" jacking rates 281
7.4.6 Short, medium, and long equalization periods 281
7.5 NOTES AND REFERENCES . . . . . 282

# 7.1 INTRODUCTION

## 7.1.1 The Canons Park Project

The Canons Park Project was established in 1985 as a follow-up to the work of Jardine,[1] who had installed and tested a fully instrumented pile at the site in 1984. The programme of research involved installation and testing of a further seven piles and excavation of an inspection trench. The full Programme-of-Works is shown in Figure 7.1.

Most displacement piles are driven into the ground, and ideally *all* the test piles would have been installed in this way. Fear of damaging the transducers during pile driving led to the *instrumented* piles being jacked instead. The question of whether a jacked pile behaves like a driven one was addressed as a separate exercise.

It was recognized at the outset that the value of the pile test data would be enhanced considerably if experiments were performed on carefully taken samples of clay from around the piles. Greatest priority was given to studying the soil's fabric in the immediate vicinity of the pile shaft, since this might provide valuable information about the shearing mechanisms controlling pile behaviour. A 4.5m inspection trench was excavated around two of the piles and over 150 samples of various kinds were taken for subsequent laboratory testing. As shown in Chapter 13, this part of the project gave extremely valuable information which helped immensely in interpreting the pile test results.

## 7.1.2 Outline of Chapters 7 and 8

The purpose of this chapter is to describe the overall scope of the research project (Section 7.2); explain the strategy adopted for the series of pile tests (Section 7.3); and to define the system of notation used to identify the tests (Section 7.4). The following chapter (Chapter 8) describes the equipment used to install and test the piles; and explains the experimental procedures that were followed.

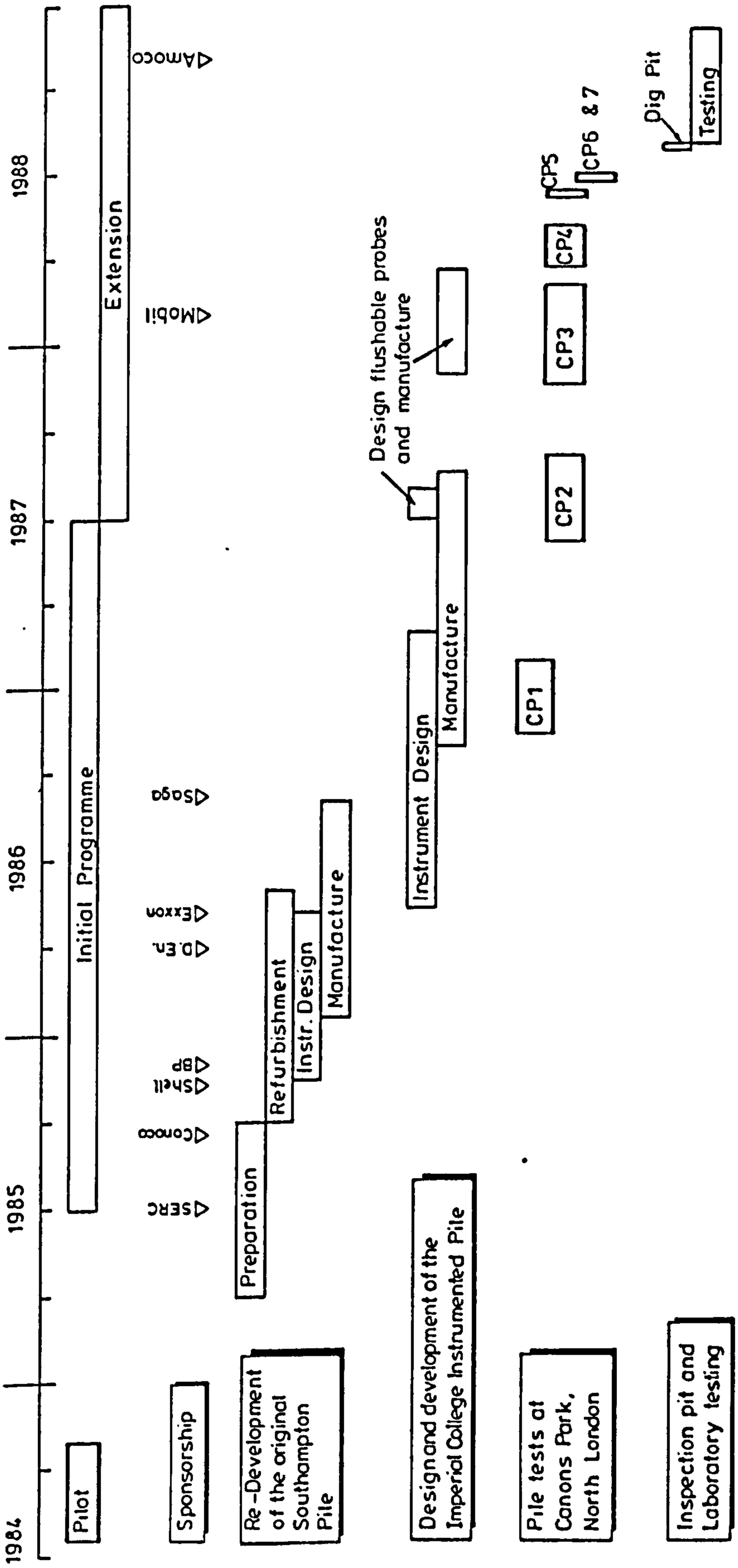



Figure 7.1 Programme-of-Works for the Canons Park Project

## 7.2 SCOPE OF THE RESEARCH PROGRAMME

### 7.2.1 Programme-of-Works

A major part of the project involved the design and development of the instrumented piles that were used in five of the seven field experiments (CP1-5). These piles were jacked into the ground to avoid damaging the transducers. The programme of tests at Canons Park also included two experiments (CP6-7) on uninstrumented driven piles, in order to assess how the method of installation affects the piles' subsequent load-displacement behaviour.

Figure 7.2 illustrates the piles' depths of penetration and the positions of the instruments relative to the soil profile.

### 7.2.2 Instrument development

The equipment used in the Pilot Test (CP0) originated at Southampton University, where it had been employed for research into the effects of electro-osmosis on the shaft capacity of piles.[2] The Southampton Pile required extensive refurbishment before being re-used (in Test Series CP1), and the opportunity was taken to re-design some of its transducers. Unfortunately, it proved impossible to waterproof the Southampton Pile completely, and several instruments gave unreliable data during the equalization stage of CP1 (a long-term experiment).

To overcome these difficulties, two completely new piles were designed and manufactured at Imperial College between May 1986 and August 1987. The first was commissioned prior to Test Series CP2, and immediately produced data of the required quality. The second pile was commissioned prior to Test Series CP4. Apart from adding a flushable pore pressure system to this second pile (see below), the design of the equipment had been finalized by February 1987.

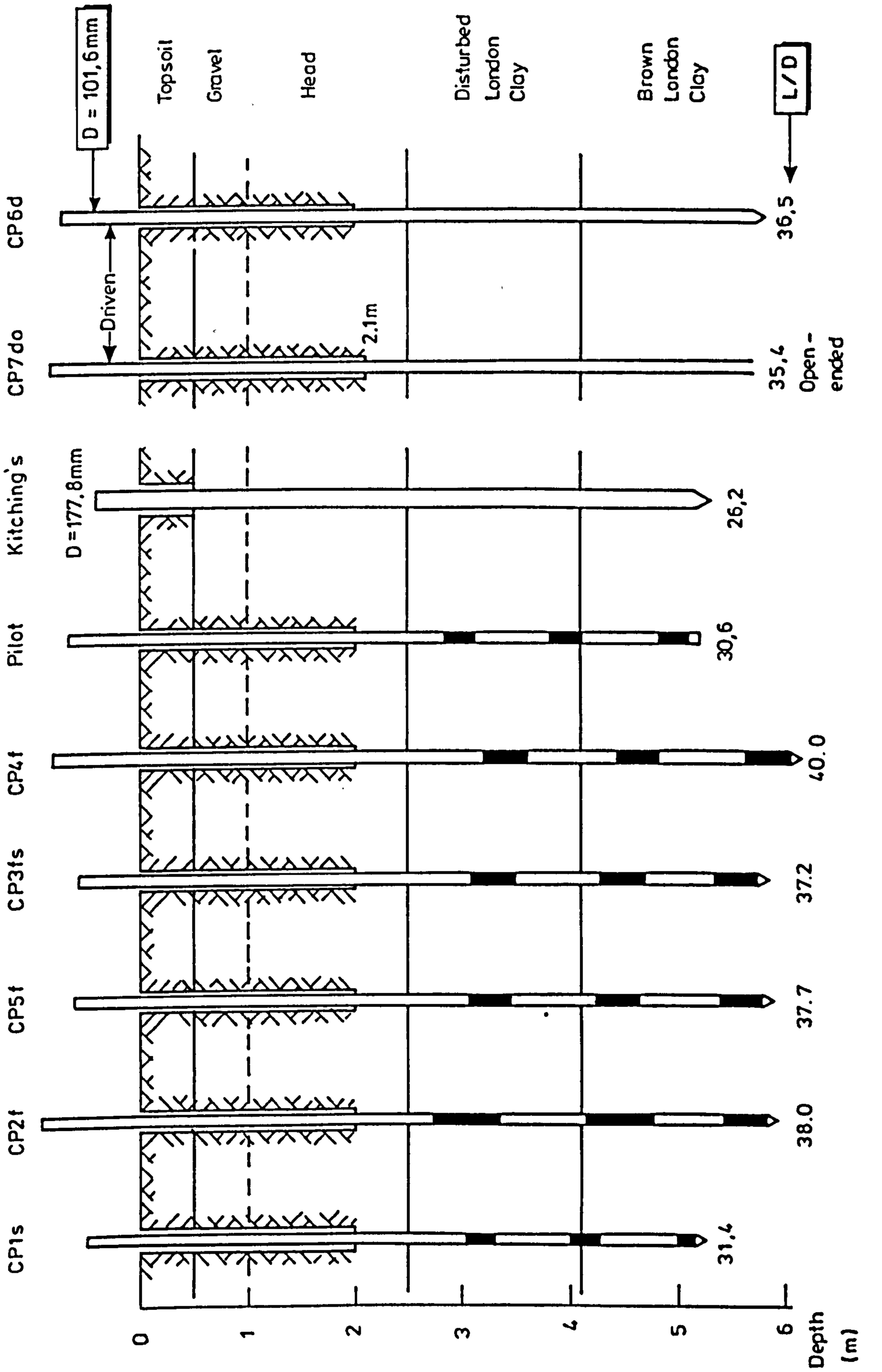



Figure 7.2 Piles installed at Canons Park by Imperial College

### 7.2.3 Field work at Canons Park

The installation and testing of the seven piles took place between November 1986 and June 1988. The first test was only a partial success, as explained earlier. Tests CP2 and CP3, however, were both extremely productive, providing a clear indication of the factors that govern pile behaviour in overconsolidated clays.

The one remaining technical difficulty at this stage (February 1988) was the accurate measurement of the long-term pore water pressures adjacent to the pile. The "standard" piezometer system on the Imperial College Instrumented Pile incorporates fast-acting pore pressure probes, which produce erratic signals if gas enters the system from the surrounding ground. In order to tackle this problem, a new piezometer system was designed and manufactured between July 1987 and April 1988 (see Chapter 6). The design allows the probes to be flushed periodically with de-aerated water. This "flushable" system was introduced in Test Series CP4 and the results obtained endorsed the use of the "standard" (fast acting) piezometer system in the short-term tests, without any modification.

The final instrumented pile (CP5) and the two driven piles (CP6 and CP7) were installed and tested in June 1988. CP5 was the control experiment for the driven pile tests, and in fact provided the clearest data in the entire programme. For this reason CP5 has been chosen as the "model" against which all the other tests are compared.

Shortly after completion of the driven tests, an inspection trench was dug around two of the piles, one of which had been installed by driving (CP6) and the other by jacking.[3] The trench was excavated to 4.5m below ground level, and over 150 samples were taken for subsequent testing in the laboratory. This part of the research programme is described in full in Chapter 13.

## 7.3 STRATEGY ADOPTED FOR THE PILE TESTS

### 7.3.1 Main parameters of interest

The review of previous research into the behaviour of displacement piles in clay (see Chapters 2-4) suggested that the behaviour of the piles installed at Canons Park would depend mainly on:

- Method of installation (slow-jacked/fast-jacked/driven)
- Equalization time (short/medium/long)
- "Direction" of first loading (compression/tension)

The strategy adopted for the pile tests at Canons Park allowed the influence of each of these factors to be examined in a systematic and

Table 7.1 Summary of pile tests at Canons Park

| Test Series | Rate of installation... | | | Equalization period..... | | | First load test in... | |
|---|---|---|---|---|---|---|---|---|
| | Slow | Fast | Driven | Short | Med. | Long | Tension | Comp |
| Pilot | | O | | | | ooo | ⇑ | |
| CP1s | ⊙ | | | | | ooo | | ⇓ |
| CP2f | | O | | | | ooo | | ⇓ |
| CP3fs | ⊙——— | O | | o | | | | ⇓ |
| CP4f | | O | | | oo | | ⇑ | |
| CP5f | | O | | o | | | ⇑ | |
| CP6d | | | ⊗ | o | | | ⇑ | |
| CP7do | | | ⊗ | o | | | ⇑ | |

economical way. Figure 7.3 shows the completed programme of tests and Table 7.1 summarizes how the main parameters were varied from one experiment to another. (For a full definition of the terms used see Section 7.4.)

### 7.3.2 Pile installation

Most displacement piles are driven into the ground, and ideally the instrumented piles would have been installed in the same way (for

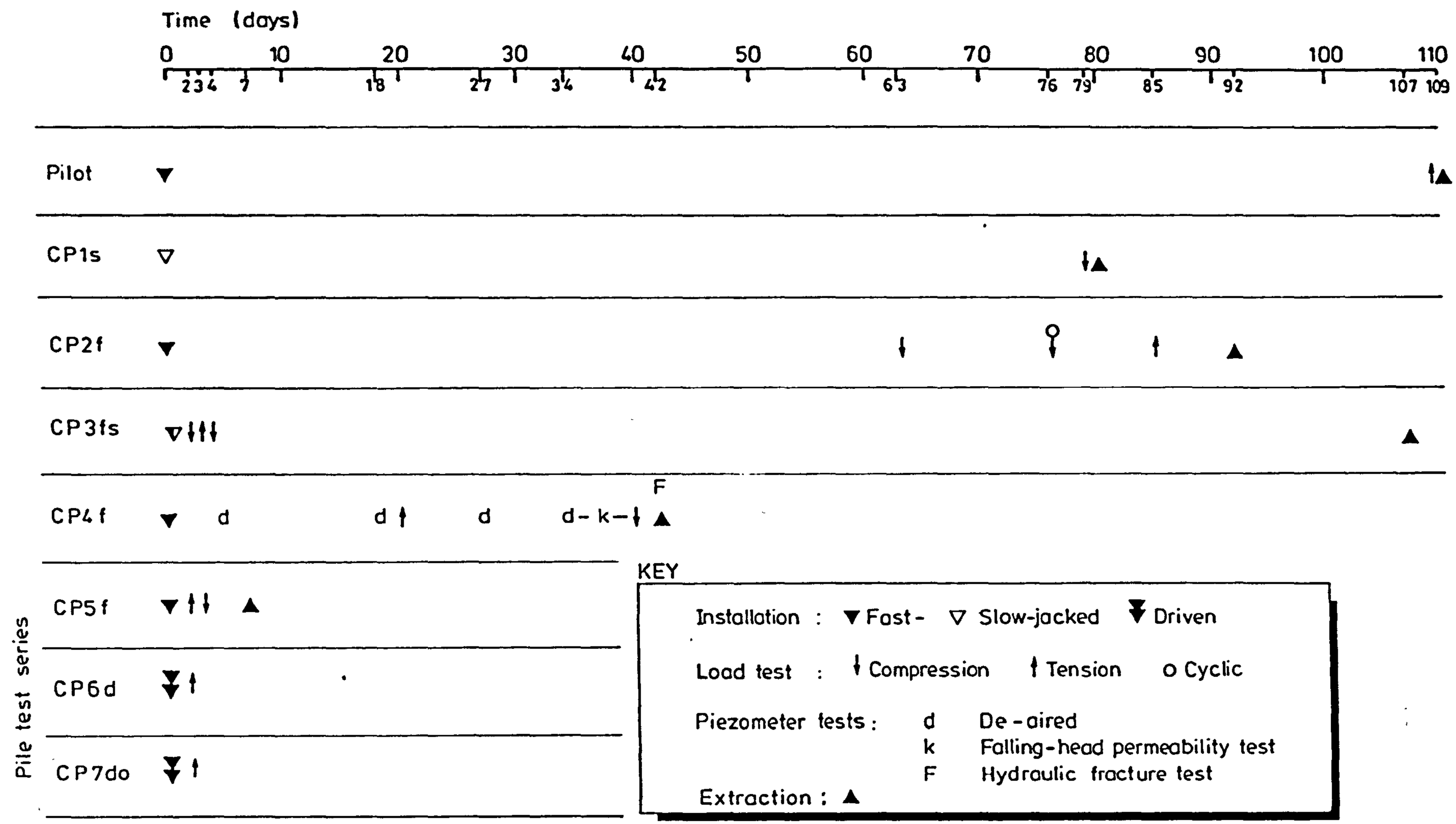



Figure 7.3 Programme of pile tests at Canons Park

similitude). However, the instrumented piles' strain-gauged devices would not have survived the accelerations due to pile driving, and so CP0-5 were installed by jacking instead. One advantage of using jacked piles (in place of driven) is that the their rate of penetration into the ground can be controlled. The question of whether a jacked pile behaves like a driven one was addressed in the final part of the test programme (see Chapter 12).

The jacking procedure allowed us to identify the strong influence that the rate of penetration has on the piles' load capacity. A distinction was made between fast- and slow-jacked piles (see p281) and experiment

Table 7.2 Installation details for piles CP0-7

| Test number | Rate of installation (mm/min) | Category | Penetration (m) | L/D | First load test after... (days) |
|---|---|---|---|---|---|
| CP0f | ≈500 ±100? | Fast | 5.20 | 30.6 | 109 |
| CP1s | 94 ±22 | Slow | 5.275 | 31.4 | 79 |
| CP2f | 426 ±34 | Fast | 5.945 | 38.0 | 63 |
| CP3fs | 403 ±94 | Fast | 4.08 | 19.6 | |
| | 81 ±15 | Slow | 5.87 | 37.2 | 2 |
| CP4f | 488 ±45 | Fast | 6.155 | 40.0 | 20 |
| CP5f | 445 ±55 | Fast | 5.92 | 37.7 | 2 |
| CP6d | 101 ±34 | Driven | 5.80 | 36.5 | 2 |
| CP7do | 53 ±14 | Driven | 5.70 | 35.4 | 2 |

CP3fs was designed to show how the mobilized shaft friction changes when the pile's velocity is reduced suddenly during installation.

The rates of jacking in each of the instrumented pile tests are given in Table 7.2.

### 7.3.3 Equalization times

It is generally believed that all piles benefit from the effects of "set-up", whereby a pile's capacity increases with time through re-consolidation of the surrounding soil following pile installation. Contrary to this expectation, the series of tests on driven and jacked piles reported by Tomlinson[4] show little or no set-up effect in heavily overconsolidated London clay (over a period of one year).

A primary goal of the present research was to investigate this apparent anomaly. Therefore the piles were load tested after widely differing set-up (equalization) periods, as shown in Table 7.2.

### 7.3.4 Loading direction: first-time loading

Load tests on pile CP0-7

| Test Series | Load tests... |
|---|---|
| CP0f | L1T |
| CP1s | L1C |
| CP2f | L1C, L2C, L3T |
| CP3fs | L1C, L2T, L3C |
| CP4f | L1T, L2C |
| CP5f | L1T, L2C |
| CP6d | L1T |
| CP7do | L1T |

The advent of tethered offshore platforms has generated greater interest in the behaviour of tension piles. This programme of research has addressed the question of whether the piles' behaviour is the same in tension as it is in compression. Since repeated tests to failure on the same pile can have a lasting influence on its behaviour, the present work has concentrated on first-time loading - although a number of repeat tests have also been performed, as shown in the adjacent box.

## 7.4 NOMENCLATURE

### 7.4.1 Main numbering system

A standard set of terms has been employed to identify the various pile experiments. The system of notation is illustrated in Figure 7.4 and explained in more detail below.

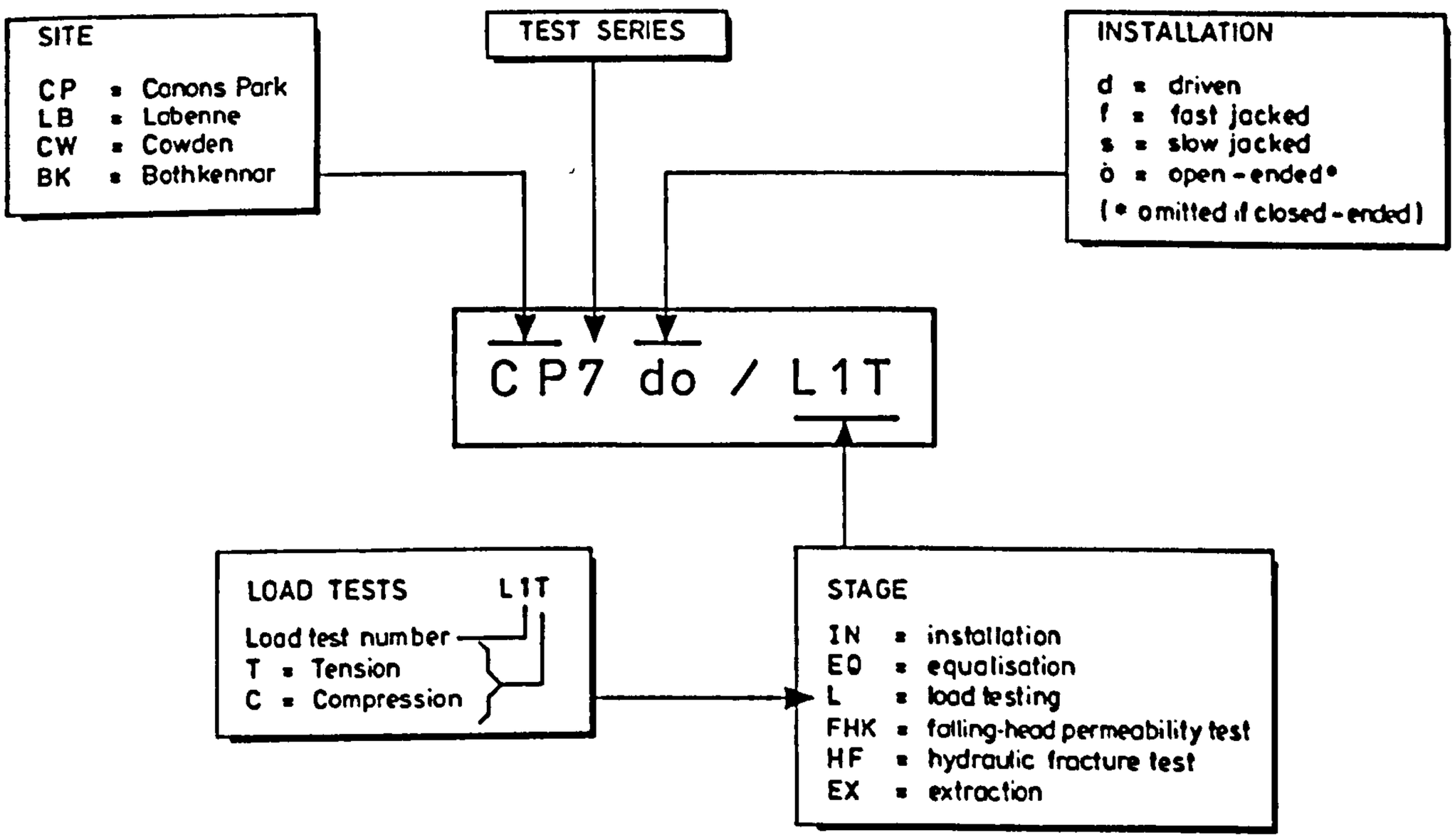



Figure 7.4 Notation used to describe the pile Test Series

Each Test Series has been numbered from one to seven, in chronological order.* The prefix "CP" signifies that the experiments were performed at Canons Park. The letters appended to the test number indicate whether the pile was installed by driving (d), "fast" jacking (f), or "slow" jacking (s) - see page 281 for a definition of these terms. The letter "o" signifies that the pile was open-ended; and its absence that the pile was closed-ended.

*For convenience, the Pilot Test is referred to as CP0f

## 7.4.2 Individual stages of a Test Series

The system of notation defined in Figure 7.4 discriminates between the individual stages of a pile test, as shown in the adjacent box. Since most of the piles were loaded more than once, it is important to differentiate the various load tests as well. In each case the first experiment is always denoted L1, the second L2, and the third L3. The letter which <u>follows</u> the test number indicates whether it was loaded in compression (C) or in tension (T). Hence the third load test (in compression) on pile CP3 would be specified by the code CP3fs/L3C.

Stages of a pile test

| Stage | Code |
|---|---|
| Installation | IN |
| Equalization | EQ |
| Load testing | L# |
| Extraction | EX |

Two other symbols have been used, to identify special experiments conducted during Test Series CP4. They are: FHK, standing for "falling-head permeability test"; and HF, for "hydraulic fracture test".

## 7.4.3 Parameters measured by the Instrumented Pile

The group of parameters that can be determined with the Imperial College Instrumented Pile are listed below. The first five are measured directly and the others are derived from them.

Main symbols used

| Symbol | Represents the... |
|---|---|
| Q | axial load along the pile |
| $\sigma_{rr}$ | radial total stress |
| $\tau_{rz}$ | shear stress on a vertical plane |
| u | pore water pressure (gauge) |
| T | temperature |
| $f_s$ | shaft friction* (analogous to $\tau_{rz}$) |
| $\sigma'_{rr}$ | radial effective stress, $\sigma_{rr}$ - u |
| $\mu$ | coefficient of friction, $\tau_{rz}/\sigma'_{rr}$ |
| $\delta$ | angle of wall friction, $\tan^{-1}\mu$ |

*$f_s = (1/\pi D)(\delta Q/\delta l)$, where $(\delta Q/\delta l)$ is the rate of change of Q along the length of the pile (l); and D is the pile's diameter

A distinction has been made between shaft friction ($f_s$) and shear stress ($\tau_{rz}$): the latter is measured at specific locations (i.e. it is a "local" measurement), whereas the former represents the <u>average</u> value of shear stress over a much larger area of

the pile (over ≈1m of its length).

### 7.4.4 Leading, following, and trailing instrument positions

The positions of the instruments along the pile's shaft have been classified as "leading", "following", or "trailing" depending on the value of the ratio z/R, where z is the instrument's distance behind the pile tip and R the pile's radius.

Instrument positions

| Position | z/R |
|---|---|
| Leading | ≤10 |
| Following | 10-30 |
| Trailing | 30-60 |

### 7.4.5 "Fast" and "slow" jacking rates

As shown in Chapter 9, the rate of installation of a jacked pile has a significant bearing on its subsequent load capacity. In describing this rate effect, it is convenient to classify the rates of steady jacking as shown alongside.

Definition of jacking rates

| Rate | mm/min |
|---|---|
| fast | 400-600 |
| slow | 50-100 |

### 7.4.6 Short, medium, and long equalization periods

For the purposes of the Canons Park experiments, the time allowed between pile installation and first-time load testing (i.e. the length of the "equalization period") has been categorized as shown on the right.

Equalization times

| Length | days |
|---|---|
| Short | <5 |
| Medium | 5-50 |
| Long | >50 |

## 7.5 NOTES AND REFERENCES

[1]Jardine R.J. (1985). Investigations of pile-soil behaviour, with special reference to the foundations of offshore structures. PhD Thesis, Univ. of London (Imperial College), 2 vol., 789pp. See Chapter 9.

[2]Johnston I.W. (1972). Electro-osmosis and porewater pressures; their effect on the stresses acting on driven piles. PhD Thesis, Southampton Univ.

[3]The pile installed in 1983 by Kitching. See Kitching D.N. (1983). A study into the microfabric of clays adjacent to jacked piles. MSc Dissertation, Univ. of London (Imperial College), 31pp+.

[4]Tomlinson M.J. (1970a). Adhesion of piles in stiff clays. CIRIA Report 26, Construction Industry Research and Information Association, London, 47pp.

# Chapter 8

# Instrumented pile tests: test procedures

# CONTENTS OF CHAPTER 8


8.1 GENERAL TEST PROCEDURES . . . . . 286
8.1.1 Introduction 286
8.1.2 Pile preparation 286
8.1.3 Installation of the instrumented piles 286
8.1.4 Load testing 289
8.1.5 Pile extraction 291
8.2 SPECIAL PROCEDURES FOR TEST SERIES CP4 . . . . . 293
8.2.1 Introduction 293
8.2.2 Falling-head permeability test: CP4f/FHK 293
8.2.3 Hydraulic fracture tests: CP4f/HF 293
8.3 DATA ACQUISITION . . . . . 295
8.3.1 Outline of the data acquisition system 295
8.3.2 Logging intervals 296
8.3.3 Data reduction 296
8.4 NOTES AND REFERENCES . . . . . 298

# 8.1 GENERAL TEST PROCEDURES

## 8.1.1 Introduction

This chapter summarizes the procedures followed during installation and load testing of the instrumented piles, CP1 to CP5. The arrangements for applying both compression and tension loads to the piles are described, and brief details are given of the special techniques that were employed in Test Series CP4 for the falling-head permeability and hydraulic fracture tests (see Section 8.2). The data acquisition system is described in Section 8.3.

## 8.1.2 Pile preparation

Tests[1,2] in the ring shear apparatus suggest that the frictional resistance of clay sheared against a rigid interface is strongly dependent on the interface's initial surface roughness. Offshore piles typically have a surface roughness $R_a$ (centre-line average) of around 10$\mu$m,[3,4] whereas metal surfaces produced by milling and turning have roughnesses between 0.4 and 6$\mu$m.[5]

The Southampton Pile's machined finish had been left un-roughened prior to the Pilot Test, and was subsequently found[6] to have an $R_a$ value of $\approx$0.54$\mu$m. In order to reproduce a more realistic level of surface roughness, all of the Southampton Pile's existing components were grit-blasted prior to experiment CP1; and the instruments for the Imperial College Instrumented Pile immediately after their manufacture. The resultant surface roughness was between 7 and 10$\mu$m.

## 8.1.3 Installation of the instrumented piles

All of the piles were installed through 2m deep cased boreholes. This ensured that they made no contact with the gravel layer that covers the site (see Chapter 5).

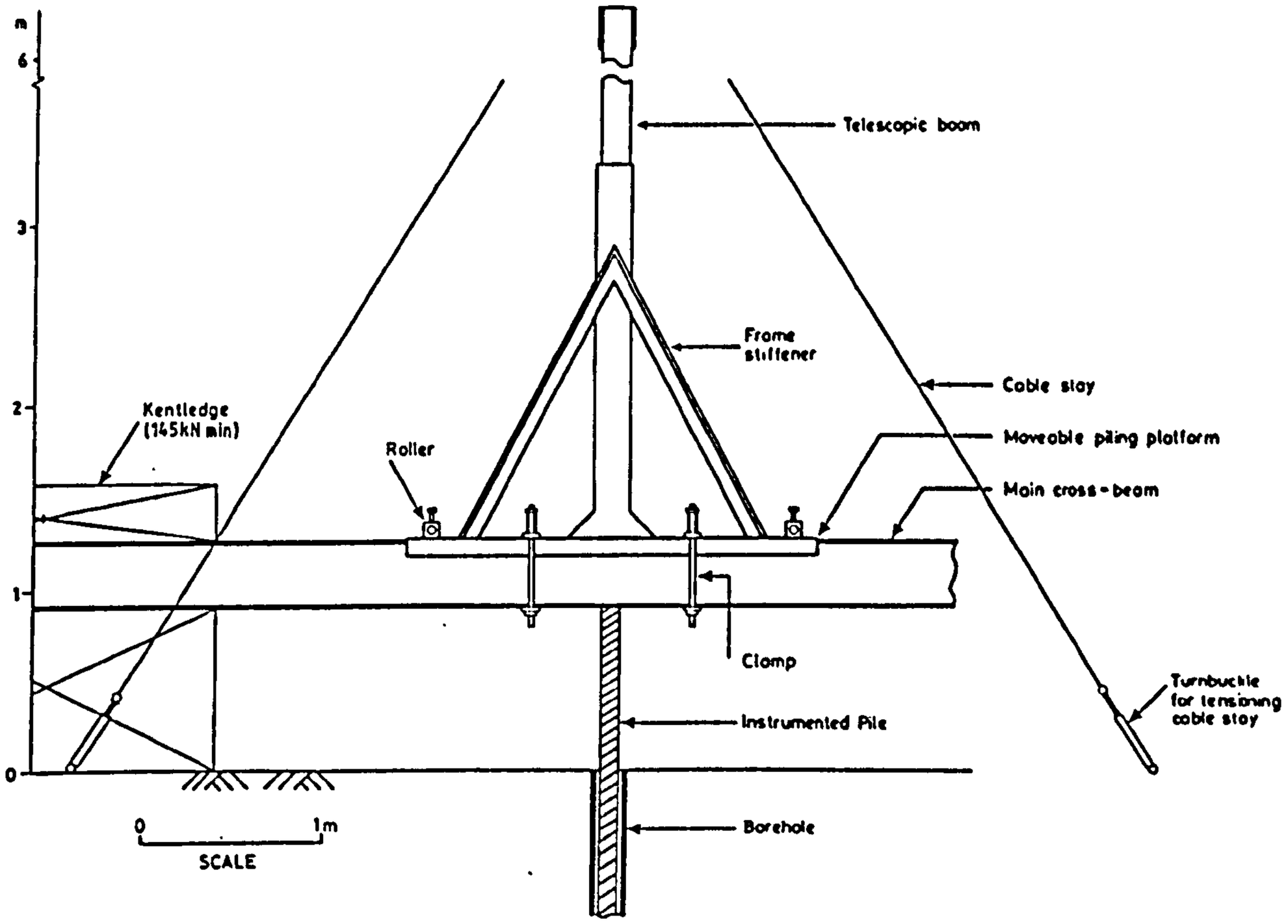



Figure 8.1 Loading frame used at Canons Park

A double-acting, hollow jack provided propulsion to the pile during installation, by reacting against the loading frame[7] shown in Figure 8.1. The frame's main components were:

- A telescopic boom mounted on a moveable platform;
- Two main cross-beams* which supported the platform;
- ≈145kN of kentledge at each end of the cross-beams; and
- Four cables which helped to stabilize the loading frame.

The jack itself was bolted to a cross-head which could be moved up and down the piling frame, as shown in Figure 8.2. The compressive loads applied to the pile passed through a ball-bearing located in two ball-seats positioned between the jack and the pile head.

*10m long, 356mm x 171mm universal beams

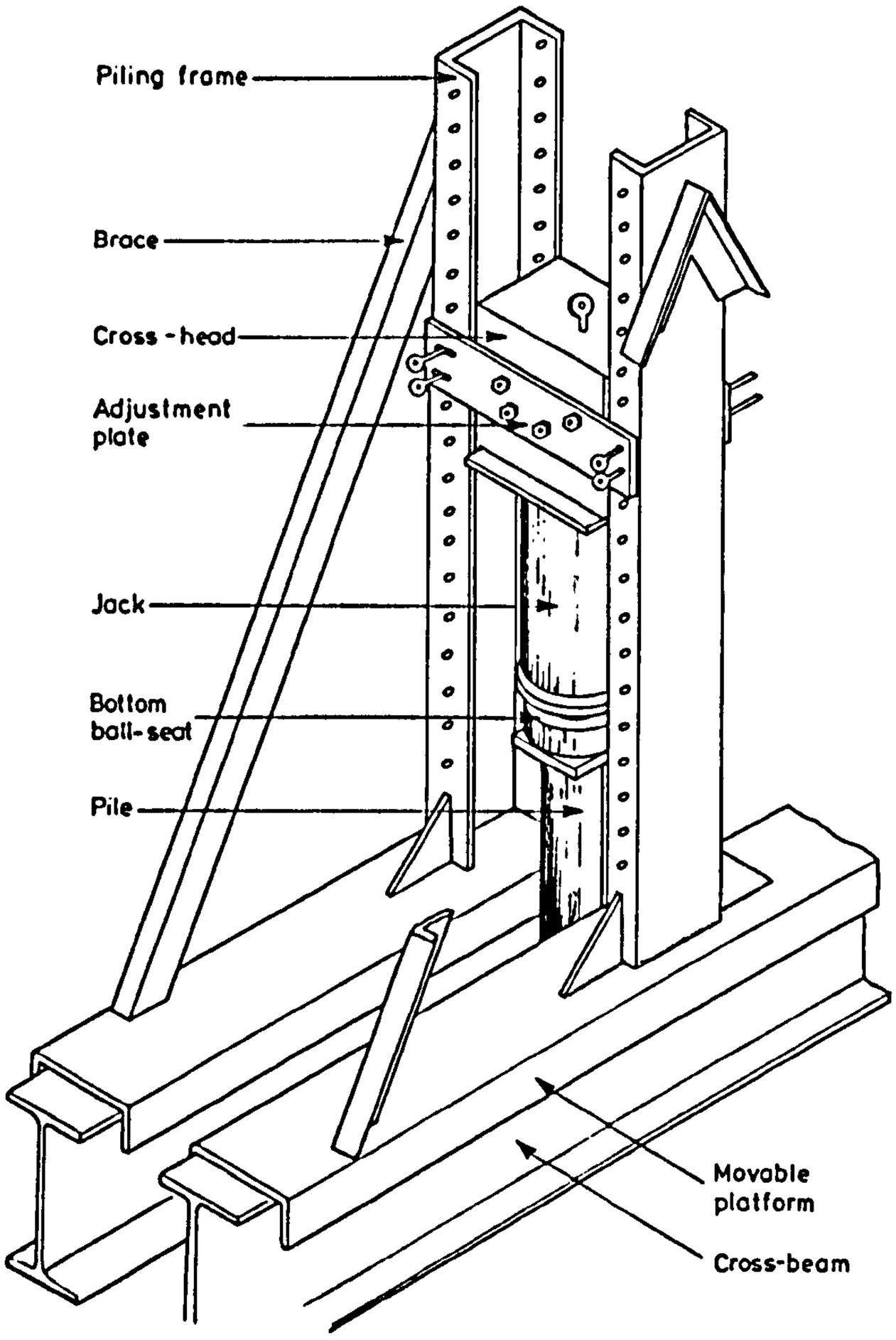



Figure 8.2 Arrangement for installing the instrumented piles

During pile installation, the jack was driven by a hydraulic power unit. This allowed the pile to be jacked at a steady velocity, which could be altered by changing the oil pressure produced by the hydraulic unit.

The jack's full stroke was about 225mm. For a slow installed pile each "push" lasted between 2¼ and 4½ minutes; and for a fast installed pile between 22 and 35 seconds (see Chapter 7 for the definition of "fast" and "slow" jacking). The time taken to reset the jack was typically between one and three minutes, and each pile required around twenty pushes for it to reach its final penetration.

The pile's average velocity was determined by measuring the speed at which the piston came out of the jack. A separate assessment was made by dividing the net distance travelled during a push by the duration that the pile was under full load. Both methods gave similar results.

The top two extension tubes were omitted from the pile at the start of installation, to improve its stability against buckling. Once the pile had been pushed far enough to make it safe to do so, the first section

of tubing was added by threading it along the cable loom that issued from the top of the pile. Likewise the second tube was inserted at a later stage in the proceedings. These additions took about 30 minutes in total.

Typically, pile installation took about 3h to complete, allowing for the delays noted above.

### 8.1.4 Load testing

a) Loading arrangement

Load tests were run both in compression and in tension. The loading frame used to install the jacked piles also provided the reaction for the loading tests.

The system for loading the piles is illustrated in Figure 8.3. In addition to the axial load cell at the pile's head, a 100 ton hollow load cell (NCB/MRE type 440, with a full-scale output of 2.4mV/V) was employed to measure the applied force.

Three displacement transducers and one dial gauge measured the displacement of the pile head. They were carried by an approximately 3.5m long steel reference beam, made from 152mm deep x 102mm wide box section. Details of the supports to the reference beam are given by Kitching.[8]

One disadvantage of the Canons Park site is that the London Underground's Jubilee Line runs along its boundary, no more than 100m or so away from the College's test area (see Chapter 5). During loading tests, we were careful to note whether a passing train had any effect on the dial gauge readings: the conclusion was that the reference beam was <u>not</u> affected by the passage of the train, but that the pile's creep rate (into or out of the ground) increased slightly as the train passed. As soon as the train had gone the creep rate returned to its previous magnitude.

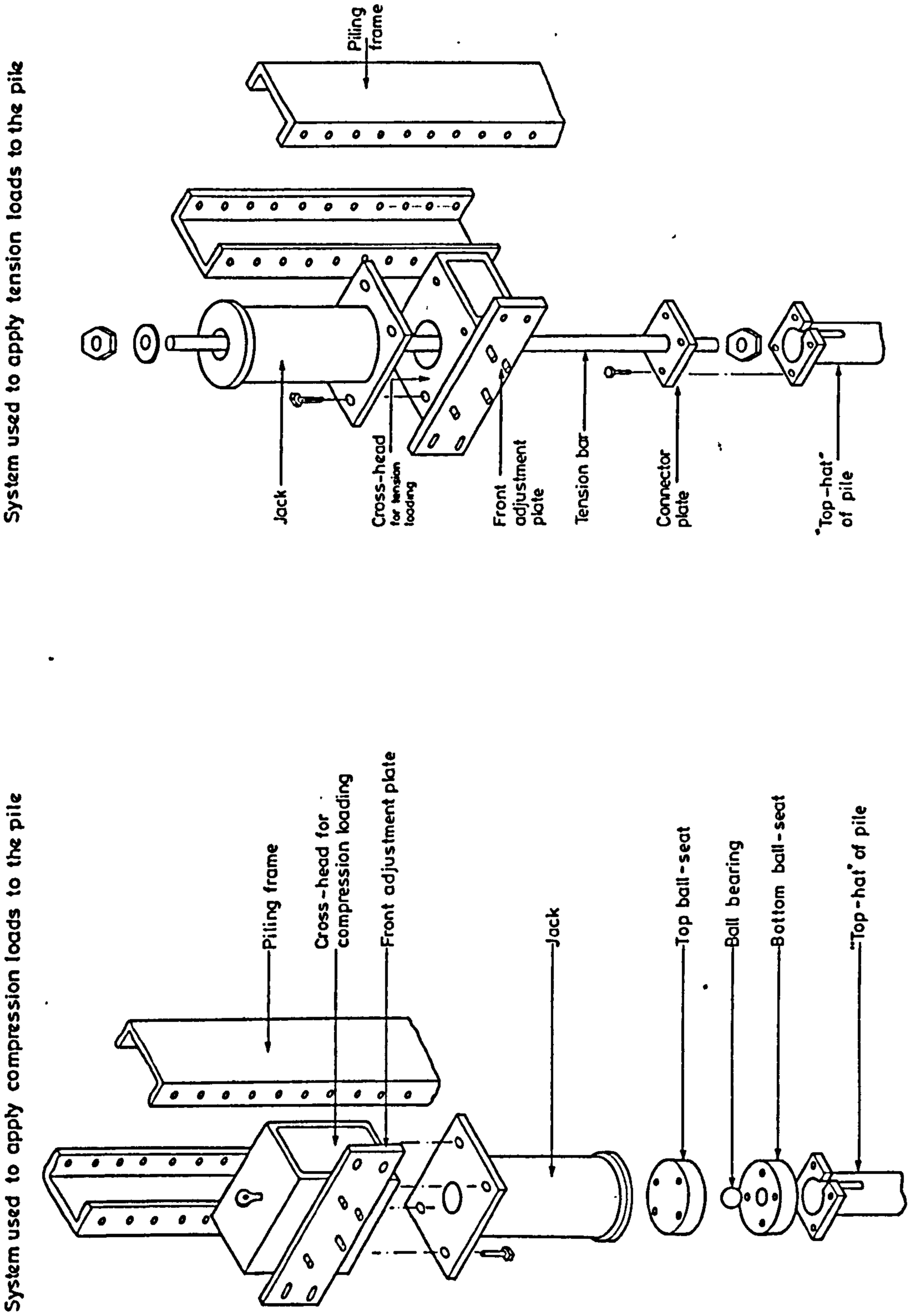



Figure 8.3 Arrangements for load testing the piles

b) Testing procedure

The piles were tested according to a modified version of the Laboratoires des Ponts et Chaussées (LPC) procedure, which is commonly used in France.[9] A major advantage of the LPC procedure is that it gives very good control of a pile test. This is especially important when attempting to define the pile's failure load in a brittle material such as the London clay.

The test procedure was as follows. Once the jack had been erected, and the displacement transducers and dial gauge fixed on the reference beam, a small "nip" load (≤5kN) was imposed on the pile in order to engage the reaction system. The load was then increased in a series of small increments, each load being maintained for a set "holding" period. The pile would creep into (or out of) the ground during the holding period.

Holding times were typically 2 minutes at low loads, increasing to 4, 8, and sometimes 16 minutes as the pile's peak capacity was approached. The loads themselves were increased in steps of ≈10kN initially, being reduced to 5, 2½, and sometimes 1kN near failure.

A test's progress was monitored by plotting "creep diagrams" (see Figure 8.4) showing the change in displacement with time for each loading step. A marked increase in the displacement rate occurs once a critical "creep failure load" has been exceeded, and failure of the pile is imminent.

In a typical tension test (for example CP5f/L1T), the pile's creep rate at low loads would be <0.01mm/min. At 50% of the final load capacity, the velocity might be 0.02mm/min, increasing to 0.03mm/min at about 75% of capacity. Only at 99% of capacity (creep rate 0.06mm/min) would the pile show signs that failure was imminent.

## 8.1.5 Pile extraction

The instrumented piles were extracted from the ground at the end of each Test Series, in a manner similar to their installation. For the first

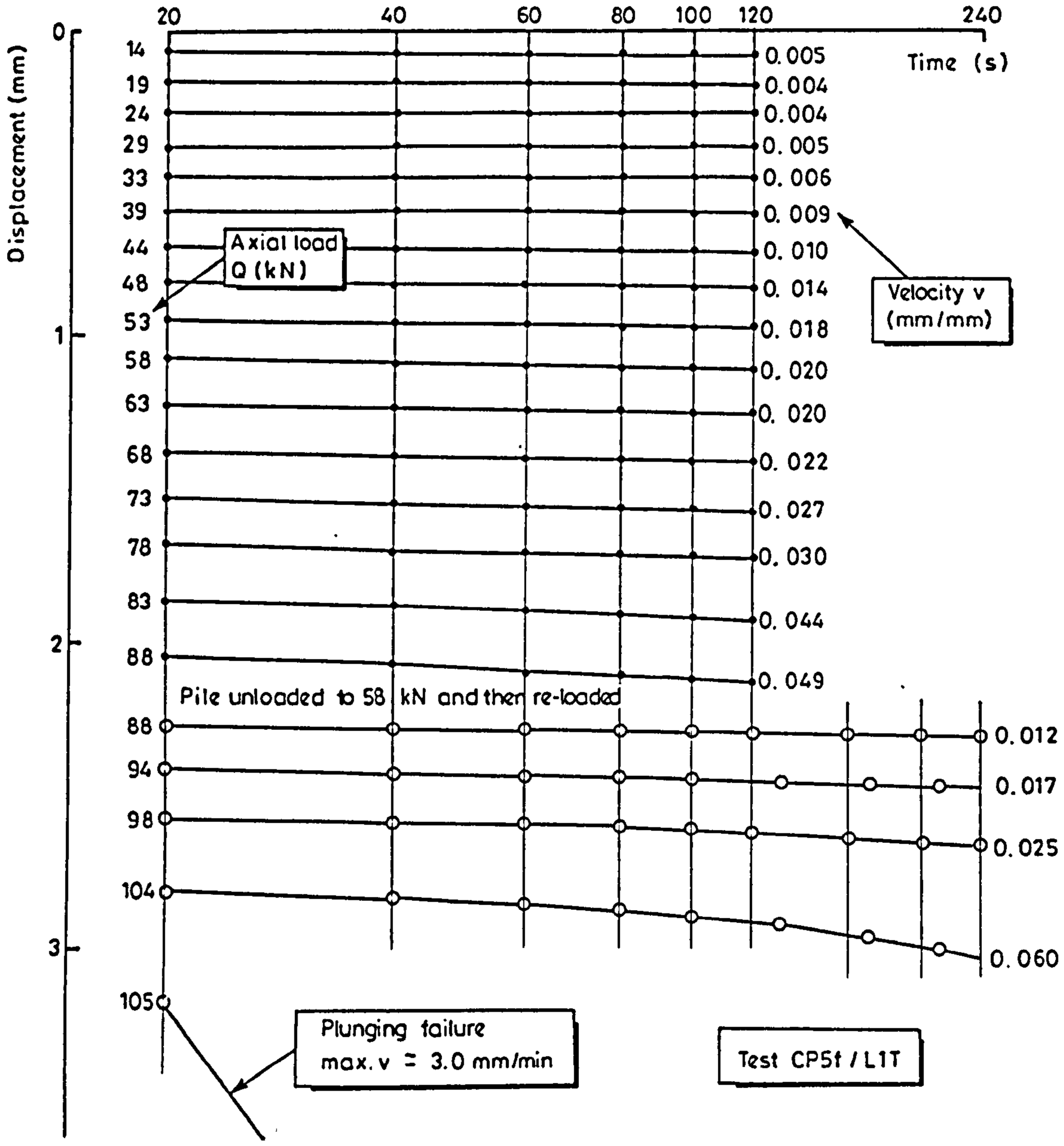



Figure 8.4 Creep diagram for load test CP5f/L1T

pull on the pile the jack was controlled by a hand pump, so that an accurate assessment of the pull-out load could be obtained. For subsequent stages, however, the jack was connected to the hydraulic power unit.

## 8.2 SPECIAL PROCEDURES FOR TEST SERIES CP4

### 8.2.1 Introduction

Pile CP4 was equipped with three flushable pore pressure probes, each of which required periodic purging with de-aerated water. In addition, a falling-head permeability test and a hydraulic fracture test were run on the flushable probes, as described in more detail below.

### 8.2.2 Falling-head permeability test: CP4f/FHK

Three falling-head permeability tests were run concurrently during the period between the first and second loading tests on pile CP4. The hydraulic lines to all of the flushable probes were de-aerated before the start of the permeability tests. The test procedure was as follows.

Three lengths of small bore tubing (cross-sectional area $\approx 2mm^2$) were mounted on a vertical board alongside a graduated ruler. The tubes were then connected to the valves at the top of the probes' "down" lines (see Figure 6.13 on p257), having previously been filled with de-aerated water. The height (above ground level) of the meniscus in each tube was noted, the valves were opened, and the permeability tests began. (The valves to the return lines were kept closed throughout.)

The levels of the menisci were noted at regular time intervals over the next six days, and from these readings the permeability of the soil was calculated.

### 8.2.3 Hydraulic fracture tests: CP4f/HF

All three flushable probes were used to perform hydraulic fracture tests, on the same day that CP4 was extracted from the ground. The test procedure was as follows.

The down line to each probe was connected to a gas/water interface, with a paraffin burette interposed between them, the hydraulic portion having

previously been de-aerated. Nitrogen gas was used to apply a known pressure to the interface, and thereby to the water contained within the down line (with the valve at the top of the down line open, but the return line valve closed - see Figure 6.12 on p257). The flow of water into the down line, and hence into the soil, was measured with the burette.

The pressure was increased monotonically in a series of steps until the flow rate increased dramatically (from 2mm$^3$/s to 100-200mm$^3$/s, typically). The pressure was then reduced in steps until the flow rate had returned to near its initial value (or had even gone negative - i.e. water had been given up by the ground). In the early parts of each test, the steps in pressure were set at 50 or 100kPa, and any given pressure was maintained for two minutes (three minutes for P56F) before being increased/decreased.

## 8.3 DATA ACQUISITION

### 8.3.1 Outline of the data acquisition system

The data acquisition system employed for the Canons Park experiments is shown schematically in Figure 8.5. The instruments were energized by a constant voltage power supply (set nominally at 5V), and their output

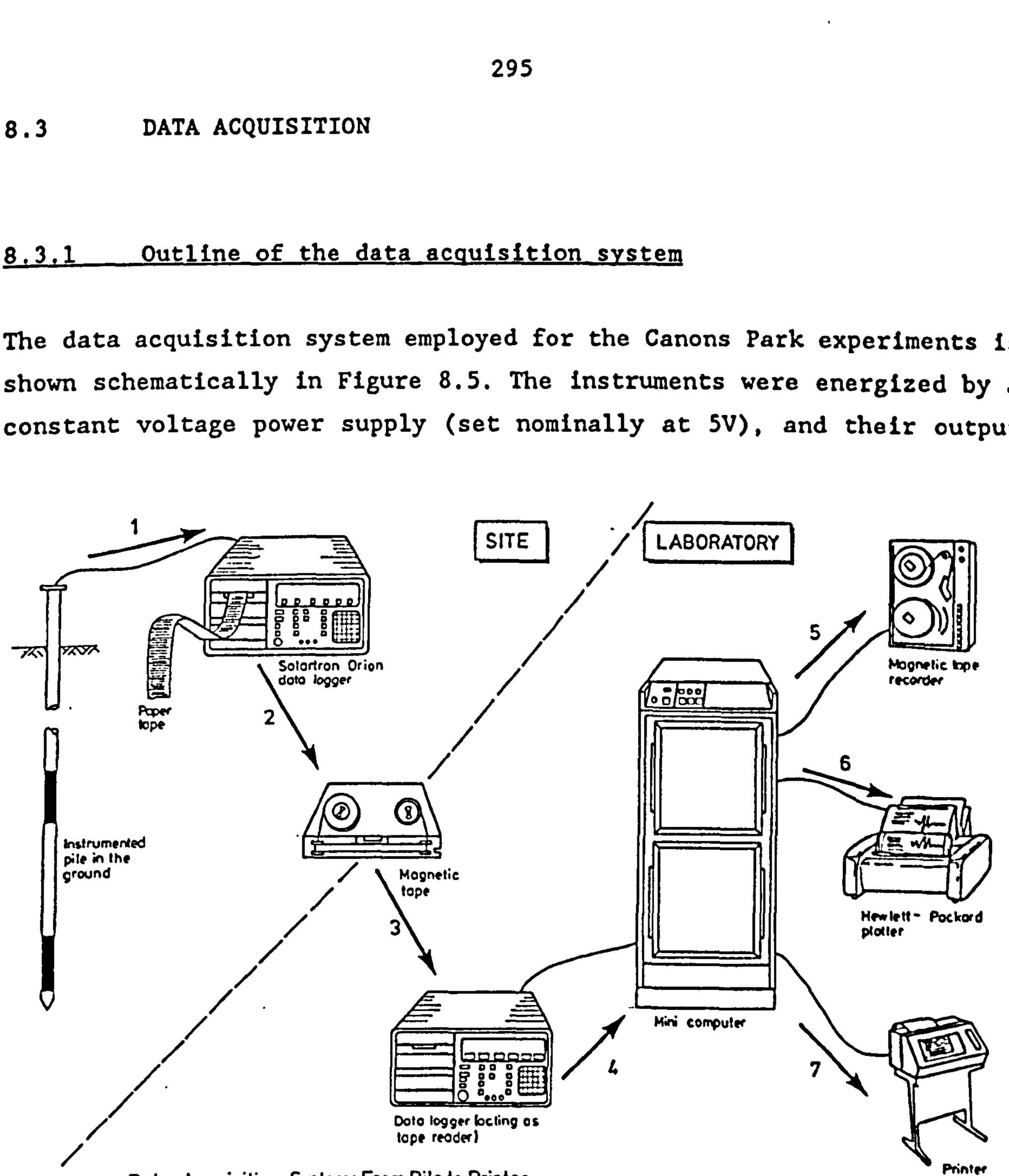



Figure 8.5 Data acquisition system: from pile to printer

voltages were digitized and recorded by a Solartron 3530A Orion data logger (Step 1). "Observations" were made at set intervals throughout all stages of the Test Series (including pile extraction): every observation comprised 23 readings, one for each circuit; the instruments' input voltage was also recorded.

The complete set of readings were stored on magnetic tape[10] (Step 2), with a partial set being printed onto paper tape (as a back-up). At suitable points in each experiment, the data was transferred from the magnetic

tape (via a second Orion data-logger) to a Prime mini computer located in the soil mechanics laboratory at Imperial College (Steps 3 and 4). A duplicate of the data was immediately written to magnetic tape (Step 5) and a "hard copy" was provided by the printer (Step 7). In addition, graphs were produced, for subsequent inspection, showing the variations in the signals against time (Step 6).

### 8.3.2 Logging intervals

The signals were recorded at frequent intervals throughout all stages of the pile experiments (see Table 8.1). During installation, data was logged at 3 or 10s intervals whilst the pile was moving: at least nine such observations were obtained in every 225mm push. In total, about 500 sets of observations were recorded during installation, i.e. 11 500 readings. A further 200 observations (4 500 readings) were made over the first 24h of the equalization period. Finally, in each load test between 850 and 1000 observations (22 000-26 000 thousand readings) were recorded onto magnetic tape.

Table 8.1 Typical data-logging intervals

| Stage | | Interval | Duration |
|---|---|---|---|
| Installation | a | 3-10s | 45-150s |
| | b | 15s | 2min |
| | c | 1-2min | 10min |
| | d | 5min | ∞ |
| Equalization | a-b | As installation | |
| | c | 1min | 2h |
| | d | 10min | 4h |
| | e | 30min | 8h |
| | f | 1h | 36h |
| | g | 4h | ∞ |
| Load testing | a | 10s | 2min |
| | b | 20s | 3min |
| | c | 30s | 5min |
| | d | 45s | 6min |
| | e | 60s | ∞ |
| Extraction | a-d | As installation | |

### 8.3.3 Data reduction

A suite of purpose-written computer programs were used to convert the instruments' (digitized) output voltages into engineering units; to process and sort the vast quantities of data; and to produce graphs and listings of the results.

A total of five independent programs were needed (see Figure 8.6) to process the data: "Sort", "Process", and "Canon" were written specially for this purpose; whereas "Dump" and "Dataac" are used for general data manipulation by my colleagues in the soil mechanics laboratory at Imperial College.[11]

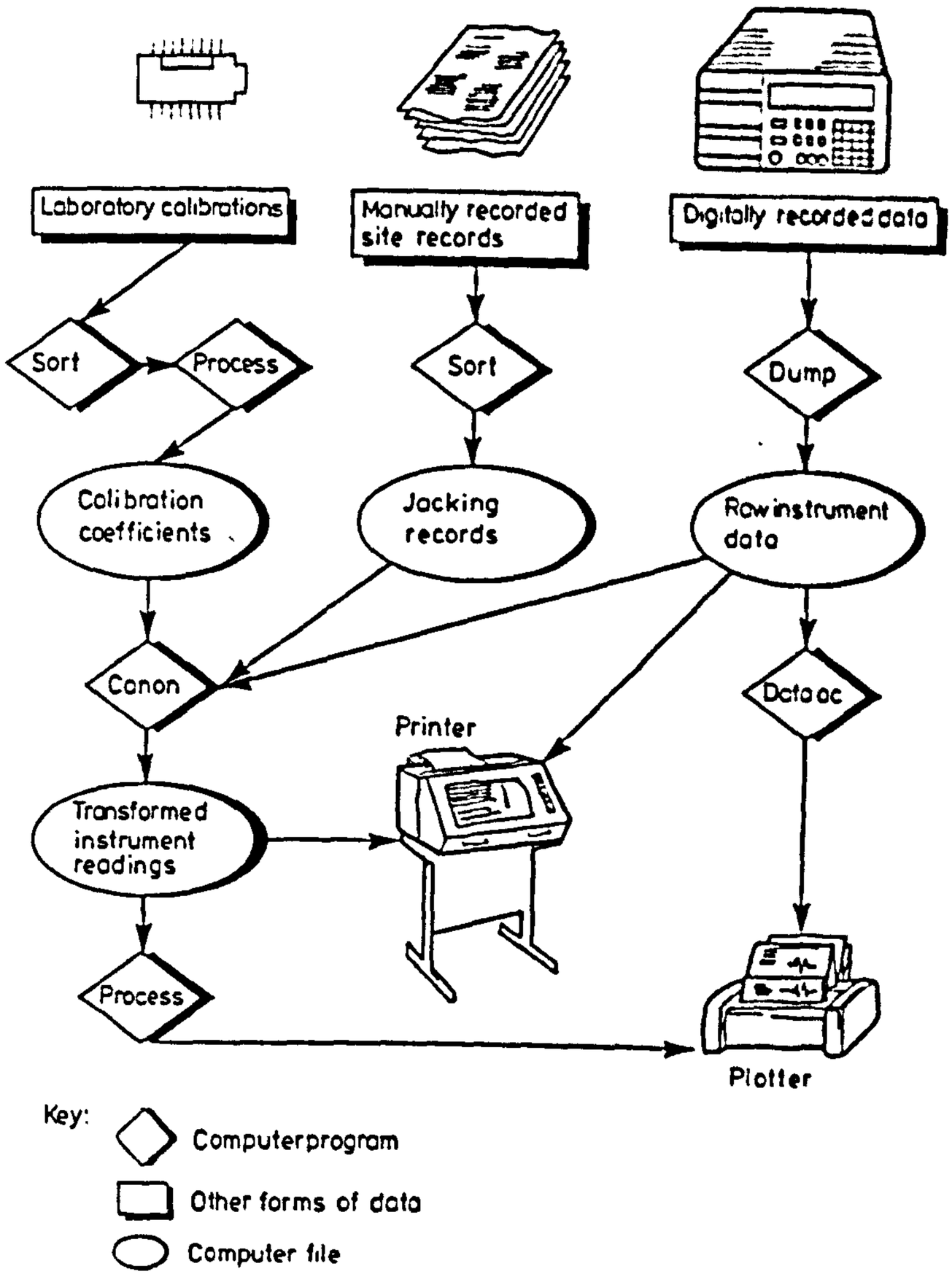



Figure 8.6 Computer programs used for data reduction

## 8.4 NOTES AND REFERENCES

[1]For the results of interface tests involving clay soils, see p490 and Figure 9-9 of: Lemos L.J.L. (1986). The effect of rate on residual strength of soil. PhD Thesis, Univ. of London (Imperial College), 540+pp.

[2]Tika T. (1989). The effect of fast shearing on the residual strength of soils. PhD Thesis, Univ. of London (Imperial College).

[3]Geotechnical Consulting Group (1984). Report no C/22-141/83 for Shell UK Ltd.

[4]Geotechnical Consulting Group (1985). Report no C/22-168/84 for Shell UK Ltd.

[5]See, for example, Chapter 10 (and in particular Table 10.1) of British Standards Institution (1984). Manual of British Standards in engineering metrology. (Editor: K. Brooker.) BSI in association with Hutchinson, London, 235pp.

[6]Resin was poured onto the surface of the pile, to create a replica with the same surface roughness. The roughness was then measured using a stylus-type instrument (a Talysurf machine), operated by the Metrology Section of Imperial College's Mechanical Engineering Department.

[7]See also Figure 25 of: Kitching D.N. (1983). A study into the microfabric of clays adjacent to jacked piles. MSc Dissertation, Univ. of London (Imperial College), 31pp+; and Figure 9.5 of: Jardine R.J. (1985). Investigations of pile-soil behaviour, with special reference to the foundations of offshore structures. PhD Thesis, Univ. of London (Imperial College), 2 vol., 789pp.

[8]See Kitching (1983), loc. cit., Figures 15 and 18.

[9]Bustumante M. (1982). The pile loading test. In "Foundation Engineering, vol. 1, Soil properties - foundation design and construction". (Editor: G.Pilot.) Presse de l'école nationale des Ponts et Chaussées, pp263-273.

[10]Scotch DC 100A or Hewlett-Packard certified data cartridges.

[11]Sort is a general utility program; Process allows data to be filtered, plotted, and otherwise manipulated; and Canon performs the various calculations needed to convert the raw data into engineering information. The programs Dump and Dataac were written at Imperial College (by Dr David Toll).

# Chapter 9

# Results of instrumented pile tests: pile installation

# CONTENTS OF CHAPTER 9


9.1 INTRODUCTION . . . . . 302
9.1.1 Outline of Chapters 9-14 302
9.1.2 Presentation of the data 302
9.1.3 Coop's test at Canons Park 303
9.2 PORE PRESSURES . . . . . 305
9.2.1 Traces from CP5f/IN 305
9.2.2 Summary diagrams for Test Series CP2-5 307
9.3 RADIAL TOTAL STRESSES . . . . . 309
9.3.1 Traces from experiment CP4f/IN 309
9.3.2 Summary diagrams for Test Series CP0-5 309
9.3.3 The "z/R effect" 313
9.3.4 Comparison with existing theories 314
9.3.5 Radial total stresses at the end of installation 315
9.4 RADIAL EFFECTIVE STRESSES . . . . . 317
9.4.1 Summary diagrams for Test Series CP2-5 317
9.4.2 The z/R effect 318
9.4.3 Comparison with existing theories 319
9.5 SHEAR STRESSES . . . . . 320
9.5.1 Traces from experiment CP4f/IN 320
9.5.2 Summary diagrams for Test Series CP0-5 321
9.5.3 Correlations with the clay's undrained shear strength 321
9.5.4 The rate effect in terms of average $\alpha$ values 323
9.5.5 The z/R effect 325
9.6 DISCUSSION . . . . . 326
9.7 NOTES AND REFERENCES . . . . . 328

# 9.1 INTRODUCTION

## 9.1.1 Outline of Chapters 9-14

The remainder of this Thesis concentrates on presenting and discussing the results of the field experiments at Canons Park.

Data from the instrumented pile tests (CP0-5) are reported in Chapters 9-11, each one dealing with an individual stage in the pile's "lifetime". The current chapter concentrates on the results obtained during pile installation; Chapter 10 considers the changes in earth and pore water pressures around the piles throughout the equalization period; and Chapter 11 reports the piles' behaviour during load testing.

Chapter 12 describes both the execution of and the results from the driven pile tests, CP6 and 7. Chapter 13 covers the work associated with the excavation of an inspection trench around two in situ piles. Finally, Chapter 14 discusses the main findings of this programme of research programme, placing the results in context by recalling the review of pile behaviour presented in Chapters 2-4.

## 9.1.2 Presentation of the data

Graphs and diagrams are used as the principal means of reporting the results of the instrumented pile tests. In many cases the data from all six instrumented pile tests (CP0-CP5) are presented collectively on summary diagrams, with the intention of:

- Demonstrating the repeatability of the results
- Establishing the trends for the main parameters of interest
- Determining the sensitivity of these parameters to the main variables*
- Presenting the data in a concise format

---

*e.g. the rate of installation of the pile; the length of the equalization period; and the direction of first loading

In some instances it is more appropriate to study the detailed results from individual experiments. In these cases experiment CP5f is used as the model fast-jacked pile test and CP3fs as the model slow-jacked, although data from other experiments is used on occasion to support the evidence from these tests.

In presenting the results, each of the measured parameters is considered in turn, and the factors that govern their response are identified and discussed. Pore pressures are considered first (in Section 9.2); then the radial total and radial effective stresses (Sections 9.3-9.4); and finally the shear stresses (Section 9.5).

Wherever possible the results are compared with data from the independent pile test conducted at Canons Park by Coop (as described below); and the significance of the findings are demonstrated by reference to current theories of pile behaviour (reviewed in Chapter 3).

### 9.1.3 Coop's test at Canons Park

An independent pile test was conducted at Canons Park in February 1986 by Dr Matthew Coop, using the Oxford University Instrumented Model Pile (IMP). The data presented in Coop's 1987 PhD Thesis[1] relates to:

- Pile installation
- Partial equalization of the earth pressures and excess pore pressures (over a period of 2.8h only)

Coop did not perform any load tests with the IMP at Canons Park.

Wherever appropriate Coop's data is plotted on the summary diagrams, to provide an independent check on the results of the current test programme. However, in making these comparisons it is necessary to remember that the Oxford University and the Imperial College piles have dissimilar length-to-diameter ratios and surface textures, and use quite different instrumentation systems.

The Oxford radial stress sensors suffer from far larger cell action effects (if used without a balancing back pressure) than do the IC surface stress transducers. Their relatively high compliance would lead to a serious under-registration of any stress changes during equalization and load testing (when the pile is relatively stationary). During installation, however, the cell action effects are probably less important. (See Chapter 4 for further details.)

Coop's pore pressure probes, which employed sintered bronze porous discs as filters, were mainly of the strain-gauged diaphragm type and were saturated with a mixture of water and glycerine. It was found in Tests CP0 and CP1 that water does <u>not</u> make a good saturating fluid in strongly dilating soils, since the probes de-saturate during pile installation and take too long to recover once penetration has ceased. Inspection of Coop's pore pressure traces suggests that his devices suffered from the same adverse effects. For this reason (and because his tests involved only *partial* equalization) Coop's pore pressure and effective stress data will not be compared with the results from the current test programme.

## 9.2 PORE PRESSURES

### 9.2.1 Traces from CP5f/IN

Figure 9.1 shows the data recorded by the leading pair of pore pressure probes during installation of pile CP5f. Figure 9.2 does likewise for the following pair. Several observations are worth making:

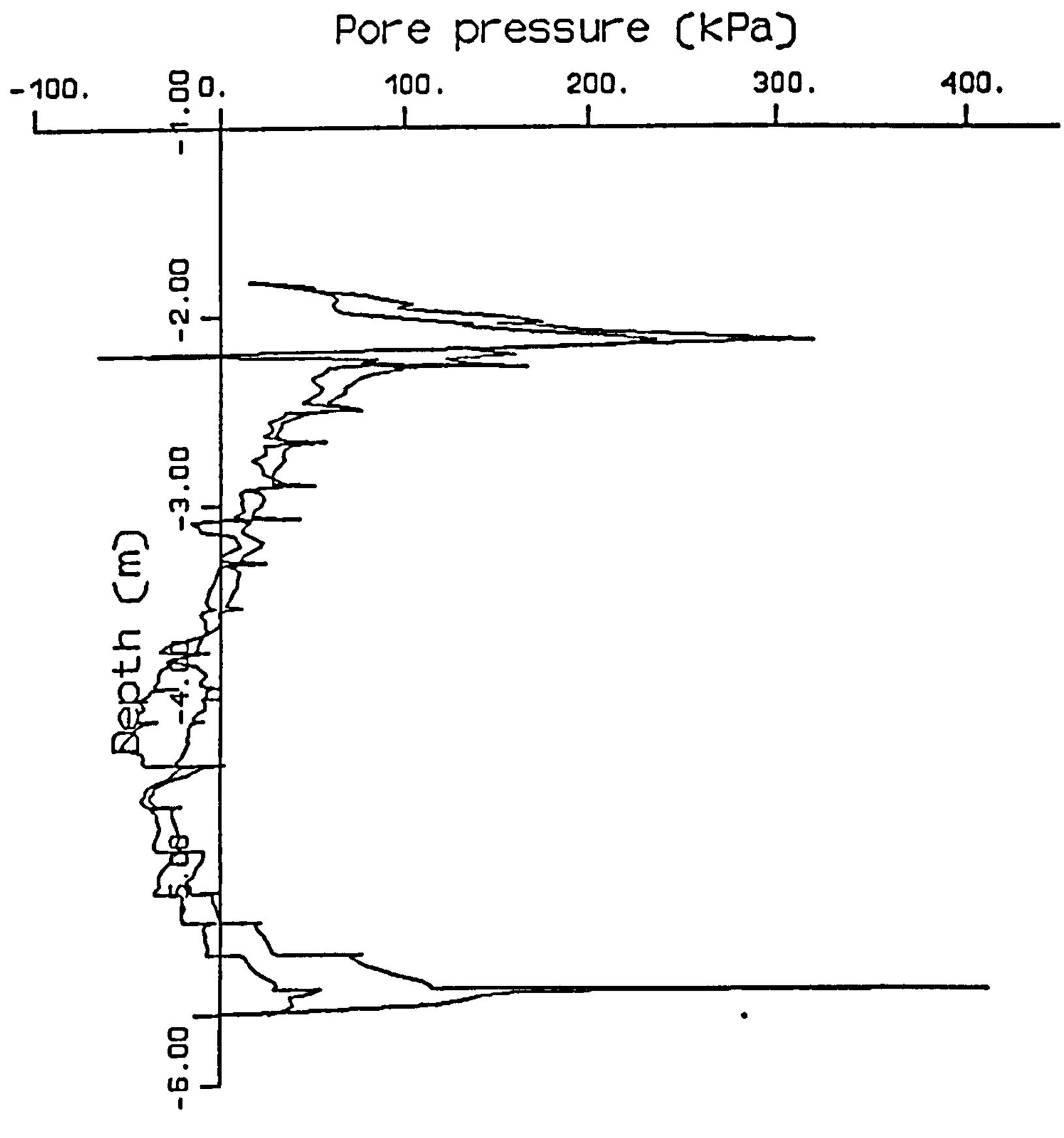



Figure 9.1 Pore pressures recorded by leading instruments during pile installation, Test CP5f

- The spikiness of the traces signifies fast response times for all the probes, the spikes being caused by excess pore pressure re-distribution during pause periods whilst jacking (it took 2-5 minutes to reset the jack between each push)

- The results from any one instrument agree remarkably well with the readings from its twin located at the same level (but on the opposite side of the pile)
- Positive pore pressures are recorded in the head material (to a depth of 2.5m), but negative pore pressures throughout the heavily overconsolidated London clay (below it); at a depth of ≈5.5m there is a marked change in behaviour, the leading traces rising sharply to high positive values; however, these high pressures are only recorded during the <u>pause</u> periods between pushes: when the pile starts to move again, the pore pressures dive down to (generally) negative values
- There is excellent agreement between traces recorded in Test Series CP2f, CP3fs, CP4f, and CP5f - see Appendix 11 for proof[2]

Although the pore pressure traces from CP0, CP1, and Coop's test show qualitative agreement with those obtained with the fast-acting pore pressure probes, the data is of poorer quality and cannot be relied on in any quantitative interpretation of the piles' behaviour.

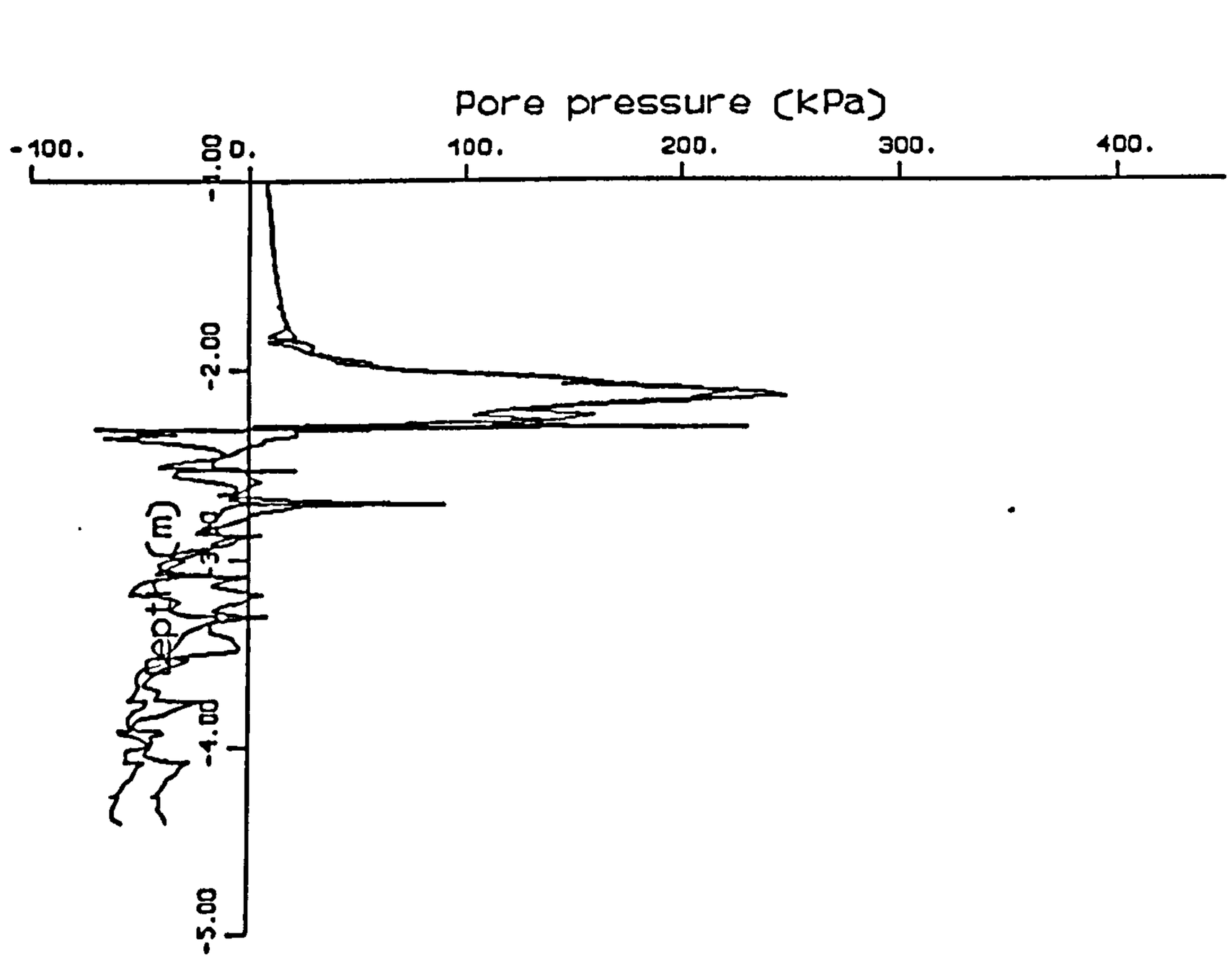



Figure 9.2 Pore pressures recorded by following instruments during pile installation, Test CP5f

I am not aware of any theory of pile behaviour which predicts this form of pore pressure response.

## 9.2.2 Summary diagrams for Test Series CP2-5

Because of their complexity, the superposition of too many pore pressure traces is unsightly and uninformative. Therefore the next two diagrams show the upper and lower *bounds* to the data recorded in Test Series CP2-5 (derived from seven traces in all). Figure 9.3 presents these bounds for the leading probes (at z/R = 5.25); and Figure 9.4 for the following ones (at z/R ≈ 28).

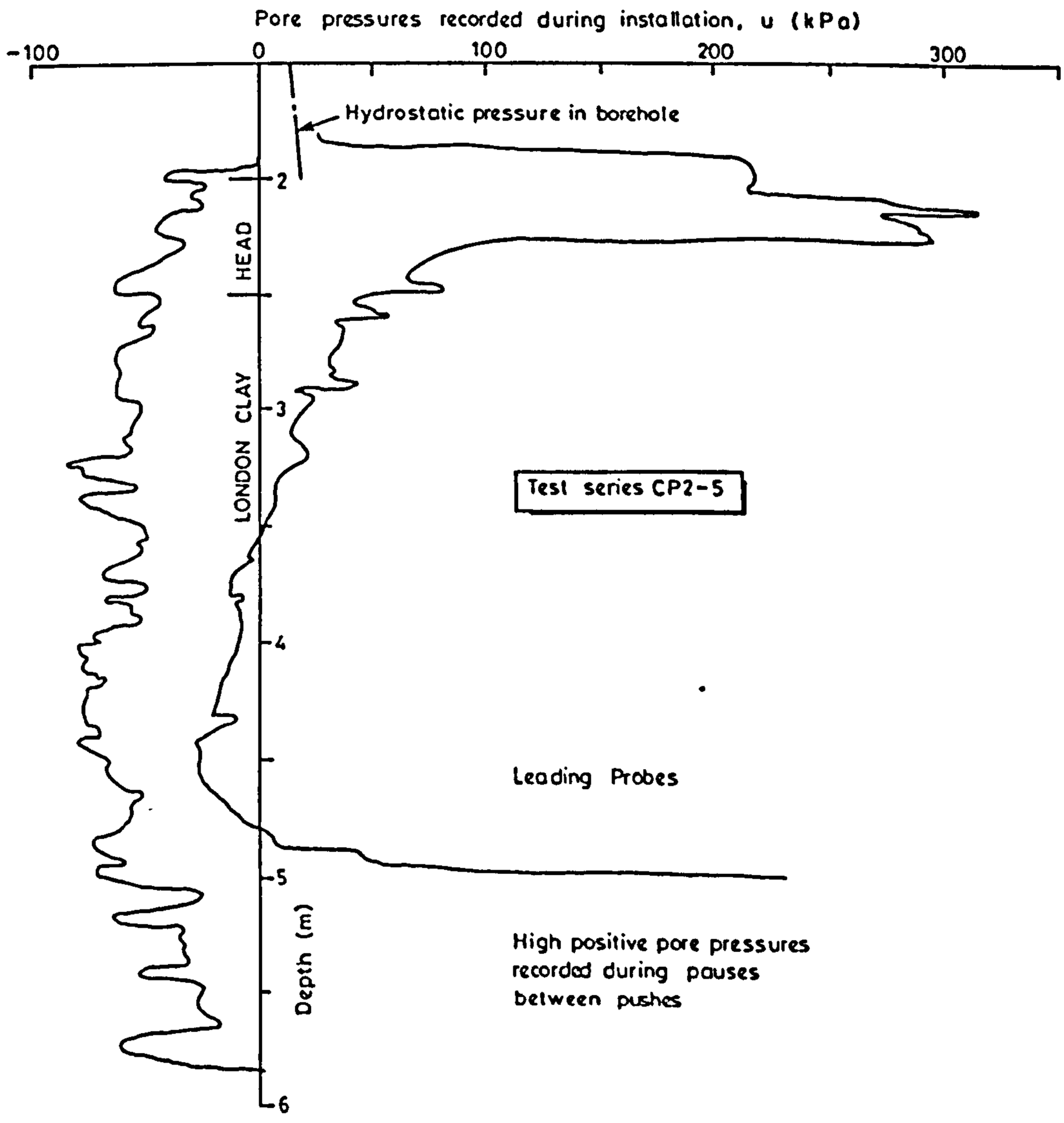



Figure 9.3 Summary diagram: pore pressures recorded by leading instruments during installation, Tests CP2-5

Both figures clearly demonstrate the excellent repeatability of the readings. For the leading probes the spread of the results in the brown London clay (2.5-4.1m deep) is less than ±40kPa; and for the following probes it is much the same. In both cases there is no doubt that the pore pressure is negative (i.e. less than atmospheric). It is slightly more negative for the leading than for the following probes.

Neither the cavity expansion method nor the strain path method (see Chapter 3) predicts negative pore pressures during pile installation.

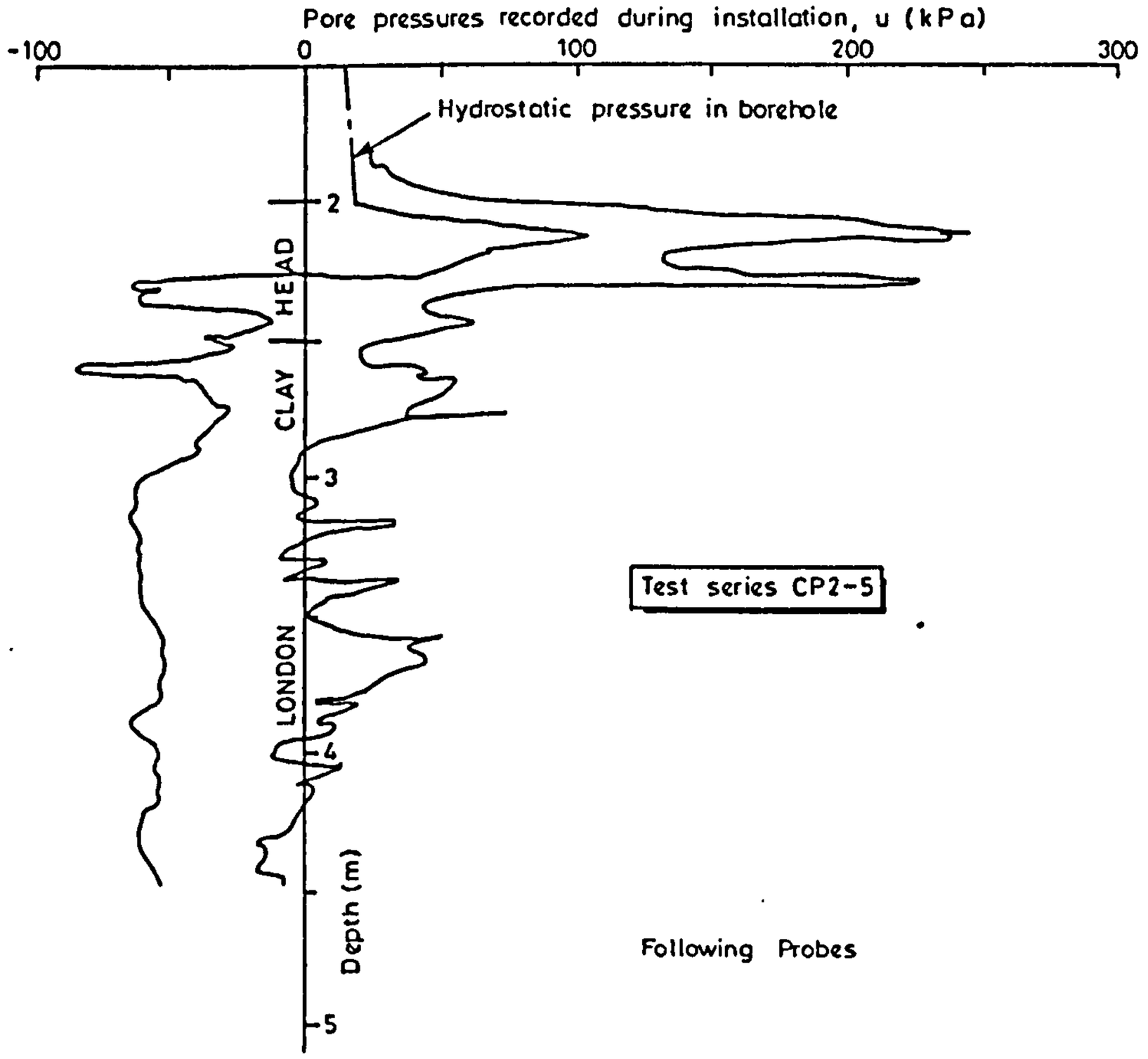



Figure 9.4 Summary diagram: pore pressures recorded by following instruments, Tests CP2-5

## 9.3 RADIAL TOTAL STRESSES

### 9.3.1 Traces from experiment CP4f/IN

Figure 9.5 shows the radial total stresses that were recorded during installation of the fast-jacked pile CP4f. The surface stress transducers were mounted at three different positions along the pile, approximately one metre apart (as indicated on the figure).

Considering the leading instrument first, we see that $\sigma_{rr}$ increased steadily with depth from about 300kPa at the top of the London clay (2.5m) to more than 1000kPa at 5.5m. However, as the figure clearly demonstrates, $\sigma_{rr}$ varies not only with depth below ground level, but also with position relative to the pile's tip. For example, the value of $\sigma_{rr}$ recorded by the leading instrument in the layer of soil at 3.5m depth was ≈400kPa, whereas the following and trailing instruments recorded about 300 and 150kPa respectively. This phenomenon (the "z/R effect") has been observed in all six instrumented pile tests at Canons Park[3] and is discussed further in Section 9.3.3 below.

### 9.3.2 Summary diagrams for Test Series CP0-5

The measurements of radial total stress $\sigma_{rr}$ during installation of all six instrumented piles are presented in Figure 9.6 and Figure 9.7, for the leading and the following instruments, respectively.

There are three main conclusions to be drawn from these figures. Firstly, it is clear from both diagrams that the results are highly repeatable. Secondly, there is no systematic difference between the readings from the "slow" jacked piles (CP1s and CP3fs) and the readings from the "fast" ones (the remainder) - thereby implying that the radial total stress is not sensitive to the rate of installation of the pile. Finally, there is close agreement between the measurements from the latest design of stress transducer (as used in Tests CP2 to CP5) and the results obtained with the earlier versions of these instruments (as used in the CP0 and CP1).

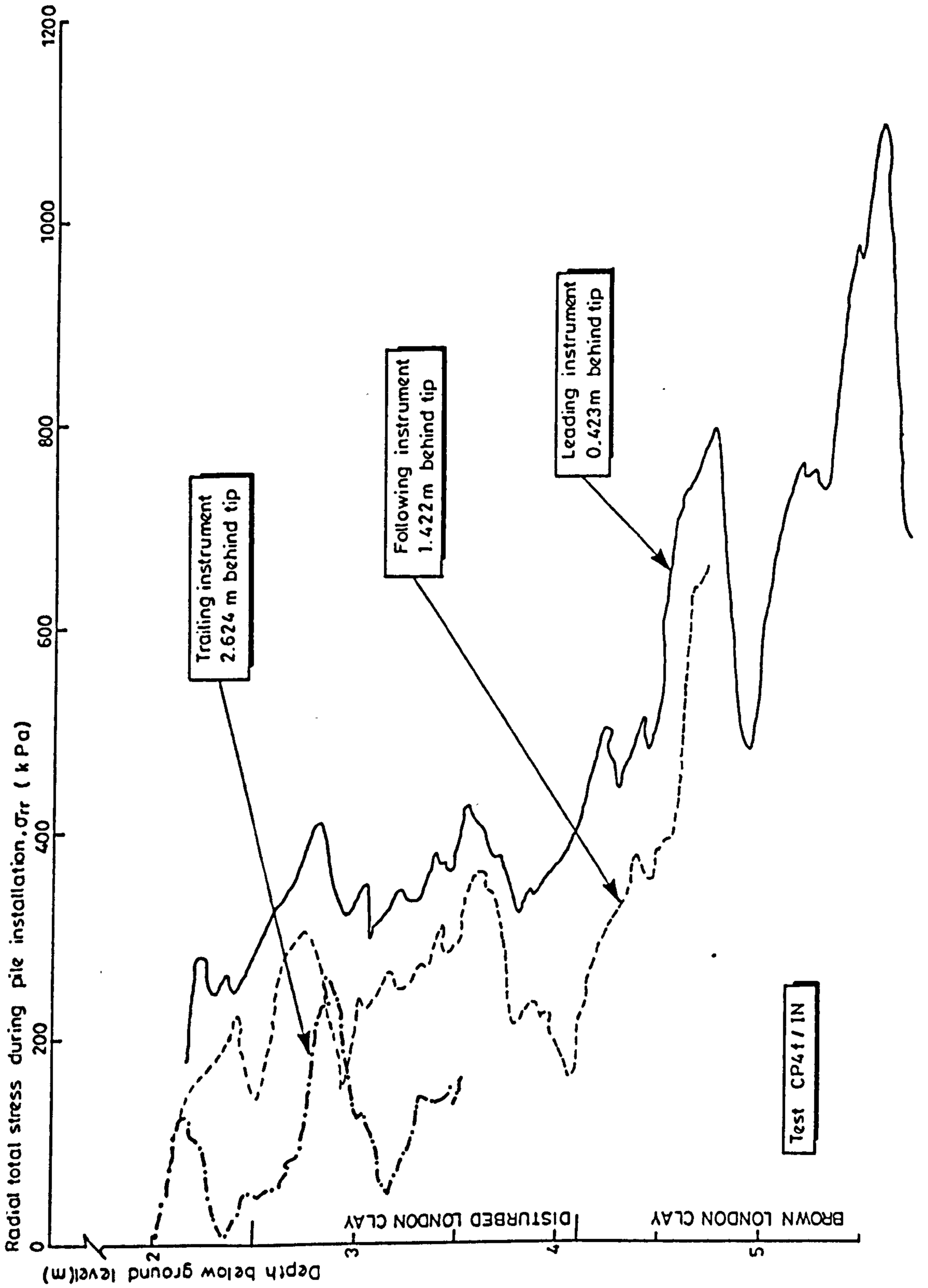



Figure 9.5 Radial total stresses recorded during installation of pile CP4f

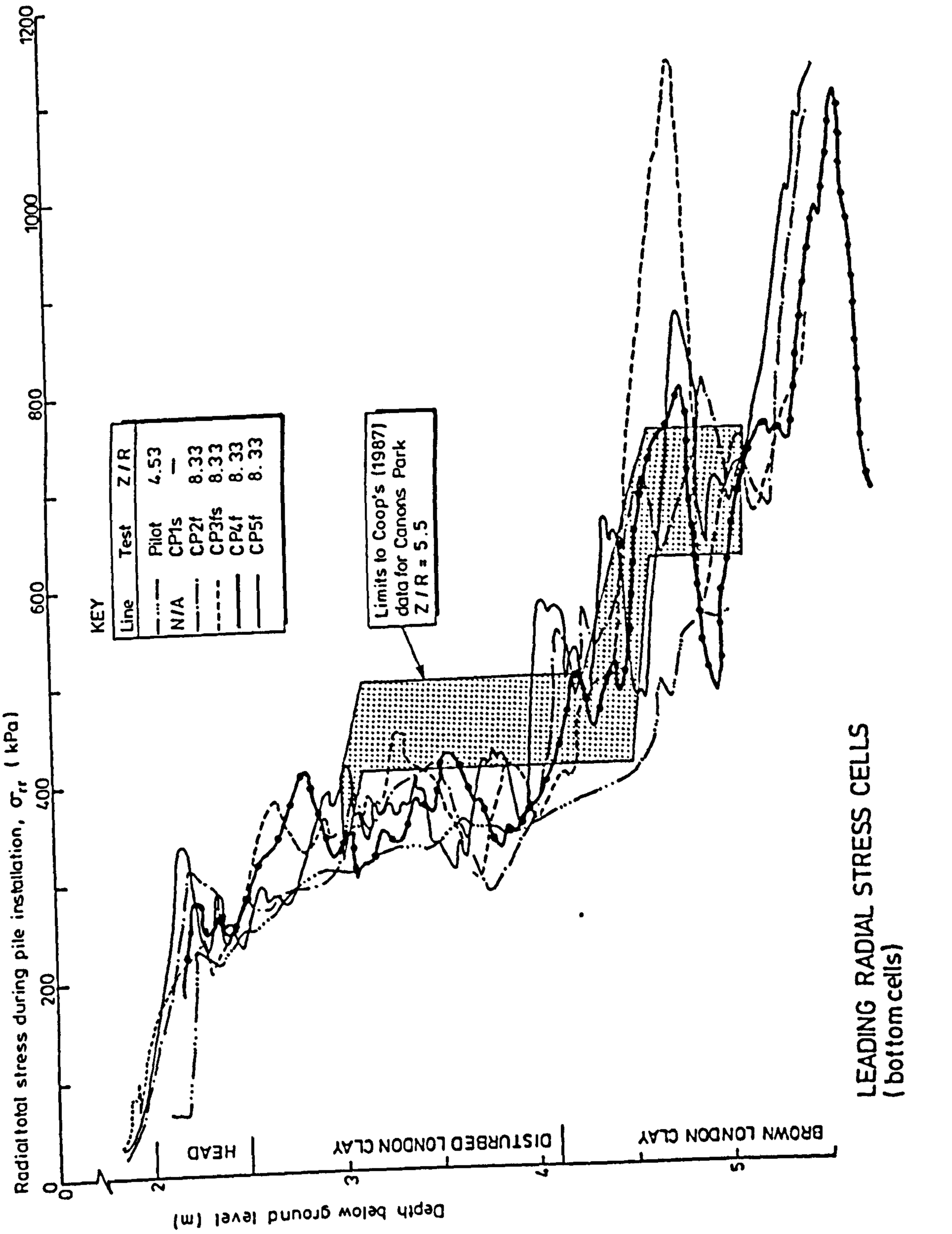



Figure 9.6 Summary diagram: radial total stresses recorded by leading instruments during pile installation, Tests CP0-5

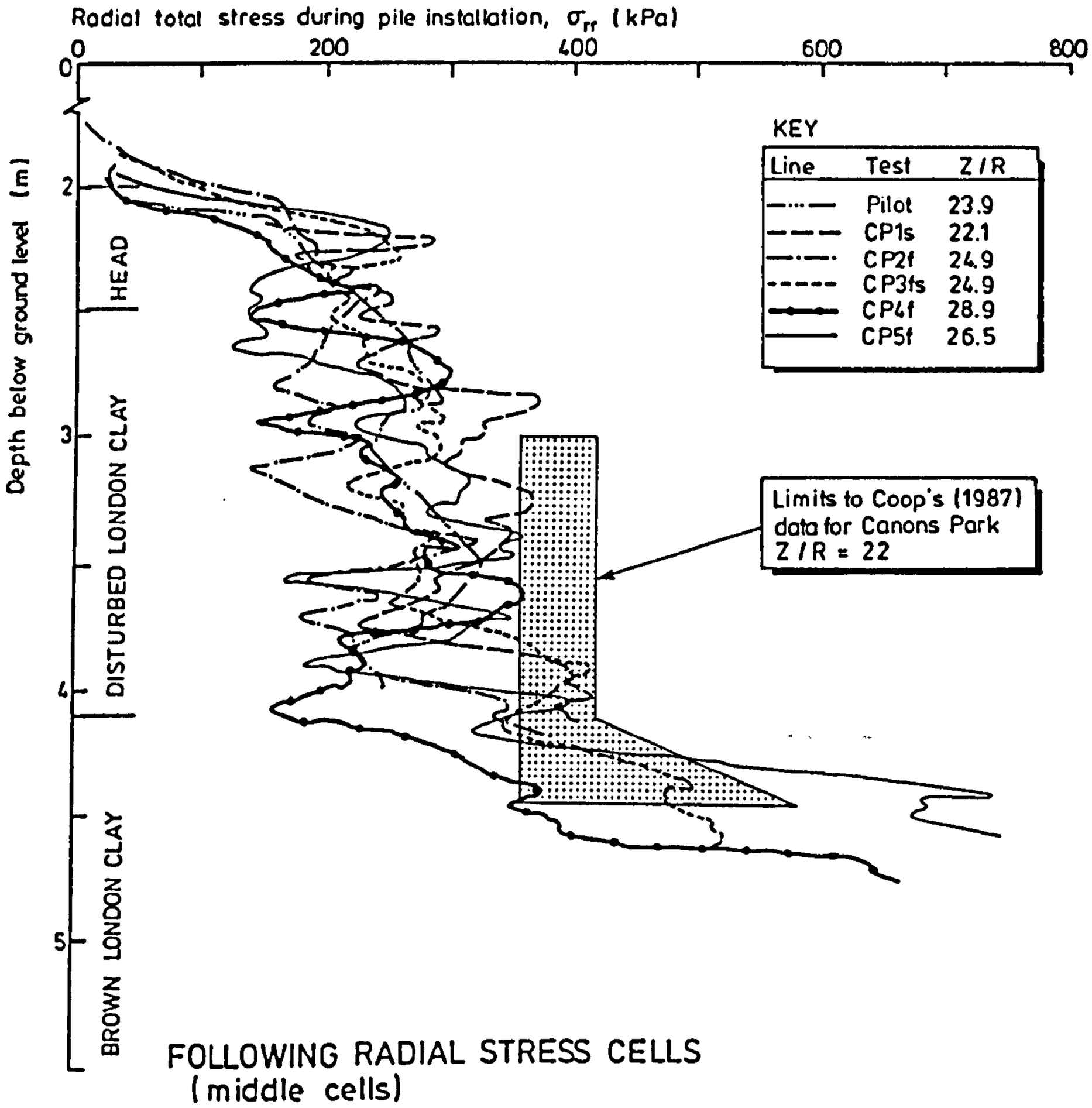



Figure 9.7 Summary diagram: radial total stresses recorded by following instruments during pile installation, Tests CP0-5

Superimposed on both figures are the results obtained by Coop[4] at Canons Park. Coop recorded slightly higher values of $\sigma_{rr}$ in the disturbed London clay (410-500kPa for his leading instruments as opposed to 300-400kPa in Tests CP0-5), but almost identical values of $\sigma_{rr}$ in the (undisturbed) brown London clay. This result is not surprising, since the strain path method predicts steep gradients in $\sigma_{rr}$ with distance behind the pile tip for $z/R$ = 0 to 10, but little variation in $\sigma_{rr}$ for $z/R > 10$ (see Chapter 3).

## 9.3.3 The "z/R effect"

The variation in radial total stress with distance behind the pile tip (z) is shown in Figure 9.8 for four separate soil "horizons", as recorded in a single test (CP5f/IN). It is clear from the left-hand diagram that there is a strong and consistent tendency for $\sigma_{rr}$ to reduce with increasing values of z. The right-hand diagram portrays this relationship in terms of the normalized stress $\sigma_{rr}/(\sigma_{rr})_{z/R=10}$, where $(\sigma_{rr})_{z/R=10}$ is the (interpolated) value of $\sigma_{rr}$ at z/R = 10. We see from this figure that the percentage fall in $\sigma_{rr}$ with distance behind the tip is reasonably independent of the value of $\sigma_{rr}$ that acts upon the pile.

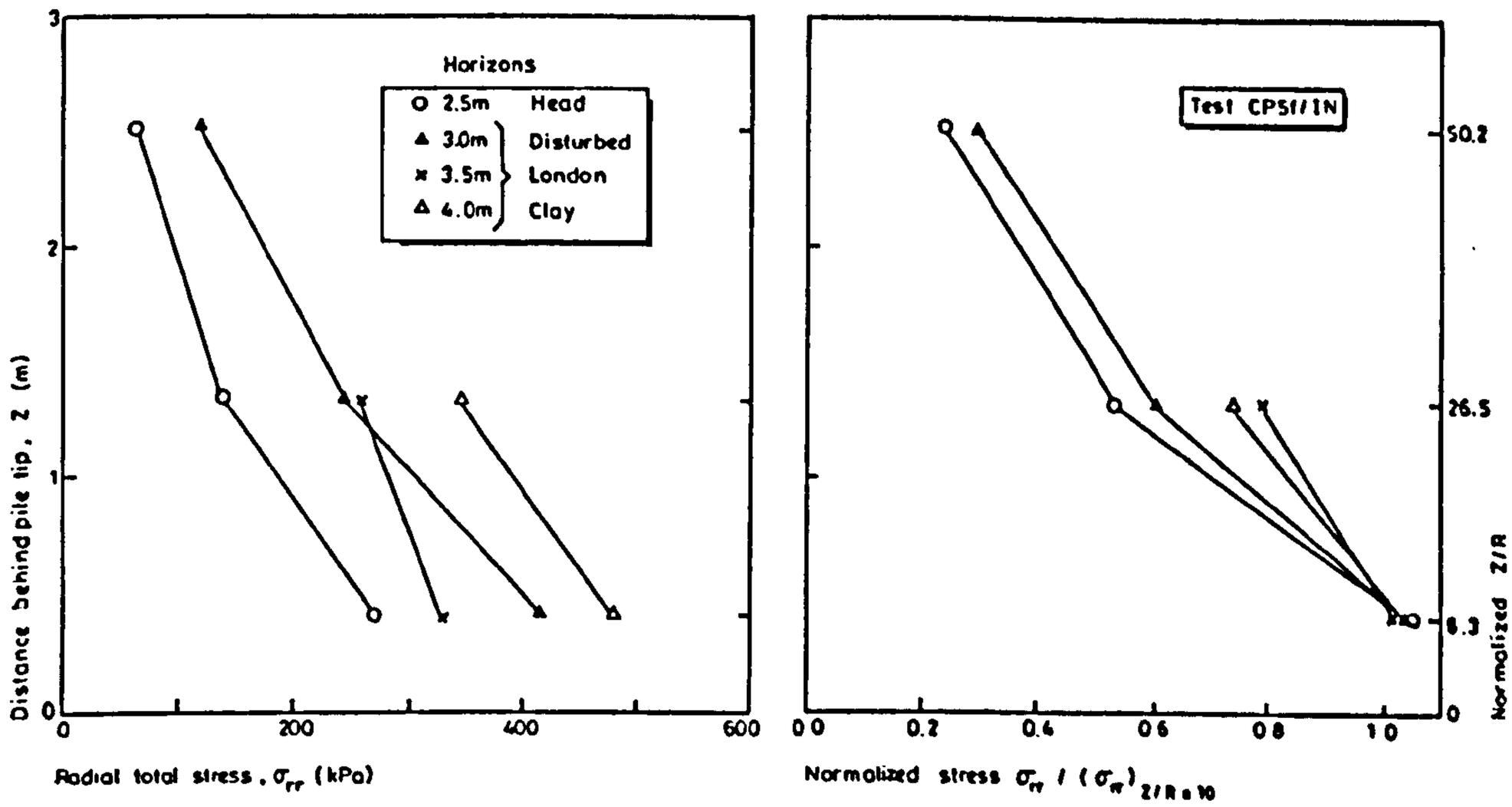



Figure 9.8 Variation in radial total stress with distance behind the pile tip, Test CP5f/IN

Figure 9.8 presents data from a single test (CP5), whereas Figure 9.9 summarizes the results from *four* tests (CP2 to CP5). The left-hand diagram shows the readings obtained at the 3m horizon (in the disturbed London clay); and the right-hand diagram compiles the results four separate horizons.

There is fairly good agreement between the results from the various experiments (the scatter being typically less than ±10% of the mean value of $\sigma_{rr}$, at the 3m horizon). Although the scatter on the normalized diagram

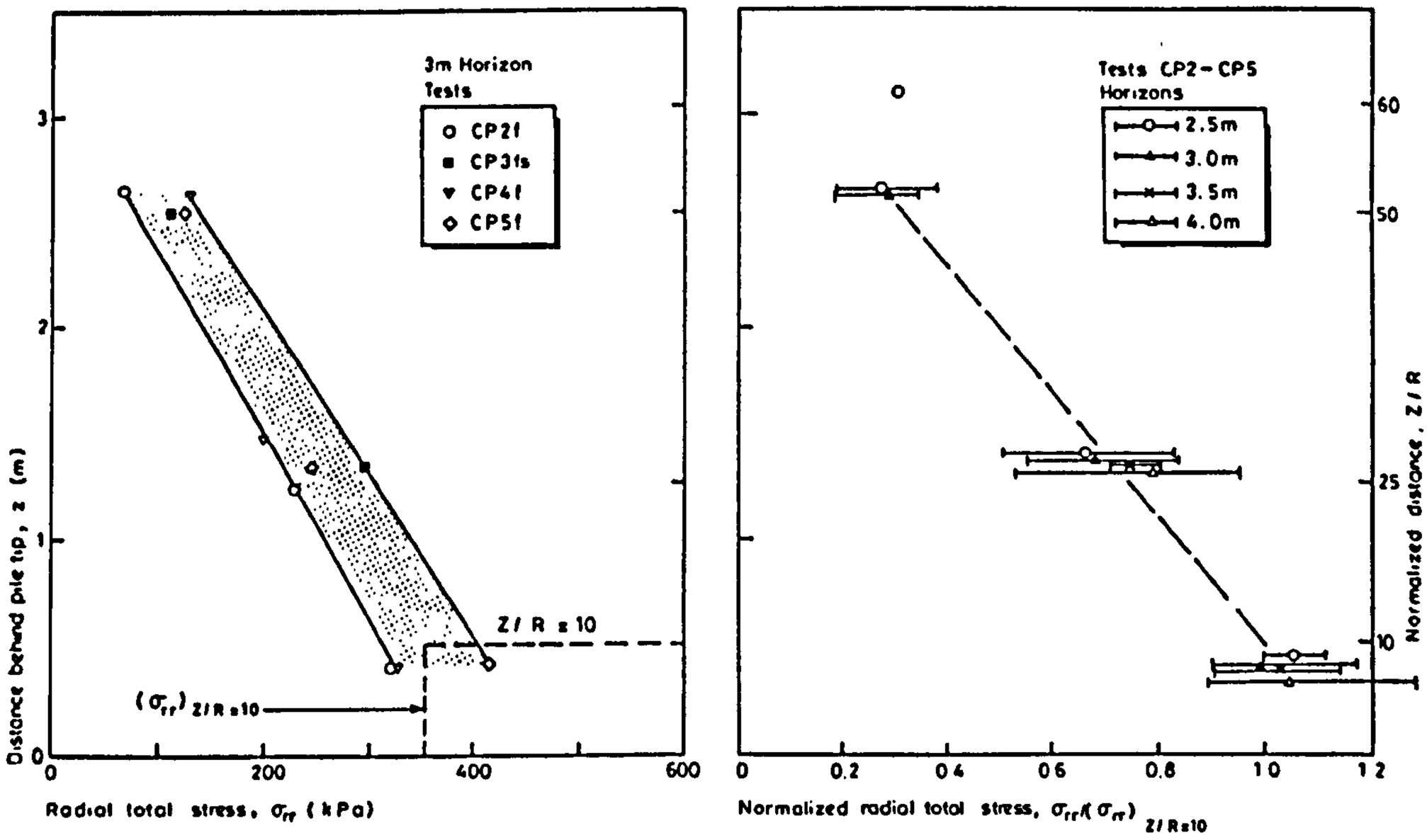



Figure 9.9 Variation in radial total stress with distance behind the pile tip, Tests CP2-5

is quite large at each instrument position (±30%), the trend of the data is clear, with $\sigma_{rr}/(\sigma_{rr})_{z/R=10}$ falling markedly with increasing values of z/R. It is important to appreciate the magnitude of the reduction in $\sigma_{rr}$ with z/R: at a point fifty times the pile radius behind the tip $\sigma_{rr}$ is just under 30% of the value it reached at z/R = 10.

Because the radial total stress varies with position along the shaft, instruments that take measurements at only one location, such as the Piezo-Lateral Stress Cell,[5] cannot provide a complete definition of the stresses developed along the whole length of a pile.

### 9.3.4 Comparison with existing theories

Turning now to comparisons with available theories of pile behaviour: perhaps the most appropriate way to assess the significance of the radial total stress measurements is to compare values of $\sigma_{rr}$ with predictions from the cavity expansion method (CEM) of analysis. A convenient way of doing this is to compare values of $\sigma_{rr}$ with the limit pressures ($p_{lim}$) deduced from self-boring pressuremeter (SBPM) tests.

The starting point for the cavity expansion method is to assume that $\sigma_{rr}$ at the end of pile installation equals the limit pressure, $p_{lim}$. The limit pressure may be estimated by theory or obtained directly, by extrapolating the SBPM pressure vs strain curves to cavity strains equal to infinity. As discussed in Chapter 5, the SBPM tests conducted at Canons Park have been re-interpreted to obtain $p_{lim}$ (see Figure 5.11 on p206). A comparison with the results shown in the summary diagrams (Figure 9.6 and Figure 9.7) reveals that:

- The basic shape of the SBPM limit pressure curve (at a cavity strain $\epsilon_c = \infty$) agrees quite well with the trend shown by the leading radial stress cells
- The limit pressure curve over-predicts the radial total stresses recorded by the leading cells by ≈50%
- Since the following and trailing instruments record lower values of $\sigma_{rr}$ than the leading ones, the over-prediction is even greater as we move further up the pile
- Hence the cavity expansion method is inaccurate for predicting the radial total stresses acting on very long piles, particularly in heavily overconsolidated clays

### 9.3.5 Radial total stresses at the end of installation

To conclude this section, Figure 9.10 portrays the radial total stresses that act on the pile at the end of installation. There is good agreement between the results from all six experiments, and also with the independent test by Coop. Note that the original in situ horizontal total stress, $\sigma_{ho}$, appears to form a lower bound to the values of $\sigma_{rr}$. The SBPM limit curve is the (putative) upper bound to $\sigma_{rr}$.

Also shown on this diagram is the direction in which $\sigma_{rr}$ changes over the first 36h following pile installation. At the lower levels $\sigma_{rr}$ drops sharply, whereas higher up it generally rises. The tendency for $\sigma_{rr}$ to increase with time suggests that the radial stresses recorded during installation over the depths 2.5-3.5m may be reduced through pile wobble (which should die out with depth).

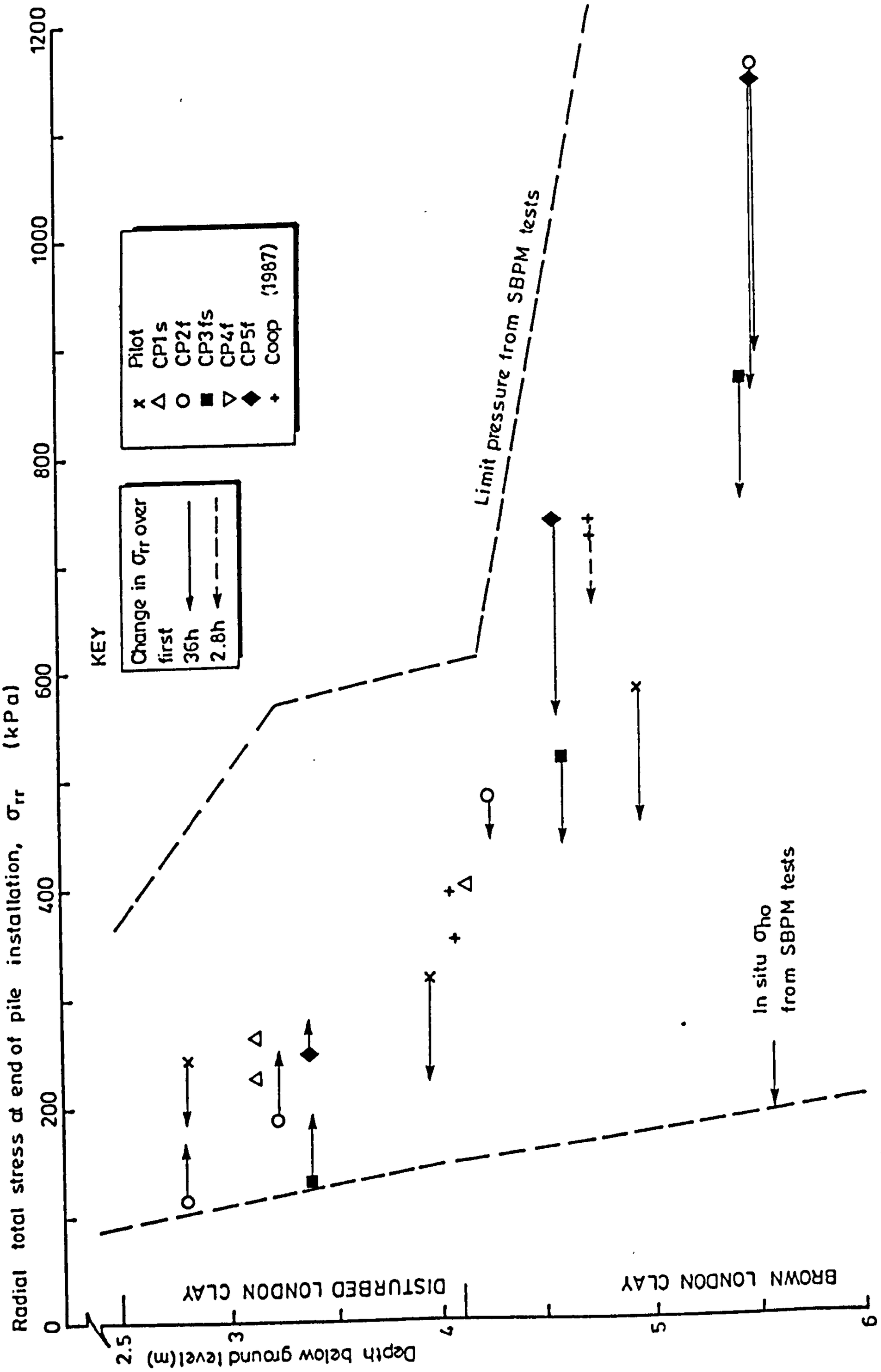



Figure 9.10 Radial total stress along the pile at the end of installation, Tests CP0-5

## 9.4 RADIAL EFFECTIVE STRESSES

### 9.4.1 Summary diagrams for Test Series CP2-5

The radial effective stresses recorded during installation of piles CP2 to CP5 are shown in Figure 9.11 and Figure 9.12, for the leading and following instrument positions (respectively).

Values of $\sigma'_{rr}$ have been calculated by subtracting the average of two pore pressure readings at each instrument level from the (single) measurement of radial total stress. Note that the pore pressure probes are located between 157 and 266mm away from the surface stress transducers, and hence there will be a small error in the calculated values of $\sigma'_{rr}$ because of this. Nevertheless, the figures reveal good agreement between the results of the four tests, particularly for the leading instruments.

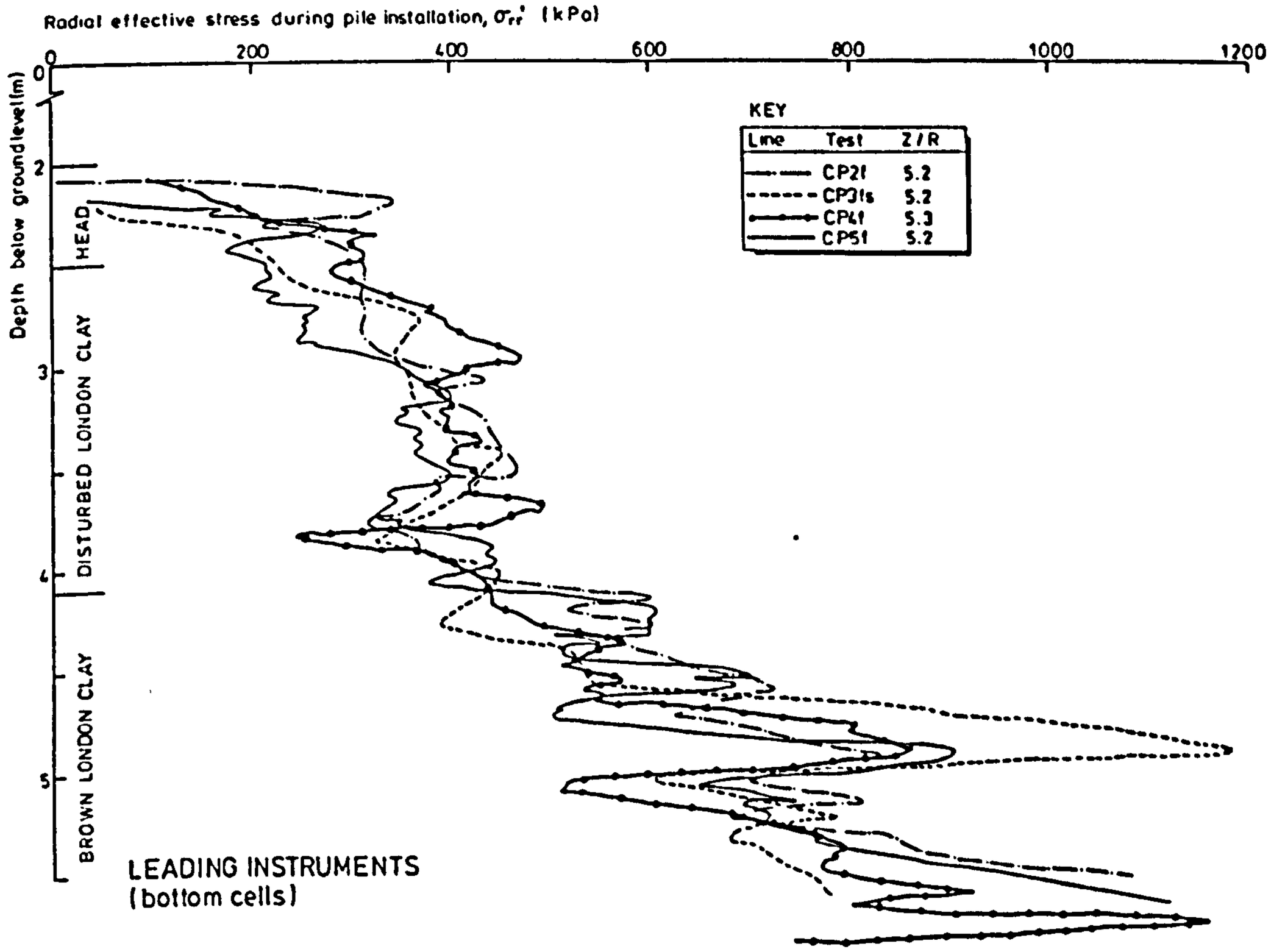



Figure 9.11 Summary diagram: radial effective stresses recorded by leading instruments during pile installation, Tests CP2-5

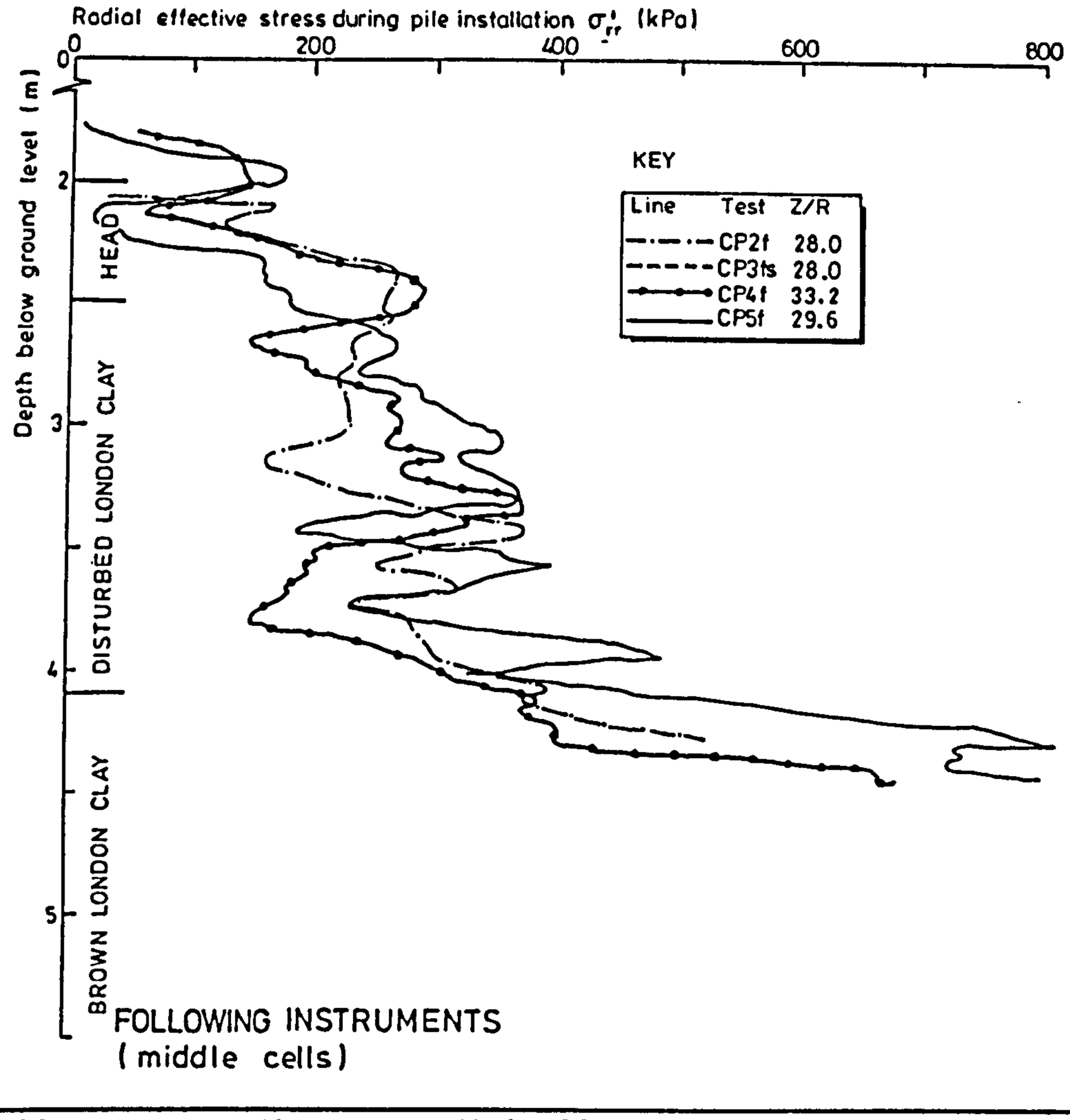



Figure 9.12 Summary diagram: radial effective stresses recorded by the following instruments during pile installation, Tests CP2-5

## 9.4.2 The z/R effect

Figure 9.13 demonstrates the degree to which $\sigma'_{rr}$ falls with increasing values of z/R, in CP2 to CP5. The left-hand diagram gives the absolute values of $\sigma'_{rr}$ measured at the 3m horizon; and the right-hand one the normalized values $\sigma'_{rr}/(\sigma'_{rr})_{z/R=10}$ at four separate horizons. As noted with $\sigma_{rr}$, the normalized curves reveal a consistent trend which is reasonably independent of the soil horizon. The reduction in $\sigma'_{rr}$ with increasing values of z/R is similar to (perhaps slightly less than) the corresponding reduction in $\sigma_{rr}$.

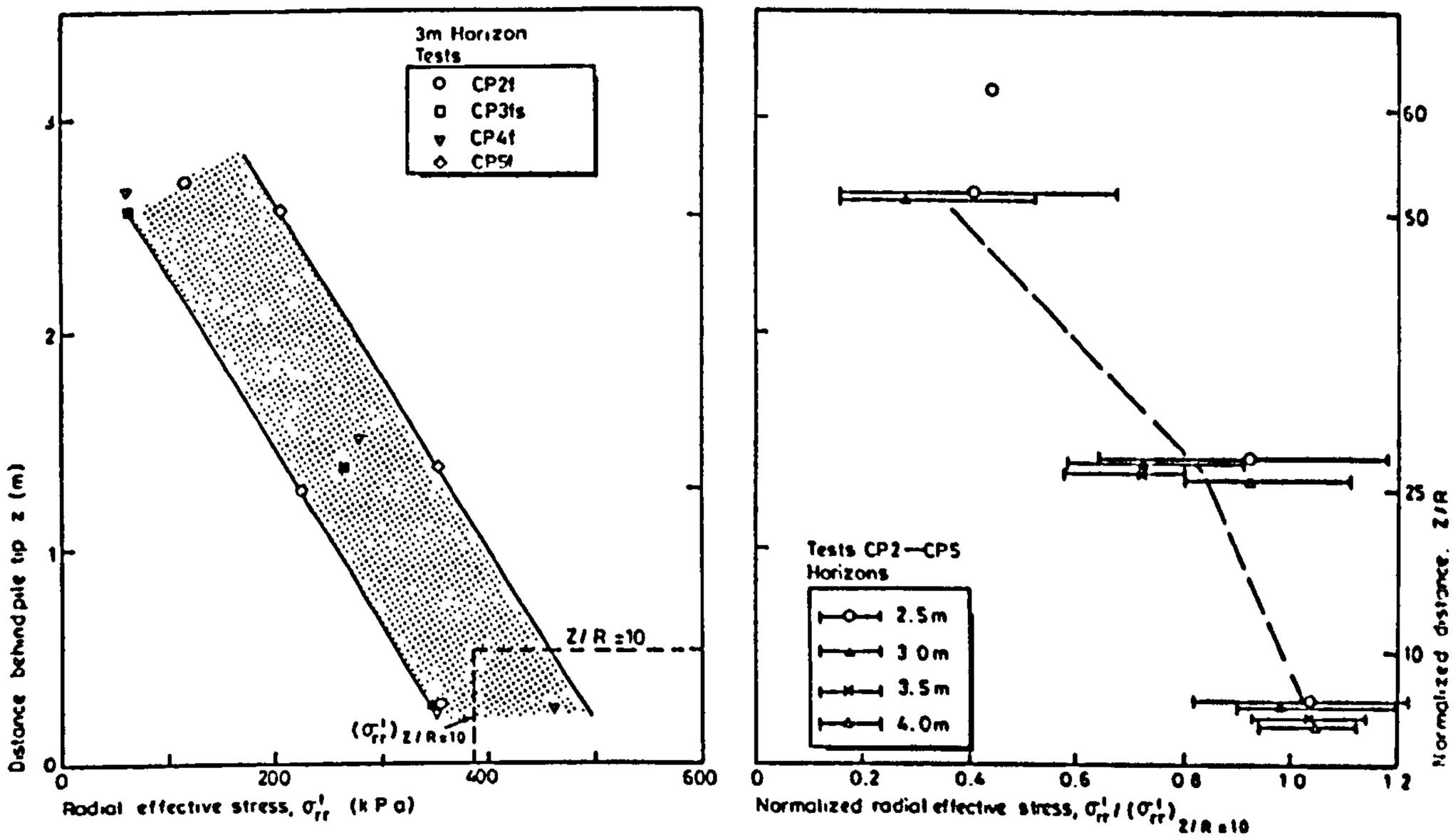



Figure 9.13 Variation of radial effective stress with distance behind the pile tip, Test Series CP2-5

## 9.4.3 Comparison with existing theories

The radial effective stresses at the end of pile installation can be compared with predictions given by the cavity expansion method (CEM), which were reviewed in Chapter 3. For London clay with an over-consolidation ratio of 32, the CEM predicts $K_i$ (= $[\sigma'_{rr}]_i/\sigma'_{vo}$) = 10.4 <u>for a point far behind the pile tip</u>. The measured values of $K_i$ are: 11.3-17.8 at leading; 8.2-10.3 at following; and 3.5-5.7 at trailing instrument positions. The OCR at Canons Park is estimated to be 25-40 over the depths at which these measurements were made (see Chapter 5). The CEM clearly over-estimates the value of $K_i$ where the method is supposed to have its greatest application - at the *trailing* instrument positions.

Strain path predictions have not yet been published for high OCR clays.

## 9.5 SHEAR STRESSES

### 9.5.1 Traces from experiment CP4f/IN

Figure 9.14 shows the shear stresses that were recorded during installation of pile CP4f. The surface stress transducers were mounted at three positions along the pile, approximately one metre apart. Although there is a slight tendency for $\tau_{rz}$ to decrease with distance behind the pile tip, the "z/R effect" is not as strong at that observed for $\sigma_{rr}$.

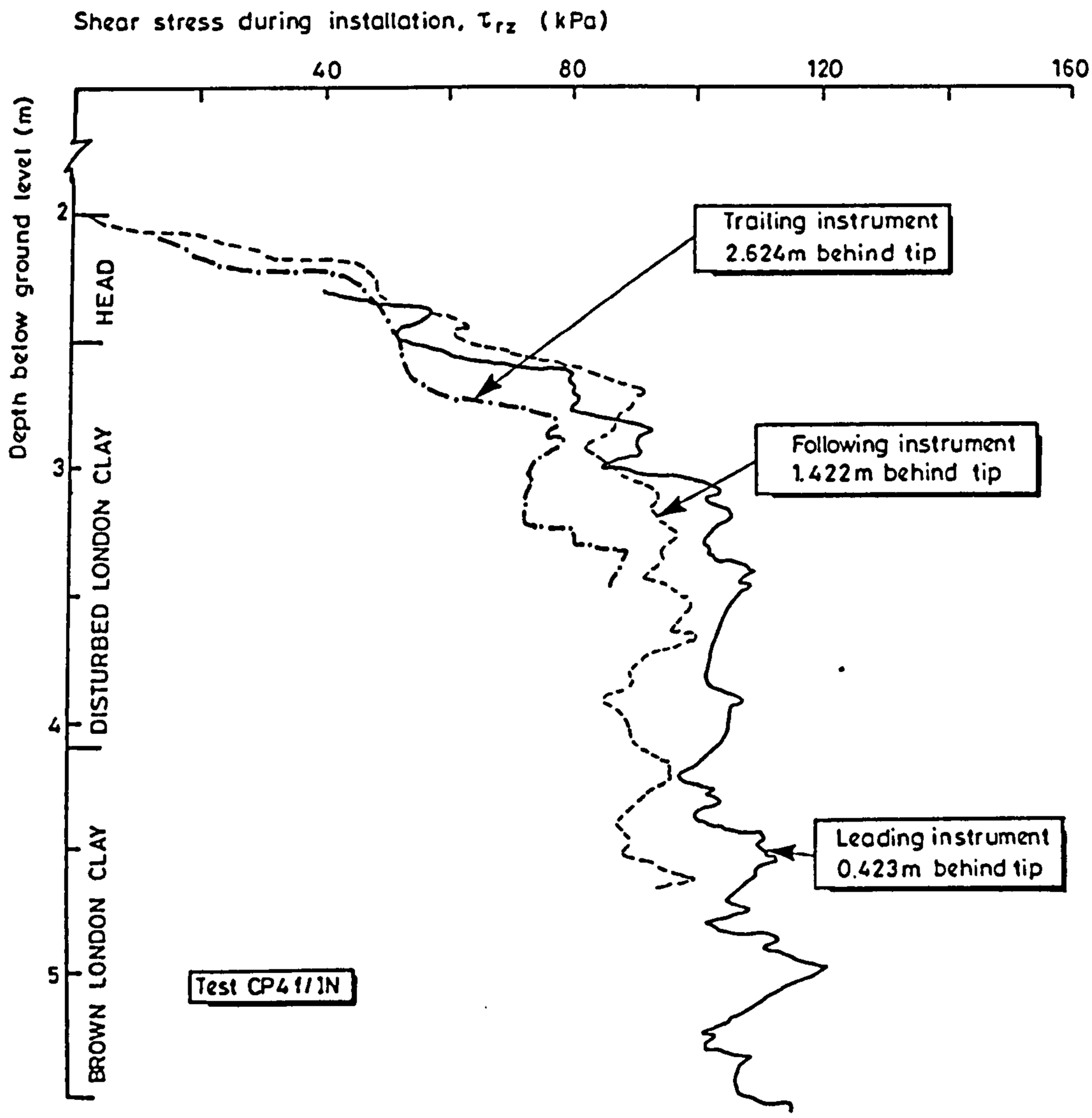



Figure 9.14 Shear stresses recorded during installation of pile CP4f

An independent measurement of the shear stress is provided by computing the shaft friction $f_s$ that acts on the pile, from the axial load cell readings.* There is excellent agreement (to within ±5%) between the readings of $r_{rz}$ and $f_s$ (not shown).

### 9.5.2 Summary diagrams for Test Series CP0-5

Figure 9.15 and Figure 9.16 show the shear stresses recorded during pile installation by the leading and following surface stress transducers (respectively), for Test Series CP0 to CP5. All of the piles were installed at a fast rate, save for CP1s (installed slowly throughout) and CP3fs (whose jacking rate was changed from fast to slow for the final 1.8m of penetration).

The first conclusion to be drawn from these diagrams is that the slow installed piles mobilize 50% less shearing resistance than the fast installed ones.

The acid test of this conclusion is experiment CP3fs, in which the rate of installation was reduced suddenly from fast to slow when the pile tip had reached a depth of 4.08m. The corresponding depths of the instruments when this change was made are highlighted on the diagrams by the star symbols. The behaviour of the leading cell in unequivocal, showing an immediate drop in $r_{rz}$. The traces for the following cell re-adjust more slowly; but nevertheless they migrate away from the family of curves for the fast-jacked piles (CP2f, CP4f, and CP5f), and towards the two (independent) traces recorded by the slow-jacked pile CP1s. (Note that in Test CP1s there were no leading surface stress transducers, but dual sensors were mounted at the following instrument position.)

### 9.5.3 Correlations with the clay's undrained shear strength

By correlating the shear stress measurements with the clay's original undrained shear strength, we can comment on the fundamental basis of the

---

*$f_s = (1/\pi D)(\delta Q/\delta l)$, where $(\delta Q/\delta l)$ is the rate of change of Q along the pile's length (l); and D is the pile's diameter

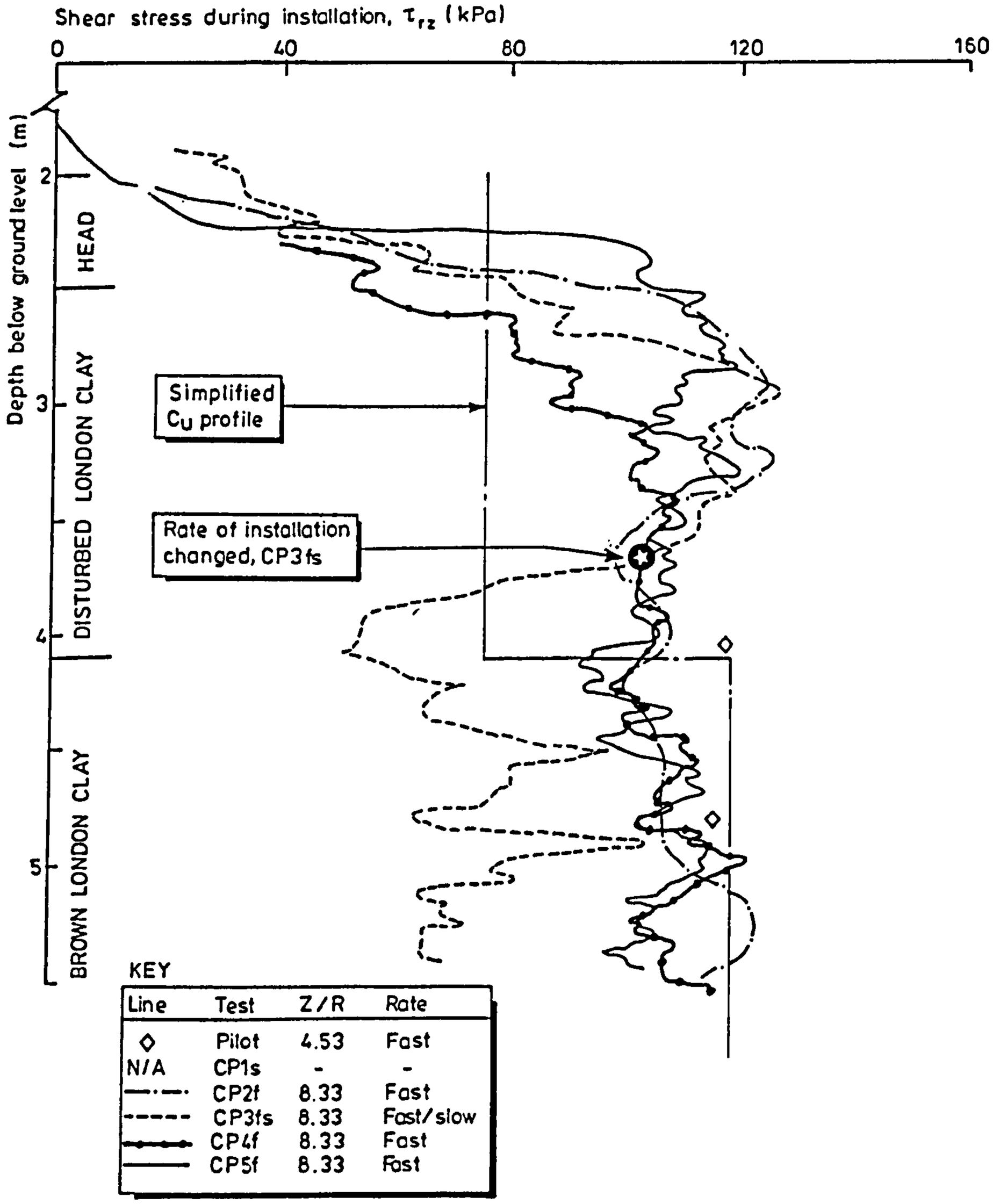



Figure 9.15 Summary diagram: shear stresses recorded by leading instruments during pile installation, Tests CP0-5

total stress approach to pile design (the $\alpha$-method).

As Figure 9.15 and Figure 9.16 reveal, there is little correspondence between the profiles of $\tau_{rz}$ and $c_{uo}$. In particular, the traces of $\tau_{rz}$ do not respond to the sharp jump in $c_{uo}$ at a depth of 4.1m, i.e. at the junction between the disturbed and the brown London clay. The consequence of the above is that the "local" values of $\alpha$ ($= \tau_{rz}/c_{uo}$) vary greatly along the pile. (Note that the values of $\alpha$ for the subsequent pile tests

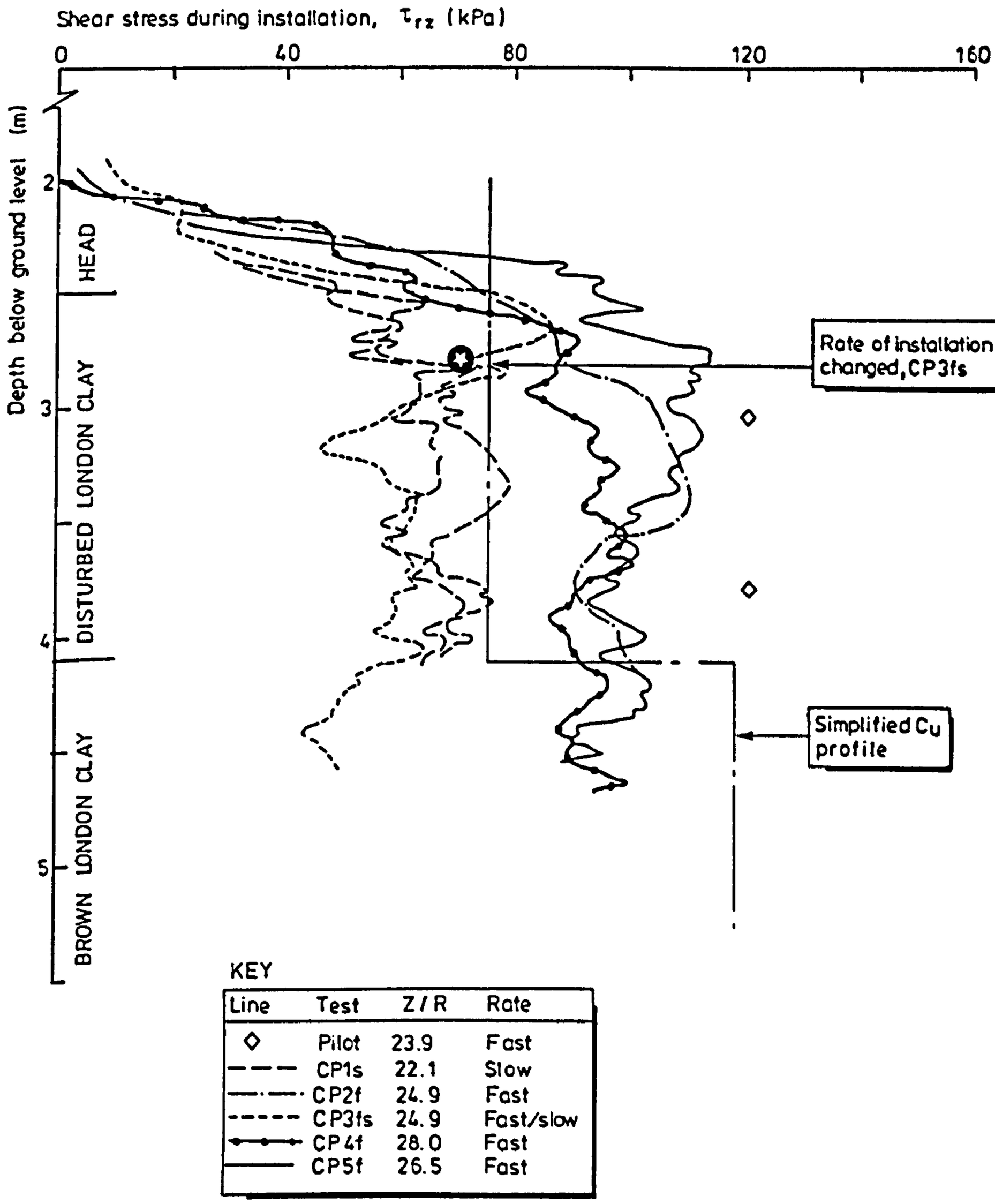



Figure 9.16 Summary diagram: shear stresses recorded by following instruments during pile installation, Tests CP0-5 [n.b. there are two *independent* traces for CP1s]

are based on the undrained shear strength profile shown in these diagrams.)

## 9.5.4 The rate effect in terms of average α values

The large difference between the shear stresses mobilized by fast- and slow-jacked piles can be summarized by plotting the average α value for

each pile (= $Q_{shaft}/\pi DL(c_{uo})_{av}$) against its rate of installation (v) - as shown in Figure 9.17. The values of $\alpha$ and $\beta$ (= $Q_{shaft}/\pi DL(\sigma'_{vo})_{av}$) plotted on this diagram are based on the loads recorded during the final 1m of penetration. Included on the figure are the data from the other pile tests at Canons Park (by Price and Wardle,[6] Kitching,[7] and Coop[8]); and the Fugro cone-test measurements of average skin friction ($f_s$).[9] Also drawn

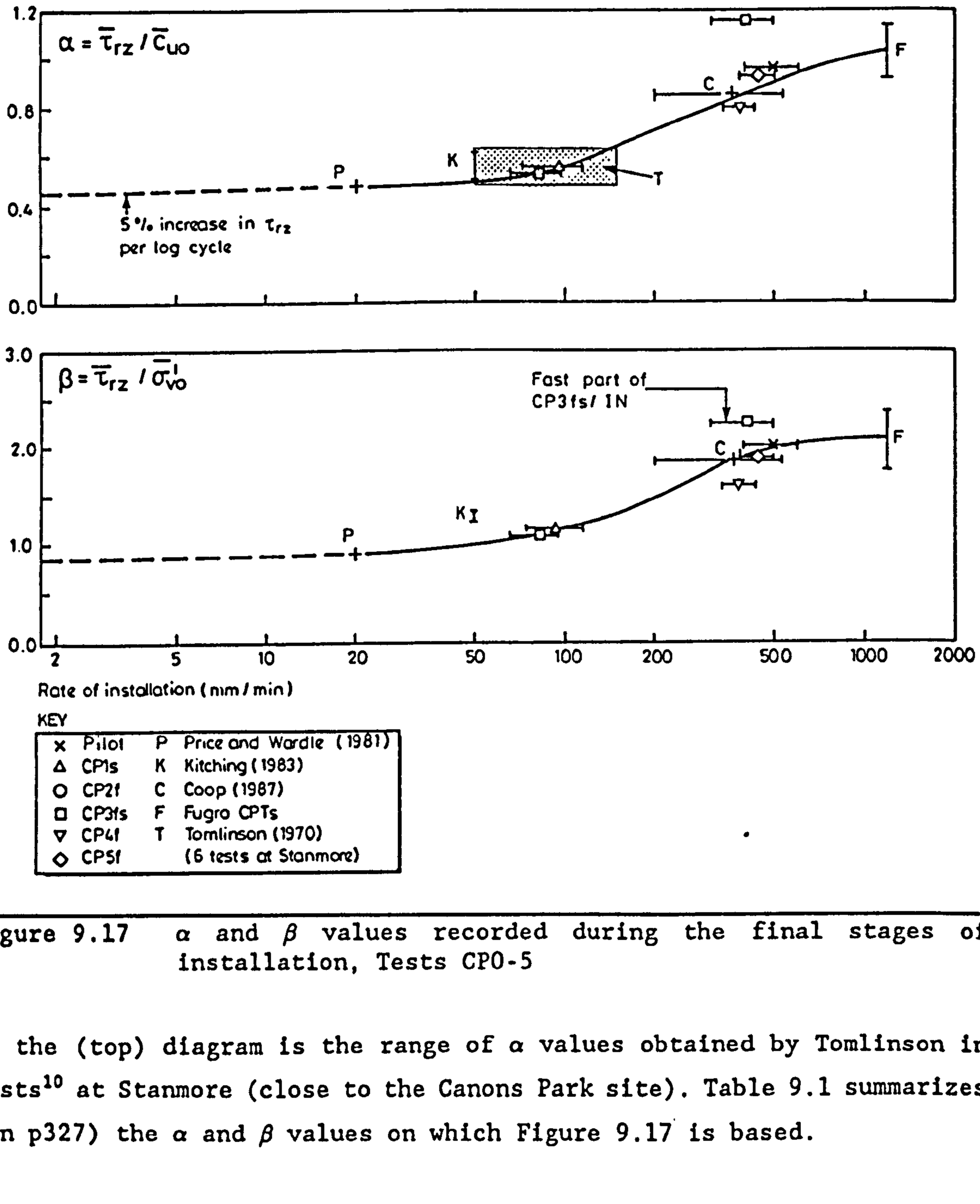



**Figure 9.17** $\alpha$ and $\beta$ values recorded during the final stages of installation, Tests CP0-5

on the (top) diagram is the range of $\alpha$ values obtained by Tomlinson in tests[10] at Stanmore (close to the Canons Park site). Table 9.1 summarizes (on p327) the $\alpha$ and $\beta$ values on which Figure 9.17 is based.

As the diagram reveals, $\alpha$ and $\beta$ are slightly rate-dependent (≈5% per log cycle) for velocities below 50mm/min; but at faster rates the trend line

through the data points climbs steeply, with a gradient of about 100% per log cycle. This remarkable rate effect closely matches that seen in laboratory tests in the ring-shear apparatus (see Chapter 5).

### 9.5.5 The z/R effect

The reduction in the value of $\tau_{rz}$ with increasing distance behind the pile tip is shown in Figure 9.18 (for Test Series CP2-5). Included on this diagram are readings of shaft friction $f_s$, plotted at the mid-points

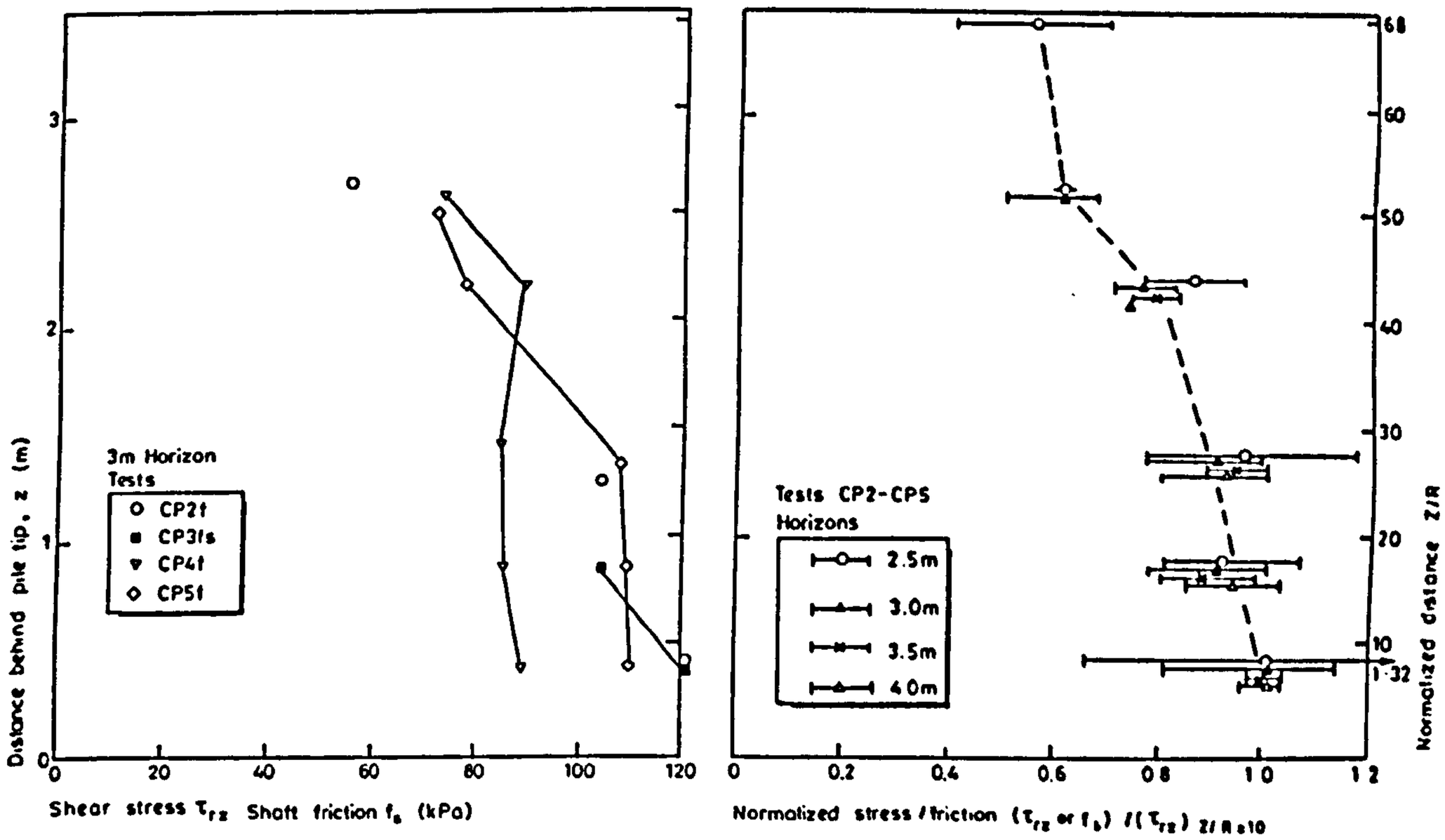



Figure 9.18 Variation in shear stress with distance behind the pile tip, Tests CP2-5

between the axial load cells. The left-hand diagram shows the absolute values of $\tau_{rz}$ recorded at the 3m horizon only (in the disturbed London clay); and the right-hand diagram shows values normalized by $(\tau_{rz})_{z/R=10}$, the interpolated value of $\tau_{rz}$ at z/R = 10, at four separate horizons.

The variation of $\tau_{rz}$ and $f_s$ with z/R is far less marked than that found for $\sigma_{rr}$: at z/R = 50, $\tau_{rz}/(\tau_{rz})_{z/R=10}$ equals 0.65, whereas the corresponding ratio for $\sigma_{rr}/(\sigma_{rr})_{z/R=10}$ was 0.3.

## 9.6 DISCUSSION

The main conclusions that arise from the results presented in this chapter are:

i) The quality of the data obtained in the present series of experiments is very high, with excellent agreement between repeated tests and between independent measurements of the principal parameters.

ii) The stress state in the ground is altered considerably by pile installation. As the pile tip approaches a particular horizon, the radial total stress increases many fold and the soil dilates strongly. The radial effective stresses recorded at the leading instrument position increase markedly with depth (at an overall rate of ≈180kPa/m), but also fluctuate in response to changes in the soil's undrained shear strength.

iii) A feature of the soil's dilation is the development of <u>negative</u> pore water pressures over most of the pile's shaft length.

iv) Once the pile tip has punched through a particular horizon, the radial stresses (both total and effective) <u>at that depth</u> tend to fall rapidly with continued penetration of the pile. This has been termed the "z/R effect". For points more than fifty pile radii above the tip, both $\sigma_{rr}$ and $\sigma'_{rr}$ reduce to less than a third of their maximum values.

v) The profiles of $\sigma_{rr}$ and $\sigma'_{rr}$ with depth at the end of installation therefore reflect both a) the variation of soil properties and the original in situ stresses; and b) the relative position of each point above the pile tip.

vi) The cylindrical cavity expansion analogy greatly over-predicts the radial total stresses acting on the pile shaft. This over-prediction increases systematically with z/R. However, at the end of installation $\sigma_{rr}$ and $\sigma'_{rr}$ exceed their original (undisturbed) values everywhere along the pile.

vii) The recorded shear stresses show less variation with depth and with z/R than the radial stresses. However, the localized (and hence the overall) skin frictions are strongly dependent on the rate of pile penetration. The radial stresses show no such rate-dependency.

viii) The variations in $\tau_{rz}$ with depth show no particular relationship either with the clay's original undrained shear strength or with the original vertical effective stress. This finding suggests that there is little fundamental basis to either the $\alpha$ or $\beta$ methods of pile design.

ix) The $\alpha$ and $\beta$ values measured towards the end of installation are surprisingly high: for fast-jacked piles $\alpha$ approaches 1.0 in the heavily overconsolidated London clay.

Table 9.1 Summary of alpha values recorded during pile installation

| Load test | Installation rate | Axial load Q (kN) Head | Toe | Shaft | $\alpha$ | $\beta$ | Rate of travel (mm/min) |
|---|---|---|---|---|---|---|---|
| CP0f | Fast | +108 | +22 | +86 | +0.96 | +1.98 | ≈500 ±20% |
| CP1s | Slow | +69.1 | +18.4 | +50.7 | +0.55 | +1.13 | 94 ±22 |
| CP2f | Fast | +123? | +20.1 | (+103) | (+0.88) | (+1.77) | 426 ±34 |
| CP3fs | Fast/ | +63.8 | +11.2 | +52.6 | +1.16 | +2.33 | 403 ±94 |
| | slow | +81.5 | +20.7 | +60.8 | +0.53 | +1.08 | 81 ±15 |
| CP4f | Fast | +126.5 | +24.5 | +102.0 | +0.80 | +1.60 | 488 ±45 |
| CP5f | Fast | +127.0 | +21.1 | +105.9 | +0.93 | +1.88 | 445 ±55 |
| Price | Slow | +164.5 | +57.6 | +106.9 | +0.48 | +0.90 | 20 ±? |
| Kitching | Slow | +158 | +40½ | +117½ | +0.53 | +1.33 | 50? |
| Coop | Fast | - | - | +18.75 | +0.85 | +1.84 | 200-540 |

$\alpha = Q_{shaft}/\pi DL(c_{uo})_{av}$; $\beta = Q_{shaft}/\pi DL(\sigma'_{vo})_{av}$
CP0-5: D = 101.6mm; for L see Table 7.2
Price & Wardle (1981): D = 168mm; L = 4.5m
Kitching (1983): D = 177.8mm; L = 4.675m
Coop (1987): D = 80mm; L = 0.74m

## 9.7 NOTES AND REFERENCES

[1]Coop M.R. (1987). The axial capacity of driven piles in clay. DPhil Thesis, Univ. of Oxford.

[2]The observations made during CP0f and CP1s must be disregarded because of the relatively slow response times of the pore pressure probes used in those experiments; Coop's pore pressure readings should be treated with circumspection for the same reason.

[3]The z/R effect can also be found in the results of pile tests in the London clay from the Hampshire Basin. See Johnston I.W. (1972). Electro-osmosis and porewater pressures; their effect on the stresses acting on driven piles. PhD Thesis, Southampton Univ; and the review of his work in Chapter 4.

[4]Coop (1987), loc. cit.

[5]Baligh M.M., Martin R.T., Azzouz A.S., and Morrison M.J. (1985). The Piezo-Lateral Stress cell. Proc. 11th Int. Conf. Soil Mech. & Fdn Engng, San Francisco, 2, pp841-844.

[6]Price G. and Wardle I.F. (1982). A comparison between cone penetration test results and the performance of small diameter instrumented piles in stiff clay. Proc. 2nd Eur. Symp. on Penetration Testing (ESOPT II), Amsterdam, 2, pp775-780. A.A. Balkema, Rotterdam, 1982.

[7]Kitching D.N. (1983). A study into the microfabric of clays adjacent to jacked piles. MSc Dissertation, Univ. of London (Imperial College), 31pp+.

[8]Coop (1987), loc. cit.

[9]Fugro Limited (1980). Static cone penetration tests at Canons Park, London. Project no U0662. Soils investigation report, 2pp + figures.

[10]Tomlinson M.J. (1970a). Adhesion of piles in stiff clays. CIRIA Report 26, Construction Industry Research and Information Association, London, 47pp. Data from the jacked pile tests only. Note that Tomlinson's $\alpha$ values were based on unrealistically low (calculated) values of end-bearing: the $\alpha$ values shown on the figure herein have been re-calculated on the basis of an $N_k$ value of 16.5.

# Chapter 10

# Results of instrumented pile tests: equalization period

CONTENTS OF CHAPTER 10


10.1 INTRODUCTION . . . . . 332

10.2 PORE PRESSURE DISSIPATION . . . . . 333

10.2.1 Typical pore pressure response over the first two days 333

10.2.2 The excess pore pressure ratio, $\Delta u/\sigma'_{vo}$ 334

10.2.3 Values of the coefficient of horizontal consolidation 336

10.3 RELAXATION OF RADIAL TOTAL STRESSES . . . . . 338

10.3.1 Results of long-term experiments CP0 and CP2 338

10.3.2 The normalized horizontal total stress H 338

10.3.3 Radial total stresses after 36h 341

10.4 CHANGES IN RADIAL EFFECTIVE STRESS . . . . . 342

10.4.1 Changes in radial effective stress over the first two days 342

10.4.2 Radial effective stresses after 36h 343

10.4.3 Comparison with existing theories 343

10.5 RESULTS OF SPECIAL TESTS ON PILE CP4f . . . . . 345

10.5.1 Falling-head permeability tests CP4f/FHK 345

10.5.2 Hydraulic fracture tests CP4f/HF 346

10.6 DISCUSSION . . . . . 349

10.7 NOTES AND REFERENCES . . . . . 350

## 10.1 INTRODUCTION

A notable feature of the instrumented pile tests was the way in which the earth and pore water pressures changed very rapidly during the first few days following pile installation. As explained in Chapter 7, set-up periods of between 2 and 109 days were allowed before load testing, and the information gathered in the long-term tests enabled the equilibrium conditions around the piles to be assessed.

This chapter presents the data recorded during the equalization period, looking in turn at the dissipation of pore pressures (Section 10.2); the relaxation of the radial total stresses (Section 10.3); and finally the resultant changes in radial effective stresses (Section 10.4).

The results of the falling-head permeability and hydraulic fracture tests on pile CP4f are reported (briefly) in Section 10.5.

## 10.2 PORE PRESSURE DISSIPATION

### 10.2.1 Typical pore pressure response over the first two days

Figure 10.1 displays the pore pressures measured over the first 44h[1] of equalization in Test Series CP5f. The dissipation curves for Tests CP1-4 are given in Appendix 12. These traces reveal the following important features:

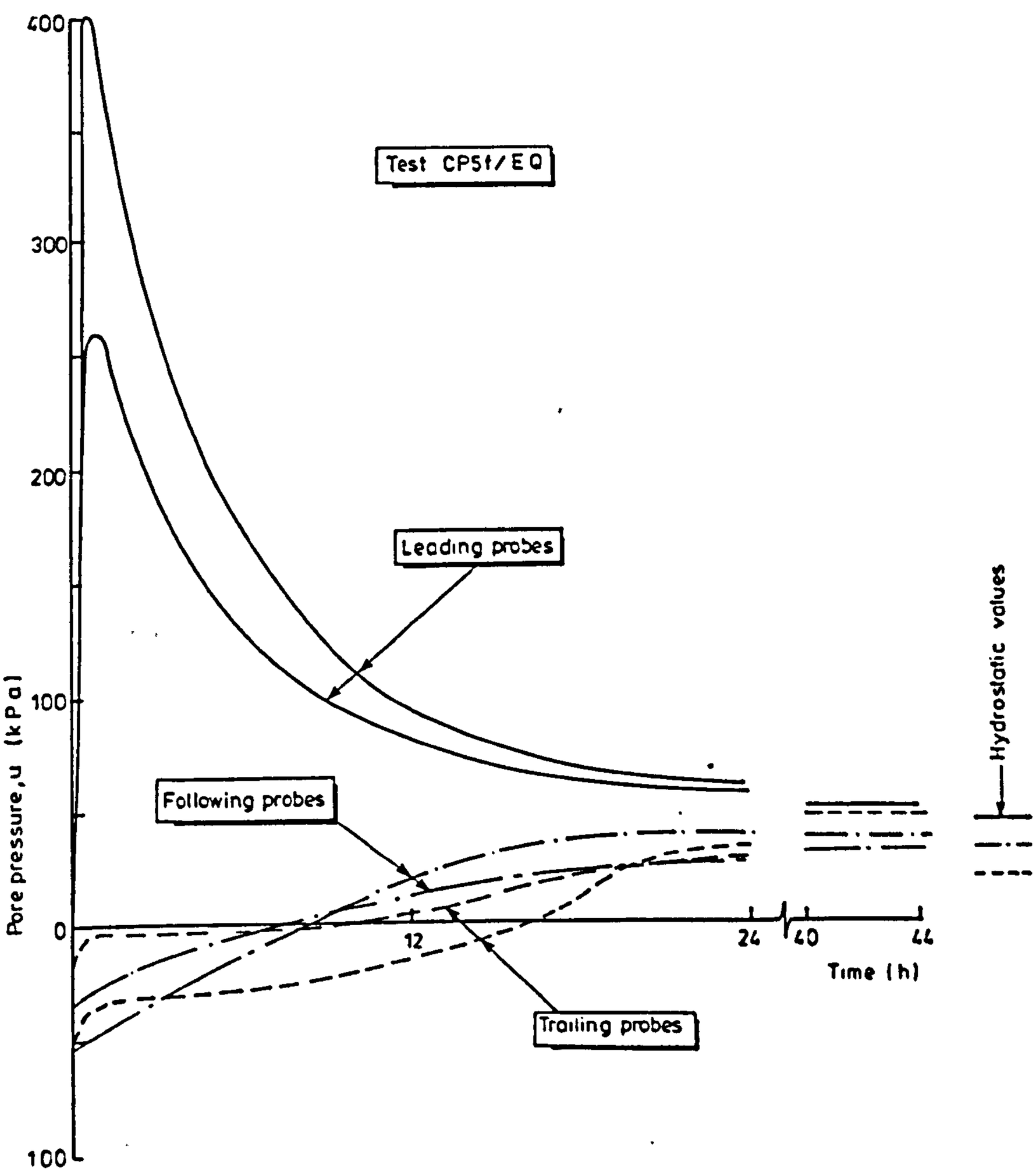



Figure 10.1 Pore pressure response during first 44h after pile installation, Test CP5f

- At *leading* instrument positions large positive pore pressures develop shortly after installation and then decay to just above hydrostatic values within ≈40h
- At *following* and *trailing* positions the pore pressures rise slowly from their negative, end-of-installation values, and approach hydrostatic levels after ≈40h
- The sole difference between the results from Tests CP2f, CP3fs, CP4f, and CP5f is in the response recorded at the following instrument positions: in CP2f the pore pressures rose significantly above the hydrostatic value (more than 200kPa above), and then dropped from their peak values along decay curves similar to those observed by the *leading* probes (see Appendix 12 for further details)

### 10.2.2 The excess pore pressure ratio, $\Delta u/\sigma'_{vo}$

The best way to compare the dissipation curves from different tests is to normalize the excess pore pressures by the original vertical effective stress in the ground ($\sigma'_{vo}$). The "excess pore pressure ratio" ($\Delta u/\sigma'_{vo}$) is defined as:

$$\Delta u/\sigma'_{vo} = (u - u_o)/\sigma'_{vo}$$

Figure 10.2 portrays the variation of $\Delta u/\sigma'_{vo}$ with time (plotted to a logarithmic scale) in Test Series CP2-5. In these experiments the pore pressures were measured using the fast-acting probes described in Chapter 6. (The readings from CP1 - using a different design of probe - have been omitted, because of slow response times during pile installation - see Appendix 9.)

The dissipation curves shown in Figure 10.2 follow one of two basic patterns, depending on whether they were recorded by *leading* or *following* probes. The *leading* traces display the following features:

- The pore pressures rise sharply as soon as the pile stops moving, and then fall steadily and monotonically with time

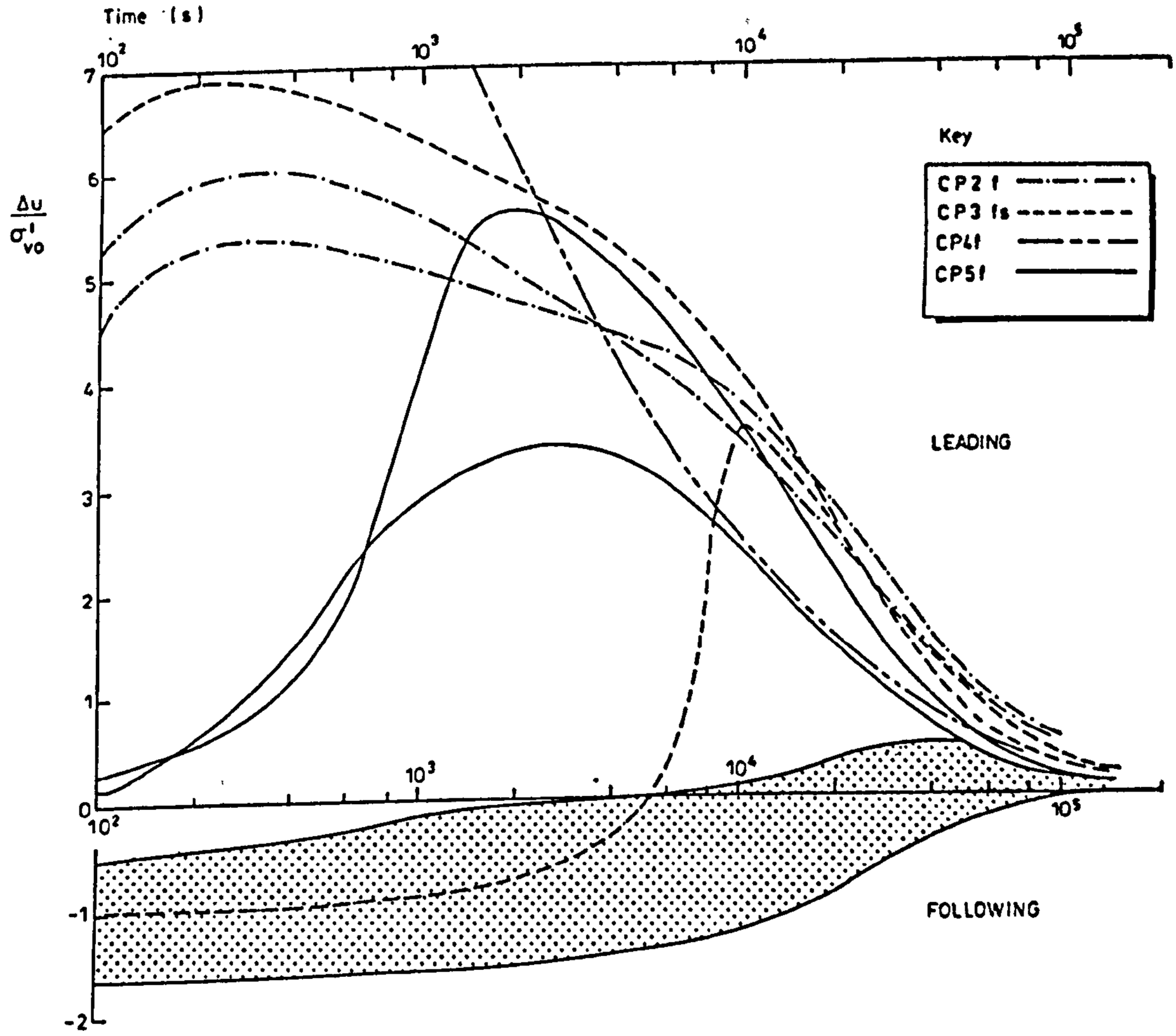



Figure 10.2 Excess pore pressure ratio vs log time, Tests CP2-5

- The pore pressure ratio at the start of equalization ($\Delta u_i/\sigma'_{vo}$) is typically less than 1.5, and in three cases is less than zero (note that Figure 10.2 doesn't show the rise in pore pressure over the first 100 seconds)
- The maximum pore pressure recorded by the leading probes is conditioned by their speed of response: in general, the faster the "rise time" the greater the value of $\Delta u_{max}/\sigma'_{vo}$
- The rise times vary from 103s (1.7 minutes) in Test CP4f to $2.5 \times 10^3$s (42 minutes) in CP5f (the trace from CP3fs with the rise time of $\approx 10^4$s is out of sync with its partner, suggesting that the sluggishness of this trace is due to a problem with the probe's response time)
- Between $10^4$s and $10^5$s (2.8 and 28h), all but two of the dissipation curves fall within a very narrow band

- The largest pore pressure recorded in any experiment (783kPa in Test CP4f) gives $\Delta u_{max}/\sigma'_{vo}$ = 11.1; however, in all the other tests $\Delta u_{max}/\sigma'_{vo}$ is in the range 5.6-6.9 (taking the higher of the two values recorded in each test)

The pore pressure response at the *following* instrument positions is completely different to that described above. As the shaded band on Figure 10.2 shows:

- The excess pore pressure ratio ($\Delta u/\sigma'_{vo}$) is *negative* at the start of the equalization period, and remains negative for a long time thereafter
- *Positive* excess pore pressures are not recorded until at least 1½h ($5 \times 10^3$s) into the equalization period, and in some cases not even after thirty hours ($10^5$s) have elapsed
- The values of $\Delta u_{max}/\sigma'_{vo}$ in Tests CP3fs, CP4f, and CP5f are very small (based on the higher of the two values recorded in each test, $\Delta u_{max}/\sigma'_{vo}$ = 0.83, 0.35, and 0.21 respectively)
- The only exception to this pattern is the behaviour recorded in Test CP2f (these curves are not shown on Figure 10.2 - see Appendix 12 instead): in this experiment the following traces repeat the pattern of the leading ones, but have slower rise times and hence smaller maxima*

In all five experiments (CP1-5), the traces recorded at *trailing* instrument positions were similar to those obtained at the following positions.

## 10.2.3 Values of the coefficient of horizontal consolidation

From Figure 10.1 it is clear that the bulk of the pore pressure changes occur within 36h of pile installation, despite the clay's low permeability ($\approx 10^{-11}$m/s according to the falling-head permeability tests

---

*The reason for this behaviour is not known, although if the response of the leading probes is attributed to their location in a more permeable stratum than the other probes (see Chapter 14) then perhaps the following probes in CP2f were also in a more permeable layer of soil

described in Section 10.5.1). Values of $c_h$, the coefficient of horizontal consolidation,* can be determined from these curves only if the initial pore pressure distribution around the pile is known. There is no current theory that predicts negative pore pressures adjacent to displacement piles, and hence no reliable theory for determining $c_h$.

One approach to the problem is to match the theoretical decay curves given by linear consolidation theory with the "post-peak" decline in pore pressure at the leading instrument positions (this cannot be done with the traces recorded by the *following* and *trailing* probes). This approach ignores the rise in pore pressure that occurs over the first 2000s (half an hour), and concentrates instead on the fall in pressure from its *maximum* value ($\Delta u_{max}$).

The selection of suitable theoretical curves for comparison with the field data is not an easy matter. The decay of pore pressure at the pile wall is strongly influenced by the *distribution* of pressures in the soil at the start of the equalization period (or rather ½h into it). For this exercise I have used the pore pressure field predicted by the strain path method (see Chapter 3). The decay curves for this case are given in Teh's PhD Thesis[2] and are reproduced here in Figures 3.17 and 3.18 (see pp101-102). $\Delta u/\Delta u_{max}$ replaces $\Delta u/\Delta u_i$ on the left-hand scale of these diagrams.#

According to this highly approximate analysis, the value of $c_h$ (as calculated from the leading traces in Tests CP2-5) is between 1.17 and 2.38mm$^2$/s (37 and 75m$^2$/year). Note the similarity between these figures and the values of $c_h$ that have been deduced for other clay soils (see Table 2.1 on p34).

---

*For non-linear materials $c_h$ is not a constant and so cannot be defined as a soil property

#I have used Teh's time factor $T^* = c_h t/R^2\sqrt{(G/c_{uo})}$, with $G/c_{uo} = 100$

## 10.3 RELAXATION OF RADIAL TOTAL STRESSES

### 10.3.1 Results of long-term experiments CP0 and CP2

Three of the Canons Park experiments involved load tests after a long equalization period (≥ 50 days). These were the Pilot Test (CP0), CP1, and CP2. Unfortunately, the radial total stresses recorded during CP1 became unreliable after just a few days, and so these readings have had to be ignored. Figure 10.1 shows the changes in $\sigma_{rr}$ as observed in the other two tests.

The radial total stress $\sigma_{rr}$ reduces rapidly at the *leading* instrument positions (marked with the letter L), and also falls (but less dramatically) at the *following* positions (F). Further up the pile, at the *trailing* positions (T) $\sigma_{rr}$ either rises (Test CP2) or falls (Pilot Test).

As Figure 10.1 shows, the major change in $\sigma_{rr}$ occurs over the first five days. There is a 26% drop in radial total stress at the *leading* transducer in Test CP2f (i.e. at 5.52m), with a further 3% drop over the next 58 days. For the *following* instrument the fall in $\sigma_{rr}$ is only 10% over the first five days (but with an extra 3% drop by day 63).

### 10.3.2 The normalized horizontal total stress H

A convenient way to compare these curves is to calculate the "normalized horizontal total stress" H, which is defined as (see Chapter 3):

$$H = (\sigma_{rr} - u_o)/\sigma'_{vo}$$

Figure 10.4 portrays the variation in H with time (on a logarithmic scale) for Tests CP2, 3, and 5 - i.e. for the tests which gave the most reliable data. (The surface stress transducers' waterproofing failed in Test CP4f [see Appendix 9] - hence readings of $\sigma_{rr}$ are unreliable in this experiment.)

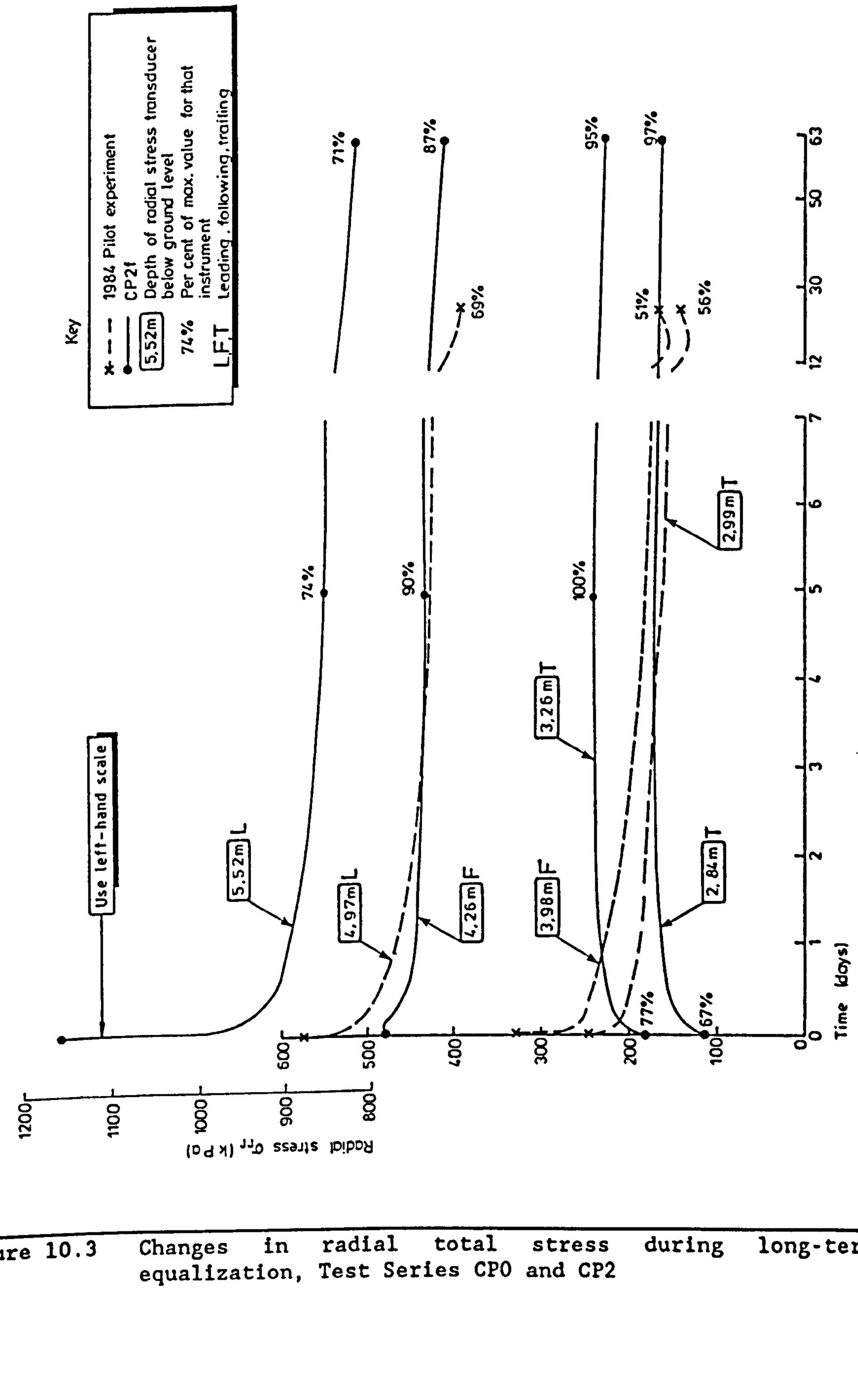



Figure 10.3 Changes in radial total stress during long-term equalization, Test Series CP0 and CP2

Figure 10.4 reveals a number of consistent trends, as described in the following paragraphs.

At depths greater than 4.1m (i.e. in the undisturbed London clay), H falls during the equalization period (from maximum values of between 9 and 18) and appears to approach an equilibrium condition (H = 8-13) after about 10 days (albeit with some signs of creep between days 10 and 63).

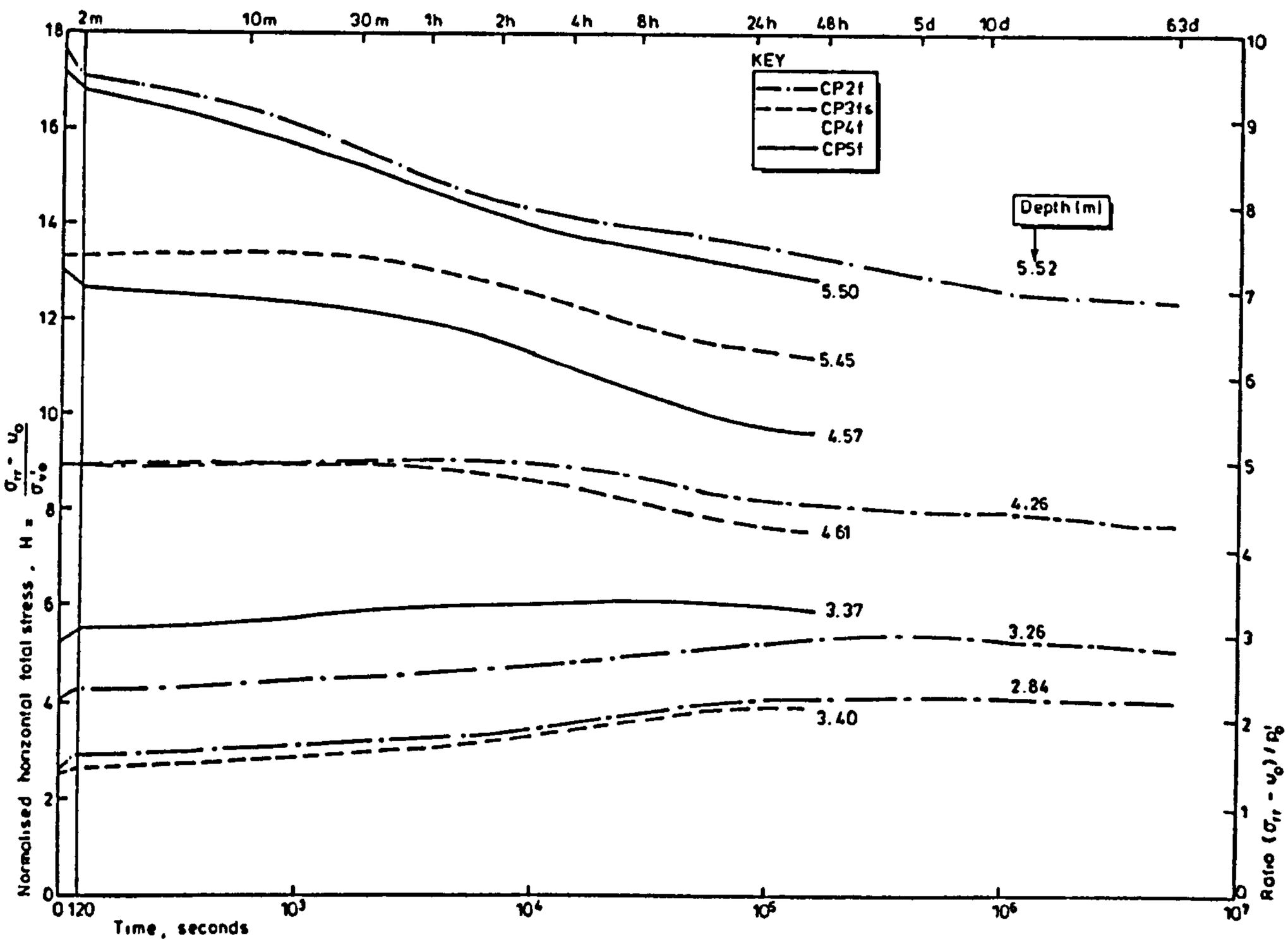



Figure 10.4 Variation of the normalized horizontal total stress during the equalization period, Tests CP2-5

At shallower depths (in the disturbed London clay), the value of H rises (from between 2½ and 5½) and appears to reach a stable plateau (H = 4-5) after ≈48h.

For comparison, in Piezo-Lateral Stress cell experiments[3] in Boston blue clay (see Chapter 4), H fell from ≈2.4 at the end of installation, to ≈0.6 at the end of equalization, 2½ days later.

## 10.3.3 Radial total stresses after 36h

Figure 10.5 shows the radial total stresses that act on the pile 36h after installation, when the soil has reached a condition close to equilibrium. The trends of $(\sigma_{rr})_{36h}$ with depth are compared with the soil's original in situ horizontal total stress ($\sigma_{ho}$) and the limit pressures ($p_{lim}$) obtained from the self-boring pressuremeter tests. Note that the increase in $(\sigma_{rr})_{36h}$ with depth is very similar in all the tests and is approximately 200kPa/m. Note also that the measurements fall roughly

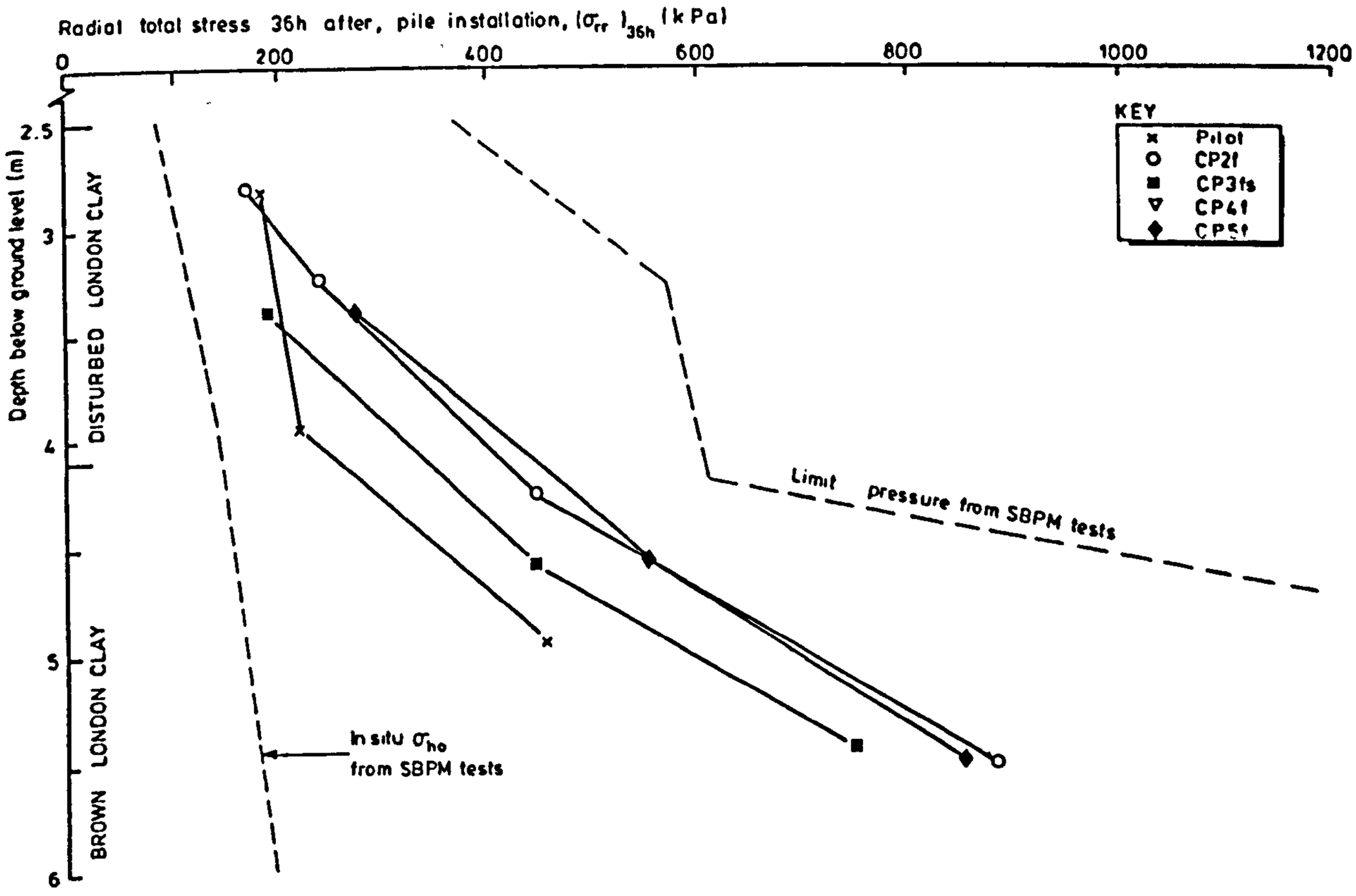



Figure 10.5 Radial total stresses along the pile, 36h after installation, Tests CP2-5

midway between the profiles of $\sigma_{ho}$ and $p_{lim}$.

There is currently no satisfactory theoretical explanation for these results.

## 10.4 CHANGES IN RADIAL EFFECTIVE STRESS

### 10.4.1 Changes in radial effective stress over the first two days

The changes in radial total stress and pore pressure are reflected in the variations in radial effective stress. Figure 10.6 shows the values of $\sigma'_{rr}$ recorded over the first 48h in Test CP5f.

At the *leading* instrument level (where the radial effective stress is greatest), $\sigma'_{rr}$ falls to a minimum in the short-term, but then rises to a steady value after about 20h. Elsewhere along the pile the behaviour is

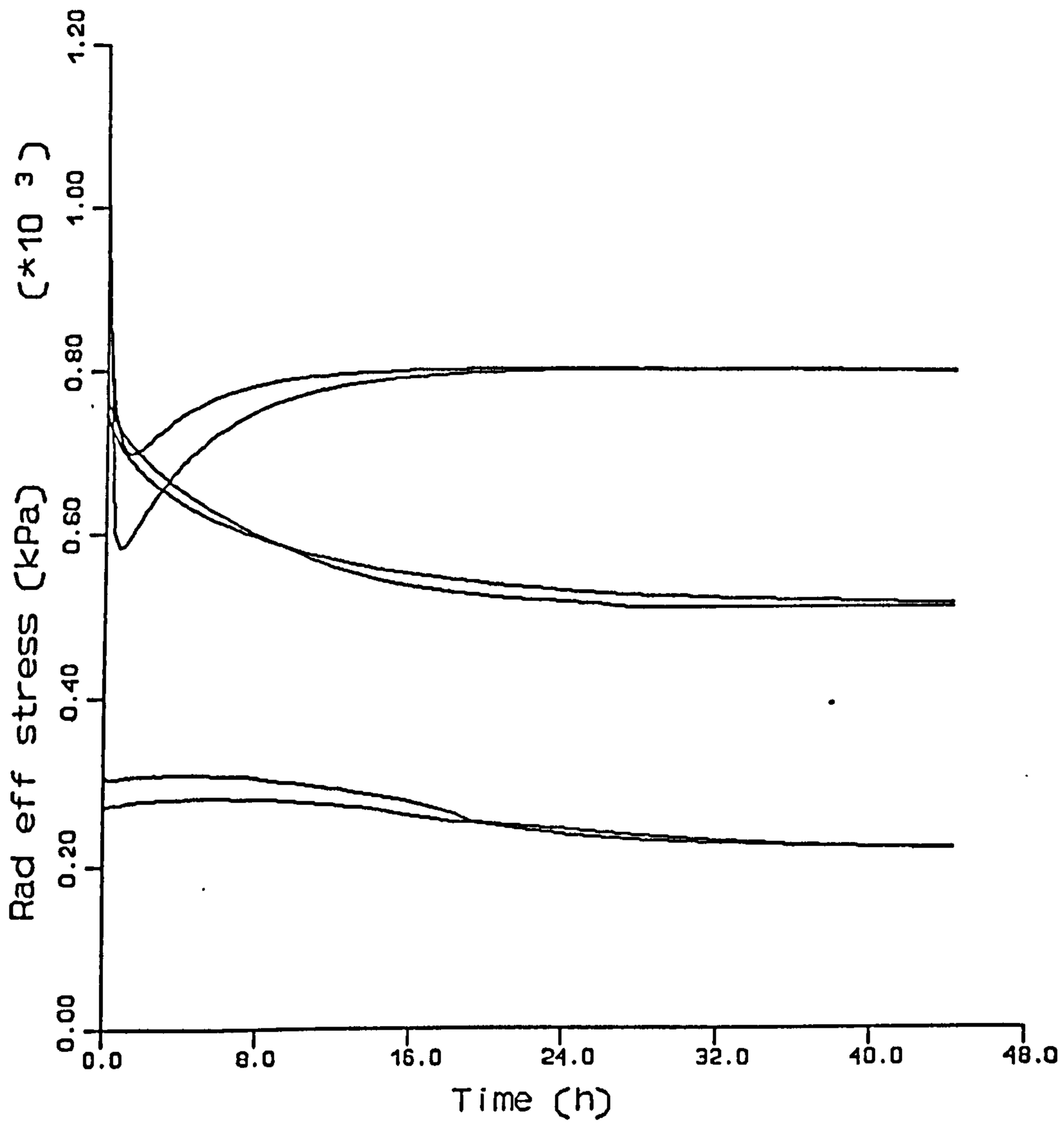



**Figure 10.6** Changes in radial effective stresses over the first 48h after pile installation, Test CP5f

very different. $\sigma'_{rr}$ falls steadily and significantly at the *following* position; but only slightly at the *trailing* position. The results of Test Series CP2f and CP3fs are in good agreement with those of CP5f.

### 10.4.2 Radial effective stresses after 36h

The radial effective stresses that act on the pile 36h after the end of installation are shown in Figure 10.7, together with a profile of the original in situ horizontal effective stress $\sigma'_{ho}$, and the prediction for $\sigma'_{rr}$ given by the cavity expansion method[4] ($\sigma'_{rr} = 5.8c_{uo}$). The field measurements tend towards the cavity expansion prediction in the deeper soil, but fall well below $5.8c_{uo}$ over most of the pile's length. It is also clear from this diagram that the ratio $\sigma'_{rr}/\sigma'_{ho}$ is not a constant, but varies with depth (from about 2 at 3.25m to 5½ at 5.5m depth).

### 10.4.3 Comparison with existing theories

Theoretical predictions for $K_c$ ($= [\sigma'_{rr}]_c/\sigma'_{vo}$) compare rather unfavourably with the results shown in Figure 10.7. According to the cavity expansion method, $K_c = 18.2$ for London clay with an overconsolidation ratio of 32 (see Chapter 3), whereas the measured values of $K_c$ are 11.0-13.0 at the leading, 7.1-9.7 at the following, and 4.0-5.9 at the trailing instrument positions. The cavity expansion method clearly over-predicts $K_c$ by a large margin, especially at the *trailing* instrument positions (where the method is supposed to have its greatest application).

There are currently no strain path predictions available for high OCR clays, such as the London clay.

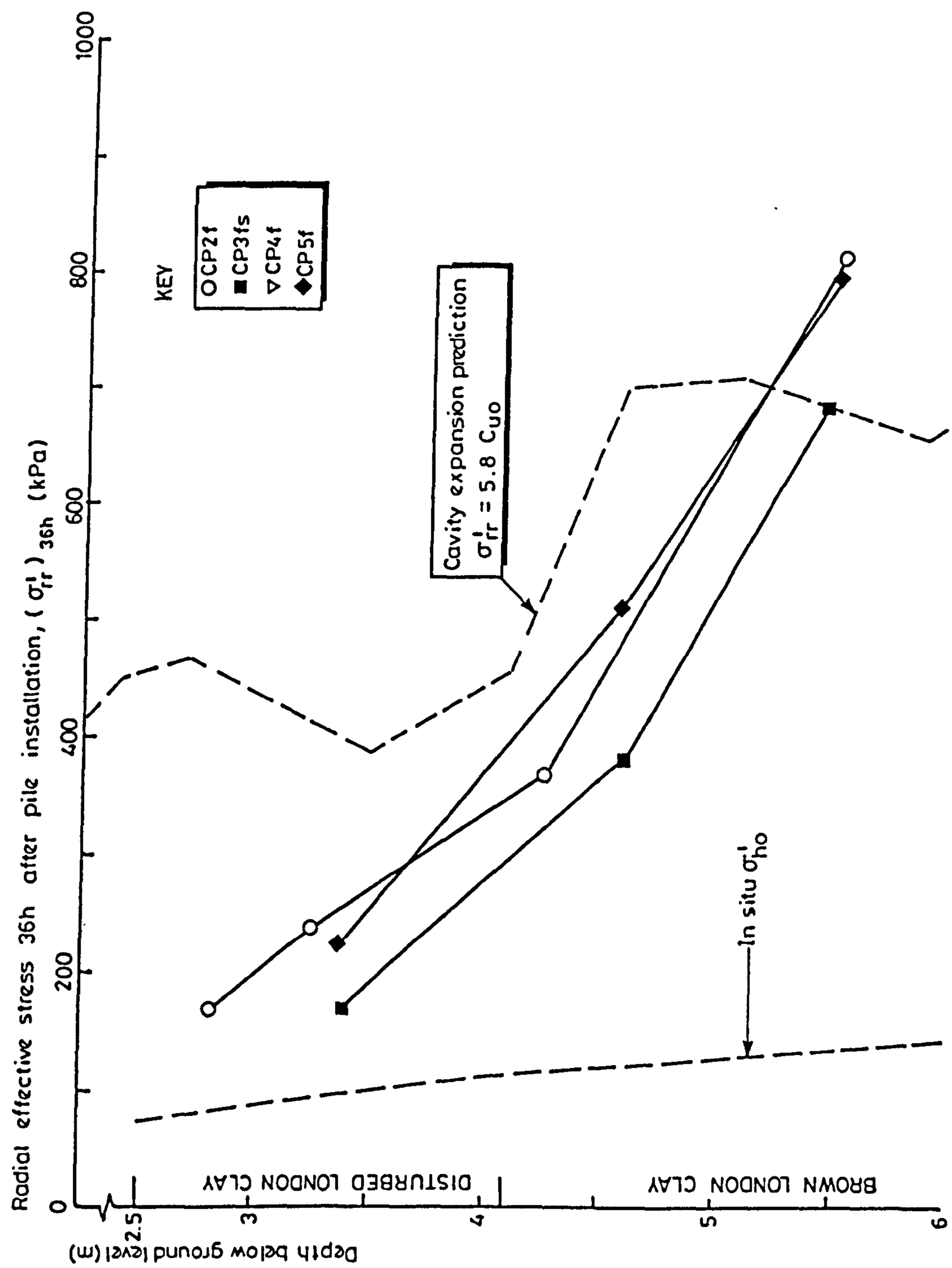



Figure 10.7 Radial effective stresses acting on the pile, 36h after installation, Tests CP2-5

## 10.5 RESULTS OF SPECIAL TESTS ON PILE CP4f

### 10.5.1 Falling-head permeability tests CP4f/FHK

The results of the falling-head permeability tests are shown in Figure 10.8. Three tests were performed, one on each of the flushable probes (P52F, P54F, and P56F) on pile CP4f. Details about the test

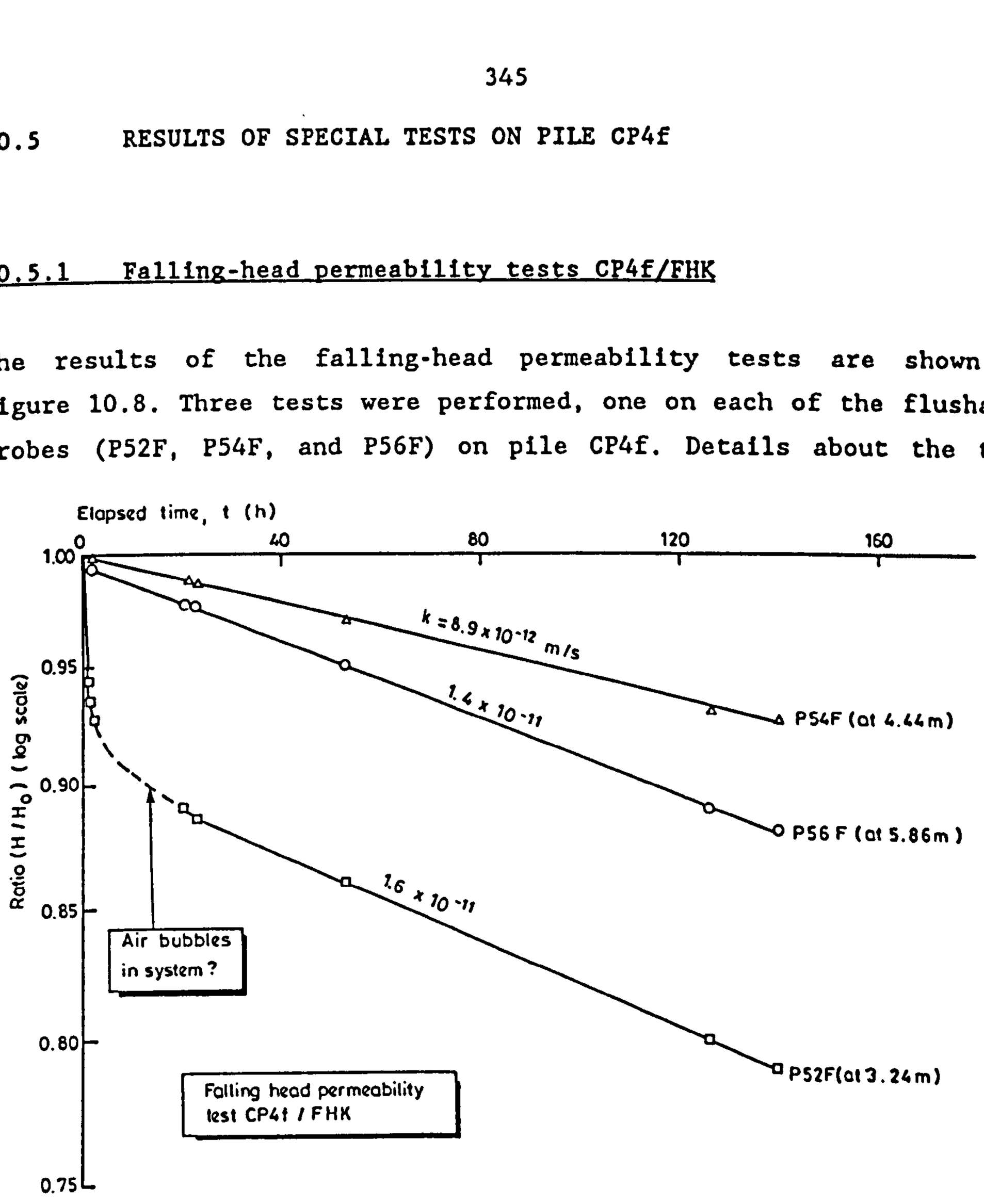



Figure 10.8 Results of falling-head permeability tests CP4f/FHK

procedures are given in Chapter 8 (see p293).

The permeability tests have been interpreted in accordance with Hvorslev's theory[5] for the flow of water through incompressible soil. (Details about this interpretation are given in a note[6] at the end of the chapter.)

The radial permeability of the clay lies between $8.9 \times 10^{-12}$ and $1.6 \times 10^{-11}$m/s. These figures are entirely consistent with measurements of the (undisturbed) clay's *vertical* permeability ($k_v$), as determined[7] in

oedometer tests. ($k_v$ is in the range $5 \times 10^{-12}$ to $2 \times 10^{-11}$m/s.)

## 10.5.2 Hydraulic fracture tests CP4f/HF

The results of the hydraulic fracture tests are presented in Figure 10.9. Three tests were performed, one each on the flushable probes P52F, P54F, and P56F. Details about the test procedures are given in Chapter 8 (see

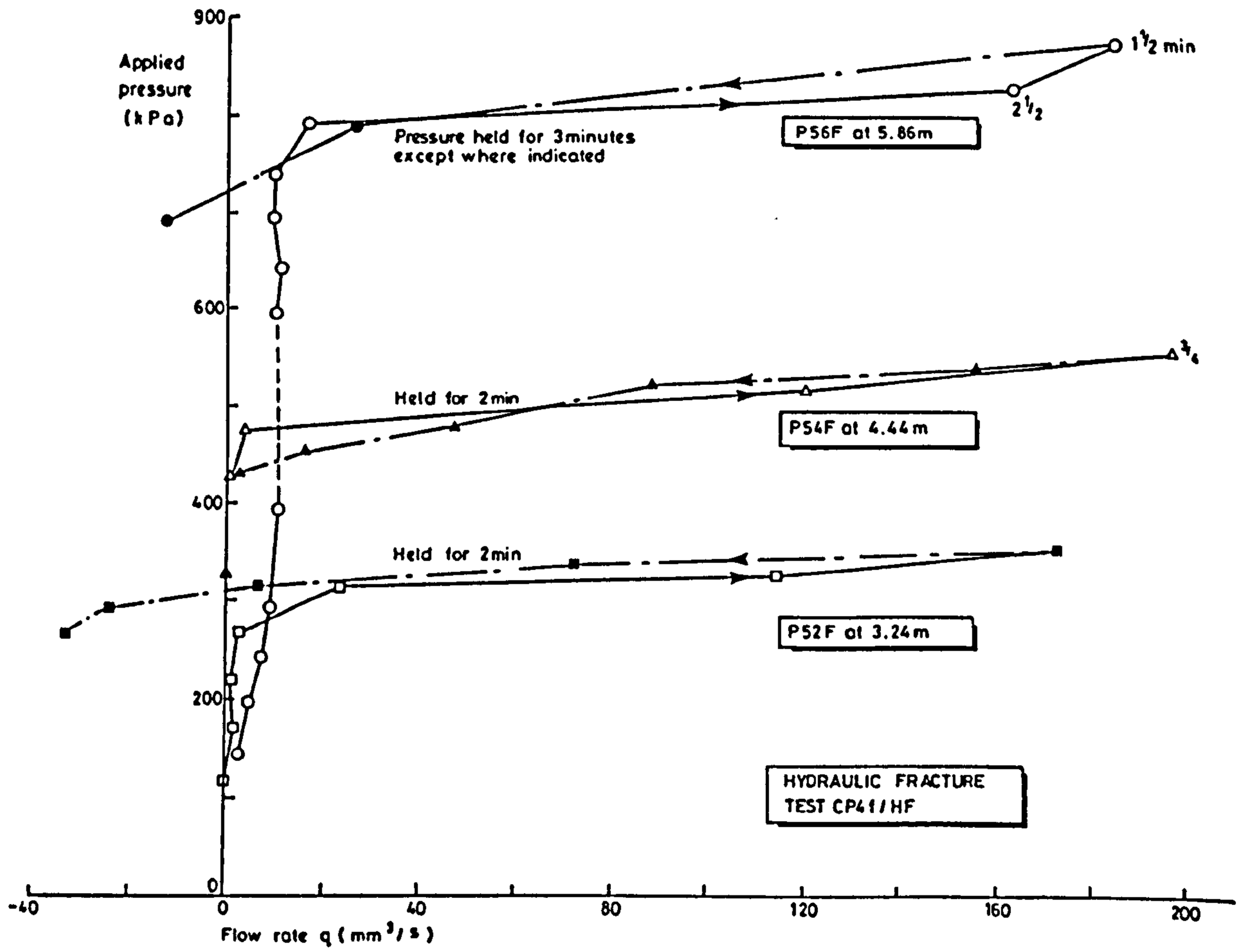



Figure 10.9 Results of hydraulic fracture tests CP4f/HF

pp293-294).

The best way to understand the data presented in Figure 10.9 is to follow one of the tests in chronological sequence. For example, consider the test on probe P56F. As the applied pressure is increased (points o), a small amount of water (<10mm3/s) flows into the soil that surrounds the pile. At some "threshold" pressure ($\sigma_{th} \approx 785$kPa) the flow rate suddenly

increases to between 100 and 200mm$^3$/s. At this stage the pressure is reduced (points •), and the flow rate drops. Below a certain "closure" pressure ($\sigma_{cl} \approx 775$kPa), the flow rate once again becomes negligible (less than 10mm$^3$/s).

Table 10.1 summarizes the values of $\sigma_{th}$ and $\sigma_{cl}$ (the threshold and closure pressures) that were deduced from Figure 10.9. In all three tests $\sigma_{th}$ and $\sigma_{cl}$ are almost identical.

Also given in the table are the radial total stresses measured *on day 42* in Test CP2f (as noted earlier, the measurements of $\sigma_{rr}$ in Test CP4f are unreliable). The hydraulic fracture tests were performed on day 42 of CP4f/EQ. Allowing for the fact that they were recorded in different

Table 10.1 Results of hydraulic fracture tests

| Test | Depth (m) | Threshold pressure (kPa) | Closure pressure (kPa) | $\sigma_{rr}$ (kPa) † | Maximum pressures... applied* (kPa) | measured# (kPa) |
|---|---|---|---|---|---|---|
| P52F | 3.24 | ≈310 | 310-325 | 232 | 350 | 308 |
| P54F | 4.44 | 450-472 | 435-495 | 420 | 520 | 445 |
| P56F | 5.86 | ≈785 | ≈775 | 824 | 875 | 825 |

†as measured on day 42 of CP2f/EQ (the SSTs had malfunctioned in CP4f/EQ)
*to the flushable probe
#by the probe on the opposite side of the pile

tests, the values of $\sigma_{rr}$ and $\sigma_{th}$ are reasonably similar to one another at any particular depth, suggesting that the soil surrounding the pile was not *fractured* by the applied pressure, but instead was pushed away from the surface of the pile, in the way that a pressuremeter forces soil to expand radially. The evidence to support this suggestion is given in the next paragraph.

One of the most notable features of each "hydraulic fracture" test was the way in which the fast-acting probe (on the other side of the pile) would respond to a pressure being applied to the soil via the flushable probe. For example, consider the probes P55 and P56F at 5.86m depth. At pressures below $\sigma_{th}$ the fast-acting probe (P55) showed no sign whatsoever that anything was happening, but as soon as the pressure applied to P56F

exceeded $\sigma_{th}$, P55 immediately registered a large increase in pore pressure. As Table 10.1 reveals, the "measured" pressure was about 50kPa less than the applied pressure at each level.

These results do indeed suggest that the soil was pushed away from the surface of the pile, and - if my interpretation is correct - these "hydraulic fracture" tests (perhaps I should call them *pressuremeter* tests) provide independent measurements of the radial total stresses acting on the pile.

## 10.6 DISCUSSION

The equalization process, in this high OCR clay, differs considerably from the simple process of monotonic consolidation that is considered by most theories of pile behaviour. The key features of the equalization process are that:

- Swelling takes place near the pile surface
- Most of the excess pore pressures dissipate in the first 36h (whereas the radial total stresses continue to change over the first five days*)

Hence the earth and pore water pressures around the pile reach a condition close to equilibrium within a few days of installation.

The radial effective stresses acting on the pile once equilibrium has been reached are very different to the stresses predicted by the cavity expansion method of analysis. The ratio of $(\sigma'_{rr})_c$ to the original in situ vertical effective stress, $\sigma'_{vo}$, (i.e. $K_c$) is not a constant, but varies markedly with distance behind the pile tip.

*Further changes in $\sigma_{rr}$ over the next sixty days are about 3% of the maximum radial total stress recorded, and are probably the result of the soil creeping

## 10.7 NOTES AND REFERENCES

[1]The readings are thought to be reliable over the first <u>five</u> days following pile installation, but may suffer from gassing-up thereafter. Long term values of the pore pressures have been obtained (during Test CP4f) using flushable pore pressure probes.

[2]Teh C.-I. (1987). An analytical study of the cone penetration test. DPhil Thesis, Univ. of Oxford.

[3]Baligh et al. (1985), loc. cit.

[4]Wroth C.P., Carter J.P., and Randolph M.F. (1979). Stress changes around a pile driven into cohesive soil. In "Recent developments in the design and construction of piles", Instn Civ. Engnrs, London, pp345-354.

[5]Hvorslev M.J. (1951). Time lag and soil permeability in ground-water observations. Bulletin No 36, Waterways Experimental Station, Corps of Engineers, Vicksburg, Mississippi, 50pp.

[6]Since $\mu$ is very small, the flow of water out of the probes during the permeability tests is given by Hvorslev's equation $q = FkH$ (where F is the shape factor of the piezometer, k is the clay's permeability, and H is the driving head of water). At time t, the head of water in the piezometer tubing depends on the initial head ($H_o$) and the cross-sectional area (A) of the tubing, and is given by:

$$\log_e(H/H_o) = Fkt/A$$

(see the book by Clayton et al., pp261-264, for the derivation of this formula). Therefore, the permeability k can be calculated from the slope of the straight lines plotted on Figure 10.8.

Reference: Clayton C.R.I., Simons N.E., and Matthews M.C. (1982). Site investigation. Granada Publishing, London, 424pp.

[7]Jardine R.J. (1985). Investigations of pile-soil behaviour, with special reference to the foundations of offshore structures. PhD Thesis, Univ. of London (Imperial College), 2 vol., 789pp. See p161 and Figure 7.17 (p583).

# Chapter 11

# Results of the instrumented pile tests: behaviour during load testing

CONTENTS OF CHAPTER 11


11.1 INTRODUCTION . . . . . 354
11.1.1 Outline of chapter 354
11.1.2 Importance of the rate of installation 354
11.2 LOAD-DISPLACEMENT CHARACTERISTICS . . . . . 356
11.2.1 Fast-jacked pile CP5f 356
11.2.2 Slow-jacked pile CP3fs 358
11.2.3 Summary of $\alpha$ and $\beta$ values 360
11.3 PORE PRESSURES DURING PILE LOADING . . . . . 363
11.3.1 Load tests on fast-jacked pile CP5f 363
11.3.2 Load tests on slow-jacked pile CP3fs 364
11.3.3 Summary of pore pressure changes 366
11.4 RADIAL TOTAL STRESSES . . . . . 367
11.4.1 Load tests on fast-jacked pile CP5f 367
11.4.2 Load tests on slow-jacked pile CP3fs 368
11.4.3 Summary of radial total stress changes 369
11.5 RADIAL EFFECTIVE STRESSES . . . . . 370
11.6 SHEAR STRESSES . . . . . 372
11.6.1 Shear stresses mobilized by fast-jacked pile CP5f 372
11.6.2 Shear stresses mobilized by slow-jacked pile CP3fs 374
11.7 COEFFICIENTS OF FRICTION . . . . . 376
11.7.1 Introduction 376
11.7.2 Load tests on fast-jacked pile CP5f 376
11.7.3 Load tests on slow-jacked pile CP3fs 378
11.8 EFFECTIVE STRESS PATHS FOLLOWED DURING PILE LOADING . . 379
11.8.1 Introduction 379
11.8.2 Load tests on fast-jacked pile CP5f 379
11.8.3 Load tests on slow-jacked pile CP3fs 381
11.9 DISCUSSION . . . . . 383
11.9.1 Key findings from load-displacement data 383
11.9.2 Summary of the behaviour in terms of effective stresses 383
11.10 NOTES AND REFERENCES . . . . . 386

# 11.1 INTRODUCTION

## 11.1.1 Outline of chapter

Although a sound understanding of pile installation and equalization is essential for the development of a complete theory of pile behaviour, it is a pile's response to loading that is of primary engineering importance. As discussed in earlier chapters, for given ground conditions the three major variables that control a pile's response to loading are:

- Its rate of installation
- The length of the equalization period
- The direction of first loading (compression or tension)

Section 11.2 examines the influence of these parameters on the load-displacement characteristics of the Canons Park piles. Sections 11.3 to 11.7 present the measurements of the earth and pore water pressures that were obtained during load testing, the purpose being to explain the results in terms of the effective stresses acting on the pile's shaft.

Section 11.8 presents the *stress paths* followed during pile loading. These provide the most satisfactory explanation yet of the fundamental mechanisms that govern pile behaviour in overconsolidated clays.

## 11.1.2 Importance of the rate of installation

As discussed in Chapter 9, the load capacities of fast- and slow-jacked piles differ considerably during installation. Figure 9.17 (see p324) shows the $\alpha$ and $\beta$ values recorded during installation of more than ten piles at Canons Park. A clear jump in shaft friction is evident ($\alpha$ and $\beta$ increasing by 60-75%) as the rate of installation increases from 100mm/min (slow) to 500mm/min (fast). This matches the behaviour observed in laboratory ring-shear tests on samples of clay from Canons Park (see Chapter 5, p208 et seq.), and corresponds to a change in the mechanism of shearing. Both viscous- and fabric-related phenomena contribute to this remarkable rate effect.

It follows from the above that one of the key objectives in interpreting the (static) load tests (performed *after* equalization of the surrounding soil) should be to determine how much the rate of jacking permanently affects the piles' subsequent load capacity by modifying the soil fabric at the pile/soil interface.

The following sections report the results from the loading tests in the two "model" experiments, CP5f and CP3fs. The results from the former are typical of a fast-jacked pile, and the latter typical of a slow-jacked pile. In both cases the load tests took place within a few days of pile installation, and reliable pore pressure readings were obtained throughout.

## 11.2 LOAD-DISPLACEMENT CHARACTERISTICS

### 11.2.1 Fast-jacked pile CP5f

Figure 11.1 shows the complete loading cycle applied to the fast-jacked pile, CP5f. L1T is the first load test (in tension) and L2C the second (in compression). Table 11.1 (see p362) presents the calculated values of $\alpha$ and $\beta$ at various points during these tests. The pile's load-displacement curves are shown in more detail in Appendix 13.

Several features of the pile's behaviour are worth noting:

- A significant part (≈25%) of the end bearing mobilized during pile installation remains locked in at the pile's toe at the start of load test L1T
- The load-displacement curve in test L1T is noticeably non-linear up to peak load, with the pile's capacity being mobilized after 3.2mm displacement
- The $\alpha$ value at peak load in test L1T is marginally smaller than the value recorded during the final push of installation (0.90 as opposed to 0.93) - despite a change in loading direction and allowing two days for "set-up"
- Post-peak, the capacity of the pile falls to 78% of its maximum value
- $\alpha$ does not increase when the pile is re-loaded in compression: in test L2C its maximum value is slightly lower (0.64) than the post-peak value in L1T; both are very much lower than the value of $\alpha$ recorded during installation (0.9)
- Once $\alpha$ has reached its peak in test L2C it continues to fall with further displacement (to ≈0.51); only when the *rate* of displacement is increased significantly (to ≈10mm/min) does $\alpha$ pick up (and then only to 0.58)

It is clear from the above that continued displacement of this fast-jacked pile causes gradual degradation of the pile's shaft capacity, regardless of the direction of that displacement. It follows that the

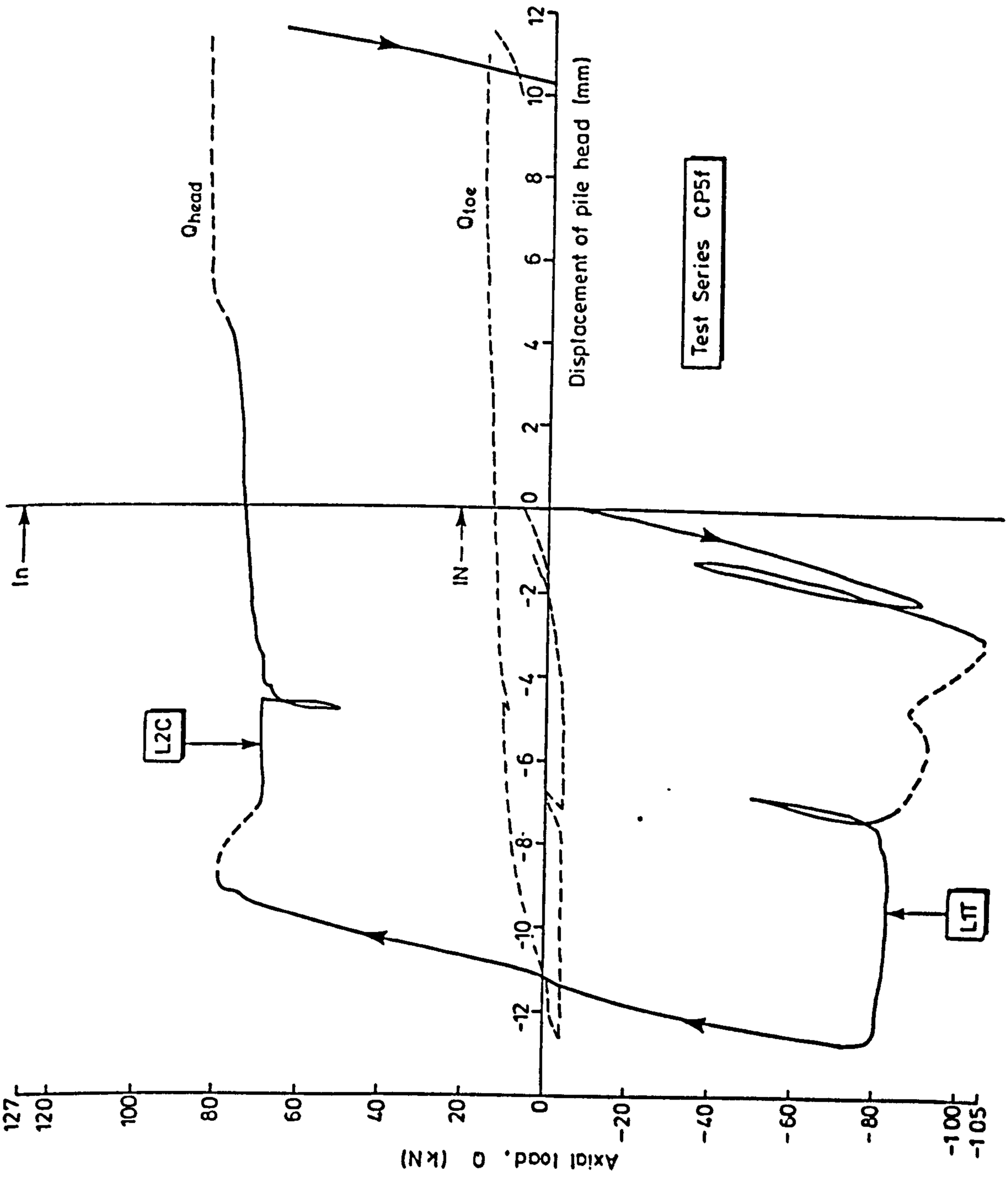



Figure 11.1 Complete loading cycle for Pile CP5f

results from multiple tests on the same pile should not be used to determine the effects of (for example) set-up time or loading direction, on the first-time loading capacity of piles.

### 11.2.2 Slow-jacked pile CP3fs

Figure 11.2 illustrates the complete loading cycle for the model slow-jacked pile CP3fs. L1C is the first load test (in compression), L2T the second (in tension), and L3C the third (in compression). Table 11.2 (see p362) gives the calculated values of $\alpha$ and $\beta$ at various stages during these tests. The load-displacement curves are given in more detail in Appendix 13.

The following points are worth noting:

- As with CP5f, significant end-bearing remains locked into the pile toe at the start of the first load test
- The load-displacement curve in L1C is noticeably non-linear and, up to 60kN load, shows a very similar shape to that of CP5f/L1T
- The $\alpha$ value at peak load in L1C is slightly smaller than that recorded during the final push of installation (0.49 as opposed to 0.53)
- The pile's peak $\alpha$ value on first-loading is only 54% of that mobilized by the fast-jacked pile CP5f
- The pile's response is ductile throughout load test L1C, although it is brittle in the subsequent tests (both of which involved a change in loading direction)
- As with CP5f, increasing the displacement rate in the load test increases the shaft capacity by about 7-15% per log cycle
- The toe resistance becomes progressively softer with each loading cycle

The ductile response in Test CP3fs/L1C is compatible with the postulate that slow-jacked piles fail by sliding along a highly-polished, continuous, "principal displacement shear" that was formed close to the pile shaft during installation (see Chapter 4). However, to prove this hypothesis conclusively we need to have measurements of the effective

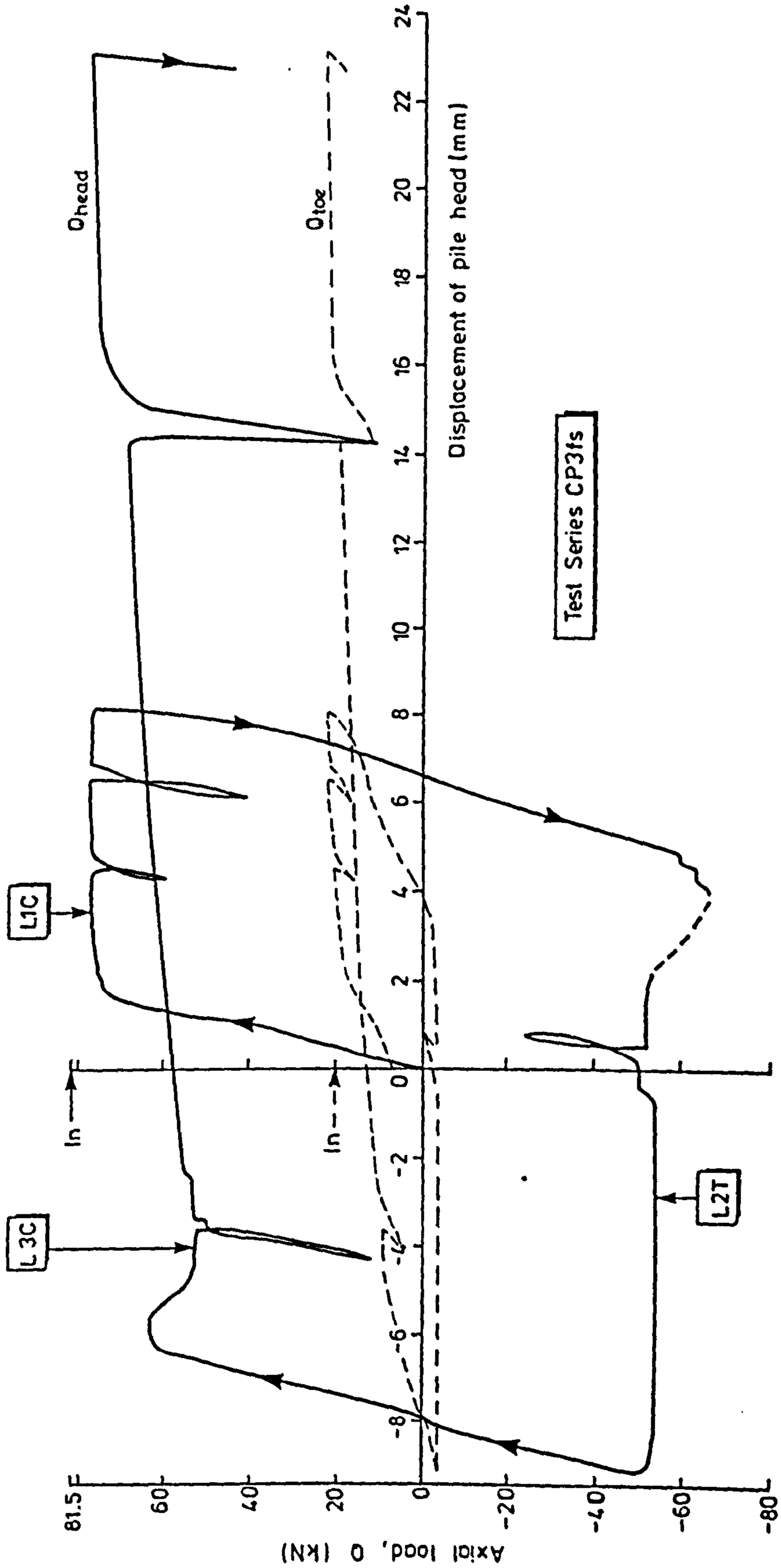



Figure 11.2 Complete loading cycle for Pile CP3fs

stresses at the pile/soil interface, and also *visual* evidence (from observations of the soil's fabric) that these highly polished slip surfaces really do exist.

### 11.2.3 Summary of $\alpha$ and $\beta$ values

The results from CP5f and CP3fs demonstrate major differences between the load capacities of fast- and slow-jacked piles. Both piles were tested for the first time two days after installation. As indicted in Chapter 7, the programme of tests at Canons Park involved several other combinations of the three main variables that are listed in Section 11.1.1.

To summarize the data, Figure 11.3 shows how the $\alpha$ and $\beta$ values vary with set-up time (the period between installation and first-time loading) for piles CP0-5. Some load tests were run in compression and others in tension. The main points to note are:

- It is the rate of installation that has the most influence on the piles' shaft capacity
- A pile installed at 500mm/min mobilizes 60% more shaft friction than one installed at 20mm/min; remembering that the radial effective stresses are not affected by the rate of installation, this reinforces the hypothesis that the angles of friction are strongly influenced by the fabric re-orientation caused by pile installation
- The values of $\alpha$ and $\beta$ appear to fall soon after installation, but do not change significantly with time once the first five days have elapsed; this is contrary to the set-up effect predicted by most theories of pile behaviour, but confirms the trends noted by Tomlinson[1] (see Chapter 14)
- Fast-jacked piles loaded in tension have a (15%) higher shaft capacity than in compression; the results of the repeated tests on CP3fs suggest that this difference may be much larger for slow-jacked piles, although any increase in capacity caused by load reversal is highly brittle and degrades rapidly with pile displacement

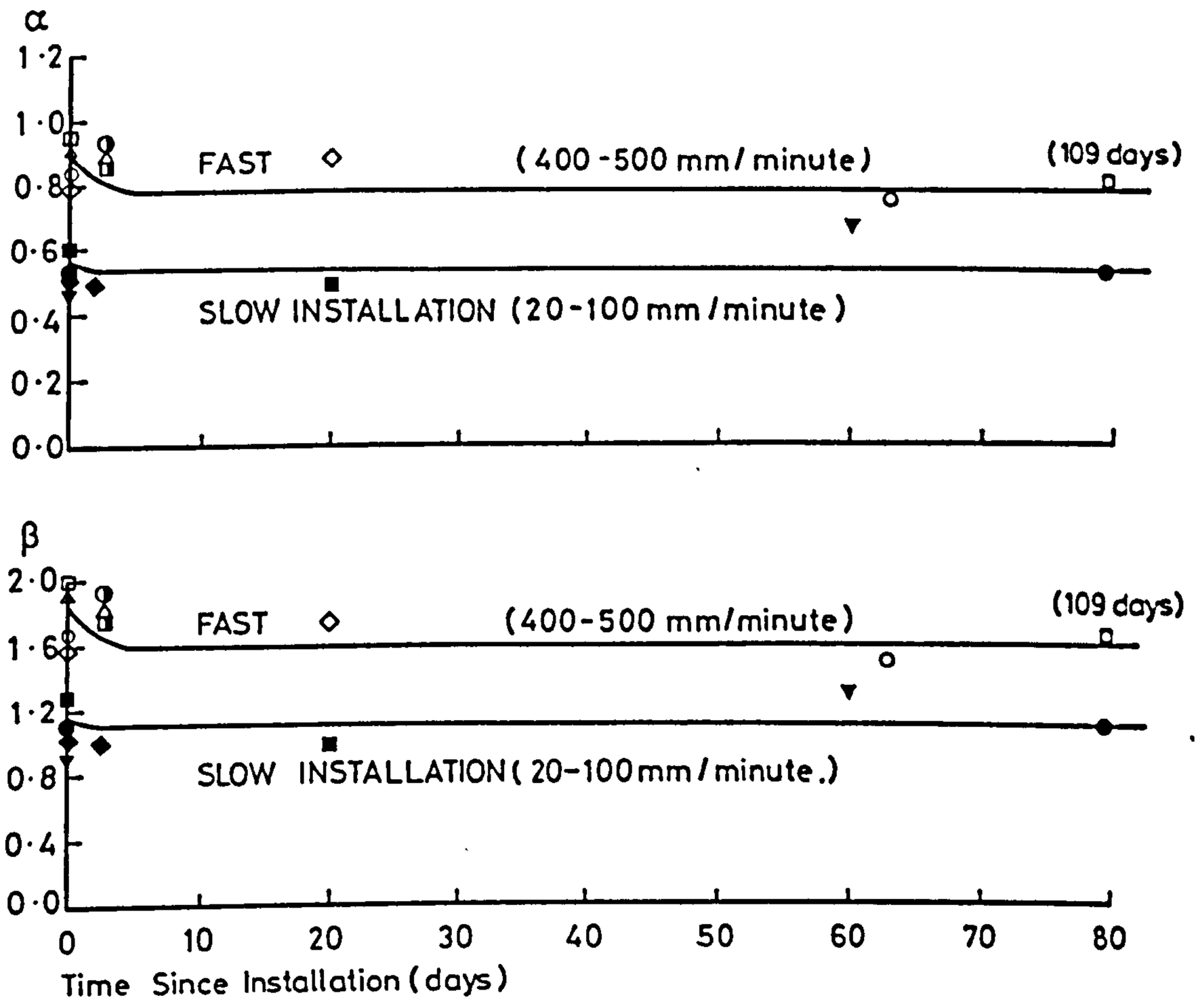



**Figure 11.3** Variation in $\alpha$ and $\beta$ values with equalization time

The practical importance of these results may be demonstrated by comparing the observed capacities with the peak capacities calculated according to the current API design codes (see Chapter 2). The codes recommend an $\alpha$ value of 0.42 ±0.03 for clays with the same undrained strength ratio as that at Canons Park ($c_{uo}/\sigma'_{vo}$ = 1.94 ±0.42). In the present series of experiments $\alpha$ values between 0.8 and 0.9 have been measured in long-term tests on fast-jacked piles.

Table 11.1 $\alpha$ and $\beta$ values recorded during Test Series CP5f

| Load test | Displacement (mm) | Axial load Q (kN) Head | Toe | Shaft | $\alpha$ | $\beta$ | Rate of travel (mm/min) |
|---|---|---|---|---|---|---|---|
| IN | - | +127.0 | +21.1 | +105.9 | +0.93 | +1.88 | ≈445 |
| L1T | 3.17 | -105.4 | -2.5 | -102.9 | -0.90 | -1.83 | - |
| | 4.18 | -95.2 | -4.4 | -90.8 | -0.80 | -1.61 | - |
| | 7.67 | -78.8 | -4.0 | -74.8 | -0.66 | -1.33 | 0.08 |
| | 8.15 | -79.5 | -4.2 | -75.3 | -0.66 | -1.34 | 0.25 |
| | 9.45 | -80.1 | -4.6 | -75.5 | -0.66 | -1.34 | 0.84 |
| L2C | 2.11 | +79.8 | +6.2 | +73.6 | +0.64 | +1.31 | - |
| | 3.48 | +74.1 | +8.7 | +65.4 | +0.57 | +1.16 | 0.12 |
| | 4.35 | +69.1 | +9.3 | +59.8 | +0.52 | +1.06 | 0.30 |
| | 6.94 | +69.0 | +10.7 | +58.3 | +0.51 | +1.03 | 0.18 |
| | 7.76 | +70.1 | +11.5 | +58.6 | +0.51 | +1.04 | 0.81 |
| | 18.70 | +82.5 | +16.2 | +66.3 | +0.58 | +1.18 | ≈10.2 |

Compression loads +ve; tension loads -ve
$\alpha = Q_{shaft}/\pi DL(c_{uo})_{av}$; $\beta = Q_{shaft}/\pi DL(\sigma'_{vo})_{av}$
$Q_{toe}$ includes the skin friction on the pile shaft below the bottom axial load cell. With $r_{rz}$ = 120kPa this axial load is ≈2.7kN (i.e. in the tension test L1T the results above suggest that suction acts at the end of the pile during plunging failure)

Table 11.2 $\alpha$ and $\beta$ values recorded during Test Series CP3fs

| Load test | Displacement (mm) | Axial load Q (kN) Head | Toe | Shaft | $\alpha$ | $\beta$ | Rate of travel (mm/min) |
|---|---|---|---|---|---|---|---|
| IN | - | +63.8 | +11.2 | +52.6 | +1.16 | +2.33 | ≈403 |
| | - | +81.5 | +20.7 | +60.8 | +0.53 | +1.08 | ≈81 |
| L1C | 2.0 | +77.2 | +19.5 | +57.7 | +0.50 | +1.02 | 0.09 |
| | 2.7 | +78.0 | +22.1 | +55.9 | +0.49 | +0.99 | 0.13 |
| | ≈5 | +78.0 | +22.8 | +55.2 | +0.48 | +0.98 | 0.18 |
| | ≈6½ | +78.0 | +23.5 | +54.5 | +0.47 | +0.96 | 0.15 |
| L2T | 2.61 | -66.6 | +0.6 | -67.2 | -0.59 | -1.19 | ≈7 |
| | | -52.0 | -2.5 | -49.5 | -0.43 | -0.88 | 0.24 |
| | | -50.2 | -1.9 | -48.3 | -0.42 | -0.85 | 0.06 |
| | | -54.5 | -3.6 | -50.9 | -0.44 | -0.90 | 0.99 |
| L3C | 1.78 | +63.3 | +5.3 | +58.0 | +0.51 | +1.03 | ≈3.4 |
| | | +53.0 | +8.6 | +44.4 | +0.39 | +0.79 | 0.10 |
| | | +68.5 | +19.5 | +49.0 | +0.43 | +0.87 | 0.95 |
| | | +77.1 | +22.8 | +54.3 | +0.47 | +0.96 | 12.9 |

## 11.3 PORE PRESSURES DURING PILE LOADING

### 11.3.1 Load tests on fast-jacked pile CP5f

The variations in pore pressure during a typical pile test are illustrated in Figure 11.4. The data is taken from the first tension load test (L1T) on pile CP5f, and represents the response of the leading pair of pore pressure probes. (The traces from the following and trailing probes are very similar - see Appendix 13 for details.) On this diagram the pore pressure is plotted as a function of pile displacement. (Note that the pile reaches its peak axial load at 3.2mm movement.) The main points to note are:

- There is a slight rise in pore pressure during initial loading
- Unloading/re-loading the pile at ≈2mm displacement has little

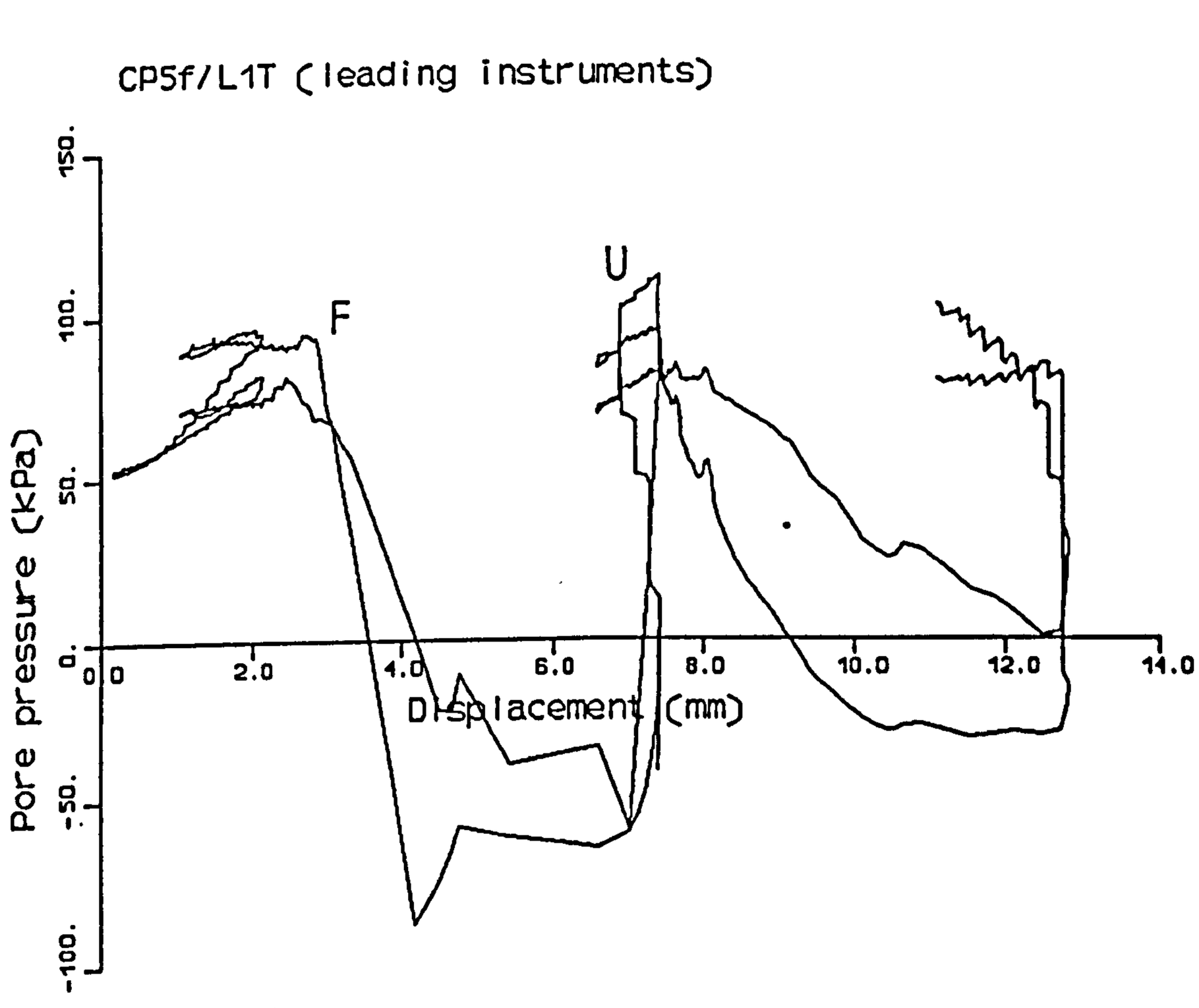



Figure 11.4 Variations in pore pressure with pile displacement during load test CP5f/L1T (leading positions)

or no effect on the pore pressures

- Once the local shaft friction has been exceeded (point F), the pore pressures plummet to negative values, and remain negative while the pile is continues to move
- On unloading at ≈7mm displacement (point U), the pore pressures rise to values similar to those recorded at point F
- On re-loading the pore pressures once again drop dramatically, and continue to fall as long as the pile is moving
- On final unloading the pore pressures re-attain their values at point F

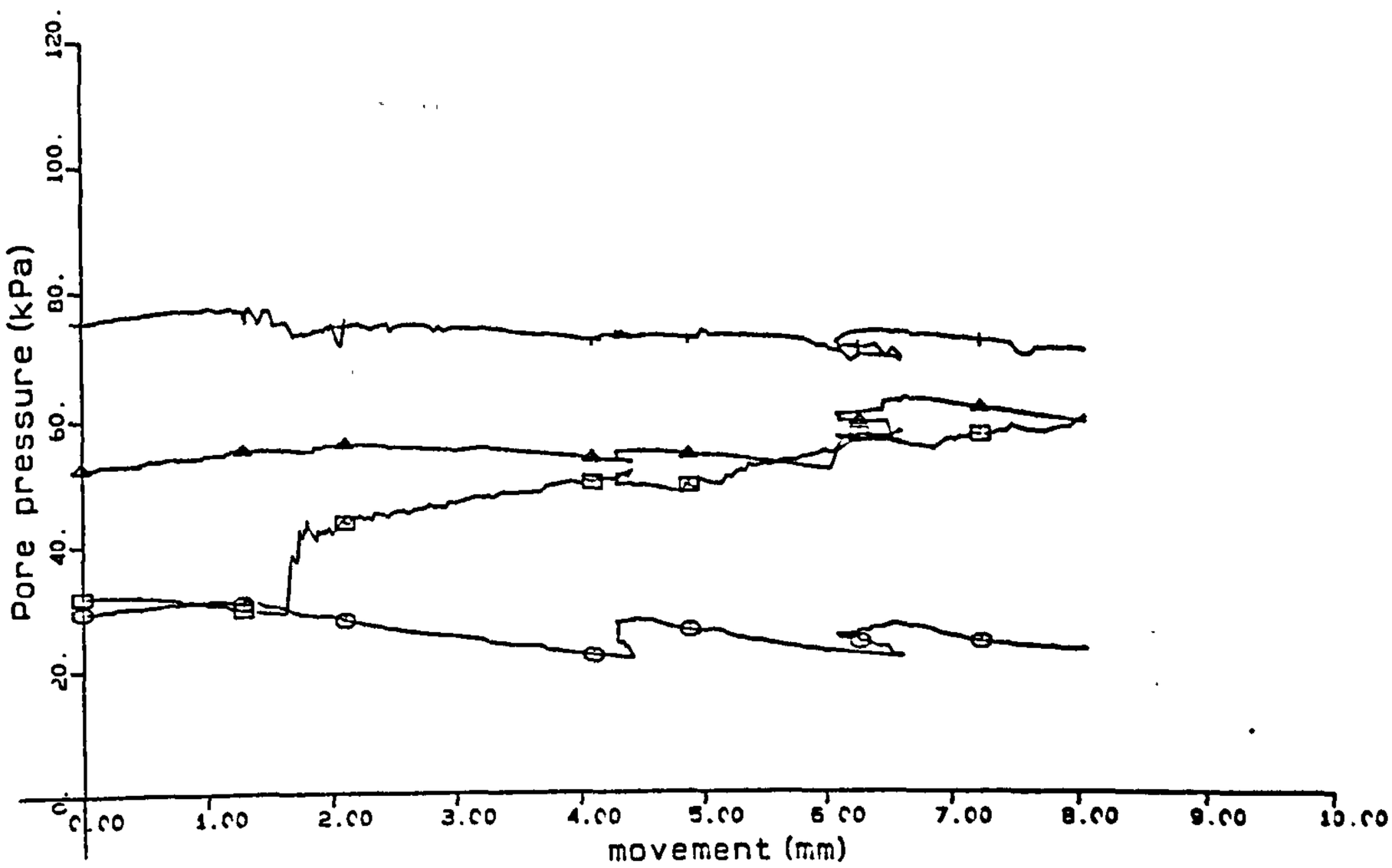
The corresponding traces (see Appendix 13) for load test CP5f/L2C (in compression) demonstrate the same response as that in the tension test L1T - i.e. unlike the behaviour of $\sigma_{rr}$ (see Section 11.4), the sign of the pore pressure changes does not switch over with a change in the direction of loading.

### 11.3.2 Load tests on slow-jacked pile CP3fs

The variation in pore pressure during the first load test (in compression) on CP3fs is illustrated in Figure 11.5.

The response at the *leading* positions is remarkably similar to that observed in CP5f/L1T at all three instrument positions (see Figure 11.4 and Appendix 13). However, the pore pressures recorded by the *following* and *trailing* probes are very different. There is virtually no change in pressure until the pile fails (after 2mm movement). And - whereas the leading probes record a drop in u of 40-80kPa during plunging - the following and trailing probes show either no change at all or a slight increase in pressure.

It is clear from the above that the clay next to the shaft of the slow-jacked pile does not dilate in the way that it does next to the fast-jacked one (except near the pile toe).



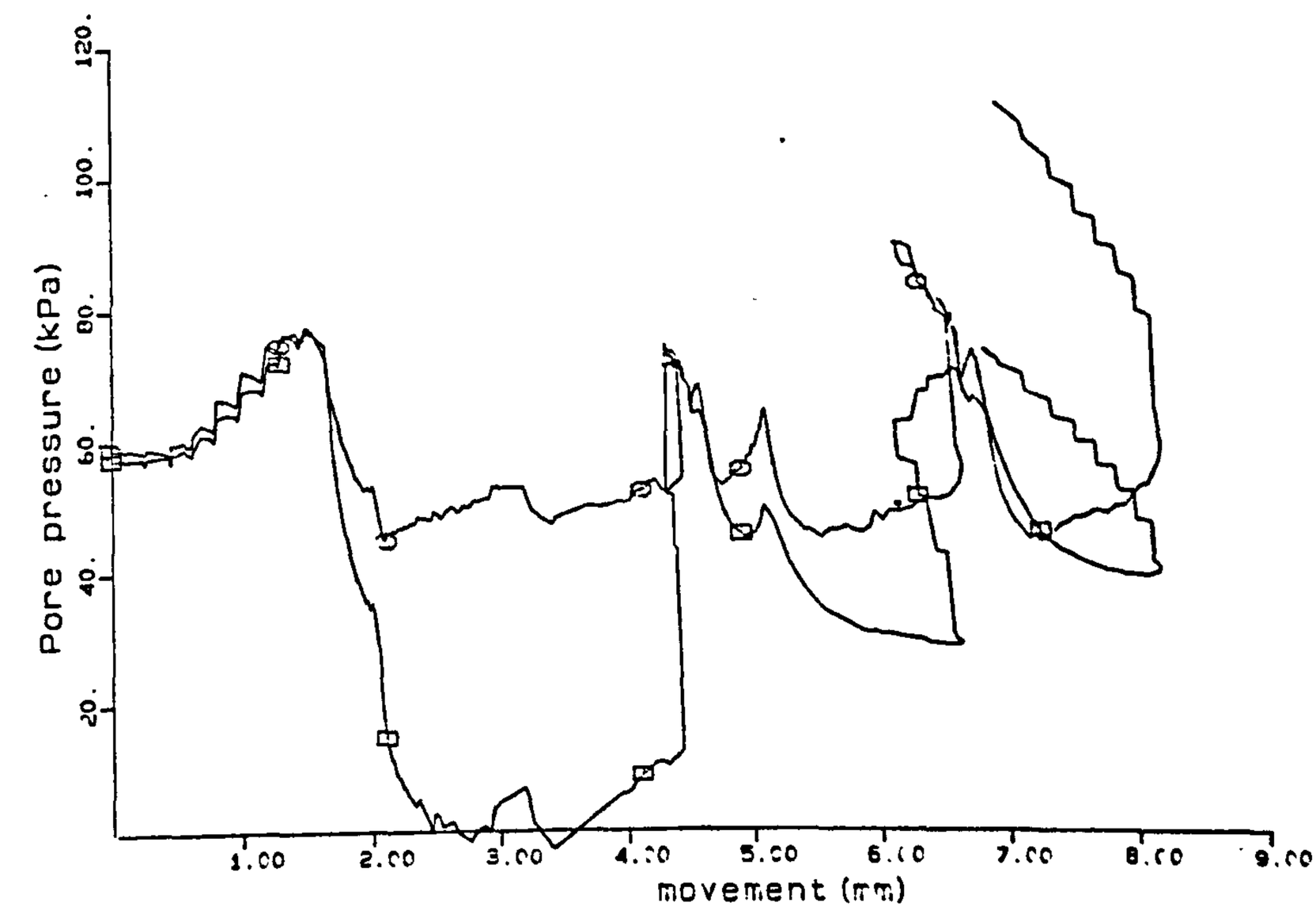




Figure 11.5 Variations in pore pressure with pile displacement during load test CP3fs/L1C: (top) following and trailing positions; (bottom) leading positions

## 11.3.3 Summary of pore pressure changes

Table 11.3 summarizes the pore pressure response during pile loading for all of the load tests at Canons Park. In all cases u rises during initial loading but falls as soon as plunging failure occurs. The response at the leading positions is always far greater than that observed at points further away from the pile tip.

Table 11.3 Changes in pore pressure during load tests, CP1-5

| Test series | Load test | Direction of loading | Changes in u Up to peak load | During plunging | On final un-loading |
|---|---|---|---|---|---|
| CP1s | L1C | Compression | X | X | X |
| CP2f | L1C | Compression | ? | Falls | Rises |
| | L2C | Compression | X | X | X |
| | L3T | Tension | X | X | X |
| CP3fs | L1C | Compression | Rises | Falls | ? |
| | L2T | Tension | Rises | Falls | Rises |
| | L3C | Compression | ? | ? | ? |
| CP4f | L1T | Tension | | | |
| | L2C | Compression | ? | ? | ? |
| CP5f | L1T | Tension | Rises | Falls | Rises |
| | L2C | Compression | Rises | Falls | Rises |

X - data not available (readings unreliable)
? - trends not clear

The *rate* of pile installation has no effect on the pore pressure response during load testing.

## 11.4 RADIAL TOTAL STRESSES

### 11.4.1 Load tests on fast-jacked pile CP5f

The variations in radial total stress during load test CP5f/L1T are illustrated in Figure 11.6. The traces from three surface stress transducers are shown: the largest stress being at the leading instrument position. (Note once again that the pile reached its peak axial load at 3.2mm movement.) Several features are worth noting:

- $\sigma_{rr}$ rises initially at all three instrument positions

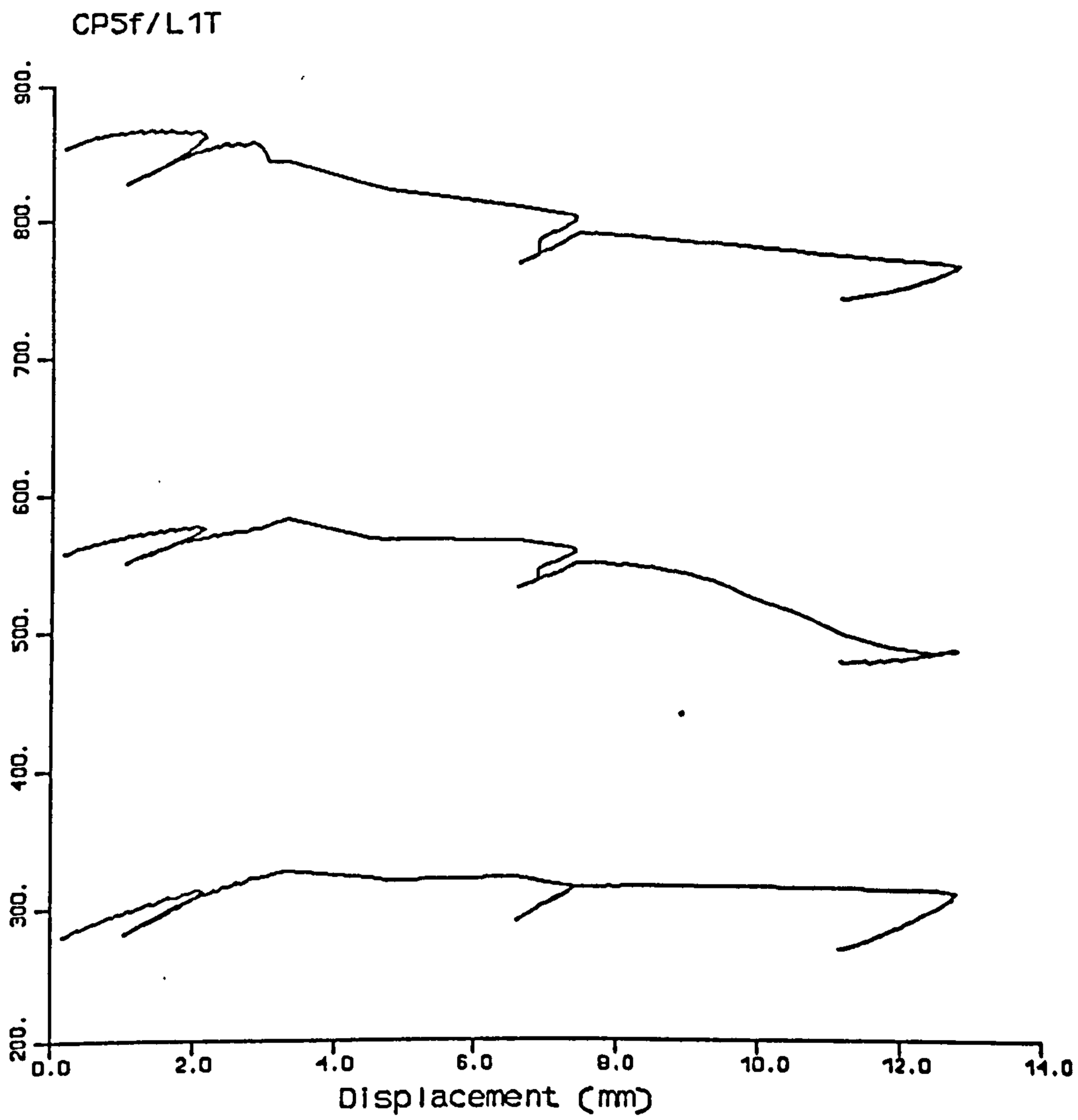



Figure 11.6 Radial total stress changes with pile displacement, load test CP5f/L1T: (top) leading, (middle) following, and (bottom) trailing instrument positions

- The radial total stress responds distinctly to any unloading/ re-loading of the pile
- During plunging failure (after 3.2mm movement), $\sigma_{rr}$ falls significantly at the leading instrument position, only slightly at the following, and hardly at all at the trailing
- On final unloading $\sigma_{rr}$ falls at all three levels

The corresponding figure for test CP5f/L2C (see Appendix 13) shows the same features as for L1T with the important exception that the changes in $\sigma_{rr}$ are of the opposite sign to those in L1T. In other words, $\sigma_{rr}$ *falls* initially, but *rises* during plunging failure.

### 11.4.2 Load tests on slow-jacked pile CP3fs

The changes in radial total stress that were recorded during the first load test (in compression) on CP3fs are shown in Figure 11.7. Note that $\sigma_{rr}$ *decreases* during loading up to failure (i.e. from 0 to ≈2.7mm

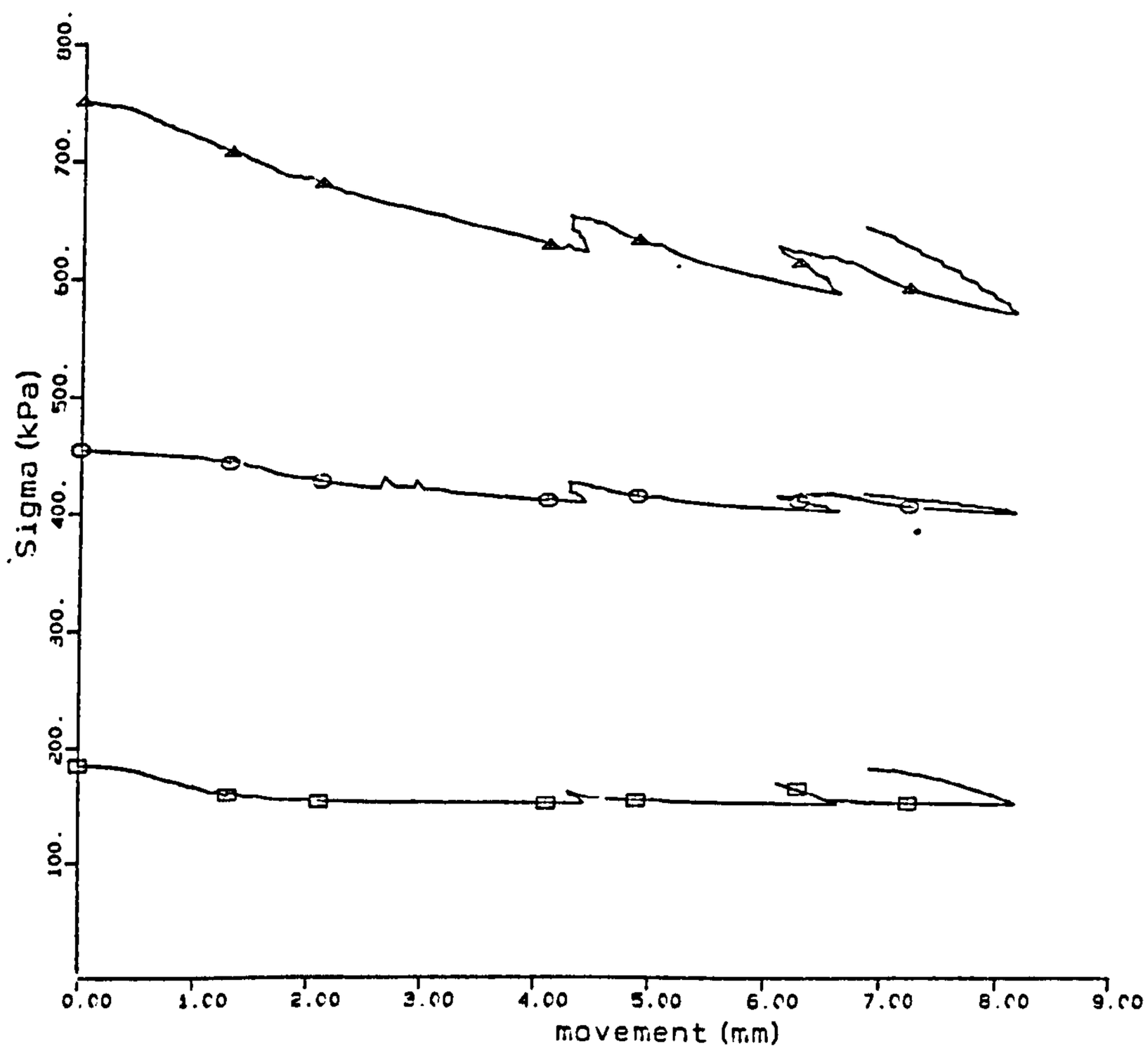



Figure 11.7 Radial total stress changes, load test CP3fs/L1C: (top) leading, (middle) following, (bottom) trailing positions

movement), whereas in CP5f/L1T $\sigma_{rr}$ *increased*. During plunging failure (2.7 to 8mm) $\sigma_{rr}$ also decreases - which matches the response in CP5f/L1T.

The corresponding figure for test CP3fs/L2T is given in Appendix 13. $\sigma_{rr}$ rises both initially and during plunging failure.

### 11.4.3 Summary of radial total stress changes

Table 11.4 summarizes the changes in $\sigma_{rr}$ for all of the tests at Canons Park. It is clear from the table that it is the *direction* of loading that controls the sign of the changes in $\sigma_{rr}$ during initial loading and final unloading (only). The stress changes during plunging failure do <u>not</u> show a one-to-one correspondence with loading direction.

Note that the *rate* of pile installation has no effect on the changes in radial total stress during pile loading.

Table 11.4 Changes in radial total stress during load tests, CP1-5

| Test series | Load test | Direction of loading | Changes in $\sigma_{rr}$ Up to peak load | During plunging | On final un-loading |
|---|---|---|---|---|---|
| CP1s | L1C | Compression | Falls | Both | Rises |
| CP2f | L1C | Compression | Falls | Both | Rises |
| | L2C | Compression | ? | ? | ? |
| | L3T | Tension | Rises | Both | Falls |
| CP3fs | L1C | Compression | Falls | Falls | Rises |
| | L2T | Tension | Rises | Rises | Falls |
| | L3C | Compression | Falls | Falls | ? |
| CP4f | L1T | Tension | Rises | Both | Falls |
| | L2C | Compression | Falls | Rises | Rises |
| CP5f | L1T | Tension | Rises | Falls | Falls |
| | L2C | Compression | Falls | Rises | Rises |

'Both' = at some positions $\sigma_{rr}$ falls, at others it rises
? = trends uncertain

## 11.5 RADIAL EFFECTIVE STRESSES

The combined effect of the changes in $\sigma_{rr}$ and u on the radial effective stress is rather complicated, as Figure 11.8 reveals for the leading instruments in test CP5f/L1T. During initial loading of the pile, the radial effective stress $\sigma'_{rr}$ falls, but then rises during plunging

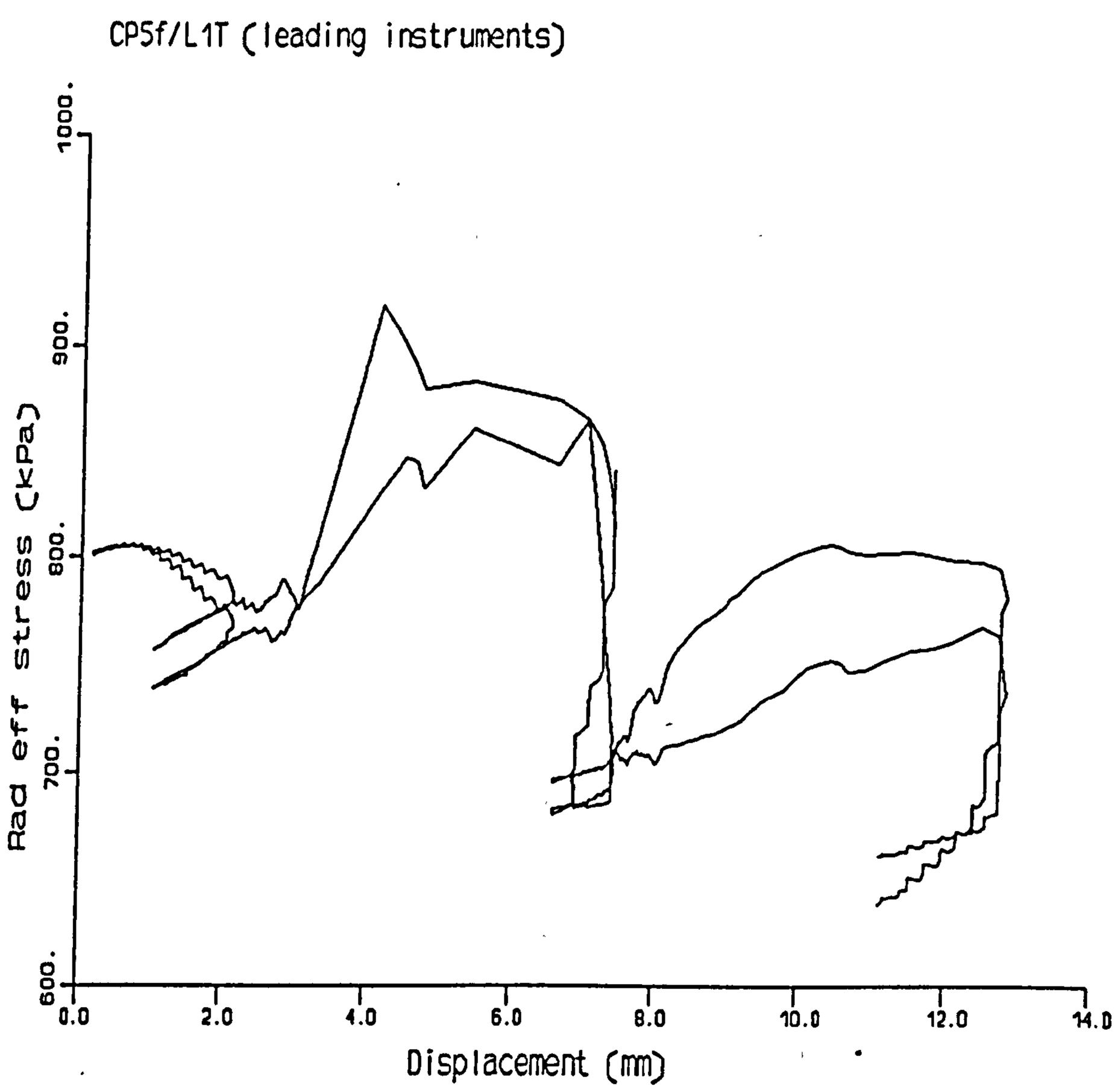



Figure 11.8 Changes in radial effective stress with pile displacement, load test CP5f/L1T (leading instruments)

failure.

The overall pattern of the results from <u>all</u> the load tests (including those on the slow-jacked pile CP3fs) is as follows. During initial loading $\sigma'_{rr}$ may rise or fall, depending on the <u>direction</u> of loading. However, during plunging failure $\sigma'_{rr}$ invariably rises.

Although the changes in $\sigma'_{rr}$ during loading are not insignificant (changes of up to ±50kPa were recorded in some tests), their magnitude is nevertheless smaller than ±15% of the value of $\sigma'_{rr}$ at the start of the test. In the terminology of Chapter 3, $0.85 \leq K_f/K_o \leq 1.15$, where $K_f$ is the lateral stress coefficient at failure, and $K_o$ at the end of equalization. (The lateral stress coefficient is defined as $K = \sigma'_{rr}/\sigma'_{vo}$.)

It is shown in Section 11.9, where the data is plotted on stress path diagrams, that the apparently arbitrary changes in $\sigma_{rr}$, u, and (hence) $\sigma'_{rr}$ during pile loading fit into a systematic pattern which is based on sound physical principles.

## 11.6 SHEAR STRESSES

### 11.6.1 Shear stresses mobilized by fast-jacked pile CP5f

The marked brittleness observed in many of the load tests[2] (see, for example, Figure 11.1) is examined further in Figure 11.9, which shows the shear stresses mobilized at the three instrument positions during load test CP5f/L1T. The pile reached its peak capacity after 3.2mm movement.

The brittleness of the soil adjacent to the pile is immediately apparent, but the degree of brittleness varies along the pile. For example, at the leading instrument position $\tau_{rz}$ falls from a peak value of ≈205kPa to ≈139kPa after 10mm displacement - i.e. a drop of 32% (of the peak value).

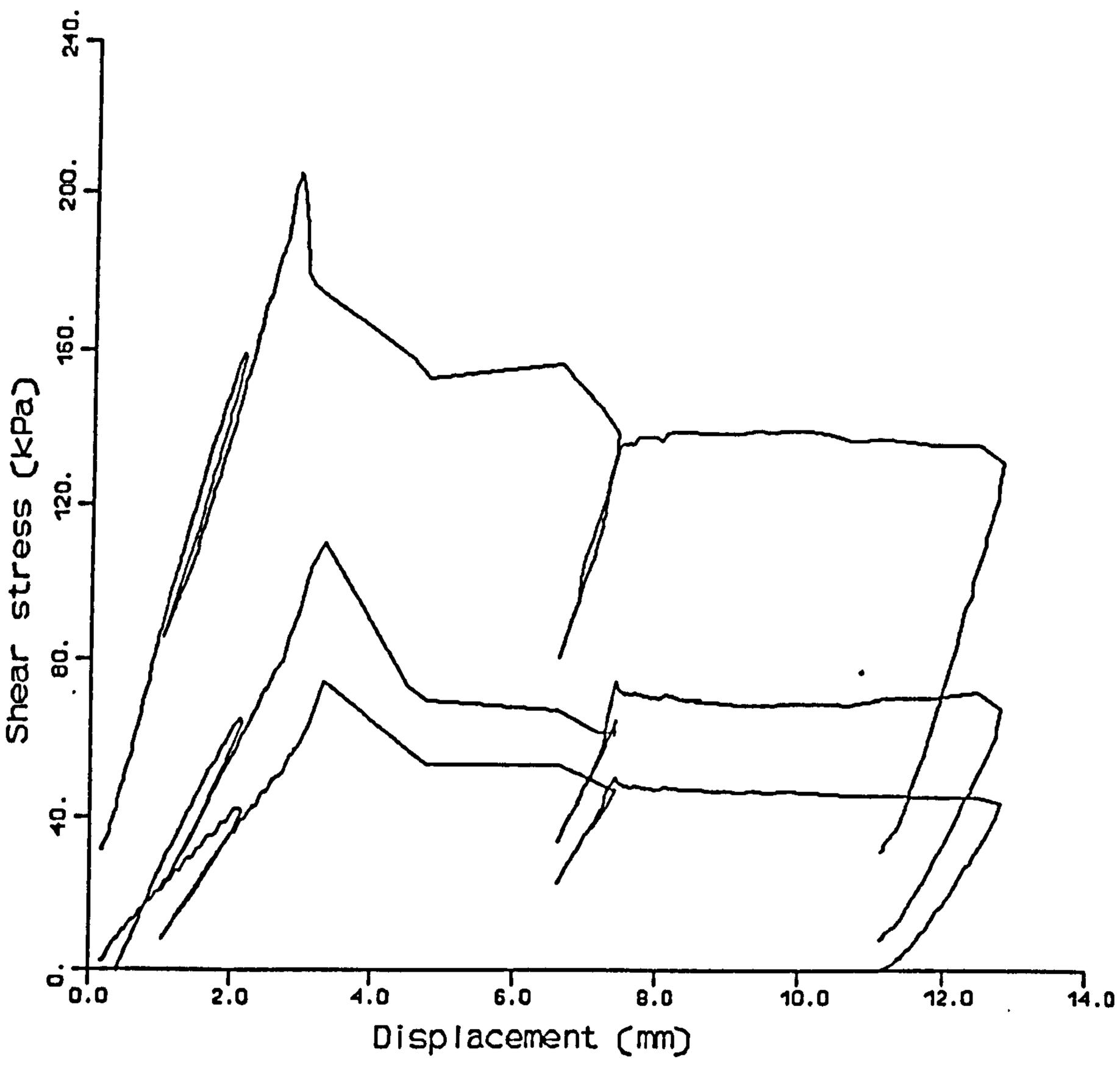



Figure 11.9 Variations in shear stresses during load test CP5f/L1T: (top) leading, (middle) following, and (bottom) trailing instrument positions

At the following position, $\tau_{rz}$ likewise falls by 36%; but at the trailing position only 20% of the peak value is lost at 10mm displacement.

The peak shear stresses are not all mobilized at the same time. Figure 11.10 shows the variation in $\tau_{rz}$ along the pile shaft at various stages during load test CP5f/L1T. Also included on this diagram

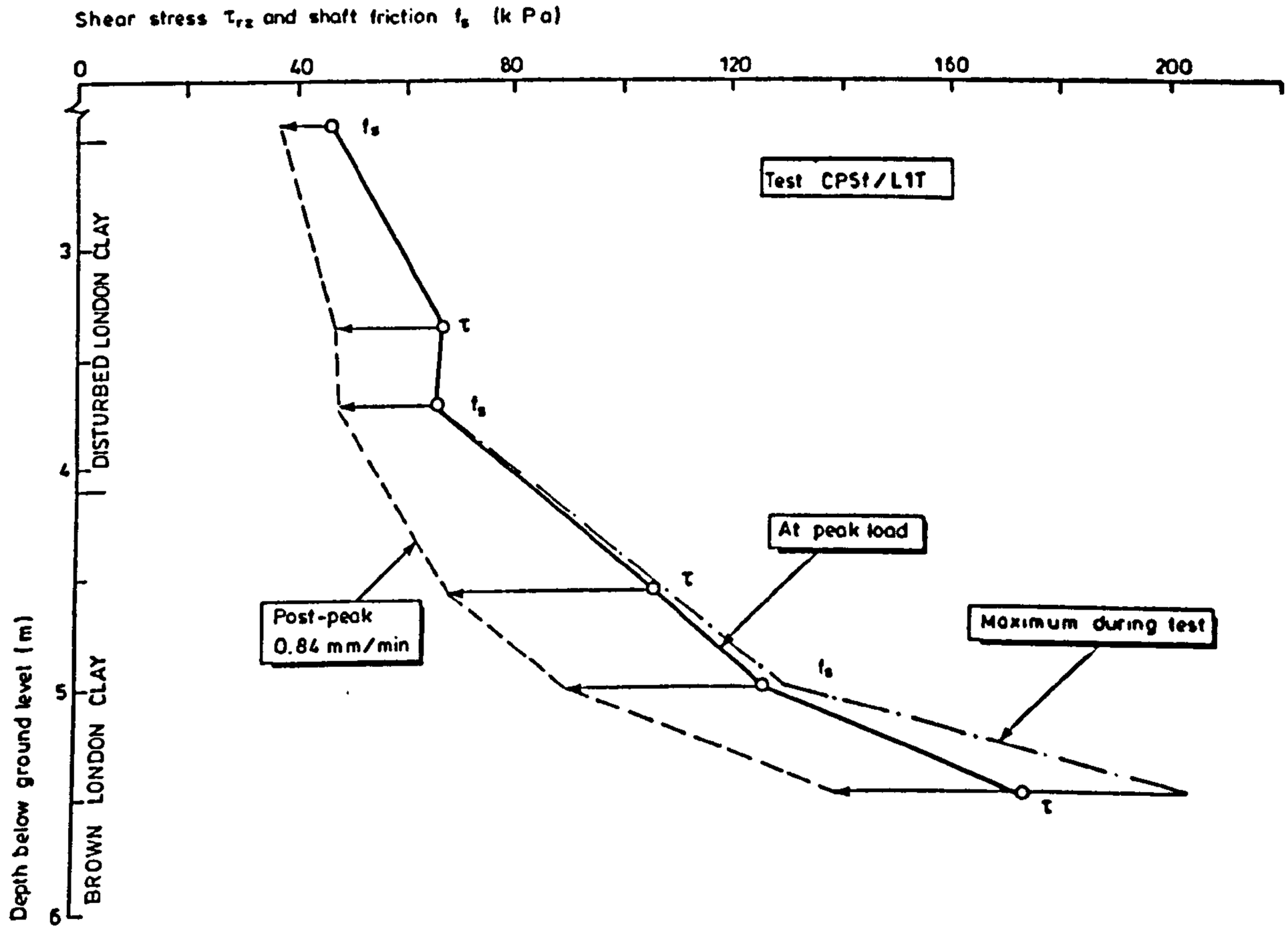



Figure 11.10 Shear stresses mobilized during load test CP5f/L1T

are the values of shaft friction, $f_s$, derived from the changes in axial load along the pile. As the figure demonstrates:

- There is good agreement between the "local" measurements of shear stress ($\tau_{rz}$) and the "average" measurements ($f_s$)
- Progressive failure occurs, starting at the pile tip (whereas most theories suggest that the pile fails from the top down)
- Significant brittleness ensues over the whole length of the pile ($I_B$ = 20-36%)*
- The variation of shear stress along the pile is very similar to

*The "brittleness index" $I_B = ([\tau_{rz}]_{peak} - [\tau_{rz}]_{residual})/[\tau_{rz}]_{peak}$

the variation of $\sigma'_{rr}$

This final point implies that there is a relatively constant angle of friction controlling the shear stresses mobilized during the load test.

Figure 11.11 presents similar profiles of $\tau_{rz}$ and $f_s$ versus depth for load test CP5f/L2C. The pattern of behaviour in this second test differs in three ways from that observed during CP5f/L1T. Firstly, the pile fails <u>before</u> the leading and following instruments have registered peak values

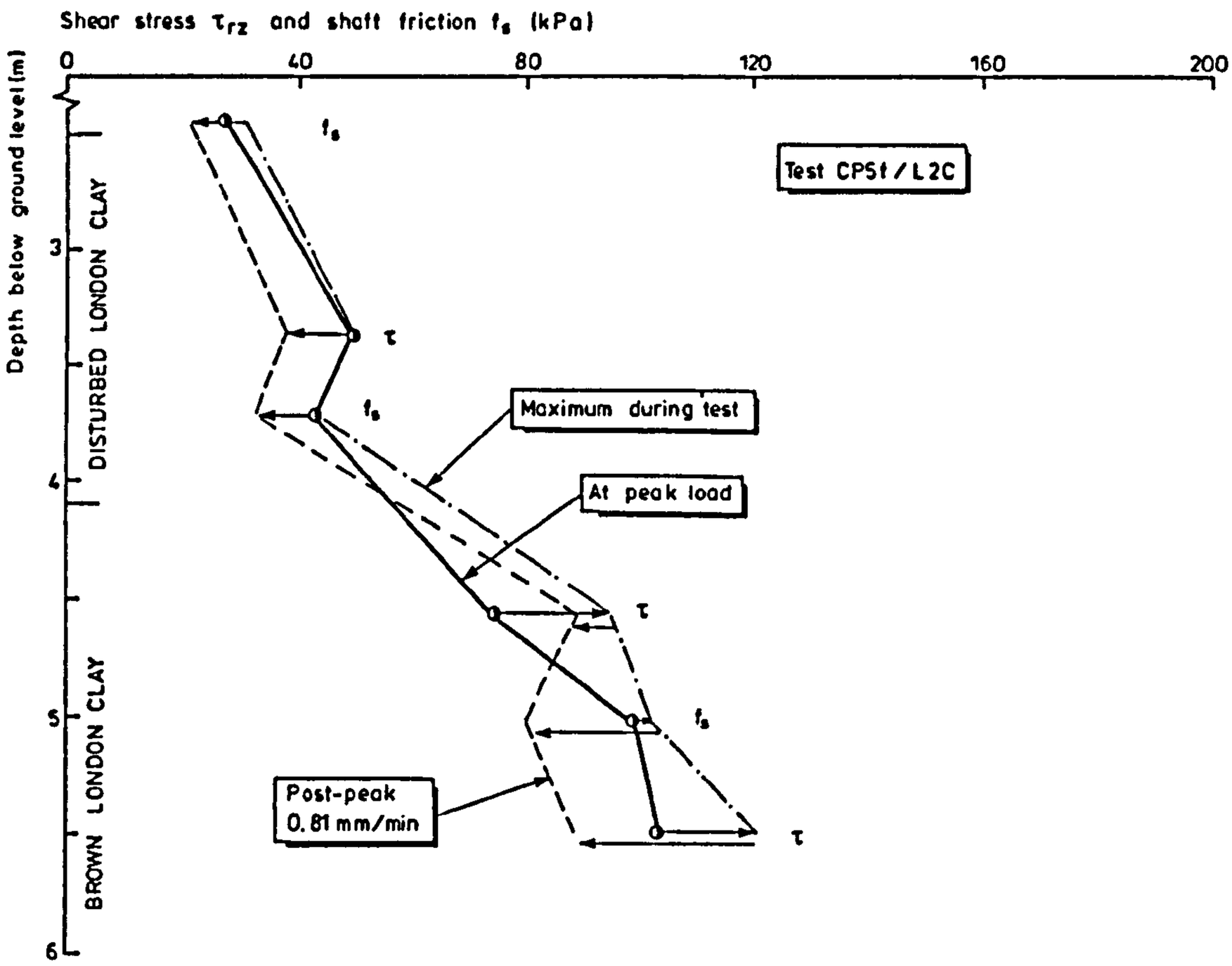



Figure 11.11 Shear stresses mobilized during load test CP5f/L2C

for $\tau_{rz}$. Secondly, there is less brittleness in absolute terms than in test L1T (although about the same amount in percentage terms: $I_B$ = 21-32%). Finally, the shear stresses mobilized during L2C only reach the order of magnitude of the stress mobilized <u>post-peak</u> in test L1T.

## <u>11.6.2 Shear stresses mobilized by slow-jacked pile CP3fs</u>

Figure 11.12 shows the shear stresses that were mobilized during the first (compression) load test on pile CP3fs. The shape of the traces is

very similar to the load-displacement curve for this load test (as shown in Figure 11.2). The clay clearly gives a ductile response to pile loading over its entire length, from the leading instrument position to the trailing.

At Canons Park, the only load tests in which ductile behaviour was observed were the first loading tests in compression on the two *slow*-jacked piles (i.e. CP1s/L1C and CP3fs/L1C); and in the *second* test in compression on the fast-jacked pile CP2f. (Note that the previous load test on CP2f was also in compression, and hence by the time the second

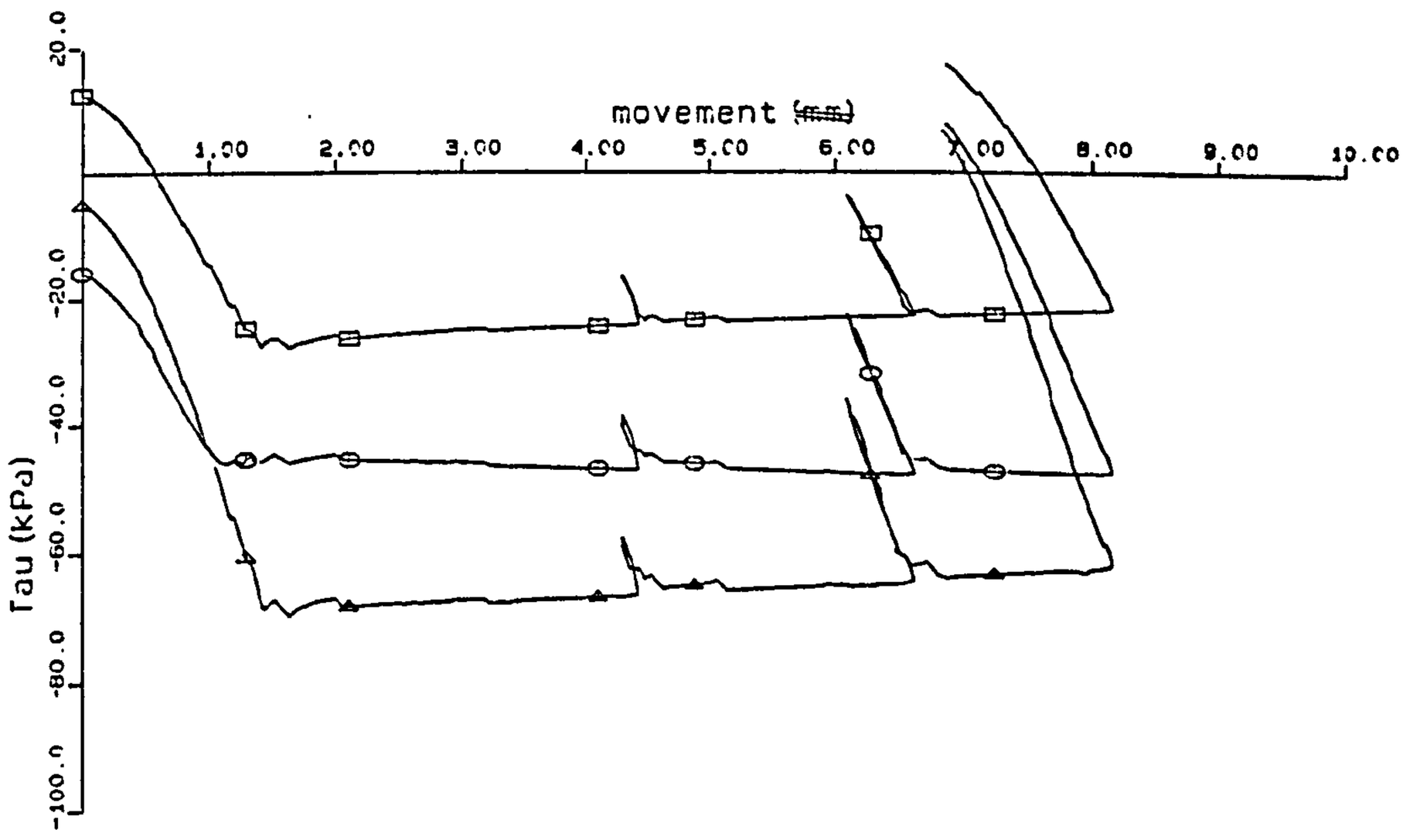



Figure 11.12 Variations in shear stresses during load test CP3fs/L1C: (top) trailing, (middle) following, (bottom) leading instrument positions

load test was performed this pile had acquired the characteristics of a slow-jacked pile.) In every other test the response of the soil was brittle.

## 11.7 COEFFICIENTS OF FRICTION

### 11.7.1 Introduction

A central step in most effective stress design methods is the assessment of the coefficient of friction to be used in calculations of shear stress. The *coefficient* of friction $\mu$ is defined as $\mu = \tau_{rz}/\sigma'_{rr}$, whereas the *angle* of friction $\delta$ equals $\tan^{-1}\mu$. As we have seen already, $\tau_{rz}$ falls quite rapidly once it has passed its peak value, whereas $\sigma'_{rr}$ does not vary greatly while this is happening. This suggests that $\mu$ can decrease markedly with pile displacement, particularly in load tests which produce brittle load-displacement curves.

### 11.7.2 Load tests on fast-jacked pile CP5f

Figure 11.13 presents the traces of $\mu$ that were recorded during load test CP5f/L1T at three different positions along the pile shaft. The following points should be noted:

- The peak values of $\mu$ on first time loading are between 0.20 and 0.25 ($11\frac{1}{2}° < \delta < 14°$); for comparison, the critical state friction angle for the London clay is $\phi_{cs} \approx 22\frac{1}{2}°$
- Values of $\mu$ in subsequent tests are all lower than 0.20 and drop towards an ultimate value of about 0.13 ($\delta \approx 7°$)
- By comparison, the friction coefficients recorded during pile installation showed a far wider range of values: at the trailing instrument level, $\mu$ exceeded 0.3 ($\delta = 16\frac{1}{2}°$), whilst at the leading position values as low as 0.075 ($\delta = 4°$) were recorded! (although $\mu \approx 0.2$ [11°] is a more typical value)
- Problems of different instrument response times may be the reason for the very low readings of $\mu$ near the pile tip during pile installation, although the very large radial effective stress variation along the pile may also be a contributory factor - this is discussed further in Chapter 14

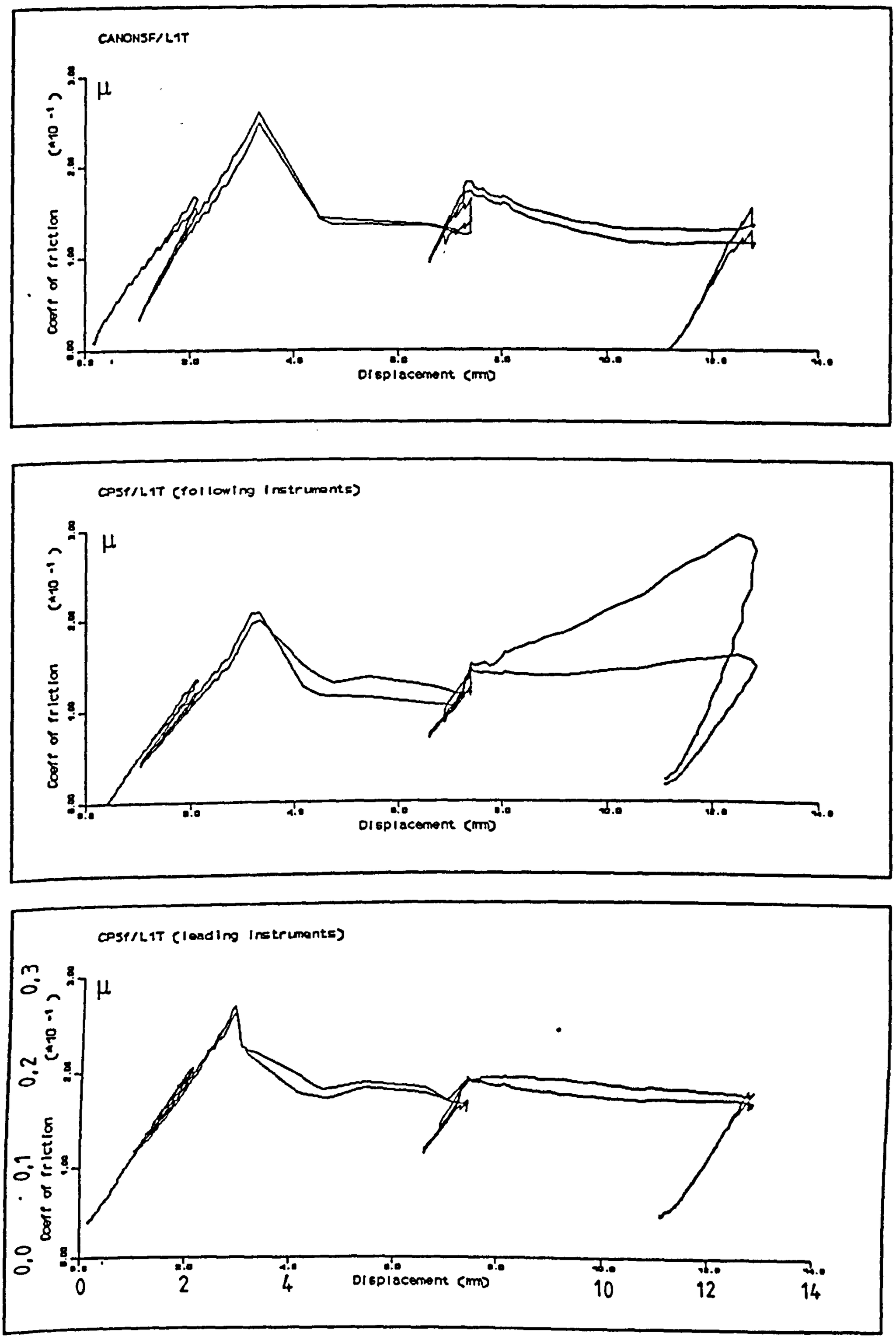



Figure 11.13 Coefficients of friction recorded during pile test CP5f/L1T: (top) trailing, (middle) following, and (bottom) leading instrument positions

## 11.7.3 Load tests on slow-jacked pile CP3fs

Figure 11.14 shows the coefficients of friction that were recorded at the following and trailing positions in Test CP3fs/L1C. The results from test CP3fs/L2T are given in Appendix 13.

- At the leading and following positions $\mu$ does not exceed 0.14 (8°) during first loading (i.e. in test CP3fs/L1C), except at the trailing position, where $\mu$ = 0.21-0.24 (12-13½°) at peak load
- Reversing the loading direction (in CP3fs/L2C) gives peak values of $\mu$ equal to 0.24 ±0.01; but $\mu$ quickly degrades towards an ultimate value of 0.14 ±0.02

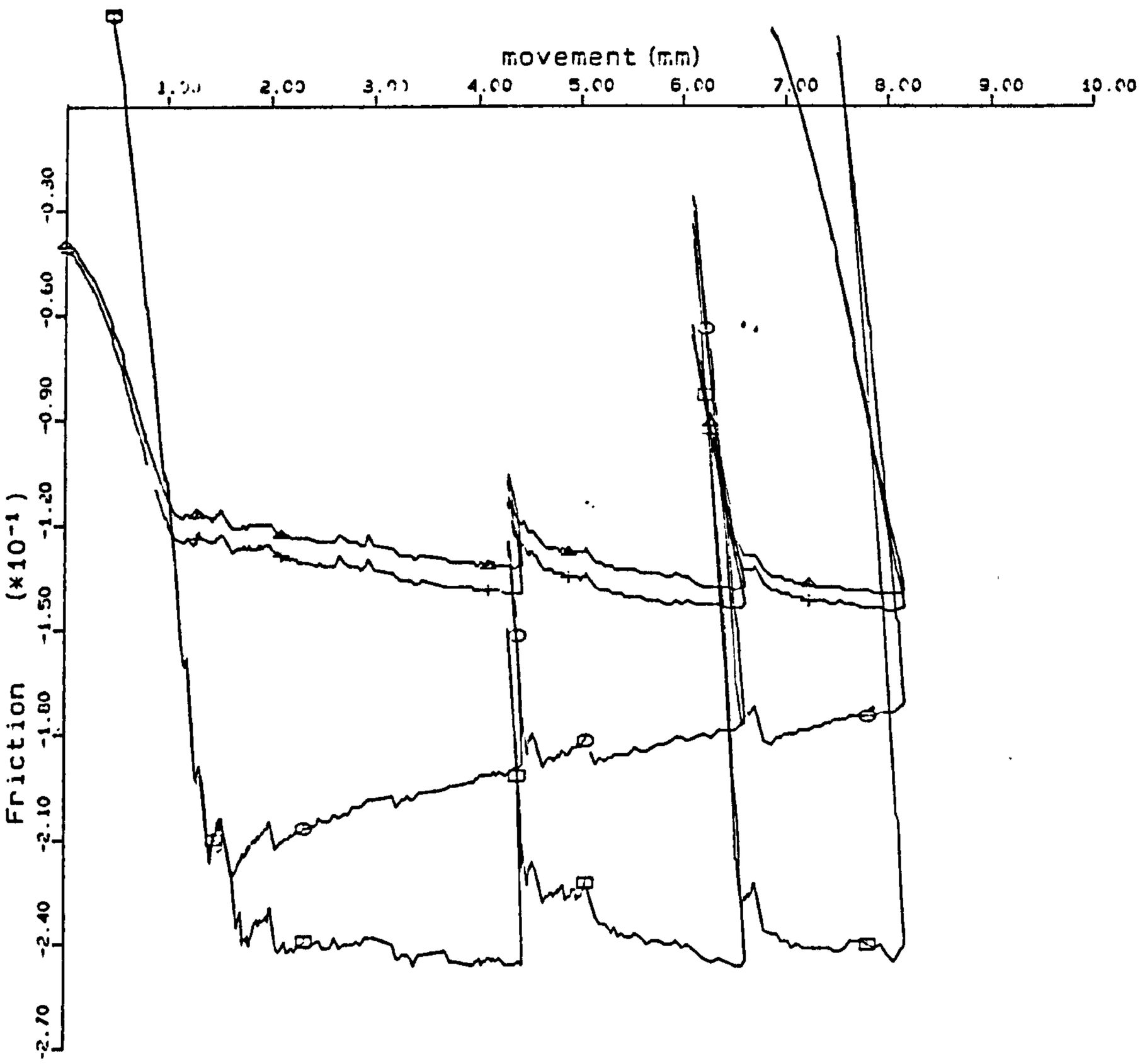



Figure 11.14 Coefficients of friction from following and trailing instruments, during load test CP3fs/L1C (2 traces per position; following instruments shown by Δ and +)

## 11.8 EFFECTIVE STRESS PATHS FOLLOWED DURING PILE LOADING

### 11.8.1 Introduction

A clear way to identify the basic mechanisms of shearing adjacent to the pile shaft is to follow the effective stress paths for separate soil elements during pile loading. Graphs of $\tau_{rz}$ against $\sigma'_{rr}$ allow us to combine, in one diagram, data from the radial total stress and shear stress circuits with that from the pore pressure probes. To my knowledge, *reliable* plots of this kind have not been published in the Literature, possibly because the data required must be of exceptionally good quality (see Chapter 4). One of the major achievements of this research is being able to report the $\tau_{rz}$ vs $\sigma'_{rr}$ stress paths for load tests on slow- and fast-jacked piles (CP3fs and CP5f).

### 11.8.2 Load tests on fast-jacked pile CP5f

Figure 11.15 shows the stress paths followed in load tests CP5f/L1T and L2C.

Consider the tension test first. As Figure 11.15 shows, the initial trend is for $\sigma'_{rr}$ to increase slightly as the pile is loaded (points A to B). Applying an unload/re-load cycle (B-C-B) makes little difference to the value of $\sigma'_{rr}$. However, once the pile has reached its peak load (point D), the soil dilates strongly and $\sigma'_{rr}$ increases (D to E). At the same time the coefficient of friction $\mu$ (= $\tau_{rz}/\sigma'_{rr}$) falls with continuing displacement. When the soil reaches a lower bound value of $\mu$ ($\approx$0.14 at E) the soil stops dilating and $\sigma'_{rr}$ starts to reduce. Between E and F the pile is plunging so fast that the load cannot be maintained at the pile head.

Figure 11.15 also shows the stress paths for load test CP5f/L2C. Re-loading the pile in compression (i.e. in the opposite direction to the first test) leads to further reductions in $\sigma'_{rr}$, until yield occurs (somewhere around point B). The soil then dilates strongly (points C to D), with $\mu$ simultaneously reducing from about 0.2 to a final value around

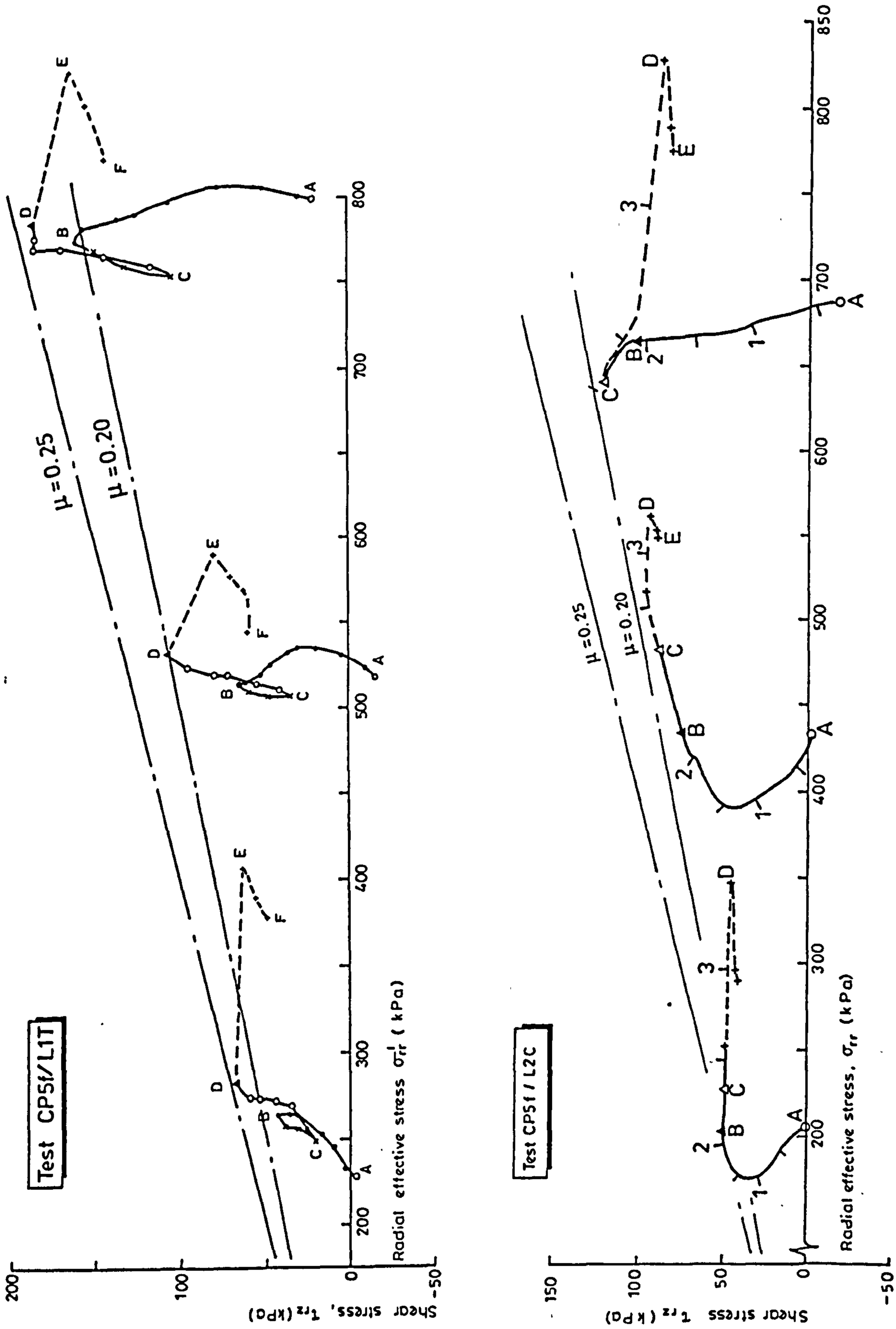



Figure 11.15 Stress paths followed in load tests CP5f/L1T and L2C

0.14. The ultimate value of $\mu$ is the same as was mobilized at the end of dilation in test L1T. From D to E the radial effective stresses reduce, but $\mu$ remains fairly constant.

### 11.8.3 Load tests on slow-jacked pile CP3fs

The stress paths for the first two load tests (L1C and L2T) on pile CP3fs are presented together in Figure 11.16. In the first test (in compression), the radial effective stresses decrease steadily with displacement until the pile reaches its peak capacity at point B. The soil then yields, and dilates slightly at the leading instrument position (right-hand stress path, points B to C) before contracting on further displacement (C to E). Elsewhere along the pile the soil contracts (B-D-E), with $\mu$ increasing slightly as $\tau_{rz}$ remains constant and $\sigma'_{rr}$ reduces. This is the opposite of the behaviour seen next to the fast-installed pile.

When re-loaded in the opposite direction (i.e. in tension), CP3fs displays many of the features seen in the first (tension) load test on the fast-installed pile (i.e. CP5f/L1T). $\sigma'_{rr}$ changes very little up to peak load (A to B), and the friction coefficients at points B ($\mu$ = 0.20-0.25) are close to the corresponding values in CP5f/L1T. However, the soil next to slow-jacked pile dilates far less than the soil next to the fast one; although the coefficient of friction falls far more rapidly.

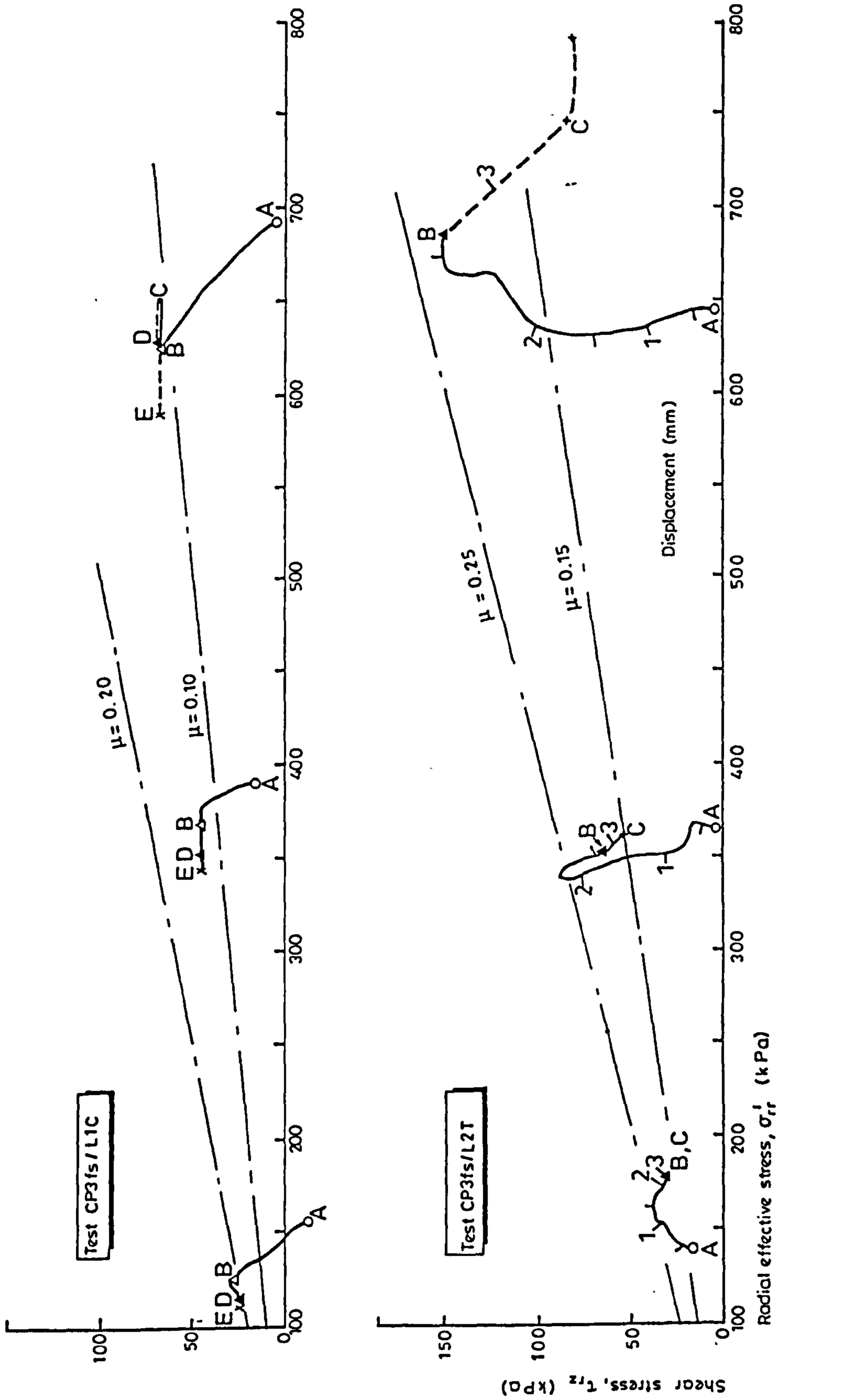



Figure 11.16 Stress paths followed in load tests CP3fs/L1C and L2T

## 11.9 DISCUSSION

### 11.9.1 Key findings from load-displacement data

As discussed in Section 11.2.1, continued displacement of fast-jacked piles causes gradual degradation of their shaft capacity, regardless of the direction of displacement. The results from multiple tests on the same pile should not be used to determine the effects of set-up time or loading direction, on the first-time loading capacity of piles.

The ductile response of slow-jacked piles (see Section 11.2.2) suggests that they fail by sliding along a highly-polished, continuous, "principal displacement shear" that was formed close to the pile shaft during installation. *Visual* evidence to support this hypothesis is presented Chapter 13.

### 11.9.2 Summary of the behaviour in terms of effective stresses

The effective stress data from the load tests on the slow- and fast-jacked piles fits into a simple pattern of behaviour which can be summarized in two flow diagrams (see pp384-385). This *modus operandi* helps to explain the behaviour of displacement piles in terms of effective stresses acting at the pile/soil interface. It clearly demonstrates that the pile's response depends on:

- Its rate of installation (slow or fast)
- Its loading history (i.e. what load tests have previously been conducted on it)
- The current direction of loading (whether tension or compression)

# SLOW-JACKED PILES

1st loading, compression (L1C)

Ductile response. Small (5-20%) reductions in $\sigma'_{rr}$ up to yield. Initial failure with $\mu$ = 0.12-0.20. $\sigma'_{rr}$ reduces with further displacement (contraction), with no change in $\tau_{rz}$. The final value of $\mu$ is within 0.01 of its peak value.
[See CP1s/L1C & CP3fs/L1C.]

2nd loading, compression (L2C)

Re-loading in compression produces behaviour similar to L1C, i.e. a ductile response.
[See CP3fs/L2C re-load.]

2nd loading, in tension (L2T)

Little change in $\sigma'_{rr}$ up to yield, at $\mu$ = 0.2-0.25, followed by rapid reduction in $\mu$ and dilation to ultimate conditions.
[See CP3fs/L2T.]

1st loading, in tension (L1T)

Brittle response. Small increases in $\sigma'_{rr}$ up to yield. Initial failure with $\mu$ = 0.2-0.25, followed by slight increases in $\sigma'_{rr}$ with further displacement, while $\tau_{rz}$ and $\mu$ reduce sharply to $\mu \approx 0.16$(?).
[Probable behaviour, based on CP3fs/L2T.]

2nd loading, compression (L2C)

Brittle response.
[See CP3fs/L3C.]

2nd loading, in tension (L2T)

Re-loading in tension produces ductile response. Small increases in $\sigma'_{rr}$ up to yield, failure with $\mu$ = 0.12-0.18 (cf. L1C).
[Based on CP3fs/L2T re-load.]

# FAST-JACKED PILES

1st loading, compression (L1C)

Moderately brittle response. Small reductions in $\sigma'_{rr}$ up to yield. Initial failure with $\mu$ = 0.2-0.25, followed by large increases in $\sigma'_{rr}$ (dilation) until $\mu$ reaches an ultimate value of ≈0.16 (?).
[Probable behaviour: based on CP2f/L1C.]

2nd loading, compression (L2C)

Re-loading in compression produces ductile response.
[See CP2f/L2C.]

2nd loading, in tension (L2T)

Data not available

1st loading, in tension (L1T)

Brittle response. Small (0-20%) increases in $\sigma'_{rr}$ up to yield. Initial failure with $\mu$ = 0.21-0.24. Then $\sigma'_{rr}$ increases with further displacement (dilation) but $\tau_{rz}$ falls (by up to 25%). As a result the final value of $\mu$ is between 0.16 and 0.19.
[See CP4f/L1T & CP5f/L1T.]

2nd loading, compression (L2C)

Moderately brittle response. Small reductions in $\sigma'_{rr}$ up to yield. Failure with $\mu$ = 0.19-0.25, followed by large increases in $\sigma'_{rr}$ (dilation). Ultimate $\mu$ = 0.14-0.16.
[See CP4f/L2C & CP5f/L2C.]

2nd loading, in tension (L2T)

Ductile response likely. Small increases in $\sigma'_{rr}$ up to yield. Ultimate $\mu$ = 0.12-0.17.
[Probable behaviour based on CP4f/L1T re-load & CP5f/L1T re-load.]

## 11.10 NOTES AND REFERENCES

[1]Tomlinson M.J. (1970a). Adhesion of piles in stiff clays. CIRIA Report 26, Construction Industry Research and Information Association, London, 47pp.

[2]The only load tests in which there was a ductile response were CP1s/L1C and CP3fs/L1C. In other words, all fast-jacked piles were brittle on first-time loading no matter whether they were loaded in tension or compression. All the piles (both fast- and slow-jacked) gave a brittle response when the loading direction was changed.

# Chapter 12

# Driven pile tests

## CONTENTS OF CHAPTER 12


12.1 INTRODUCTION . . . . . 390

12.2 FABRICATION, INSTALLATION, AND LOAD TESTING . . . . . 391

12.2.1 Fabrication of the driven piles 391

12.2.2 Pile installation 391

12.2.3 Load testing 392

12.2.4 Pile extraction 392

12.3 RESULTS OF TENSION TESTS ON DRIVEN PILES . . . . . 393

12.4 DISCUSSION . . . . . 395

12.5 NOTES AND REFERENCES . . . . . 396

## 12.1 INTRODUCTION

The main purpose of the driven pile tests at Canons Park was to determine whether the method of installation has any significant effect on the pile's subsequent load-displacement characteristics. The aims were i) to compare the behaviour of closed-ended jacked and closed-ended driven piles; and ii) to assess any differences in behaviour between closed-ended driven and open-ended driven piles. The value of the results from the instrumented pile tests would be greatly enhanced if it was shown that these piles, which were jacked into the ground, had the same load-displacement characteristics as driven piles.

Two uninstrumented driven piles (CP6 and 7) were installed at Canons Park and were tested in the same way as the "control" instrumented jacked pile CP5. All three piles were loaded two days after installation; CP5f was fast-jacked and closed-ended; CP6d driven and closed-ended; and CP7do driven but open-ended. The tests were all carried out in tension to avoid the problem of estimating the end-bearing of the driven piles.

## 12.2 FABRICATION, INSTALLATION, AND LOAD TESTING

### 12.2.1 Fabrication of the driven piles

Piles CP6 and CP7 were fabricated from hot-finished, seamless steel tubing, 100mm in diameter and with a wall thickness of 9.525mm. As with the jacked piles, both were grit-blasted prior to installation in order to simulate the surface roughness of a typical rusty pile. A steel cone (apex angle 60°) was welded to the end of pile CP6d whereas CP7do was left open-ended.

Key features of piles CP6d and CP7do

| | CP6d | CP7do |
|---|---|---|
| Pile type | Closed-ended tube | Open-ended tube |
| Overall length | 6.52m | 6.52m |
| Penetration | 5.80m | 5.70m |
| Embedded length L | 3.71m | 3.60m |
| Ratio (L/D) | 36.5 | 35.4 |
| Instrumentation | None | None |
| Installation | Driven | Driven |
| Equalization | Short | Short |
| Load tests | L1T | L1T |

### 12.2.2 Pile installation

CP6 and 7 were driven using an Atlas Copco PH5 double-acting air hammer. This weighs about 390kg and delivered approximately 250 blows/minute (its nominal impact rate is 310 blows/minute). The pile's average velocity was determined by monitoring the progress of a series of marks placed at 50mm intervals along its shaft. Table 12.1 summarizes the main details regarding driving.

Table 12.1 Summary of driven pile tests at Canons Park

| Pile | Embedded length (m) | Average velocity (mm/min) | Hammer rate (blows/min) | Driving time (min) |
|---|---|---|---|---|
| CP6d | 5.80 | 101 ±34 | 256 ±12 | ≈17 |
| CP7do | 5.70 | 53 ±15 | 258 ±14 | ≈34 |

The rates of movement achieved on installing CP6d and CP7do were significantly different. The most likely cause was the loss in impact energy that resulted from the loosening of bolts securing the steel dolly during installation of CP7. At the end of driving, a 1.68m long plug of soil had formed in the bottom of the open-ended pile.

### 12.2.3 Load testing

The loading frame used to install the jacked piles also provided the reaction for the loading tests on the driven piles. The frame itself was reassembled for these tests, having been removed temporarily to allow the piles to be driven.

CP6d and CP7do were load tested in tension two days after installation. During the load test on CP6d, the displacement of the pile's head was kept to a minimum to avoid disturbing the soil fabric around the pile, since an inspection trench was to be excavated around it (see Section 12.2.4). Therefore as soon as the peak capacity had been determined, and one small unload/re-load loop followed, the pile was unloaded completely. Total displacement was less than 6mm.

### 12.2.4 Pile extraction

CP6d was one of two piles that were unearthed when the inspection trench was dug (see Chapter 13), the other being Kitching's[1] slow-jacked pile. Samples were taken of the soil adjacent to the piles for later examination in the laboratory. Since the fabric of the soil was of particular interest, the displacement of pile CP6d was kept to a minimum during load test L1T in order not to disturb it. CP7do was not extracted from the ground.

## 12.3 RESULTS OF TENSION TESTS ON DRIVEN PILES

The load-displacement curves resulting from the tension tests on piles CP6d and CP7do are presented in Figure 12.1. These curves should be compared with that presented earlier for load test CP5f/L1T (see Figure 9.1 on p357 and Appendix 13).

The following are the main points of interest:

- The load-displacement curves for CP6d and CP7do are noticeably non-linear up to peak load (likewise for CP5f)
- The load capacity is higher for the closed-ended pile (CP6d) than for the open-ended one (CP7do), and both are comparable with that of CP5f
- The difference in capacity is partly due to the slightly different lengths of the three piles; there is far less difference between their $\alpha$ values at peak load
- Pile CP6d shows marked brittleness post-peak (as does CP5f); the load capacity of CP7do also falls with continued displacement, but not so conspicuously - nevertheless, at ≈12mm displacement both CP5f and CP7do mobilize only 80% of their peak loads

Table 12.2 summarizes the peak load capacities for these piles, together with the alpha values that have been deduced from them.

Table 12.2 Results of tension load tests on driven piles

| Pile test | Displacement at failure (mm) | Peak axial load (kN) | $\alpha$ | $\beta$ |
|---|---|---|---|---|
| CP5f | 3.2 | -105.4 | -0.90 | -1.83 |
| CP6d | 3.0 | -104.6 | -0.93 | -1.90 |
| CP7do | 3.0 | -93.5 | -0.87 | -1.73 |

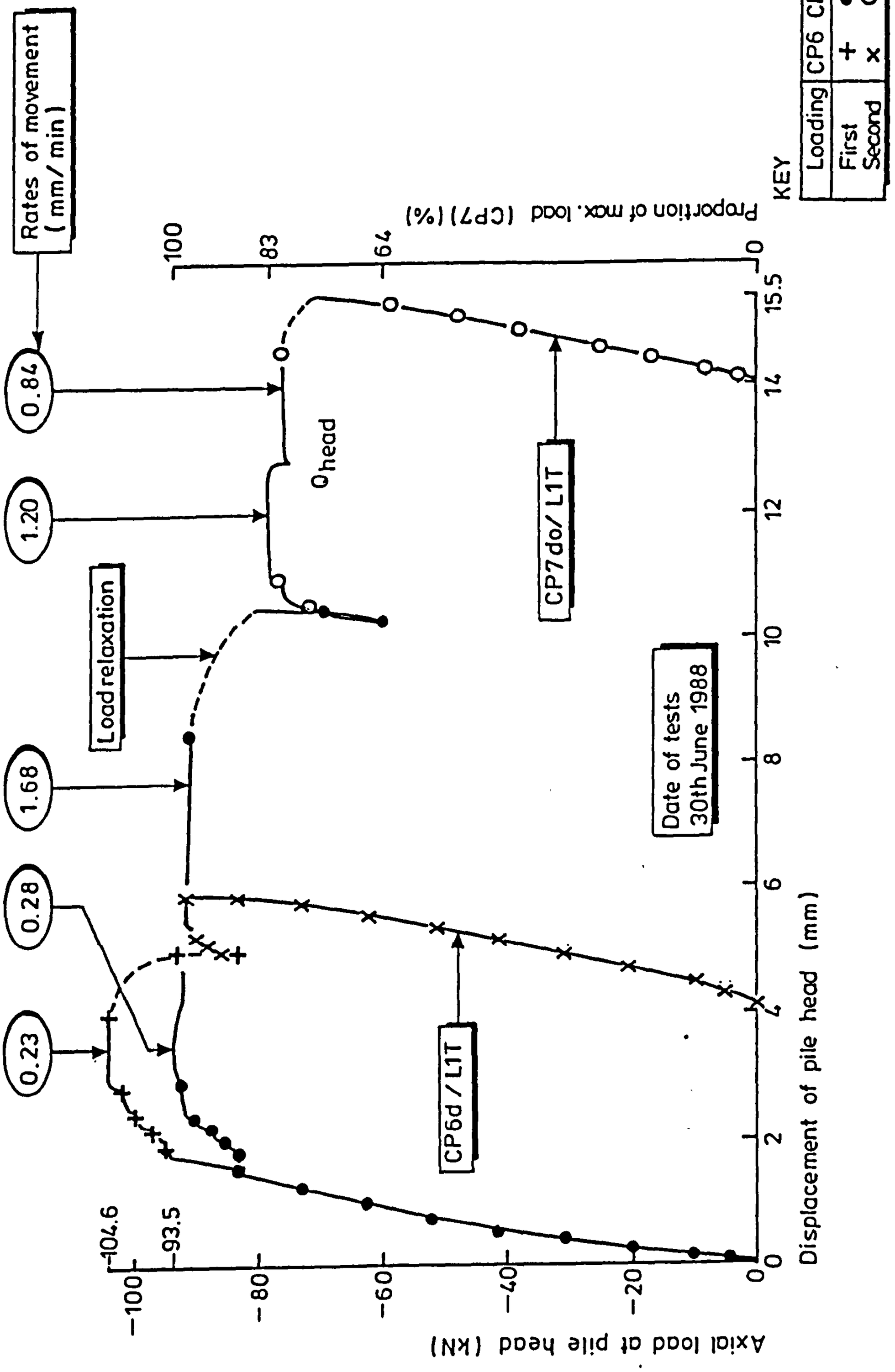



Figure 12.1 Load-displacement curves for load tests CP6d/L1T and CP7do/L1T

## 12.4 DISCUSSION

These observations suggest that - for the soil conditions at Canons Park - there is little or no difference between the behaviour of a fast-jacked pile and a driven pile (at least in first time loading). Slight discrepancies exist between the behaviour of the open-ended and closed-ended piles, but only after failure has occurred.

The earlier Test Series at Canons Park (as described in Chapter 11) show that fast-jacked piles are considerably stronger in first time loading than slow-jacked piles. It therefore follows that significant differences should exist between the behaviour of driven and slow-jacked piles in soils such as the London clay. Evidence to support this conclusion can be found in the tests reported by Tomlinson[2] (see Chapter 4).

## 12.5 NOTES AND REFERENCES

[1]Kitching D.N. (1983). A study into the microfabric of clays adjacent to jacked piles. MSc Dissertation, Univ. of London (Imperial College), 31pp+.

[2]Tomlinson M.J. (1970a). Adhesion of piles in stiff clays. CIRIA Report 26, Construction Industry Research and Information Association, London, 47pp.

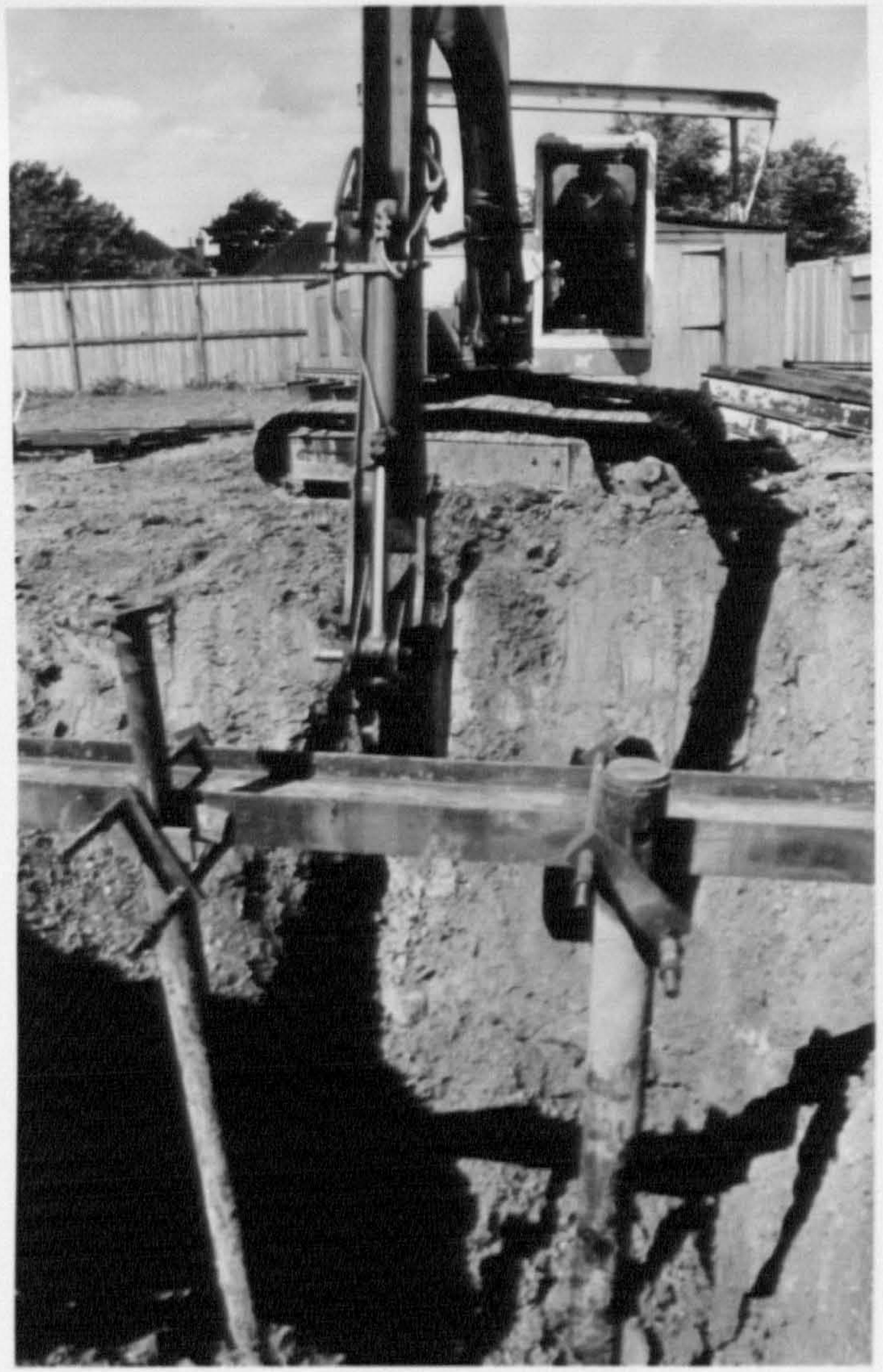
# Chapter 13

# Pile inspection trench

## 13.1 INTRODUCTION

The final element of the research programme at Canons Park comprised excavating an inspection trench around two piles, one of which had been jacked into the ground, and the other driven. The main purpose of the exercise was to examine the fabric of the soil and, in particular, to look for shear surfaces adjacent to the piles. At the same time, samples could be taken for subsequent laboratory testing and a number of simple in situ tests could be performed.

This chapter is divided into five main sections. The first (13.2) describes the general features of the trenching operations; 13.3 gives details of the sampling techniques and in situ test procedures; 13.4 presents the variation of the soil's properties with radial distance from the piles; and Section 13.5 describes the distortion to the soil's fabric caused by pile installation and testing. Finally, Section 13.6 synthesizes these findings and attempts to tie them into the general understanding of pile behaviour obtained from the instrumented pile tests.



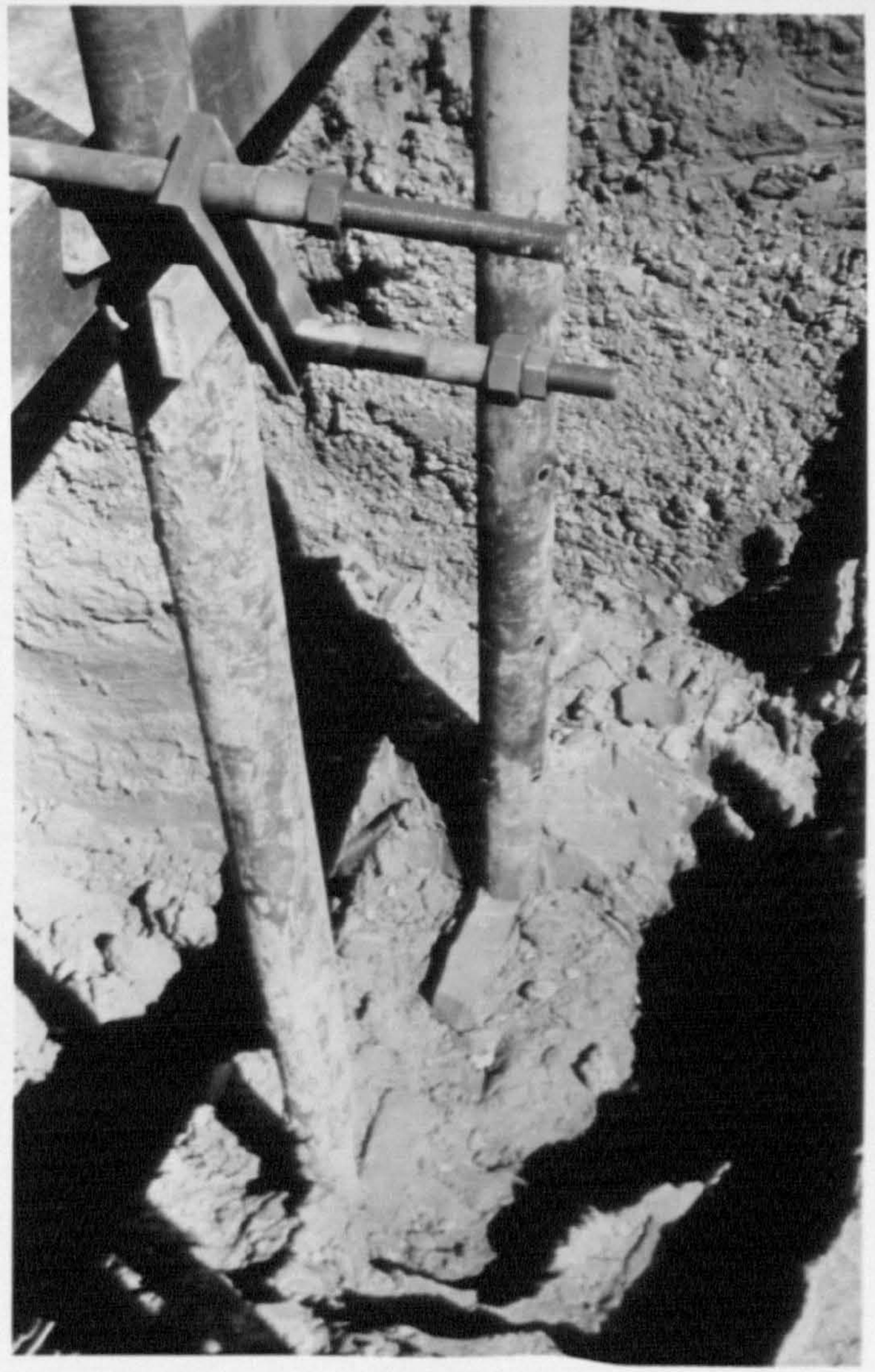


Plate 6 Views of the inspection trench: (a) excavation in progress (left);
(b) working platform between the piles (right) [photos: A. Bond]

## 13.2 GENERAL FEATURES OF THE INSPECTION TRENCH

### 13.2.1 Excavation of the inspection trench

The inspection trench was excavated to a depth of 4.5m, around i) the slow-jacked* pile installed by Kitching[1] (in the summer of 1983) and ii) the driven pile CP6d (installed on 28th June 1988). The trenching operations were completed over a three day period (from 25th to 27th July 1988). Thus, before being unearthed these piles had been in the ground for five years and one month (respectively). Both piles had been load tested (once only) shortly after installation.

Plate 6 presents two views of the inspection trench, showing: (a) excavation in progress; and (b) a close up of the sampling area between the piles. In both photographs the driven pile is on the left. The inspection trench was approximately 5m wide x 8m long on plan.

The bulk of the digging was done by a Poclain excavator operating from ground level. Great care was taken not to disturb the clay in the places where samples were required: hand-held, pneumatically powered, clay-spades were employed to rough out the clay in these areas. The final cuts around each sample were made with a cheese wire.

Both piles were clamped at ground level to a universal beam that straddled the trench, to prevent them from moving during excavation (see Figure 13.1 and Plate 6). This was done both as a safety precaution and for fear of disturbing the clay next to the piles. The toes of both piles remained embedded in the ground throughout.

---

*See Chapter 7 for the definition of "slow" jacking

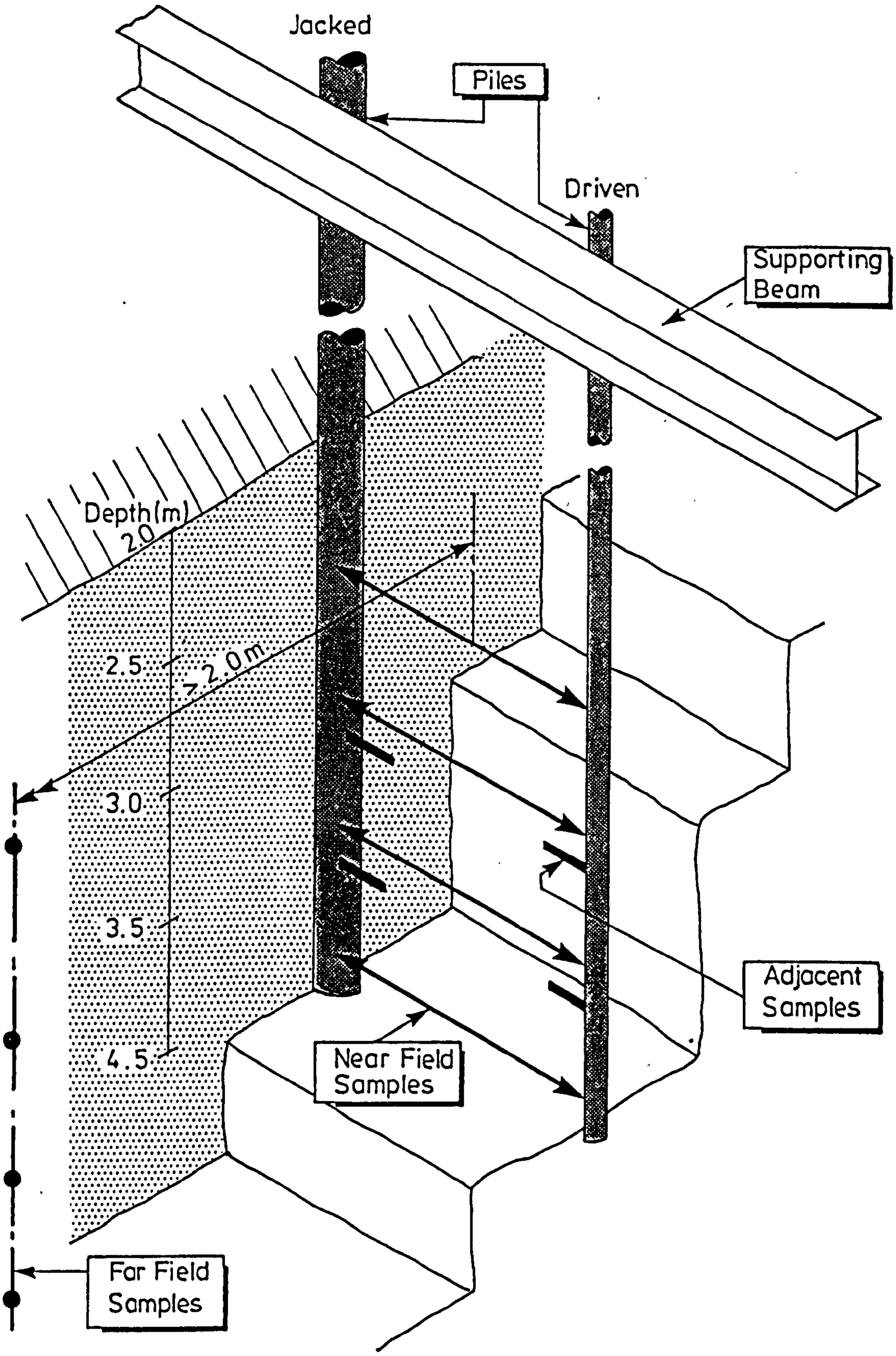



Figure 13.1 General scheme of the inspection trench

## 13.2.2 Sampling/test schedule

### a) Location of samples/in situ tests

Figure 13.1 shows the general scheme of the trenching operations. Samples were taken both from the "near-field" (between the two piles) and from the "far-field" (more than 2m away). Some of the near-field samples were taken specifically to investigate the soil fabric close to the piles (<300mm away): these are termed "adjacent" samples.

Many more samples were taken than were required for the anticipated laboratory test programme, and consequently not all of the samples recovered have been tested to date.

### b) Notation for identifying individual samples

Each sample has been given a reference number comprising three main elements: a sample code (shown in the box below); the sample's depth below ground level (in metres); and a letter designating whether it was adjacent to the driven (d) or to the jacked (j) pile. Far-field samples have been designated by the letters "ff" (instead of d or j).

Various sample types

| Code | Sample type |
|---|---|
| W | Water content |
| FP | Filter paper |
| AD | Air-dried |
| TS | Thin section |
| X | X-ray |
| O | Oedometer |
| D | Dissipation |
| B | Block |

For example, according to this system the air-dried sample from 3.10m, next to the jacked pile, would be denoted AD3.10j; and an oedometer sample (horizontally oriented) from 2.24m in the far-field as OH2.24ff. (This notation will be particularly helpful in the discussion of the thin-sections and X-rays.)

### c) Near-field/adjacent samples

The near-field samples promised to supply the key information in this investigation: Figure 13.2 illustrates the density of samples that were recovered from between the two piles.

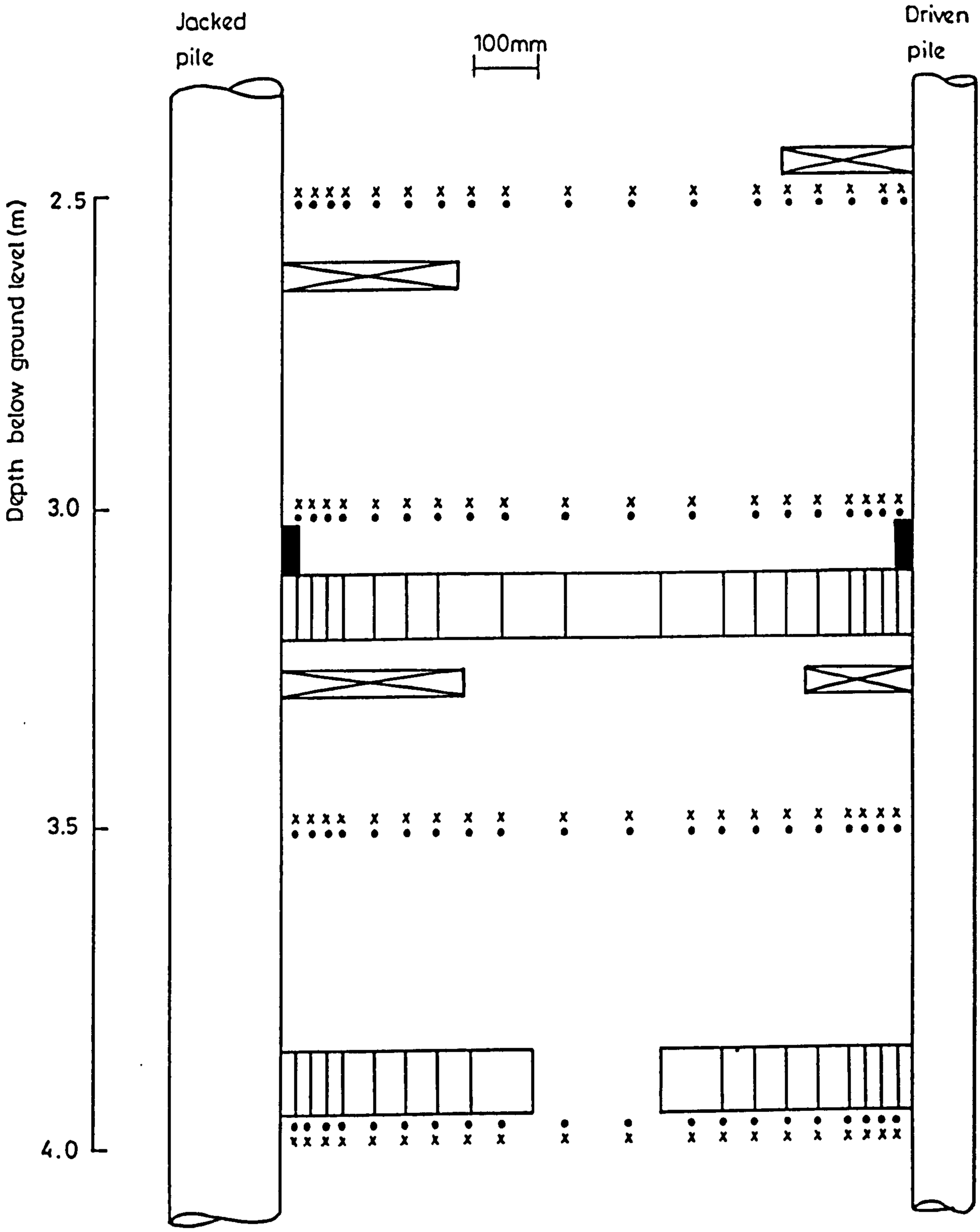



**Figure 13.2** Inspection trench: schedule of samples recovered from between the two piles

The samples and tests shown on Figure 13.2 can be divided into two broad groups: those that were useful for studying the soil's fabric (the air-dried, X-ray, and thin-section samples); and those that could provide a measure of the soil's properties (water content and soil suction measurements; and pocket penetrometer tests).

The procedures followed for taking the samples and in conducting the in situ tests are described in detail in Section 13.3.

d) Far-field samples

A number of far-field samples were taken from positions more than 2m away from the piles, as itemized below.

Water contents were determined at 0.1m intervals from 0.8 to 2.5m (and also at 2.24, 3.18, and 4.03m); pocket penetrometer tests were performed in the same places. Five block samples were cut to provide material suitable for testing in the triaxial apparatus (if required); both vertically and horizontally oriented samples were retrieved for oedometer tests; and further samples were recovered for possible tests in the dissipation cell.

## 13.3 SAMPLING AND IN SITU TEST PROCEDURES

### 13.3.1 Water content samples (W)

Samples were taken at four levels and at various positions between the two piles, to determine the variation in water content with radial distance from their centres.

The following procedure was adopted for taking the samples. Each moisture content tin was filled with soil from a specified position and its lid was securely fitted. The tin was then placed inside a sealable plastic bag, in order to prevent any loss of moisture from the soil. Once all of the samples had been taken from a particular level, the tins were taken to one of the site huts for immediate weighing. Thus the weight of the wet soil was determined within a few minutes of the sample being taken. (Failure to follow a strict procedure such as this contributed to the scatter in the results obtained by the BRE at Cowden.[2]) The subsequent drying and weighing of the samples followed the guidance given in BS1377[3] (but with water contents accurate to ±0.1%).

The water content results are presented in Section 13.4.2.

### 13.3.2 Pocket penetrometer tests (PP)

A measure of the consistency* of the London clay between the two piles was obtained using two pocket penetrometers. One was a standard device and the other a modified instrument whose plunger was smaller in diameter. The modified instrument provided a test range beyond that of the standard penetrometer.

The penetrometer results are presented in Section 13.4.3.

---

*"Consistency" is the estimated undrained shear strength of intact blocks of soil

## 13.3.3 Measurements of soil suction

### a) Introduction

Although the experiments with the instrumented piles provide information about the stresses in the adjacent soil, they give no indication of how these stresses vary with radial distance away from the piles. The excavation of the inspection trench, however, provided the opportunity to estimate the mean effective stress ($p'$) in the soil between the piles, from measurements of the suction ($p_k$) in the recovered samples.

There are two main difficulties in making such estimates of $p'$:

- How do we measure the soil suction?
- How do we relate $p'$ to $p_k$?

The following sections attempt to answer these questions.

### b) Measuring the soil suction

The capillary suction $p_k$ remaining in a sample after it has been removed from the ground can be determined in several ways, with varying degrees of certainty. The principal methods involve:

i) Measuring the pore pressure in the sample (u) when it has reached undrained equilibrium under an <u>all round total stress</u> $\sigma$ [$p_k$ then equals $(\sigma - u)$][4]

ii) Measuring the pore pressure in the sample ($u_w$) when it has reached undrained equilibrium under an <u>elevated air pressure</u> $u_a$ [$p_k$ then equals $(u_a - u_w)$]

iii) Employing the <u>filter-paper technique</u>,[5] in which a dry filter-paper wets up to a water content ($w_{FP}$) in equilibrium with the soil suction [$p_k$ is related to $w_{FP}$ by a pre-determined calibration]

Of these methods, the last two have been employed to determine $p_k$.

The filter-paper method is both simple and quick to perform - and with over 40 samples to test, speed was a critical factor in selecting which technique to use. Two disadvantages of the method are that it relies on a pre-determined calibration relating $p_k$ to the water content of the filter-paper $w_{FP}$, and that the published calibrations may not be completely reliable in the suction range of interest to the piling work. Therefore, in order to check the values of $p_k$ obtained with the filter-papers, a series of independent measurements were made in the pressure-plate apparatus. This apparatus allows an elevated air pressure to be imposed on the sample (method ii above). The procedures involved in both tests are described in detail in Sections 13.3.4 and 13.3.5 below.

c) Relating p′ to $p_k$

Having determined the soil suction $p_k$, the next step is to relate it to p′, the mean effective stress in the soil, where:

$$p' = (\sigma'_{rr} + \sigma'_{\theta\theta} + \sigma'_{zz})/3$$

If we assume that the sampling process is 'perfect' (i.e. consists only of a release of deviator stress) and that the clay behaves as an <u>isotropic linear-elastic material</u> which remains <u>fully saturated</u> (B = 1),[6] then the suction in the sample is given by $p_k = p'$. However, if the sample becomes de-saturated (B < 1) then $p_k$ is less than p′; likewise, it can be shown (see Appendix 15) that if the sample is anisotropic, $p_k$ is probably less than p′. Thus, although an estimate of p′ can be obtained from measurements of soil suction, the absolute value of the mean effective stress is not reliably determined by this method.

## <u>13.3.4 Filter-paper samples (FP)</u>

a) General outline of the test method

Perhaps the simplest method of determining soil suction is the filter-paper technique described by Chandler and Gutierrez:

> "The method involves placing a piece of filter-paper against the soil sample... and sealing the whole to prevent evaporation.

> The filter-paper then wets up to a water content in equilibrium with the magnitude of the soil suction, and careful measurement of [this] water content... enables the soil suction to be obtained from a previously established correlation."[7]

A total of 41 filter-paper samples were taken from between the two piles, in four groups: FP3.10d; FP3.86d; FP3.10j; and FP3.86j.

Figure 13.3 illustrates the way in which the filter-papers were placed in contact with the soil, one on the inside of the sample and one each against the two outer faces.

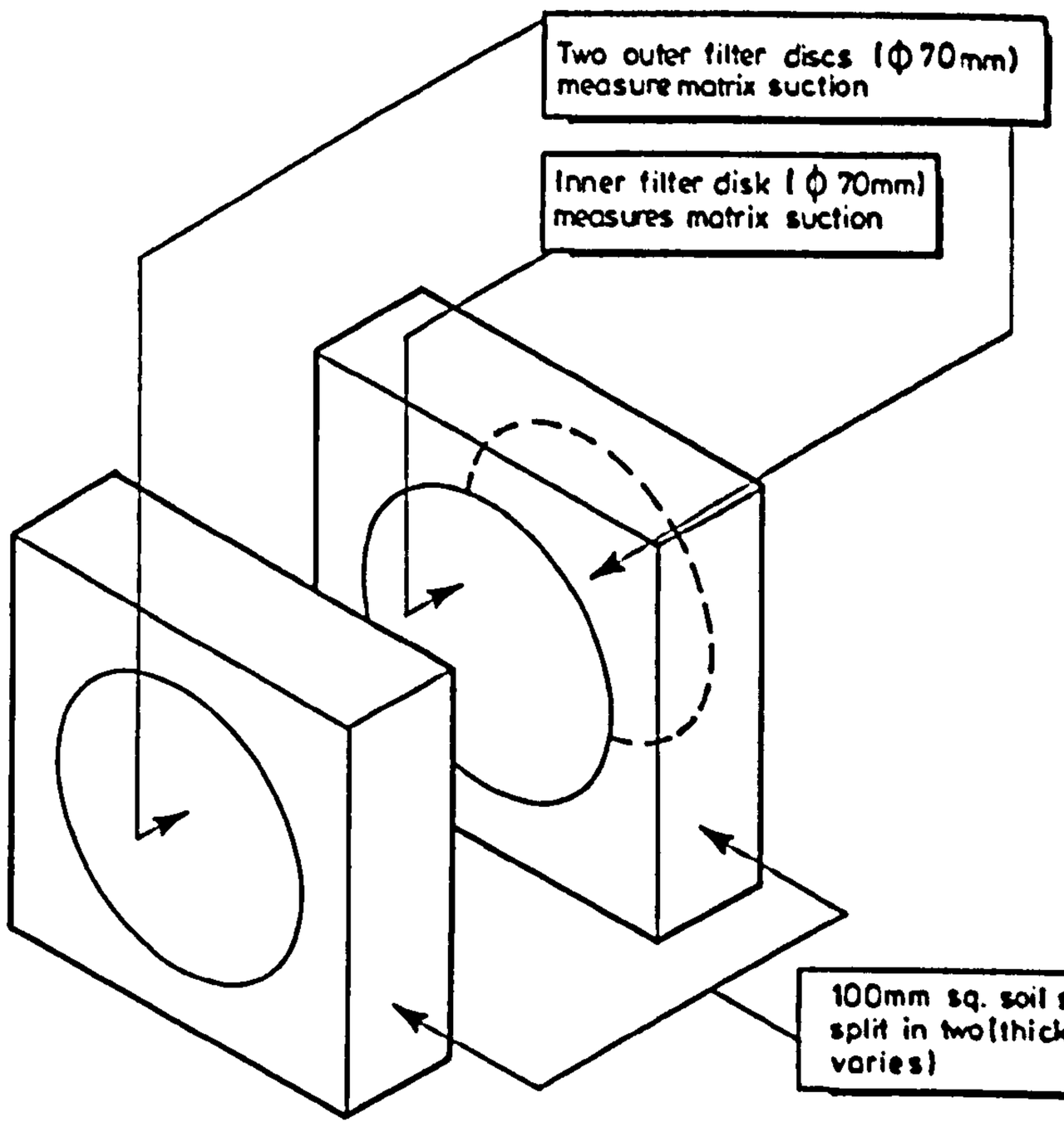



Figure 13.3 Filter-paper samples

Full details of the experimental technique are given in Appendix 15. The filter-paper measurements are presented in Section 13.4.4.

### 13.3.5 Pressure-plate measurements of soil suction

In order to obtain a second estimate of the soil's suction, a limited number of samples were tested in the pressure-plate apparatus.[8] The specimens were cut from soil that had been used for the filter-paper experiments: namely, nine samples from the group FP3.86d. I would expect these tests to give higher values of $p_k$ than the filter-paper method, since the pressure-plate experiments were performed on samples that will

inevitably have dried out slightly during handling between the tests.

The pressure-plate measurements are also presented in Section 13.4.4.

### 13.3.6 Air-dried samples (AD)

Two samples were recovered from a depth of 3.10m for later visual examination in the laboratory. One came from next to the driven pile (AD3.10d) and the other from next to the jacked pile (AD3.10j). Both were wrapped in cling film and then coated in wax, to prevent premature drying during transportation to the laboratory. Care was taken not to damage the samples' curved surfaces, which carried the piles' imprints.

Once their protective wrapping had been removed, the samples were photographed and then inspected by eye, using a sharp knife to cut into the soil. Initially it proved impossible to expose any shear surfaces without smearing the clay. However, after the samples had been left to dry slightly in the warm laboratory air (for about one to two hours) they were re-examined with more success.

The appearance of the air-dried samples is described in Section 13.5.2.

### 13.3.7 X-ray specimens (X)

Four X-ray specimens (X2.43d; X3.25d; X2.61j; and X3.25j) were recovered from the positions shown in Figure 13.2. In the laboratory, the specimens were reduced in size (by careful paring with a sharp knife) to the dimensions shown in Figure 13.4. The side faces of each sample were made as smooth and as parallel as possible, to ensure that the sample's thickness did not vary significantly along its length.

X-ray photographs were taken of all four specimens, in the Geology Department of Imperial College.[9] Pieces were then cut from the ends closest to the pile, to provide samples from which thin-sections could be prepared.

The X-ray photographs are presented and described in Section 13.5.3.

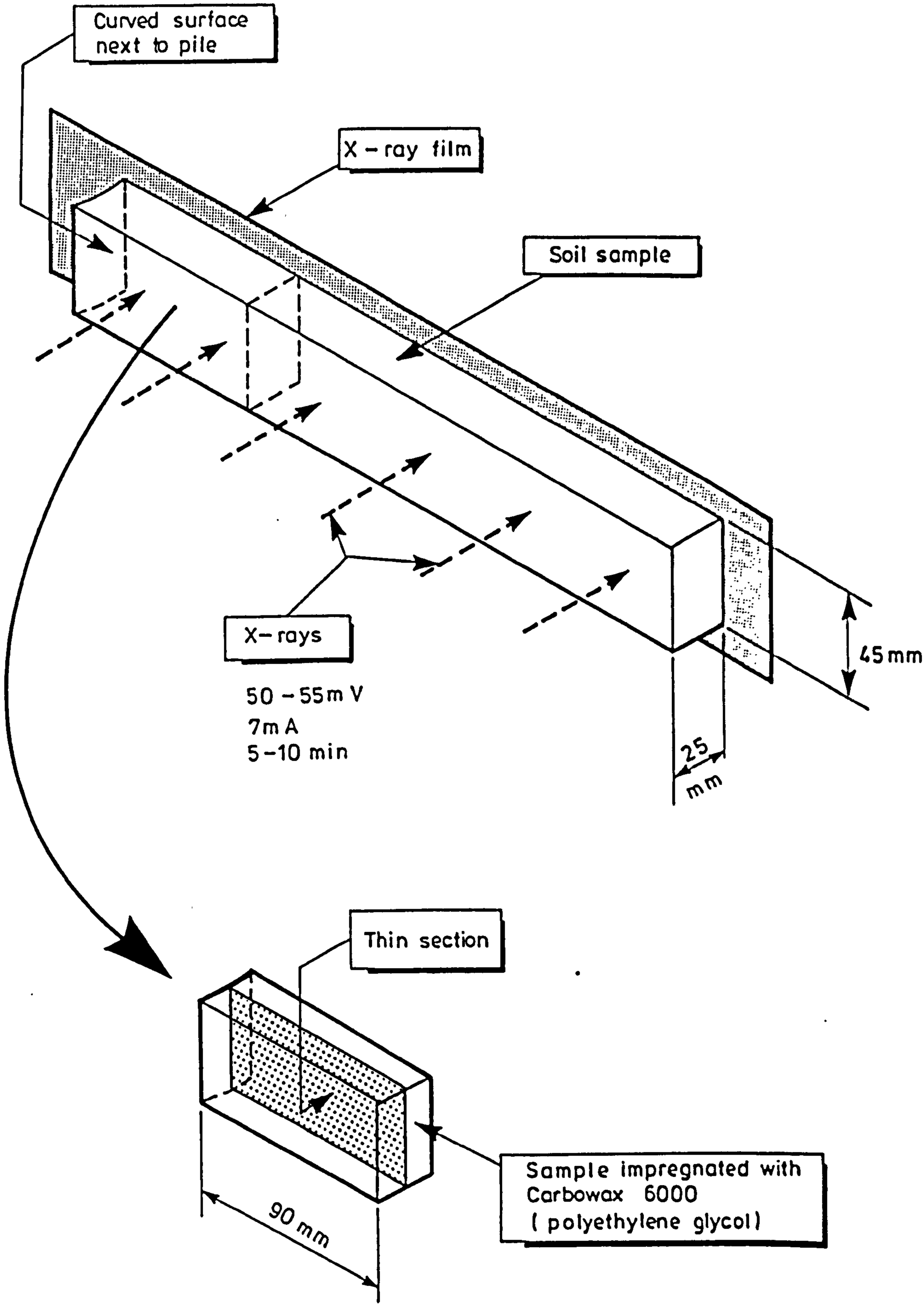



Figure 13.4 X-ray and thin-section samples

## 13.3.8 Thin-sections (TS)

### a) Schedule of samples

Thin-sections were produced from samples of soil that had been carefully cut from next to one or other of the two piles. The majority of the thin-sections were aligned vertically (denoted TSV), but a couple were aligned horizontally (TSH).

Some thin-sections were made from pieces cut from the X-ray specimens (see Section 13.3.7) and others from separate samples that were recovered specifically for the purpose. The sections taken from the X-ray specimens are denoted TSVX (all were aligned vertically).

### b) Sample impregnation

All the thin-section samples were impregnated with Carbowax 6000,* following the procedure recommended by Tchalenko.[10] Carbowax is used to replace the water in the soil's pores, making the sample rock-hard at room temperature. It can then be ground into a thin-section and mounted on a glass slide for examination under a microscope.

### c) Photographs of the thin-sections

Clay particles are bi-refringent: if they are viewed under cross-polarized light they will transmit that light at varying intensity, depending on their alignment relative to the light's optical axes. Random particle alignment produces no variation in the intensity of transmitted light. On the other hand, if the clay particles are oriented in a particular direction, then either a minimum or a maximum light intensity will be seen (depending on the orientation of the polarized light).

The thin-sections were photographed onto black-and-white film, under cross-polarized light. Prints of these photographs are presented on pages

---

*Polyethylene glycol (PeG) with a molecular weight of ≈6000

433-435, and they are discussed in detail in Section 13.5.4. In this work, the light was polarized in such a way that cracks in the specimens appear as black lines; white lines reveal the preferred orientation of the clay particles; and random structures appear as mid-grey in tone. For detailed study, prints were produced at a scale of four times real life, and line drawings were made from these enlarged prints. A total of eleven thin-sections were manufactured, and photographs of eight of them are presented herein.[11]

## 13.4 VARIATIONS IN THE SOIL'S PROPERTIES BETWEEN THE PILES

### 13.4.1 Introduction

This section presents the results of the water content determinations (13.4.2); the pocket penetrometer tests (13.4.3); and the measurements of soil suction (13.4.4).

### 13.4.2 Water content variation

Figure 13.5 shows the variation of water content between the two piles, as determined at four different levels. The jacked pile (Kitching's) is situated at the left-hand end of the distance scale, and the driven pile (CP6d) at the right-hand end. (Because CP6 was driven at a slight angle to the vertical, the distance between the piles is not the same at each level.)

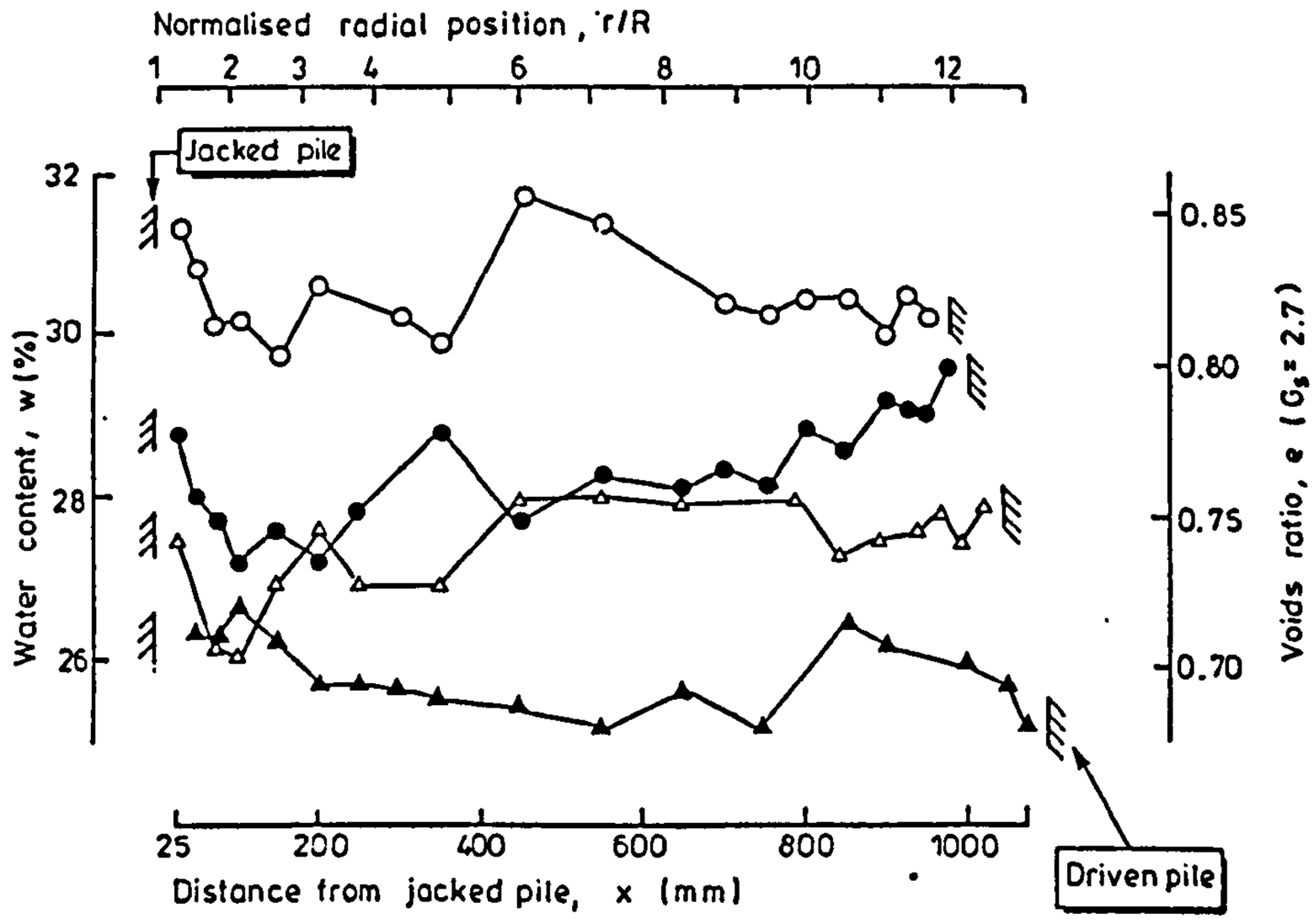



Figure 13.5 Variation in water content between driven and jacked piles (black Δ 2.50m; white Δ 2.99m; • 3.49m; o 3.96m)

Before discussing the results, it is important to note that Kitching's pile had small portholes cut through its wall, at 0.5m intervals along its entire length.[12] The water that had collected on the inside of the pile whilst in the ground was removed by baling at the start of excavation. However, the soil immediately adjacent to Kitching's pile may have been affected by contact with the standing water inside the pile, and so water content measurements here may be in error.

As Figure 13.5 reveals, the water content readings (w) show no conclusive trend at any of the four levels considered, given that the slight increase in moisture content next to Kitching's pile may be misleading. The undisturbed water content in the far-field at these depths (2.50-4.0m) is 29½ ±3% (see Chapter 7); and the moisture contents shown on Figure 13.5 fall essentially within the same range of values. It is clear that the marked variation in water content observed, for example, by the Norwegian Geotechnical Institute adjacent to piles installed in the contractive Haga clay[13] (see Chapter 4) does not occur in the dilating London clay.

### 13.4.3 Variations in the soil's consistency

Figure 13.6 presents the results of the pocket penetrometer tests.* They are expressed in terms of an index value (PPI), to highlight the fact that these are measurements of the consistency of the soil (i.e. very imprecise estimates of $c_u$) rather than accurate measurements of its undrained shear strength.

The index shows no particular trend at any of the four levels investigated, the values generally falling within the range $30 \leq PPI \leq 40$. The undrained shear strength of the undisturbed clay at 2.5m is approximately 76kPa (see Chapter 7): at this depth in the far-field the pocket penetrometer index was 25-30 (as shown by the bar on the top diagram of Figure 13.6). There is, therefore, a tendency for the PPI between the piles to be (perhaps) ≈25% higher than the far field value, but we should not place too much reliance on this result given the imprecise nature of the test.

---

*The readings shown were obtained using the standard pocket penetrometer: those from the modified instrument show a similar (i.e. no!) trend

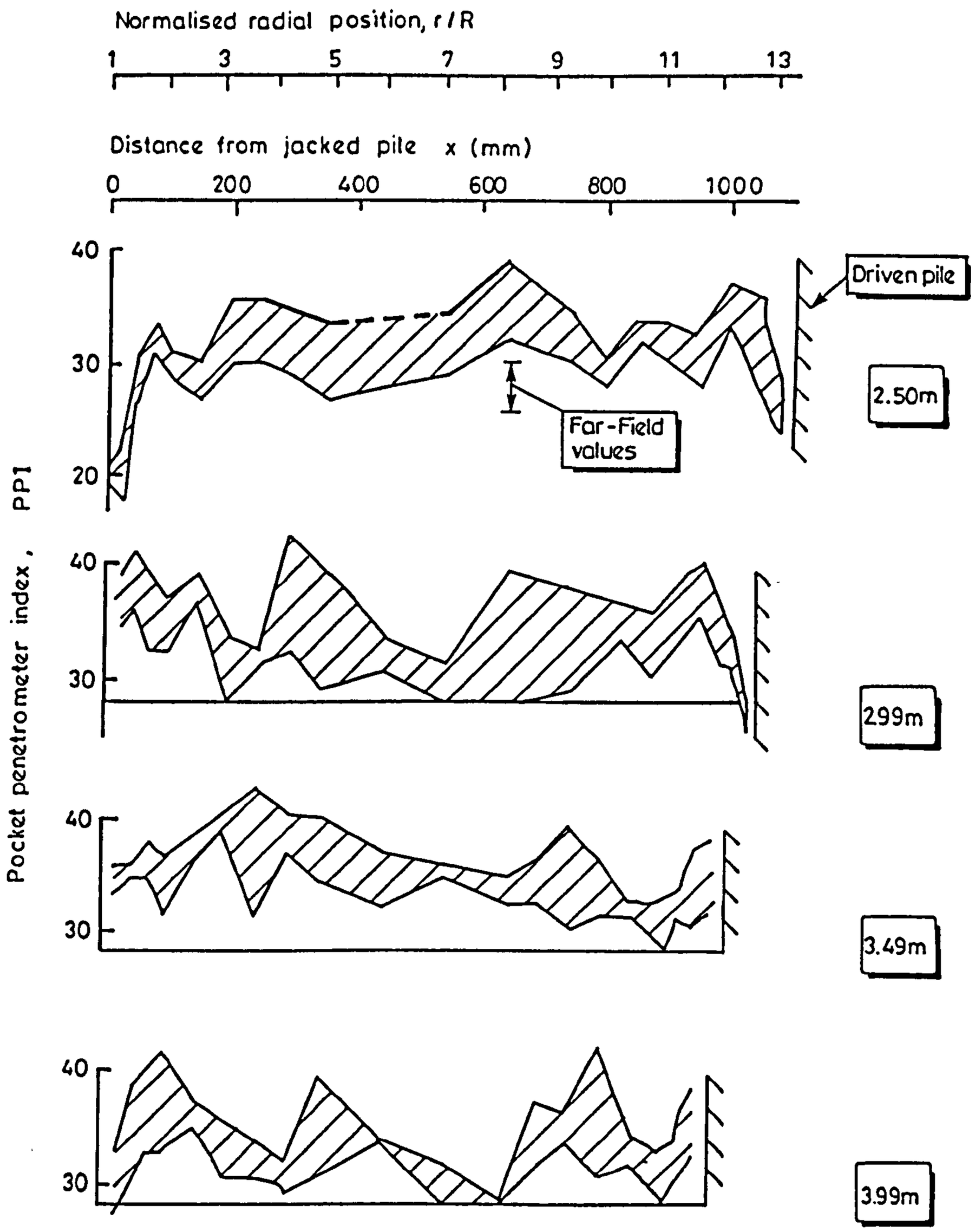



Figure 13.6 Pocket penetrometer readings

## 13.4.4 Variations in soil suction

Figure 13.7 presents measurements of the suction in the samples taken at 3.86m depth, from close to the driven pile (group FP3.86d). The values of $p_k$ were obtained using the filter-paper technique (see Section 13.3.4) and with the pressure-plate apparatus (see Section 13.3.5). The following points should be noted:

- The pressure-plate measurements are significantly (50-100%) higher than the values determined by the filter-paper technique (as mentioned earlier, the pressure plate measurements were expected to over-read $p_k$)
- The inner filter papers (black symbols) generally gave lower values of $p_k$ than the outer papers (white symbols): i.e. the outer discs had lower water contents

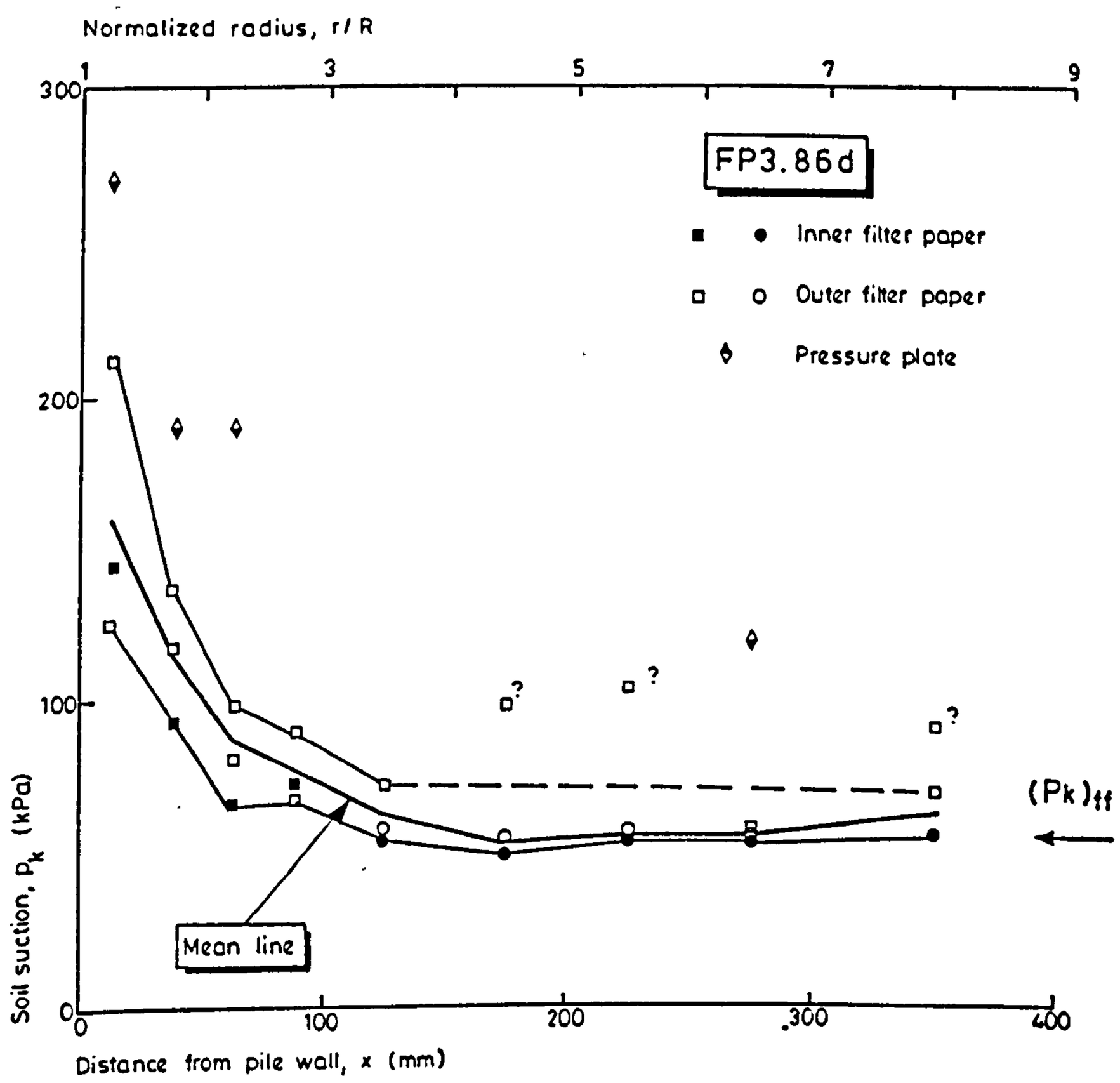
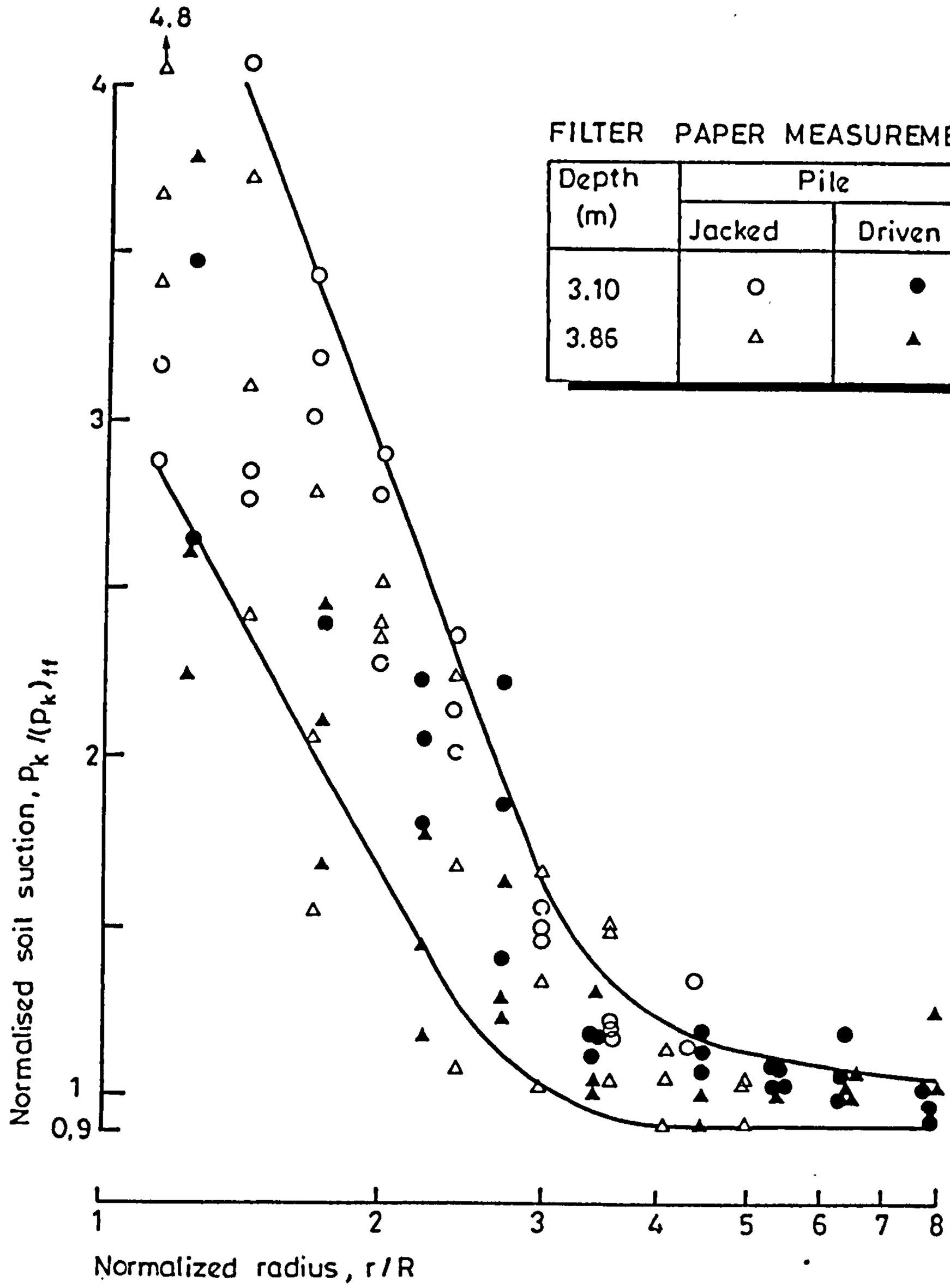



Figure 13.7 Soil suction at 3.86m near to the driven pile

- The filter-paper $p_k$ values for $r/R > 4$ are about 40% lower than the estimated far-field mean effective stress $p'_o$ (assuming $K_0$ = 2.5 at 3.86m)

The results of the filter-paper measurements, from next to both piles, are presented in Figure 13.8. On this diagram the values of soil suction ($p_k$) have been normalized by the far-field value $(p_k)_{ff}$, and the radial




FILTER PAPER MEASUREMENTS

| Depth (m) | Pile | |
|---|---|---|
| | Jacked | Driven |
| 3.10 | ○ | ● |
| 3.86 | △ | ▲ |

**Figure 13.8** Normalized soil suction from filter-paper measurements

position (r) by the appropriate pile radius (R). It should be noted that the measurements of $p_k$ were taken at different distances (z) behind the pile tips: for samples at 3.86m and 3.10m depth, the z/R values are (respectively) 16 and 25 for the jacked pile; and 38 and 53 for the driven.

Although the scatter of the results is quite large (typically ±25% for $r/R < 3$), the trend is clear. The most important conclusions to arise from this figure are:

- Most of the readings fall within a well defined band, <u>regardless</u> of the method of pile installation
- The suction in samples at $r/R = 1$ (i.e. those in contact with the piles) are 3-4 times the far-field value
- Close to the pile ($r/R \leq 3$), the normalized soil suction falls linearly with the logarithm of r/R
- Further away from the pile ($4 \leq r/R \leq 8$) the soil suction is essentially constant
- The filter-paper $p_k$ values for $r/R > 4$ are about 40% lower than the estimated far-field (undisturbed) mean effective stress

The first two of these findings are the most important. Despite the marked differences between the load capacities of these two piles ($\alpha$ = 0.6 for the slow-jacked pile and 0.93 for the driven) the effective stress regime appears to be essentially the same around both of them. This provides further evidence that the piles' shaft capacity is governed by the (rate-dependent) residual strengths developed at the pile-soil interface during installation.

No conclusions could be drawn about the effect of z/R on the soil suction.

## 13.5 EXAMINING THE SOIL FABRIC NEXT TO THE PILES

### 13.5.1 Introduction

This section presents the results of the examination of the soil's fabric next to the piles. Three techniques have been employed in these studies: visual examination of the soil's fabric (Section 13.5.2); X-ray photography (Section 13.5.3); and microscopic examination of the soil using thin-sections (Section 13.5.4).

### 13.5.2 Visual examination

#### a) Field observations

During trenching operations, attempts were made to examine the fabric of the soil adjacent to the piles. Several oblique and discontinuous polished surfaces (less than 5mm in length) were noted in the clay - but one continuous shear surface could not be found. Regrettably, the shear surfaces could not be logged in a systematic fashion, because it was impossible to separate samples from the piles' surfaces without destroying the structure of the soil. There appeared to be no clear difference between the structures observed next to the driven pile and those next to the jacked.

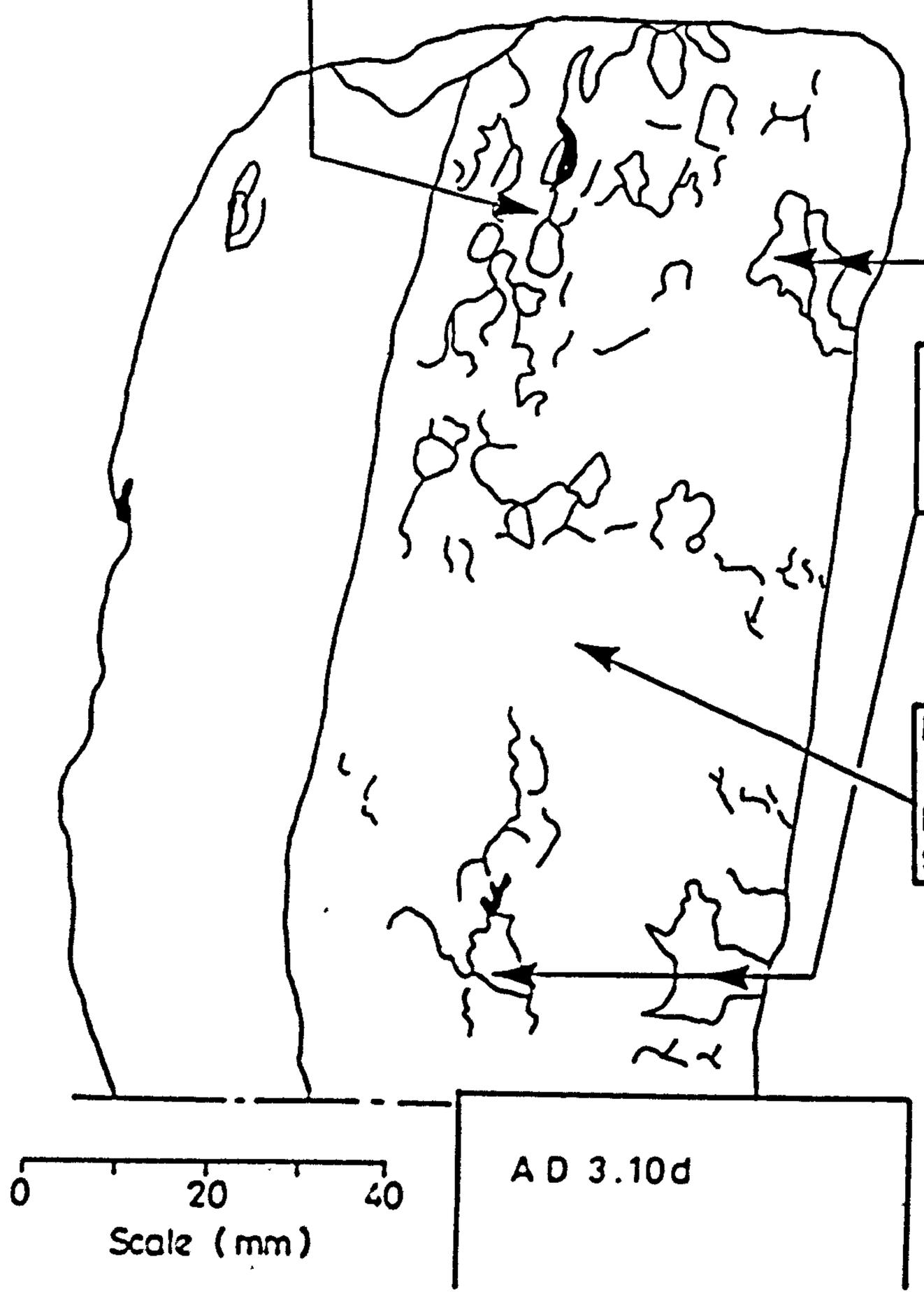
#### b) Laboratory observations

Observations of the soil's fabric were made from the air-dried samples AD3.10d and AD3.10j, photographs of which are shown on Plate 7. The sample from next to the driven pile is on the left, and that from next to the jacked pile on the right. The main features that were noted when examining these samples are listed below, and are summarized on the transparency that overlays Plate 7.

Frequent knobs of clay, irregular size (typically 2-5mm)

Smooth, striated surface (exposed) beneath 1.4mm surface layer

Main surface: matt texture with pile imprint, rust-stained throughout



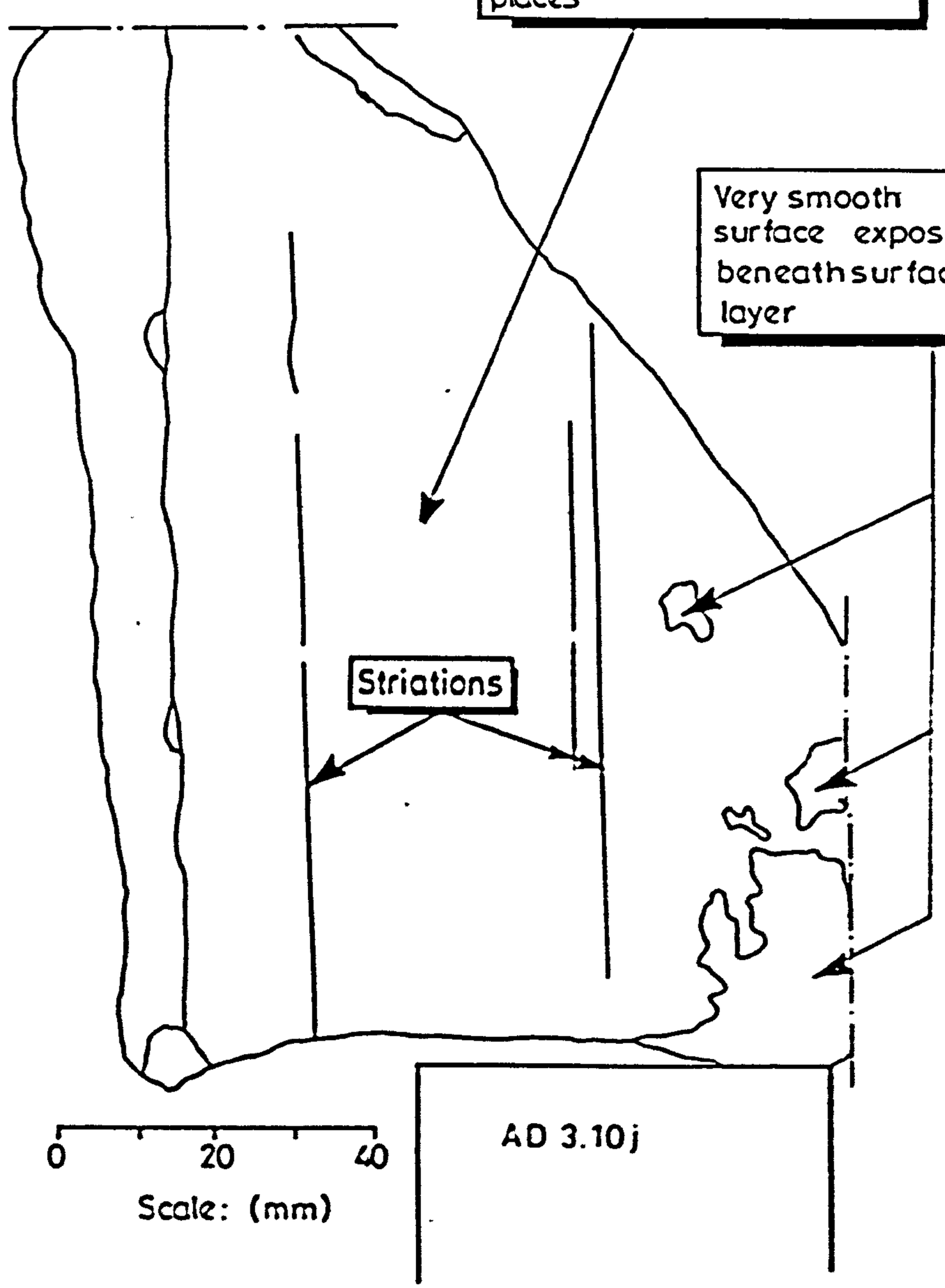
0 20 40
Scale (mm)

AD 3.10d

Main surface: smooth, rust-stained and roughened in places

Very smooth surface exposed beneath surface layer

Striations



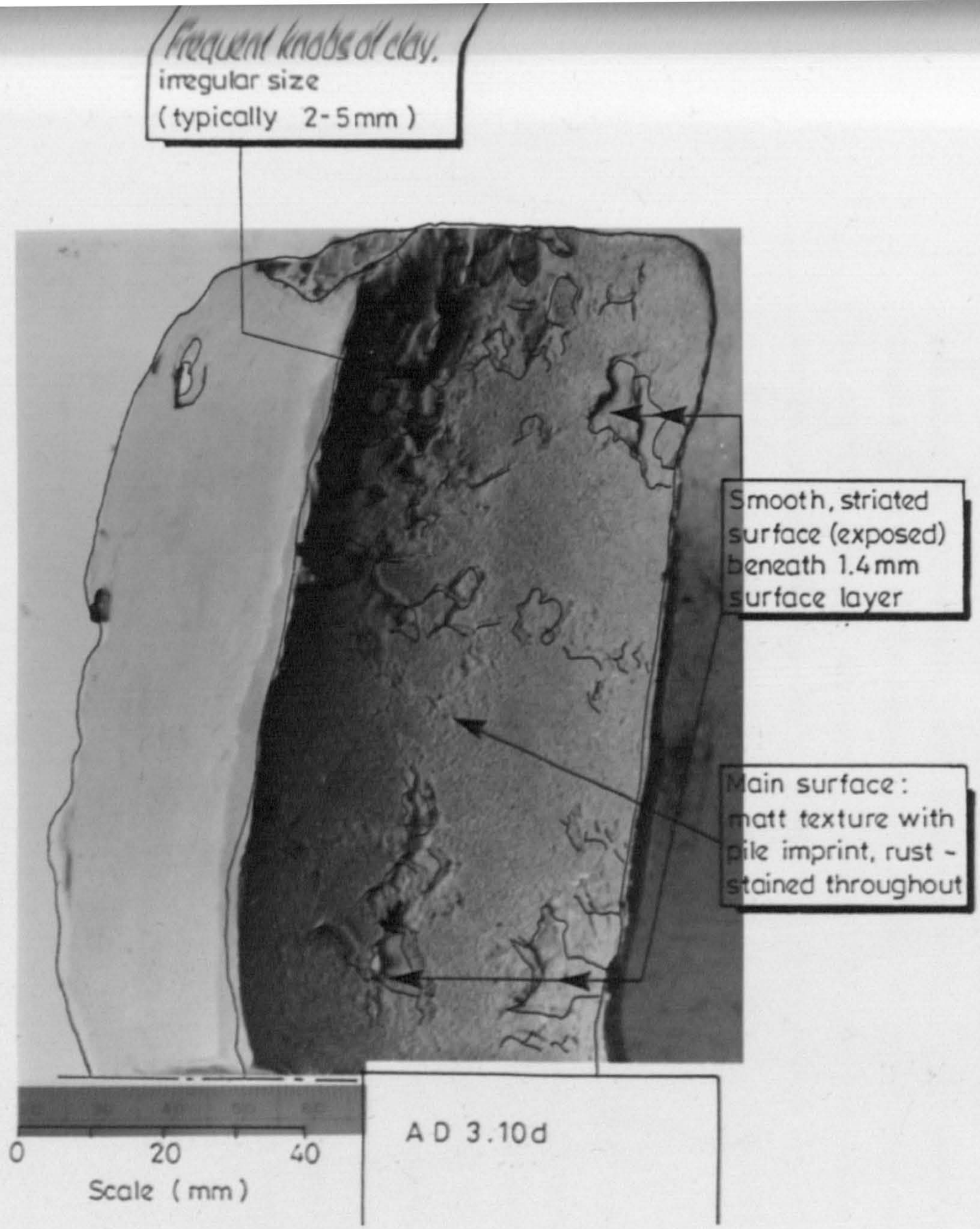
0 20 40
Scale: (mm)

AD 3.10j





Plate 7 Air-dried samples from (a) driven pile (left, AD3.10d); (b) jacked pile (right, AD3.10j) (photos: A. Bond)



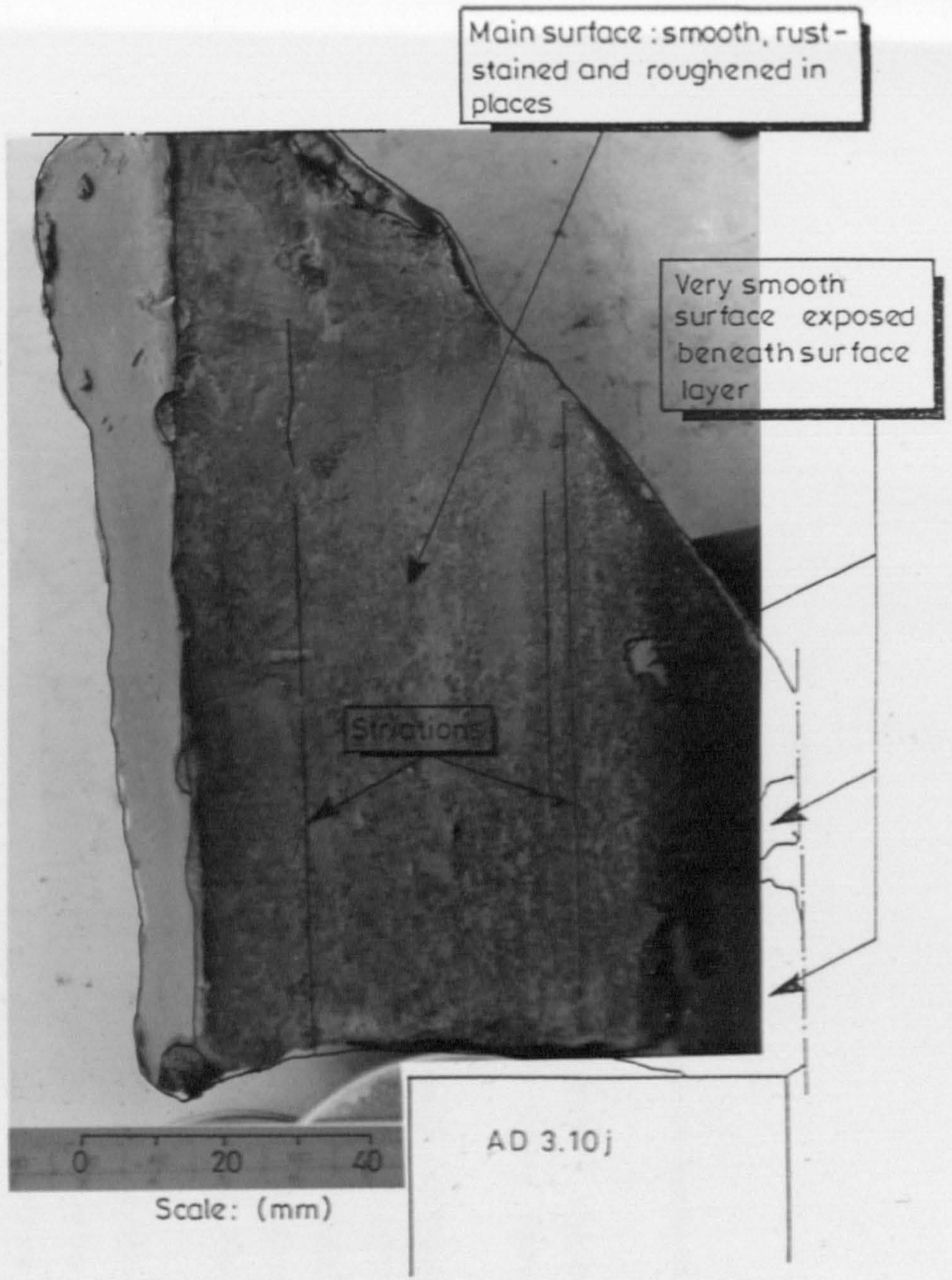




Plate 7 Air-dried samples from (a) driven pile (left, AD3.10d); (b) jacked pile (right, AD3.10j) [photos: A. Bond]

- Both samples were rust-stained where they had been in contact with the piles
- Both samples had a surface skin (0.75 to 1.4mm thick) which displayed the pile's imprint, and beneath which there were several smooth (shear) surfaces
- Next to the driven pile (see AD3.10d), the main (outer) surface was rather knobbly in appearance, especially in the top left-hand corner; the lumps of clay were of irregular size (typically 2-5mm across); and where the outer surface was flat it carried the mirror image of the pock marks caused by grit-blasting the pile
- Next to the jacked pile (AD3.10j), the main surface was smooth but striated (like the surface of the pile itself); there were no signs of the lumps seen on AD3.10d; and the outer surface looked like a thin skin on top of a second (smoother) surface lying beneath it
- The underlying surface beneath the skin of AD3.10j was <u>highly polished</u> in appearance, and extended over a large part of the sample (part of it is exposed in the bottom right-hand corner)
- In contrast, below the outer surface of AD3.10d there were several <u>discontinuous</u> small shear surfaces (<10mm in length), aligned in random directions, and all of which were uneven in appearance

On cutting into the sample from next to the driven pile, it was clear that there existed several layers of shear surfaces, rather than one distinct and continuous surface, i.e. there was no evidence of the existence of a "principal displacement shear" (as described by Skempton[14] for landslides in stiff clays). The sample's overall appearance was comparable to that of an onion skin. On the other hand, the sample from next to the jacked pile showed signs that a principal displacement shear may have existed, together with other discontinuous shear surfaces.

## 13.5.3 X-ray examination

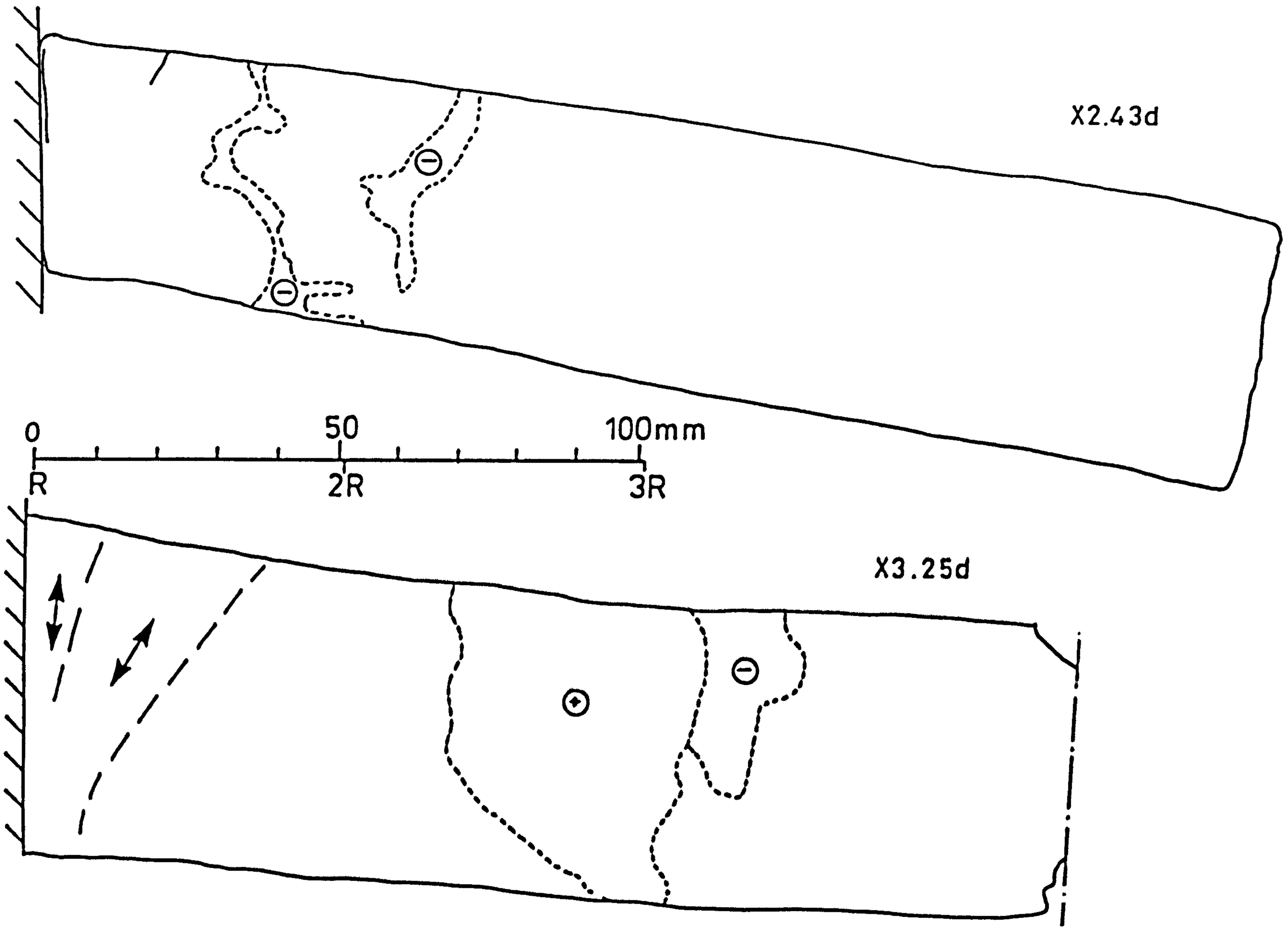
Photographs of the four X-rays are shown on Plate 8 (for the driven pile) and Plate 9 (for the jacked); in each case the pile was located at the left hand edge. Careful examination of these photographs reveals strong particle re-orientation in the vicinity of the piles, with less disturbance to the soil further away. There appears to have been far greater re-orientation next to the jacked pile than next to the driven, although the fabric is not so clearly seen on X2.43d (Plate 8(a), top) as on the other X-rays.

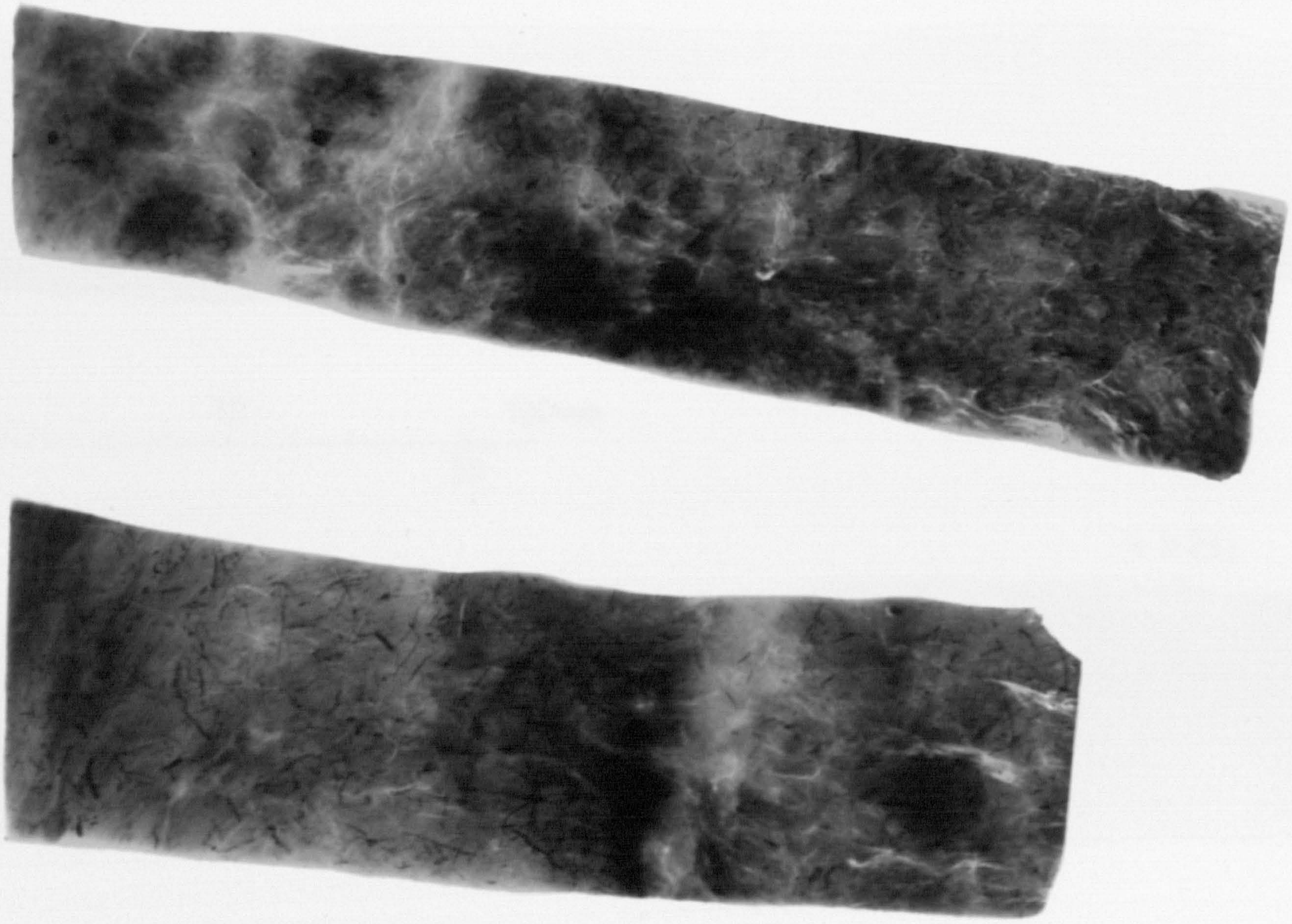
The corresponding overlays summarize my analysis of these photographs. The symbols ⊕ and ⊖ designate areas where a samples' density was greater than (⊕) or less than (⊖) that of the adjacent soil; the arrows (↕) indicate the general orientation of the fabric; and the full lines (|) mark several obvious linear features.

The distance over which the soil's fabric has visibly been re-oriented is approximately 40mm (r/R = 1.8) for the driven pile, and approximately 100mm (r/R = 2.1) for the jacked. However, these are very rough estimates, based solely on visual examination of the photographs. Little can be said about the variations in density across the samples: there appears to be no pattern.*

---

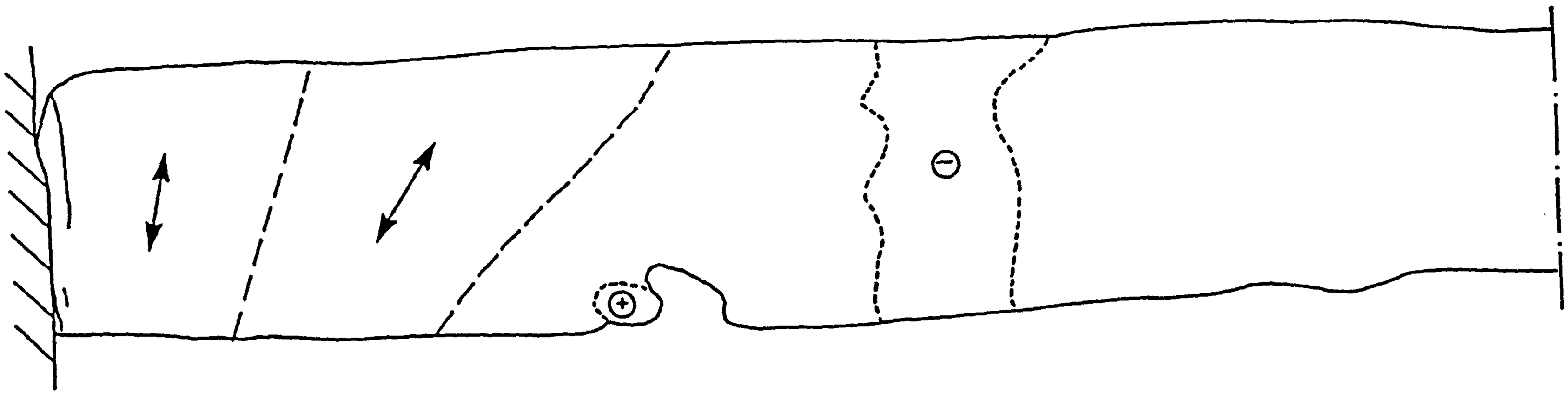
*Some areas of higher density are caused by stones present in the soil - e.g. there is a small one in X2.61j midway along the bottom of the sample; and a larger one at the top of X3.25j, 40-50mm from the pile wall

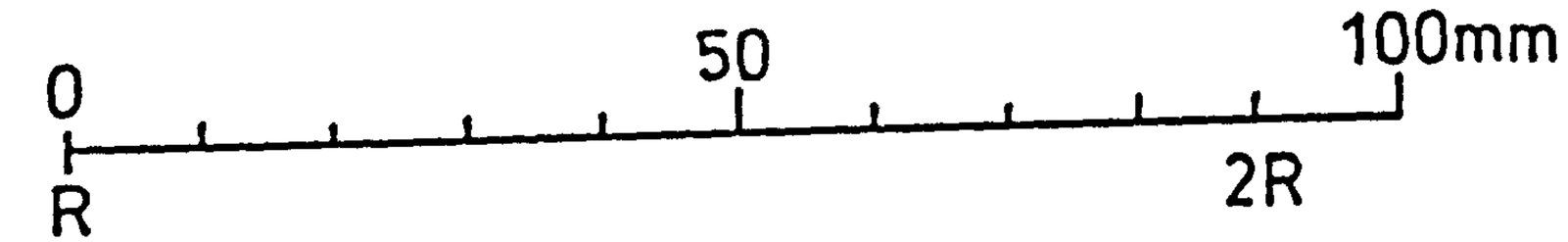

X2.43d
0
50
100mm
R
2R
3R
X3.25d



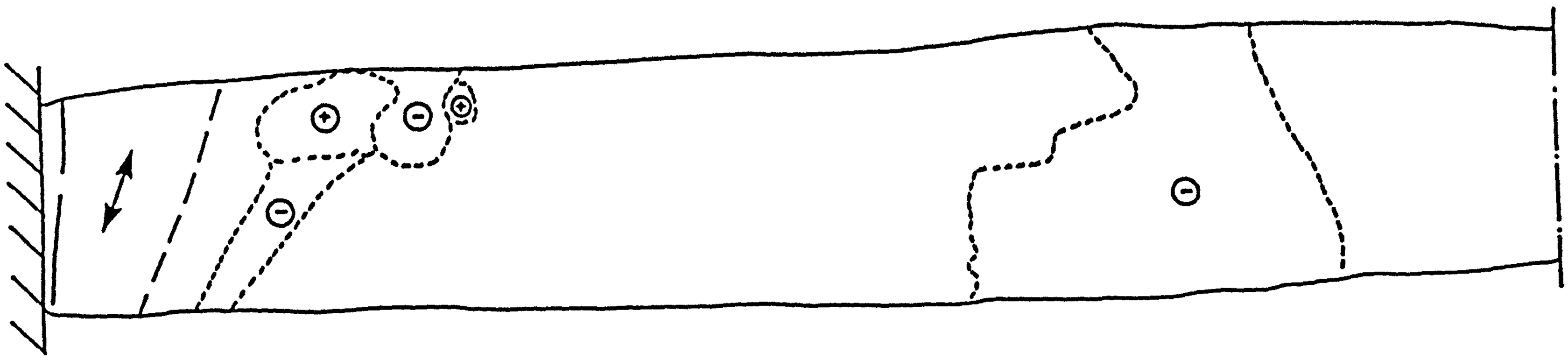
10mm Plate 8 X-rays of samples adjacent to driven pile: X2.43d (top); X3.25d (bottom) [X-rays: M. Gill; photos: A. Chipling]

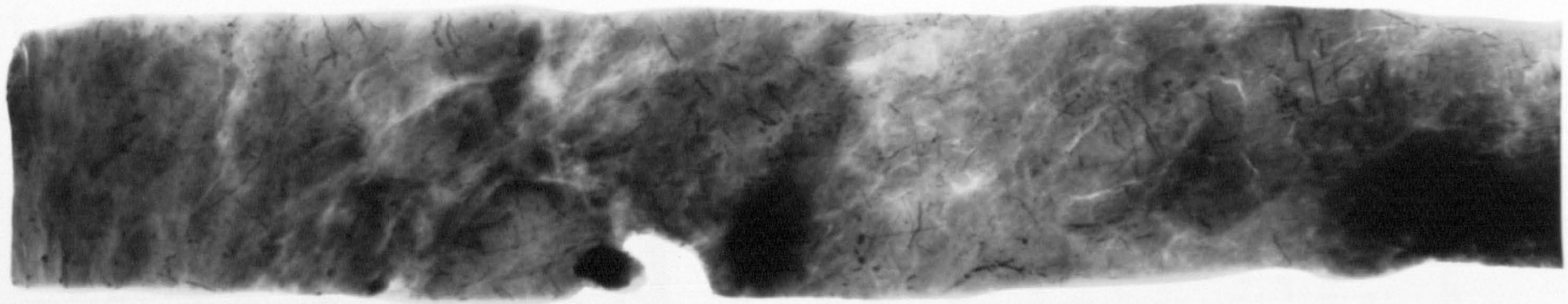
X 2.61j

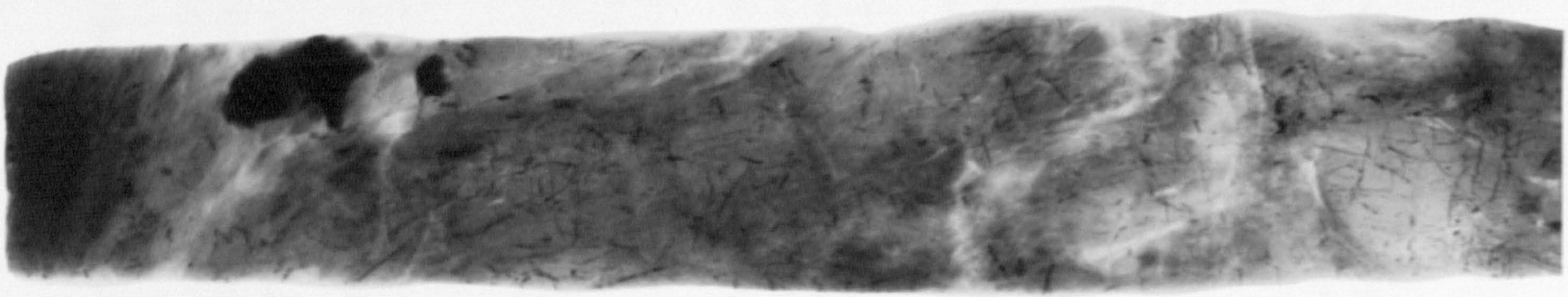





X 3.25j

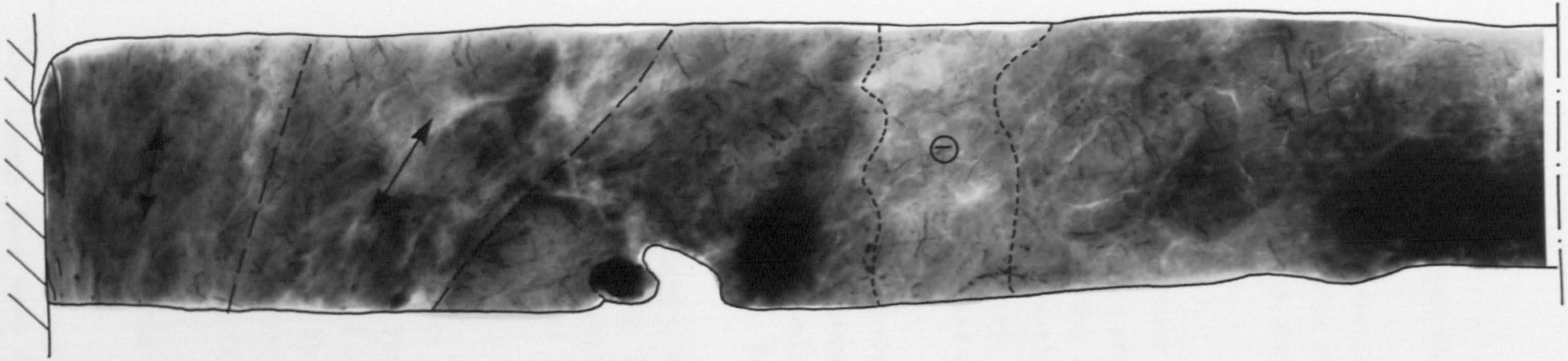






10mm Plate 9 X-rays of samples adjacent to jacked pile: X2.61j (top); X3.25j (bottom) [X-rays: M. Gill; photos: A. Chipling]

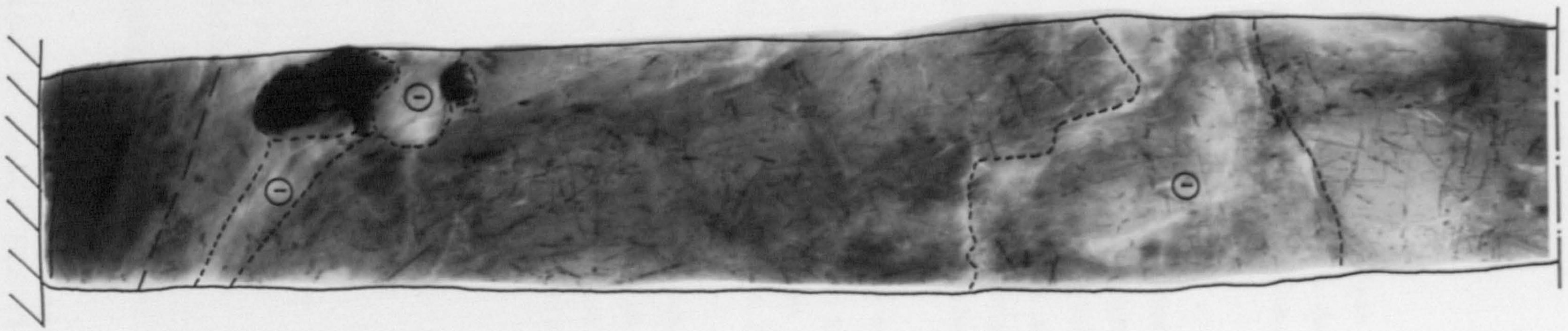
X 2.61j



0 50 100mm

R 2R

X 3.25j



10mm

Plate 9 X-rays of samples adjacent to jacked pile: X2.61j (top); X3.25j (bottom) [X-rays: M. Gill; photos: A. Chipling]

## 13.5.4 Micro-fabric observations

Photographs of the vertical thin-sections are presented on Plate 10 to Plate 13, together with overlay line drawings that show the main features of each one. In each case, the pile was situated at the left-hand edge of the thin-section.

As mentioned in Section 13.3.8.c, cracks* in the specimens appear as black lines on the photographs; white lines reveal the preferred orientation of the clay particles (i.e. potential shear surfaces); and where the soil's particles are randomly aligned the photograph appears mid-grey in tone. On the overlays these features have been portrayed by full lines (cracks) and chain dotted lines (potential shear surfaces).

The re-orientation of the clay next to the piles is immediately evident on viewing the photographs. There are potential shear surfaces running parallel to the pile wall - within 1-2mm of it - in at least five out of eight cases (TSV2.61j; TSV3.25j; TSVX3.25j; TSV2.43d1; and TSV3.25d).

The particle alignment is very steep in a narrow zone next to the pile wall; but its angle to the vertical ($\theta$) increases with radial distance from the pile. To quantify this effect, the line drawings have each been divided into four zones (I-IV), depending on the degree of particle re-orientation:

i) In Zone I there is strong particle re-orientation, the majority of potential shear surfaces being near vertical (i.e. inclined at $\theta \leq 20°$)
ii) In Zone II the degree of particle re-orientation decreases rapidly with increasing distance away from the pile, but the fabric is still steeply inclined ($\theta$ = 20-45°)
iii) In Zone III the fabric is gently inclined ($\theta$ = 45-70°)

---

*The cracks form when the specimens shrink on removal from the warm Carbowax

iv) In Zone IV the fabric is near horizontal ($\theta > 70°$), but there is still evidence of disturbance to the soil's structure

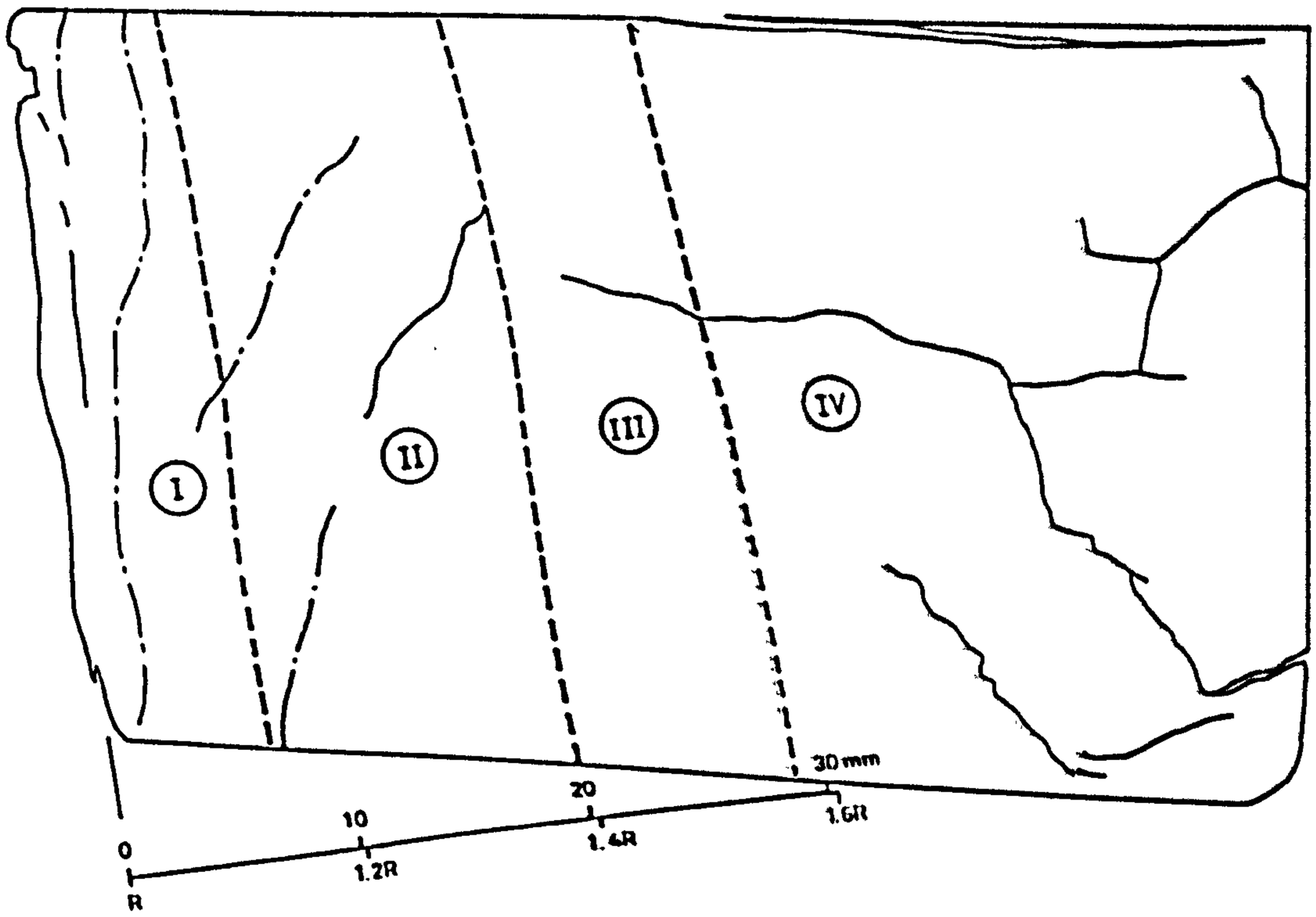
The boundaries between the various zones have been determined for each of the vertical thin sections (nine in total) and marked on the line drawings by the broken lines (----). Table 13.1 summarizes the distances of these boundaries from the two piles, in terms of the normalized radial distance $r_z/R$ (where $r_z$ is the outer radius of the boundary and R is the radius of the pile).

Table 13.1 Orientation of potential shear surfaces on thin-sections

| Zone | Orientation | θ | Normalized radius $r_z/R$ Driven pile | Jacked pile |
|---|---|---|---|---|
| I | Near vertical | ≤20° | 1.24 ±0.08 | 1.21 ±0.06 |
| II | Steeply inclined | 20-45° | 1.49 ±0.12 | 1.45 ±0.08 |
| III | Gently inclined | 45-70° | 1.70 ±0.15 | Not determined |
| IV | Near horizontal | >70° | | |
| Nearest potential shear surface | | | 0.75-1.0mm | 0.75-1.0mm |

The values of $r_z/R$ given in Table 13.1 suggest that the boundaries between the various zones occur at the same normalized radial positions for both the driven and the jacked pile. However, the distance of the nearest potential shear surface from the pile wall is the same absolute value in both cases.

TSVX 2.43d




TSVX 3.25d

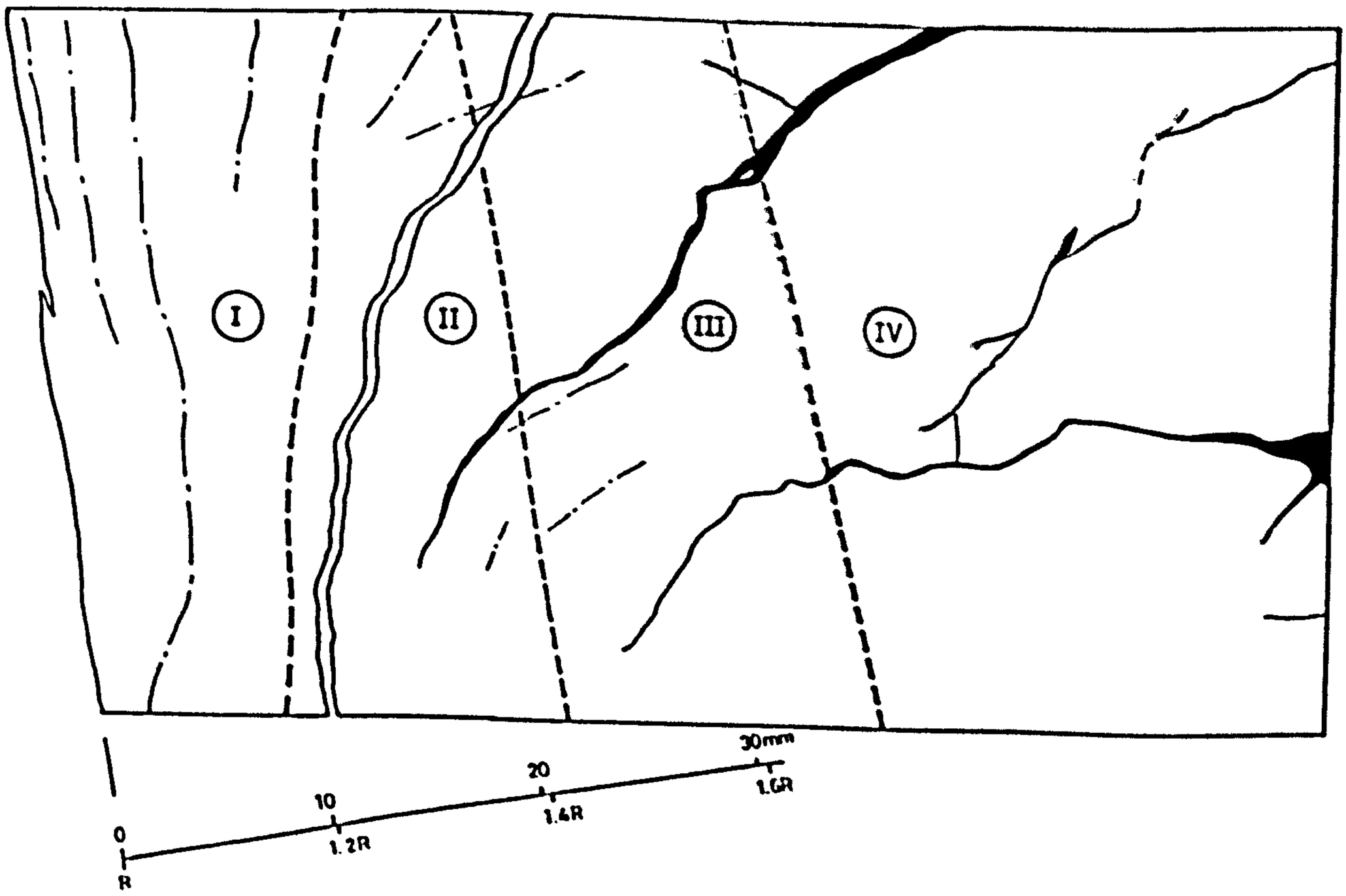





Plate 10(a) Thin section TSVX2.43d, from adjacent to driven pile

[section: K. Schrapel; photo: A. Bond/A. Chipling]




Plate 10(b) Thin section TSVX3.25d, from adjacent to driven pile

[section: K. Schrapel; photo: A. Bond/A. Chipling]

TSVX 2.43d

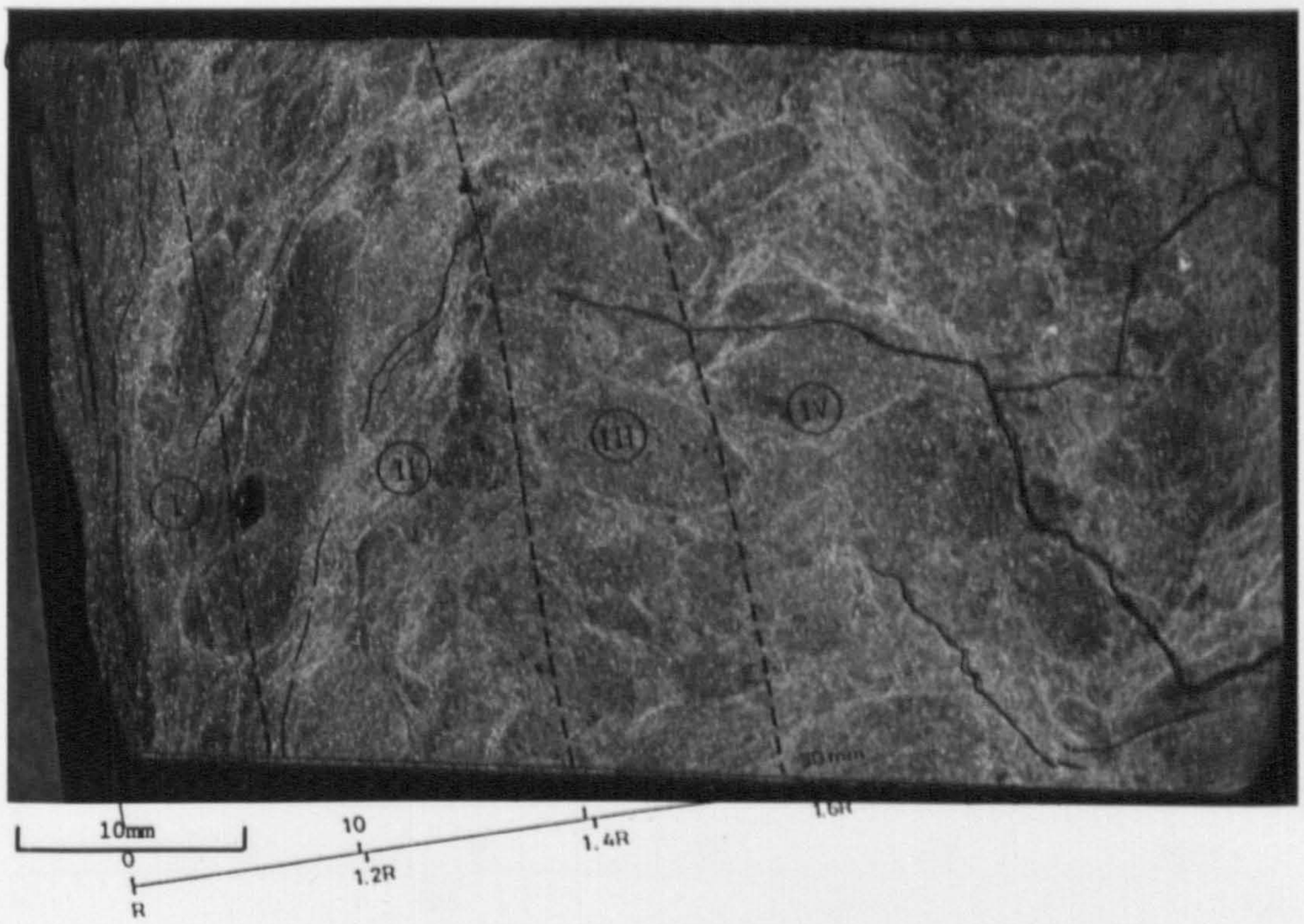



Plate 10(a) Thin section TSVX2.43d, from adjacent to driven pile

[section: K. Schrapel; photo: A. Bond/A. Chipling]

TSVX 3.25d

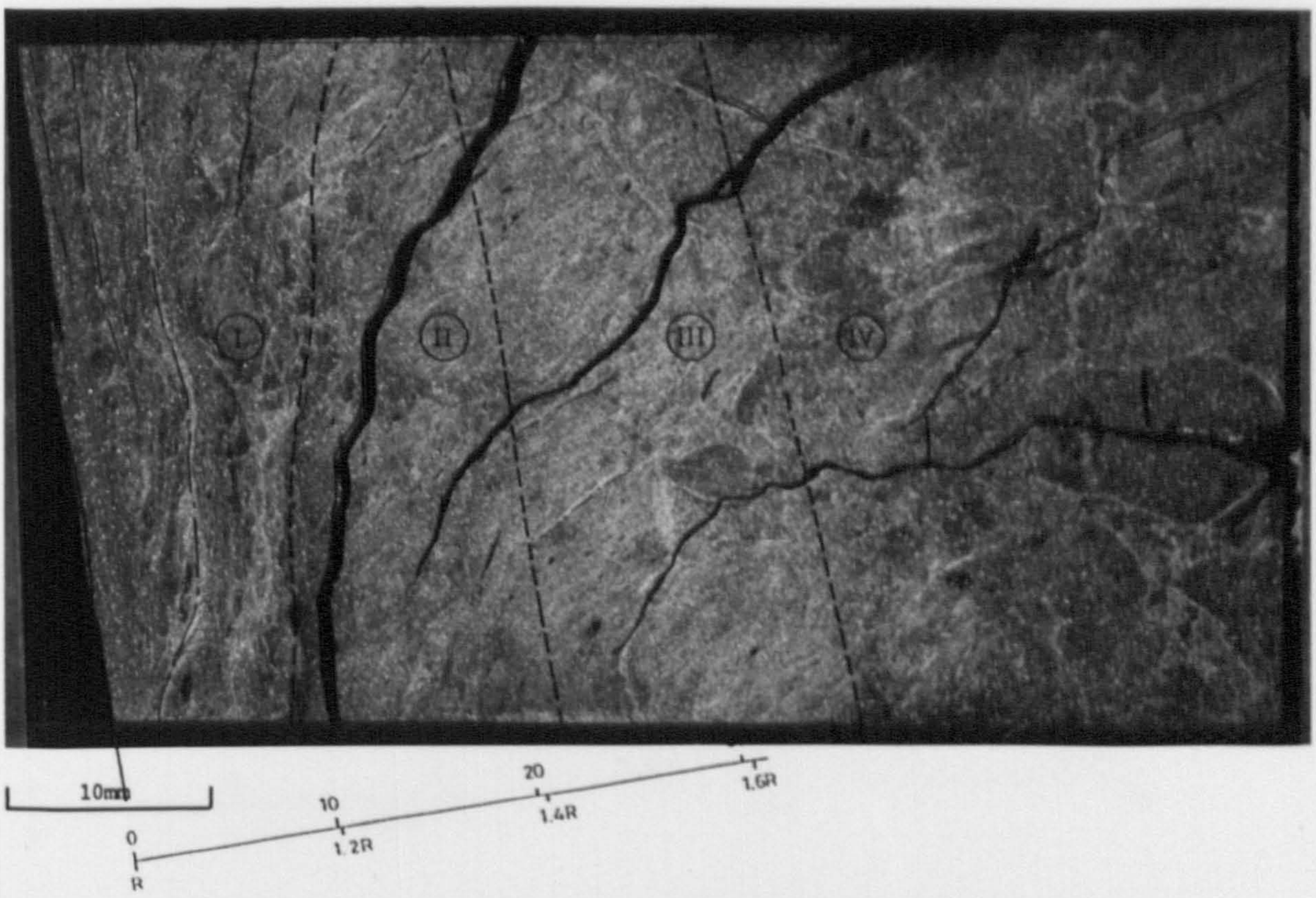
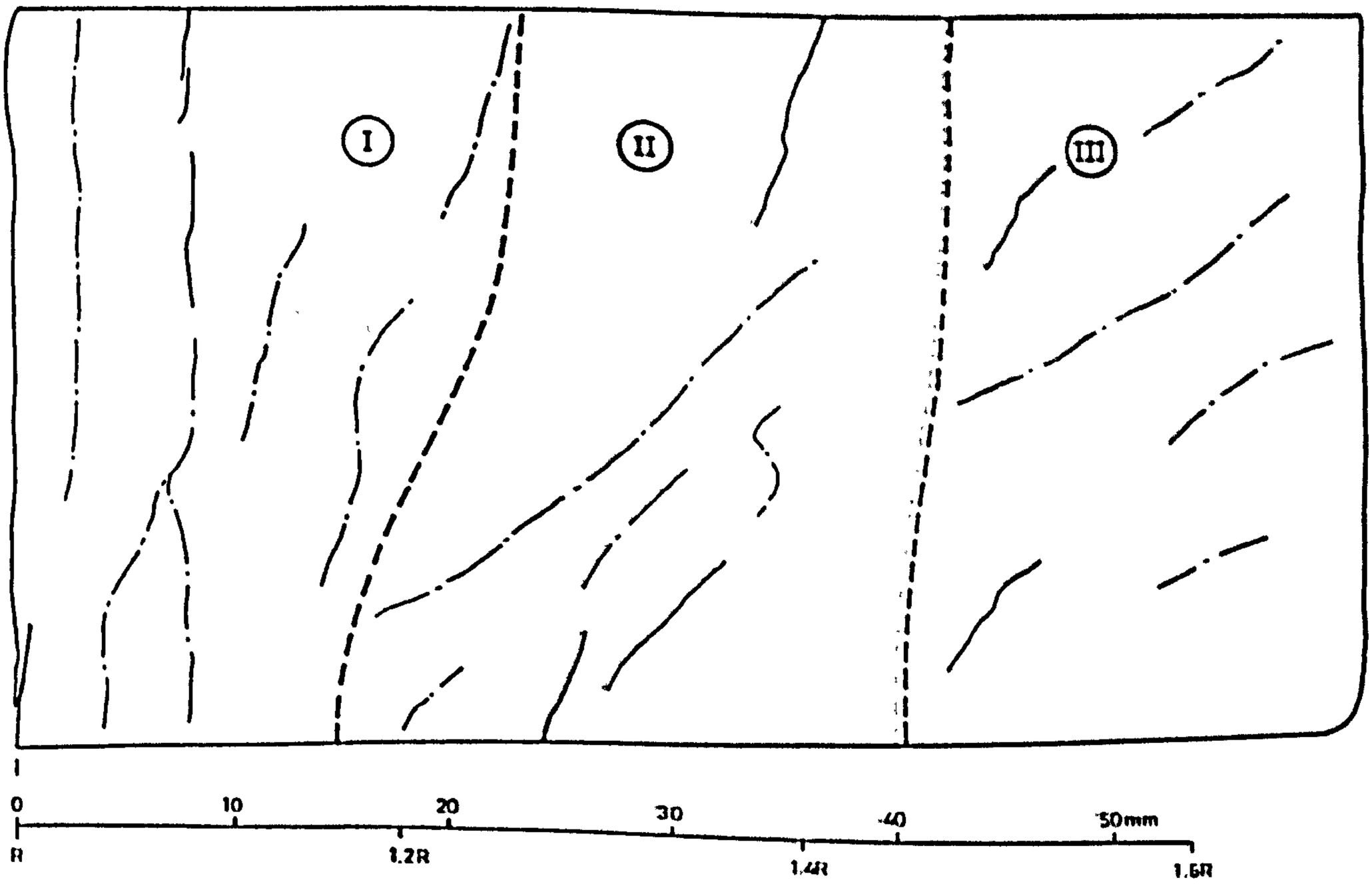


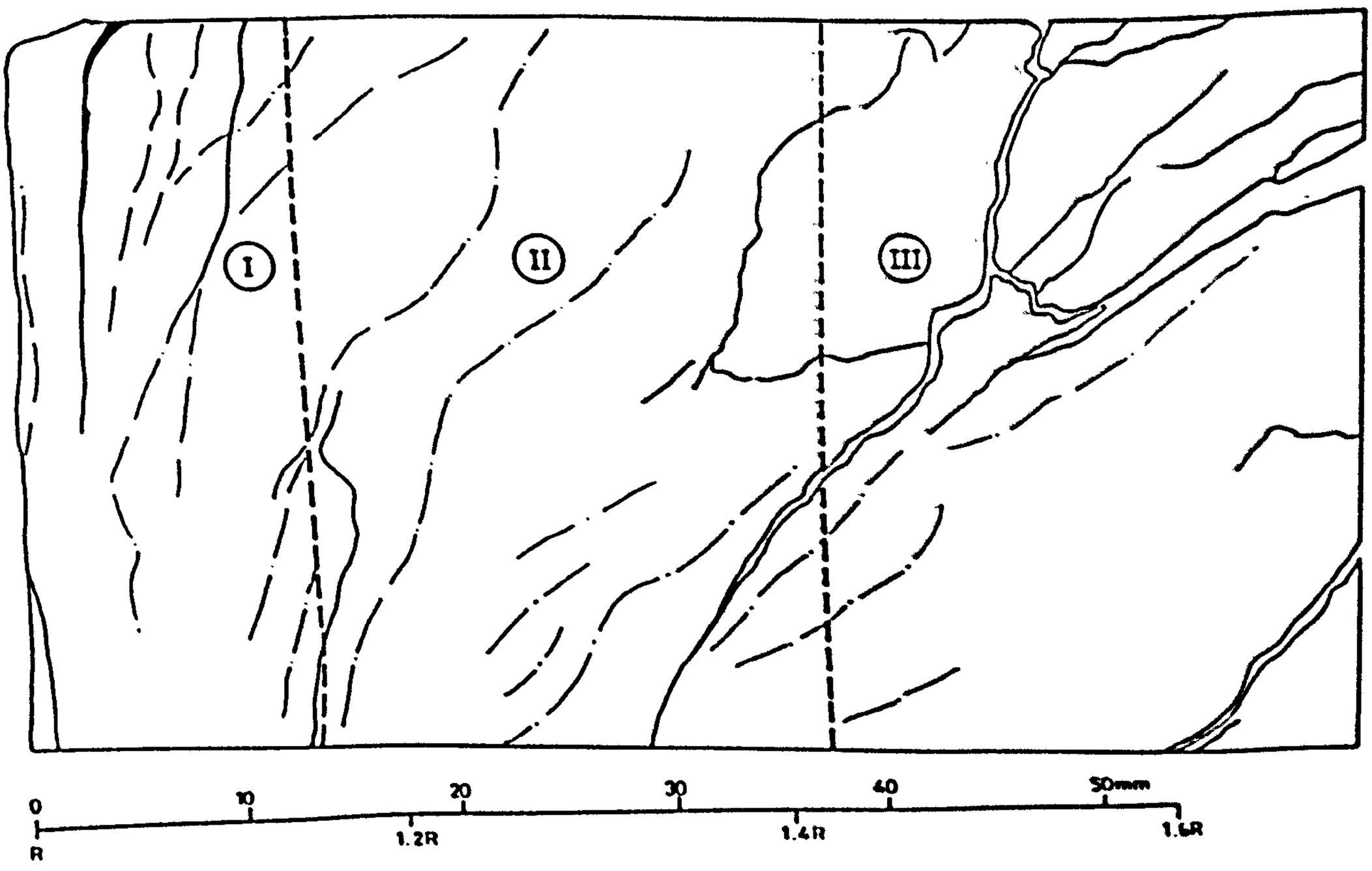

Plate 10(b) Thin section TSVX3.25d, from adjacent to driven pile

[section: K. Schrapel; photo: A. Bond/A. Chipling]

TSVX 2.61 j




TSVX 3.25j



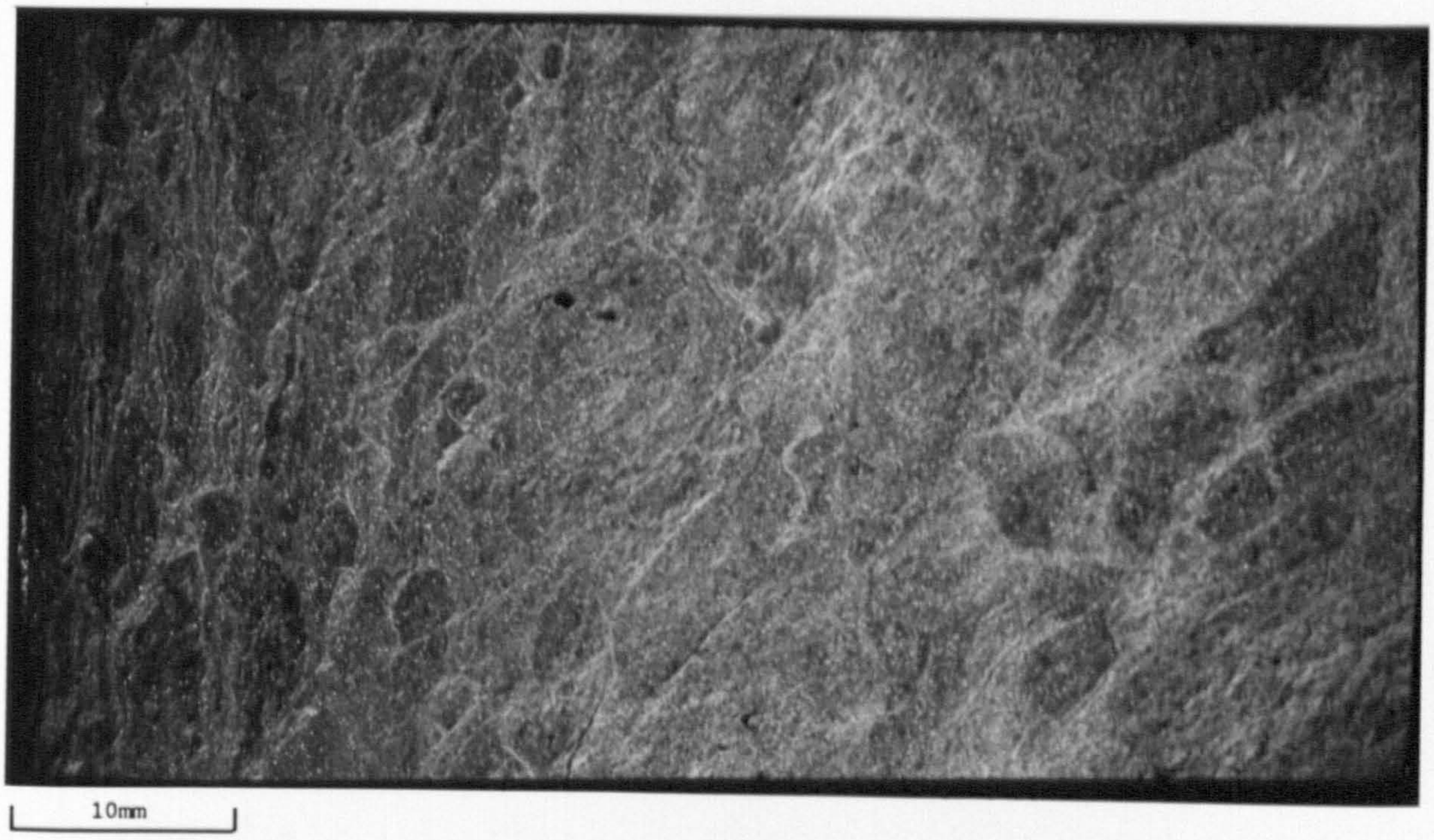



Plate 11(a) Thin section TSVX2.61j, from adjacent to jacked pile

[section: K. Schrapel; photo: A. Bond/A. Chipling]

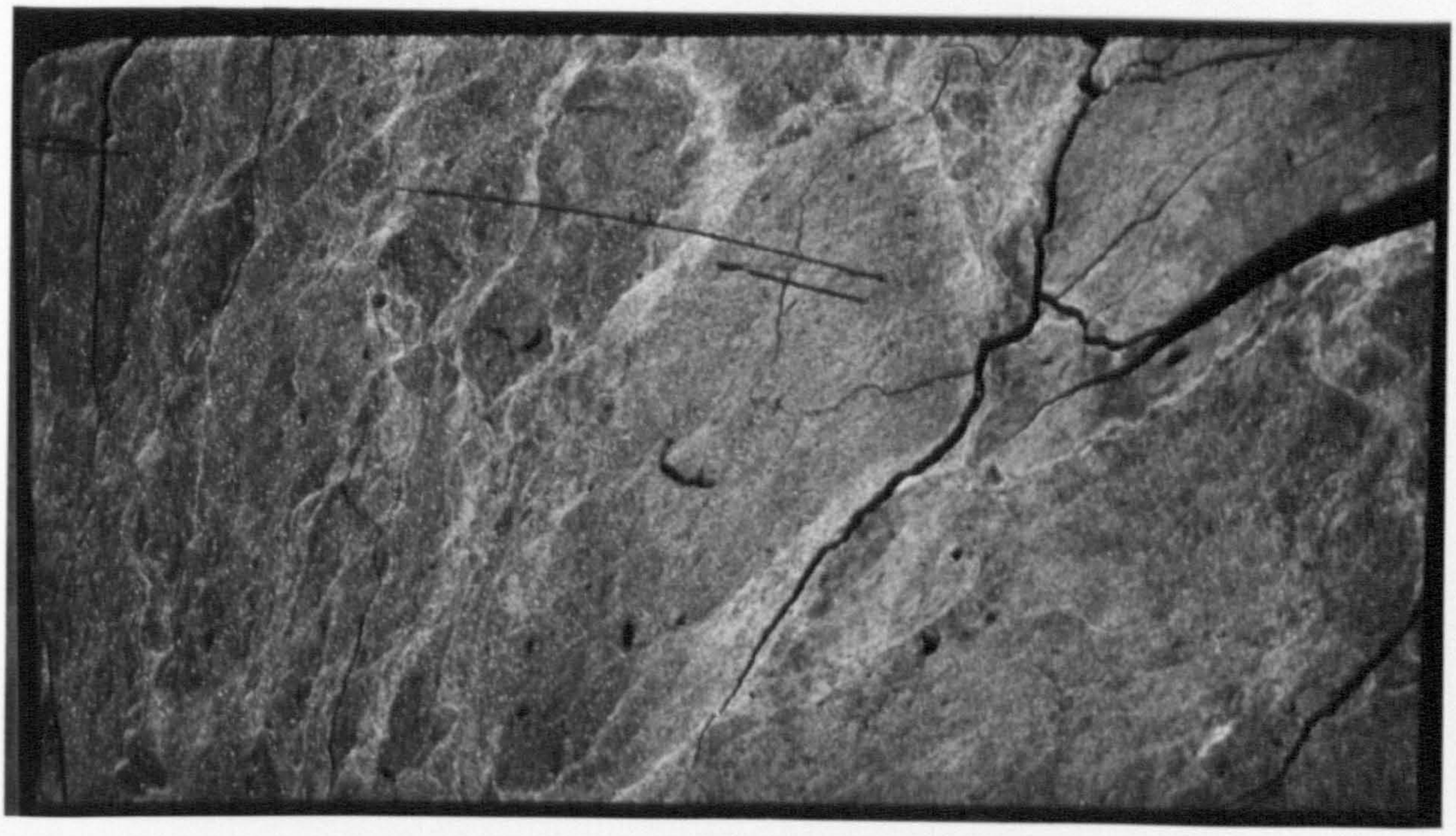



Plate 11(b) Thin section TSVX3.25j, from adjacent to jacked pile

[section: K. Schrapel; photo: A. Bond/A. Chipling]

TSVX 2.61 j

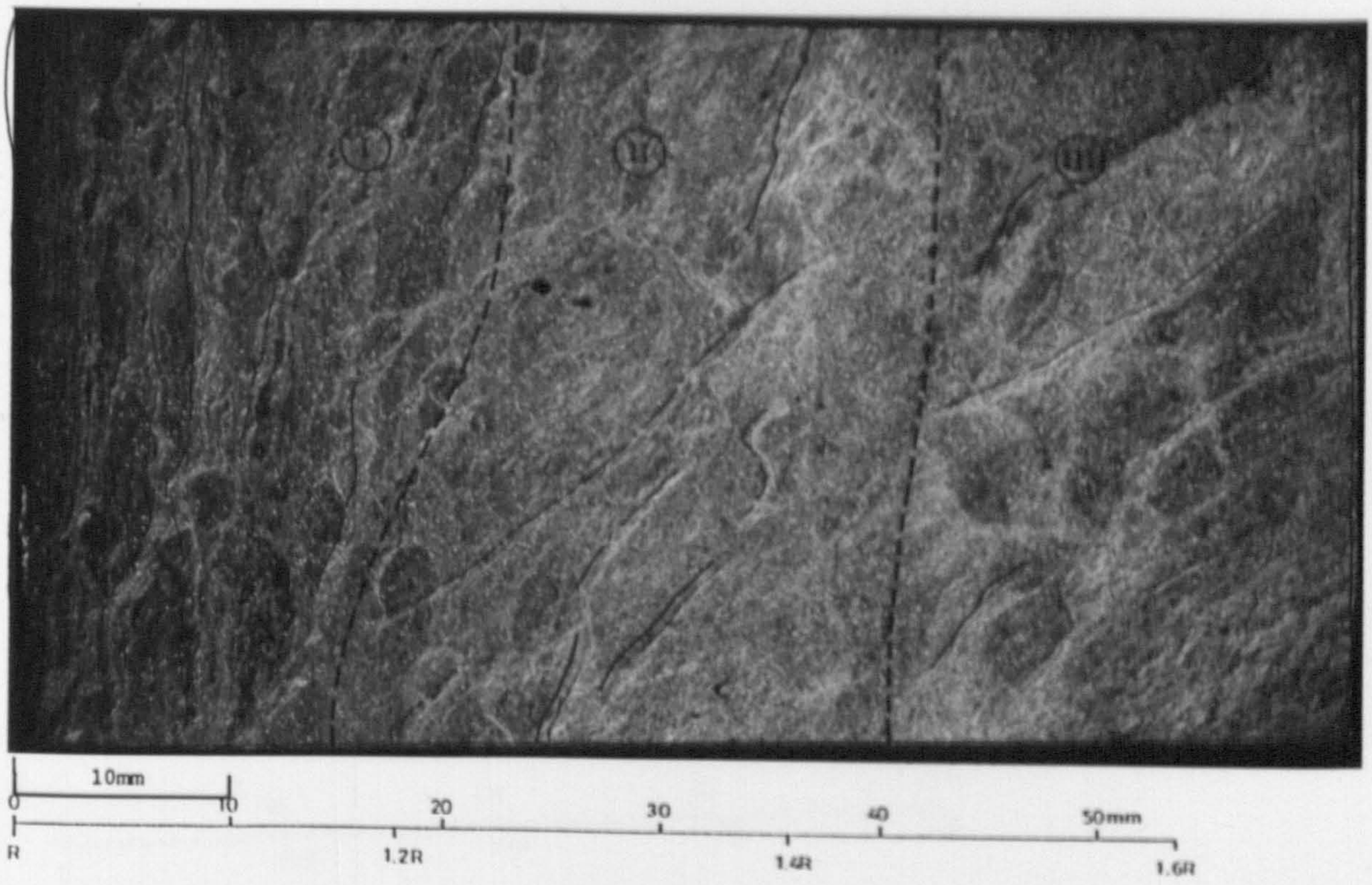



Plate 11(a) Thin section TSVX2.61j, from adjacent to jacked pile

[section: K. Schrapel; photo: A. Bond/A. Chipling]

TSVX 3.25j

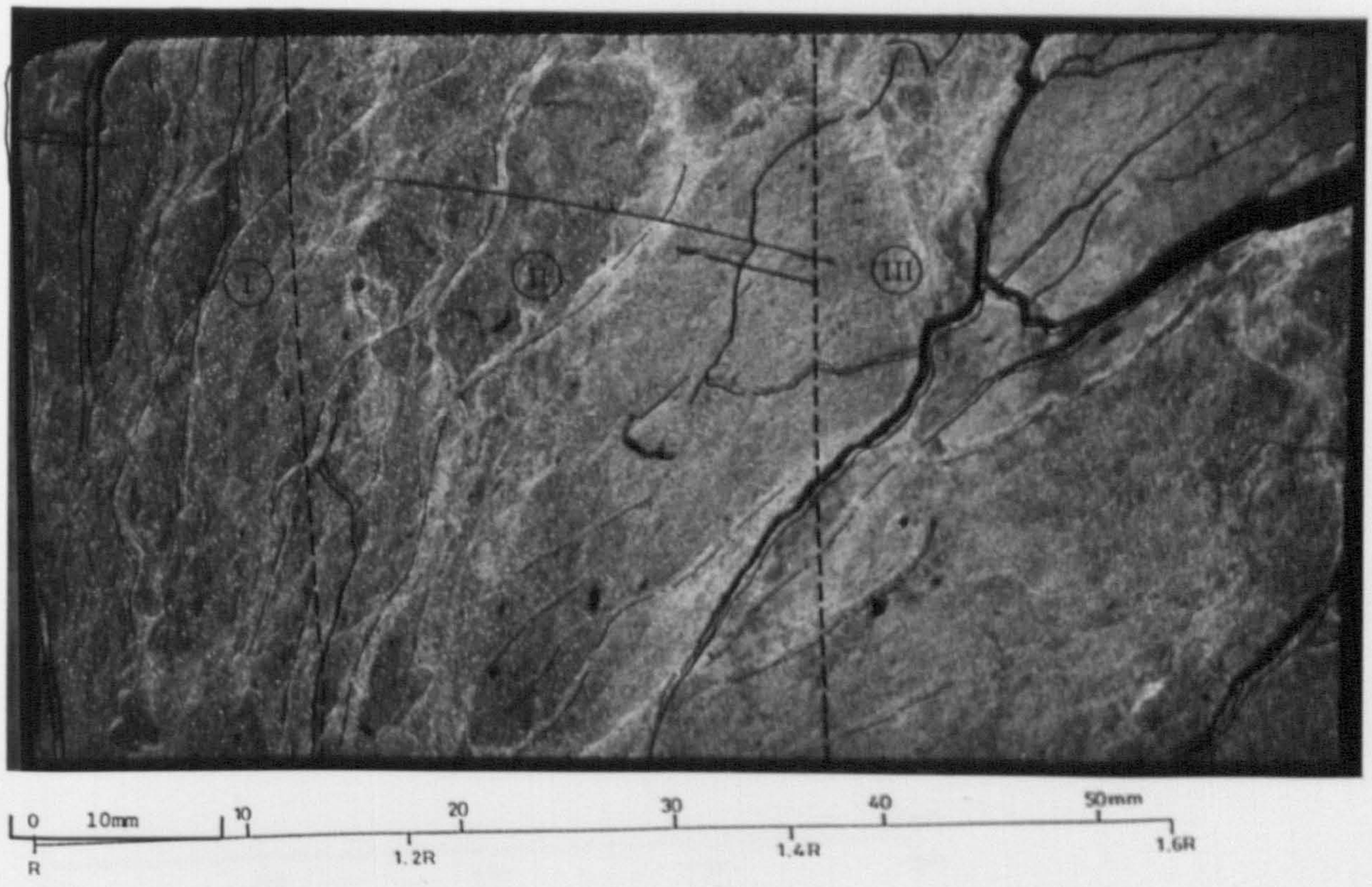
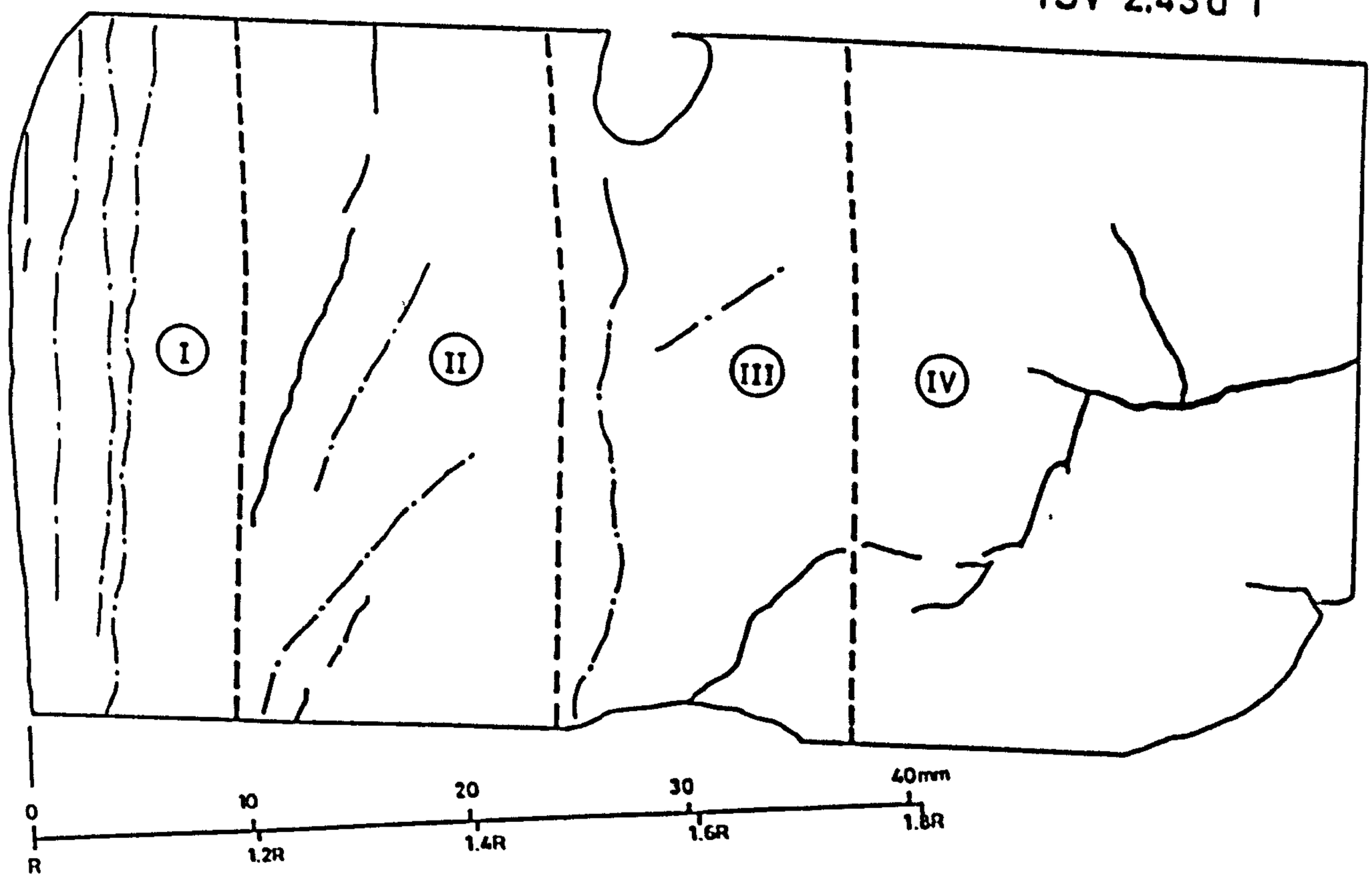


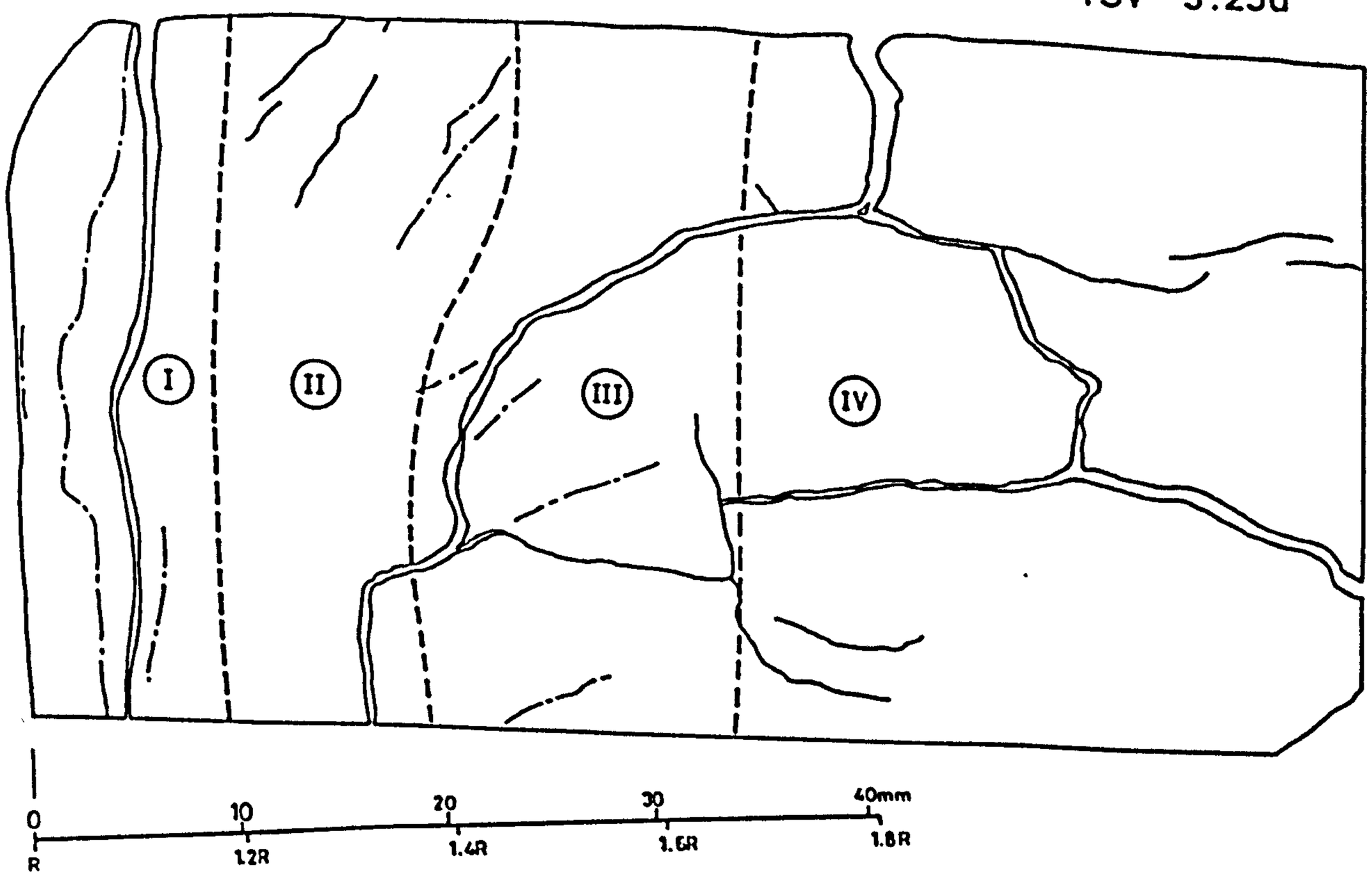

Plate 11(b) Thin section TSVX3.25j, from adjacent to jacked pile

[section: K. Schrapel; photo: A. Bond/A. Chipling]

TSV 2.43d 1




TSV 3.25d



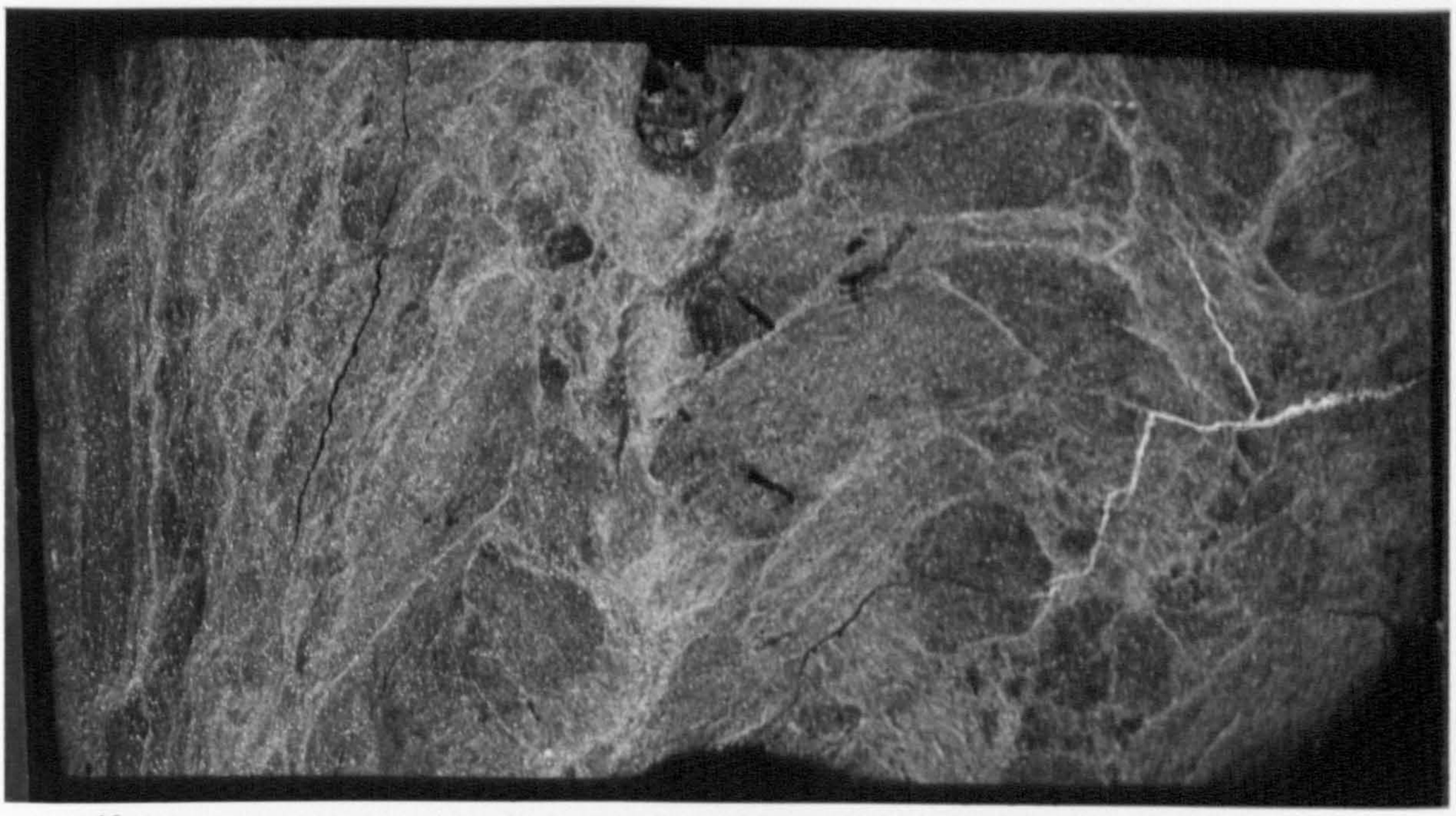



Plate 12(a) Thin section TSV2.43d1, from adjacent to driven pile

[section: K. Schrapel; photo: A. Bond/A. Chipling]

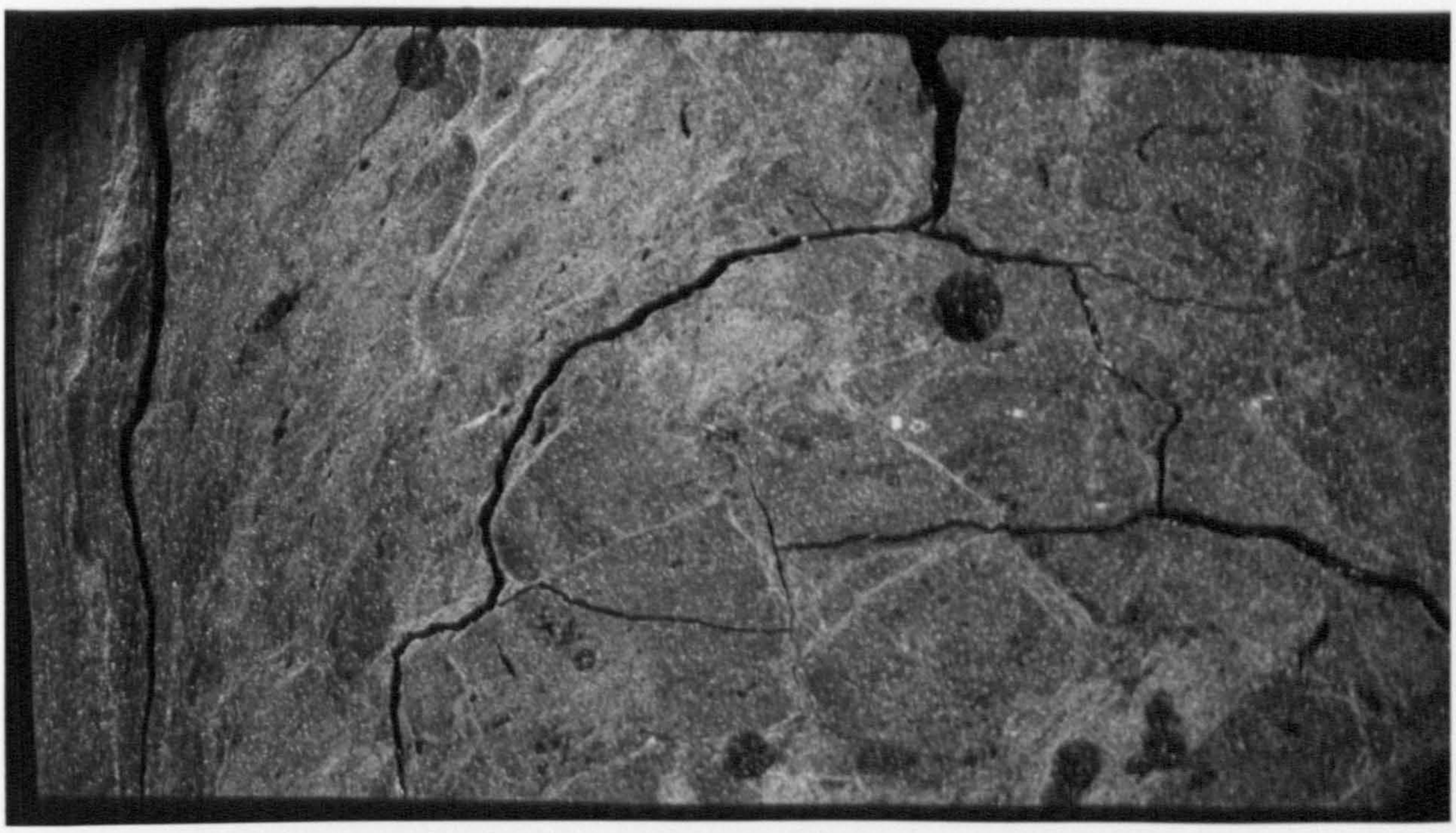



Plate 12(b) Thin section TSV3.25d, from adjacent to driven pile

[section: K. Schrapel; photo: A. Bond/A. Chipling]

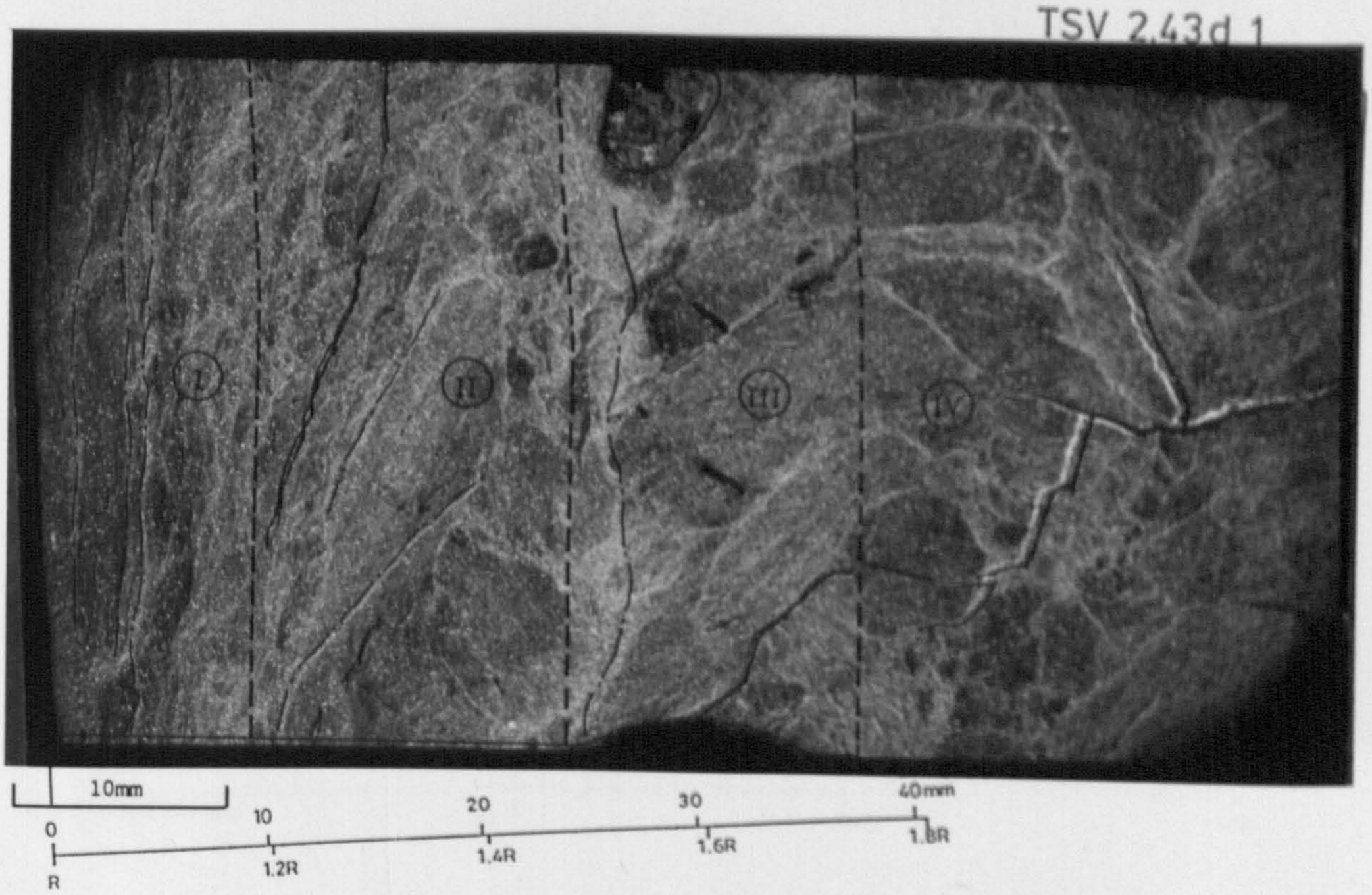



Plate 12(a) Thin section TSV2.43d1, from adjacent to driven pile

[section: K. Schrapel; photo: A. Bond/A. Chipling]

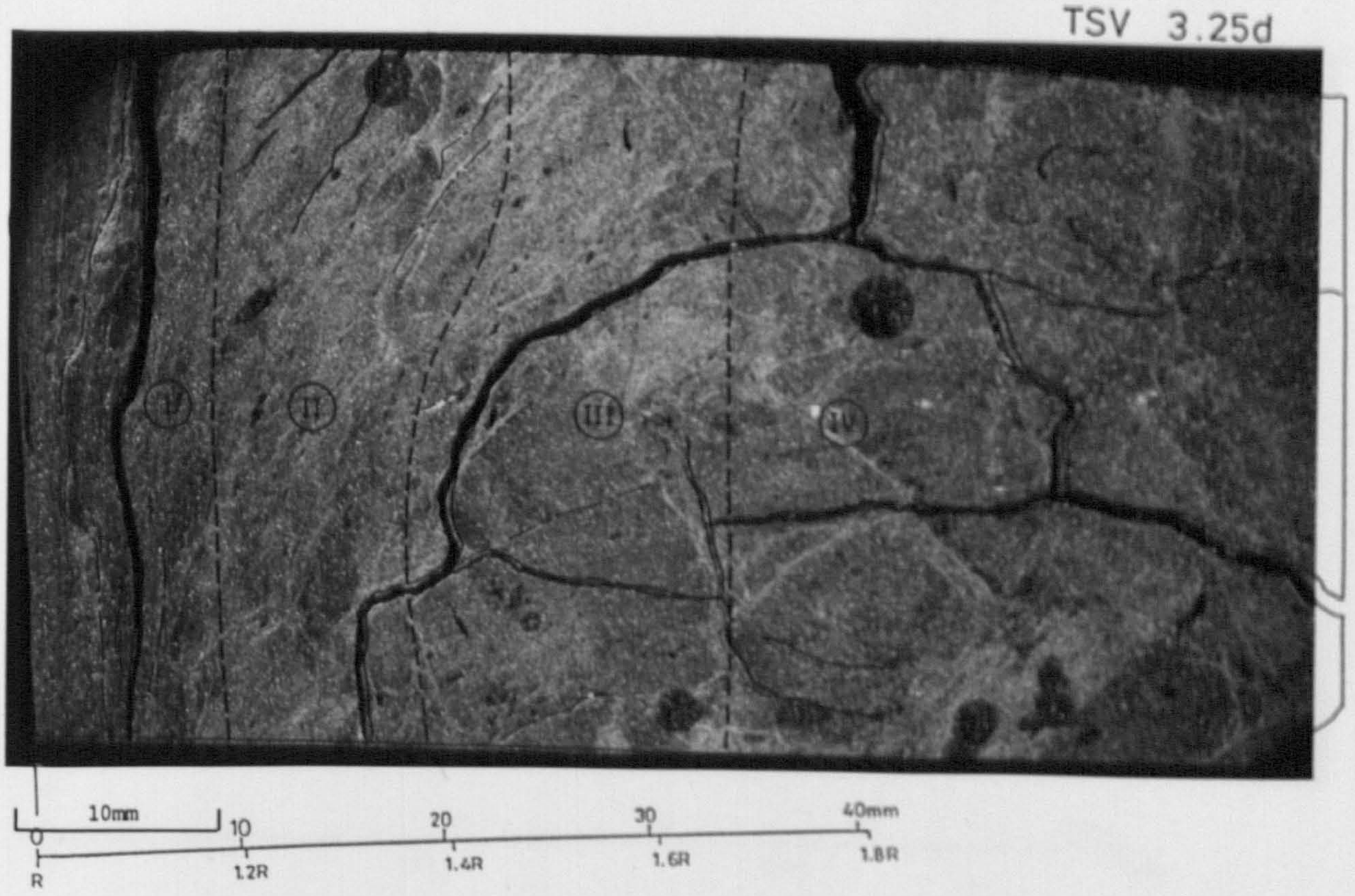
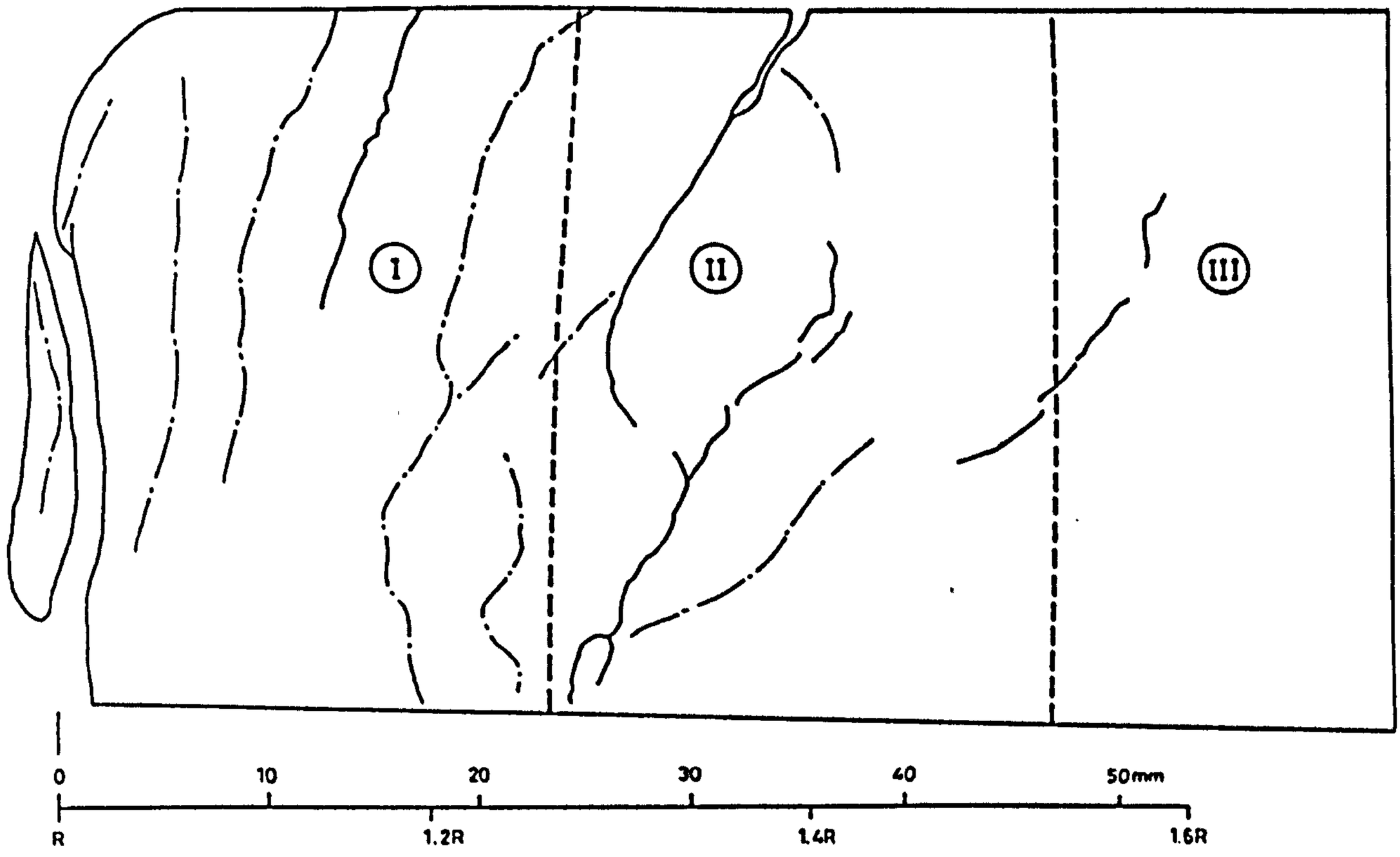


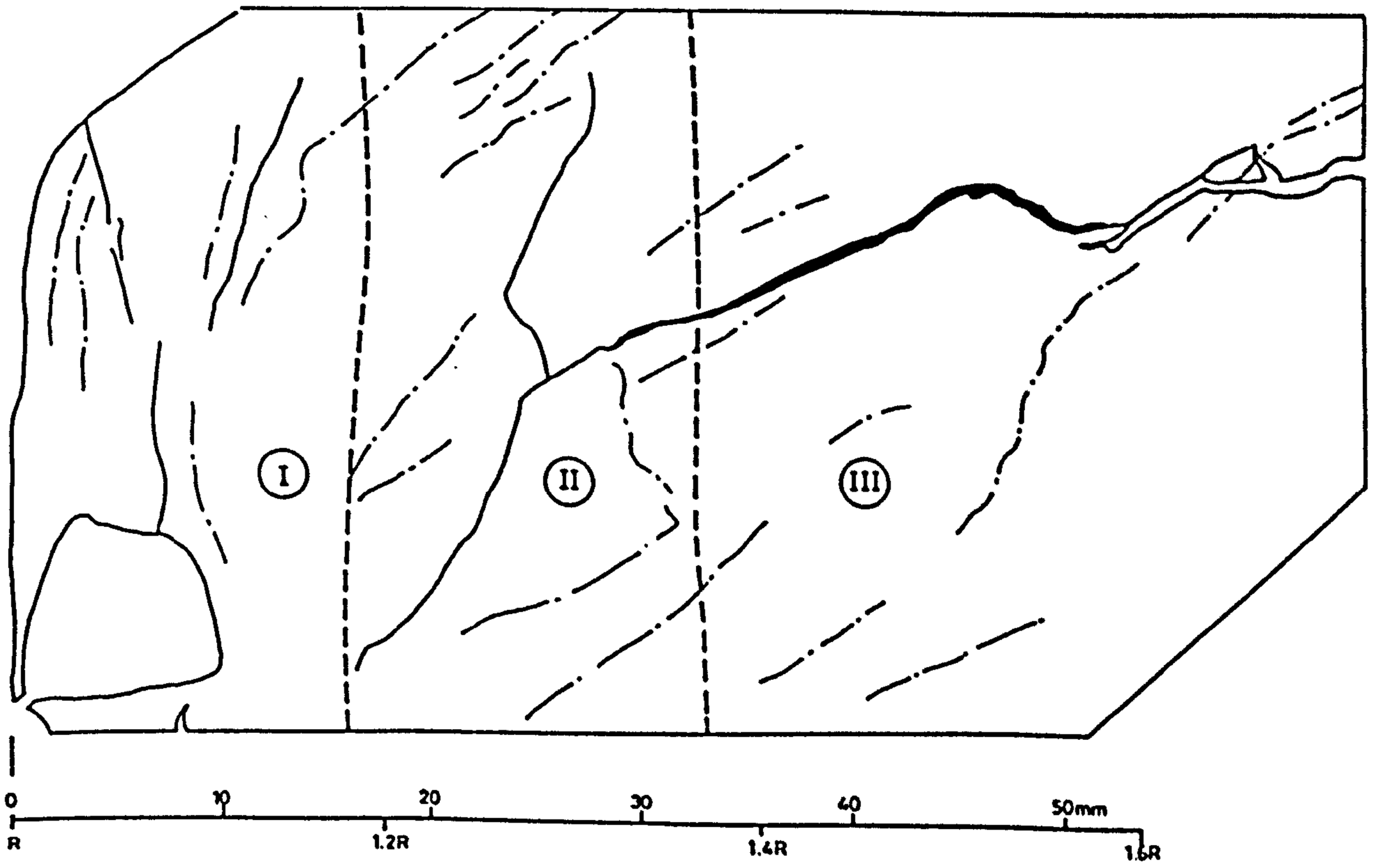

Plate 12(b) Thin section TSV3.25d, from adjacent to driven pile

[section: K. Schrapel; photo: A. Bond/A. Chipling]

TSV 2.61j




TSV 3.25j



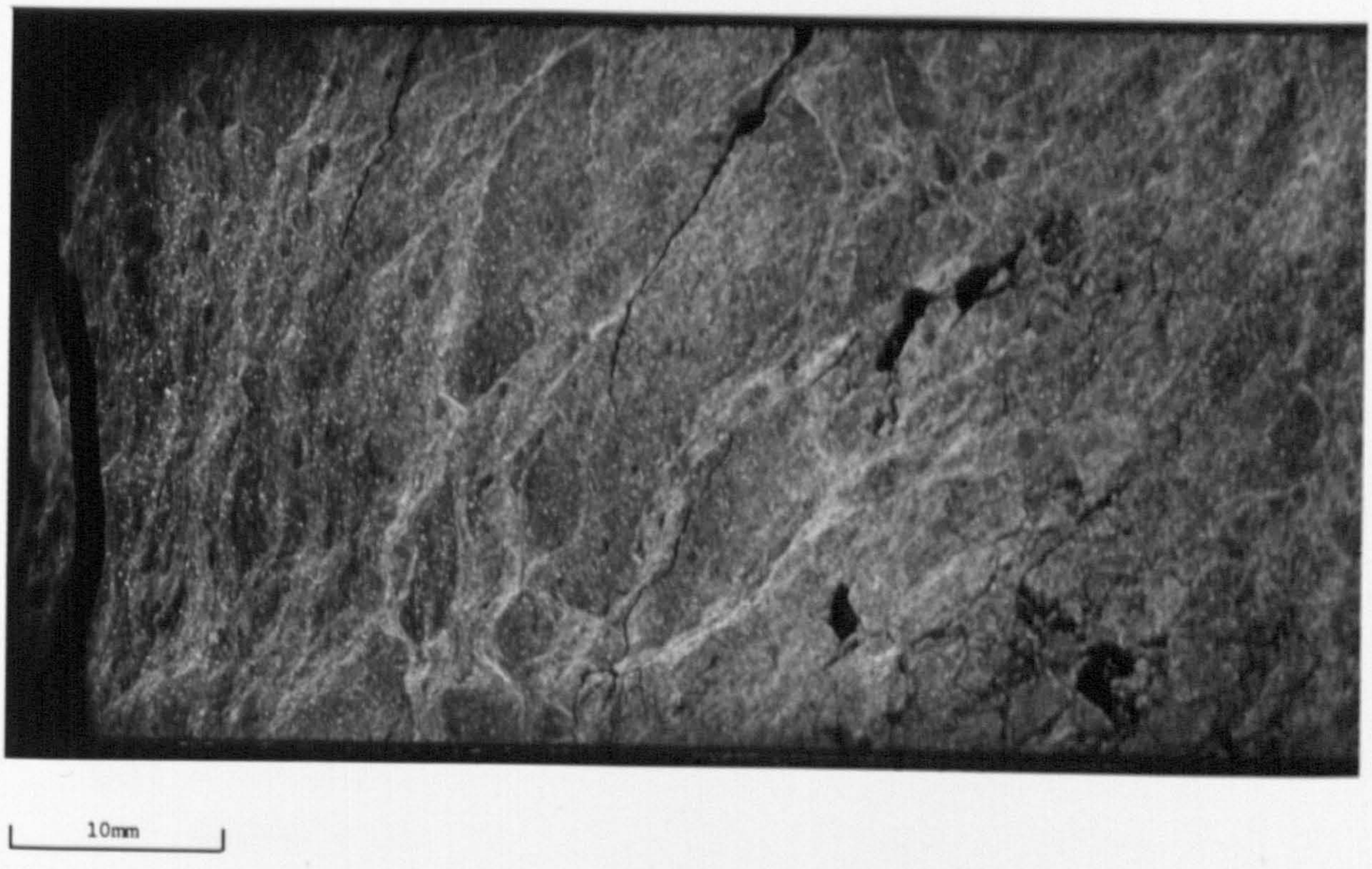



Plate 13(a) Thin section TSV2.61j, from adjacent to jacked pile

[section: K. Schrapel; photo: A. Bond/A. Chipling]




Plate 13(b) Thin section TSV3.25j, from adjacent to jacked pile

[section: K. Schrapel; photo: A. Bond/A. Chipling]

TSV 2.61j

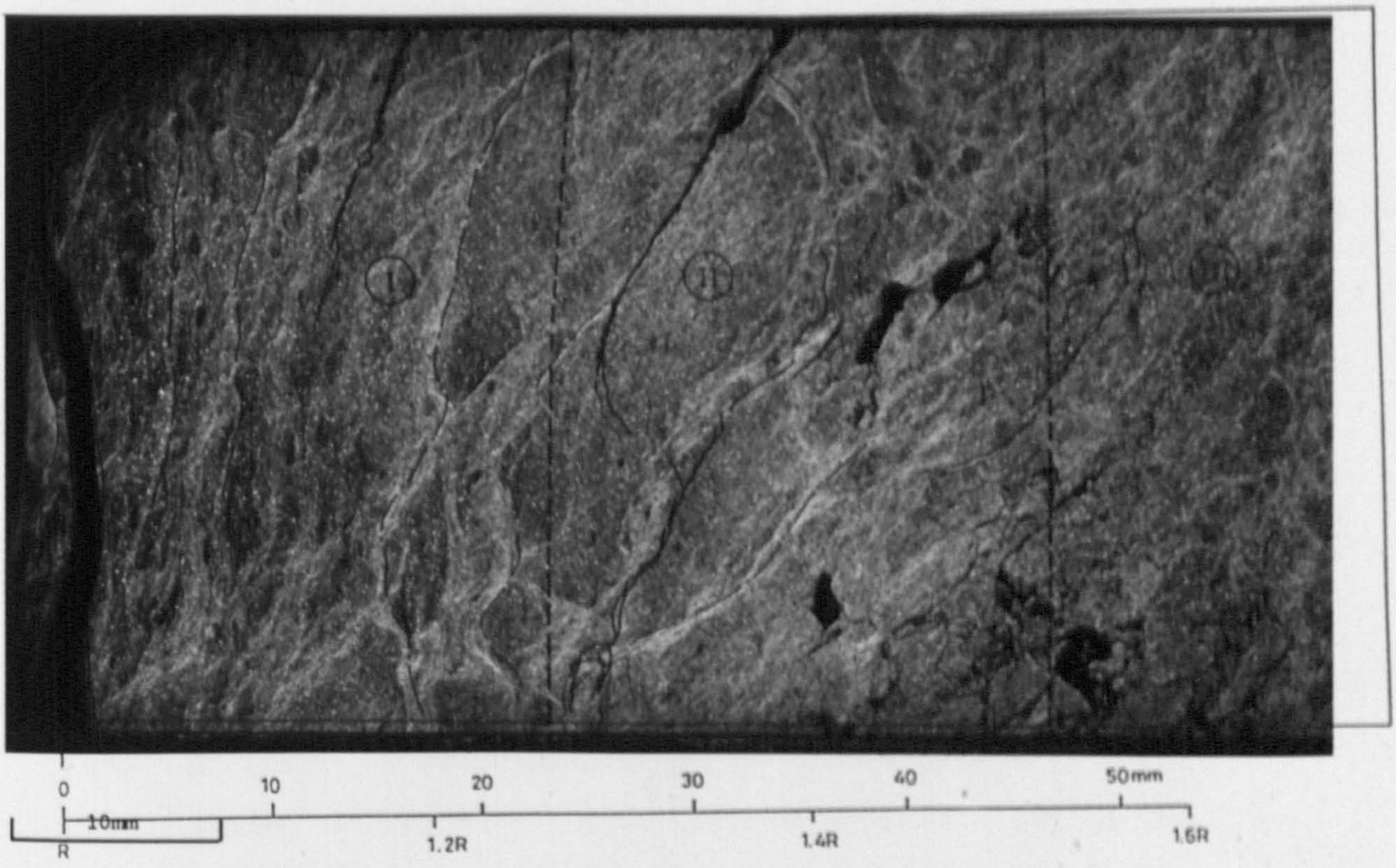



Plate 13(a) Thin section TSV2.61j, from adjacent to jacked pile

[section: K. Schrapel; photo: A. Bond/A. Chipling]

TSV 3.25j

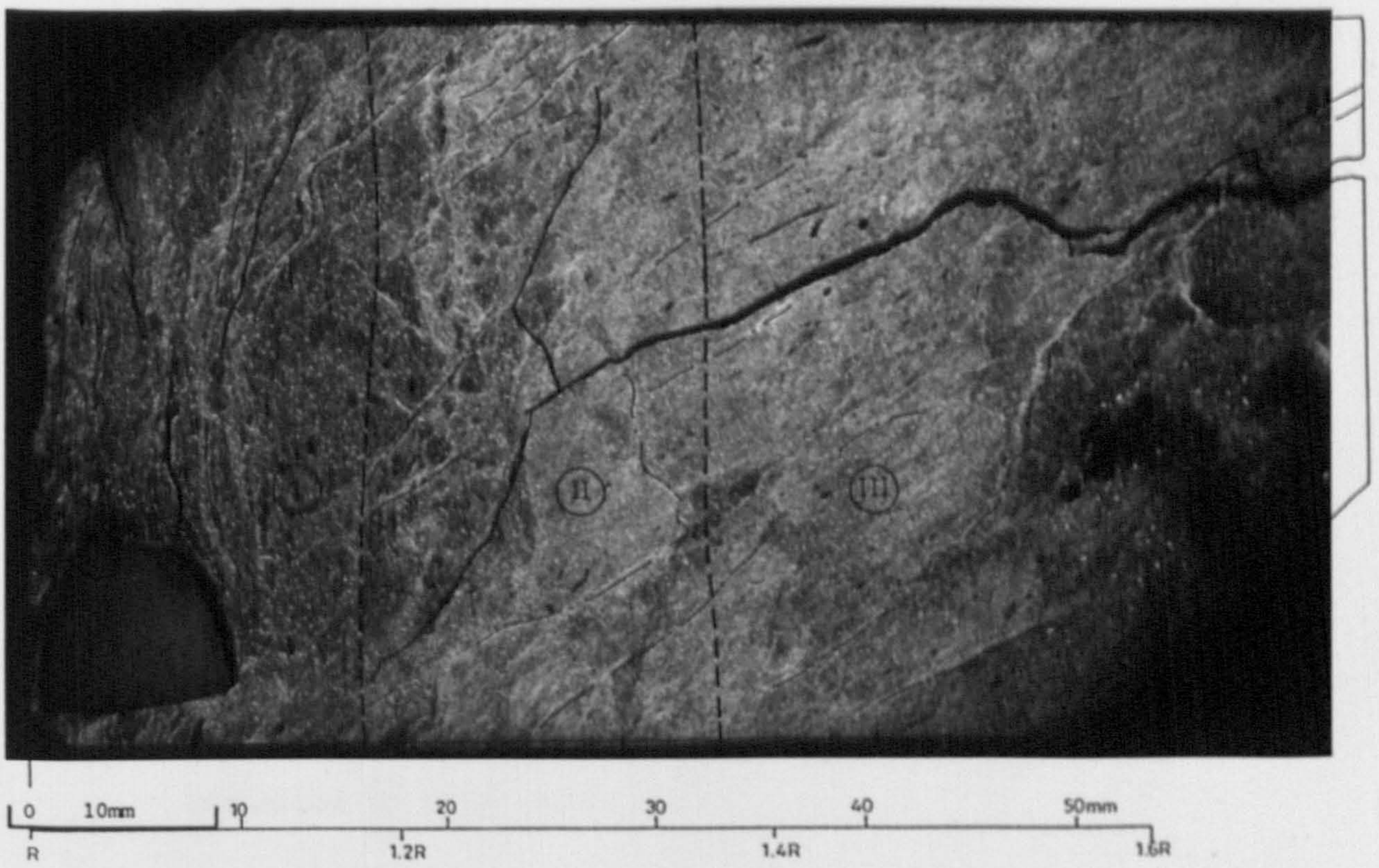



Plate 13(b) Thin section TSV3.25j, from adjacent to jacked pile

[section: K. Schrapel; photo: A. Bond/A. Chipling]

## 13.6 DISCUSSION

The following are the main conclusions that can be drawn from the work described in this chapter:

i) The soil around a displacement pile is <u>not</u> remoulded by the action of installing the pile: instead there is systematic shear distortion of the soil which diminishes with distance away from the pile wall.

ii) In stiff clays, the fabric is re-oriented in a near vertical direction within a zone extending to 1.2 times the pile radius ($r/R = 1.2$).

iii) A "principal displacement shear" may form next to <u>slow-jacked</u> piles (for which the disturbance caused by installation is minimal): this is a highly polished slip surface which is between 0.75 and 1.0mm away from the pile.

iv) Next to <u>driven</u> piles the shearing is more turbulent in nature, and causes the soil's fabric to be less even (the texture is knobbly). There is evidence, however, of frequent <u>discontinuous</u> shear surfaces which are irregular in size and alignment. The overall texture is akin to that of a multi-layered "onion skin".

v) Further away from the pile ($r/R > 1.2$), there is little to distinguish between jacked and driven piles: the orientation of the fabric declines towards the vertical at the same rate for both. The "contours" between the various zones listed in Table 13.1 are at the same normalized radius $r/R$; and there appears to be no difference in the variation with $r/R$ of the soil parameters that have been measured (water content, consistency, and soil suction).

vi) The outer extent of the disturbance to the clay is about 4R - much less than is commonly assumed for piles installed in stiff clays.

## 13.7 NOTES AND REFERENCES

[1]Kitching D.N. (1983). A study into the microfabric of clays adjacent to jacked piles. MSc Dissertation, Univ. of London (Imperial Coll.), 31pp+.

[2]Ove Arup and Partners (1986). Research on the behaviour of piles as anchors for buoyant structures. Dept of Energy, Offshore Technology Report, OTH 86 215. HMSO, London, 80pp. See p57: "...the scatter in results was large and no firm conclusions could be drawn. There was, however, a long delay between sampling and the time at which the water contents were measured."

[3]BS 1377: 1975. Methods of test for soils for civil engineering purposes. British Standards Institution, London, 143pp.

[4]Skempton A.W. (1961). Horizontal stresses in an overconsolidated Eocene clay. Proc. 5th Int. Conf. Soil Mech. & Fdn Engng, Paris, 1, pp351-357. See pp354-355, "Determination of Capillary Pressure", method (iii).

[5]Chandler R.J. and Gutierrez C.I. (1986). The filter-paper method of suction measurement. Géotechnique, 36(2), pp265-268.

[6]Skempton A.W. (1954). The pore-pressure coefficients A and B. Géotechnique, 4, pp143-147.

[7]Chandler and Gutierrez (1986), loc. cit. The filter-paper method "provides a measure of the matrix suction, which is assumed to be the same numerically as the capillary pressure" (p265).

[8]For a description of this apparatus, see Chapter 8 of: Schreiner H.D. (1988). Volume change of compacted highly plastic African clays. PhD Thesis, Univ. of London (Imperial College), 313pp. Dr Deneys Schreiner kindly performed the pressure-plate tests described herein.

[9]X-rays taken by Mr Martin Gill, Dept of Geology, Imperial College.

[10]Tchalenko J.S. (1967). The influence of shear and consolidation on the microscopic structure of some clays. PhD Thesis, Univ. of London (Imperial College), 2vols, 221pp + 171 figures. See pp36-42; and 196-200.

[11]Of those omitted, the TSH2.61j and TSH3.25j fail to show anything of value and TSV2.43d2 is similar in appearance to TSV2.43d1.

[12]See Kitching (1983), loc. cit., Figures 7, 8, 9, and 22.

[13]Ove Arup and Partners (1987). Comparison of British and Norwegian research on the behaviour of piles as anchors for buoyant structures. Dept of Energy, Offshore Technology Report, OTH 86 218. HMSO, London, 43pp.

[14]Skempton A.W. (1967). The strength along structural discontinuities in stiff clays. Proc. Geotech. Conf., Oslo, 2, pp29-46.

# Chapter 14

# Discussion of test results

CONTENTS OF CHAPTER 14


14.1 INTRODUCTION . . . . . 446
14.1.1 Outline of the chapter 446
14.1.2 Summary of results from Canons Park 446
14.1.3 Comparisons with other high quality field experiments 447
14.1.4 Comparisons with theory 448
14.2 PILE INSTALLATION . . . . . 449
14.2.1 Pore pressure response 449
14.2.2 Radial total stresses 454
14.2.3 Radial effective stresses 458
14.2.4 Coefficients of friction 460
14.3 EARTH AND PORE PRESSURE EQUALIZATION . . . . . 465
14.3.1 Pore pressure dissipation 465
14.3.2 Relaxation of radial total stress 470
14.3.3 Changes in radial effective stress 471
14.4 PILE LOADING . . . . . 473
14.4.1 Introduction 473
14.4.2 Radial effective stress at the end of equalization 474
14.4.3 Changes in radial effective stress during pile loading 478
14.4.4 Coefficients of friction 479
14.5 DESIGN METHOD FOR DISPLACEMENT PILES IN HIGH OCR CLAYS . 482
14.5.1 A new design method for high OCR clays 482
14.5.2 Limitations of the new method 483
14.5.3 Determining the parameters needed for the new design method 483
14.5.4 Worked example 485
14.6 NOTES ON THE SELECTED CASE HISTORIES . . . . . 487
14.7 NOTES AND REFERENCES . . . . . 488

## 14.1 INTRODUCTION

### 14.1.1 Outline of the chapter

The results of the Canons Park Project have major implications for the design of displacement piles in overconsolidated clays. The present chapter attempts to highlight the most important findings of this Project, and to put them into context by comparing them with the results of instrumented pile tests in other clay soils.

The discussion follows the pattern of previous chapters by considering, in turn, the three separate stages in the lifetime of a pile. Section 14.2 covers pile installation; 14.3 earth and pore pressure equalization; and 14.4 pile loading. Finally, Section 14.5 describes a new method for designing displacement piles installed in heavily over-consolidated clays.

Sections 14.2 to 14.4 each contain at least three sub-sections. One of these summarizes the results of the instrumented pile tests at Canons Park. The emphasis here is to discuss the observed behaviour in terms of effective stresses, based on the data presented in Chapters 9-11. Another of the sub-sections compares the results with data from other high quality field experiments (see Section 14.1.3). Finally, another sub-section compares the Canons Park data with theoretical predictions of pile behaviour (where these are available) - see Section 14.1.4.

### 14.1.2 Summary of results from Canons Park

The discussion in this chapter concentrates on the values of four main parameters:

- The excess pore pressure ratio, $\Delta u/\sigma'_{vo} = (u - u_o)/\sigma'_{vo}$
- The normalized horizontal total stress, $H = (\sigma_{rr} - u_o)/\sigma'_{vo}$
- The lateral stress coefficient, $K = \sigma'_{rr}/\sigma'_{vo}$
- The coefficient of friction, $\mu = \tau_{rz}/\sigma'_{rr}$

We are interested in the values of these parameters during i) pile installation (denoted by the subscript "i", as in $\Delta u_i/\sigma'_{vo}$, $H_i$, and $K_i$); ii) at the end of equalization (denoted "c"); and iii) at the point of failure during loading tests (denoted "f"). By definition, $K_i = H_i - \Delta u_i/\sigma'_{vo}$ and $H_c = K_c$ (since $\Delta u_c/\sigma'_{vo} = 0$).

The numerical values of these parameters, as recorded in the tests at Canons Park, are given in Appendix 11.

### 14.1.3 Comparisons with other high quality field experiments

The best way to demonstrate the importance of the Canons Park results is to compare them with the findings of instrumented pile tests in other clay soils. Very few high quality field tests have been reported in sufficient detail for such a comparison to be made. For example, in only eight of the thirty-four cases listed in Table 4.2 (see pp132-133) can the data be regarded as being of "very good" quality.

I have selected three of these tests for comparison with the Canons Park experiments. Two are in soft to firm, sensitive clays and the other in a stiff, insensitive clay. The tests are as follows:

- The Norwegian Geotechnical Institute's (NGI's) experiments at Haga, in Sweden (Case 12 of Table 4.2)[1]
- The Massachusetts Institute of Technology's (MIT's) experiments in the Boston blue clay at Saugus, Massachusetts, USA (Case 10)[2]
- Oxford University's tests in the Gault clay at Madingley, England (Case 17a)[3]

Brief details about each of these experiments are given at the end of the chapter (see Section 14.6), together with a summary of the soil properties at each site.

## 14.1.4 Comparisons with theory

Chapter 3 describes the two modern theories that have contributed the most to recent debates about pile behaviour in clay soils, i.e. the cavity expansion and strain path methods.

The cavity expansion method has been used to predict the behaviour of piles installed in London clay, at overconsolidation ratios (OCRs) from one to thirty-two. These predictions, which are discussed at length in Chapter 3, are compared with the data from Canons Park at various points throughout this chapter.

The strain path method has also been used to predict the behaviour of displacement piles in clays, but at present only for soils with low OCRs (i.e. less than or equal to four). However, as noted on p144, Professor Whittle and I hope to publish predictions for the London clay at a later date.

## 14.2 PILE INSTALLATION

### 14.2.1 Pore pressure response

a) Discussion of the Canons Park data

Negative pore water pressures are generated during pile installation in heavily overconsolidated clays. The evidence from Canons Park is unequivocal: the traces recorded by the leading, following, and trailing instruments (see Figures 9.1 and 9.2, pp305-306) all show a sudden switch from positive to negative values as each instrument passes from the head material and into the (disturbed) London clay at 2.5m depth.

The pore pressures that are measured during pile installation ($u_i$) consist of three separate components: the original pressure in the soil ($u_o$); the excess pressure that results from the increase in mean total stress ($\Delta u_{ts} > 0$); and a shear-induced excess pore pressure ($\Delta u_{sh}$), which is positive if the soil *contracts* and negative if it *dilates*. The relative magnitude of these three components determines the pore pressures recorded by the piezometers mounted on the pile. The *excess* pore pressure ($\Delta u_i$) is given by the sum of the last two components, i.e.:

$$\Delta u_i = (u_i - u_o) = (\Delta u_{ts} + \Delta u_{sh})$$

The fact that *negative* pore pressures ($u_i < 0$) were registered during the instrumented pile tests at Canons Park implies that the shear-induced pressure is both negative ($\Delta u_{sh} < 0$) *and* much larger than the increase in total stress ($|\Delta u_{sh}| >> |\Delta u_{ts}|$). This form of response is typical of clay soils that dilate strongly when sheared.

The spikiness of individual pore pressure traces (for example, see Figure 9.1) reflects the soil's attempts to come into equilibrium during pauses in installation (while the jack was being re-set). These delays generally lasted between two and five minutes (although sometimes they stretched to 3/4h). The size of the spikes reveals subtle differences between i) the response of the soil above and below a depth of 5m; and ii) the

pressures recorded at any one horizon, but by different probes.

The best way to illustrate these points is to examine the readings obtained during a typical installation. Table 14.1 lists the readings obtained with the *leading* pore pressure probe* in Test Series CP4f. (The corresponding visual trace is given in Appendix 11.)

Table 14.1 Pore pressure response at the leading instrument position during installation of pile CP4f

| End of push | Depth (m) | Pile moving $u_i$ (kPa) | Stationary $u_{max}$ (kPa) | Rise time (mins:secs) | Total pause (mins:secs) |
|---|---|---|---|---|---|
| 8 | 3.34 | -61.5 | +240.4 | 1:00 | 7:09 |
| 9 | 3.84 | -32.2 | +119.3† | 6:12 | 6:12 |
| 10 | 4.06 | -46.2 | +131.6 | 3:15 | 31:01 |
| 11 | 4.29 | -66.9 | +124.2 | 5:18 | 14:31 |
| 12 | 4.46 | -60.6 | +69.7 | 5:24 | 9:33 |
| 13 | 4.69 | -70.0 | +175.4 | 9:18 | 26:35 |
| 14 | 4.86 | -68.4 | +303.6 | 5:21 | 43:49 |
| 15 | 5.07 | -58.5 | +531.3 | 2:03 | 5:03 |
| 16 | 5.27 | -75.9 | +230.2† | 2:14 | 2:14 |
| 17 | 5.51 | -44.9 | +527.6† | 2:08 | 2:08 |
| 18 | 5.73 | -54.3 | +534.9† | 3:55 | 3:55 |
| 19 | 5.94 | +13.4* | +707.6 | 1:16 | 5:14 |
| 20 | 6.16 | -67.3# | +783.2 | 1:43 | 20 days |

†Still rising at the start of the next push
*$u_i$ fluctuated between +13.4kPa and +148.0kPa, and #$u_i$ between -67.3kPa and +184.6kPa

As the table shows, the pore pressure recorded by the leading transducer is less than atmospheric ($u_i < 0$) <u>while the pile is moving</u>,# although it soon rises to a (large) positive value once the pile is stationary. The *maximum* pore pressure registered during the pause periods ($u_{max}$) depends on the transducer's depth below ground level. Above 5m, $u_{max}$ is generally between +125 and +300kPa; whereas below 5m it exceeds +500kPa.

In the other tests at Canons Park the rise in pore pressure during the pause periods was far less dramatic than that recorded in CP4f (e.g. see Figure 9.1, p305), *except in the soil below 5m* where the response was similar.

---

*In this experiment there was only <u>one</u> fast-acting pore pressure probes in each instrument cluster - the other was one of the flushable variety

#Except perhaps during pushes 19 and 20, when the large *positive* pressures that exist at the start of push are not completely negated by the dilation of the clay

The response of the *following* and *trailing* probes in Test CP4f was different to that described above. The pressures recorded *while the pile is moving* were generally <u>less</u> negative than at the leading position, and during the pause periods the pressure rose no higher than +50kPa. There is no indication that the following or trailing probes were any slower to respond than the leading ones (their saturation was identical) - hence this behaviour reflects the <u>true</u> response of the soil.

At first glance these results appear highly unusual. This is because most people's expectations of the behaviour during pile installation are conditioned by the results of tests in low OCR clays. This is the first time that *reliable* pore pressure readings have been reported for a heavily overconsolidated clay. Evidence to support the Canons Park data can be found in the results of Coop's test at the same site and in piezocone soundings in other high OCR clays (see Section 14.2.1.b.).

b) Comparison with selected test cases

As noted in Chapter 4, previous attempts to measure the pore pressures generated next to piles installed in heavily overconsolidated clays have been singularly unsuccessful. The only person to obtain credible readings in such soils is Coop, and there are doubts about the response of his piezometers during pile installation (see Chapter 4, pp142-143). Successful pore pressure measurements have been obtained in *contractive* clays, partly because the demands made on the piezometer system are far less severe than in dilating soils.

Before comparing the results from the Canons Park experiments with the data from the three "test cases" at Haga, Saugus, and Madingley (see p447), it is appropriate to summarize the performance of the pore pressure probes that were used in each experiment:

- NGI/Haga (Haga clay): pressures recorded at end of installation <u>only</u>; *reliability*: VERY HIGH
- MIT/Saugus (Boston blue clay): pressures measured at one location <u>only</u> (z/R = 50); *reliability*: VERY HIGH

- Oxford University/Madingley (Gault clay): cavitation during installation: traces "died"; *reliability*: LOW
- This thesis/Canons Park (London clay): cavitation during installation: traces remained "alive"; *reliability*: HIGH

The pore pressure readings that were obtained in the London clay at Canons Park are compared below with the results of the tests at Haga, Saugus, and Madingley mentioned above. In the *contractive* soils, large *positive* excess pore pressures are generated during pile installation; whereas in the *dilating* soils, *negative* pore pressures are recorded.

| Haga clay | CONTRACTIVE/DILATING | London clay |
|---|---|---|
| $3 \leq \Delta u_i/\sigma'_{vo} \leq 4$ | $\Delta u_i/\sigma'_{vo}$ and $u_i > 0$ | |
| $2 \leq \Delta u_i/\sigma'_{vo} \leq 3$ | $\Delta u_i/\sigma'_{vo}$ and $u_i < 0$ | |
| Boston blue clay | | Gault clay |

In addition to seven tests at Madingley, Coop[4] also performed a (single) instrumented pile test at Canons Park, at a location 20m away from the Imperial College test area (see Figure 5.2 on p189). Although his probes were slow to respond during pile installation (see pp142-143), they generally recorded *negative* pore water pressures ($u_i < 0$) below a depth of 2.5m, at both the leading and following positions (see Figure 4.3 on p142). This is in complete agreement with the results of my own experiments at Canons Park. (Coop's probes failed to notice any change in the soil's response below 5m, owing to their slow response times.)

Indirect evidence to support the Canons Park results comes from the series of piezocone soundings performed by Lunne et al.[5] in the dilating clays at Brent Cross (London clay), Madingley (the Gault), and Cowden (glacial till). *Negative* pore pressures ($u_i < 0$) were recorded at each site by piezocones with porous filters behind the cone shoulder (i.e. the van den Berg and Delft cones), but not by those with filters at the cone tip or face (i.e. the McClelland and Fugro cones).*

---

*At Cowden, the Fugro piezocone recorded negative pore pressures from 2.5 to 12.5m, but positive pore pressures elsewhere; Lunne at al. attributed this response to the presence of stones in the soil

As noted in Section 14.2.1.a, the pore pressures that are measured during undrained penetration are the combination of three separate components: $u_o$, $\Delta u_{ts}$, and $\Delta u_{sh}$ (see p449). The results of the piezocone tests by Lunne at al. indicate that, within a very short distance of the cone tip, the shear-induced pressures - which in dilating clays are *negative* - are much bigger than the (positive) pressures caused by the increase in total stress. In other words, $|\Delta u_{sh}| >> |\Delta u_{ts}|$. This is despite the fact that the total-stress component $\Delta u_{ts}$ is very large beneath the cone tip (and therefore very large just behind the cone shoulder?).

These results corroborate one of the principal conclusions of the instrumented pile tests at Canons Park: that *negative* pore pressures are generated along the shaft during pile installation in high OCR clays.

c) Comparison with theory

As discussed in Chapter 4 (see pp143-145), the cavity expansion method (CEM) fails to predict *negative* pore pressures next to displacement piles installed in high OCR clays. As Figure 14.1 shows, the cavity expansion method predicts excess pore pressure ratios ($\Delta u_i/\sigma'_{vo}$) in excess of seven in clays with OCRs greater than twenty. This is much higher than has been recorded in the Gault and London clays (these being the only high OCR clays for which reliable measurements exist).

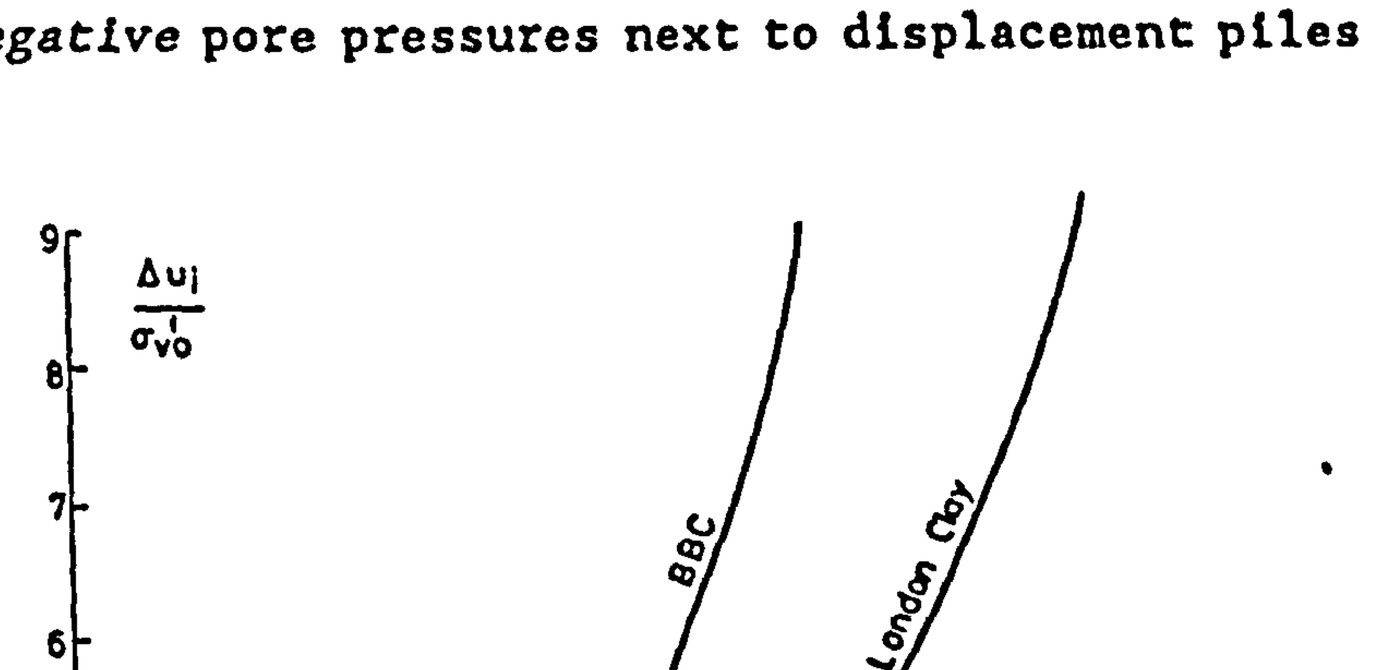



Figure 14.1 Comparison of theoretical and measured values of $\Delta u_i/\sigma'_{vo}$

## 14.2.2 Radial total stresses

### a) Discussion of the Canons Park data

The two outstanding features of the radial total stress measurements at Canons Park are: i) the absolute magnitude of $\sigma_{rr}$; and ii) its strong variation with distance behind the pile tip.

As Figure 9.10 (p316) shows, the radial total stresses at the end of installation are much smaller than the limit pressures measured in self-boring pressuremeter (SBPM) tests. However, they are far higher than the original *in situ* horizontal total stresses ($\sigma_{ho}$) in the soil.

The radial total stresses are also much higher than the stresses measured in low OCR clays. This is demonstrated on Figure 14.2, which plots the normalized horizontal total stress ($H_i$) against OCR, for a wide range of clays. The Canons Park results are given by the square symbols, and lie in the range $2.55 \leq H_i \leq 17.7$ (inside the elongated balloon).

The measurements of $H_i$ from Canons Park vary with distance behind the pile tip, falling from 13-17½ at $z/R \approx 8$ to 2½-5 at $z/R \approx 50$. The precise values of $H_i$ are given in Appendix 11. They are in good agreement with the limited data that is available in other high OCR clays (i.e. Coop's tests in the Gault clay at Madingley, and at Canons Park). They are very different from the

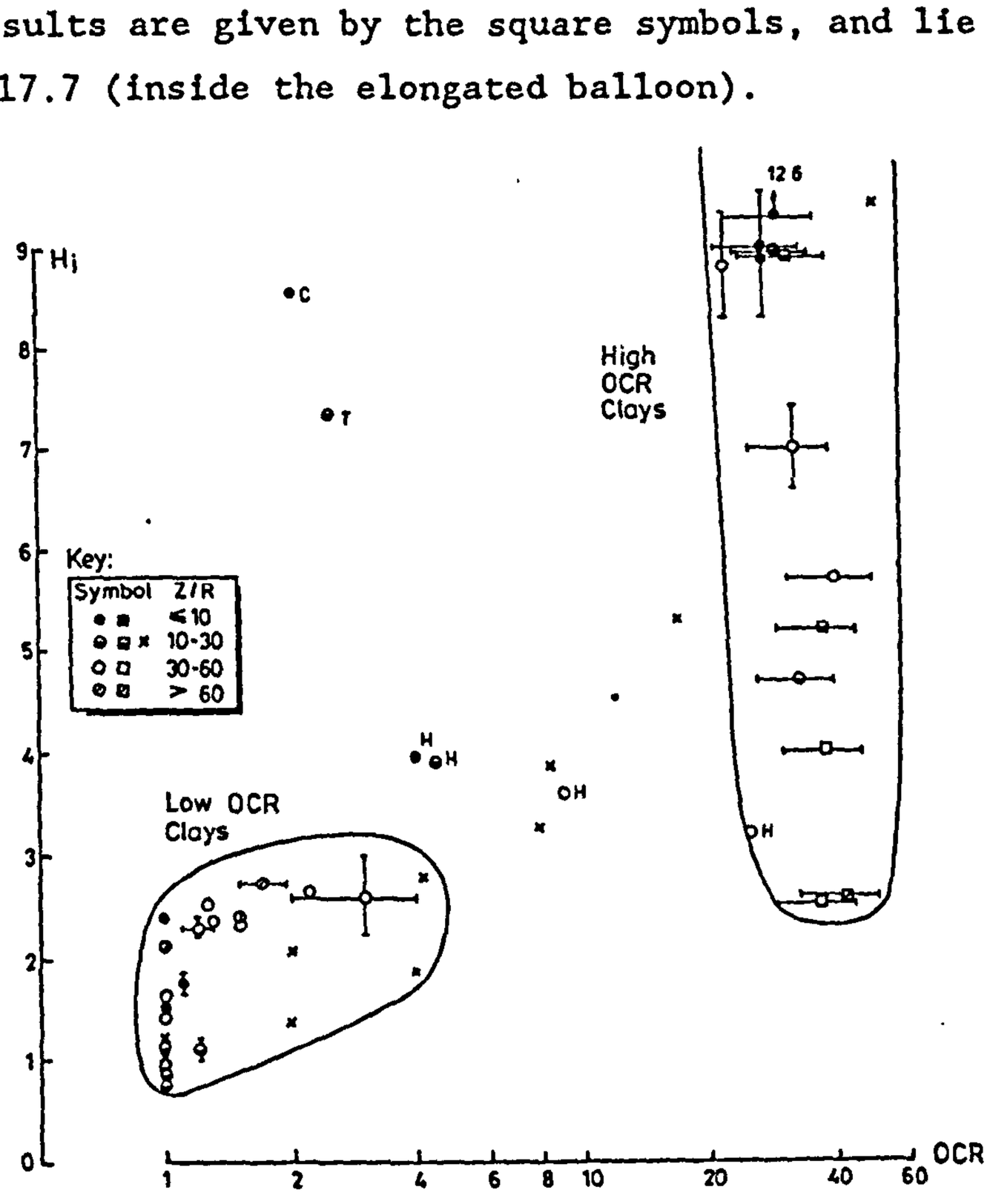



Figure 14.2 Normalized horizontal total stress $H_i$ vs OCR (Canons Park data given by square symbols)

results for the low OCR clays, for which $H_i < 3$ even at $z/R < 10$.

b) The "z/R effect"

One of the key findings of the Canons Park experiments was the discovery of a strong "z/R effect", whereby the radial total stress acting on the pile varies with distance behind the pile tip. In essence, the radial total stress at any particular horizon relaxes once the pile tip has passed through it on its way to full penetration.

The value of $H_i$ at any given horizon depends on the overconsolidation ratio (OCR) at that depth, and on the length of pile that has passed through it (i.e. its distance behind the pile tip, z). Mathematically, this relationship can be written in terms of the non-dimensional variables OCR and z/R (where R is the pile's radius), as follows:

$$H_i = f(OCR,\ z/R)$$

Since OCR varies with depth (and hence with z/R), there is no simple way to determine the relationship between $H_i$ and z/R. One approach is to calculate the *percentage* drop in $\sigma_{rr}$ at specific soil horizons as each instrument passes through them. This is the method adopted in Chapter 9, where $\sigma_{rr}/(\sigma_{rr})_{z/R=10}$ is plotted against z/R for horizons at 2.5, 3.0, 3.5, and 4.0m (see Figures 9.8 and 9.9, pp313-314). The symbol $(\sigma_{rr})_{z/R=10}$ represents the value of $\sigma_{rr}$ at a given soil horizon, when the tip is a distance equal to ten pile radii below it.*

Since for any soil horizon $u_o$, $\sigma'_{vo}$, and OCR are all constant, we can write the parameter $\sigma_{rr}/(\sigma_{rr})_{z/R=10}$ as:

$$\sigma_{rr}/(\sigma_{rr})_{z/R=10} = (H\sigma'_{vo} + u_o)/(H_{z/R=10}\sigma'_{vo} + u_o) \approx H/H_{z/R=10}$$

where the final equality holds since (in the Canons Park experiments) $H\sigma'_{vo} >> u_o$. The parameter $H_{z/R=10}$ represents the value of H at the given

---

*Note that, since the leading instruments on the Imperial College Instrumented Pile are located at $z/R \approx 8$, $(\sigma_{rr})_{z/R=10}$ is interpolated from the readings at the leading and following positions

soil horizon when the pile tip is a distance z/R = 10 below it.

Figure 9.9 (p314) shows the relationship between $\sigma_{rr}/(\sigma_{rr})_{z/R=10}$ and z/R, as determined in Test Series CP2-5. As the diagram implies, $\sigma_{rr}$ (and hence H) reduces in a systematic fashion with increasing z/R, <u>independent</u> of the horizon being considered. It follows that the reduction in $\sigma_{rr}$ is reasonably independent of OCR.

The z/R effect can be identified in the results of instrumented pile tests in other clay soils. For example, a re-analysis of Johnston's experiments[6] in the London clay at Southampton University reveals a

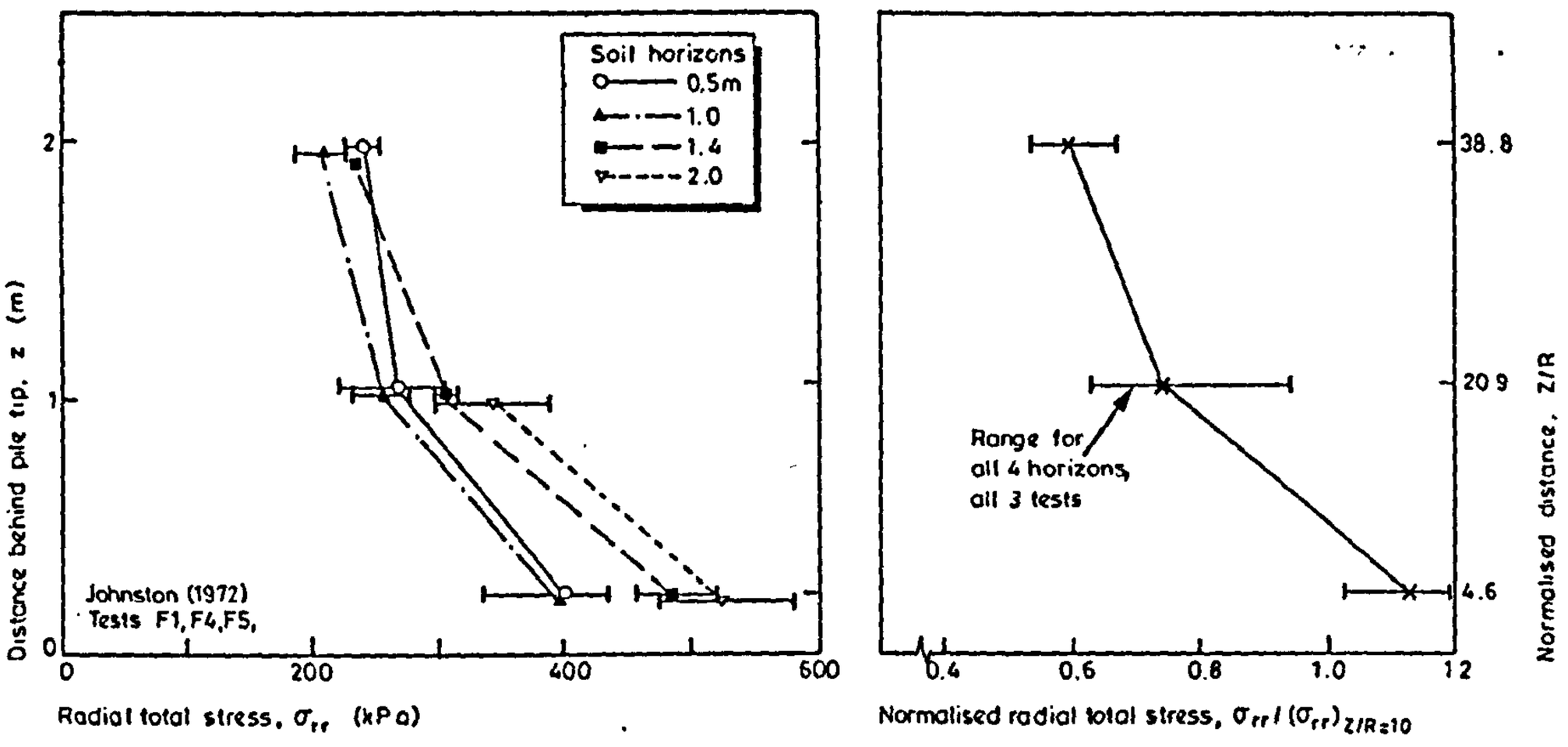



Figure 14.3 The z/R effect, as measured in Johnston's tests

similar relationship between $\sigma_{rr}/(\sigma_{rr})_{z/R=10}$ and z/R to that obtained at Canons Park. This is apparent if Figure 14.3 (in this chapter) is compared with Figure 9.9 (on p314). Quantitatively, the two sets of readings agree remarkably well (the spread of the readings helps to ensure that).

The z/R effect is not limited to high OCR clays. The radial total stresses measured by Kenney[7] in the quick Oslo clay (OCR ≈ 1) also show a significant reduction with increasing distance behind the pile tip. The drop in $\sigma_{rr}$ from z/R = 7.5 to z/R = 27 is about 60%.

c) Comparison with selected test cases

The radial total stresses recorded at Haga, Saugus, and Madingley are summarized in the following boxes. The normalized horizontal total stress ($H_i$) in the *contractive* clays is between two and four, whereas in the *dilating* clays it is generally very much larger. The z/R effect is also far more significant (in absolute terms) in the dilating clays.

| Haga clay | CONTRACTIVE/DILATING | | London clay | | |
|---|---|---|---|---|---|
| $H_i$ = 3.2 | @ z/R ≈ 61 | (OCR ≈ 25) | $H_i$ ≈ 2½ | @ z/R = 61 | (OCR ≈ 42) |
| $H_i$ = 3.6 | @ z/R ≈ 43 | (OCR ≈ 9) | $H_i$ = 2½-5 | @ z/R ≈ 50 | (OCR ≈ 37) |
| $H_i$ = 3.9 | @ z/R ≈ 23 | (OCR ≈ 4½) | $H_i$ = 8-13 | @ z/R ≈ 25 | (OCR ≈ 30) |
| $H_i$ = 4.0 | @ z/R ≈ 5 | (OCR ≈ 4) | $H_i$ = 13-18 | @ z/R ≈ 8 | (OCR ≈ 25) |
| $H_i$ = 2-3 | @ z/R = 50 | (OCR = 2-4) | $H_i$ ≈ 9 | @ z/R = 22 | (OCR ≈ 22) |
| $H_i$ ≈ 2.3 | @ z/R = 50 | (OCR = 1.2) | $H_i$ ≈ 9 | @ z/R = 5 | (OCR ≈ 27) |
| Boston blue clay | | | Gault clay | | |

d) Comparison with theory

Values of $H_i$ for high OCR clays are compared on Figure 14.4 with theoretical predictions based on the cavity expansion method (CEM/MCC). The curve labelled "London clay" is in reasonable agreement with the radial total stresses recorded by the *leading* instruments at Canons Park, but overestimates the stresses at the *following* and *trailing* positions (by a very large margin). The agreement with the stresses recorded by

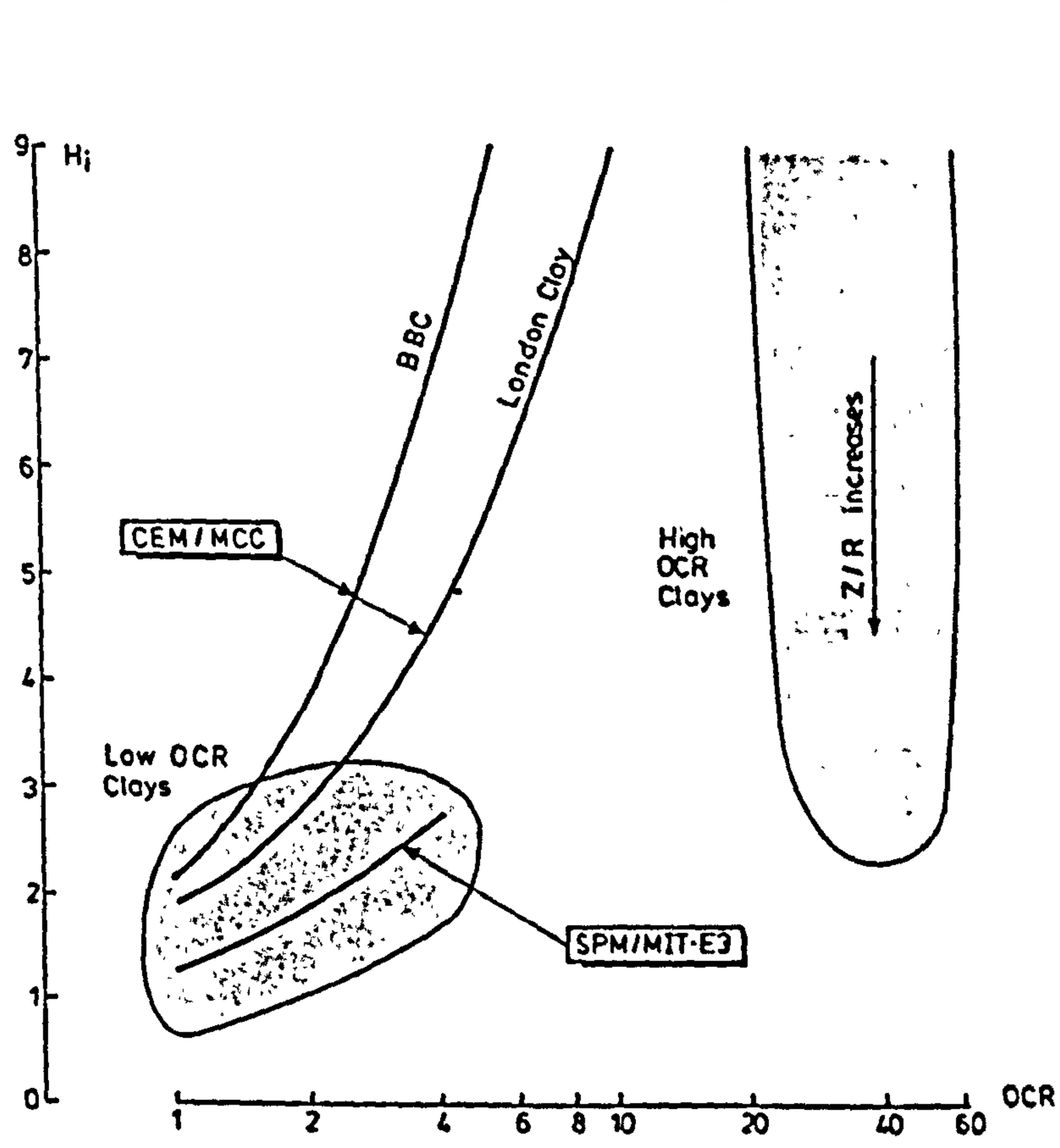



Figure 14.4 Comparison of theoretical and measured values of $H_i$

the leading instruments* is purely coincidental, since the cavity expansion method is supposed to apply only at positions that are far from the ends of the pile.

Another test of the cavity expansion hypothesis is to compare the experimental results with the limit pressures ($p_{lim}$) determined from self-boring pressuremeter tests. According to this hypothesis, $(\sigma_{rr})_i$ should equal $p_{lim}$. As Figure 9.10 shows (see p316), this is <u>not</u> true for the London clay at Canons Park.

Finally, one of the most important conclusions from the radial total stress data is that pile installation is not a *one*-dimensional process (as assumed in the cavity expansion method), but is *two*-dimensional (as assumed in the strain path method).

### <u>14.2.3 Radial effective stresses</u>

a) Discussion of the Canons Park data

The radial effective stresses acting on the pile ($\sigma'_{rr}$) are calculated from the radial total stresses ($\sigma_{rr}$) and pore pressures (u) measured in each instrument cluster ($\sigma'_{rr} = \sigma_{rr} - u$). The uncertainty in the magnitude of the suction in the soil (see Appendix 11) means that the effective stresses <u>during installation</u> are not reliably known. Since the suction is probably under-registered, then so too is the radial effective stress ($\sigma'_{rr} = \sigma_{rr} - u = \sigma_{rr} + p_k$, where $p_k$ is the suction).

If we take the pore pressure readings at face value, then the lateral stress coefficient ($K_i = \sigma'_{rr}/\sigma'_{vo}$) is slightly bigger than the normalized horizontal total stress (since $u_i < 0$ and $K_i = H_i - \Delta u_i/\sigma'_{vo}$).

Figure 14.5 compares the results of the Canons Park experiments with those from tests in other clay soils. The Canons Park data is given by the square symbols, and lies in the range $3.5 \leq K_i \leq 17.8$ (inside the

---

*$H_i$ (predicted) is ≈20 for OCR = 32 (see Tables 3.3 and 3.4, pp88 & 92); the measurements at z/R ≈ 8 were between 13.3 and 17.7 (for OCR ≈ 25)

balloon marked "high OCR clays"). Precise values of $K_i$ for Canons Park are given in Appendix 11.

As Figure 14.5 indicates, the lateral stress coefficient in the high OCR clays is very much higher than the value of $K_i$ in the low OCR soils. $K_i$ is also greater than $K_0$, in the high OCR clays (at Canons Park, $K_0 \approx$ 2-2.5).

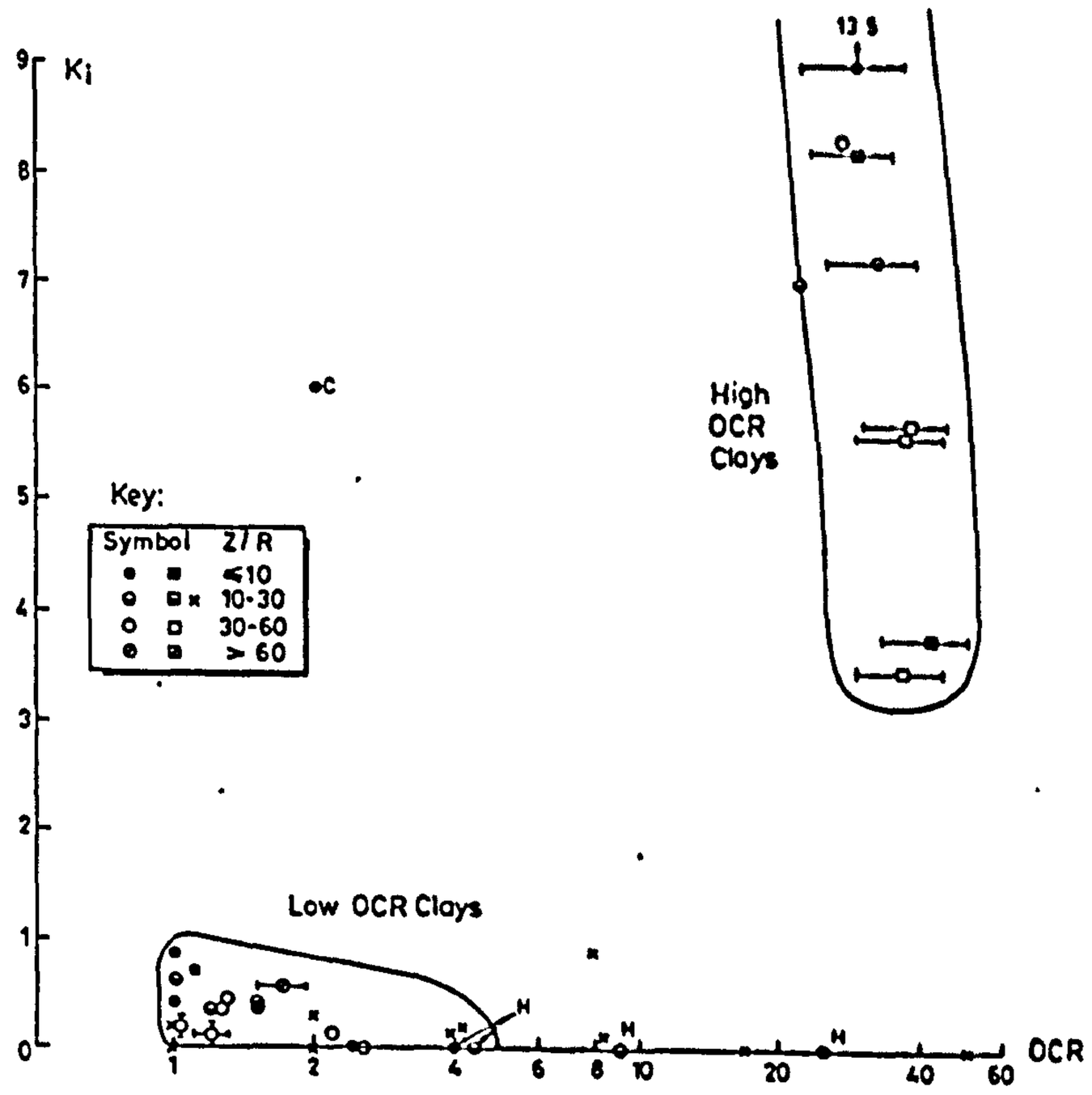



Figure 14.5 Lateral stress coefficient $K_i$ vs OCR (Canons Park data given by square symbols)

The z/R effect (see Section 14.2.2.b, [illegible]) is clearly evident in the readings of $(\sigma'_{rr})_i$ at Canons Park. This is not surprising, since $K_i$ and $H_i$ are almost equal. ($K_i \neq H_i$ in low OCR clays, since $\Delta u_i/\sigma'_{vo} > 0$: note from Figure 14.5 that the z/R effect is not so readily apparent in these soils.)

b) Comparison with selected test cases

The Canons Park data is compared in the following boxes with the results from the selected test cases at Haga, Saugus, and Madingley.

The behaviour of the two stiff clays is clearly very different to that of the softer soils. In the *contractive* clays the radial effective stress is virtually zero during pile installation; whereas in the *dilating* clays $K_i$ is very large.

| Haga clay | CONTRACTIVE/DILATING | | | London clay |
|---|---|---|---|---|
| $K_i \approx 0$ (all z/Rs) | $K_i \approx 4$ | @ z/R = 61 | (OCR ≈ 42) | |
| | $K_i$ = 3½-6 | @ z/R ≈ 50 | (OCR ≈ 37) | |
| | $K_i$ = 10-15 | @ z/R ≈ 25 | (OCR ≈ 30) | |
| | $K_i$ = 11-18 | @ z/R ≈ 8 | (OCR ≈ 25) | |
| $K_i$ = 0.05-0.20 (z/R = 50) | $K_i \approx 7$ | @ z/R = 22 | (OCR ≈ 22) | |
| | $K_i \approx 8$ | @ z/R = 5 | (OCR ≈ 27) | |
| Boston blue clay | | | | Gault clay |

c) Comparison with theory

Values of $K_i$ for the London and Gault clays are compared with cavity expansion predictions for $K_i$ on Figure 14.6. The method over-estimates the radial effective stresses in these high OCR clays, particularly as z/R increases. Once again, the experimental data demonstrates the <u>two</u>-dimensional nature of pile installation.

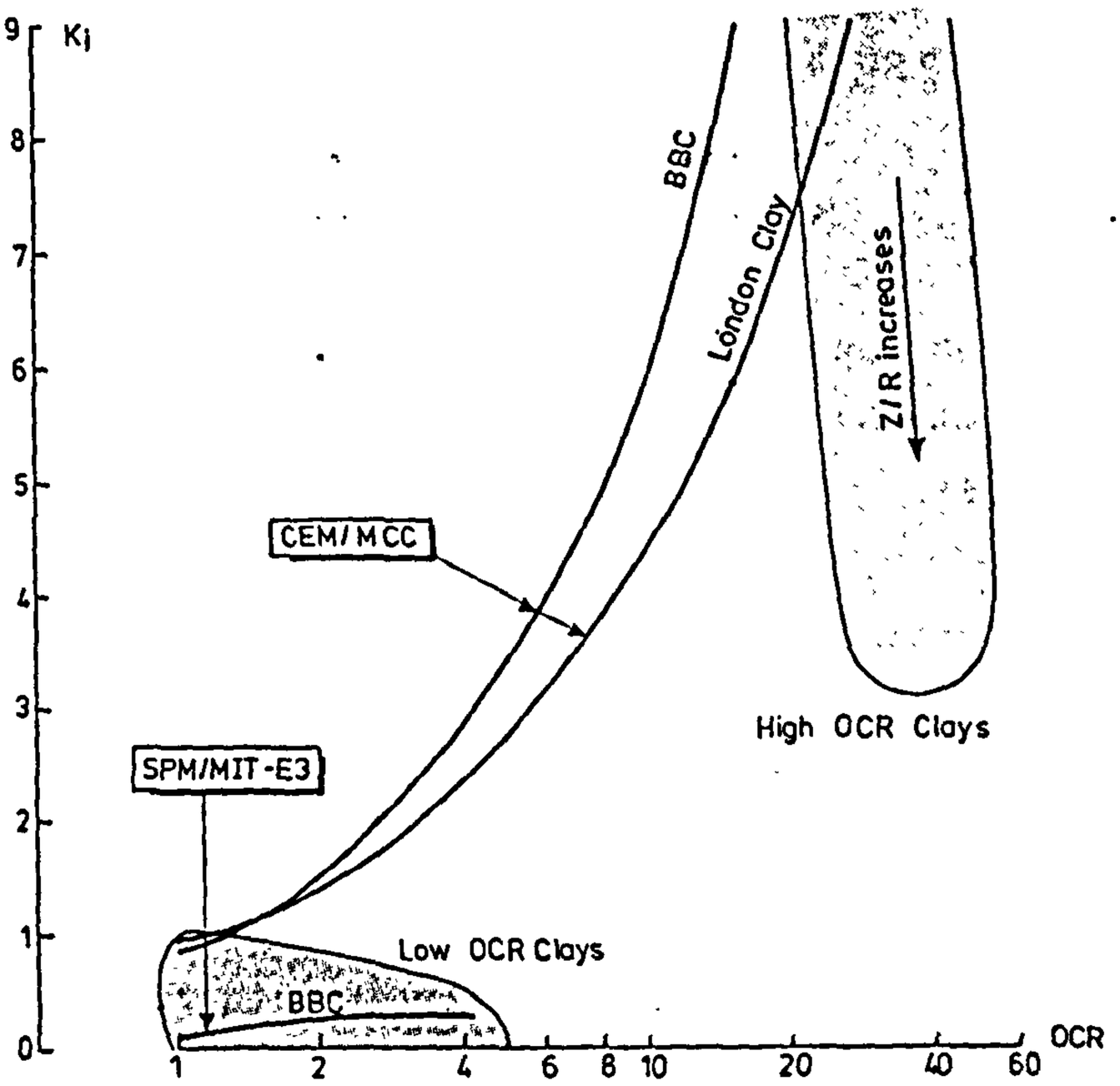



Figure 14.6 Comparison of measured and theoretical values of $K_i$

## 14.2.4 Coefficients of friction

a) Rate-effects during pile installation

The experiments at Canons Park reveal important differences between the frictional characteristics of fast- and slow-jacked piles,* both during installation and in subsequent (static) loading tests.

*These terms are defined on p281

Figure 14.7 illustrates the remarkable jump in shearing resistance that was discovered in the experiments at Canons Park. The average shear stress on the pile (as represented by the alpha and beta factors) rises

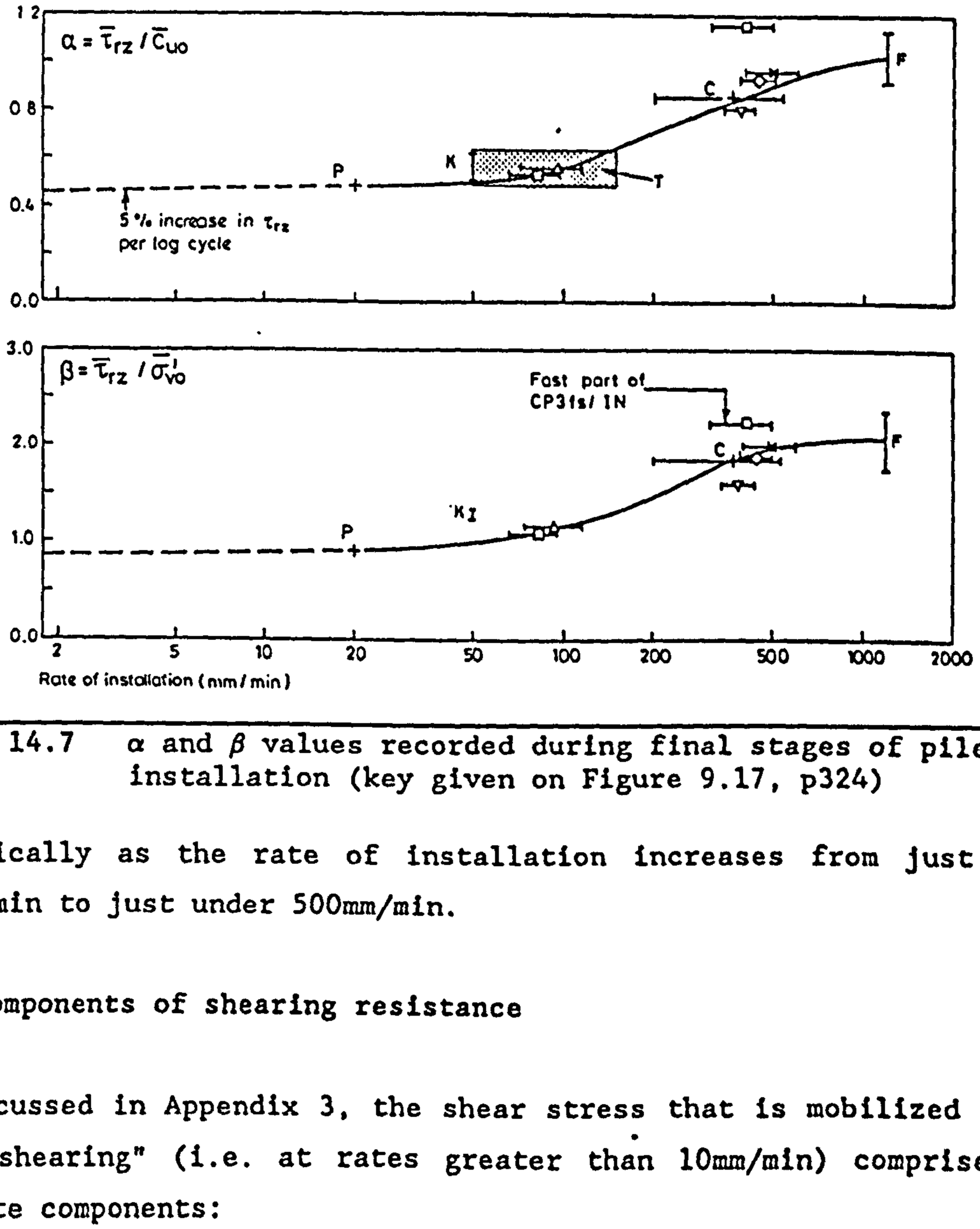



Figure 14.7 $\alpha$ and $\beta$ values recorded during final stages of pile installation (key given on Figure 9.17, p324)

dramatically as the rate of installation increases from just under 100mm/min to just under 500mm/min.

b) Components of shearing resistance

As discussed in Appendix 3, the shear stress that is mobilized during "fast shearing" (i.e. at rates greater than 10mm/min) comprises two separate components:

- A *viscous* (i.e. velocity-dependent) component
- A *frictional* (i.e. fabric-controlled) component

The <u>viscous</u> component ($r_{viscous}$) is present during pile installation and dynamic loading, but is absent during slow - a.k.a. "static" - loading (i.e. at velocities below 1mm/min). Although it depends on the velocity of shearing, the viscous element may or may not be related to the radial

effective stress that acts on the pile.

The <u>frictional</u> component ($\tau_{friction}$) is governed by the re-orientation of the soil's fabric during pile installation (see Chapter 12), and depends strongly on whether the pile was slow-jacked, fast-jacked, or driven. Although, in the past, it has been assumed that the frictional resistance is directly proportional to the radial effective stress acting on the pile ($\tau_{friction} \propto \sigma'_{rr}$), the experiments at Canons Park are the first ones that <u>prove</u> this assumption conclusively (see Figures 11.15 and 11.16, pp380 & 382).

The viscous component of shearing can be estimated from the results of ring-shear tests at fast and slow rates of displacement (see Figure 5.14 on p213). The peak stress ratio measured at fast rates, $(\tau/\sigma_n)_{fp}$, combines both the viscous and the frictional components of resistance; whereas the peak ratio measured in <u>slow</u>-loading tests *on soil that had previously been sheared at a fast rate*, $(\tau/\sigma_n)_{sp}$, contains the frictional element <u>alone</u>. (See pp210-213 for further explanation of these terms.) For London clay sheared *initially* at 500mm/min, $(\tau/\sigma_n)_{fp}$ is about 0.35 and $(\tau/\sigma_n)_{sp}$ about 0.23 (for $\sigma_n$ = 250-530kPa).

Subtracting $(\tau/\sigma_n)_{sp}$ from $(\tau/\sigma_n)_{fp}$ provides a rough estimate of the viscous component of resistance. In this case, the difference is ≈0.12. This *over*-estimates the value of $\tau_{viscous}/\sigma'_n$, since the London clay generates *negative* pore pressures when sheared at fast rates, and so $\sigma_n < \sigma'_n$.

By writing the shear stress $\tau_{rz}$ as $\tau_{viscous} + \tau_{friction}$, and normalizing by the radial effective stress acting on the pile, we get:

$$\tau_{rz}/\sigma'_{rr} = \tau_{viscous}/\sigma'_{rr} + \tau_{friction}/\sigma'_{rr} = \tau_{viscous}/\sigma'_{rr} + \mu$$

where $\mu$ is the *coefficient of friction*.

The remainder of this discussion concentrates on the frictional resistance (i.e. $\mu$), as measured during pile installation. Section 14.4.4 discusses the values of $\mu$ recorded during slow loading tests.

### c) Discussion of the Canons Park data

Figure 14.8 shows the values of the coefficient of friction ($\mu$) that were recorded by the *leading* instruments during installation of the fast-jacked piles CP2f, CP4f, and CP5f. $\mu$ has been calculated from:

$$\mu = \tau_{rz}/(\sigma_{rr} - u)$$

where $\tau_{rz}$ is the shear stress; $\sigma_{rr}$ the radial total stress; and u the pore water pressure measured at the pile wall. This equation ignores the viscous component of shearing resistance, and therefore *over*-estimates the true value of $\mu$. (There is a further error in $\mu$ because the pore water suction is under-registered during installation - see Appendix 11.)

The repeatability of the results is quite remarkable, given that the coefficient of friction is calculated from three <u>independent</u> measurements ($\tau_{rz}$, $\sigma_{rr}$, and u).

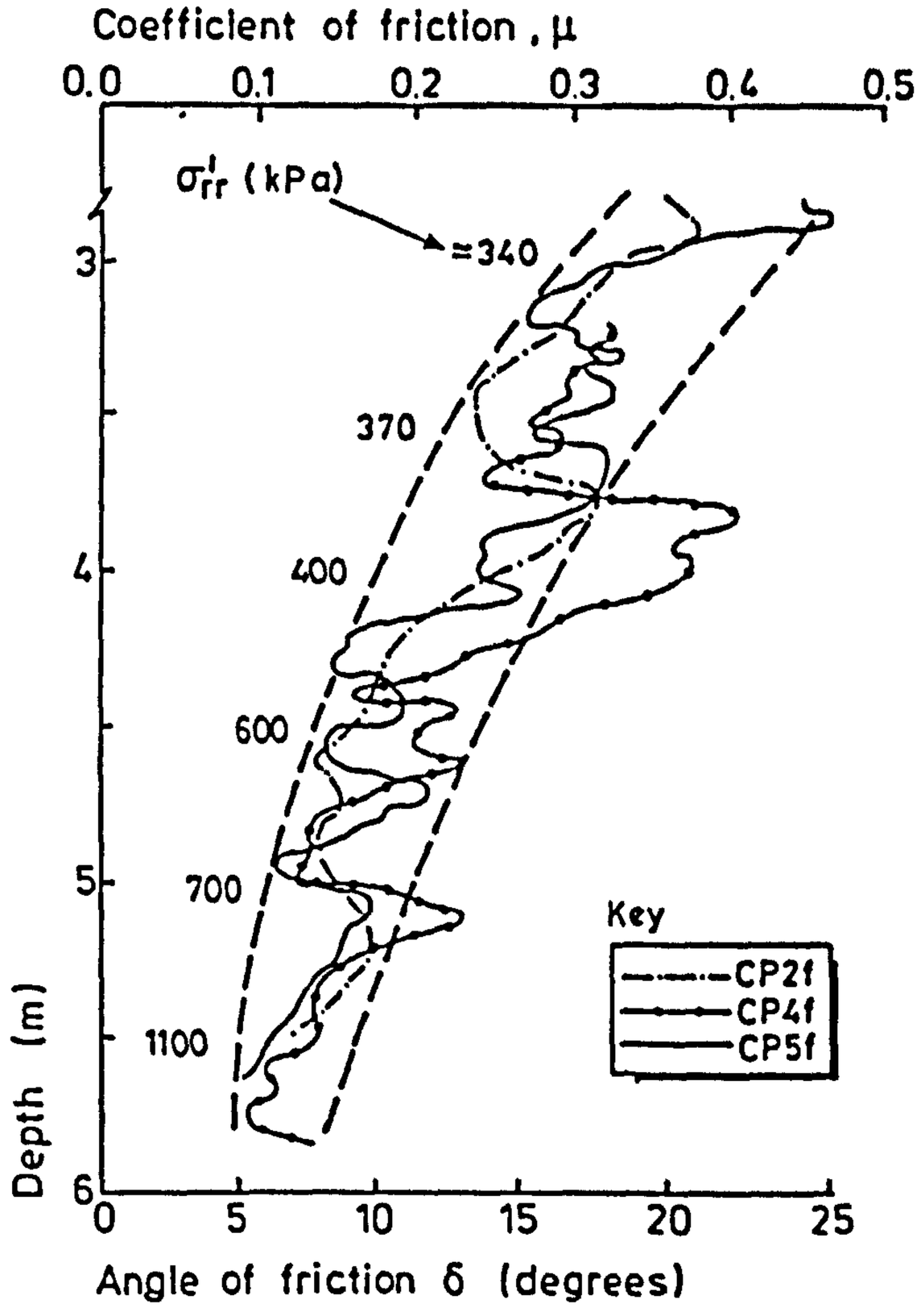



Figure 14.8 Profile of $\mu$ during pile installation: leading instruments (CP2f, 4f, & 5f)

As Figure 14.8 shows, the *angle* of friction ($\delta = \tan^{-1}\mu$) reduces from 16½-23° at 3m, to 5-9° at 5.5m.* This means that, in the undisturbed clay (below 4.1m), the angle of friction is close to <u>or below</u> the slow residual angle of the soil ($\phi_R$ = 10-11½°).

*Note that Coop obtained $\delta$ = 9-13° over the depths 2½-4½m, with a pile jacked at 200mm/min - see Figure 4.3 on p142

The angle of friction is also below that recorded in the subsequent static load tests on the fast-jacked piles. For example, in CP5f/L1T the coefficient of friction $\mu$ was 0.22 ($\delta$ = 12.4°), as opposed to $\mu$ = 0.075 ($\delta$ = 4.3°) during installation.

The reduction in $\mu$ with depth can be explained in part by the corresponding increase in radial effective stress ($\sigma'_{rr}$). As indicated on Figure 14.8, $\sigma'_{rr}$ rises from about 400kPa at 4m, to 1100kPa at 5.5m. Experiments in the ring-shear apparatus[8] have shown that $\phi_R$ drops from ≈11½° at a normal stress $\sigma_n$ = 248kPa, to 10° at $\sigma_n$ = 490kPa. Extrapolating this trend suggests that $\delta$ is less than 9° at $\sigma_n$ = 1000kPa. This is still far higher than the measured coefficients below 5.5m. Regrettably, I have no satisfactory explanation for these very low values of $\mu$ - especially since the coefficient of friction is probably *over*-estimated.

The coefficients of friction recorded at leading instrument positions, during installation of the slow-jacked pile CP3fs, were in the range 0.074 to 0.109 ($\delta$ = 4.2-5.6°) at 5.5m.

d) Comparison with other data

Interestingly, Coop and Wroth report values of $\mu$, from tests in the normally consolidated clay at Huntspill, that are "very much lower than measured in the Bromhead ring shear apparatus".[9] For tests at Madingley they quote $\mu$s which are typically between 0.13 and 0.21 (i.e. $\delta$ = 7½-12°), with an average $\mu$ of 0.16 ($\delta \approx 9°$). However, at some depths $\delta$ falls to as little as 5.3°. At both sites the pile was jacked at ≈200mm/min.

In addition, Butterfield and Johnston argued that although they did not record the pore pressures next to their instrumented pile:

> "The simultaneous measurement of shear and radial stress allows an effective interface friction angle ($\delta$) to be assessed and from some 200 values obtained 46% of them fall within the range $\delta$ = 10° ±2°."[10]

As at Canons Park, the angle of friction was lower near the pile tip than elsewhere along the shaft: at z/R = 4.6, $\delta$ = 8.3 ±2.3° (97 readings).

## 14.3 EARTH AND PORE PRESSURE EQUALIZATION

### 14.3.1 Pore pressure dissipation

**a) Discussion of the Canons Park data**

The excess pore pressures that were generated during pile installation at Canons Park took about thirty-six hours to dissipate. During this time, the readings followed one of two basic patterns, as shown on Figure 10.2 (see p335).

At *leading* instrument positions the pore pressures rise to very high values, implying that large *positive* pressures exist in the soil at the end of installation, but at points that are distant from the pile shaft. Since the rise times are so short, the positive pore pressures can only be a few millimetres away. A simple calculation[11] shows that this distance is between 25 and 50mm. Since the pile tip is 266mm away (i.e. five to ten times further), it seems most unlikely that the rise in pore pressure at the leading probes is caused by *vertical* flow of water up the pile shaft. It seems probable that the bulb of high pressure surrounding the pile tip extends some distance behind it, and this may be the source of high (positive) pressure that flows *radially* towards the pile. Evidence presented by Coop and Wroth[12] also supports the conclusion that the water does not flow vertically.

The pore pressure response at *following* and *trailing* positions is entirely different to that described above. As Figure 10.2 (p335) shows, the excess pore pressure ratio ($\Delta u/\sigma'_{vo}$) is *negative* at the start of the equalization period, and remains negative for a long time thereafter. *Positive* excess pore pressures are not recorded until at least 1¼h ($5 \times 10^3$s) into the equalization period, and in some cases not even after thirty hours ($10^5$s) have elapsed.

The pore pressure readings during installation and equalization, and the filter-paper measurements of soil suction (see Chapter 13, pp418-421), allow us to explain these observations in terms of the response of three

distinct zones of soil surrounding the pile:

- In the *inner* zone (which is a few millimetres thick at most), negative pressures are generated during pile installation through strong dilation of the clay (in the notation of Section 14.2.1.a, $|\Delta u_{sh}| >> |\Delta u_{ts}|$); the inner zone corresponds to the region next to the pile wall where the shearing of the clay is most intense
- In the *middle* zone (which extends to a normalized radius $r/R \approx 4$, and where the dilation is weaker), the <u>positive</u> pore pressures caused by the increase in mean total stress overwhelm any shear-induced pore pressures ($|\Delta u_{ts}| >> |\Delta u_{sh}|$)
- In the *outer* zone ($r/R > 4$), pile installation has a relatively minor effect on the ground; small (positive) excess pore pressures are generated, which die out rapidly with increasing distance from the pile wall

The differences between the behaviour at leading and following positions can be explained by the relative sizes of the *inner* and *middle* zones, and by the magnitude of the (positive or negative) pore pressures that are generated in each one. Consider the leading positions first:

- The *inner* zone must be small since the pore pressure rise times are small (see p465 and note[11])
- Very large (positive) pressures are generated in the *middle* zone, which leads to large positive pore pressures being recorded by the leading probes some time after the pile ceases penetration

At the *following* and *trailing* positions:

- Since the rise times are extremely long, either the *inner* zone is large,* or the positive pressures generated in the *middle* zone ($|\Delta u_{ts}|$) are relatively small

---

*A similar calculation to that given in note 11 implies that the inner zone could extend to r/R = 10-30

- The observation that the radial total stress at any given horizon relaxes with continued penetration of the pile (the "z/R effect") supports the hypothesis that - in the *middle* zone at least - $|\Delta u_{ts}|$ is far lower at the following and trailing positions than at leading ones

b) Comparison with selected test cases

The pore pressure readings from the three "test" cases listed on p447 and from Canons Park are summarized below. Once again, the response of the ground appears to hinge on whether the clay *contracts* when sheared or *dilates*. (The time factor $T_1$ has been calculated using the formula $T_1 = c_h t/R^2$, with $c_h$ assumed equal to $1mm^2/s$ - see pp32-34.)

| Haga clay | CONTRACTIVE/DILATING | London clay |
|---|---|---|
| Pressures decay monotonically<br>Equalization in 7 days<br>$T_1 \approx 100$ | | Pressures rise and fall<br>Equalization in ≈ 36h<br>$T_1 \approx 50$ |
| Pressures decay monotonically<br>Equalization in ≈ 28h<br>$T_1 \approx 250$ | | Pressures rise and fall<br>Equalization in ≈ 11½ days<br>$T_1 \approx 600$ |
| Boston blue clay | | Gault clay |

c) Comparison with theory

There is currently no theory of pile behaviour that predicts the rise and fall in pore pressures that were recorded at Canons Park. However, it is still possible to draw some (tentative) conclusions from the experimental results, by comparing them with pore pressure decay curves derived from a simplified study of the dissipation process. This allows us to obtain a provisional estimate for the shape and size of the pore pressure field at the end of pile installation.

The dissipation of pore pressure next to the pile wall is controlled to a large extent by the pore pressure isochrone at the end of installation. This is illustrated by the dissipation curves shown on Figure 14.9. The full lines are based on a "constant" initial isochrone, which extends to a normalized radius $\lambda$ (see the inset diagram on Figure 14.9); whereas the

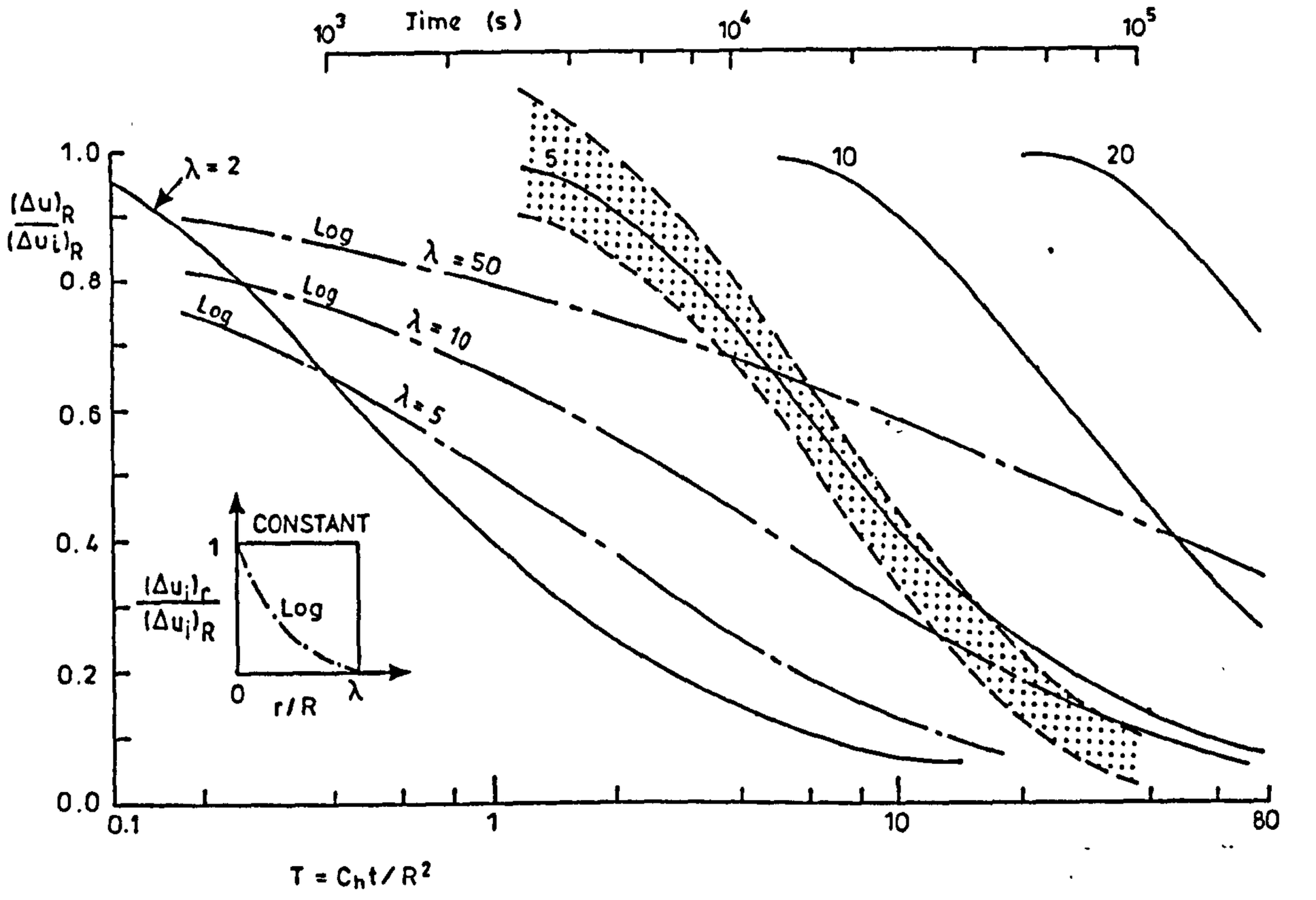



Figure 14.9 Comparison between observed pore pressure decay and simple theoretical decay curves

broken-lines (marked "Log") are based on a "logarithmic" isochrone. These curves were derived by Levadoux[13] using <u>linear</u> consolidation theory (see Chapter 3). The functions $f(r/R) = (\Delta u_i)_r/(\Delta u_i)_R$ that define the initial isochrones are given in a note[14] at the end of the chapter.

As the inset diagram shows, the parameter $\lambda$ represents the *size* of the pore pressure field at the start of equalization; whereas the function $f(r/R)$ represents its *shape*. The curves derived from the constant isochrone represent $\lambda = 2$, 5, 10, and 20; whereas the "Log" curves are for $\lambda = 5$, 10, and 50. (Changing the value of $\lambda$ merely shifts the curves to left or right, without rotating them.)

The shaded band on Figure 14.9 represents the pore pressures that were recorded by the *leading* probes in Test Series CP2-5. The data is taken from Figure 10.2 (on p335). The time factors for these experiments have been calculated on the assumption that $c_h = 1mm^2/s$ (which is reasonable for London clay - see Chapter 2, pp32-34, and Chapter 10, pp336-337).

In plotting the experimental data, I have ignored the rise in pore

pressure that was observed over the first ≈2500s (see Figure 10.2). In other words, Figure 14.9 shows the <u>fall</u> in pore pressure from its *maximum* value ($\Delta u_{max} \approx 5.0\sigma'_{vo}$, according to Figure 10.2). To allow direct comparison with the theoretical curves, the experimental data has been plotted as $(\Delta u)_R/(\Delta u_{max})_R$ [note that the theoretical curves are shown in terms of $(\Delta u)_R/(\Delta u_i)_R$, where $(\Delta u_i)_R$ is simultaneously the initial and the maximum pore pressure at the pile wall].

Several conclusions can be drawn from Figure 14.9:

- Looking first at the <u>shape</u> of the curves, we see that the *constant* initial isochrone gives a much better match to the observed decay of pore pressures than the *logarithmic* isochrone
- Looking next at the <u>position</u> of the curves, we see that the experimental data falls closest to the curve based on the *constant* initial isochrone with $\lambda = 5$ (assuming, of course, that $c_h = 1mm^2/s$)
- Reducing $\lambda$ from fifty to five shifts the *logarithmic* curve well away from the experimental data - <u>unless</u> $c_h$ is simultaneously reduced to 0.02-0.1$mm^2/s$ (in which case the curve would hardly move); *neither* $\lambda = 50$ nor $c_h \leq 0.1mm^2/s$ are realistic values for the experiments at *Canons Park (see below)*

The *logarithmic* distribution of pore pressures clearly does not match the experimental data from Canons Park, whereas the *constant* (i.e. "square") distribution reproduces the essential features of the observed pore pressure decay. The cavity expansion method predicts initial isochrones which are logarithmic in shape, whereas the strain path method predicts isochrones that are basically "square" (see Chapter 3, pp84-88, and especially Figure 3.8).

Evidence to support the conclusion that $\lambda \approx 5$ is provided by the measurements of soil suction described in Chapter 13 (see pp418-421). When the excess pore pressures that are generated during pile installation dissipate, the mean effective stress in the soil (p') inevitably changes. As Figure 13.8 (p420) shows, beyond $r/R \approx 4$, the mean effective stress at the end of equalization ($p'_c$) is unchanged from its

original (i.e. the far-field) value* ($p'_o$). This implies that any excess pore pressures that are generated during pile installation must be negligible in the soil beyond r/R ≈ 4.

Figure 13.8 also implies that the mean effective stress at the end of equalization varies with the *logarithm* of r/R. Note that this is not necessarily incompatible with an initial pore pressure isochrone that is square in shape.

### 14.3.2 Relaxation of radial total stress

a) Discussion of the Canons Park data

The radial total stresses follow one of two basic patterns, as shown on Figure 10.4 (p340). At *leading* and *following* positions (i.e. below 4m), the normalized horizontal total stress H falls very rapidly over the first 24h following pile installation, but stabilizes five days into the equalization period. However, at the *trailing* positions (above 4m), H rises from its end-of-installation value (by almost 50% in one case), before stabilizing on or around the fifth day.

Table 14.2 $H_c/H_i$ and $K_i/K_c$ as recorded in Tests CP2-5

| Instrument position | z/R | $H_c/H_i$ | $K_i/K_c$ |
|---|---|---|---|
| Lagging | 61 | 1.76 | 0.82 |
| Trailing | ≈51 | 1.04-1.46 | 0.87-1.04 |
| Following | ≈26 | 0.74-0.82 | 1.39-1.53 |
| Leading | ≈ 8 | 0.72-0.83 | 1.03-1.39 |

The values of the "relaxation coefficient" ($H_c/H_i$) that were recorded in the Canons Park experiments are summarized in Table 14.2.

b) Comparison with selected test cases

The Canons Park data is compared in the following boxes with the results from the three "test" cases listed on page 447.

---

*Note that $p'_c/p'_o = p_k/[p_k]_{ff}$ and $p_k/[p_k]_{ff} = 1$ for r/R > ≈4

| Haga clay | CONTRACTIVE/DILATING | London clay |
|---|---|---|
| $H_c/H_i$ = 0.29-0.34 (for all z/Rs) | | $H_c/H_i$ = 1.04-1.76 for z/R > 50<br>$H_c/H_i$ = 0.72-0.83 for z/R < 30 |
| $H_c/H_i$ = 0.26-0.35 (for z/R = 50) | | $H_c/H_i$ = 0.69-0.76 for z/R < 30 |
| Boston blue clay | | Gault clay |

c) Comparison with theory

The values of the relaxation coefficient $H_c/H_i$ from the Canons Park experiments (see Table 14.2) can be compared with the cavity expansion predictions given in Chapter 3 (see Table 3.7 on p105).

The cavity expansion method predicts $H_c/H_i$ = 0.87 ±0.03 for London clay, regardless of overconsolidation ratio (based on Modified Cam Clay). Hence the method fails to predict the *increase* in radial total stress that was observed far behind the pile tip (at z/Rs greater than fifty). The agreement between the theoretical predictions and the values of $H_c/H_i$ that were measured at the leading and following instrument positions is purely coincidental, since the cavity expansion method is supposed to apply only for positions far from the ends of the pile.

## 14.3.3 Changes in radial effective stress

a) Discussion of Canons Park data

The variation in radial effective stress during Test Series CP5f is shown on Figure 14.10. In general the radial effective stress decreases during equalization, which explains why the pile's overall load capacity decreases with time - as demonstrated in Figure 11.3 (p361).

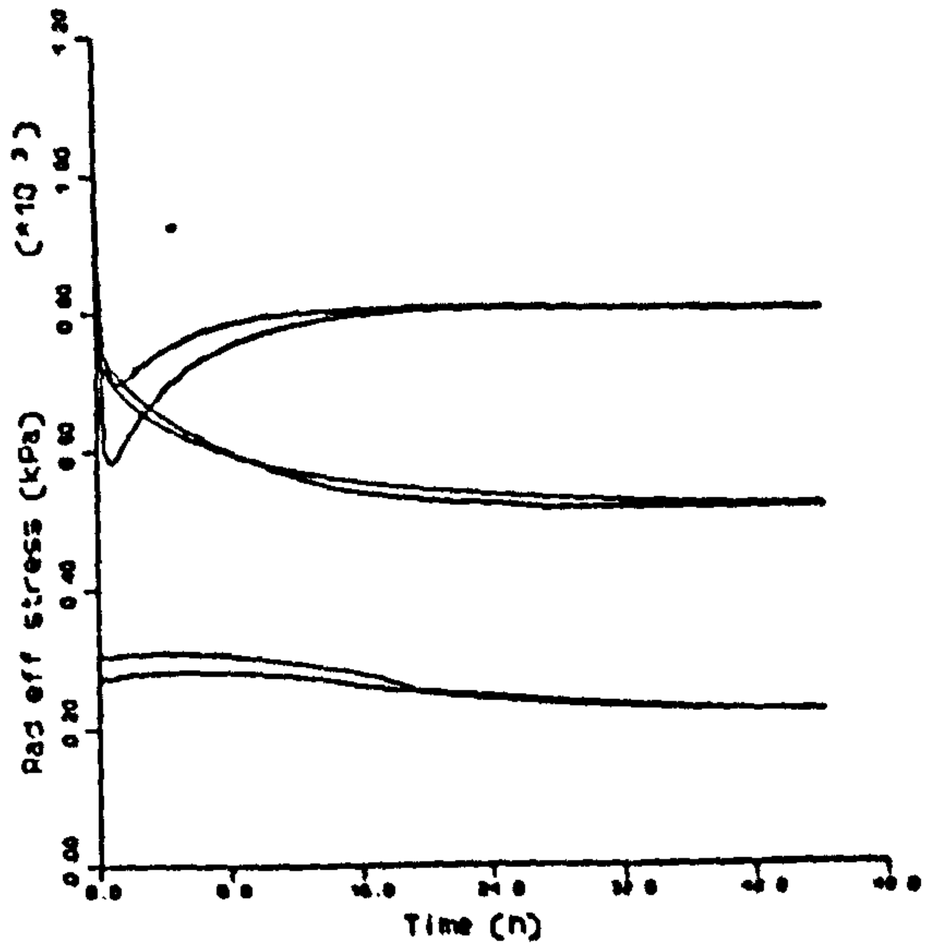



Figure 14.10 Changes in $\sigma'_{rr}$ during CP5f/EQ

Short-term minima in $\sigma'_{rr}$ (like the one recorded by the *leading* instruments) have been observed in

instrumented pile tests in other clay soils, namely the quick clay at Oslo[15] and the Gault at Madingley.[16]

The "set-up coefficients" ($K_i/K_c$) for the Canons Park experiments are listed in Table 14.2.

b) Comparison with selected test cases

The variations in radial effective stress are compared with the data from Haga, Saugus, and Madingley below. Once again, the soil's behaviour depends primarily on whether it is a *contractive* or a *dilating* material.

| Haga clay | CONTRACTIVE/DILATING | London clay |
|---|---|---|
| $K_i/K_c$ = 0.15-0.71 (for all z/Rs) | | $K_i/K_c$ = 0.82-1.04 for z/R > 50<br>$K_i/K_c$ = 1.03-1.53 for z/R < 30 |
| $K_i/K_c$ = 0.08-0.33 (for z/R = 50) | | $K_i/K_c$ = 1.04-1.36 for z/R < 30 |
| Boston blue clay | | Gault clay |

The decrease in radial effective stress during equalization helps to explain the *negative* set-up reported by Tomlinson[17] in load tests on driven and jacked piles installed in London clay at Stanmore.

c) Comparison with theory

The set-up coefficients ($K_i/K_c$) from the Canons Park experiments (see Table 14.2) can be compared with the cavity expansion predictions given in Chapter 3 (see Table 3.7 on p105).

The cavity expansion method predicts $K_i/K_c$ = 0.57 (i.e. an *increase* in radial effective stress) for London clay, regardless of overconsolidation ratio (based on Modified Cam Clay). The method fails to predict the *decrease* in radial effective stress that was observed near the pile tip (i.e. at z/Rs less than thirty); and it over-estimates the increase in K at the following and "lagging" positions (i.e. at z/R > 50).

## 14.4 PILE LOADING

### 14.4.1 Introduction

As discussed in Chapters 3 and 4 (see pp109 and 163), the shaft capacity of a pile can be calculated from the equation:

$$Q_{shaft} = \pi D \int_L \tau_{rz} dz$$

Effective stress theories of pile behaviour assume that the shear stress ($\tau_{rz}$) is related to the radial effective stress *at failure* ($[\sigma'_{rr}]_f$) by the following equation:

$$\tau_{rz} = \mu(\sigma'_{rr})_f$$

where $\mu$ is the coefficient of friction. As noted in Section 14.2.4.b, this equation ignores viscous components of shear, and hence only applies to static loading tests.

If we express $\sigma'_{rr}$ in terms of the coefficient of lateral stress ($K = \sigma'_{rr}/\sigma'_{vo}$), then:

$$Q_{shaft} = \pi D \int_L \mu K_f \sigma'_{vo} dz = \pi D \int_L \mu (K_f/K_c) K_c \sigma'_{vo} dz$$

where $K_c$ and $K_f$ are the values of K at the end of equalization and at failure (respectively).

The last equation effectively divides $\tau_{rz}$ into four separate components:

- The original vertical effective stress in the ground ($\sigma'_{vo}$)
- The lateral stress coefficient at the end of equalization ($K_c$)
- The <u>change</u> in radial effective stress during pile loading, as represented by the ratio $K_f/K_c$
- The coefficient of friction mobilized at the pile/soil interface *at failure* ($\mu$)

Sections 14.4.2 to 14.4.4 examine the last three components in some detail, by comparing the results of the Canons Park experiments with i) data from other instrumented pile tests and ii) theoretical predictions for $K_c$, $(K_f/K_c)$, and $\mu$. As a result of this analysis, I have devised a new design method for displacement piles installed in heavily over-consolidated clays - see Section 14.5.

## 14.4.2 Radial effective stress at the end of equalization

### a) Discussion of the Canons Park data

As noted in Section 14.3.1.a, the excess pore pressures that were generated during pile installation at Canons Park took about thirty-six hours to dissipate. The radial effective stresses at the end of this period, $(\sigma'_{rr})_{36h}$, are shown on Figure 10.7 (see p344). They are generally smaller than the cavity expansion predictions for $\sigma'_{rr}$ - and yet far higher than the original *in situ* horizontal effective stress $(\sigma'_{ho})$.

The corresponding values of the lateral stress coefficient $(K_c)$ are plotted on Figure 14.11, against the overconsolidation ratio (OCR). The Canons Park data is given by the square symbols, and lies in the range $4.0 \leq K_c \leq 13.0$ (inside the balloon marked "high OCR clays"). The numerical values of $K_c$ are listed in Appendix 11.

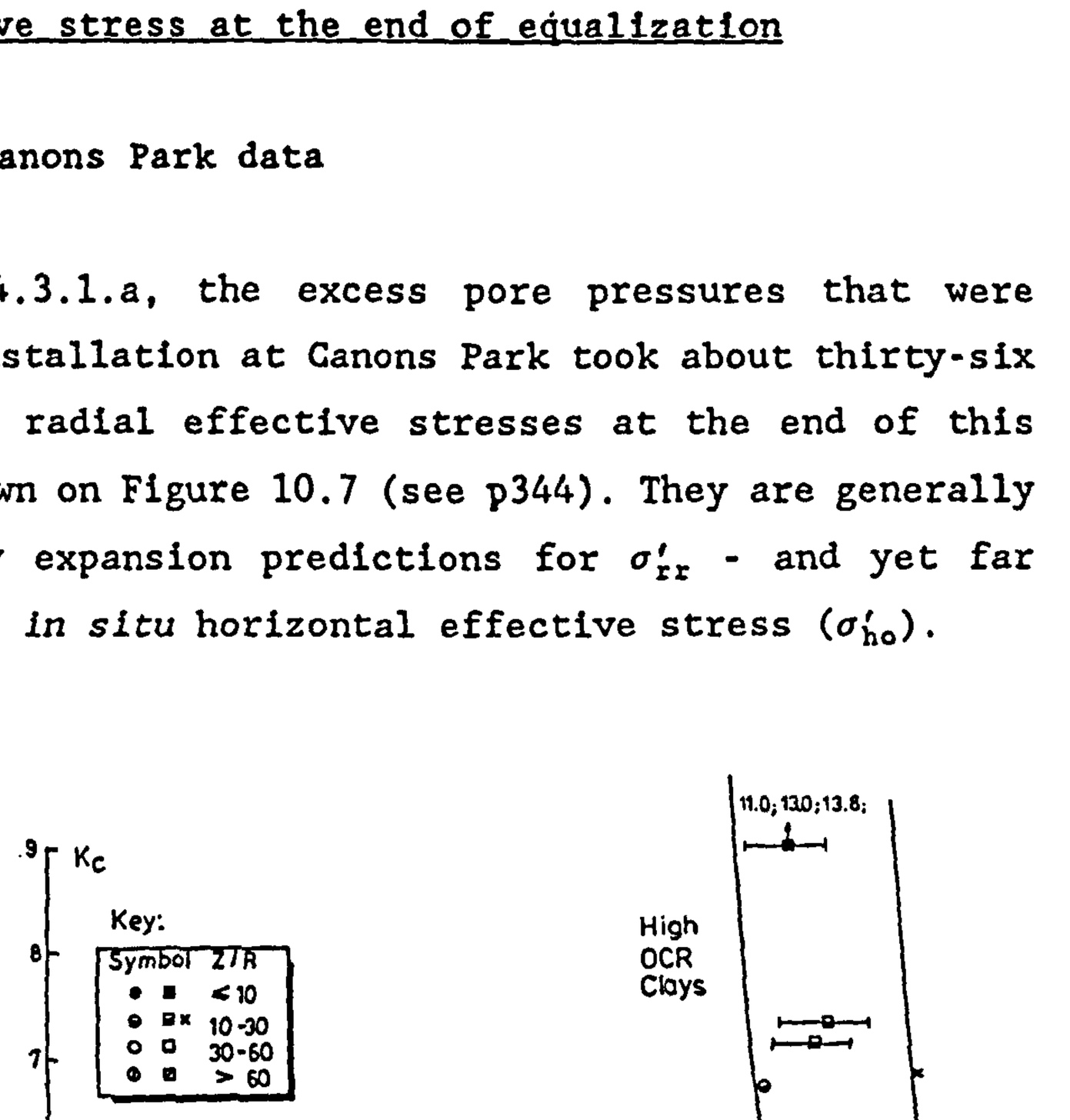



Figure 14.11 Lateral stress coefficient $K_c$ vs OCR (Canons Park data given by square symbols)

These readings show

reasonable agreement with the limited data that is available in other heavily overconsolidated clays: i.e. Coop's tests in the Gault clay at Madingley (at Canons Park, Coop removed his pile from the ground before the end of equalization). $K_c$ is clearly much greater in the high OCR clays than in the low OCR ones.

b) The "z/R effect"

As Figure 14.11 demonstrates, the value of $K_c$ depends both on the over-consolidation ratio (OCR) of the soil and on the value of z/R, i.e.:

$$K_c = f(OCR,\ z/R)$$

where $f(OCR,\ z/R)$ is some unknown function of OCR and z/R. Since OCR varies with depth (and hence with z/R), there is no simple way* to determine the precise relationship between $K_c$, OCR, and z/R.

Because the variation in the overconsolidation ratio at Canons Park is not great (in percentage terms), there is only a small error involved in splitting the function $f$ into two separate functions, one involving z/R and the other involving OCR:

$$K_c = f(OCR,\ z/R) = \psi(z/R)\Omega(OCR)$$

Figure 14.12 illustrates the general form of the relationship between $K_c$ and z/R, by plotting the normalized parameter $K_c/(K_c)_{z/R=8}$ against the normalized distance z/R. $(K_c)_{z/R=8}$ is the value of $K_c$ at the *leading* instrument position (i.e. at z/R = 8). The results, which are taken from Test Series CP2f, CP3fs, and CP5f, show very good agreement with one another.

---

*One way to determine this relationship would be to perform multiple tests with piles of different length. The measurements of $K_c$ would have to be obtained at the same depths in each test, in order to avoid inevitable variations in OCR

c) Comparison with the test results from Kjelsås

Also included on this diagram are the results of Kenney's[18] instrumented pile test in the quick clay at Kjelsås, near Oslo. This is the only case history I can find where reliable measurements were made at enough points along the pile shaft for the relationship between $K_c$ and z/R to be established.

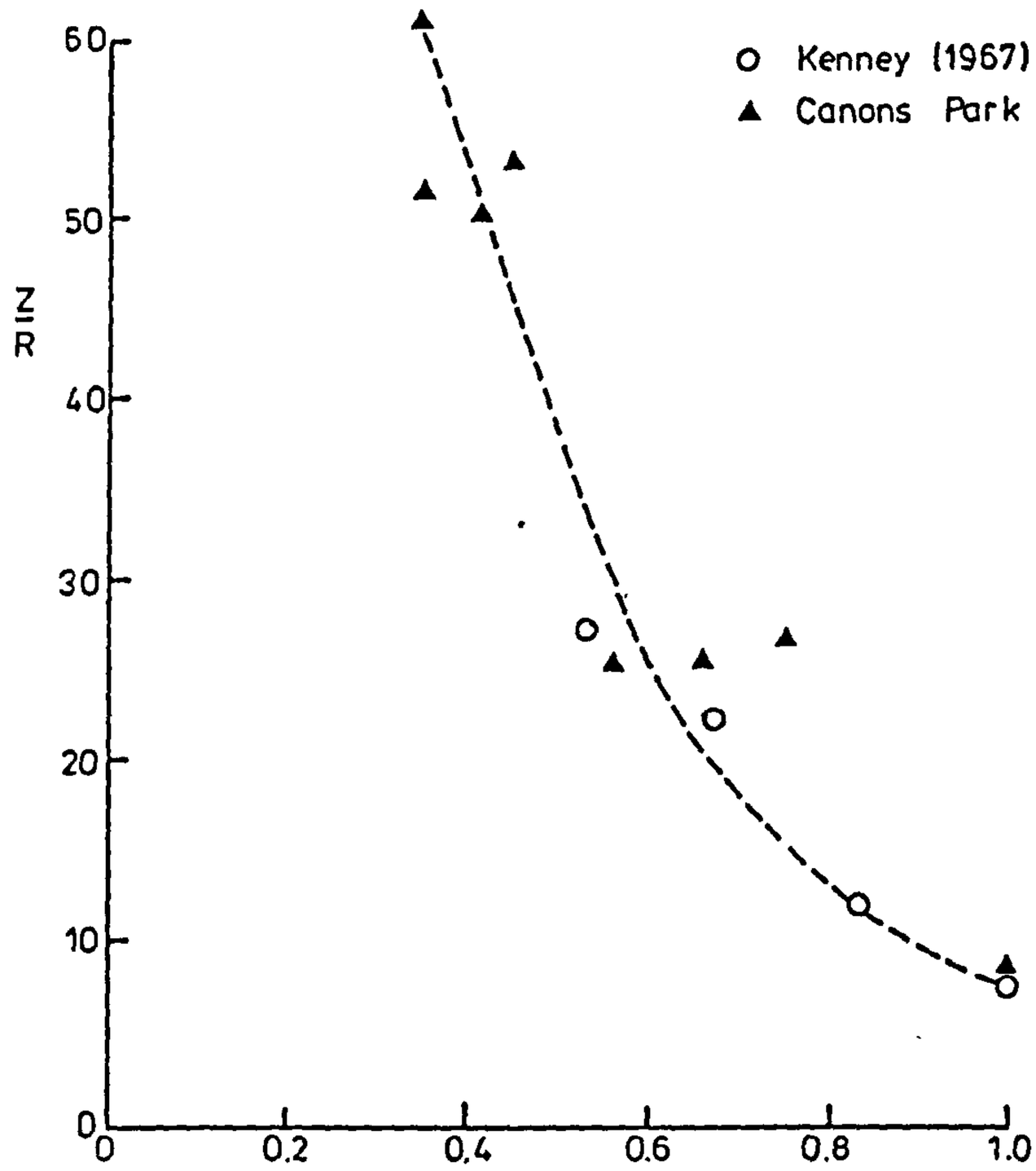



Figure 14.12 Relationship between $K_c$ and z/R for London & Oslo clays

The broken line on Figure 14.12 is based on results from two sites only, and therefore should be regarded as provisional. Nevertheless, the data suggests a similar relationship between $K_c/(K_c)_{z/R=8}$ and z/R for these two (very different) soils.

(As noted in Table 4.4, p136, the quick clay at Kjelsås has a low plasticity index [$I_p$ = 7%], very high sensitivity [$S_t$ > 100], and a low undrained shear strength [$(c_{uo})^{FV} \approx$ 5kPa]. Its OCR is ≈1 throughout the deposit, and its $K_0$ is between 0.5 and 0.6.)

d) Comparison with selected test cases

The radial effective stresses that were recorded in the experiments at Canons Park are compared below with the results from the high quality field tests at Haga, Saugus, and Madingley.

| Haga clay | CONTRACTIVE/DILATING | London clay |
|---|---|---|

| | | | | | |
|---|---|---|---|---|---|
| $K_c$ = 0.9 | @ z/R ≈ 61 | (OCR ≈ 25) | $K_c$ ≈ 4½ | @ z/R = 61 | (OCR ≈ 42) |
| $K_c$ = 1.2 | @ z/R ≈ 43 | (OCR ≈ 9) | $K_c$ = 4-6 | @ z/R ≈ 50 | (OCR ≈ 37) |
| $K_c$ = 1.3 | @ z/R ≈ 23 | (OCR ≈ 4½) | $K_c$ = 7-9½ | @ z/R ≈ 25 | (OCR ≈ 30) |
| $K_c$ = 1.1 | @ z/R ≈ 5 | (OCR ≈ 4) | $K_c$ = 11-13 | @ z/R ≈ 8 | (OCR ≈ 25) |
| | $K_c/K_0$ = 1-1½ | | | $K_c/K_0$ = 1½-6 | |

| | | | | | |
|---|---|---|---|---|---|
| $K_c$ ≈ 0.9 | @ z/R = 50 | (OCR = 2-4) | $K_c$ ≈ 7 | @ z/R = 22 | (OCR ≈ 22) |
| $K_c$ ≈ 0.6 | @ z/R = 50 | (OCR ≈ 1.2) | $K_c$ ≈ 6 | @ z/R = 5 | (OCR ≈ 27) |
| | $K_c/K_0$ ≈ 1 | | | $K_c/K_0$ = 2½-3 | |

Boston blue clay — Gault clay

Once again, the comparison with the three test cases indicates that the soil's behaviour depends on whether it is a *contractive* or a *dilating* material.

e) Comparison with theory

Values of the lateral stress coefficient at the end of equalization are compared with the cavity expansion predictions for $K_c$ on Figure 14.13.

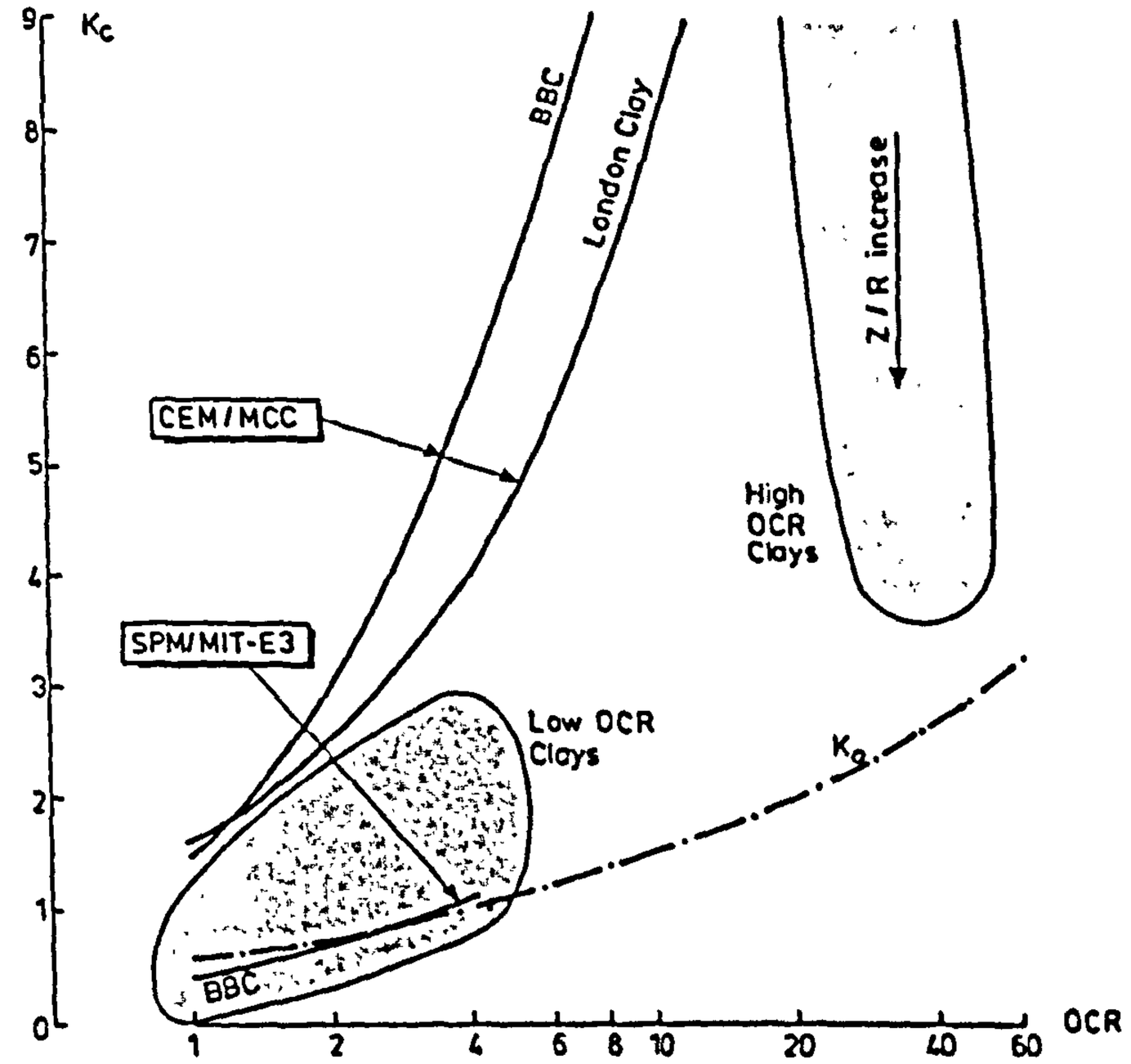



Figure 14.13 Comparison between measured and theoretical values of $K_c$

The cavity expansion method clearly overestimates the value of $K_c$ for both high and low OCR clays. The divergence between the predictions and the observations increases both with OCR and with z/R.

Note also from Figure 14.13 how the lateral stress coefficient in the high OCR clays is significantly higher than the value of $K_0$ for the undisturbed ground. According to Meyerhof[19] (see Chapter 2, pp35-41) the ratio $K_s/K_0$ (= $K_c/K_0$) is between one and two. The data from Canons Park

suggests that $K_c/K_0$ = 5.1-6.1 at leading, 3.2-4.3 at following, and 1.6-2.4 at trailing instrument positions.

## 14.4.3 Changes in radial effective stress during pile loading

a) Drained or undrained loading?

The load tests at Canons Park, which typically took four to five hours to complete, were all *undrained* tests. The evidence for this comes from observations of changes in the excess pore pressures during breaks in load testing. Since it is difficult, while the load test is being performed, to distinguish between pore pressure changes due to dissipation and changes due to variations in total stress, the breaks in testing were designed so that the excess pore pressures could dissipate while the total stresses remained fairly constant. The fact that there were no noticeable changes in pressure during breaks lasting more than one hour implies that the soil surrounding the pile was effectively undrained throughout the load tests.

b) Discussion of the Canons Park data

The changes in radial effective stresses that occur during pile loading are generally very small, as can be seen from the effective stress paths presented in Figures 11.15 and 11.16 (see pp380 and 382). At leading and following positions, $K_f/K_c$ = 0.98 ±0.08; and at trailing positions $K_f/K_c$ = 1.00 ±0.28.

The shape of the effective stress paths implies that the London clay behaves elastically during pile loading, with failure occurring when the stress paths reach their "cut-off" points, corresponding to the peak values of $\mu$ that can be mobilized at the pile/soil interface.

c) Comparison with selected test cases

The ratios of $K_f$ to $K_c$ that were measured at the Haga, Saugus, and Madingley test sites are summarized in the following boxes.

| Haga clay | CONTRACTIVE/DILATING | London clay |
|---|---|---|
| $K_f/K_c$ = 1.05 ±0.22<br>Incremental loading tests<br>Stress paths confidential at present | | $K_f/K_c$ = 1.00 ±0.28 for z/R > 50<br>$K_f/K_c$ = 0.98 ±0.08 for z/R < 30<br>LPC load test procedure<br>Stress paths on Figs 11.15-11.16 |
| $K_f/K_c$ = 0.45-0.83<br>($K_f$ not determined accurately)<br>Rapid load test<br>Stress paths similar to results of direct simple shear tests? | | $K_f/K_c \approx 1$<br>($K_f$ not determined accurately)<br>Rapid load test<br>Stress paths not reported |
| Boston blue clay | | Gault clay |

The results of these experiments suggests that $K_f/K_c$ is close to 1.0 in the dilating clays; whereas the limited evidence available for the contractive clays suggests that they yield prior to pile failure, with K reducing significantly both before and after this happens.

## 14.4.4 Coefficients of friction

### a) Discussion of the Canons Park data

The evidence from Chapters 11 and 12 proves conclusively that piles installed in London clay fail by sliding on residual shear surfaces, close to - but not at - the pile/soil interface. The frictional strength depends critically on the rate at which the piles are installed, which forces us to distinguish between slow- and fast-jacked piles.

The essential feature of *slow*-jacking is that it creates a "principle displacement shear" next to the pile shaft, 1-2mm away. The shear surface is highly polished and acts as a plane of weakness in all the subsequent loading tests on the slow-jacked pile.

As the flow-chart on p384 shows, if a slow-jacked pile is loaded in the *same* direction as in its previous loading, it fails in a ductile manner, with a coefficient of friction ($\mu$) between 0.12 and 0.20 (i.e. close to the slow-minimum value $\mu_{sm}$ - see Chapter 5, pp210-213). Loading in the *opposite* direction produces a brittle response, with $\mu$ increasing to its slow-peak value ($\mu_{sp}$ = 0.2-0.25). The increase in $\mu$ is caused by the stresses acting on the shear surface realigning themselves, in order to

accommodate the change in loading direction.

*Fast*-jacked piles behave very differently to this, in several ways. During pile installation failure occurs in a shear band rather than on a single displacement shear. The shear band is not very wide (10mm at most) and comprises a series of inter-connected shear surfaces which may be likened to the layers of an onion skin. The shearing that takes place in this zone during installation is *transitional* between the turbulent and sliding modes described by Lupini et al.[20] (see Chapter 5, pp208-210). The "skin" of re-oriented clay acts as a *zone* of weakness next to the pile, such that $\mu$ cannot reach its critical state value ($\tan \phi_{cs}$ = 0.41) in any of the subsequent load tests on the fast-jacked pile.

When the fast-jacked pile is loaded slowly, the maximum resistance that can be obtained from the shear zone is close to the slow-peak residual strength (see Chapter 5, pp210-213), i.e. $\mu = \mu_{sp}$ (= 0.20-0.25). With continued displacement, the soil particles become more uniformly aligned, and the $\mu$ drops towards its slow-minimum value $\mu_{sm}$ (≈0.15). When the loading direction changes, the coefficient of friction rises to $\mu_{sp}$, since the clay particles are not aligned for movement in the new direction. (These changes in $\mu$ are summarized by the flow-chart on p385.)

The switch from transitional to sliding shear occurs at a *threshold* velocity, which, for the London clay, is between 100 and 500mm/min. This has been confirmed both in the field tests at Canons Park (see Figure 9.17, p324) and by ring-shear experiments (see Figure 5.14, p213).

The evidence presented in Chapter 12 suggests that *driven* piles behave identically to fast-jacked piles.

b) Tests on other piles jacked into London clay

A number of experiments have been conducted on piles in London clay which were jacked at rates below the threshold velocity. In each case the pile gave a ductile response to first-time loading in compression, whereas the *driven* piles tested by the some of these authors gave a brittle response:

- Tomlinson[21]/Stanmore (piles jacked at 50-200mm/min; compression tests gave ductile load-displacement curves with $\alpha < 0.55$: driven piles gave brittle response on first loading, with $\alpha$ = 0.62-0.93; repeated loading reduced $\alpha$ to 0.49-0.66 [see Figure 4.20, p169])
- Cooke and Price[22]/Hendon (pile jacked at 5mm/min; compression test gave a ductile response with $\alpha$ = 0.46; subsequent tension test gave slightly brittle response, with $\alpha$ = 0.54)
- Cooke et al.[23]/Hendon (pile jacked at 15mm/min; $\alpha$ = 0.45)
- Price and Wardle[24]/Canons Park (pile jacked at 20mm/min gave ductile response in compression; driven pile, brittle)

These results are consistent with the description of residual sliding given above.

c) Comparison with selected test cases

The coefficients of friction that were recorded at Canons Park are compared below with the results from Haga, Saugus, and Madingley. Once again, the soil's behaviour depends on whether it is a *contractive* or a *dilating* material.

| Haga clay | CONTRACTIVE/DILATING | London clay |
|---|---|---|
| $\mu$ = 0.40-0.47 (below 2m) ⇒ $\delta$ = 22-25° (cf. $\phi_{tc}$ = 33°)<br>No variation in $\mu$ with z/R<br><br>N.b. "average" not "local" $\tau_{rz}$<br>No evidence of residual shear surfaces next to the pile (from an examination of the soil's fabric after load testing) | | Fast-jacked piles: many discontinuous shear surfaces in a 10mm thick shear zone<br>L1C & L1T: $\mu = \mu_{sp}$ = 0.20-0.25 ⇒ $\delta$ = 11-14° (cf. $\phi_{tc} \doteq 22\frac{1}{2}°$)<br><br>Slow-jacked: one continuous "principal displacement shear", 1-2mm from the shaft<br>L1C: $\mu = \mu_{sm}$ = 0.12-0.20 ⇒ $\delta$ = 7-11°<br>L1T: $\mu = \mu_{sp}$ = 0.20-0.25 ⇒ $\delta$ = 11-14°<br><br>Subsequent tests<br>Change in direction ⇒ $\mu_{sp}$; no change ⇒ $\mu_{sm}$<br><br>No variation in $\mu$ with z/R |
| $\mu$ = 0.3-0.62 ⇒ $\delta$ = 17-32°<br>(cf. $\phi_{tc}$ = 33°)<br>Values of $\mu$ unreliable<br>Measurements at z/R = 50 only<br>"Average" not local $\tau_{rz}$<br>Non-standard test procedures | | $\mu \approx$ 0.15-0.19? ⇒ $\delta$ = 8½-11°<br>(cf. $\phi_{tc}$ = 24°)<br>Ductile response ⇒ "slow-jacked" pile (jacked at ≈200mm/min)<br>"Average" not local $\tau_{rz}$<br>Non-standard test procedures |
| Boston blue clay | | Gault clay |

## 14.5 DESIGN METHOD FOR DISPLACEMENT PILES IN HIGH OCR CLAYS

### 14.5.1 A new design method for high OCR clays

The information given in Section 14.4 can be used to formulate a new method for calculating the (static) shaft capacity of displacement piles in high OCR clays.

The pile's shaft capacity ($Q_{shaft}$) can be expressed in terms of the four main parameters that are listed in Section 14.4 ($\mu$, $K_f/K_c$, $K_c$, and $\sigma'_{vo}$). The equation relating these parameters to $Q_{shaft}$ is (see p473):

$$Q_{shaft} = \pi D \int_L \tau_{rz} dz = \pi D \int_L \mu (K_f/K_c) K_c \sigma'_{vo} dz \qquad \ldots.[1]$$

As a first approximation, it appears that i) $\mu$ is independent of z/R (see Section 14.4.4.c above); and ii) that $K_f/K_c \approx 1$ (at least for medium and high plasticity clays, see Section 14.4.3.c). Under these conditions, equation [1] can be simplified to:

$$Q_{shaft} = \pi D \mu \int_L K_c \sigma'_{vo} dz \qquad \ldots.[2]$$

According to the arguments put forward in Section 14.4.2.b, the lateral stress coefficient ($K_c$) can be expressed in terms of two functions, one involving z/R and the other OCR:

$$K_c = \psi(z/R)\Omega(OCR) \qquad \ldots.[3]$$

The data plotted on Figure 14.11 suggests that - for constant z/R - the relationship between $K_c$ and OCR is given by a power function, i.e. $(K_c)_{constant} = \Omega(OCR) = aOCR^b$ (where a and b are constants). The function $\psi(z/R)$ is reasonably independent of OCR (see Section 14.4.2.a), and can be written as $\psi(z/R) = K_c/(K_c)_{z/R=\infty}$. Choosing the constant a so that $(K_c)_{constant} = (K_c)_{z/R=\infty}$ allows us to write:

$$(K_c)_{z/R=\infty} = K_c/\psi(z/R) = aOCR^b \qquad \ldots.[4]$$

Combining equations [2] and [4] then gives:

$$Q_{shaft} = \pi D \mu a \int_L \psi(z/R) OCR^b \sigma'_{vo} dz \quad \ldots\ldots[5]$$

## 14.5.2 Limitations of the new method

Equation 5 has been derived by assuming that the radial effective stress does not change during pile loading (i.e. $K_f/K_c = 1$). Therefore the equation does not hold for soils, like the Boston blue clay, that contract markedly before the pile fails. Of course, if sufficient experimental evidence became available to justify a different value for $K_f/K_c$, then equation 5 (with suitable modification) could still be used for these soils (provided also that $\mu$ can be determined).

Equation 5 also assumes that we are dealing with a deposit that has a uniform coefficient of friction ($\mu$). In layered deposits this may not be true. In addition, for very long piles, progressive failure may result in $\mu$ taking different values at different points along the pile shaft. In these cases equation 5 should be amended to:

$$\Delta Q_{shaft} = \pi D \mu a \int_{\Delta L} \psi(z/R) OCR^b \sigma'_{vo} dz \quad \ldots\ldots[6]$$

where $\Delta Q_{shaft}$ is the capacity of an individual element of the pile shaft, of length $\Delta L$. The total shaft capacity is then calculated by summing the capacities of the individual elements ($Q_{shaft} = \Sigma \Delta Q_{shaft}$).

## 14.5.3 Determining the parameters needed for the new design method

If equation 5 is to be used to estimate the shaft capacity of piles in clay soils, then six independent parameters must be determined: the function $\psi(z/R)$; the vertical effective stress ($\sigma'_{vo}$) and over-consolidation ratio (OCR); the empirical factors a and b; and the coefficient of friction ($\mu$).

The paucity of good quality data (see Chapter 4) means that the relationship between $K_c$ and z/R cannot, at present, be established with the required degree of certainty. Provisionally, the broken line

on Figure 14.12 can been used to define $\psi(z/R)$.

Although the vertical effective stress in the ground ($\sigma'_{vo}$) is easy to determine, the true value of OCR is not, especially in heavily over-consolidated clays (see Chapter 4, pp139-140). If the results of high-pressure oedometer tests are not available,* then the factor $OCR^b$ could be estimated from geological records, Marchetti dilatometer tests, or the soil's undrained strength ratio. A lower bound value for OCR leads to a conservative estimate of shaft capacity.

The factors a and b can be determined by correlating $(K_c)_{z/R=8}$ (= $K_c/\psi[z/R]$) against OCR (see equation 4). Table 14.3 gives details of a

Table 14.3 Statistical analysis of relationship between $K_c$ and OCR

Least-squares regression between $K_c/\psi$ (= $[K_c]_{z/R=8}$) and OCR: assumptions and limitations

1. Function $\psi(z/R)$ is given by the broken line on Figure 14.12
2. Data taken from Table 4.4 (pp136-137) and Appendix 11
3. Data points with $8 \leq z/R < 61$ are included, others ignored
4. Unrepresentative cases have been ignored, including: Cases 2 (Tokyo clay, very sensitive); 9 (laboratory tests in kaolin); and 12 (Haga clay, apparent OCR caused by leaching)
5. Questionable data (marked ? in Table 4.4) has been ignored
6. To avoid excessive weighting to the Canons Park data, $K_c$ taken from Tests CP2f and CP5f only

Relationship obtained from regression analysis on 26 data points:

$$K_c/\psi(z/R) = (0.82 \pm 0.16)OCR^{(0.83 \pm 0.11)}$$

with a correlation coefficient $r^2 = 0.911$ ($r = 0.955$). The ± figures indicate ±95% confidence limits

statistical analysis that I have performed on the data summarized in Table 4.4 (pp136-137) and in Appendix 11. The data represents the results of instrumented pile tests in a wide range of clay soils, including two of the tests at Canons Park (CP2f and CP5f). The study reveals a very good correlation between $K_c/\psi(z/R)$ and OCR (correlation coefficient $r^2$ = 0.91), and suggests that a and b are (coincidentally) both equal to ≈0.8.

Based on this study I have prepared a design chart (see Figure 14.14) showing values of $K_c$ as a function of OCR and z/R. For comparison, I have plotted on this chart the experimental data from Canons Park and from Cases 1-3a, 7, 9-12, 15, and 17a (see Table 4.4, pp136-137). These test results are discussed in detail in Section 14.4.2.

---

*The values of a and b depend on the method used to determine OCR, and in particular the method used to determine the OCRs of the heavily over-consolidated clays

Finally, the coefficient of friction ($\mu$) can be measured in the laboratory, using the ring-shear apparatus. The soil should be tested against a suitably roughened interface and at an appropriate rate of displacement. Direct shear tests (also against an interface) may possibly provide values for $\mu$, although this needs to be investigated further.

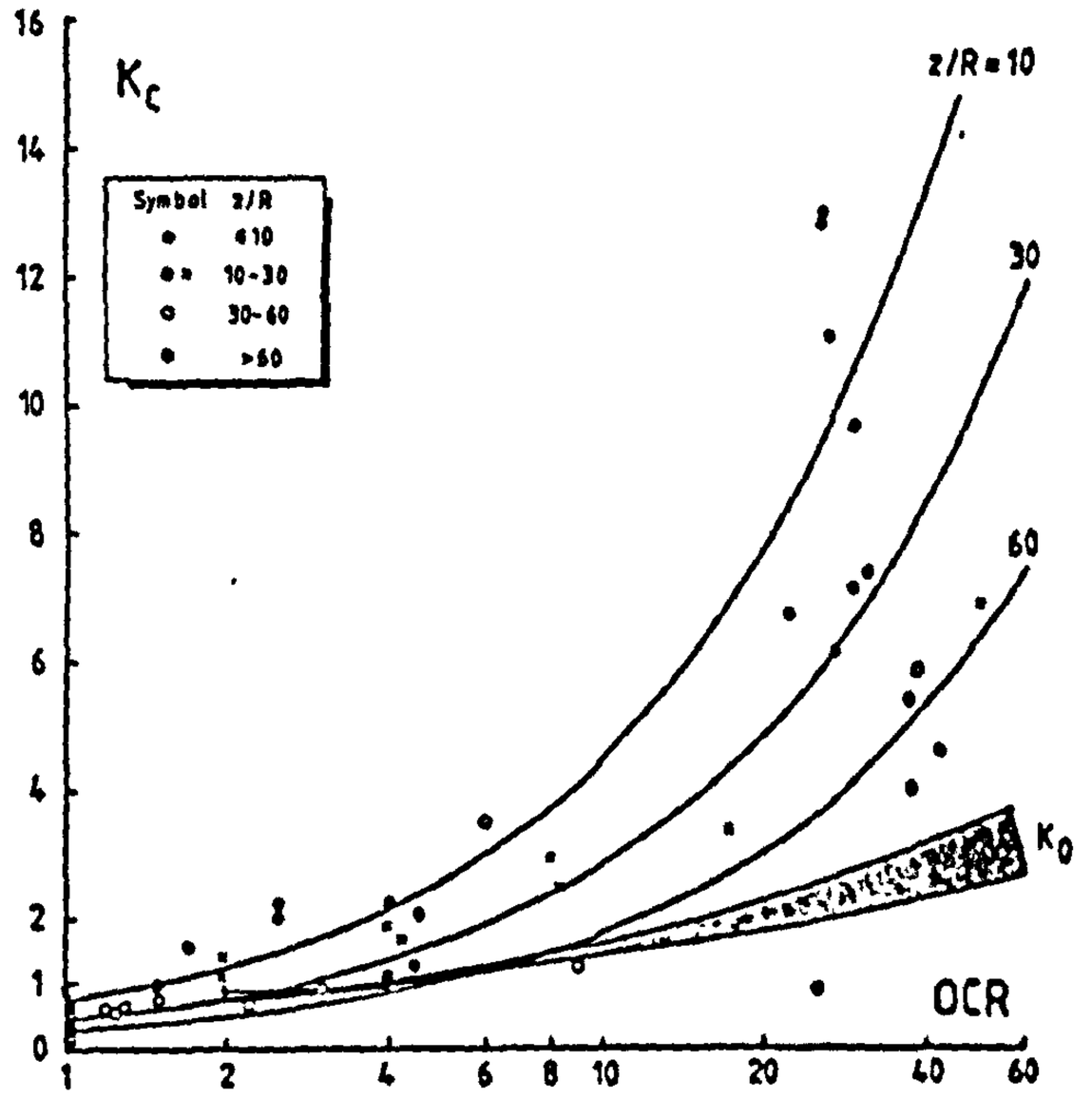



Figure 14.14 Design chart giving values of $K_c = f(OCR, z/R)$

## 14.5.4 Worked example

The conclude this discussion I present a worked example based on the new design method, in order to illustrate how it can used to determine the shaft capacity of piles in clays. The example concentrates on the 82m long, 2.13m diameter piles that were installed in the layered soil profile at the offshore Magnus field. Information about the soil

Table 14.4 Worked example for Magnus foundations

| Layer | Depth (m) | $\sigma'_{vo}$ (kPa) | OCR | z/R | $\mu$ | $\psi$(z/R) † | a·OCR$^b$ ‡ | $K_c$ | $\tau_{rz}$ (kPa) |
|---|---|---|---|---|---|---|---|---|---|
| A | 1 | 12 | 52.0 | 75.9 | 0.47 | 0.35 | 18.9 | 6.6 | 37.3 |
| | -6 | -72 | -17.0 | -71.2 | | | -7.7 | -2.7 | -91.4 |
| B | 7 | 84 | 14.0 | 70.3 | 0.47 | 0.35 | 6.6 | 2.3 | 91.3 |
| | -10 | -120 | -9.6 | -67.5 | | | -4.9 | -1.7 | -96.4 |
| C | 11 | 132 | 26.0 | 66.5 | 0.47 | 0.35 | 10.8 | 3.8 | 235.4 |
| | -16 | -192 | -13.0 | -61.9 | | | -6.2 | -2.2 | -196.7 |
| D | 17 | 204 | 22.0 | 60.8 | 0.47 | 0.35 | 9.5 | 3.3 | 318.3 |
| | -20 | -240 | -15.0 | -58.1 | | | -7.0 | -2.4 | -276.3 |
| E | 21 | 252 | 4.9 | 57.2 | 0.47 | 0.35 | 2.9 | 1.0 | 118.9 |
| | -40 | -467 | -3.4 | -39.4 | | -0.45 | -2.1 | | -211.3 |
| F | 41 | 478 | 3.6 | 38.4 | 0.35 | 0.46 | 2.2 | 1.0 | 172.2 |
| | -50 | -574 | -2.9 | -30.0 | | -0.57 | -1.9 | -1.1 | -213.5 |
| G | 51 | 585 | 1.0 | 29.1 | 0.35 | 0.58 | 0.8 | 0.5 | 95.0 |
| | -76 | -855 | | 5.6 | | -1.06 | | -0.8 | 253.7 |
| H | 77 | 866 | 3.7 | 4.7 | 0.35 | 1.09 | 2.3 | 2.5 | 749.1 |
| | -82 | -921 | -3.3 | -0.0 | | -1.22 | -2.1 | | 814.4 |

† $\psi(z/R) = 0.35 + 0.865(1 - [z/R]/60)^2$ ; $\Psi \geq 0.35$
‡ a = 0.8 and b = 0.8

conditions at this site (i.e. $\sigma'_{vo}$, OCR, and $\mu$) is given by Jardine.[25] The piles' overall shaft capacity ($Q_{shaft}$) has been calculated by summing the individual loads carried by each one metre section, using the formula $Q_{shaft} = \pi D \Sigma \tau_{rz} \Delta L$, where $\tau_{rz} = \mu K_c \sigma'_{vo}$, $K_c = \psi(z/R)^a OCR^b$, and $\Delta L$ = 1m. Table 14.4 summarizes the results of these calculations, and Figure 14.15 shows the variation in skin friction ($f_s = \tau_{rz}$) along the pile shaft.

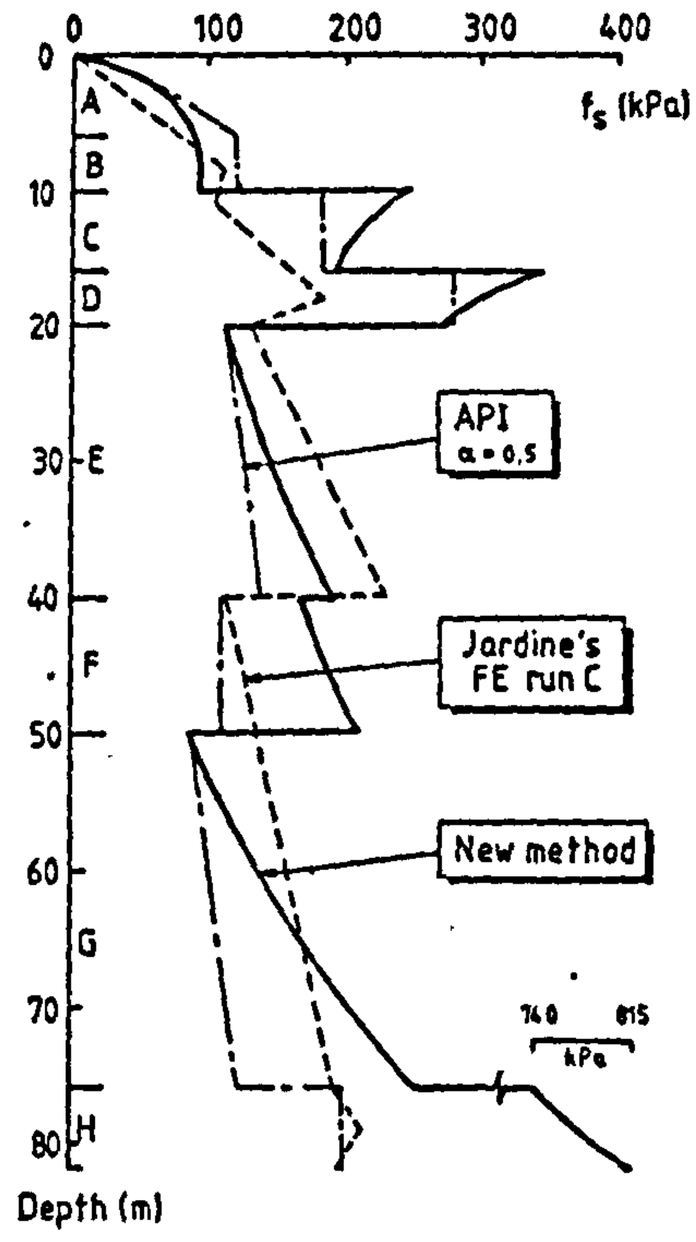



Figure 14.15 Estimates of skin friction for the Magnus piles

According to the new design method, the piles' overall shaft capacity is 110.8MN. Other estimates of $Q_{shaft}$ - and the design methods on which they are based - are as follows:

- 72.0MN - API recommendations[26] ($\alpha$ = 0.5, see the predicted profile of $f_s$ on Figure 14.15)
- 79.4MN - Jardine's[27] finite element analysis, with a limiting ratio of $\tau_{rz}/\sigma'_{rr}$ at the pile wall (see the predicted profile of $f_s$ on Figure 14.15)
- 79.7MN - the $\beta$ method[28] (see the predicted profile of $f_s$ on Figure 2.11, p45)
- 94.3MN - Randolph and Murphy's modified $\alpha$ approach[29]
- 106.8MN - Semple and Rigden's modified $\alpha$ approach[30]

The main difference between the predictions of the new design method and those based on the other methods is the skin friction in layer H (where z/R is small and the OCR high). Clearly further research is needed before we can decide whether the pile is able to mobilize such enormous shear stresses near the pile tip.

## 14.6 NOTES ON THE SELECTED CASE HISTORIES

The following boxes summarize the main features of the instrumented pile tests that have been selected for comparison with the experiments at Canons Park (see Section 14.1.3). The information given includes:

- The name of the institution (Inst'n)
- The method and rate of installation of the pile (Install)
- Whether the pile was open- or closed-ended (End)
- The pile diameter and length (D x L)
- Its aspect ratio (length to diameter ratio) (L/D)
- The instruments carried (Device): PP = pore pressure probe; EP = earth pressure cell; SS = shear stress cell; AL = axial load cell; SG = strain gauges; TS = temperature sensor
- The position of these instruments relative to the pile tip, in terms of z/R (z/R)
- Whether an inspection trench was excavated around the pile(s) (Trench?)
- The soil's plasticity index ($I_p$); sensitivity ($S_t$); overconsolidation ratio (OCR); undrained shear strength (in unconsolidated undrained triaxial compression tests, $[c_{uo}]^{UU}$); and undrained strength ratio ($c_{uo}/\sigma'_{vo}$)

**NGI/Haga (Haga clay)**

| | |
|---|---|
| Inst'n | NGI |
| Device | Pile |
| Install | Jacked ≈61mm/min |
| End | Closed |
| D x L | ϕ153mm x 5.15m |
| L/D | 33.7 |
| Devices | 4PP; 4EP; 1AL; 6SG; TS |
| z/R | 4.6-60.8 |
| Trench? | Yes: water content & $c_u$ variation with radius; X-ray & micro-fabric studies |
| Soil | Haga clay |
| Type | Leached, sensitive, low plasticity, firm marine clay |
| Age | Quaternary (possibly 10 000 years old) |
| $I_p$ | 15% [CL] / 35-40% [CI] |
| $S_t$ | 5-6 [sensitive] |
| OCR | 2-20 |
| $(c_{uo})^{UU}$ | ≈65kPa [firm] |
| $c_{uo}/\sigma'_{vo}$ | 0.7-1.8 |

**Canons Park (London clay)**

| | |
|---|---|
| Inst'n | Imperial College |
| Device | ICIP |
| Install | Jacked 80-490mm/min |
| End | Closed |
| D x L | ϕ102mm x 3.18-4.07m |
| L/D | 31.4-40.0 |
| Devices | 6PP; 3EP; 3SS; 4AL; 3TS |
| z/R | 8.3-61.2 |
| Trench? | Yes: water content, $c_u$, & $p_k$ variation with radius; X-ray & micro-fabric studies |
| Soil | London clay |
| Type | Medium plasticity, firm to stiff, silty marine clay (fissured) |
| Age | Eocene (> 30 million years old) |
| $I_p$ | 42-58% [CI] |
| $S_t$ | Insensitive |
| OCR | > 30 |
| $(c_{uo})^{UU}$ | 60-130kPa [firm-stiff] |
| $c_{uo}/\sigma'_{vo}$ | 1.6-2.1 |

**MIT/Saugus (Boston blue clay)**

| | |
|---|---|
| Inst'n | MIT |
| Device | PLS cell |
| Install | Jacked 1200mm/min |
| End | Closed |
| D x L | ϕ38.4mm x variable |
| L/D | - |
| Devices | 1PP; 1EP; 1AL; 1TS |
| z/R | Usually 50 |
| Trench? | No |
| Soil | Boston blue clay |
| Type | Sensitive, low plasticity, soft to firm, marine clay |
| Age | Late Pleistocene (14 000 years old) |
| $I_p$ | 18-27% [CL] |
| $S_t$ | 7 ±2 [sensitive] |
| OCR | 1.2-6 |
| $(c_{uo})^{UU}$ | ≈25-45kPa [soft-firm] |
| $c_{uo}/\sigma'_{vo}$ | 0.2-0.36 |

**Oxford Univ./Madingley (Gault clay)**

| | |
|---|---|
| Inst'n | Oxford University |
| Device | Oxford IMP |
| Install | Jacked ≈200mm/min |
| End | Closed/open |
| D x L | ϕ80mm x 5-9m |
| L/D | 65-110 |
| Devices | 5PP; 4EP; 3AL; TS |
| z/R | 5.5 and 22 |
| Trench? | No |
| Soil | Gault clay |
| Type | High plasticity, stiff, silty marine clay (fissured) |
| Age | Cretaceous (> seventy million years old) |
| $I_p$ | 45-65% [CH] |
| $S_t$ | Insensitive |
| OCR | > 30 |
| $(c_{uo})^{UU}$ | 105-150kPa [stiff] |
| $c_{uo}/\sigma'_{vo}$ | ≈2.4 |

## 14.7 NOTES AND REFERENCES

[1]Karlsrud K. and Haugen T. (1985a). Axial static capacity of steel model piles in overconsolidated clay. Proc. 11th Int. Conf. Soil Mech. & Fdn Engng, San Francisco, 3, pp1401-1406; Karlsrud K. and Haugen T. (1985b). Behaviour of piles in clay under cyclic axial loading - results of field model tests. Proc. 4th Int. Conf. on the Behaviour of Offshore Structures (BOSS 1985), Delft, pp589-600. Elsevier, Amsterdam.

[2]Morrison M.J. (1984). In-situ measurements on a model pile in clay. PhD Thesis, Massachusetts Institute of Technology, c687pp; Azzouz A.S. and Morrison M.J. (1988). Field measurements on model pile in two clay deposits. J. Geotech. Engng, Am. Soc. Civ. Engrs, 114(1), pp104-121.

[3]Coop M.R. (1987). The axial capacity of driven piles in clay. DPhil Thesis, Univ. of Oxford; Coop M.R. and Wroth C.P. (1989). Field studies of an instrumented model pile in clay. Géotechnique (in press).

[4]Coop (1987), loc. cit.

[5]Lunne T., Powell J.J.M., Quarterman R.S.T., and Eidsmoen T.E. (1986). Piezocone testing in overconsolidated clays. Proc. 39th Can. Geotech. Conf. on 'Insitu Testing and Field Behaviour', Carlton Univ., Ottawa, Canada, pp209-218.

[6]Johnston I.W. (1972). Electro-osmosis and porewater pressures; their effect on the stresses acting on driven piles. PhD Thesis, Southampton Univ.

[7]Kenney T.C. (1967). Field measurements of in situ stresses in quick clays. Proc. Geotech. Conf. on Shear Strength Properties of Natural Soils and Rocks, Oslo, 1, pp45-55.

[8]Tika T. (1989). The effect of fast shearing on the residual strength of soils. PhD Thesis, Univ. of London (Imperial College). Tests 38-42 were on blue London clay from Canons Park. See Figure 4.41 in particular.

[9]Coop and Wroth (1989), loc. cit.

[10]Butterfield R. and Johnston I.W. (1973). The stress acting on a continuously penetrating pile. Proc. 8th Int. Conf. Soil Mech. & Fdn Engng, Moscow, 2.1, pp39-45. See p43.

[11]Assume that the negative pressures (equal to $u^-$) extend to a radius $\lambda R$, and that for $r > \lambda R$ the pore pressures are everywhere constant and positive (equal to $u^+$). If we regard the excess pore pressure as being $\Delta u = (u - u^+)$, we can write: $\Delta u = (u^- - u^+)$ for $r/R \leq \lambda$ and $\Delta u = 0$ for $r/R > \lambda$. Hence in the terminology given in note 14 (q.v.), $(\Delta u_i)_R = (u^- - u^+)$; $f(r/R) = 1$ for $1 \leq r/R \leq \lambda$; and $f(r/R) = 0$ for $r/R > \lambda$. This is the same definition as Levadoux's "constant" initial isochrone (see Section 14.3.1.c and note 14).

Using decay curves similar to those shown on Figure 14.8, we can determine the magnitude of $\lambda$ from the time taken for the negative pore pressures to rise up to within 5% of $u^+$.

According to Figure 10.2, (p335), the 95% "rise times" at the pile wall ($t_{g5}$) are between 100 and 120s (and at the very extreme might equal 1000s). The corresponding time factor $T_{g5}$ is given by $T_{g5} = c_h t_{g5}/R^2$, where $c_h$ is the coefficient of horizontal consolidation (= 1.6mm$^2$/s at Canons Park) and R the pile's radius (50.8mm). Hence $T_{g5}$ = 0.06-0.07 (and at the extreme 0.6).

The following table lists the values of $T_{95}$ for different values of $\lambda$, from which it can be seen that $\lambda$ lies between 1½ and 2 (and in the extreme between two and five).

| $\lambda$ | $T_{95}$ | $t_{95}$ | $(\lambda - 1)R$ |
|---|---|---|---|
| 1.5 | 0.031 | $\approx 5.0 \times 10^1$s | ≈25mm |
| 2.0 | 0.113 | $\approx 1.8 \times 10^2$s | ≈50mm |
| 5.0 | 1.59 | $\approx 2.6 \times 10^3$s | ≈203mm |
| 10.0 | 7.55 | $1.2 \times 10^4$s | |
| 15.0 | 17.7 | $2.8 \times 10^4$ | |
| 20.0 | 31.8 | $5.2 \times 10^4$ | |
| 30.0 | 72.8 | $1.2 \times 10^5$ | |
| 40.0 | 130. | $2.1 \times 10^5$ | |
| 50.0 | 204. | $3.3 \times 10^5$ | |

[12]Coop and Wroth (1989), loc. cit. Commenting on a similar rise in pore pressure in the field tests at Madingley, Coop and Wroth state:

> "The source of these pore pressures is uncertain, but since the tip transducer registers the increase last, they cannot result from high pore pressures near the tip spreading back along the shaft. It is more likely that there is a pore pressure maximum during installation which is radially remote from the shaft."

[13]Levadoux J.-N. (1980). Pore pressures in clays due to cone penetration PhD Thesis, Massachusetts Institute of Technology. See Table H.7, p617.

[14]In the following equations, the excess pore pressure in the soil at time factor (T) and radius (r) is denoted $(\Delta u)_r$.

On Figure 14.9, the *initial* pore pressure in the soil, $(\Delta u_i)_r$, is given by the equation:

$$(\Delta u_i)_r / (\Delta u_i)_R = f(r/R)$$

where $(\Delta u_i)_R$ is the initial pore pressure at the pile wall ($r = R$). R is the pile's radius; and $f(r/R)$ is some function of $r/R$.

The *constant* initial isochrone shown on Figure 14.9 is defined by the equations:

$$f(r/R) = 1 \text{ for } 1 \leq r/R < \lambda$$
$$f(r/R) = 0 \text{ for } r/R \geq \lambda$$

where $\lambda$ represents the *size* of the (initial) pore pressure field and $f(r/R)$ its *shape*.

The *logarithmic* initial isochrone is defined by the equations:

$$f(r/R) = 1 - \log_e(r/R)/\log_e(\lambda) \text{ for } 1 \leq r/R < \lambda$$
$$f(r/R) = 0 \text{ for } r/R \geq \lambda$$

The excess pore pressure <u>at the pile wall</u> at time factors T is denoted $(\Delta u)_R$, and on Figure 14.9 has been normalized by the initial excess pore pressure <u>at the pile wall</u>, $(\Delta u_i)_R$.

[15]Kenney (1967), loc. cit.

[16]Coop (1987), loc. cit.

[17]Tomlinson M.J. (1970a). Adhesion of piles in stiff clays. CIRIA Report 26, Construction Industry Research and Information Association, London, 47pp.

[18]Kenney (1967), loc. cit.

[19]Meyerhof G.G. (1976). Bearing capacity and settlement of pile foundations. The 11th Terzaghi Lecture. J. Geotech. Engng Div., Am. Soc. Civ. Engrs, 102(GT3), pp197-228.

[20]Lupini J.F., Skinner A.E., and Vaughan P.R. (1981). The drained residual strength of cohesive soils. Géotechnique, 31(2), pp181-213.

[21]Tomlinson (1970a), loc. cit.

[22]Cooke R.W. and Price G. (1973). Strains and displacements around friction piles. Proc. 8th Int. Conf. Soil Mech. & Fdn Engng, Moscow, 2, pp53-60.

[23]Cooke R.W., Price G., and Tarr K. (1979). Jacked piles in London Clay: a study of load transfer and settlement under working conditions. Géotechnique, 29(2), pp113-147.

[24]Price G. and Wardle I.F. (1982). A comparison between cone penetration test results and the performance of small diameter instrumented piles in stiff clay. Proc. 2nd Eur. Symp. on Penetration Testing (ESOPT II), Amsterdam, 2, pp775-780. A.A. Balkema, Rotterdam, 1982.

[25]Jardine R.J. (1985). Investigations of pile-soil behaviour, with special reference to the foundations of offshore structures. PhD Thesis, Univ. of London (Imperial College), 2 vol., 789pp. See Chapters 6 and 10.

[26]American Petroleum Institute (1980). API RP2A (11th edition), Recommended practice for planning, designing, and constructing fixed offshore platforms. American Petroleum Institute, Dallas, Texas. See also Figure 2.4 and pp27-28 in this Thesis.

[27]Jardine (1985), loc. cit. See Chapter 10 for a full discussion of Jardine's calculations (I have made my comparisons with Run C).

[28]See pp43-46 of this Thesis.

[29]Randolph M.F. and Murphy B.J. (1985). Shaft capacity of driven piles in clay. Proc. 17th Offshore Technology Conf., Houston, Texas, 1, pp371-378 (Paper OTC 4883). $\alpha$ depends on $c_{uo}/\sigma'_{vo}$, as shown on p29 in this Thesis. For this calculation I have assumed S = 0.25.

[30]Semple R.M. and Rigden W.J. (1984). Shaft capacity of driven pipe piles in clay. Proc. Symp. on Codes and Standards, Am. Soc. Civ. Engnrs National Convention, San Francisco. In "Analysis and design of pile foundations" (ed. J.R. Meyer), Am. Soc. Civ. Engnrs, New York, pp59-79. Repeated in Ground Engng, 19(1), Jan, pp11-19. $\alpha$ depends on $c_{uo}/\sigma'_{vo}$, see note 29 on p55 of this Thesis and the text on p31.

# Chapter 15

# Conclusions

# TABLE OF CONTENTS

15.1 INTRODUCTION . . . . . 494

15.2 PRINCIPAL EXPERIMENTAL RESULTS . . . . . 495

15.2.1 Pile installation (495)

15.2.2 Equalization stage (496)

15.2.3 Pile loading (497)

15.3 CONCLUSIONS CONCERNING EXISTING PILE THEORIES . . . . . 499

15.4 SUGGESTIONS FOR FURTHER RESEARCH . . . . . 500

## 15.1 INTRODUCTION

The aim of this Thesis has been to explain the behaviour of displacement piles in terms of effective stresses.

The research described herein involved a series of field experiments using instrumented model piles jacked into London clay. The field work was performed at the Building Research Establishment's (BRE's) test-bed site at Canons Park, north London. A total of five instrumented pile tests were performed, in which earth and pore water pressures were measured along the pile shaft during installation, equalization, and load testing. In addition, the experimental programme involved tests on two (uninstrumented) driven piles, and the excavation of an inspection trench around a driven and a jacked pile.

The following sections summarize the conclusions that have been drawn from this research project. Section 15.2 presents the principal experimental results, dealing in turn with the three stages in the lifetime of a pile, i.e.: installation (Section 15.2.1), equalization (15.2.2), and pile loading (15.2.3). The results were obtained in a heavily overconsolidated, medium plasticity clay, and some of the conclusions may not apply to other soil types.

Section 15.3 lists conclusions regarding existing theories of pile behaviour; and Section 15.4 gives some suggestions for future research.

## 15.2 PRINCIPAL EXPERIMENTAL RESULTS

### 15.2.1 Pile installation

1 Large increases in radial stress. The radial total stresses ($\sigma_{rr}$) and radial effective stresses ($\sigma'_{rr}$) are increased enormously by pile installation. However, $(\sigma_{rr})_i$ is much less than the limit pressure measured in self-boring pressuremeter tests ($p_{lim}$). The lateral stress coefficient ($K_i = [\sigma'_{rr}]_i/\sigma'_{vo}$) is between 1½ and 8½ times the coefficient of earth pressure at rest ($K_0$).

2 Negative pore pressures. Pile installation generates *negative* pore water pressures ($u_i < 0$) over most of the pile shaft. The suction does not exceed 100kPa, owing to the pore water in the soil cavitating.

3 Strong rate effect. The rate at which the pile penetrates the ground has a marked effect on its shaft resistance. Piles jacked at speeds below 100mm/minute have just over half the shaft capacity of piles jacked at speeds above 400mm/min. The former have been termed "slow-jacked" and the latter "fast-jacked" piles.

4 The "z/R effect". Once the pile tip has passed through a particular soil horizon, continued penetration causes the radial stresses at that level to fall. The percentage decrease in $(\sigma_{rr})_i$ and $(\sigma'_{rr})_i$ is independent of the horizon considered (and hence is independent of the overconsolidation ratio, OCR). This geometrical process has been termed the "z/R effect" (z is the distance behind the pile tip, and R the pile's radius), and demonstrates the strongly two-dimensional nature of pile installation. The shear stress and pore pressure show a much weaker z/R effect than the radial stresses. The coefficient of friction appears to be independent of z/R.

5 Systematic distortion. Studies of the soil's fabric show that pile penetration distorts the ground in a systematic manner, and not in the random fashion implied by the term "remoulding"

6 Residual shear surfaces. During installation, a *slow-jacked pile* forms a "principal displacement shear" close to the pile shaft, which is highly polished and continuous along the length of the pile. This residual shear surface is less than 1mm away from the

pile, and acts as a plane of weakness in subsequent pile tests on the slow-jacked pile. The pile fails by *sliding* on the principal displacement shear. A *fast-jacked pile* forms a series of discontinuous shear surfaces within a shear zone no more than 10mm thick. The soil next to the pile fails in a *transitional* mode, part sliding and part *turbulent*.

7 Changes in soil properties. There is little change in the water content or undrained shear strength of the soil due to pile installation. However, measurements of soil suction indicate that the mean effective stress (p') is increased within a region which extends to $r/R \approx 4$.

### 15.2.2 Equalization stage

1 Fast equalization. The equalization of pore pressures at the pile/soil interface is very fast, despite the low permeability of the clay. This implies either i) the clay is very stiff (the coefficient of consolidation, $c_h$, is large); or ii) the pore pressure gradients at the start of equalization are very steep.

2 Equalization involves swelling. The pore water pressures initially rise during equalization, in some places displaying a monotonic climb towards their equilibrium values, in others reaching a maximum and then falling. At the same time, the radial total stresses generally fall. The equalization process therefore involves both swelling and consolidation of the soil surrounding the pile.

3 Pore pressure response near the pile tip. Near the pile tip (at $z/R \approx 8$), the pore pressure rises to a maximum value ($\Delta u_{max}/\sigma'_{vo} \approx 5½$-11) in less than half an hour. Thereafter the pore pressure falls monotonically towards its equilibrium value.

4 Pore pressure response along the pile shaft. Along the pile shaft (at $z/R > 20$), the pore pressures rise very slowly, taking more than 1½h for the excess pressure ($\Delta u = u - u_o$) to become positive. In some cases the pore pressure next to the pile never exceeds its equilibrium value (i.e. $\Delta u \not> 0$).

5 Relaxation of radial total stresses. The radial total stresses ($\sigma_{rr}$) vary greatly during the first few hours of equalization, and

generally fall during this period. The radial total stresses reach a state of equilibrium within two to five days of pile installation.

6 Negative "set-up". The radial effective stresses at the pile/soil interface generally *fall* during equalization. Hence, near the pile shaft, equalization involves *swelling* rather than consolidation. This is consistent with the observation that the piles' shaft capacity reduces slightly with time.

7 Radial effective stresses at the end of equalization. At the *end* of equalization, the radial effective stress is between 3½ and 18 times the vertical effective stress ($\sigma'_{vo}$), depending on distance behind the pile tip. The lateral stress coefficient $K_c$ (= $[\sigma'_{rr}]_c/\sigma'_{vo}$) is much greater than $K_0$ ($K_c/K_0$ = 1.6-6.1), and generally less than the cavity expansion prediction ($K_c \approx 5.8c_{uo}/\sigma'_{vo}$). The measurements of soil suction indicate that, at the pile wall, the mean effective stress $p'_c$ is more than three times its original value ($p'_o$).

## 15.2.3 Pile loading

1 The effective stress equation holds. The pile's shaft capacity is controlled by the effective stresses acting at the pile/soil interface. The *local* shear resistance ($\tau_{rz}$) is linked to the radial effective stress at failure ($[\sigma'_{rr}]_f$) by the equation: $\tau_{rz} = \mu\sigma'_{rr}$, where $\mu$ is the coefficient of friction. The shaft capacity of the pile can be written as $Q_{shaft} = \pi D\int_L \mu(K_f/K_c)K_c\sigma'_{vo}dz$, where $K = \sigma'_{rr}/\sigma'_{vo}$ and the subscripts f and c denote stresses at the point of failure and at the end of equalization (respectively).

2 Variation in radial effective stress during undrained loading. The radial effective stress acting on the pile does not vary greatly during pile loading (until failure occurs). Hence $K_f/K_c \approx 1$.

3 Values of the coefficient of friction. The coefficient of friction ($\mu$) is independent of z/R, but its value depends strongly on the rate at which the pile was installed and on whether there is a change in loading direction.

4 Slow-jacked piles. A pile installed by *slow*-jacking gives a ductile response and at failure mobilizes a friction coefficient between 0.12 and 0.2 ($\delta$ = 7-11°). The soil surrounding the pile contracts after yielding (with $\mu$ increasing slightly or staying constant).

The (global) alpha value of the pile is close to 0.5. On loading in tension, the *slow*-jacked pile would be expected to give a brittle response and mobilize a friction coefficient between 0.2 and 0.25 ($\delta$ - 11-14°).

5 Fast-jacked piles. A *fast*-jacked pile loaded in either direction gives a brittle response and mobilizes a friction coefficient between 0.2 and 0.25 ($\delta$ - 11-14°). The soil surrounding the pile dilates after yielding (with $\mu$ decreasing). The (global) alpha value of the pile is close to 0.9.

6 Changes in loading direction. Reversing the direction of loading increases the brittleness of the pile and raises the coefficient of friction.

7 Continued displacement in the same direction. Continued displacement without a change in direction produces a ductile response to loading, with $\mu$ gradually reducing to somewhere between 0.12 and 0.20.

8 Driven piles. Driven piles behave in a similar fashion to fast-jacked piles, regardless of whether they are open- or closed-ended. Their load-displacement curves and first-time load capacities are identical to that of a fast-jacked pile (and therefore much different to that of a *slow*-jacked one). The results of load tests on slow-jacked piles should not be included in data-bases which are supposed to represent the behaviour of driven piles.

## 15.3 CONCLUSIONS CONCERNING EXISTING PILE THEORIES

1 Main conclusion. There is currently no theory of pile behaviour that correctly predicts the piles' response throughout installation, equalization, and pile loading.

2 Alpha method. The data provides little support for current empirical design rules. The measured alphas for the driven/fast-jacked piles are twice the value recommended by the current API code (0.78-0.93 as opposed to 0.42).

3 Beta method. There is no simple relationship between shaft friction and vertical effective stress (contrary to the assumption made in the beta method).

4 Cavity expansion theory. The cavity expansion method fails to predict the correct pore pressures, radial total stresses, or radial effective stresses over the entire range of OCRs (from 1 to 32). The discrepancy between the theory and the available test results widens as OCR increases. The cavity expansion method should not be used as a basis for designing piles in clays.

5 Strain path method. The strain path method gives reasonable predictions for the behaviour of displacement piles in low OCR clays. Predictions are not yet available for soils with OCRs greater than four.

## 15.4 SUGGESTIONS FOR FURTHER RESEARCH

One of the major conclusions from this research project is that current design methods do not reflect the underlying processes that govern pile behaviour. The long-term aim of any future research project should be to develop a rational design method based on an effective stress theory.

The first step in this direction is taken in Chapter 14, where a new method is proposed for designing piles in high OCR clays. Some of the assumptions on which the method is based require verification. The best way to achieve this is to conduct further *high quality* instrumented pile tests, in a wide range of clay soils. These tests should concentrate on:

- Verifying the relationship between the radial effective stress at the end of equalization and overconsolidation ratio of the soil (i.e. between $K_c = \sigma'_{rr}/\sigma'_{vo}$ and OCR)
- Establishing the relationship between $K_c$ and z/R for a number of soil types
- Recording the effective stress paths ($\tau_{rz}$ vs $\sigma'_{rr}$) during pile loading, with particular attention being paid to the values of $K_f/K_c$ and $\mu$

These tests should be conducted in a wide range of soils, with simultaneous measurement of the pore pressures and radial stresses <u>at several points</u> along the shaft. Care should be taken to ensure complete saturation of the pore pressure probes; and the earth pressure cells that are used should be stiff enough to nullify the effects of arching. Any load tests that are performed should follow well-established procedures.

In conjunction with the experimental work suggested above, efforts should be made to develop a reliable *theoretical* method for predicting the behaviour of piles, especially in high OCR clays. The cavity expansion method is not soundly-based, and gives poor predictions of the main parameters of interest over a wide range of OCRs. The first task should be to extend the strain path method to cover pile installation in heavily overconsolidated clays. As noted on p144, work has already started on this problem.

BIBL. LONDIN. UNIV.